

INITIATING MECHANISMS OF AORTIC VALVE DISEASE:
A ROLE FOR THE ENDOTHELIUM

A Dissertation

Presented to the Faculty of the Graduate School

of Cornell University

In Partial Fulfillment of the Requirements for the Degree of

Doctor of Philosophy

by

Emily Jean Farrar

August 2015

© 2015 Emily Jean Farrar

INITIATING MECHANISMS OF AORTIC VALVE DISEASE:
A ROLE FOR THE ENDOTHELIUM

Emily Jean Farrar, Ph.D.

Cornell University 2015

The objective of this thesis was to unveil initiating mechanisms of aortic valve disease, a serious and prevalent cardiovascular pathology affecting 2.8% of Americans over the age of 75. Currently, valve disease has no known causes and no existing treatments except for cardiothoracic surgery. Identification of initiating mechanisms will lead to new diagnostic markers and treatment strategies that would allow for early intervention and eventually the prevention of valve disease.

This work primarily focuses on the influence of the inflammatory cytokine tumor necrosis factor- α (TNF α) on the endothelial cells that line the aortic valve. By focusing on inflammation and the endothelium, both “first responders” to disease conditions in the valve environment, we hoped to unveil new mechanisms that could govern early stages of the disease. In this thesis, we have demonstrated that TNF α causes adult valve endothelial cells to produce destructive free radicals, dysregulating the delicate oxidate stress state of the valve. TNF α also drives endothelial cells to become mesenchymal via NF κ B signaling, a reactivation of an embryonic pathway important to shaping the valve leaflets *in utero*. We further found that NF κ B signaling

drives endothelial participation in the later stages of valve calcification, showing *in vivo* that NFκB is a critical mediator of valve dysfunction. We have also demonstrated a role for the stem cell transcription factor Oct4 in governing how valve endothelial cells change phenotype throughout disease. These findings have led to improved understanding of how NFκB and Oct4 govern interstitial cell calcification, in the later stages of valve disease. Finally, we have used the biomechanical engineering strengths of our lab to investigate how the regulation of valve interstitial cell contractility is crucial to progression of calcification in the valve.

My hope is that the results presented in this thesis will create a basic science foundation for the development of diagnostics and therapies to help patients suffering from aortic valve disease, especially those ineligible for surgical amelioration. Our *in vitro* and *in vivo* findings regarding the role of inflammation in endothelial dysfunction provide new evidence for the design of drugs targeting the NFκB pathway for aortic valve disease.

BIOGRAPHICAL SKETCH

Emily Farrar (née Howell) received a B.S. in Engineering, concentration in Mechanical Engineering, from Messiah College, Mechanicsburg, PA in May 2010. She graduated *summa cum laude* and was the recipient of the full-tuition Trustee's Scholarship as well as the James T. Scroggin Excellence in Engineering Award. Emily received her Master's in Biomedical Engineering in 2013 from Cornell University in the Cardiovascular Developmental Bioengineering Laboratory, led by Dr. Jonathan Butcher, where she also completed her doctoral dissertation research. She has been the recipient of numerous honors and awards, including the Cornell Sloan Fellowship for Diversity in Engineering and the National Science Foundation Graduation Research Fellowship. Emily has presented her work at numerous international and domestic conferences, including the Society for Heart Valve Disease and the American Heart Association's annual meetings. Her work has been published in numerous peer-reviewed journals, including *Arteriosclerosis, Thrombosis, & Vascular Biology* and the *Public Library of Science*.

Emily's doctoral dissertation work, "Initiating mechanisms of aortic valve disease: A role for the endothelium" was supervised by Dr. Jonathan Butcher, with committee members Dr. Cynthia Reinhart-King and Dr. Natasza Kurpios. She will begin as an Assistant Professor of Engineering at Messiah College in August 2015.

For MJF, my husband

“When I think of what life is, and how seldom love is answered by love; it is one of the moments for which the world was made.”

E.M. Forster, *A Room with a View*

ACKNOWLEDGMENTS

My doctoral work was funded by a National Science Foundation graduate research fellowship and a Cornell University Sloan Diversity Fellowship. Research materials and laboratory infrastructure were supplied by Dr. Jonathan Butcher, funded by grants from the National Science Foundation (CBET-0955172 and MRSEC DMR-1120296), the National Institutes of Health (HL110328 and HL118672), the Hartwell Foundation, and the LeDucq Foundation (MITRAL project). My conference travel for presentation of this research were additionally funded by Cornell Diversity Programs in Engineering, the Cornell Engineering Communications Program, the Cornell Center for Vertebrate Genomics, and the Cornell Graduate School.

I will always be grateful for my time at Cornell, because of the family that I found here. I discovered the loving environment of Bethel Grove Bible Church as a first year graduate student and it has never ceased to be my spiritual family in Ithaca. In 2010, I met my husband at Cornell and came to love him through our mutual work in the church. Now we have a beautiful daughter together, Clara Rose. My parents have been pivotal to my perseverance through the most challenging parts of my Ph.D. and self-sacrificial in their love for my family and me. My mother willingly gave up three months of her own time to help with Clara while I was writing this thesis, making it possible for both me and Matt to finish our work at Cornell in the best possible way. This work is the culmination of the efforts of many, and I am truly humbled by their love.

TABLE OF CONTENTS

Biographical Sketch.....	iv
Dedication.....	v
Acknowledgments.....	vi
Table of Contents.....	vii
List of Figures.....	x
List of Tables.....	xiii
List of Abbreviations.....	xiv
Preface.....	xviii
Chapter 1 Introduction	
1.1 Aortic valve structure and function.....	1
1.2 Aortic valve mechanics.....	4
1.3 Model systems.....	5
1.4 Aortic Valve Disease.....	7
1.5 Aims of this dissertation.....	28
REFERENCES.....	31
Chapter 2 Endothelial-derived oxidative stress drives myofibroblastic activation and calcification of the aortic valve	
2.1 Abstract.....	49
2.2 Introduction.....	51
2.3 Materials and Methods.....	54
2.4 Results.....	67
2.5 Discussion.....	85
REFERENCES.....	93
Chapter 3 Inflammatory cytokines promote mesenchymal transformation in embryonic and adult valve endothelial cells	
3.1 Abstract.....	101
3.2 Introduction.....	102
3.3 Materials and Methods.....	105
3.4 Results.....	117
3.5 Discussion.....	147
REFERENCES.....	153
Chapter 4 Heterogeneous Susceptibility of Valve Endothelial Cells to Mesenchymal Transformation in Response to TNF-alpha	
4.1 Abstract.....	163
4.2 Introduction.....	164
4.3 Materials and Methods.....	167
4.4 Results.....	173
4.5 Discussion.....	186
4.6 Conclusion.....	192

REFERENCES	194
Chapter 5 NFκB regulates endothelial to mesenchymal transformation and susceptibility to calcification in the aortic valve	
5.1 Abstract	199
5.2 Introduction.....	200
5.3 Materials and Methods.....	204
5.4 Results.....	209
5.5 Discussion.....	227
REFERENCES	231
Chapter 6 Characterization of the role of Oct4 in adult aortic valve disease	
6.1 Abstract.....	240
6.2 Introduction.....	241
6.3 Materials and Methods.....	244
6.4 Results.....	247
6.5 Discussion.....	259
REFERENCES	263
Chapter 7 Valve interstitial cell contractility directs calcification and extracellular matrix remodeling processes via RhoA signaling	
7.1 Abstract.....	269
7.2 Introduction.....	271
7.3 Materials and Methods.....	273
7.4 Results.....	284
7.5 Discussion.....	299
REFERENCES	307
Chapter 8 Future Directions & Conclusions	
8.1 Future Directions	313
REFERENCES	345
8.2 Conclusions.....	349
Chapter 9 Learning Spatial Visualization: Beyond Drills and into Early Mastery	
9.1 Abstract.....	352
9.2 Introduction.....	353
9.3 Course description and research methodologies.....	356
9.4 Results.....	360
9.5 Discussion.....	369
REFERENCES	371
Chapter 10 Valvular Heart Diseases in the Developing World: Developmental Biology Takes Center Stage	
10.1 Abstract.....	375
10.2 Introduction.....	376
10.3 Rheumatic Heart Disease.....	378

10.4 Endomyocardial Fibrosis	381
10.5 Developmental Biology Perspectives	383
10.6 Paths Forward	388
REFERENCES	390
Appendix A.....	396

LIST OF FIGURES

- Figure 1.1 Valves of the human heart. 1
- Figure 1.2 Relevant sources and effects of superoxide and nitric oxide in VEC. 12
- Figure 1.3 Sources and suppression of oxidative stress in valve endothelial cells. 14
- Figure 1.4 Mechanism of TNF α stimulation of NF κ B (p65/RelA sub-unit). 19
- Figure 1.5 Overlap between valvulogenic and pathogenic mechanisms in the aortic valve. 23
- Figure 1.6 Summary of the aims of this thesis. 27
- Figure 2.1 Elevated superoxide in the endothelium of calcified human aortic valves. 68
- Figure 2.2 Superoxide dismutase in calcified human valves. 69
- Figure 2.3 TNF α drives eNOS uncoupling. 71
- Figure 2.4 TNF α caused increased superoxide expression in VEC. 72
- Figure 2.5 eNOS protein expression in 48 hour VEC with TNF α or H₂O₂. 73
- Figure 2.6 VEC cultured *in vitro* on 3D hydrogels for 48 hours with TNF α +antioxidants. 73
- Figure 2.7 Effects of blocking eNOS uncoupling. 75
- Figure 2.8 VE-cadherin, eNOS, and VCAM1 protein expression in 48 hour VEC. 76
- Figure 2.9 Apoptosis in *ex vivo* AV leaflets cultured for 21 days. 77
- Figure 2.10 TNF α induces side-specific endothelial oxidative stress *ex vivo*. 78
- Figure 2.11 TNF α induces endothelial dysfunction *ex vivo*. 80
- Figure 2.12 eNOS, VE-cad, α SMA protein expression in *ex vivo* AV leaflets. 81
- Figure 2.13 TNF α induces early calcification and ECM changes *ex vivo*. 83
- Figure 2.14 q-rtPCR analysis of *ex vivo* AV leaflets with TNF α +antioxidants. 84
- Figure 2.15 Valve endothelial oxidative stress contributes directly to aortic valve disease. 86
- Figure 3.1 TNF α drives EndMT in postnatal VEC. 116
- Figure 3.2 Exposure to inflammatory cytokines induces EndMT in PAVEC. 119
- Figure 3.3 Exposure to inflammatory cytokines induces EndMT. 121
- Figure 3.4 NF κ B activation in PAVEC exposed to inflammatory cytokines. 122
- Figure 3.5 Diseased human aortic valve immunohistochemistry. 123
- Figure 3.6 Healthy human pediatric valve immunohistochemistry. 124
- Figure 3.7 Healthy human pediatric valve. 125
- Figure 3.8 Exposure to inflammatory cytokines induces EndMT in embryonic VEC. 127
- Figure 3.9 NF κ B expression in QEE+ TNF α , 48 hours. 128
- Figure 3.10 Inflammatory cytokine dose response migration and proliferation in QEE. 129
- Figure 3.11 Inflammatory gene expression in embryonic valve forming regions. 130
- Figure 3.12 TNF α induces EndMT through Akt/MAPK/NF κ B in PAVEC. 132
- Figure 3.13 IL-6 induces EndMT through Akt/NF κ B in PAVEC. 133
- Figure 3.14 TNF α induces EndMT through Akt/MAPK/NF κ B in QEE. 135
- Figure 3.15 IL-6 induces EndMT through Akt/NF κ B in QEE. 136
- Figure 3.16 Akt and MEK1 inhibitor effects on AKT1 and MEK1 in PAVEC. 137
- Figure 3.17 Akt and MEK1 inhibitor effects on AKT1 and MEK1 in QEE. 138
- Figure 3.18 Embryonic endocardial monolayers co-opt TGF β in TNF α -EndMT signaling. 140
- Figure 3.19 Exogenous TGF- β 1 induces EndMT in PAVEC. 142
- Figure 3.20 Embryonic endocardial monolayers co-opt TGF β in IL-6-EndMT signaling. 143
- Figure 3.21 Adult cells do not require TGF β in inflammatory-EndMT signaling. 145
- Figure 3.22 EndMT in development and disease. 146
- Figure 4.1 Membrane-based platform for VEC culture and evaluation of EndMT. 168
- Figure 4.2 Characterization of membrane culture system and EndMT response to TNF α . 174
- Figure 4.3 Imaging of TNF α -EndMT process. 176
- Figure 4.4 Time-dependent expression of EndMT genes in VEC treated with TNF α . 179

Figure 4.5	Expression of EndMT proteins in non-transformed and transformed cells.	180
Figure 4.6	Comparison of genes in transformed and non-transformed VEC.	183
Figure 4.7	Collagen fibers surrounding transformed and non-transformed VEC.	186
Figure 5.1	Characterization of the effect of IKK β deletion on valve function.	210
Figure 5.2	p65 and VCAM-1 expression in AVD and AVD+IKK $\beta^{fl/fl}$ mice.	212
Figure 5.3	Inactivation of NF κ B prevents development of aortic valve calcification.	214
Figure 5.4	Valve function changes with AVD or AVD+IKK $\beta^{fl/fl}$.	215
Figure 5.5	Cardiac function and aortic plaques are improved by NF κ B inactivation.	217
Figure 5.6	Aortic root diameter and distensibility.	218
Figure 5.7	NF κ B activation is necessary and sufficient for aortic valve EndMT.	220
Figure 5.8	NF κ B activation enables endothelial osteogenic differentiation.	222
Figure 5.9	NF κ B modulates interstitial cell calcification.	225
Figure 6.1	Oct4 in healthy human aortic valve leaflets.	248
Figure 6.2	Oct4 in calcified human aortic valve leaflets.	249
Figure 6.3	Delivery of ASOct4 and Oct4 plasmids to PAVEC.	251
Figure 6.4	Oct4 protein expression in PAVIC and PAVEC after 14 days.	251
Figure 6.5	Effect of Oct-4 modulation on VEC inflammatory EndMT.	252
Figure 6.6	Oct4 mRNA in 14 day valve cell co-culture (+OGM, + TNF α).	254
Figure 6.7	Oct4 over-expression enables VEC calcification and pro-osteogenic signaling.	255
Figure 6.8	Effect of Oct4 over-expression or inhibition on VIC calcification.	257
Figure 6.9	Oct4 expression in healthy and diseased adult mouse aortic valves.	258
Figure 7.1	Design and manufacturing of system to measure VIC contractility.	274
Figure 7.2	Calibration of system to measure VIC contractility.	276
Figure 7.3	Characterization of system to measure VIC contractility.	285
Figure 7.4	Pro-osteogenic environment disrupts native mechanical activity of VIC.	287
Figure 7.5	Pro-osteogenic environment increases VI. NC myofibroblastic signaling.	289
Figure 7.6	Pro-osteogenic environment disrupts VIC organization of collagen matrix.	292
Figure 7.7	Nodules and osteogenic signaling in mechanically active VIC hydrogels.	294
Figure 7.8	RhoA inhibition blocks osteogenic response of VIC.	296
Figure 7.9	Collagen fiber dynamics correlate with VIC mechanical activation.	298
Figure 7.10	Dynamics of collagen, cells, and calcification in VIC in tensioned hydrogels.	299
Figure 7.11	Interactions between cells, collagen, signaling molecules, and tension.	300
Figure 8.1	Effect of SOD-mimetic Tempol on 30 minute TNF α -VEC oxidative stress.	314
Figure 8.2	Effect of Akt inhibition on 30 minute TNF α -VEC oxidative stress.	315
Figure 8.3	Acute eNOS response of adult valve endothelial cells to TNF α .	316
Figure 8.4	Apoptotic and NF κ B signaling response of VEC to TNF α .	317
Figure 8.5	Interplay between EndMT and OxS signaling in VEC+TNF α .	319
Figure 8.6	Effect of VEC-specific NF κ B inactivation on aortic valve disease <i>in vivo</i> .	325
Figure 8.7	VEC+NF κ B microarray results for EndMT and calcification genes.	330
Figure 8.8	VEC+NF κ B microarray results for AVD and reprogramming genes.	330
Figure 8.9	Network 1 for NF κ B Data	334
Figure 8.10	Network 18 for NF κ B Data	335
Figure 8.11	Network 25 for NF κ B Data	336
Figure 8.12	Oct4 expression in adult mouse aortic valves.	338
Figure 8.13	Interplay between NF κ B and Oct4 signaling in PAVEC.	340
Figure 8.14	Interplay between NF κ B and Oct4 signaling in PAVIC.	341
Figure 8.15	Effect of changing cantilevered spring stiffness on VIC phenotype.	344
Figure 8.16	Conclusion of findings contained in this thesis.	346
Figure 9.1	SV Project “Nuclear Squeeze” data from faculty client.	362
Figure 9.2	Partial worksheet for the Nuclear Squeeze project.	363

- Figure 9.3 Structure and components of spatial visualization course. 364
- Figure 9.4 Visuals created by students working on the Nuclear Squeeze project. 367
- Figure 9.5 Frequency of student use of different terms in peer evaluation of SV projects. 368
- Figure 10.1 Mortality due to RHD in developing countries compared to Western nations. 378
- Figure 10.2 Valve deformity in rheumatic heart disease. 380
- Figure 10.3 Pathology of endomyocardial fibrosis. 382
- Figure 10.4 Similar pathways in valve development and disease. 385

LIST OF TABLES

Table 1.1	Endothelial cell oxidants, sources, and inhibitors	15
Table 1.2	Effects of diet and timing on the aortic valve of LDLR ^{-/-} mice	20
Table 3.1	Primer sequences for q-rtPCR on pig and chick mRNA	110
Table 4.1	Quantitative rt-PCR primers used in membrane-EndMT assays	172
Table 5.1	Mouse groups, genotypes, and diet conditions	206
Table 5.2	Offspring ratios of Nfatc1 ^{Cre} ;IKKβ ^{fllox} ;LDLR ^{KO} mice	207
Table 7.1	Quantitative rt-PCR primers	280
Table 8.1	NFκB Networks	333
Table 8.2	DNA binding targets of Oct4 in aortic valve interstitial cells	342

LIST OF ABBREVIATIONS

3-D	three-dimensional
ACTA2	smooth muscle aortic alpha-actin
Akt	protein kinase B
Akt XI	inhibitor of Akt
Alk2/5	activin receptor-like kinase 2 and 5
ALP	alkaline phosphatase
ANOVA	analysis of variance
AoV	aortic valve
ARS	alizarin red s
ASc	aortic sclerosis
ASOct4	antisense-Oct4
AV	aortic valve
AVD	aortic valve disease
AVS	aortic valve stenosis
BAV	bicuspid aortic valve
BAY11-7082	irreversible inhibitor of phosphorylation of I κ B α
BH ₄	tetrahydrobiopterin
BMP	bone morphogenetic protein
BrdU	bromodeoxyuridine
BSA	bovine serum albumin
CAD	computer-aided design
CAVD	calcific aortic valve disease
CD31	cluster of differentiation 31, also known as PECAM-1
cHAV	calcified human aortic valve
ChIP	chromatin immunoprecipitation
CM-H ₂ DCF-DA	chloromethyl derivative of 2',7'-dichlorodihydrofluorescein diacetate
COL1A1	collagen type 1, alpha 1
COL2A1	collagen type 2, alpha 1
COL3A1	collagen type 3, alpha 1
CTL	control
CUES	cornell university engineering success
CVD	cardiovascular disease
DHE	dihydroethidium
DI water	deionized water
DIC	differential interference contrast
DMEM	Dulbecco's modified Eagle's medium
DN-RhoA	dominant-negative RhoA
DNA	deoxyribose nucleic acid
DN κ B	dominant-negative I κ B
DPE	Diversity Programs in Engineering

Draq5	far-red DNA stain
EC	endothelial cells
ECM	extracellular matrix
ECP	Engineering Communications Program
EDTA	ethylenediaminetetraacetic acid
EKV	ECG-Gated Kilohertz Visualization
EMF	endomyocardial fibrosis
EMT	epithelial to mesenchymal transformation
EndMT	endothelial to mesenchymal transformation
eNOS	endothelial nitric oxide synthase
EPC	endothelial progenitor cells
FBS	fetal bovine serum
FGC	first-generation college
GAG	glycosaminoglycans
GAPDH	glyceraldehyde 3-phosphate dehydrogenase
GFP	green fluorescent protein
H ₂ O ₂	hydrogen peroxide
HH14 ⁻	Hamburger Hamilton stage 14-
HIV	human immunodeficiency virus
HVD	heart valve disease
hVEC	human valve endothelial cells
hVIC	human valve interstitial cells
ICAM-1	intercellular cell adhesion molecule 1
ICM	inner cell mass
IKK β	inhibitor of nuclear factor kappa-B kinase subunit beta
IL-6	interleukin-6
IL6RA	interleukin-6 receptor A
IntDen/ μm^2	integrated density per micron-squared
IPA	Ingenuity Pathway Analysis
iPS	induced pluripotent stem cell
I κ B α	nuclear factor of kappa light polypeptide gene enhancer in B-cells inhibitor, alpha
kDa	kiloDalton
L-NAME	L-NG-Nitroarginine methyl ester
lacZ	structural gene of the lac operon
LDLR	low density lipoprotein receptor
LV	left ventricular
MAPK	mitogen-activated protein kinase
MATLAB	mathematics laboratory software, developed by MathWorks
MEK1	activator of MAPK
mM	milliMolar
MMP-9	matrix metalloproteinase-9

mRNA	messenger RNA
Msx2	msh homeobox-2
mtROS	mitochondrial reactive oxygen species
NADPH	nicotinamide adenine dinucleotide phosphate-oxidase
NaF	sodium fluoride
NaOH	sodium hydroxide
NaVO ₄	sodium orthovanadate
NEMO	NFκB essential modulator
Nfatc1	nuclear factor of activated T-cells, cytoplasmic protein 1
NFκB	nuclear factor kappa B
Ng/mL	nanograms per milliliter
NO	nitric oxide
NOS3	nitric oxide synthase 3
NSF	National Science Foundation
NT-VEC	non-transforming valve endothelial cells
nVIC	normal valve interstitial cells
obVIC	osteoblast-like valve interstitial cells
OCN	osteocalcin
Oct4	octamer-binding transcription factor-4
OFT	outflow tract
OGM	osteogenic media
ONOO ⁻	peroxynitrite
OPN	osteopontin
OxS	oxidative stress
P4	passage 4
PAEC	porcine aortic endothelial cells
PAVEC	porcine aortic valve endothelial cells
PAVIC	porcine aortic valve interstitial cells
PBS	phosphate buffered saline
PCR	polymerase chain reaction
PD98059	selective inhibitor of MAPK
PDMS	polydimethylsiloxane
PDTC	pyrrolidine-dithiocarbamate
PECAM-1	platelet endothelial cell adhesion molecule, also known as CD31
Peg-SOD	pegylated superoxide dismutase
PET/CT	positron emission tomography-computed tomography
PFA	paraformaldehyde
PjBL	project-based learning
PpYLKTK	cell-permeable STAT3 inhibitor peptide
PSVT	Purdue Spatial Visualization Test
q-rtPCR	quantitative real time polymerase chain reaction
QEE	quail endocardial explants

QH1	quail endothelial marker
RANKL	receptor activator of nuclear factor kappa-B ligand
RHD	rheumatic heart disease
RIPA	radioimmunoprecipitation assay
RLT buffer	proprietary lysis buffer, Qiagen RNeasy kit
RNA	ribonucleic acid
ROSA26	ROSA β geo26 gene locus for generalized expression
RT	room temperature
Runx2	runt-related transcription factor 2
SB 431542	selective inhibitor of TGF- β 1 Alk receptors
SDS	sodium dodecyl sulfate
SEM	standard error of the mean
SMC	smooth muscle cells
SOD	superoxide dismutase
STAT3	signal transducer and activator of transcription 3
STEM	Science, Technology, Engineering, and Mathematics
STEP	Science, Technology, Engineering, and Mathematics Talent Expansion Program
SV	Spatial Visualization
SYBR Green	asymmetrical cyanine dye used as a nucleic acid stain in molecular biology
T-VEC	transformed valve endothelial cells
TEHV	tissue engineered heart valve
TGF β	transforming growth factor-beta
TNFR1	tumor necrosis factor receptor 1
TNFRSF1A	tumor necrosis factor receptor super family 1A
TNF α	tumor necrosis factor-alpha
Tris	tris(hydroxymethyl)aminomethane
TUNEL	terminal deoxynucleotidyl transferase dUTP nick end labeling
Tween-20	polysorbate 20
U/mL	units of activity per milliliter
URM	under-represented minority
UV	ultraviolet
VCAM-1	vascular cell adhesion molecule 1
VE-cadherin	vascular endothelial cadherin
VEC	valve endothelial cells
VEGF	vascular endothelial growth factor
VIC	valve interstitial cells
WT	wild type mouse
α SMA	alpha smooth muscle actin

PREFACE

This thesis focuses primarily on the initiating mechanisms of valve disease, following a trajectory from inflammation to oxidative stress, to EndMT, NFκB, and transdifferentiation (Chapters 2-6). All these elements focus on the endothelium of the aortic valve. However, the Butcher Lab has great strengths in development of novel bioreactors for studying the complex mechanical elements of the valve and my background is mechanical engineering. Thus, I also chose to explore the contractile mechanics of valve interstitial cells through the collaborative design and development of a novel device to grow and measure the tensile stress of valve interstitial cells (Chapter 7). The biomedical engineering research portion of this thesis concludes with a discussion and future directions in chapter 8. However, I also wished to present publications from two of my other areas of interest, engineering education (Chapter 9) and biomedical engineering for the developing world (Chapter 10). I am fortunate to be able to say that these three interests: biomedical engineering research, engineering education, and work for the developing world, will coalesce in my career as an engineering professor at Messiah College, starting in Fall 2015. I hope that my future students who read this thesis will see how my path was shaped by the pursuit of seemingly disconnected endeavors and be encouraged.

“Life is easy to chronicle, but bewildering to practice.”

E.M. Forster, *A Room with a View*

CHAPTER 1

INTRODUCTION

1.1 Aortic valve structure and function

The aortic valve is a tri-leaflet structure that sits at the base of the aorta, superior to the left ventricle (Figure 1.1). The primary function of the aortic valve is to preserve unidirectional flow out of the ventricle and into circulation, preventing regurgitation.

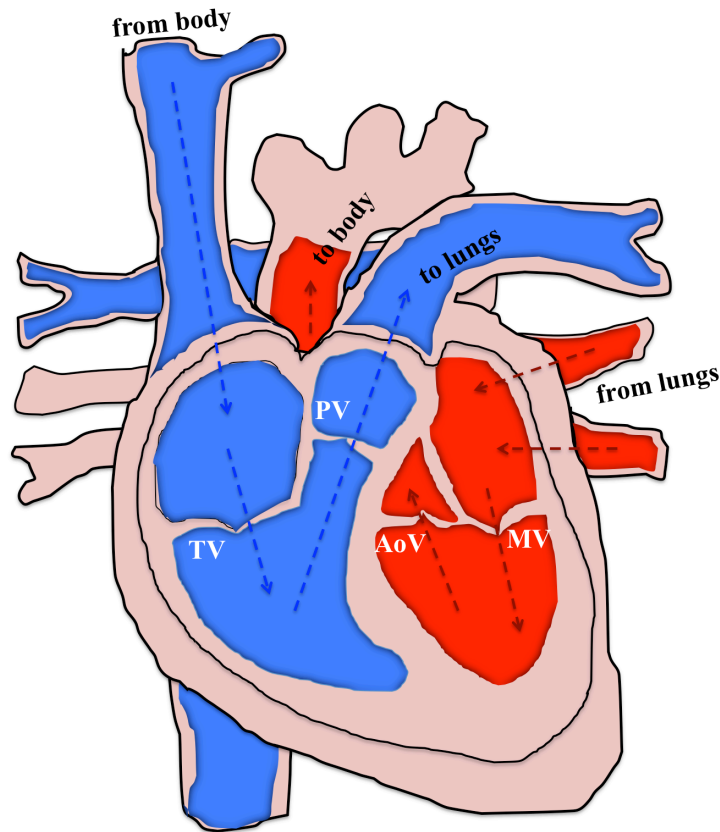


Figure 1.1 Valves of the human heart.

Oxygenated blood from the lungs is in red, deoxygenated blood from the body is in blue. The aortic valve (AoV) sits at the base of the aortic. The mitral valve (MV), the tricuspid valve (TV), and the pulmonary valve (PV) are also noted for reference.

The valve has two main cell types, valve interstitial cells (VIC) and valve endothelial cells (VEC). VIC reside within the matrix of the valve tissue; VEC line the surface of the valve. There is also a small sub-population of cells of extravalvular origin. The aortic valve extracellular matrix (ECM) is made up of collagen, glycosaminoglycans, and elastin. Preservation of the native valve structure is crucial to the proper function of the heart and ultimately the health and function of the human body [1].

Valve interstitial cells

VIC play an active role in maintaining the health of valve tissue and in valve pathology. VIC originate from endocardial cells in the developing heart that undergo an endothelial to mesenchymal transition [2]. In the mature valve, VIC reside within the valve ECM. A number of different VIC phenotypes have been identified [3], but the primary populations are quiescent VIC and activated VIC, differentiated by the presence of the myofibroblastic protein alpha-smooth muscle actin in the latter [4]. Importantly, VIC are distinct from other populations of mesenchymal cells in the body. They have a unique contractile phenotype and a characteristic secretion of protein and ECM components in culture [5]. The specificity of this cell population highlights the importance of understanding the active contribution of VIC to valve degeneration in order to develop effective therapies [6].

Valve endothelial cells

VEC line the surface of the aortic valve, continuous with the endothelial cell populations that cover the adjacent blood vessels. VEC are a typical endothelial cell population, flat and polarized so as to bind with the basal lamina on their underside and to be hemodynamically sensitive on their outer surface [7]. They form a barrier between the blood and the valve tissue, are first responders to circulating biochemical cues, and are mechanically sensitive to shear, stiffness, and strain [8]. VEC are distinct from other endothelial populations, most notably in hemodynamic response [9] and in propensity towards endothelial to mesenchymal transformation (EndMT) [10,11]. It is still disputed whether VEC EndMT, whereby endothelial cells invade their underlying matrix and become mesenchymal cells, is a normal homeostatic process [12,13] or a feature of disease [14]. Dysregulation of the valve endothelium is a well-established feature of early valve disease in humans [15]. Understanding the pathobiological contribution of VEC to valve degeneration is an important step towards developing effective diagnostic and treatment strategies.

Cells of extravalvular origin

Aortic valves also play host to cells of extravalvular origin, recruited as a feature of both normal valve maintenance and in disease. Mouse models have shown homeostatic recruitment of bone marrow derived cells to the aortic valve as a source of new VIC [16]. The role of endothelial progenitor cells (EPC) has been subject to intense scrutiny. Some groups hypothesize that a sub-group of native VEC are progenitors that help replenish VIC populations [13]. Others identify circulating EPC

(CD34⁺;CD133⁺) as the primary population of interest, especially as fewer EPC from the circulating peripheral blood are found in diseased valves compared to healthy [17]. In diseased valves, EPC are co-localized with inflammatory cells [18] and osteoblast-like cells [19], pointing towards their active role in disease.

Valve extracellular matrix

The aortic valve is organized into three layers, distinguished by their primary extracellular matrix components. The fibrosa is closest to the aortic side of the valve. It is characterized by collagen fibers that provide tensile strength and durability during valve flexure. The spongiosa is the middle layer, characterized by proteoglycans that provide cushioning against the intense mechanical deformations undergone by the valve during a normal cardiac cycle. The final layer is the ventricularis, which is characterized by its elastin fibers [20,21]. The fibrosa layer is most prone to the formation of calcific nodules, possibly due to the exposure of the arterial side of the valve to the circulating blood flow patterns of the aortic root [22].

1.2 Aortic valve mechanics

The aortic valve is a complex mechanical tissue that resides within an even more mechanically complex environment. Both VIC and VEC actively modulate the mechanical properties of the valve tissue, and each ECM component fine-tunes the valve structure. As a whole tissue structure, the valve is subject to shear stress from the blood rushing past its surface and to bending stress as the leaflets open and shut [23]. The valve undergoes contractile changes throughout each cardiac cycle [24] and

changes in stiffness when diseased [25]. All the elements combine to make the aortic valve a compelling structure for biomedical engineering investigation.

The case for the mechanical environment as a master regulator of aortic valve cellular function arose from examination of bicuspid aortic valves (BAV). Patients with BAV have two leaflet aortic valves, rather than the typical three-leaflet structure. These patients progress to aortic valve stenosis (AVS) more quickly and at higher rates than those with tricuspid aortic valves [26]. One explanation of this propensity for disease is that BAV experience different stress, strain, and shear patterns *in vivo* than their tricuspid aortic valve counterparts. Thus, many different bioreactors have been constructed to understand the effect of mechanical environment on valve cell phenotype. Elevated strain influences ECM remodeling [27,28], EndMT [11], calcific nodule morphogenesis [29], and apoptosis [30]. Conversely, valve cells play an active role in shaping their mechanical environment [28,31,32] [8,33]. Consideration of both the “outside-in” and “inside-out” interplay between valve cells and their environment is an important component of aortic valve mechanobiology.

1.3 Model systems

Both *in vivo* and *in vitro* systems are used to study aortic valve pathobiology. There is no animal model that completely recapitulates human aortic valve disease (AVD), but there are many different approaches that capture specific elements. Wild type mice do not spontaneously develop AVD at any age. Therefore, mouse models of AVD rely on a genetic, diet-induced, or combination approach. Some genetic approaches

recapitulate elements of AVD that arise in valvulogenesis, such as bicuspid aortic valve (ex. eNOS^{-/-}, Periostin^{-/-}). AVD in these models develops exceedingly quickly, as soon as 6 weeks postnatal [34]. Other genetic approaches are modeled after known human genetic mutations associated with AVD, primarily Notch1 mutations [35]. Diet-induced AVD in mice is typically achieved using a high-fat diet known as the “Western diet”, with 42% of calories from fat and elevated cholesterol. The Western diet can induce certain elements of AVD in C57/Bl6 wild type mice, with enhanced effects when administered to mice with pro-hypercholesterolemic genetic alterations [36,37]. Herein, we have chosen to use a low-density lipoprotein receptor knock-out (LDLR^{-/-}) mouse with four months of the Western diet. This model induces calcific deposition in the leaflets, chronic inflammation, and elevation of transvalvular velocities [38,39].

Although they do not progress to calcification, pig valves develop spontaneous lesions with age and are widely used in cardiovascular research [40,41]. The pig genome is homologous to humans and porcine valves are often used to as human valve replacements [42]. Porcine VEC have been shown to recapitulate fundamental aspects of AVD such as side-specific phenotypic changes [43], VEC-VIC signaling [44], and heterogeneity in susceptibility to disease [45]. Pig hearts are widely available, inexpensive, and large enough to provide a robust valve cell source for primary culture. Porcine VEC maintain their phenotype for up to six passages after primary isolation [14] and porcine VIC for up to seven passages [5]. Both have been characterized in three-dimensional co-culture systems by our lab [5] and others [46].

1.4 Aortic Valve Disease

Statistics

Valvular heart disease has a prevalence of 2.5% in the overall population of the United States. Aortic stenosis (AS) and regurgitation contributes 0.9%, with increasing prevalence with age. The prevalence of moderate or severe AS is 2.8% in patients older than 75 years [47]. About half of diagnosed AS patients undergo cardiothoracic surgery for replacement of the aortic valve, the only existing treatment for AS [48,49]. No efficacious medical therapies have been identified, despite early indications that statin therapy could slow ASc progression [50-52]. Transcatheter aortic valve replacement is the most common and most cost-effective surgical intervention, with a one-year cost of \$106,076 per patient on average [53]. Therefore, approximately 336,000 Americans undergo aortic valve replacement each year, with a total burden on the United States economy of \$35 billion in health care expenses per year due only to aortic stenosis.

Etiology

Clinical aortic valve disease (AVD) typically presents in two stages: aortic sclerosis (ASc) and the more severe aortic stenosis (AS). ASc is the thickening and/or calcification of the aortic valve with no hemodynamic changes, considered an early and subclinical form of AVD. ASc is considered a necessary but not sufficient step towards AS; some ASc patients will never progress to AS [54]. However, ASc is independently associated with increased risk of other cardiovascular events and all-

cause mortality [55]. AS is characterized by hemodynamic changes, primarily increased velocity and pressure gradient through the valve [56].

New imaging techniques are shedding light on early mechanisms, important to understanding what initiates and causes progression of ASc to AS [57-59]. PET/CT studies reveal that calcification of the aortic valve appears to be its own distinct phenomenon in both initiation and mechanism, despite sharing risk factors with atherosclerosis [60]. AVD involves mineralization more often and earlier in the process than atherosclerosis [61].

Tissue injury is another known contributor to AVD initiation. AVD increases in prevalence with age, leading to the hypothesis that the “wear and tear” associated with ageing can disrupt the collagen structure of the valve tissue and promote calcification [62]. Aortic valve calcific deposits are frequently localized to areas of maximal cusp flexion, pointing to mechanical stress as an initiating factor in AVD [63]. Recently, it was shown in wild type mice that direct injury to the valve leaflet can induce AS [64], supporting the tissue injury hypothesis.

Tissue injury, inflammation, oxidative stress, and physical forces activate valve cells in early stages of disease, initiating valve degeneration [65]. Both VIC and VEC are considered active and necessary contributors to AVD, with additional participation from circulating extravalvular cells such as osteoprogenitors [66].

Valve interstitial cells in aortic valve disease

Improvements in cell culture methods have allowed researchers to move from a descriptive, histopathology-based understanding of cell participation in AVD to a mechanistic approach [3]. VIC are the majority cell type in the aortic valve. VIC differentiate into osteoblast-like cells under the influence of osteogenic media (DMEM+ascorbic acid and β -glycerophosphates), enhanced by bone morphogenetic proteins and cytokine TGF- β [67]. VIC pro-osteogenic activity is most often monitored by alkaline phosphatase assays and alizarin red staining for calcium, as well as activation of pro-calcific cell signaling pathways and formation of nodules [68]. VIC osteogenesis is regulated by their mechanical [69] and inflammatory environment [70,71].

Valve endothelial cells in aortic valve disease

It is certain that VEC play an active role in the initiation and progression of AVD, but their mechanisms of contribution are not well understood [7]. VEC are important protectors of healthy valve function; endothelial dysfunction correlates with progression of AVD [15]. Many recent studies have shown that VEC regulate the function of VIC [72], maintaining VIC quiescence and promoting valve health [73]. One mechanism of VEC influence on VIC is via production of the vasoreactive agent nitric oxide, which protects against VIC calcification [44] and regulates Notch1 signaling [74].

VEC also play an independent, active role in AVD apart from their effect on VIC. For example, endothelial-specific deletion of Notch signaling *Jag1* leads to valve calcification in mice [75]. VEC actively regulate the mechanical properties of the aortic valve [33], which leads to downstream changes in both VIC and VEC signaling and disease propagation. VEC from the disease-prone fibrosa side of the valve have different DNA [45] and micro-RNA [76] profiles than the ventricularis side. This spatial heterogeneity is observed but not explained; it may relate to the different hemodynamic environments experienced by these VEC populations.

Inflammation in AVD

That inflammation is a feature of AVD has been known for some time [77]. Recent advances in imaging have revealed that inflammation of the valve actually precedes calcification [78]. Inflammation is proportional to degree of calcification in AVD throughout the course of the disease [79]. VEC are first-responders to inflammatory signals [80]. Circulating immune cells activate inflammatory adhesion molecules on the protective VEC layer early and persistently [81]. The expression of these molecules, such as ICAM-1 and VCAM-1, selectively modulates disease progression [82]. VEC inflammatory activation also acts in a dynamic feedback loop with changes in mechanics as the valve [83], evidence of ongoing cross-talk between inflammation and valve degeneration throughout AVD.

Oxidative stress in AVD

Oxidative stress is well-described in late-stage valve disease [84] and is known to exacerbate osteogenic activation in aortic sclerosis, but it is not known why or how oxidative stress becomes elevated. Tightly regulated in vitro studies can elucidate the cellular mechanism behind increased oxidative stress and reveal new therapeutic targets with high clinical impact.

Previous studies have suggested that valve oxidative stress is fundamentally different than vascular oxidative stress, in that reactive oxygen species (ROS) arise not from NADPH oxidases, but from uncoupling of endothelial nitric oxide synthase (eNOS) [85]. The antioxidant effects of statins arise from inhibition of NADPH oxidase and upregulation of catalase, thus bypassing any effect on eNOS [86]. Therefore, answering the question of eNOS involvement in oxidative stress would contribute to understanding of why lipid-lowering agents have largely proved ineffective in CAVD [87].

Evidence for a unique role of valve endothelial cells in disease [88] supports close investigation of this cell type in oxidative stress initiation. Oxidative stress from the endothelium can be both protective, in the form of nitric oxide, and degenerative when there is excess superoxide (Figure 1.2). It is important to understand the balance of benefit and degradation when examining valve endothelial oxidative stress.

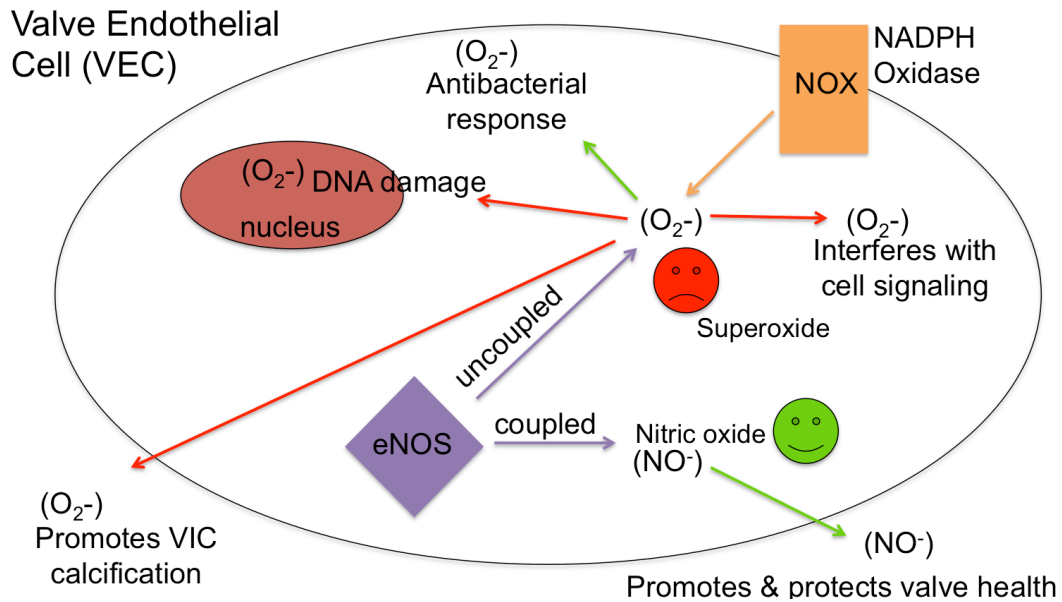


Figure 1.2 Relevant sources and effects of superoxide and nitric oxide in valve endothelial cells.

Detrimental effects are denoted by red arrows. Beneficial effects are denoted by green arrows. Cellular oxidative stress is complex and should be seen as a continuum, rather than an on/off mechanism.

For example, in addition to an active role of endothelial cells in initiating oxidative stress, oxidative stress itself could degrade the protective role of the endothelium, especially through reduced nitric oxide and increased permeability, further propagating valve degeneration. Lastly, oxidative stress in the form of superoxide (O_2^-) is known to activate osteogenic transcription factor Runx-2 in atherosclerosis [89], suggesting that reactive oxygen species secreted by the endothelium could participate in activation of underlying interstitial cells towards an osteogenic phenotype.

Nitric oxide synthases are enzymes that produce nitric oxide, a free radical. There are three isoforms, endothelial, neuronal, and inducible NOS. Endothelial NOS (eNOS) is found in endothelial cells, typically associated with the plasma membrane, membranes of golgi bodies, and the perinuclear region during activation [90]. Constitutive levels of Ca^{2+} activate eNOS to secrete basal levels of nitric oxide (NO), which regulates vasculature tone and valve stiffness [91, 92]. Reduced bioavailability of NO is considered permissive of aortic valve disease ([93, 84]), but the mechanism of protection is unknown. Neuronal NOS is similar to eNOS in that it is activated by calcium in its basal state, but it is mainly found in neuronal and skeletal muscle tissue. Inducible NOS is slightly different in that basal levels of active iNOS have not been detected and it is not dependent on calcium. iNOS also is typically triggered at later time points than eNOS and nNOS, which respond within minutes [95] (Figure 1.3A).

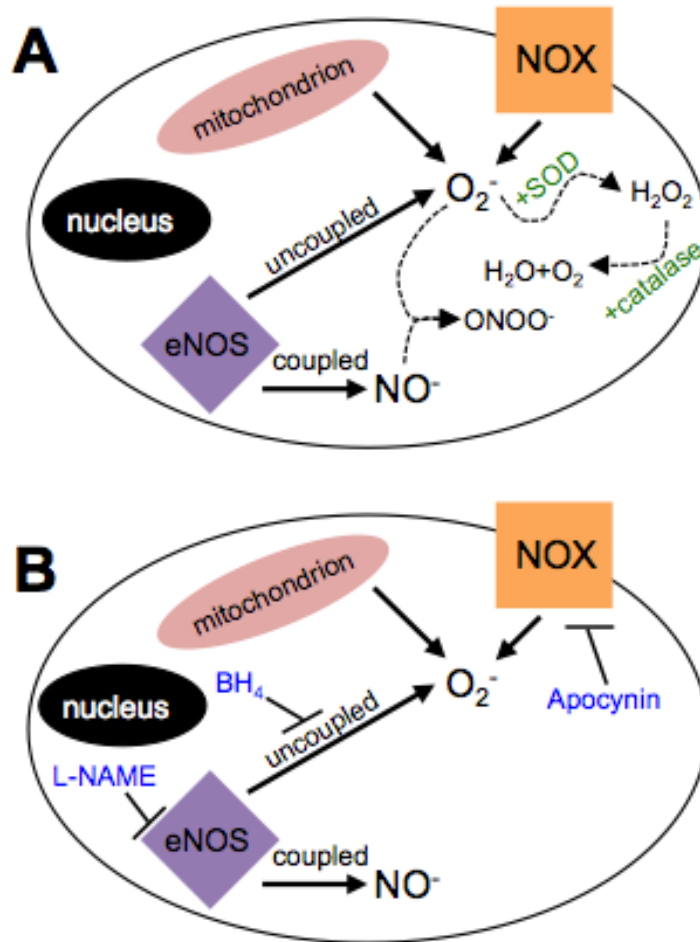


Figure 1.3 Sources and suppression of oxidative stress in valve endothelial cells.

A. NADPH oxidases (NOX), endothelial nitric oxide synthase (eNOS), and mitochondria are sources of superoxide (O_2^-) in valve endothelial cells. O_2^- becomes hydrogen peroxide (H_2O_2) or peroxynitrite ($ONOO^-$). Superoxide dismutase (SOD) and catalase are native intracellular enzymes that work to breakdown O_2^- into harmless water and molecular oxygen. B. Exogenous treatments (blue) can be added to inhibit or mitigate different components of endothelial oxidative stress, including eNOS cofactor tetrahydrobiopterin (BH_4) and L-arginine competitor L-NAME.

Nitric oxide was discovered by Joseph Priestley in 1772 as a colorless, odorless gas. Its properties as a vasodilator were discovered in 1980 by Furchgott and Zawadzki, as well as its origins in the endothelium, though the connection between this function and the NO gas was only made in 1987 by a separate group [96] [97]. It is synthesized by one of the three NOS isoforms from the amino acid L-arginine in a two step process, dependent on calmodulin binding [98]. nNOS and eNOS also require Ca²⁺ for NO synthesis, but iNOS is independent of Ca²⁺ levels [95]. After calmodulin binding, reduced NADPH at the cell membrane donates an electron to the NOS complex, which reduces a molecular oxygen at the heme site, within the oxidase domain. The oxidase domain also binds the cofactor tetrahydrobiopterin (BH₄) and L-arginine. The reduced oxygen then converts L-arginine to L-citrulline via interaction with the guanidino group, with NO as a byproduct (review: [99]).

N^G-nitro-L-Arginine (L-NNA) is an analogue of L-arginine with a chemically altered guanidino group. When administered to cells, L-NNA competitively binds with the NOS complex, making it dysfunctional and decreasing NO synthesis. L-NNA is only marginally water-soluble, thus a more soluble precursor to L-NNA, L-N^G-Nitroarginine methyl ester (L-NAME) is used rather than L-NNA in most *in vitro* experiments. L-NAME does however require intracellular hydrolysis of its methyl ester group in order to be a fully functional inhibitor, reducing its usefulness *in vivo* [100].

Although generally synonymous with healthy endothelial function, eNOS can become detrimental to cellular function if improperly regulated. The most important case involves the cofactor tetrahydrobiopterin (BH₄). Insufficient BH₄ has been implicated in a phenomenon known as eNOS uncoupling, where eNOS produces superoxide rather than nitric oxide [101]. Without BH₄ in the NOS oxidase domain, the electron from NADPH binds to an oxygen molecule rather than to L-arginine, producing superoxide (O₂⁻) rather than NO.

Hydrogen peroxide (H₂O₂) is a highly oxidizing free radical that can be broken down into oxygen and water by the enzyme catalase. Both H₂O₂ and superoxide are elevated in stenotic aortic valves [86]. H₂O₂ activates osteogenic transcription factor Runx-2 in atherosclerosis [90] and was recently shown to act similarly in aortic valve interstitial cells [158]. The half-life of H₂O₂ in vivo is much longer than that of NO or superoxide, from 60 minutes to 4 hours depending on cell type [102]. This characteristic of H₂O₂ contributes to the role of H₂O₂ as a major signaling molecule in endothelial cells [103]. Thus, tuning of the levels of intracellular H₂O₂ is preferable to complete eradication of H₂O₂.

Superoxide is formed by a one-electron reduction of O₂, resulting in O₂⁻. It is biologically toxic. Superoxide release by leukocytes is used in pathogen destruction [104]. Intracellular, superoxide damages proteins, lipids, catalase, and DNA (via the Haber-Weiss reaction) [105]. Superoxide can also react with nitric oxide to form peroxynitrite, reducing the overall bioavailability of nitric oxide in the cell (review:

[106]). Superoxide can be produced by NADPH oxidase, a membrane-bound enzyme complex that creates the O_2^- molecule by transferring an electron to an intracellular oxygen molecule. NADPH oxidase is an important component of antibacterial response and has been implicated in the progression of atherosclerosis [107]. Superoxide can also be produced by mitochondria, when electrons “leak” from the electron transport chain during synthesis of ATP [108]. This superoxide rarely leaves the mitochondrial space in its isolated form; rather, it binds with NO to form peroxynitrite or is dismutated into H_2O_2 by superoxide dismutase.

Superoxide dismutase (SOD) converts superoxide to hydrogen peroxide; reductions in SOD have been linked to cardiovascular disease [86]. There are three isoforms of SOD: SOD1, SOD2, and SOD3. SOD1 is Copper-Zinc-SOD (CuZn-SOD), found throughout the intracellular space. SOD1 is thought to be the most prevalent form of SOD in endothelial cells [109] and it is modulated by changes in shear stress [110], making it highly relevant to valve pathology. SOD2 is manganese-SOD (MnSOD), found in the mitochondrial compartment. It converts mitochondrial O_2^- to H_2O_2 before the O_2^- can leave the mitochondrial compartment, unless the mitochondria are producing an excessive amount of O_2^- . SOD3 is extracellular SOD (ecSOD), a protein secreted by cells into the extracellular space. SOD3 is sometimes associated with heparin sulfate and is thought to be involved in the progression of hypertension in the vasculature [111] (Figure 1.3B).

Several inhibitors are available to elucidate sources of oxidative stress *in vitro*. Apocynin, or acetovanillone, is an organic compound known to have potent anti-oxidant effects, due to its ability to suppress NADPH oxidase activity [112, 113]. It is FDA-approved for a number of applications and has shown to be efficacious in treating atherosclerosis [107]. Superoxide can be dismutated into hydrogen peroxide by the native enzyme superoxide dismutase (SOD). SOD for *in vitro* experiments can be bought in the form of SOD isolated from bovine erythrocytes. SOD can also be purchased with pegylated ethylene glycol synthetically attached (peg-SOD), which increases the half-life of SOD in the blood and facilitates uptake of the SOD enzyme by cells. L-NAME, as mentioned above, prevents the function of the eNOS enzyme. Addition of BH₄ to cultured cells mitigates eNOS uncoupling by providing an excess of the BH₄ cofactor that is deficient during uncoupling. Exogenous catalase facilitates the breakdown of H₂O₂. A summary of these inhibitors is found in Figure 1.3B and Table 1.1.

Table 1.1 Endothelial cell oxidants, sources, and inhibitors.

Oxidant	Source	Inhibitor	Inhibitor Mechanism
Nitric Oxide	Coupled eNOS	L-NAME	L-arginine analog, competitively binds NOS
Superoxide	Uncoupled eNOS	BH ₄	Cofactor, facilitates electron transfer from NOS oxidase to L-arginine
	NADPH oxidase	Apocynin;	Inhibits intracellular assembly of NADPH oxidases
	Mitochondria; leakage of electrons during ATP synthesis	Superoxide Dismutase (SOD2, Manganese-SOD)	Dismutates superoxide into H ₂ O ₂ ; natively found only in mitochondrial space
	All sources	Superoxide Dismutase	Dismutates superoxide into H ₂ O ₂ ; see text
Hydrogen Peroxide	Peroxisomes, mitochondria, many cellular enzymes	Catalase	Catalyzes the decomposition of H ₂ O ₂ into water and O ₂

NFκB signaling in AVD

The role of NFκB in atherosclerosis has been studied extensively [113], showing that NFκB is an integrator of many of the central pathological mechanisms in plaque formation and endothelial dysfunction. A recent study found that genetic inhibition of NFκB signaling in the endothelium protects mice from atherosclerosis [114]. It is a first responder to changes in hemodynamics [115], inflammation [116], and oxidative stress [117], all of which are also key elements of aortic valve disease.

Recent evidence from our lab implicates NFκB signaling in the pathogenesis of aortic valve disease, through inflammatory activation of the endothelium and induction of a mesenchymal transformation in aortic endothelial cells [118]. NFκB has been

associated with osteoclast activity [119], suggesting that in addition to driving endothelial dysfunction, it may play a direct role in valve calcification. It has been shown that $TNF\alpha$, which activates $NF\kappa B$, accelerates valve interstitial cell calcification [120], and that inflammation correlates with degree of calcification [121]. Taken together, this evidence suggests that $NF\kappa B$ is a promising target as an integrative regulator of valve disease as it progresses from inflammation to calcification.

NFκB structure and function

Nuclear factor kappa-light-chain-enhancer of activated B cells ($NF\kappa B$) is a family of transcription factors that is present in most animal cell types. It can regulate cell response to stress, inflammation, DNA damage, viral attack, and free radicals by triggering transcription of a wide range of genes controlling cell proliferation, survival, immune response, and differentiation. It belongs to a specific family of “rapid-acting” transcription factors because it is continually present in the cytoplasm in its inactive state and therefore is readily activated and translocated to the nucleus upon stimuli.

There are five $NF\kappa B$ proteins, each with a different subset of transcriptional targets: RelA, RelB, c-Rel, $NF\kappa B1$ (p105/p50), and $NF\kappa B2$ (p100/p52). All five share a Rel homology domain; only $NF\kappa B1$ and $NF\kappa B2$ have an additional region of ankyrin repeats which mediate protein-protein interactions, including cytoplasmic binding of $I\kappa B$'s (review: [122]). $NF\kappa B$ levels are tightly regulated by an auto-feedback

mechanism in which NF κ B triggers transcription of I κ B α , which then acts to sequester NF κ B in the cytoplasm. This results in a characteristic oscillatory activation as the NF κ B is released and sequestered [123].

IKK β is a kinase that phosphorylates the inhibitor of kappa B (I κ B). I κ B binds NF κ B in its inactive state; phosphorylation of I κ B causes it to be degraded, allowing freed NF κ B to enter the nucleus and transcribe various downstream targets (Figure 1.4). This pathway is the canonical NF κ B activation pathway that has been implicated in aortic valve disease [118] and arterial inflammation [124], involving the RelA (p65) sub-unit of NF κ B. Non-canonical pathways involving IKK α and NF κ B2 precursor protein have not been linked to aortic valve disease.

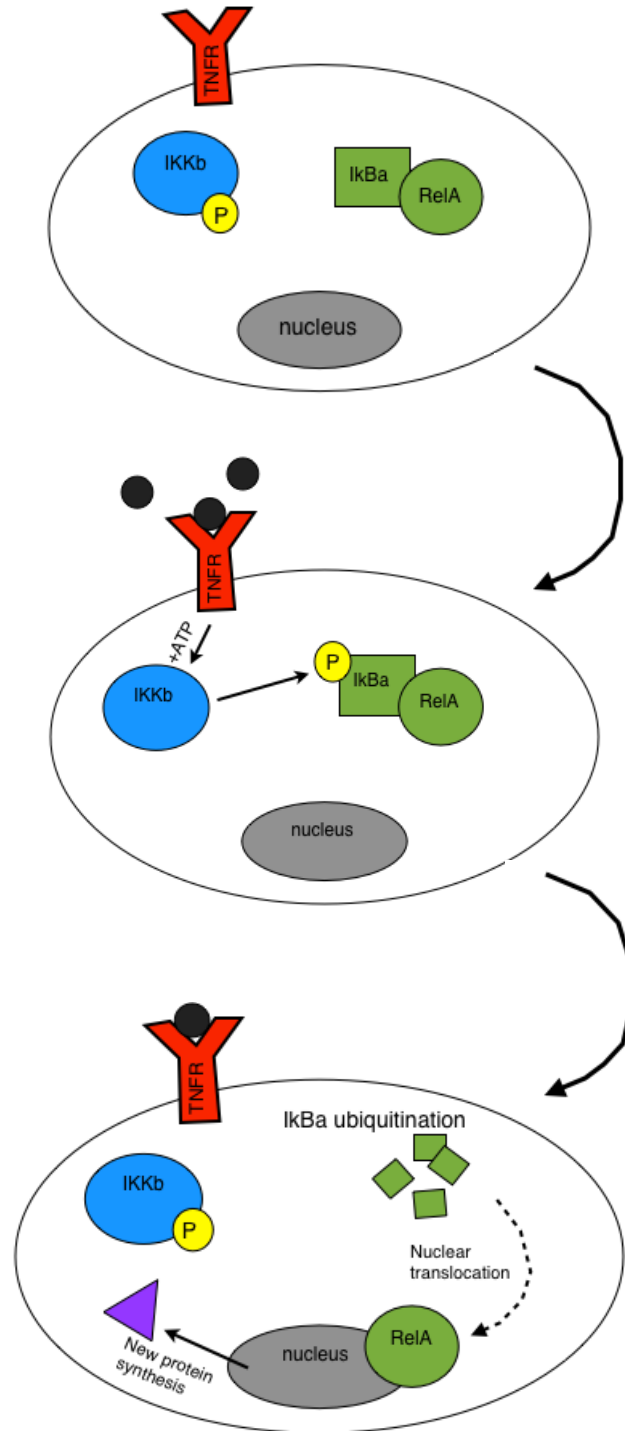


Figure 1.4 Mechanism of TNF α stimulation of NF κ B (p65/RelA sub-unit).

TNF α binds with TNF receptor (TNFR), triggering IKK β to phosphorylate I κ B α . This causes ubiquitin-mediated protein degradation of I κ B α , releasing RelA to enter the nucleus, where can trigger transcription of a number of genes, including VCAM-1.

Murine models allowing for endothelial-specific regulation of NFκB in the context of aortic valve disease

Mice with genetic ablation of the low density lipoprotein receptor (Ldlr^{-/-} mice) have been well characterized as a cardiovascular disease model, with substantial examination of effects aortic valve disease [125-131]. Ldlr^{-/-} mice lack the low-density lipoprotein (LDL) receptor which allows endothelial cells of the cardiovascular system to remove cholesterol-rich LDL from the bloodstream, thereby controlling plasma cholesterol levels [132]. The resulting excess LDL collects on the walls of blood vessels, forming atherosclerotic plaques.

Table 1.2 Effects of diet and timing on the aortic valve of LDLR^{-/-} mice

Diet; time	Effect on valve	Reference
42% fat, 0.2% chol.; 4 mo	Mineral deposition	[130]
42% fat, 0.15% chol.; 4 mo	Mineralization, osteoblasts, superoxide, calcification	[126]
Normal diet; 20 mo	Calcification, superoxide, decreased orifice area	[125]
42% fat, 0.15% chol.; 4 mo	Decreased orifice area, decreased eNOS, myofibroblast and osteoblast activation	[127]
15.8% fat, 1.25% chol.; 1 mo	Elevated TNFα, increased ICAM1, increased leukocyte adhesion (observed in postcapillary venules)	[133]

As shown in Table 1.2, 16 weeks of a high fat/high cholesterol diet is sufficient to induce aortic valve disease and preliminary calcification in Ldlr^{-/-} mice. The most common diet used to induce valve disease in Ldlr^{-/-} mice is the TD.88137 diet, also

known as the “Western diet”. The Western diet is 0.2% cholesterol and derives 42% of its calories from fat.

A study by Weiss et al. in 2006 [125] included an additional transgenic modification that removes all apolipoproteins except Apolipoprotein B, which binds with high specificity to the LDL receptor, thereby exacerbating the hyperlipidemic phenotype. These mice spontaneously develop valve dysfunction in old age (20 months) without a high-fat diet, but the end phenotype is very similar to ApoB-WT *Ldlr*^{-/-} mice with a four-month Western diet.

The *Ldlr*^{-/-} model is distinct from the commonly used Apolipoprotein-E ^{-/-} model (ex. [134]). Apolipoproteins act by binding with lipids in the circulation in such a way that the hydrophobic lipid particle becomes hydrophilic, allowing it to be transported through the blood stream. The LDL receptor removes LDL from plasma, but Apolipoprotein E facilitates removal of very-low density lipoprotein (VLDL) from the bloodstream. VLDL is a precursor of LDL. VLDL contains ApoE both in its nascent form (in the liver) and in its mature form (in the bloodstream). In the mature form, ApoE allows the VLDL molecule to bind to LDL receptors, thereby exiting the circulation. Without ApoE, VLDL remains in the circulation longer, creating more LDL and plaques. However, ApoE is also involved in regulating immune response, inflammation and oxidation [135], so ApoE knock-out can cause confounding peripheral effects in studies of inflammation and early valve disease.

Other options for mouse model choice include Notch^{+/-} [136], eNOS^{-/-} [137], and periostin^{-/-} [138]. These models are congenitally derived, meaning that aortic valve degeneration begins with morphological malformations *in utero* that then propagate into postnatal pathologies. This was not ideal in our case because we examine the early inflammatory stage of valve disease and wanted to exclude confounding morphological or mechanical effects that might arise in a congenital mouse model.

Developmental origins of AVD

During valvulogenesis, the valve interstitium is populated via endothelial to mesenchymal transition (EndMT) of valve endocardial cells (review: [139]). EndMT is necessary for healthy cell migration, matrix digestion, cell separation, and growth in the developing valve. Many of these same events occur in valve disease, including activation of endothelial cells, matrix disorganization, proliferation, and cell migration, suggesting overlap between valvulogenesis and early AVD (Figure 1.5, [140]).

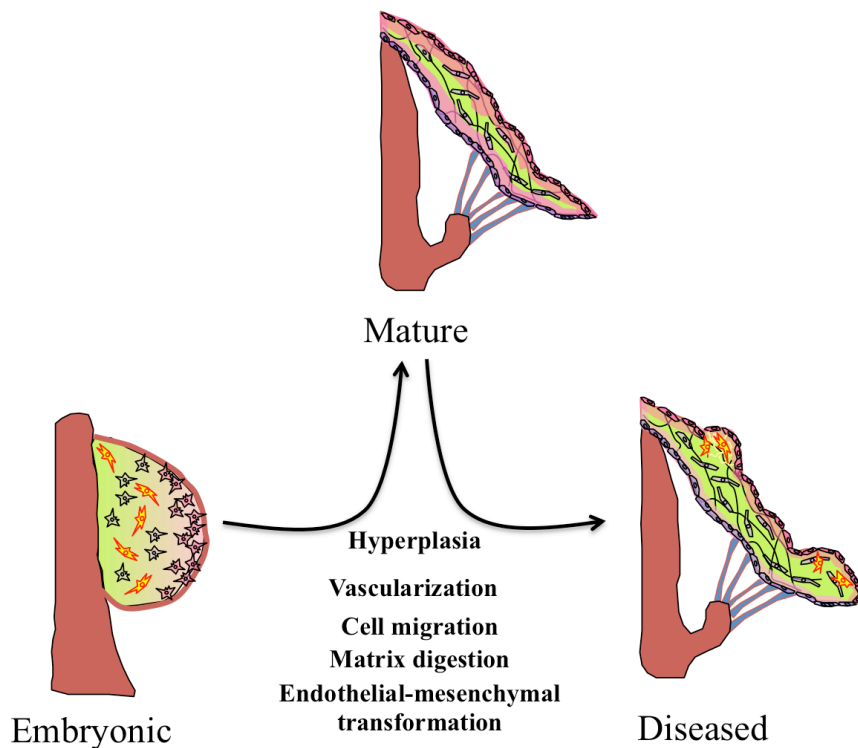


Figure 1.5 Share mechanisms between valve embryonic development and disease.

Mechanisms such as vascularization, ECM organization, and cell migration that feature in embryonic valvulogenesis are reactivated in valve disease.

Recently, we have shown that EndMT occurs in postnatal valve disease due to inflammatory stimulus, via similar pathways as in the developing heart [141]. Other groups have shown postnatal valve EndMT as a consequence of strain [142], shear stress [143], or Notch signaling [144]. Similarities between postnatal and developmental EndMT (review: [145]) suggests that EndMT may provide a source of valve cells in the interstitium with increased differentiation potential in the beginning stages of valve disease. However, the phenotype of the transformed endothelial cells has not been established, nor has their downstream function in disease. Recent studies have shown that adult aortic valves contain a subpopulation of cells with phenotypic

plasticity, collectively known as “mesenchymal progenitors”. These valve interstitial cells (VIC) can differentiate into osteogenic, adipogenic, chondrogenic, and myofibroblast lineages [146]. The origin of these cells is currently unknown. One source is circulating endothelial progenitor cells, but these account for only 4% of cells with demonstrated phenotypic plasticity in sclerotic valves [147, 148]. This points to a hypothesis that VIC with increased phenotypic plasticity in adult valves are transformed valve *endothelial* cells, populating the valve mesenchyme due to inflammatory EndMT. In this thesis, the role of TNF α initiation of endothelial cell “reprogramming”, whereby VEC undergo EndMT, gain increased differentiation potential, and participate in valve pathology via osteogenic or myofibroblastic differentiation is investigated.

Reprogramming and Oct4 governance of cell differentiation and fate

One mechanism by which valve endothelial cell reprogramming may occur is through upregulation of stem-cell regulating transcription factors in transformed endothelial cells. Octamer binding transcription factor 4 (Oct4), also known as POU5F1, is a critical regulator of self-renewal and differentiation in stem cells [149]. Oct4 belongs to the Pit-Onc-Unc (POU) gene family of transcription factors, which share a DNA binding domain with affinity for ATGCAAAT. Oct4 contains the homeobox domain, which regulates morphogenesis through synthesis of DNA binding domains with the characteristic helix-turn-helix structure. It is strongly expressed in the inner cell mass (ICM) and repressed in the trophoectoderm [150]. The Puceat lab has identified tight

regulation of Oct4 as essential to direction of embryonic stem cells towards a cardiac lineage [151], suggesting that Oct4 has a unique role in the heart.

Recent studies have highlighted the role of Oct4 in the generation of induced pluripotent stem cells, along with transcription factors Nanog, Klf4, and Sox9, among others [152, 153]. Oct4 was demonstrated to be essential to induction of pluripotency in adult cells in 1990 [154]. In 2006, Takahashi and Yamanaka identified Oct4 as one of four genes required to induce pluripotency in mouse fibroblasts [155]. More recently, induced pluripotent stem cells (iPSC) were created from porcine somatic cells using only Oct4 and Klf4 [156], further establishing the role of Oct4 as a master regulator. Oct4 is persistently expressed in cardiac progenitors that have been used in regeneration post-myocardial infarction [157]. Taken together, these studies suggest Oct-4 as a likely candidate for regulating reprogramming of postnatal valve endothelial cells in the early stages of disease.

1.5 Aims of this dissertation

This dissertation aims to elucidate initiating mechanisms of aortic valve disease from three angles. First, we seek to understand the role of inflammation, specifically tumor necrosis factor- α , in driving dysregulation of oxidative stress in valve endothelial cells and the downstream effects of that stress on valve health. Second, we seek to understand the role that NF κ B-mediated endothelial to mesenchymal transformation plays in valve disease, as a consequence of inflammatory stimulation of the valve endothelium. This component includes a novel transgenic mouse model of valve-

specific NF κ B inactivation. Finally, we seek to understand the role of the somatic cell reprogramming factor, Oct4, in guiding transdifferentiation of valve endothelial cells as they contribute to valve degeneration. We also explored how mechanical contractility of valve interstitial cells guides valve calcification. Through these aims, we hope to contribute new understanding of the mechanisms that underlie aortic valve disease, in order to facilitate the development of clinical diagnostic and therapeutic targets (Figure 1.5).

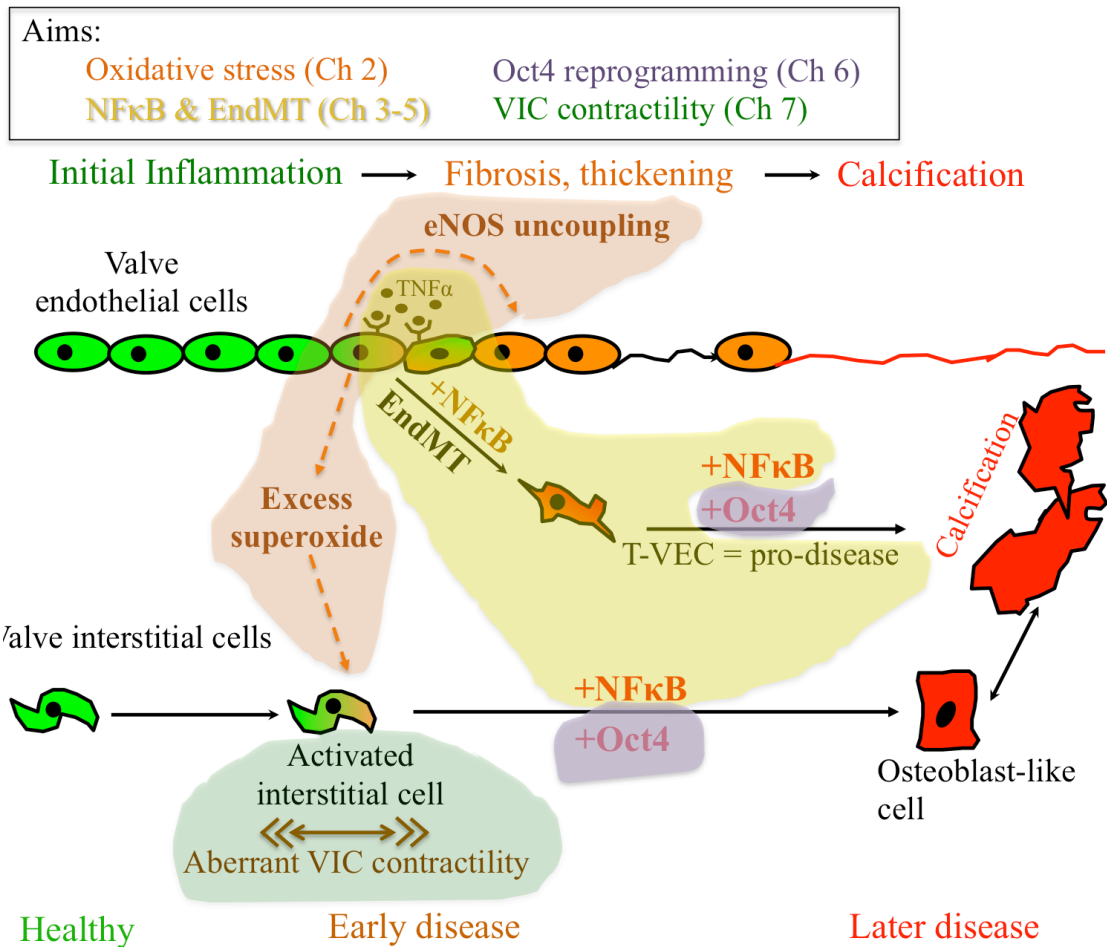


Figure 1.3 Summary of the aims of this thesis.

This thesis aims to explore three main contributions of endothelial cells to early aortic valve disease: oxidative stress (orange), NFκB signaling in both endothelial and interstitial cells (yellow), and the role of Oct4 in valve cell reprogramming (purple). This thesis also explores the role of aberrant interstitial cell contractility in the transition from quiescent to activated to osteogenic VIC (green).

REFERENCES

1. Piazza N, de Jaegere P, Schultz C, Becker AE, Serruys PW, et al. (2008) Anatomy of the Aortic Valvar Complex and Its Implications for Transcatheter Implantation of the Aortic Valve. *Circulation: Cardiovascular Interventions* 1: 74–81.
2. Butcher JT, Markwald RR (2007) Valvulogenesis: the moving target. *Philosophical Transactions of the Royal Society B* 362: 1489–1503.
3. Liu AC, Joag VR, Gotlieb AI (2007) The Emerging Role of Valve Interstitial Cell Phenotypes in Regulating Heart Valve Pathobiology. *The American Journal of Pathology* 171: 1407–1418.
4. Taylor PM, Batten P, Brand NJ, Thomas PS, Yacoub MH (2003) The cardiac valve interstitial cell. *The International Journal of Biochemistry & Cell Biology* 35: 113–118.
5. Butcher J, Nerem R (2004) Porcine aortic valve interstitial cells in three-dimensional culture: Comparison of phenotype with aortic smooth muscle cells Vol. 13. pp. 478–485.
6. Rajamannan NM, Evans FJ, Aikawa E, Grande-Allen KJ, Demer LL, et al. (2011) Calcific Aortic Valve Disease: Not Simply a Degenerative Process. *Circulation* 124: 1783–1791.
7. Tao G, Kotick JD, Lincoln J (2012) Heart Valve Development, Maintenance, and Disease: The Role of Endothelial Cells. *Current Topics in Developmental Biology* 100: 204–223.
8. Butcher JT, Nerem RM (2007) Valvular endothelial cells and the mechanoregulation of valvular pathology. *Philosophical Transactions of the Royal Society of London Series B: Biological Sciences* 362: 1445–1457.
9. Butcher JT, Penrod AM, Garcia AJ, Nerem RM (2004) Unique Morphology and Focal Adhesion Development of Valvular Endothelial Cells in Static and Fluid Flow Environments. *Arteriosclerosis, Thrombosis, & Vascular Biology* 24: 1429–1434.

10. Mahler GJ, Farrar EJ, Butcher JT (2013) Inflammatory Cytokines Promote Mesenchymal Transformation in Embryonic and Adult Valve Endothelial Cells. *Arteriosclerosis, Thrombosis, & Vascular Biology* 33: 121–130.
11. Balachandran K, Alford P, Wylie-Sears J, Goss JA, Grosberg A, et al. (2011) Cyclic strain induces dual-mode endothelial- mesenchymal transformation of the cardiac valve. *Proceedings of the National Academy of Sciences*: 1–6.
12. Paranya G, Vineberg S, Dvorin E, Kaushal S, Roth SJ, et al. (2001) Aortic Valve Endothelial Cells Undergo Transforming Growth Factor-beta-Mediated and Non-Transforming Growth Factor-beta-Mediated Transdifferentiation in Vitro. *The American Journal of Pathology* 159: 1335–1343.
13. Bischoff J, Aikawa E (2011) Progenitor Cells Confer Plasticity to Cardiac Valve Endothelium. *J of Cardiovasc Trans Res* 4: 710–719.
14. Farrar EJ, Butcher JT (2013) Heterogeneous Susceptibility of Valve Endothelial Cells to Mesenchymal Transformation in Response to TNF α . *Annals of Biomedical Engineering* 42: 149–161.
15. Poggianti E, Venneri L, Chubuchny V, Jambrik Z, Baroncini LA, et al. (2003) Aortic valve sclerosis is associated with systemic endothelial dysfunction. *Journal of the American College of Cardiology* 41: 136–141.
16. Hajdu Z, Romeo SJ, Fleming PA, Markwald RR, Visconti RP, et al. (2011) Recruitment of bone marrow-derived valve interstitial cells is a normal homeostatic process. *Journal of Molecular and Cellular Cardiology* 51: 955–965.
17. Matsumoto Y, Adams V, Walther C, Kleinecke C, Brugger P, et al. (2008) Reduced number and function of endothelial progenitor cells in patients with aortic valve stenosis: a novel concept for valvular endothelial cell repair. *European Heart Journal* 30: 346–355.
18. Skowasch D, Schrepf S, Wernert N, Steinmetz M, Jabs A, et al. (2005) Cells of primarily extravalvular origin in degenerative aortic valves and bioprostheses. *European Heart Journal* 26: 2576–2580.

19. Gössl M, Khosla S, Zhang X, Higano N, Jordan KL, et al. (2012) Role of Circulating Osteogenic Progenitor Cells in Calcific Aortic Stenosis. *Journal of the American College of Cardiology* 60: 1945–1953.
20. Hinton RB, Lincoln J, Deutsch GH, Osinska H, Manning PB, et al. (2006) Extracellular matrix remodeling and organization in developing and diseased aortic valves. *Circulation Research* 98: 1431–1438.
21. Gross L, Kugel MA (1931) *Topographic Anatomy and Histology of the Valves in the Human Heart**.
22. Otto CM (2008) Calcific aortic stenosis--time to look more closely at the valve. *N Engl J Med* 359: 1395.
23. Sacks MS, Merryman WD, Schmidt DE (2009) On the biomechanics of heart valve function. *Journal of Biomechanics* 42: 1804–1824.
24. Kershaw JD, Misfeld M, Sievers HH, Yacoub MH, Chester AH (2004) Specific regional and directional contractile responses of aortic cusp tissue. *Journal of Heart Valve Disease* 13: 798–803.
25. Freeman RV, Otto CM (2005) Spectrum of Calcific Aortic Valve Disease: Pathogenesis, Disease Progression, and Treatment Strategies. *Circulation* 111: 3316–3326.
26. Beppu S, Suzuki S, Matsuda H, Ohmori F, Nagata S, et al. (1993) Rapidity of progression of aortic stenosis in patients with congenital bicuspid aortic valves. *The American Journal of Cardiology* 71: 322–327.
27. Balachandran K, Sucusky P, Jo H, Yoganathan AP (2009) Elevated cyclic stretch alters matrix remodeling in aortic valve cusps: implications for degenerative aortic valve disease. *AJP: Heart and Circulatory Physiology* 296: H756–H764.
28. Ku C, Johnson P, Batten P, Sarathchandra P, Chambers R, et al. (2006) Collagen synthesis by mesenchymal stem cells and aortic valve interstitial cells in response to mechanical stretch. *Cardiovascular Research* 71: 548–556.

29. Fisher CI, Chen J, Merryman WD (2012) Calcific nodule morphogenesis by heart valve interstitial cells is strain dependent. *Biomech Model Mechanobiol* 12: 5–17.
30. Bouchareb R, Boulanger M-C, Fournier D, Pibarot P, Messaddeq Y, et al. (2014) Mechanical strain induces the production of spheroid mineralized microparticles in the aortic valve through a RhoA/ROCK-dependent mechanism. *Journal of Molecular and Cellular Cardiology* 67: 49–59.
31. Simmons CA (2009) Aortic Valve Mechanics. *Journal of the American College of Cardiology* 53: 1456–1458.
32. Merryman WD, Schoen FJ (2013) Mechanisms of Calcification in Aortic Valve Disease: Role of Mechanokinetics and Mechanodynamics. *Curr Cardiol Rep* 15: 355.
33. El-Hamamsy I, Balachandran K, Yacoub MH, Stevens LM, Sarathchandra P, et al. (2009) Endothelium-Dependent Regulation of the Mechanical Properties of Aortic Valve Cusps. *Journal of the American College of Cardiology* 53: 1448–1455.
34. Lee TC, Zhao YD, Courtman DW, Stewart DJ (2000) Abnormal aortic valve development in mice lacking endothelial nitric oxide synthase. *Circulation* 101: 2345–2348.
35. Garg V, Muth AN, Ransom JF, Schluterman MK, Barnes R, et al. (2005) Mutations in NOTCH1 cause aortic valve disease. *Nature* 437: 270–274.
36. Sider KL, Blaser MC, Simmons CA (2011) Animal models of calcific aortic valve disease. *International Journal of Inflammation* 2011.
37. Weiss RM, Miller JD, Heistad DD (2013) Fibrocalcific Aortic Valve Disease: Opportunity to Understand Disease Mechanisms Using Mouse Models. *Circulation Research* 113: 209–222.
38. Towler DA, Bidder M, Latifi T, Coleman T, Semenkovich CF (1998) Diet-induced Diabetes Activates an Osteogenic Gene Regulatory Program in the Aortas of Low Density Lipoprotein Receptor-deficient Mice. *Journal of Biological Chemistry* 273: 30427–30434.

39. Matsumoto Y, Adams V, Jacob S, Mangner N, Schuler G, et al. (2010) Regular Exercise Training Prevents Aortic Valve Disease in Low-Density Lipoprotein-Receptor-Deficient Mice. *Circulation* 121: 759–767.
40. Skold BH, Getty R, Ramsey FK (1966) Spontaneous atherosclerosis in the arterial system of aging swine. *American Journal of Veterinary Research* 27: 257–273.
41. Skold BH, Getty R (1961) Spontaneous atherosclerosis of swine. *Journal of the American Veterinary Medical Association* 139: 655–660.
42. Guerraty M, Mohler ER III (2007) Models of Aortic Valve Calcification. *Journal of Investigative Medicine* 55: 278–283.
43. Guerraty MA, Grant GR, Karanian JW, Chiesa OA, Pritchard WF, et al. (2010) Hypercholesterolemia Induces Side-Specific Phenotypic Changes and Peroxisome Proliferator-Activated Receptor- Pathway Activation in Swine Aortic Valve Endothelium. *Arteriosclerosis, Thrombosis, & Vascular Biology* 30: 225–231.
44. Richards J, El-Hamamsy I, Chen S, Sarang Z, Sarathchandra P, et al. (2013) Side-Specific Endothelial-Dependent Regulation of Aortic Valve Calcification. *The American Journal of Pathology*: 1–11.
45. Simmons CA, Grant GR, Manduchi E, Davies PF (2005) Spatial heterogeneity of endothelial phenotypes correlates with side-specific vulnerability to calcification in normal porcine aortic valves. *Circulation Research* 96: 792–799.
46. Bowler MA, Merryman WD (2014) In vitro models of aortic valve calcification: solidifying a system. *Cardiovascular Pathology* 24: 1–10.
47. Mozaffarian D, Benjamin EJ, Go AS, Arnett DK, Blaha MJ et al. (2015) Heart Disease and Stroke Statistics - 2015 Update. *Circulation* 131: e29–e322.
48. Cawley PJ, Otto CM (2009) Prevention of calcific aortic valve stenosis—fact or fiction? *Annals of Medicine* 41: 100–108.
49. Lindman BR, Bonow RO, Otto CM (2013) Current Management of Calcific Aortic Stenosis. *Circulation Research* 113: 223–237.

50. Teo KK, Corsi DJ, Tam JW, Dumesnil JG, Chan KL (2011) Lipid lowering on progression of mild to moderate aortic stenosis: meta-analysis of the randomized placebo-controlled clinical trials on 2344 patients. *Canadian Journal of Cardiology* 27: 800–808.
51. Chan KL, Teo K, Dumesnil JG, Ni A, Tam J (2010) Effect of Lipid Lowering With Rosuvastatin on Progression of Aortic Stenosis. *Circulation* 121: 306–314.
52. Mollnau H, Wendt M, Szocs K, Lassegue B, Schulz E, et al. (2002) Effects of Angiotensin II Infusion on the Expression and Function of NAD(P)H Oxidase and Components of Nitric Oxide/cGMP Signaling. *Circulation Research* 90: 58e–65.
53. Reynolds MR, Magnuson EA, Lei Y, Wang K, Vilain K, et al. (2012) Cost-Effectiveness of Transcatheter Aortic Valve Replacement Compared With Surgical Aortic Valve Replacement in High-Risk Patients With Severe Aortic Stenosis. *Journal of the American College of Cardiology* 60: 2683–2692.
54. Coffey S, Cox B, Williams MJA (2014) The Prevalence, Incidence, Progression, and Risks of Aortic Valve Sclerosis. *Journal of the American College of Cardiology* 63: 2852–2861.
55. Otto CM, Lind BK, Kitzman DW, Gersh BJ, Siscovick DS (1999) Association of aortic-valve sclerosis with cardiovascular mortality and morbidity in the elderly. *New England Journal of Medicine* 341: 142–147.
56. Stewart BF, Siscovick D, Lind BK, Gardin JM, Gottdiener JS, et al. (1997) Clinical Factors Associated With Calcific Aortic Valve Disease. *Journal of the American College of Cardiology* 29: 630–634.
57. Halevi R, Hamdan A, Marom G, Mega M, Raanani E, et al. (2015) Progressive aortic valve calcification: Three-dimensional visualization and biomechanical analysis. *Journal of Biomechanics* 48: 489–497.
58. Singh A, Steadman CD, McCann GP (2014) Advances in the Understanding of the Pathophysiology and Management of Aortic Stenosis: Role of Novel Imaging Techniques. *Canadian Journal of Cardiology* 30: 994–1003.

59. New SEP, Aikawa E (2011) Molecular Imaging Insights Into Early Inflammatory Stages of Arterial and Aortic Valve Calcification. *Circulation Research* 108: 1381–1391.
60. Dweck MR, Khaw HJ, Sng GKZ, Luo ELC, Baird A, et al. (2013) Aortic stenosis, atherosclerosis, and skeletal bone: is there a common link with calcification and inflammation? *European Heart Journal* 34: 1567–1574.
61. Otto CM, Kuusisto J, Reichenbach DD, Gown AM, O'Brien KD (1994) Characterization of the early lesion of “degenerative” valvular aortic stenosis. Histological and immunohistochemical studies. *Circulation* 90: 844–853.
62. Mohler ER III (2000) Are atherosclerotic processes involved in aortic-valve calcification? *The Lancet* 356: 1–2.
63. Thubrikar MJ, Aouad J, Nolan SP (1986) Patterns of calcific deposits in operatively excised stenotic or purely regurgitant aortic valves and their relation to mechanical stress. *The American Journal of Cardiology* 58: 304–308.
64. Honda S, Miyamoto T, Watanabe T, Narumi T, Kadowaki S, et al. (2014) A novel mouse model of aortic valve stenosis induced by direct wire injury. *Arteriosclerosis, Thrombosis, & Vascular Biology* 34: 270–278.
65. Li C, Xu S, Gotlieb AI (2013) The progression of calcific aortic valve disease through injury, cell dysfunction, and disruptive biologic and physical force feedback loops. *Cardiovascular Pathology* 22: 1–8.
66. Towler DA (2013) Molecular and Cellular Aspects of Calcific Aortic Valve Disease. *Circulation Research* 113: 198–208.
67. Osman L, Yacoub MH, Latif N, Amrani M, Chester AH (2006) Role of human valve interstitial cells in valve calcification and their response to atorvastatin. *Circulation* 114:I-547–I-552.
68. Cloyd KL, El-Hamamsy I, Boonrunsiman S, Hedegaard M, Gentleman E, et al. (2012) Characterization of Porcine Aortic Valvular Interstitial Cell “Calcified” Nodules. *PLoS ONE* 7: e48154.

69. Yip CYY, Chen JH, Zhao R, Simmons CA (2009) Calcification by Valve Interstitial Cells Is Regulated by the Stiffness of the Extracellular Matrix. *Arteriosclerosis, Thrombosis, & Vascular Biology* 29: 936–942.
70. Wang D, Zeng Q, Song R, Ao L, Fullerton DA, et al. (2014) Ligation of ICAM-1 on human aortic valve interstitial cells induces the osteogenic response: A critical role of the Notch1-NF- κ B pathway in BMP-2 expression. *BBA - Molecular Cell Research* 1843: 2744–2753.
71. Venardos N, Nadlonek NA, Zhan Q, Weyant MJ, Reece TB, et al. (2014) Aortic valve calcification is mediated by a differential response of aortic valve interstitial cells to inflammation. *Journal of Surgical Research* 190: 1–8.
72. Butcher J, Nerem R (2006) Valvular endothelial cells regulate the phenotype of interstitial cells in co-culture: Effects of steady shear stress. *Tissue Engineering* 12: 905–915.
73. Accaoui El RN, Gould ST, Hajj GP, Chu Y, Davis MK, et al. (2014) Aortic valve sclerosis in mice deficient in endothelial nitric oxide synthase. *AJP: Heart and Circulatory Physiology* 306: H1302–H1313.
74. Bosse K, Hans CP, Zhao N, Koenig SN, Huang N, et al. (2013) Endothelial nitric oxide signaling regulates Notch1 in aortic valve disease. *Journal of Molecular and Cellular Cardiology* 60: 27–35.
75. Hofmann JJ, Briot A, Enciso J, Zovein AC, Ren S, et al. (2012) Endothelial deletion of murine Jag1 leads to valve calcification and congenital heart defects associated with Alagille syndrome. *Development* 139: 4449–4460.
76. Holliday CJ, Ankeny RF, Jo H, Nerem RM (2011) Discovery of shear- and side-specific mRNAs and miRNAs in human aortic valvular endothelial cells. *AJP: Heart and Circulatory Physiology* 301: H856–H867.
77. Mohler ER, Gannon F, Reynolds C, Zimmerman R, Keane MG, et al. (2001) Bone formation and inflammation in cardiac valves. *Circulation* 103: 1522–1528.
78. Abdelbaky A, Corsini E, Figueroa AL, Subramanian S, Fontanez S, et al. (2015) Early aortic valve inflammation precedes calcification: A longitudinal FDG-PET/CT study. *Atherosclerosis* 238: 165–172.

79. Hjortnaes J, Butcher J, Figueiredo JL, Riccio M, Kohler RH, et al. (2010) Arterial and aortic valve calcification inversely correlates with osteoporotic bone remodelling: a role for inflammation. *European Heart Journal* 31: 1975–1984.
80. Ghaisas N, Foley J, O'Briain D, Crean P, Kelleher D, et al. (2000) Adhesion molecules in nonrheumatic aortic valve disease: Endothelial expression, serum levels and effects of valve replacement. *Journal of the American College of Cardiology* 36: 2257–2262.
81. Müller AM, Cronen C, Kupferwasser LI, Oelert H, Müller K-M, et al. (2000) Expression of endothelial cell adhesion molecules on heart valves: up-regulation in degeneration as well as acute endocarditis. *The Journal of Pathology* 191: 54–60.
82. Ali OA, Chapman M, Nguyen TH, Chirkov YY, Heresztyn T, et al. (2014) Interactions between inflammatory activation and endothelial dysfunction selectively modulate valve disease progression in patients with bicuspid aortic valve. *Heart* 100:
83. Metzler SA, Pregonero CA, Butcher JT, Burgess SC, Warnock JN (2008) Cyclic Strain Regulates Pro-Inflammatory Protein Expression in Porcine Aortic Valve Endothelial Cells. *Journal of Heart Valve Disease* 17: 571–578.
84. Rajamannan NM (2011) Bicuspid aortic valve disease: the role of oxidative stress in Lrp5 bone formation. *Cardiovascular Pathology* 20: 168–176.
85. Miller JD, Chu Y, Brooks RM, Richenbacher WE, Pena-Silva R, et al. (2008) Dysregulation of Antioxidant Mechanisms Contributes to Increased Oxidative Stress in Calcific Aortic Valvular Stenosis in Humans. *Journal of the American College of Cardiology* 52: 843–850.
86. Davignon J, Jacob RF, Mason RP (2004) The antioxidant effects of statins. *Coronary Artery Disease* 15: 251–258.
87. Chan KL, Teo K, Dumesnil JG, Ni A, Tam J (2010) Effect of Lipid Lowering With Rosuvastatin on Progression of Aortic Stenosis. *Circulation* 121: 306–314.
88. Butcher JT, Tressel S, Johnson T, Turner D, Sorescu G, et al. (2005) Transcriptional Profiles of Valvular and Vascular Endothelial Cells Reveal Phenotypic Differences: Influence of Shear Stress. *Arteriosclerosis, Thrombosis, & Vascular Biology* 26: 69–77.

89. Byon CH, Javed A, Dai Q, Kappes JC, Clemens TL, et al. (2008) Oxidative Stress Induces Vascular Calcification through Modulation of the Osteogenic Transcription Factor Runx2 by AKT Signaling. *Journal of Biological Chemistry* 283: 15319–15327.
90. Sowa G, Liu J, Papapetropoulos A, Rex-Haffner M, Hughes T, et al. (1999) Trafficking of endothelial nitric-oxide synthase in living cells - Quantitative evidence supporting the role of palmitoylation as a kinetic trapping mechanism limiting membrane diffusion. *Journal of Biological Chemistry* 274: 22524–22531.
91. El-Hamamsy I, Balachandran K, Yacoub MH, Stevens LM, Sarathchandra P, et al. (2009) Endothelium-Dependent Regulation of the Mechanical Properties of Aortic Valve Cusps. *Journal of the American College of Cardiology* 53: 1448–1455.
92. Iwakiri Y, Tsai MH, McCabe TJ, Gratton JP, Fulton D, et al. (2002) Phosphorylation of eNOS initiates excessive NO production in early phases of portal hypertension. *American Journal of Physiology - Heart and Circulatory Physiology* 282: H2084–H2090.
93. Towler DA (2008) Oxidation, inflammation, and aortic valve calcification: Peroxide paves an osteogenic path. *Journal of the American College of Cardiology* 52: 851–854.
94. Stuehr DJ (1997) Structure-function aspects in the nitric oxide synthases. *Annual review of pharmacology and toxicology* 37: 339–359.
95. Ignarro LJ, Buga GM, Wood KS, Byrns RE, Chaudhuri G (1987) Endothelium-derived relaxing factor produced and released from artery and vein is nitric oxide. *Proceedings of the National Academy of Sciences* 84: 9265.
96. Palmer RMJ, Moncada S (1989) A novel citrulline-forming enzyme implicated in the formation of nitric oxide by vascular endothelial cells. *Biochemical and Biophysical Research Communications* 158: 348–352.
97. Su Z, Blazing MA, Fan D, Huntley GD (1995) The calmodulin-nitric oxide synthase interaction. *Journal of Biological Chemistry* 270: 29117–29122.
98. Verhaar MC (2004) Free radical production by dysfunctional eNOS. *Heart* 90: 494–495.

99. Mulsch A, Busse R (1990) N G-nitro-L-arginine (N 5-[imino (nitroamino) methyl]-L-ornithine) impairs endothelium-dependent dilations by inhibiting cytosolic nitric oxide synthesis from L-arginine. *Naunyn-Schmiedeberg's archives of pharmacology* 341: 143–147.
100. Wever RMF, van Dam T, van Rijn HJM, de Groot F, Rabelink TJ (1997) Tetrahydrobiopterin regulates superoxide and nitric oxide generation by recombinant endothelial nitric oxide synthase. *Biochemical and Biophysical Research Communications* 237: 340–344.
101. Gulden M, Jess A, Kammann J, Maser E, Seibert H (2010) Cytotoxic potency of H₂O₂ in cell cultures: Impact of cell concentration and exposure time. *Free Radical Biology and Medicine* 49: 1298–1305.
102. Cai H (2005) Hydrogen peroxide regulation of endothelial function: Origins, mechanisms, and consequences. *Cardiovascular Research* 68: 26–36.
103. Babior BM, Kipnes RS, Curnutte JT (1973) Biological Defense Mechanisms. The production by leukocytes of superoxide, a potential bactericidal agent. *Journal of Clinical Investigation* 52: 741–744.
104. Benov L (2001) How superoxide radical damages the cell. *Protoplasma* 217: 33–36.
105. Fukai T, Folz RJ, Landmesser U, Harrison DG (2002) Extracellular superoxide dismutase and cardiovascular disease. *Cardiovascular Research* 55: 239–249.
106. Singh U, Jialal I (2006) Oxidative stress and atherosclerosis. *Pathophysiology* 13: 129–142.
107. Li X, Fang P, Mai J, Choi ET, Wang H, et al. (2013) Targeting mitochondrial reactive oxygen species as novel therapy for inflammatory diseases and cancers. *Journal of Hematology & Oncology* 6: 1–19.
108. Cai H, Harrison DG (2000) Endothelial Dysfunction in Cardiovascular Diseases: The Role of Oxidant Stress. *Circulation Research*.

109. Inoue N, Ramasamy S, Fukai T, Nerem RM, Harrison DG (1996) Shear stress modulates expression of Cu/Zn superoxide dismutase in human aortic endothelial cells. *Circulation Research* 79: 32–37.
110. Kashiwagi A, Shinozaki K, Nishio Y, Maegawa H, Maeno Y, et al. (1999) Endothelium-specific activation of NAD(P)H oxidase in aortas of exogenously hyperinsulinemic rats. *American Journal of Physiology Endocrinol Metabolism* 277: E976–E983.
111. Hougee S, Hartog A, Sanders A, Graus YMF, Hoijer MA, et al. (2006) Oral administration of the NADPH-oxidase inhibitor apocynin partially restores diminished cartilage proteoglycan synthesis and reduces inflammation in mice. *European Journal of Pharmacology* 531: 264–269.
112. Stolk J, Hiltermann TJ, Dijkman JH, Verhoeven AJ (1994) Characteristics of the Inhibition of NADPH Oxidase Activation in Neutrophils by Apocynin, a Methoxy-Substituted Catechol. *American Journal of Respiratory Cell and Molecular Biology* 11: 95–102.
113. Van der Heiden K, Cuhlmann S, Luong LA, Zakkar M, Evans PC (2010) Role of nuclear factor κ B in cardiovascular health and disease. *Clinical Science* 118: 593–605.
114. Gareus R, Kotsaki E, Xanthoulea S, van der Made I, Gijbels MJJ, et al. (2008) Endothelial Cell-Specific NF- κ B Inhibition Protects Mice from Atherosclerosis. *Cell Metabolism* 8: 372–383.
115. Hajra L, Evans A, Chen M, Hyduk S, Collins T, et al. (2000) The NF-kappa B signal transduction pathway in aortic endothelial cells is primed for activation in regions predisposed to atherosclerotic lesion formation. *Proceedings of the National Academy of Sciences* 97: 9052–9057.
116. Molestina RE, Miller RD, Lentsch AB, Ramirez JA, Summersgill JT (2000) Requirement for NF-kappa B in Transcriptional Activation of Monocyte Chemotactic Protein 1 by *Chlamydia pneumoniae* in Human Endothelial Cells. *Infection and Immunity* 68: 4282–4288. doi:10.1128/IAI.68.7.4282-4288.2000.
117. True AL, Rahman A, Malik AB (2000) Activation of NF- κ B induced by H₂O₂ and TNF- α and its effects on ICAM-1 expression in endothelial cells. *American Journal of Physiology-Lung Cellular and Molecular Physiology* 279: L302–L311.

118. Mahler GJ, Farrar EJ, Butcher JT (2013) Inflammatory Cytokines Promote Mesenchymal Transformation in Embryonic and Adult Valve Endothelial Cells. *Arteriosclerosis, Thrombosis, & Vascular Biology* 33: 121–130.
119. Crotti TN, Smith MD, Findlay DM, Zreiqat H, Ahern MJ, et al. (2004) Factors regulating osteoclast formation in human tissues adjacent to peri-implant bone loss: expression of receptor activator NF κ B, RANK ligand and osteoprotegerin. *Biomaterials* 25: 565–573.
120. Yu Z, Seya K, Daitoku K, Motomura S, Fukuda I, et al. (2011) Tumor necrosis factor- α accelerates the calcification of human aortic valve interstitial cells obtained from patients with calcific aortic valve stenosis via the BMP2-Dlx5 pathway. *Journal of Pharmacology and Experimental Therapeutics* 337: 16–23.
121. Hjortnaes J, Butcher J, Figueiredo JL, Riccio M, Kohler RH, et al. (2010) Arterial and aortic valve calcification inversely correlates with osteoporotic bone remodelling: a role for inflammation. *European Heart Journal* 31: 1975–1984.
122. Ghosh S, May MJ, Kopp EB (1998) NF κ B and Rel Proteins: Evolutionarily Conserved Mediators of Immune Responses. *Annual Review of Immunology* 16: 225–260.
123. Sun S, Ganchi P, Ballard D, Greene W (1993) NF-kappa B controls expression of inhibitor I kappa B alpha: evidence for an inducible autoregulatory pathway. *Science* 259: 1912–1915.
124. de Winther MPJ, Kanters E, Kraal G, Hofker MH (2005) Nuclear factor κ B signaling in atherogenesis. *Arteriosclerosis, Thrombosis, & Vascular Biology* 25: 904–914.
125. Weiss RM, Ohashi M, Miller JD, Young SG, Heistad DD (2006) Calcific aortic valve stenosis in old hypercholesterolemic mice. *Circulation* 114: 2065–2069.
126. Matsumoto Y, Adams V, Jacob S, Mangner N, Schuler G, et al. (2010) Regular Exercise Training Prevents Aortic Valve Disease in Low-Density Lipoprotein-Receptor-Deficient Mice. *Circulation* 121: 759–767.

127. Schlotter F, Matsumoto Y, Mangner N, Schuler G, Linke A, et al. (2012) Regular Exercise or Changing Diet Does Not Influence Aortic Valve Disease Progression in LDLR Deficient Mice. *PLoS ONE* 7: e37298.
128. Miller JD, Weiss RM, Serrano KM, Brooks RM, Berry CJ, et al. (2009) Lowering Plasma Cholesterol Levels Halts Progression of Aortic Valve Disease in Mice. *Circulation* 119: 2693–2701.
129. Miller JD, Weiss RM, Serrano KM, Castaneda LE, Brooks RM, et al. (2010) Evidence for active regulation of pro-osteogenic signaling in advanced aortic valve disease. *Arteriosclerosis, Thrombosis, & Vascular Biology* 30: 2482–2486.
130. Towler DA, Bidder M, Latifi T, Coleman T, Semenkovich CF (1998) Diet-induced Diabetes Activates an Osteogenic Gene Regulatory Program in the Aortas of Low Density Lipoprotein Receptor-deficient Mice. *Journal of Biological Chemistry* 273: 30427–30434.
131. Sider KL, Blaser MC, Simmons CA (2011) Animal models of calcific aortic valve disease. *International Journal of Inflammation* 2011: 1-18.
132. Ishibashi S, Brown MS, Goldstein JL, Gerard RD, Hammer RE, et al. (1993) Hypercholesterolemia in low density lipoprotein receptor knockout mice and its reversal by adenovirus-mediated gene delivery. *Journal of Clinical Investigation* 92: 883-893.
133. Henninger DD, Gerritsen ME, Granger DN (1997) Low-density lipoprotein receptor knockout mice exhibit exaggerated microvascular responses to inflammatory stimuli. *Circulation Research* 81: 274-281.
134. Tanaka K, Sata M, Fukuda D, Suematsu Y, Motomura N, et al. (2005) Age-Associated Aortic Stenosis in Apolipoprotein E-Deficient Mice. *Journal of the American College of Cardiology* 46: 134–141.
135. Zhang H-L, Wu J, Zhu J (2010) The Role of Apolipoprotein E in Guillain-Barré Syndrome and Experimental Autoimmune Neuritis. *Journal of Biomedicine and Biotechnology* 2010: 1–13.
136. Nus M, MacGrogan D, Martinez-Poveda B, Benito Y, Casanova JC, et al. (2011) Diet-induced aortic valve disease in mice haploinsufficient for the Notch

pathway effector RBPJK/CSL. *Arteriosclerosis, Thrombosis, & Vascular Biology* 31: 1580–1588.

137. Lee TC, Zhao YD, Courtman DW, Stewart DJ (2000) Abnormal aortic valve development in mice lacking endothelial nitric oxide synthase. *Circulation* 101: 2345–2348.

138. Tkatchenko TV, Moreno-Rodriguez RA, Conway SJ, Molkentin JD, Markwald RR, et al. (2009) Lack of periostin leads to suppression of Notch1 signaling and calcific aortic valve disease. *Physiological Genomics* 39: 160–168.

139. Butcher JT, Markwald RR (2007) Valvulogenesis: the moving target. *Philosophical Transactions of the Royal Society B* 362: 1489–1503.

140. Farrar EJ, Butcher JT (2012) Valvular Heart Diseases in the Developing World: Developmental Biology Takes Center Stage. *The Journal of Heart Valve Disease* 21: 234–240.

141. Mahler GJ, Farrar EJ, Butcher JT (2013) Inflammatory Cytokines Promote Mesenchymal Transformation in Embryonic and Adult Valve Endothelial Cells. *Arteriosclerosis, Thrombosis, & Vascular Biology* 33: 121–130.

142. Balachandran K, Alford P, Wylie-Sears J, Goss JA, Grosberg A, et al. (2011) Cyclic strain induces dual-mode endothelial- mesenchymal transformation of the cardiac valve. *Proceedings of the National Academy of Sciences*: 1–6.

143. Mahler GJ, Frendl CM, Cao Q, Butcher JT (2014) Effects of shear stress pattern and magnitude on mesenchymal transformation and invasion of aortic valve endothelial cells. *Biotechnol Bioeng* 111: 2326–2337.

144. Yang J-H, Wylie-Sears J, Bischoff J (2008) Opposing actions of Notch1 and VEGF in post-natal cardiac valve endothelial cells. *Biochemical and Biophysical Research Communications* 374: 512–516.

145. Combs MD, Yutzey KE (2009) Heart valve development regulatory networks in development and disease. *Circulation Research* 105: 408–421.

146. Chen J-H, Yip CYY, Sone ED, Simmons CA (2009) Identification and Characterization of Aortic Valve Mesenchymal Progenitor Cells with Robust Osteogenic Calcification Potential. *The American Journal of Pathology* 174: 1109–1119.
147. Visconti RP, Ebihara Y, LaRue AC, Fleming PA, McQuinn TC, et al. (2006) An in vivo analysis of hematopoietic stem cell potential. *Circulation Research* 98: 690–696.
148. Skowasch D, Schrempf S, Wernert N, Steinmetz M, Jabs A, et al. (2005) Cells of primarily extravalvular origin in degenerative aortic valves and bioprostheses. *European Heart Journal* 26: 2576–2580.
149. Nichols J, Zevnik B, Anastassiadis K, Niwa H (1998) Formation of pluripotent stem cells in the mammalian embryo depends on the POU transcription factor Oct4. *Cell* 95: 379-391.
150. Pesce M, Schöler HR (2001) Oct-4: Gatekeeper in the Beginnings of Mammalian Development. *Stem Cells* 19: 271–278.
151. Zeineddine D, Papadimou E, Chebli K, Gineste M, Liu J, et al. (2006) Oct-3/4 Dose Dependently Regulates Specification of Embryonic Stem Cells toward a Cardiac Lineage and Early Heart Development. *Developmental Cell* 11: 535–546.
152. Shi G, Jin Y (2010) Role of Oct4 in maintaining and regaining stem cell pluripotency. *Stem Cell Research Therapy* 1: 39.
153. Sternecker J, Höing S, Schöler HR (2011) Concise Review: Oct4 and More: The Reprogramming Expressway. *Stem Cells* 30: 15–21.
154. Schöler HR, Dressler GR, Balling R, Rohdewohld H, Gruss P (1990) Oct-4: a germline-specific transcription factor mapping to the mouse t-complex. *The EMBO journal* 9: 2185-2195.
155. Takahashi K, Yamanaka S (2006) Induction of pluripotent stem cells from mouse embryonic and adult fibroblast cultures by defined factors. *Cell* 126: 663-676.

156. Liu K, Ji G, Mao J, Liu M, WANG L, et al. (2012) Generation of Porcine-Induced Pluripotent Stem Cells by Using OCT4 and KLF4 Porcine Factors. *Cellular Reprogramming* 14: 505-513.
157. Blin G, Nury D, Stefanovic S, Neri T, Guillevic O, et al. (2010) A purified population of multipotent cardiovascular progenitors derived from primate pluripotent stem cells engrafts in postmyocardial infarcted nonhuman primates. *The Journal of Clinical Investigation* 120: 1125-1139.
158. Branchetti E, Sainger R, Poggio P, Grau JB (2013) Antioxidant Enzymes Reduce DNA Damage and Early Activation of Valvular Interstitial Cells in Aortic Valve Sclerosis 33: e66-74.

CHAPTER 2

ENDOTHELIAL-DERIVED OXIDATIVE STRESS DRIVES MYOFIBROBLASTIC ACTIVATION AND CALCIFICATION OF THE AORTIC VALVE

This chapter was published in *PLoS One*:

Farrar EJ, Huntley GD, Butcher JT (2015) Endothelial-Derived Oxidative Stress
Drives Myofibroblastic Activation and Calcification of the Aortic Valve. PLoS ONE
10(4): e0123257.

2.1 Abstract

Aims:

Oxidative stress is present in and contributes to calcification of the aortic valve, but the driving factors behind the initiation of valve oxidative stress are not well understood. We tested whether the valve endothelium acts as an initiator and propagator of oxidative stress in aortic valve disease.

Methods and Results:

Calcified human aortic valves showed side-specific elevation of superoxide in the endothelium, co-localized with high VCAM1 expression, linking oxidative stress, inflammation, and valve degeneration. Treatment with inflammatory cytokine TNF α increased superoxide and oxidative stress and decreased eNOS and VE-cadherin acutely over 48 hours in aortic valve endothelial cells (VEC) and chronically over 21 days in *ex vivo* AV leaflets. Co-treatment of VEC with tetrahydrobiopterin (BH₄) but not apocynin mitigated TNF α -driven VEC oxidative stress. Co-treatment of *ex vivo* AV leaflets with TNF α +BH₄ or TNF α +peg-SOD rescued endothelial function and mitigated inflammatory responses. Both BH₄ and peg-SOD rescued valve leaflets from the pro-osteogenic effects of TNF α treatment, but only peg-SOD was able to mitigate the fibrogenic effects, including increased collagen and α SMA expression.

Conclusions:

Aortic valve endothelial cells are a novel source of oxidative stress in aortic valve disease. TNF α -driven VEC oxidative stress causes loss of endothelial protective function, chronic inflammation, and fibrogenic and osteogenic activation, mitigated differentially by BH₄ and peg-SOD. These mechanisms identify new targets for

tailored antioxidant therapy focused on mitigation of oxidative stress and restoration of endothelial protection.

2.2 Introduction

Aortic valve disease (AVD) causes approximately 15,000 deaths per year in the United States, occurring in 2.8% of Americans over the age of 75 [1]. AVD is an active process driven by complex intercellular interactions [2] that is pathobiologically unique from other cardiovascular diseases [3-5]. Valve endothelial cells (VEC), which line the surface of the valve, are phenotypically different from other endothelial cell populations [6-9] and must be investigated for unique pathological mechanisms. VEC are known to play a unique role in regulating the properties of valve tissue in response to the dynamic cardiac environment [10-11], but their role in early disease is not known. Disruption of VEC function is an early and persistent feature of AVD [12-14], but it is not known if disrupted VEC actively contribute to valve calcification. Development of treatments that would protect against AVD by maintaining VEC protective function and blocking potential active contributions to calcification are hampered by a lack of understanding of the underlying mechanisms of VEC pathology.

VEC production of nitric oxide (NO) is protective against AVD, but is reduced in calcified valves [15-18]. In vascular disease, NO is reduced due to a phenomenon known as eNOS uncoupling [19], however, it is not known if eNOS uncoupling represents a significant source of oxidative stress in AVD. Uncoupled eNOS produces superoxide rather than nitric oxide due to a lack of the eNOS co-factor tetrahydrobiopterin (BH₄) [20]. Increased superoxide reacts with NO to form peroxynitrite (ONOO⁻), further reducing the bioavailability of NO [21], or excess

superoxide is dismutated to hydrogen peroxide (H₂O₂) [22]. Superoxide and hydrogen peroxide are increased in calcifying regions of the aortic valve [23-24] and contribute to osteogenic activation of valve interstitial cells [25]. If eNOS uncoupling is a significant phenomenon in the valve endothelium, VEC-derived oxidative stress could be an important and accessible target in the development of treatments to prevent valve calcification.

Inflammation has long been clinically linked to oxidative stress [26] and eNOS uncoupling [27] in vascular endothelial cells, but it is not known whether a similar link exists in valve endothelial cells as a mechanism of valvular disease. Inflammatory activation of the endothelium correlates proportionally with calcification in AVD [28]. Inflammation induces early and sustained expression of endothelial inflammatory adhesion molecules VCAM-1 and ICAM-1 [29]. Inflammatory cytokine TNF α has been identified as a key effector of pro-inflammatory signaling in valve endothelial cells and of pro-calcific signaling in valve interstitial cells [30-32]. TNF α can also initiate a pro-disease endothelial to mesenchymal transition in adult VEC [33-34]. However, it is not known if TNF α causes VEC to actively contribute pro-calcific oxidative stress to the diseased valve environment.

In this study, we establish that inflammatory cytokine TNF α drives increased oxidative stress in the valve endothelium, identifying valve endothelial cells as a novel source of elevated oxidative stress in AVD. We show that TNF α -driven endothelial oxidative stress, in part from eNOS uncoupling, causes endothelial dysfunction and

exacerbates endothelial inflammatory response and that these effects can be prevented by treatment with TNF α +tetrahydrobiopterin (BH₄) or TNF α +peg-SOD. Results from our *ex vivo* AV leaflet culture show that blocking endothelial oxidative stress also mitigates TNF α -driven myofibroblastic activation, extracellular matrix remodeling, and calcification in the valve tissue. These findings identify a novel pathophysiological mechanism by which TNF α -driven endothelial oxidative stress initiates downstream calcification of the aortic valve. Antioxidant therapies that protect against endothelial-derived increases in oxidative stress can mitigate valve disease progression by preserving the protective capabilities of the endothelium.

2.3 Materials and Methods

Human aortic valves

Calcified human aortic valves were obtained from adults undergoing planned, non-elective valve replacement surgery at Robert Packer Hospital in Sayre, PA. The Guthrie Institutional Review Board at Robert Packer Hospital and the Institutional Review Board for Human Participants at Cornell University approved all procedures (IRB#0908-24, “Gene expression and phenotypic changes in stenotic aortic valves”). Written informed consent was obtained from all participants. The investigation conformed to the principles outlined in the Declaration of Helsinki. Patient age range was 65-90 years, with a mean age of 76.2 years, 21 samples total. 33% were female; all were diagnosed with moderate to severe aortic stenosis; one patient had concurrent peripheral vascular disease. There were no racial/ethnic-based differences in samples. Healthy, non-diseased aortic valves were obtained from patients who died from non-valve related illnesses, who had no visible valve pathology, and whose hearts were ineligible for organ donation due to non-valve related defects, provided by Dr. Jonathan Chen, Cornell-Weill Medical School and NY Presbyterian Hospital. For quantification of superoxide, VCAM-1, and superoxide dismutase in the valve endothelium, CD31 expression was used to detect presence or absence of endothelial cells along each point on the valve periphery. Superoxide, VCAM-1, and superoxide dismutase expression were quantified at each point on the periphery that was positive for CD31. This value was integrated over the fibrosa or the ventricularis endothelium and calculated as integrated density of SOD or VCAM-1 expression per micron.

Superoxide in human aortic valve sections

Calcified human aortic valve (cHAV) leaflets were decalcified in 10% sodium citrate and 22% formic acid in deionized water for 12 hours or until soft, then washed in running water for 30 minutes. Decalcified cHAV and non-diseased HAV were embedded in paraffin wax and sectioned in 6 μ m increments. Superoxide was visualized using dihydroethidium (DHE) fluorescence. Valve sections were deparaffinized, washed in 1x Hank's buffered salt solution (HBSS) (Invitrogen), and incubated in the dark in 10 μ mol/L DHE for 30 minutes. Sections were rinsed twice and imaged immediately on a Zeiss 710 (Thornwood, NY) laser scanning confocal microscope, using 488nm excitation and 585nm emission. Images were adjusted to minimize background fluorescence using controls and fluorescence intensity was mapped onto a colorimetric intensity scale using ImageJ (NIH).

Aortic valve endothelial cells

Valve endothelial cells (VEC) were harvested from porcine aortic valves (Shirk Meats, Dundee, NY). Use of porcine cells, a widely-accepted human valve analog, provided a large, controlled population of VEC that were screened for phenotype and purity using q-rtPCR and immunofluorescence for CD31, eNOS, VE-cadherin, and absence of α SMA (see Appendix A). All reagents obtained from Sigma-Aldrich, St Louis, MO, unless otherwise noted. Porcine aortic valve endothelial cells (PAVEC) were isolated as demonstrated previously¹⁶ from valves donated by Shirk Meats of Dundee, NY. PAVEC were grown in flasks coated with 50 μ g/mL rat-tail collagen I (BD Biosciences, San Jose, CA) at 37°C and 5% CO₂ in DMEM supplemented with

10% FBS (Invitrogen, Grand Island, NY), 1% penicillin-streptomycin (Invitrogen, Grand Island, NY), and 50U/mL heparin. Cells were passaged 1:3 at confluency using 0.25% Trypsin-EDTA (Invitrogen, Grand Island, NY) and media was changed every 48 hours. Purity of endothelial population was monitored via quantitative real-time PCR, western blot, and immunofluorescent assessment. Only cultures with consistent CD31 and VE-cadherin expression, cobblestone morphology, and non-detectable α SMA expression were used. α SMA levels were measured via real-time PCR (> 37 cycle threshold), western blot, and immunofluorescence. PAVEC cultures were used between passage four and six. For all experiments and assays except those requiring protein isolation for Western blot, PAVEC were cultured on 3-D collagen hydrogels composed of 10% FBS (Gemini Biosciences, West Sacramento, CA), 1x Dulbecco's modified eagle medium (D-MEM, Invitrogen, Grand Island, NY), and 2 mg/mL collagen type I (BD Biosciences, San Jose, CA), adjusted to a pH of 7.2. After one hour incubation of the hydrogels at 37°C, PAVEC were seeded at 100,000 cells/cm² and allowed to adhere overnight, as described previously [35]. For Western blot, PAVEC were cultured in 6-well plates to 70% confluence, and then treatment was added. For treatments, cells were rinsed twice in fresh 1x PBS, then human recombinant TNF α or 1 μ mol/L H₂O₂ in DMEM was added. 500 μ mol/L L-NAME was added 30 minutes prior to TNF α treatment; all other co-treatments were added concurrently with TNF α , using 1000U/mL catalase, 10 μ mol/L BH₄, 20U/mL pegylated Cu-Zn-Superoxide dismutase, or 100 μ mol/L Apocynin suspended in DMSO.

Endothelial oxidative stress state assessment

Human recombinant TNF α was administered at dosages from 10-100ng/mL and determined to have a significant inflammatory effect (VCAM-1 upregulation, NF κ B nuclear translocation) with no statistically significant VEC apoptosis at 30ng/mL, as previously shown [33]. H₂O₂ dosage (1 μ mol/L) was chosen to recapitulate peak increases in secreted H₂O₂ by VEC stimulated with 30ng/mL TNF α . Acute increases in oxidative stress due to TNF α were measured across 0-4 hours. Peak effect occurred and is presented here at 30 minutes post-treatment. Intracellular oxidative stress was assessed via DHE fluorescence and CM-H₂DCF-DA fluorescence, quantified on a microplate reader and with confocal microscopy. Cells were cultured overnight on collagen gels, then treatment was added for amount of time specified in text. Samples were then rinsed twice in 1x HBSS and 10 μ mol/L CM-H₂DCFDA in 1x HBSS was added and incubated at 37°C for one hour. Samples were rinsed twice in 1x HBSS and assessed for dye fluorescence immediately on a Gen5 micro-plate reader (BioTek, Winooski, VT) with 485/525 excitation/emission.

Secreted NO was measured using the Griess assay. Importantly, heparin was not added to the culture media used for any conditions of the Griess assay, as heparin induces precipitation upon addition of the Griess reagent. Secreted H₂O₂ was measured by the Fluoro H₂O₂TM assay (Cell Technology, Inc). Phenol-red-free D-MEM was used to culture PAVEC and PAEC in all treatments for H₂O₂ measurement experiments, in order to optimize signal to noise ratio. Standard curves for each assay

were performed using media kept in identical conditions as treatments and controls, but without cells. Mitochondrial reactive oxygen species were measured using MitoSOX™ Red assay, quantified on a microplate reader and with confocal microscopy. Efficacy of antioxidant administration was optimized for pre-treatment time and dosage. Peak effect was achieved by administering 500µmol/L L-NAME 30 minutes prior to TNFα treatment and all other co-treatments concurrently with TNFα, using 10 µmol/L BH₄, 100 µmol/L apocynin (acetovanillone), and 20U/mL Cu-Zn-Superoxide dismutase-polyethylene glycol (peg-SOD).

Dihydroethidium (DHE) was used to assess superoxide levels in PAVEC and deparaffinized *ex vivo* aortic valve leaflet sections. Time course imaging studies were performed in order to determine the optimal length of time for DHE stain incubation, as well as the degradation of the signal during imaging. 1 hour of 10uM DHE stain, 2 rinses in HBSS, and immediate imaging was found to give optimum results in terms of minimal background and bright calcific nodule (positive control). Samples were washed twice in 1x Hank's buffered salt solution (HBSS) (Invitrogen, Grand Island, NY), and incubated in the dark in 10 µmol/L DHE for 30 minutes. Sections were rinsed twice in 1x HBSS and imaged immediately on a Zeiss 710 (Thornwood, NY) laser scanning confocal microscope (488/585) or immediately on a Gen5 (BioTek, Winooski, VT) micro-plate reader (485/525). Confocal images were adjusted to minimize background fluorescence using negative controls and fluorescence intensity was mapped onto a colorimetric intensity scale using ImageJ (NIH). Micro-plate data

was adjusted to remove background fluorescence and averaged across at least three samples for each condition.

MitoSOX red mitochondrial superoxide indicator was used to detect mitochondrial O_2^- in both *in vitro* and *ex vivo* samples. Time course imaging studies were performed in order to determine the maximum MitoSOX signal produced from *in vitro* porcine VEC, as well as the optimal length of time for MitoSOX stain incubation, and the degradation of the signal during imaging (negligible over 30 minute imaging period). The *in vitro* protocol for VEC on 3-D hydrogels was as follows: treat VEC gels with $TNF\alpha$ +antioxidants as described above, incubate for 30 minutes, rinse twice in 1x PBS, add 200 μ L of 5 μ M MitoSOX in 1x HBSS to each gel. Incubate 10 minutes at 37°C, rinse 3x in 1x HBSS, and image immediately on a Gen5 (BioTek, Winooski, VT) micro-plate reader (510/590). Micro-plate data was adjusted to remove background fluorescence, averaged across at least three samples for each condition, and normalized to control samples.

Ex vivo aortic valve leaflets

Porcine aortic valve leaflets were harvested sterilely from fresh porcine hearts (Shirk Meats, Dundee, NY). Leaflets were immediately rinsed in sterile PBS, transported on ice, and transferred to Dulbecco's Modified Eagle Medium (D-MEM) within two hours. D-MEM was supplemented with 10% fetal bovine serum and 1% penicillin-streptomycin, adjusted to a pH of 7.2. 30ng/mL of $TNF\alpha$ was added directly to the media, supplemented with 10 μ mol/L BH_4 or 20U/mL peg-SOD, where noted. This

culture media was changed every 48 hours for 21 days. TUNEL assay for apoptosis was performed to confirm cell viability and DHE or MitoSOXTM Red assay were used to detect oxidative stress. For MitoSOX Red, samples were processed identical to the *in vitro* cell staining procedure, but with 10 minutes MitoSOX stain incubation at 37°C and a final co-stain with 5µM Draq5 (Cell Signaling Technology) for 10 minutes at room temperature. Slides were then rinsed 3x in 1x PBS, mounted with Permount anti-fade mounting media (Life Technologies), and imaged immediately on a Zeiss 710 (Thornwood, NY) laser scanning confocal microscope (488/585). MitoSOX staining intensity was analyzed by separating only the 590nm fluorescence channel and using ImageJ to quantify integrated pixel intensity over different regions of the leaflet: interstitium, fibrosa endothelium, and ventricularis endothelium. Data is presented for n=6 samples per condition and normalized to control leaflet intensities.

Russell-Movat pentachrome staining was used to visualize extracellular matrix components and Alizarin Red S in combination with von Kossa staining was used to assess calcification.

Immunofluorescence

PAVEC on collagen gels were rinsed twice in PBS and fixed in 4% paraformaldehyde for one hour at 37°C or overnight at 4°C. Samples were rinsed 3 times on a rocker with PBS for 15 minutes each, permeabilized with 0.2% Triton-X (VWR International, West Chester, PA) for 10 minutes on rocker, and blocked in 10% goat serum in 1% BSA solution for one hour at 37°C or overnight at 4°C. Samples were rinsed 3x for 15 minutes each in PBS and primary antibodies were added: mouse anti-pig CD31 (AbD

Serotec, 1:100), mouse anti-human eNOS (BD transduction laboratories, 1:100), rabbit anti-human VE-cadherin (Cell Signaling Technology, 1:100), rabbit anti-human VCAM-1 (Santa Cruz Biotechnology, 1:50), rabbit anti-human NF κ B (Cell Signaling Technology, 1:100), and rabbit anti-human α SMA (Abcam, 1:100). Samples were incubated overnight at 4°C, rinsed in 3x for 15 minutes each in PBS on rocker, and species-specific secondary antibodies raised in goat conjugated to Alexa Fluor® 488 or 568 fluorophores were added. Samples were incubated for 2 hours at room temperature, rinsed, then incubated for an additional 30 minutes with 1:1000 Draq5 nuclear stain (Enzo Life Sciences AG, Lausen, Switzerland). Samples were rinsed thoroughly in PBS 3 times on rocker for 15 minutes each, then imaged using a Zeiss 710 (Thornwood, NY) laser scanning confocal microscope.

Western blot

PAVEC were lysed directly on the plate using RIPA buffer (Thermo Scientific, Rockford, IL) supplemented with 25mM NaF, 1mM NaVO₄, and 0.5% Protease inhibitor cocktail, incubated for 15 min at RT, scraped and homogenized by pipetting up and down, and centrifuged at 15,000 rpm for ten minutes. Protein was mass balanced using Pierce 660nm protein assay with ionic detergent compatibility reagent (Thermo Scientific, Waltham, MA) and loaded into a 4-15% gradient gel (Bio-Rad, Hercules, CA) with 4x buffer (Li-Cor, Lincoln, NE)+10% β -mercaptoethanol at 1:3 ratio and run for one hour at 120V in 25mM Tris, 0.2M Glycine, 1% SDS running buffer. Western blot transfer to nitrocellulose membrane (Thermo Scientific, Rockford, IL) was performed at 400mA for one hour in 25mM Tris, 20% methanol

transfer buffer. After rinsing in PBS 0.1% Tween-20, membrane was blocked for one hour in Odyssey Blocking Buffer (Li-Cor, Lincoln, NE) at RT. Mouse anti-human VE-cadherin (Cell Signaling Technology, Danvers, MA) (1:1000), mouse anti-human eNOS (BD Biosciences, San Jose, CA) (1:1000), rabbit anti-human VCAM-1 (Santa Cruz, Dallas, TX) (1:1000), rabbit anti-human NFκB (Cell Signaling Technology, Danvers, MA) (1:1000) and mouse anti-human GAPDH (Invitrogen, Grand Island, NY) (1:20,000) were used in Odyssey blocking buffer+0.1%Tween-20 to detect protein expression. The membrane was washed 4x in PBS-tween, 1x in PBS, and incubated overnight with primary antibody at 4°C with gentle agitation. The same washes were then performed and the membrane was incubated in Odyssey blocking buffer +0.1% Tween-20 +0.2% SDS with 1:20,000 anti-mouse (680nm) and anti-rabbit secondary antibodies (800nm) (Li-Cor IRDye, Lincoln, NE). Blots were imaged using the Odyssey Infrared system (Li-Cor, Lincoln, NE).

Quantitative real-time polymerase chain reaction

Total RNA was extracted from lysed 3-D hydrogels using a RNeasy total RNA purification kit (Qiagen, Valencia, CA) and quantified using a Nanodrop 2000 spectrophotometer (Nanodrop, Wilmington, DE). An equal amount of RNA from each sample was reverse transcribed to cDNA using the iScript™ cDNA synthesis kit (Bio-Rad, Hercules, CA). Quantitative real-time polymerase chain reaction was performed on all samples using SYBR Green PCR master mix (Applied Biosystems, Foster City, CA), and a CFX96 or MiniOpticon Real-Time PCR Detection System (Bio-Rad, Hercules, CA). Samples amplifying at > 37 cycles were considered non-detectable.

Primer Name	Forward	Reverse
ALP	ATGAGCTCAACCGGAACA	GTGCCCATGGTCAATCCT
MMP-9	ACACACACGACATCTTCC	AAGGTCACGTAGCCCACAA
MMP-2	CGCCCATCATCAAGTTTC	TCGAGTTCGCCTGTCTG
Sox9	GGAGACTGCTGAATGAGAGC	CGTTCTTCACCGACTTTCTC
Msx2	AAGGCAATGACTTGTTTTTCG	AGGCTGGAGACCTTGACG
COL1A1	AGAAGACATCCCACCAGTCA	CGTCATCGCACAACACATTG
COL2A1	GTCTACCCCAATCCAGCAAA	GTCTACCCCAATCCAGCAAA
COL3A1	TTGGCCCTGTTTGCTTTTA	TGGTTGACAAGATGAGAACAAA

Ex vivo protein isolation

Fresh, healthy, adult pig hearts were donated by Shirk Meats of Dundee, NY. Leaflets were removed carefully from the heart and transferred immediately to ice-cold sterile PBS. In less than one hour, sterile tools were used to cut leaflets in half and transfer each half to a single well of a 24-well plate, with 0.5mL of control or treatment media in each well. Treatments were designed with identical formulations as the *in vitro* experiments. Leaflet halves were paired across control and treatment conditions to increase robustness of comparison. Six or more samples were used for each individual treatment. Plates were cultured at 37°C and 5% CO₂. 30ng/mL of TNF α was added directly to the media, supplemented with 10 μ mol/L BH₄ or 200U/mL Cu-Zn-Superoxide dismutase-polyethylene glycol, where noted. This culture media was changed every 48 hours for 21 days. TUNEL assay for apoptosis was performed to

confirm cell viability, DHE was used to detect superoxide, Russell-Movat pentachrome staining was used to visualize extracellular matrix components and Alizarin Red S in combination with von Kossa staining was used to assess calcification, as describe below.

For *ex vivo* protein isolation, leaflet halves were transferred to a sterile mortar, flash frozen with liquid nitrogen, and crushed to a fine powder with sterile pestle. Mortar and pestle were washed and sterilized between each sample. Sample powder was transferred to 100 μ L of 2x Laemmli buffer, heated to 70°C for 10 minutes, sonicated on ice, and spun down at 14,000 rpm for 10 minutes at 4°C. The supernatant was transferred to a new tube, flash frozen, and kept at -80°C until protein quantification. Protein was quantified as described for *in vitro* experiments and western blot performed as above.

Ex vivo RNA isolation

Aortic valve leaflet tissue was flash-frozen and ground to a powder, similar to protein isolation procedure. Powder was transferred to eppendorf tube and vortexed with 350 μ L of RLT lysis buffer (Qiagen, Hilden, Germany) +1% β -mercaptoethanol to mix. Any remaining un-dissolved tissue was homogenized using the QIAshredder system (Qiagen, Hilden, Germany). RNA solutions were flash frozen and stored at -80°C.

Ex vivo Histology & Immunofluorescence

Aortic valve leaflet samples were fixed in 4% PFA overnight at 4°C, and then stored in ethanol until paraffin embedding. Samples were embedded with root to free-edge view exposed. Embedded sections were sectioned in 6µm increments and mounted on glass slides. Representative sections from each sample were stained with Alizarin Red S (VWR), von Kossa, or Russell-Movat pentachrome stain (Mastertech, Lodi, CA). For ARS, cells were deparaffinized, hydrated, incubated in ARS stain for 2 minutes, rinsed in xylene and xylene-acetone (1 min each), dehydrated in 3 changes of xylene (1 min each), and mounted. Analysis of ARS was done in ImageJ, using thresholding to identify boundaries of the leaflet section. Leaflet section with background subtracted was measured for area and integrated density of ARS stain. Similar deparaffinization and hydration was performed for von Kossa, followed by a 20 minute incubation in 1% aqueous silver nitrate under UV light. Slides were rinsed in water followed by 5% sodium thiosulfate (5 min), rinsed, and counter-stained with 0.1% nuclear fast red (5 min). Dehydration and mounting performed as above. Slides were imaged and thresholded in ImageJ so that only black-brown mineral deposits were selected for analysis. Mineral deposit area was measured and normalized to valve leaflet area. Russell-Movat pentachrome stain was performed according to manufacturer's instructions, with the following adjustments: 30 seconds in 2% ferric chloride, 20 minutes in 1% alcian blue, and 1 minute in each change of 5% phosphotungstic acid. A color deconvolution algorithm [58] was used to separate individual dyes from the Russell-Movat stained sections into single-channel images. MATLAB© was used to find the integrated density of each single-channel image. Integrated density of each component (GAG = blue, collagen = yellow, elastin =

black) was normalized to the area of the valve leaflet section being examined. The resulting output was divided by the average integrated density of each dye in control samples, producing fold change expression of GAG, elastin, and collagen relative to control.

Additional sections were immunofluorescently labeled as described above, with an additional antigen retrieval step in which slides were submerged in 98°C sodium citrate buffer (10 mM Sodium citrate, 0.05% Tween 20, pH 6.0) for five minutes. Immunofluorescently labeled slides were imaged with a Zeiss 710 laser scanning confocal microscope, as described in the *in vitro* methods. TUNEL assay (Invitrogen, Grand Island, NY) was performed according to manufacturer's instructions to label apoptosis, necrosis, and cell nuclei. Leaflet sections were imaged with a Zeiss 710 laser scanning confocal microscope, analyzed, and quantified using ImageJ. Number of cell nuclei and cells positive for apoptosis per section were counted using particle analysis. Percent of cells positive for apoptosis (TUNEL stain) was presented.

Statistical Analysis

Data is expressed as mean +/- standard error of the mean (SEM). All comparisons between two groups were made using two-tailed, unpaired t-tests assuming unequal variance. Comparisons between multiple groups were made using one-way ANOVA with Tukey's post hoc tests. Differences between means were considered significant when $p < 0.05$.

2.4 Results

Calcified human aortic valves show elevated endothelial superoxide in a side-specific manner, co-localized with inflammatory activation

We first examined superoxide levels in calcified (cHAV) human aortic valves, using DHE intensity. Superoxide levels were significantly increased in calcified regions of the valves (Figure 2.1A) and in the fibrosa endothelium, but not in non-calcified regions or the ventricularis endothelium (Figure 2.1A, B). Elevated endothelial superoxide was associated with the fibrosa side of the stenotic human aortic valve, where calcific lesions are known to form. Across cHAV samples, regions of the endothelium with high levels of superoxide were positive for both VCAM-1 and CD31 (Figure 2.1C), indicating a link between inflammatory endothelial activation and elevated endothelial superoxide. The interstitial cells directly beneath the human VEC (hVEC) did not have significantly increased superoxide (arrows). hVEC on the ventricularis side were positive for CD31, but did not have significantly increased superoxide or elevated VCAM-1 expression (Figure 2.1C).

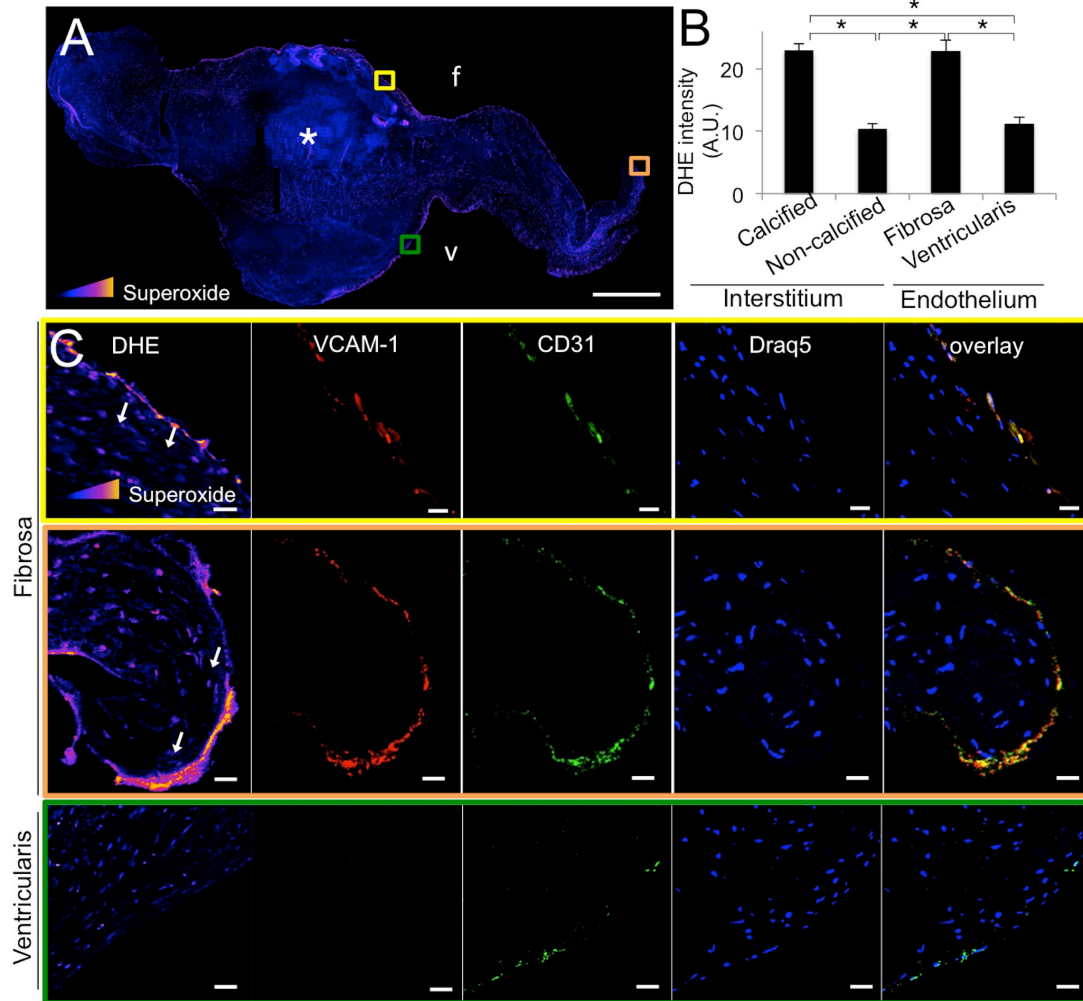


Figure 2.1 Elevated superoxide in the endothelium of calcified human aortic valves.

A, Superoxide staining (DHE) of calcified human aortic valve leaflets. Asterisks indicate calcific nodule. Intensity of superoxide staining is colorimetrically scaled, with yellow indicating most intense (inset triangle). Colored boxes indicate region magnified in lower panels; f indicates fibrosa, v indicates ventricularis. Scale bar = 1 mm. B, Quantification of DHE intensity (superoxide) across all valve samples, presented as DHE intensity in different regions of calcified valves (cHAV), n=21. * indicates $p < 0.05$ between indicated groups. C, Co-localization of elevated superoxide with VCAM-1 and CD31 expression in calcified human aortic valve leaflet endothelium. Representative images from n=21 valves. Scale bar = 20 μ m.

Side-specific expression of endothelial superoxide dismutase in calcified human aortic valves

The fibrosa endothelium of diseased valves showed little to no SOD1 expression, while the ventricularis endothelium retained strong expression of SOD1 (Figure 2.2A). Quantitative analysis of SOD1 expression in the CD31⁺ endothelial cells of cHAV confirmed that the fibrosa endothelium showed significantly less SOD1 than the ventricularis endothelium (Figure 2.2B).

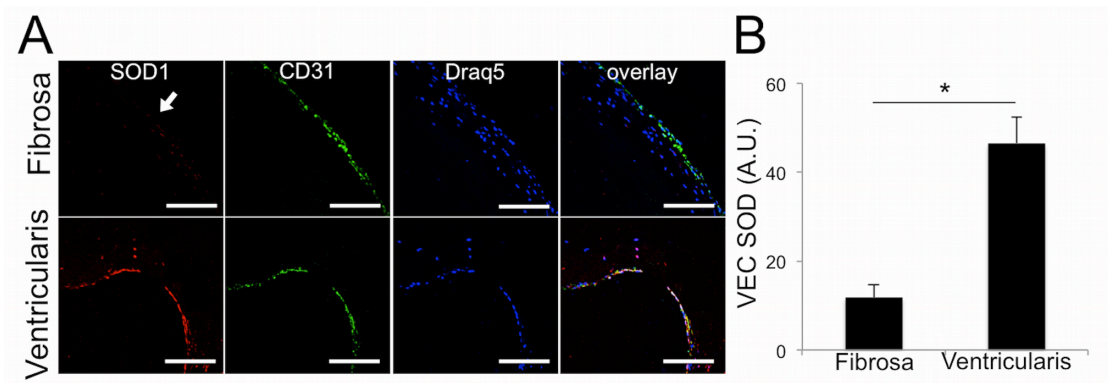


Figure 2.2 Superoxide dismutase in calcified human valves.

A. Immunofluorescence for endothelial protein CD31 and SOD1 revealed little to no expression of SOD1 (arrow) on the fibrosa endothelium of calcified aortic valve leaflets. The ventricularis showed strong SOD1 expression in the endothelium. B. Quantification of the pixel intensity of SOD1 in the CD31⁺ endothelial cells in cHAV, n=21. The fibrosa endothelium had significantly less SOD1 than the ventricularis in cHAV. * indicates $p < 0.05$ between groups, Student's t-test.

TNF α causes increased oxidative stress and decreased NO in VEC

TNF α caused a significant increase in VEC intracellular oxidative stress (Figure 2.3A), superoxide (Figure 2.4), and secreted H₂O₂ (Figure 2.3B), 30 minutes after treatment. After 48 hours, TNF α or H₂O₂ treatment decreased VEC secretion of nitric

oxide (Figure 2.3C) and decreased expression of eNOS and VE-cadherin proteins (Figure 3D, Figure 2.5).

To elucidate the source of increases in endothelial oxidative stress and the resulting endothelial dysfunction, we administered NOS inhibitor L-NAME, eNOS co-factor BH₄, NADPH oxidases inhibitor apocynin, or peg-SOD in conjunction with TNF α treatment. At 30 minutes, L-NAME, BH₄, and peg-SOD blocked TNF α -stimulated increases in VEC superoxide, but apocynin did not (Figure 2.3E). L-NAME and apocynin reduced overall oxidative stress compared to TNF α alone, and peg-SOD lowered oxidative stress further still. Only eNOS co-factor BH₄ restored VEC oxidative stress back to control levels (Figure 2.3F). Similar trends were observed in H₂O₂ secretion: co-administration of L-NAME, BH₄, or peg-SOD blocked increases in secreted H₂O₂ by VEC, but apocynin did not (Figure 2.3G). TNF α similarly drove increases in VEC mitochondrial reactive oxygen species (mtROS), which were only abrogated by peg-SOD (Figure 2.3H). Over 48 hours, only BH₄ or peg-SOD maintained control levels of nitric oxide secretion (Figure 2.3I). Catalase co-treatment was able to reduce general oxidative stress state in VEC, but was found to cause a significant increase in apoptosis, loss of VE-cadherin, nuclear translocation of NF κ B, and VCAM-1 expression (Figure 2.6). Thus, catalase treatment had off-target effects on VEC that were significant enough to prevent further investigation of its viability as a pro-endothelial valve treatment against inflammation and calcification.

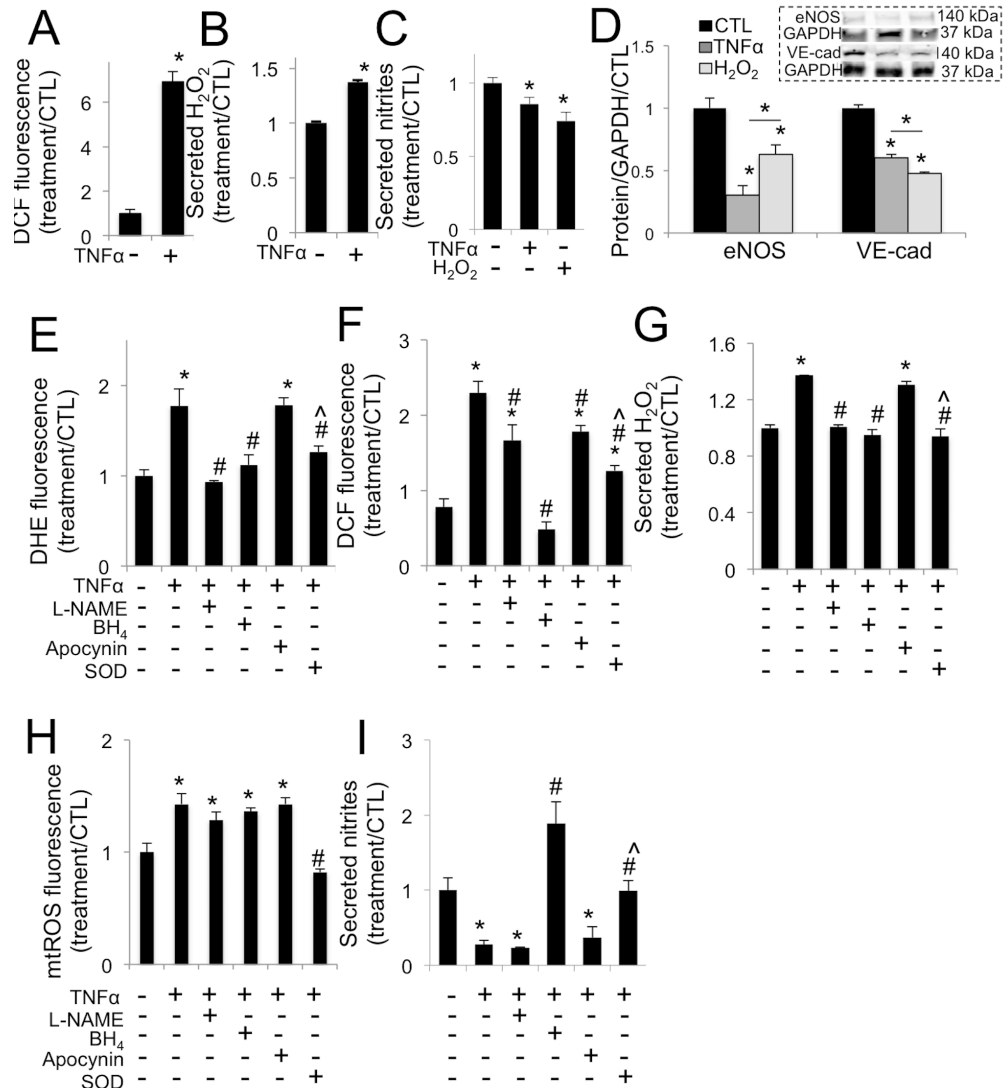


Figure 2.3 TNF α drives eNOS uncoupling.

A, TNF α increases oxidative stress in VEC at 30 minutes. B, TNF α increases hydrogen peroxide (H₂O₂) secretion from VEC at 30 minutes. C, TNF α or H₂O₂ decrease nitric oxide secretion from VEC at 48 hours (n=4). D, TNF α or H₂O₂ decrease eNOS and VE-cadherin expression in VEC at 48 hours. Representative western blot images (inset) and blot quantification. E, L-NAME, BH₄, or peg-SOD but not apocynin block increases in superoxide (DHE) in VEC caused by TNF α , at 30 minutes. F, L-NAME, apocynin, and peg-SOD mitigate increases in general oxidative stress (DCF) caused by TNF α at 30 minutes, but only BH₄ completely blocks superoxide increase, maintaining control levels. G, L-NAME, BH₄, or peg-SOD but not apocynin block increases in H₂O₂ secreted by VEC at 30 minutes caused by TNF α at 30 minutes. H, TNF α drives increased mtROS, mitigated only by co-treatment with SOD. I, BH₄, or peg-SOD but not L-NAME or apocynin block decreases in nitric oxide secretion in VEC caused by TNF α at 48 hours. * indicates p < 0.05 versus control. # indicates p < 0.05 versus TNF α . ^ indicates p < 0.05 versus apocynin. N=4.

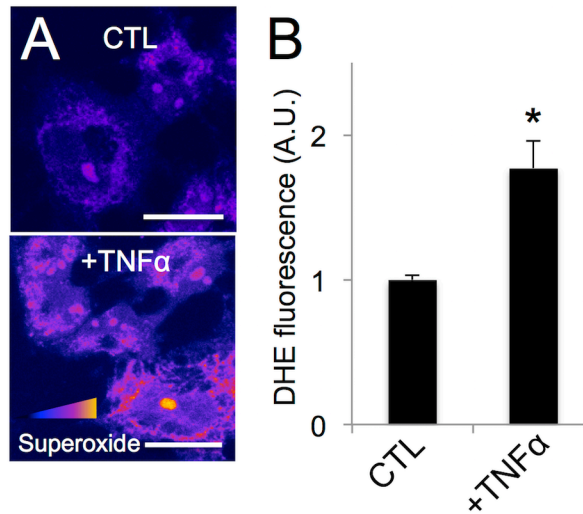


Figure 2.4 TNF α caused increased superoxide expression in VEC.

A, Intracellular superoxide in VEC+TNF α at 30 minutes after treatment. Presented using colorimetric scale to show relative DHE intensity, indicated in inset triangle. B, Quantification of superoxide production at 30 minutes using microplate assay for DHE fluorescence. * indicates $p < 0.05$ versus control. $N > 6$ for each condition. DHE fluorescence was measured using integrated pixel density in three different fields of view ($250\mu\text{m}^2$) on each sample. The three measurements were averaged within each sample, with each average corresponding to N of 1. Means were compared using unpaired Student's t-test, assuming unequal variance.

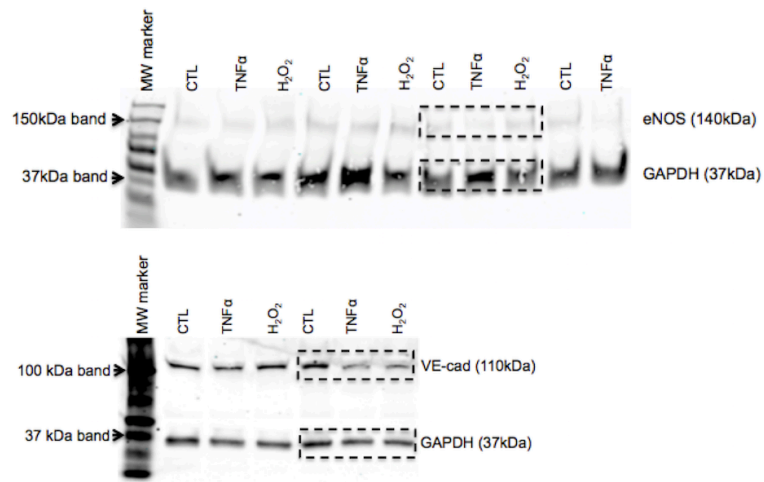


Figure 2.5 eNOS protein expression in 48 hour VEC with TNF α or H $_2$ O $_2$.

Original western blot images for Figure 3. PAVEC cultured 48 hrs on 3D hydrogels with control, +30 ng/mL TNF α , or 1 μ M H $_2$ O $_2$. Boxed regions indicate bands shown in Figure 2.3.

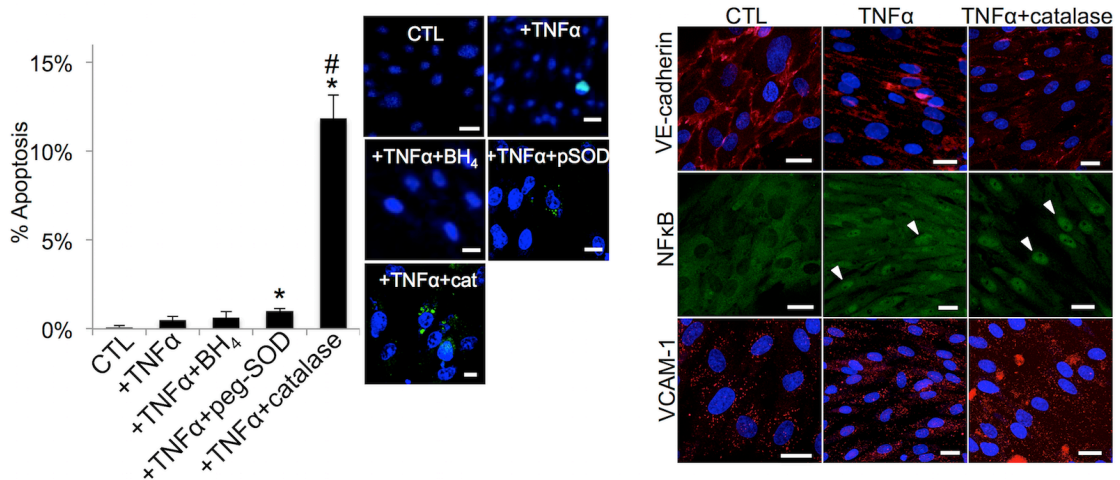


Figure 2.4 VEC cultured *in vitro* on 3D hydrogels for 48 hours with TNF α +antioxidants.

A. TNF α +catalase treatment caused a significant increase in apoptosis. B. TNF α +catalase treatment caused increased loss of VE-cadherin, increased nuclear translocation of NF κ B, and increased VCAM-1 expression compared to both control and TNF α alone. N = 3, * indicates p < 0.05 vs CTL, # indicates p < 0.05 vs TNF α . Scale bar is 20 μ m.

Mitigating the effects of TNF α -oxidative stress rescues endothelial function and abates VEC inflammatory response.

We then examined the protein-level effects of BH₄ and peg-SOD on VEC when applied in conjunction with TNF α treatment. TNF α decreased VE-cadherin and eNOS and increased VCAM-1 protein expression in VEC (Figure 2.7A, arrows). Co-treatment of VEC with BH₄ or peg-SOD protected against loss of VE-cadherin and eNOS and reduced VCAM-1 response to TNF α . Western blot analysis confirmed this result (Figure 2.7B,C, Figure 2.8).

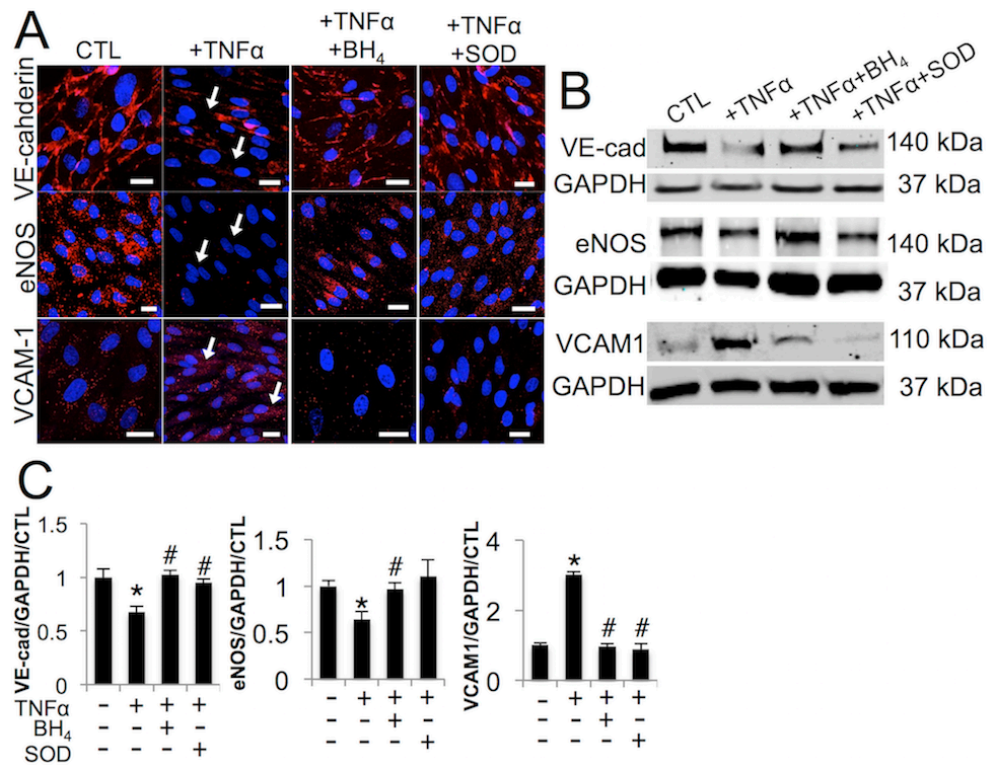


Figure 2.7 Effects of blocking eNOS uncoupling.

A, TNF α decreases VE-cadherin and eNOS expression in VEC over 48 hours (arrows), rescued by BH $_4$ or peg-SOD. TNF α increases VCAM-1 expression in VEC over 48 hours, mitigated by BH $_4$ or peg-SOD. B, Western blot analysis of VE-cadherin (VE-cad), eNOS, and VCAM-1 protein in same conditions as A, with GAPDH housekeeping protein. C, Quantification of western blot results, normalized to GAPDH and control, n=3. * indicates $p < 0.05$ versus control, # indicates $p < 0.05$ versus TNF α . Scale bar = 20 μ m. Images representative of three independent experiments.

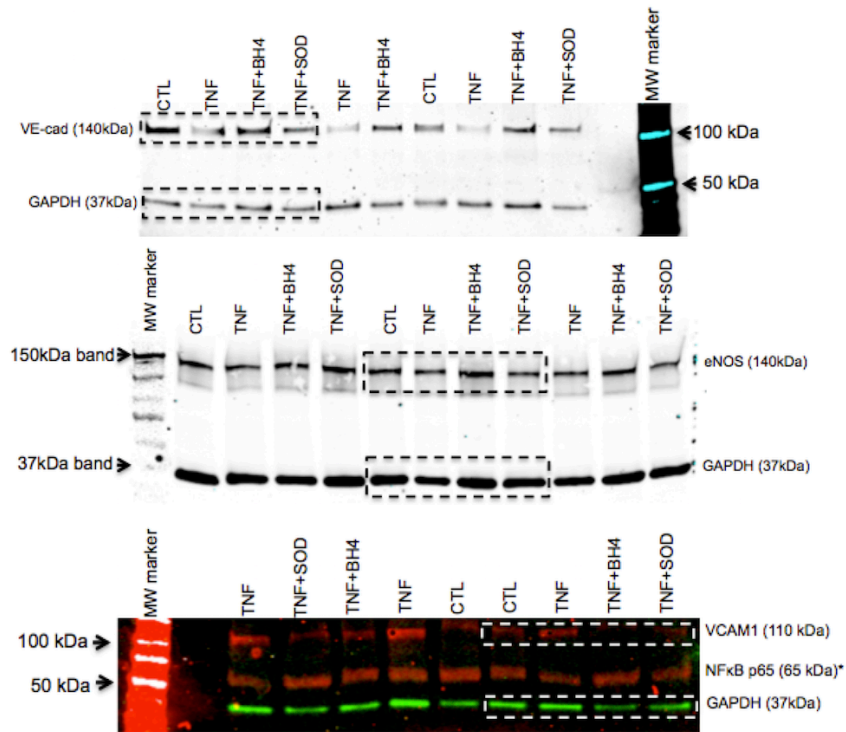


Figure 2.8 VE-cadherin, eNOS, and VCAM1 protein expression in 48 hour VEC.

PAVEC cultured 48 hrs on 3D hydrogels with control, +30 ng/mL TNF α , +30 ng/mL TNF α +10 μ M BH $_4$, or +30 ng/mL TNF α +20U/mL peg-SOD. Boxes indicate bands shown in Figure 4. *Analysis of NF κ B p65 protein expression was not used in this study.

TNF α increases VEC oxidative stress in ex vivo aortic valve leaflets, rescued by antioxidants.

We then used *ex vivo* culture of healthy porcine AV leaflets to examine tissue-level effects of TNF α -driven endothelial oxidative stress and the ability of BH $_4$ or peg-SOD to mitigate TNF α effects. No significant apoptosis was observed in the leaflets throughout the course of the experiment (Figure 2.9). Similar to our findings *in vitro*, over 21 days TNF α increased endothelial superoxide, most distinctly in the fibrosa endothelium (Figure 2.10A). BH $_4$ treatment mitigated fibrosa but not ventricularis-side increases in superoxide. Peg-SOD lowered endothelial superoxide even further than

BH₄, significantly decreasing levels on both the fibrosa and ventricularis sides (Figure 2.10B). To elucidate a potential mechanism behind differential BH₄ and peg-SOD effects, we examined the contribution of mitochondrial reactive oxygen species (mtROS) within our *ex vivo* leaflets. We found that TNF α indeed increased levels of mtROS, specifically within the ventricularis endothelium (Figure 2.10C). Quantification of mtROS fluorescence revealed a 42 \pm 9.3% increase in mtROS only in ventricularis VEC and not in fibrosa VEC or VIC, which was mitigated by co-treatment with SOD, but not BH₄ (Figure 2.10D).

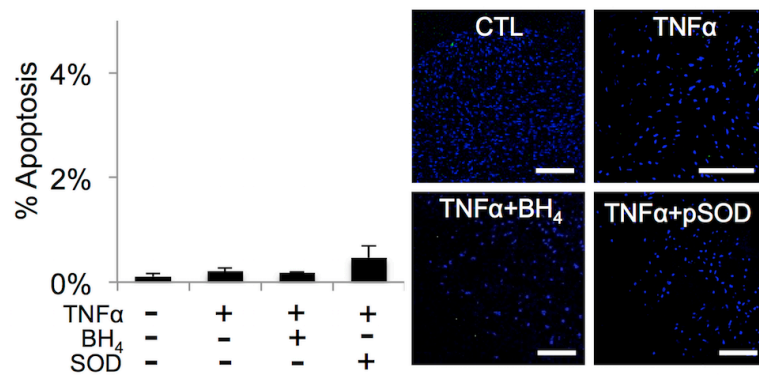


Figure 2.9 Apoptosis in *ex vivo* AV leaflets cultured for 21 days.

There was no significant apoptosis in any of AV leaflets, as measured by the TUNEL assay. N = 6 for all sample groups. Means were compared using one-way ANOVA with Tukey's post hoc test.

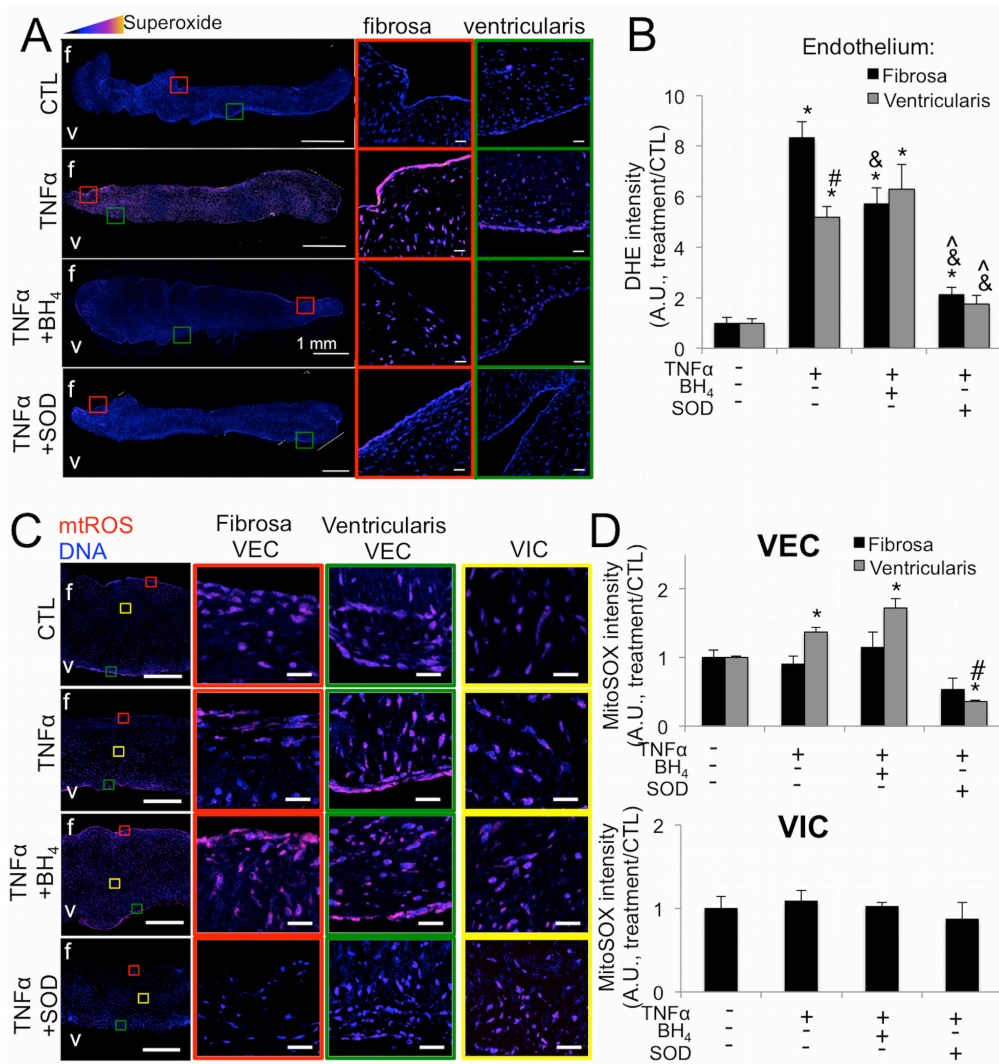


Figure 2.5 TNF α induces side-specific endothelial oxidative stress *ex vivo*.

A, TNF α causes increased superoxide in the fibrosa endothelium of *ex vivo* porcine aortic valve leaflets cultured for 21 days, revealed by DHE staining. Superoxide is mitigated on the fibrosa by co-treatment with BH₄ and on both the fibrosa and ventricularis by peg-SOD. Pixel intensity of superoxide levels is scaled colorimetrically (inset triangle) to show regions of highest superoxide. Colored boxes indicate regions magnified on right, showing endothelium on fibrosa and ventricularis sides of valve. Scale bar is 1mm in left images, 20 μ m in magnified images. B, Quantification of endothelial superoxide in *ex vivo* aortic valves stained with DHE reveals side-specific rescue-effects of BH₄ and more pronounced mitigation of superoxide on both sides of the valve by peg-SOD. C, TNF α increases mtROS in the ventricularis VEC of *ex vivo* AV leaflets. D, Quantification of mtROS fluorescence. Ventricularis-specific increases in mtROS are mitigated by peg-SOD but not BH₄. * indicates p < 0.05 versus control condition. # indicates p < 0.05 versus fibrosa endothelium in same condition. & indicates p < 0.05 versus same side endothelium in TNF α condition. ^ indicates p < 0.05 versus same side endothelium in TNF α +BH₄. N=6.

Antioxidants improve endothelial function and repress valve interstitial cell myofibroblastic activation in aortic valve leaflets.

AV leaflets cultured in TNF α for 21 days showed significant endothelial dysfunction, with decreases in CD31, VE-cadherin, and eNOS on both the fibrosa and the ventricularis. These effects were rescued by co-treatment with BH₄ or peg-SOD. TNF α also caused upregulation of VCAM-1 on both sides of the valve, which was mitigated almost entirely on both the fibrosa and ventricularis by co-treatment with BH₄ or peg-SOD. TNF α significantly increased α SMA in both the endothelium and the underlying interstitium on both sides of the valve, decreased on the fibrosa by peg-SOD and on the ventricularis by BH₄ or peg-SOD (Figure 2.11A). Loss of VE-cadherin and eNOS and increases in α SMA due to TNF α and the protective effect of antioxidants were confirmed via western blot analysis (Figure 2.11B, Figure 2.12).

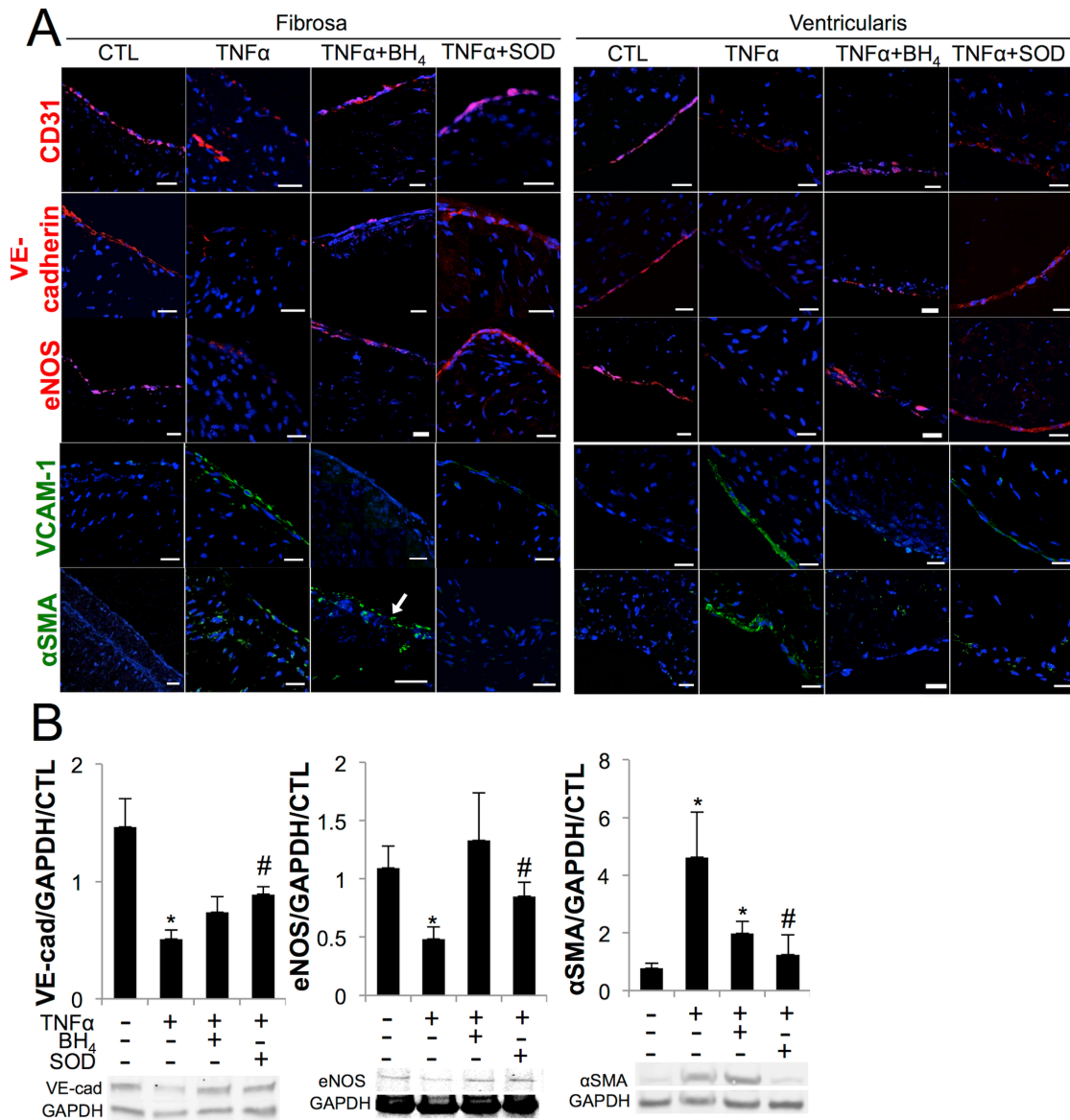


Figure 2.6 TNF α induces endothelial dysfunction *ex vivo*.

A, In *ex vivo* porcine aortic valve leaflets, TNF α decreased endothelial proteins CD31, VE-cadherin, and eNOS on both sides of the valve, rescued by BH $_4$ or peg-SOD. TNF α increased VCAM1 on both sides of the valve, mitigated by BH $_4$ or peg-SOD. TNF α increased α SMA on both sides of the valve, which was mitigated on the fibrosa by peg-SOD but not by BH $_4$ (arrow) and on the ventricularis by either BH $_4$ or SOD. B, Western blot quantification confirmed loss of VE-cadherin and eNOS and increase in α SMA in TNF α condition that is rescued by BH $_4$ or peg-SOD. * indicates $p < 0.05$ versus CTL, # indicates $p < 0.05$ versus TNF α . Scale bar = 20 μ m. N=6.

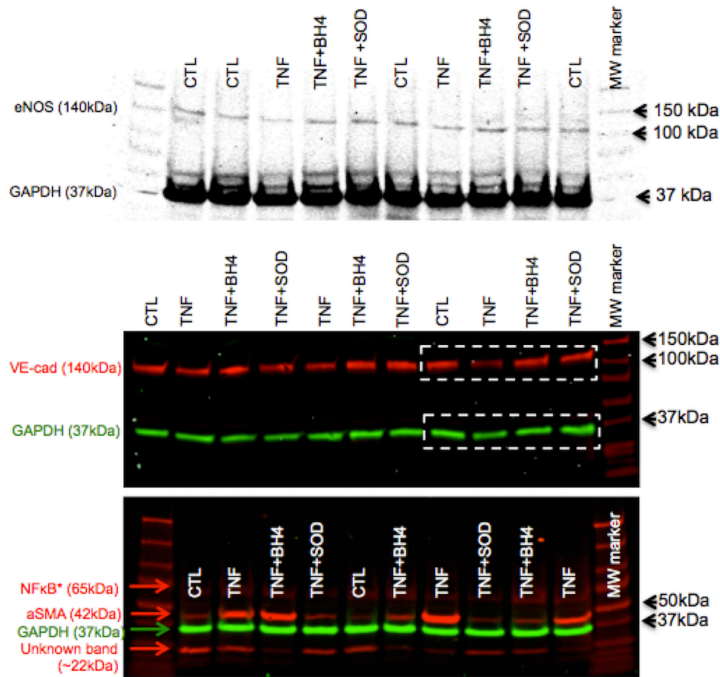


Figure 2.7 eNOS, VE-cad, α SMA protein expression in *ex vivo* AV leaflets.

Porcine AV leaflets cultured 21 days in control, +30 ng/mL TNF α , +30 ng/mL TNF α +10 μ M BH $_4$, or +30 ng/mL TNF α +20U/mL peg-SOD. Boxes indicate bands shown in Figure 6.

*Analysis of NF κ B p65 protein expression was not used in this study.

TNF α causes extracellular matrix disorganization and calcification in aortic valve leaflets, rescued by antioxidants.

Ex vivo aortic valve leaflets treated with TNF α for 21 days showed significant fibrogenesis and osteogenesis compared to controls. Control AV leaflets showed distinct trilaminar structure of the extracellular matrix (ECM), with well-defined organization of elastin fibers within the ventricularis (arrow, Figure 2.13A). Valve leaflets treated with TNF α showed ECM disorganization, marked by significantly decreased elastin and glycosaminoglycans (GAG), and significantly increased collagen. q-rtPCR analysis of the valve tissue showed increased synthesis of COL1A1

and COL3A1 mRNA with TNF α (Figure 2.13B). BH₄ protected against loss of elastin and GAG, but allowed similar increases in collagen as in TNF α alone. Peg-SOD protected against loss of elastin and GAG and provided significant protection against increases in collagen, maintaining collagen expression at control levels. Peg-SOD blocked increases in COL1A1 and COL3A1 mRNA. COL2A1 was decreased in all treatment conditions.

Alizarin red staining showed significant increase in free calcium in leaflets cultured with TNF α , localized to the fibrosa side of the leaflets (Figure 2.13C, arrows) that was mitigated by BH₄ and returned to control levels by peg-SOD. von Kossa staining showed an increase in mineralization, again on the fibrosa, in leaflets cultured with TNF α that was equally blocked by BH₄ or peg-SOD (Figure 2.13D). BH₄ caused minimal off-target effects on a range of markers regulating AV function (Figure 2.14).

TNF α increased synthesis of mRNA for alkaline phosphatase, an enzyme involved in active bone formation, which was mitigated by co-treatment with BH₄ or peg-SOD. TNF α decreased synthesis of mRNA for the anti-osteogenic transcription factor Sox9, indicating a pro-calcific phenotypic shift that was rescued by co-treatment with BH₄. TNF α also increased synthesis of mRNA for matrix metalloproteinase-9, mitigated by BH₄ or peg-SOD (Figure 2.13E).

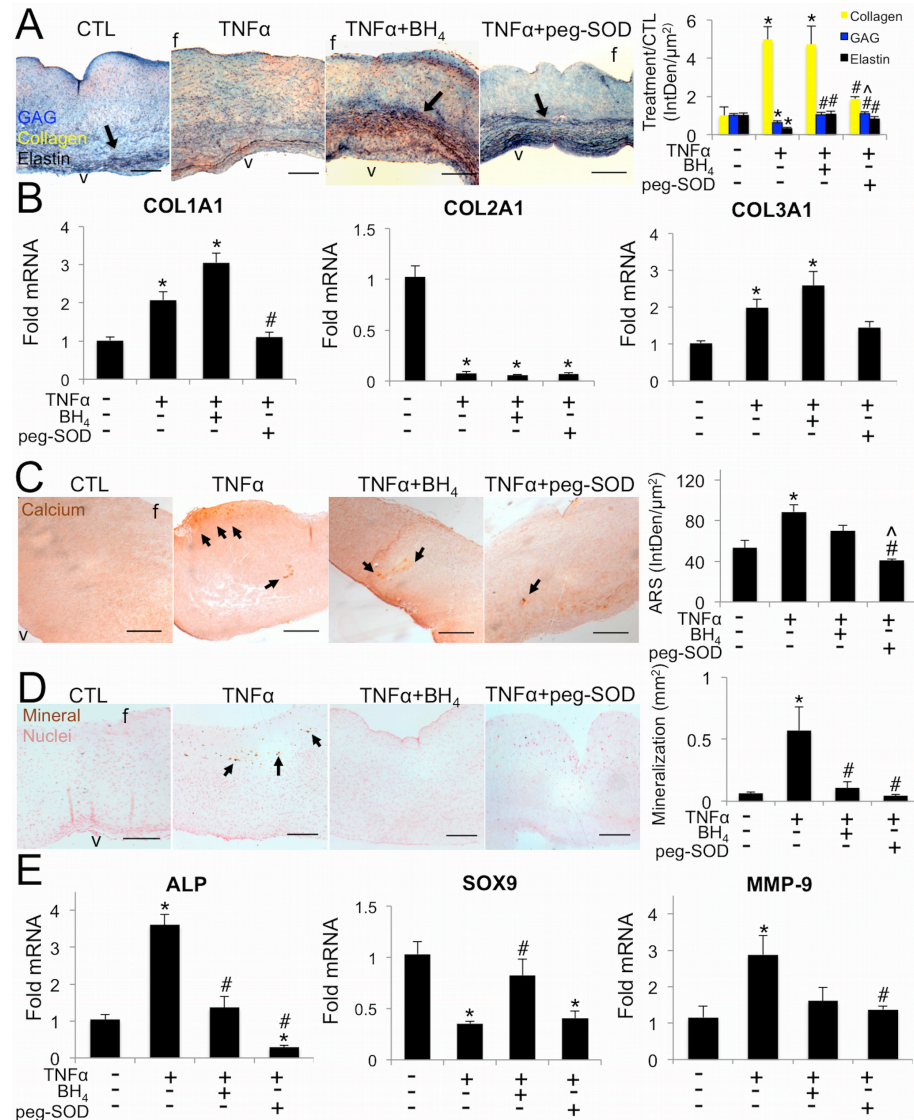


Figure 2.13 TNF α induces early calcification and ECM changes *ex vivo*.

A, TNF α increased collagen and decreased GAG and elastin (arrows). BH $_4$ maintains GAG and elastin at control levels, but does not block increases in collagen. Peg-SOD significantly reduced collagen compared to TNF α and maintained control levels of GAG and elastin (Blue: glycosaminoglycans, Red: mucins, Yellow: collagen, Black, elastin). B, TNF α increased synthesis of COL1A1 and COL3A1 mRNA, rescued by peg-SOD but not by BH $_4$. COL2A1 was decreased in all treatment conditions. * indicates $p < 0.05$ versus control, # indicates $p < 0.05$ versus TNF α . N=6. One-way ANOVA with Tukey's post hoc test were used to compare means. C, TNF α increased calcium deposition (Alizarin Red S stain) that is rescued by BH $_4$ or peg-SOD. D, TNF α increased mineralization (von Kossa stain), rescued by BH $_4$ or peg-SOD. E, TNF α increased alkaline phosphatase, decreased Sox9, and increased MMP-9 mRNA, rescued differentially by BH $_4$ or peg-SOD. Representative images from $n = 6$ leaflets per condition. Scale bar = $200\mu\text{m}$. * indicates $p < 0.05$ versus control, # indicates $p < 0.05$ versus TNF α , ^ indicates $p < 0.05$ versus TNF α +BH $_4$. N=6.

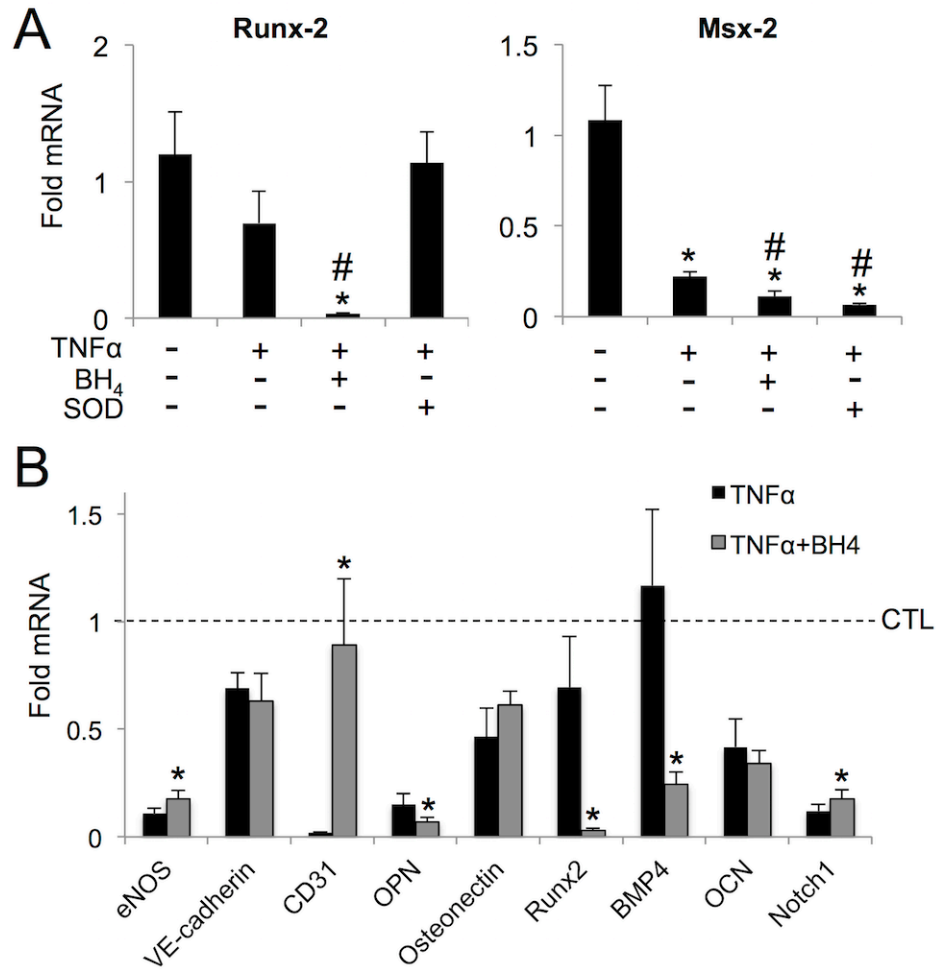


Figure 2.14 q-rtPCR analysis of *ex vivo* AV leaflets with TNF α +antioxidants.

A. Complex regulation of transcription factors Runx2 and Msx2 by TNF α and BH $_4$ or SOD. N = 6, * indicates p < 0.05 vs CTL, # indicates p < 0.05 vs TNF α . B. BH $_4$ co-treatment consistently causes either neutral or beneficial effects compared to TNF α alone. N = 6, * indicates p < 0.05 vs TNF α .

2.5 Discussion

Aortic valve disease is a pressing medical issue with few clinically useful pharmacological intervention strategies. New therapies are needed that target specific cellular mechanisms that will guard against valve degeneration. In this study, we have shown the valve endothelium to be a novel source of oxidative stress in the aortic valve when stimulated with the inflammatory cytokine TNF α (Figure 2.15). We further showed that targeting this mechanism via antioxidants directed at superoxide levels protects against loss of endothelial function, chronic inflammation response, myofibroblastic activation, calcification, and extracellular matrix disorganization.

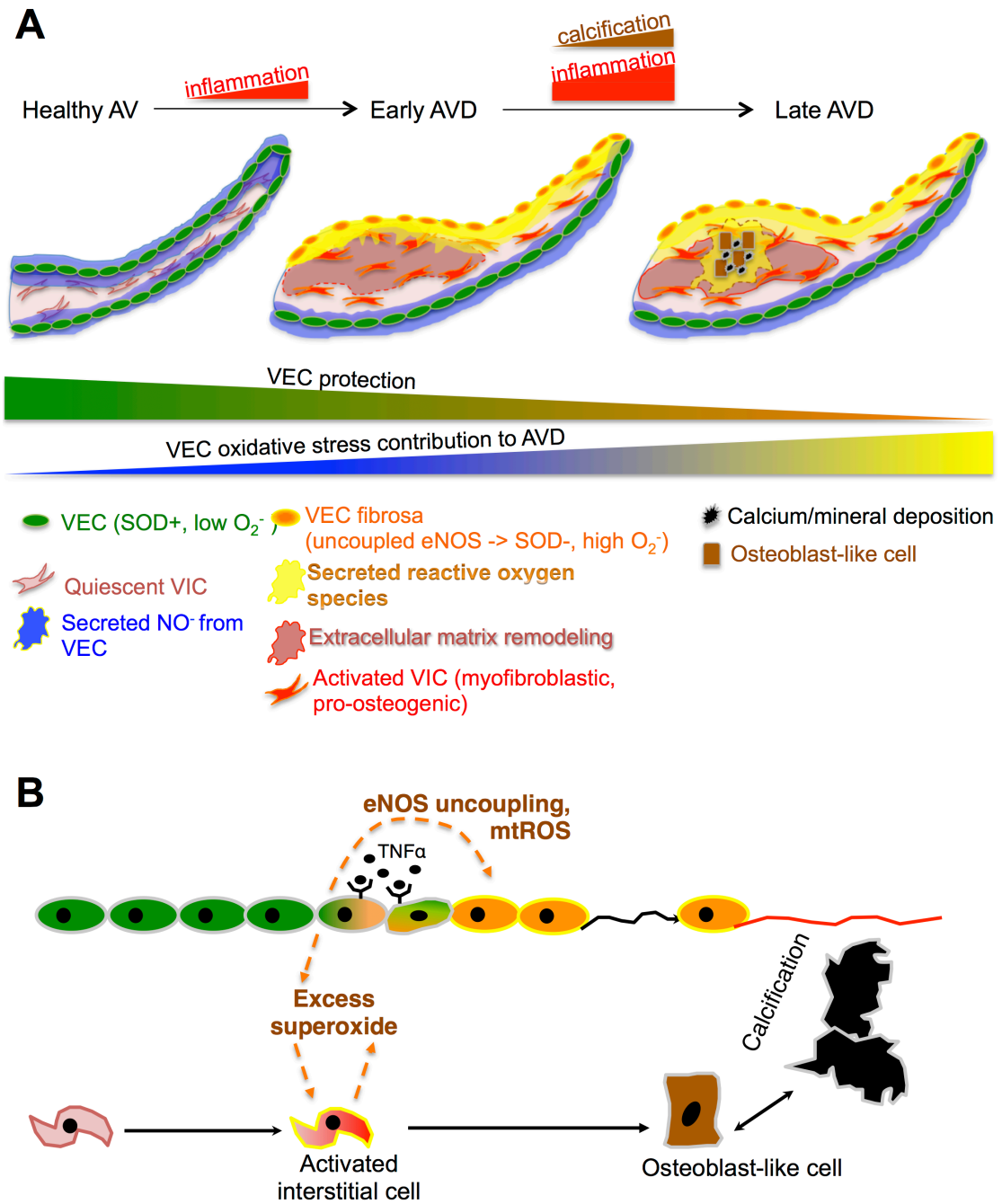


Figure 2.15 Valve endothelial oxidative stress contributes directly to aortic valve disease.

A. Valve tissue-level contribution of endothelial and interstitial oxidative stress throughout the course of AVD. B. Cellular level endothelial and interstitial contributions with specific sources of oxidative stress identified.

In a healthy valve, endothelial cells secrete protective NO, maintaining quiescence of valve interstitial cells. Early AVD is characterized by inflammation-driven side specific increase in VEC oxidative stress, in part via eNOS uncoupling, causing disorganization of the extracellular matrix and loss of protective NO secretion in the fibrosa. In late AVD, oxidative stress from VEC contributes to calcification and mineral deposition, while NO and SOD are decreased in fibrosa VEC.

We showed that regions of the calcified valve endothelium with high VCAM-1 co-localized with regions of high superoxide, linking inflammation with oxidative stress in the diseased valve endothelium. This phenomenon occurs in both mildly and heavily affected regions of the valve, specifically on the fibrosa side of the leaflet. This pervasive and side-specific co-localization of inflammatory activation and oxidative stress in the endothelium suggests that TNF α -driven endothelial oxidative stress occurs throughout mild and advanced stages of AVD. Side-specificity of endothelial oxidative stress points to a distinct involvement of this endothelial-specific mechanism with calcific lesion formation, known to develop preferentially on the fibrosa [36]. Our observation of increased superoxide levels in hVEC but not the adjacent hVIC supports a role for valve endothelial cells as a unique source of oxidative stress in the diseased valve, distinct from oxidative stress previously described in the calcifying regions of the valve [23-24] or as a result of immune cell invasion. We also observed fibrosa-specific loss of SOD1 expression in cHAV, indicating a dearth of SOD1 in the diseased fibrosa endothelium during AVD, making the valve more susceptible to increases in oxidative stress from the endothelium. Low

fibrosa SOD1 compared to the ventricularis in cHAV can also explain the preferential accumulation of superoxide that we observed in the fibrosa endothelium of calcified valves.

Recently, TNF α signaling has been implicated as a key inflammatory pathway in stenotic aortic valves [37-39]. Mouse models of hypercholesterolemia show inflammatory activation of the endothelium, increased superoxide [40], and endothelial dysfunction [41]. Here, we have demonstrated that TNF α increases endothelial oxidative stress, decreases NO secretion, and lowers VE-cadherin and eNOS protein expression in valve endothelial cells, both *in vitro* and *ex vivo*. This finding provides a mechanistic link between inflammation, endothelial dysfunction, and oxidative stress. TNF α -derived oxidative stress effects were blocked by co-treatment with eNOS co-factor BH₄, demonstrating that eNOS uncoupling is a primary mechanism of increased endothelial oxidative stress and a significant cause of endothelial dysfunction that leads to increased AV calcification via degradation of endothelial protection.

Co-treatment of VEC with TNF α +catalase did not protect the endothelium, but led to increased cellular apoptosis and elevated inflammatory activation. This agrees with previous studies that have shown that in certain cell types, H₂O₂ actually protects against TNF α –induced apoptosis and that increased levels of catalase has a neutral or negative effect [42-44]. The ability of apocynin to mitigate TNF α -driven endothelial oxidative stress levels as indicated by DCF staining shows that NADPH oxidases also

have a role to play in this phenomenon, though it appears to be less important than the uncoupling mechanism, as demonstrated by the more potent effects of BH₄. These findings define two unique mechanisms of endothelial oxidative stress contribution to AVD: via changes in eNOS activity due to uncoupling and disruption of native SOD1 and H₂O₂ levels. TNF α driven oxidative stress, in part due to eNOS uncoupling, degrades the endothelial protection that would normally mitigate valve degeneration [15, 17] and increases oxidative stress in the valve. This establishes a novel mechanism of valve oxidative stress based on endothelial inflammatory activation, distinct from existing descriptions of oxidative stress that have focused on valve interstitial cells [25, 45-47].

We further established the ability of BH₄ and peg-SOD to mitigate increases in VCAM-1 that occurred in VEC in response to TNF α . This dovetails with recent studies that implicate side-specific VCAM-1 expression in the progression and regulation of AVD [48-49]. Thus, mitigating the cellular stress imposed on VEC by TNF α -driven eNOS uncoupling may also decrease the need to activate downstream inflammatory signaling pathways. Mitigation of the symptoms of chronic inflammation could prove important to aortic valve calcification, as the TNF α signaling pathway is known to promote osteogenesis [50] and to be an active regulator of lesion formation in the vasculature [51].

Translation of our cellular-level findings into an *ex vivo* evaluation of AV leaflets allowed us to assess the specific effects of TNF α and antioxidants on the complex,

multicellular aortic valve leaflet. We found that superoxide levels in TNF α -treated valve leaflets was specifically elevated in VEC, with highest elevation on the fibrosa side, confirming that endothelial superoxide in cHAV is linked to inflammation of the valve endothelium. Interestingly, co-treatment of *ex vivo* AV leaflets with TNF α +BH $_4$ reduced oxidative stress only in the fibrosa endothelium compared to TNF α alone, whereas peg-SOD reduced oxidative stress on both sides of the valve leaflet. Examination of mitochondrial ROS provided an explanation for this difference, as peg-SOD but not BH $_4$ lowered mtROS levels within the ventricularis of *ex vivo* leaflets. We conclude that BH $_4$ treatment mitigates valve oxidative stress via direct targeting of fibrosa-specific eNOS uncoupling, whereas peg-SOD mitigates both fibrosa-specific eNOS uncoupling and mtROS within ventricularis VEC. A limitation of this study is the lack of direct experimental interrogation of mtROS as a propagator of AVD; however, the evidence presented here provides a foundation for future investigation of mitochondrial contribution to increased oxidative stress in the aortic valve in the early inflammatory stages of AVD.

Immunofluorescent staining confirmed the side-specific effect of BH $_4$. CD31, VE-cadherin, and eNOS were more robustly restored on the fibrosa with co-treatment of TNF α +BH $_4$, compared to TNF α alone. TNF α caused increased α SMA in the fibrosa, potentially due to mesenchymal transition of valve endothelial cells [34], in addition to direct myofibroblastic activation of valvular interstitial cells [31]. TNF α -induced increases in α SMA were blocked by co-treatment of valve leaflets with TNF α +BH $_4$ or TNF α +peg-SOD, demonstrating a role for both eNOS uncoupling and superoxide

from other sources such as NADPH oxidases and mtROS in driving myofibroblastic activation during AVD.

TNF α exposure caused significant disruption of the extracellular matrix organization and content of the aortic valve. TNF α increased collagen and decreased GAG and elastin, agreeing with studies that find differential GAG localization [52] and reduced elastin [53] in diseased aortic valves. GAG and elastin were preserved by BH₄ or peg-SOD. Increases in collagen were only mitigated by peg-SOD, not by BH₄. mRNA analysis showed that increased collagen was caused by increased expression of COL1A1 and COL3A1 isoforms in TNF α and TNF α +BH₄ conditions, but rescued in TNF α +peg-SOD condition. Interestingly, COL2A1 was uniformly decreased across TNF α , TNF α +BH₄, and TNF α +peg-SOD conditions, pointing to TNF α as a driver of early chondrocyte differentiation in valve cells and as an important contributor to valve calcification via a mechanism separate from the oxidative stress pathways examined here [54]. These findings indicate that protection against excess valve endothelial oxidative stress can guard against ECM changes known to feature in AVD [55] via antioxidant mitigation of inflammation, endothelial dysfunction, and oxidative stress.

TNF α accelerates calcification of aortic valve interstitial cells *in vitro* [32-33]. However, the contribution of TNF α to AVD within the complex multi-cellular environment of the native aortic valve is unknown. Here we used TNF α with and without BH₄ treatment to show that stimulation of endothelial eNOS uncoupling by

TNF α contributes to valve calcification, elucidating a novel mechanism of TNF α contribution to AVD. Increases in alkaline phosphatase point to the mechanism behind these changes, indicating that TNF α stimulates early osteogenic differentiation of valve interstitial cells, as has been observed *in vitro* under TGF- β stimulation [56], that can be protected against by preservation of endothelial function and reductions in oxidative stress.

Antioxidant therapy for AVD must be founded on specific mechanisms generating oxidative stress in order to be efficacious [57]. The evidence presented here establishes inflammatory activation of endothelial oxidative stress as a unique integrated pathobiological mechanism effecting early to late stages of aortic valve disease. Our findings support that specific targeting of eNOS uncoupling and the resulting excess superoxide may be key elements of managing AVD via antioxidant treatments.

Acknowledgements

The authors thank Dr. Sanjay Samy, Robert Packer Hospital, Sayre, PA, for generous donation of calcified aortic valve leaflets, Shirk Meats in Dundee, NY for donation of porcine aortic valve tissue, Dr. Jonathan Chen, Seattle Children's Hospital, for generous donation of non-diseased aortic valve leaflets, Kevin S. Hsu for assistance with data acquisition and analysis, and Jennifer M. Richards for assistance in the procurement and processing of diseased aortic valve tissue.

REFERENCES

1. Go AS, Mozaffarian D, Roger VL, Benjamin EJ, Berry JD, et al. (2013) Heart disease and stroke statistics--2013 update: A report from the American Heart Association. *Circulation* 127: e6–e245.
2. Rajamannan NM, Evans FJ, Aikawa E, Grande-Allen KJ, Demer LL, et al. (2011) Calcific aortic valve disease: Not simply a degenerative process. *Circulation* 124: 1783–91.
3. Teo KK, Corsi DJ, Tam JW, Dumesnil JG, Chan KL. (2011) Lipid lowering on progression of mild to moderate aortic stenosis: meta-analysis of the randomized placebo-controlled clinical trials on 2344 patients. *Can J Cardiol* 27: 800–8.
4. Shavelle DM, Takasu J, Budoff MJ, Mao S, Zhao X-Q, et al. (2002) HMG CoA reductase inhibitor (statin) and aortic valve calcium. *Lancet* 359: 1125–6.
5. Rossebø AB, Pedersen TR, Boman K, Brudi P, Chambers JB, et al. (2008) Intensive lipid lowering with Simvastatin and Ezetimibe in aortic stenosis. *New Engl J Med* 359: 1343–56.
6. Butcher JT, Penrod AM, Garcia AJ, Nerem RM. (2004) Unique morphology and focal adhesion development of valvular endothelial cells in static and fluid flow environments. *Arterioscler Thromb Vasc Biol* 24:1429–34.
7. Simmons CA, Grant GR, Manduchi E, Davies PF. (2005) Spatial heterogeneity of endothelial phenotypes correlates with side-specific vulnerability to calcification in normal porcine aortic valves. *Circ Res* 96:792–9.
8. Bischoff J, Aikawa E. (2011) Progenitor cells confer plasticity to cardiac valve endothelium. *J Cardiovasc Trans Res* 4: 710–9.
9. Farivar RS, Cohn LH, Soltesz EG, Mihaljevic T, Rawn JD, et al. (2003) Transcriptional profiling and growth kinetics of endothelium reveals differences between cells derived from porcine aorta versus aortic valve. *Eur J Cardiothorac Surg* 24: 527-34.

10. Butcher JT, Nerem RM. (2007) Valvular endothelial cells and the mechanoregulation of valvular pathology. *Philos Trans R Soc Lond B* 362: 1445–57.
11. Pompilio G, Rossoni G, Sala A, Polvani GL, Berti F, et al. (1998) Endothelial-dependent dynamic and antithrombotic properties of porcine aortic and pulmonary valves. *Ann Thorac Surg* 65: 986–92.
12. Müller AM, Cronen C, Kupferwasser LI, Oelert H, Müller K-M, et al. (2000) Expression of endothelial cell adhesion molecules on heart valves: up-regulation in degeneration as well as acute endocarditis. *J Pathol* 191: 54–60.
13. Poggianti E, Venneri L, Chubuchny V, Jambrik Z, Baroncini LA, et al. (2003) Aortic valve sclerosis is associated with systemic endothelial dysfunction. *J Am Coll Cardiol* 41:136–41.
14. Gould ST, Sriganapalan S, Simmons CA, Anseth KS. (2013) Hemodynamic and cellular response feedback in calcific aortic valve disease. *Circ Res* 113:186–97.
15. Richards J, El-Hamamsy I, Chen S, Sarang Z, Sarathchandra P, et al. (2013) Side-specific endothelial-dependent regulation of aortic valve calcification. *Am J Pathol* 182:1922-31.
16. Rajamannan NM, Subramaniam M, Stock SR, Stone NJ, Springett M, et al. (2005) Atorvastatin inhibits calcification and enhances nitric oxide synthase production in the hypercholesterolaemic aortic valve. *Heart* 91:806–10.
17. El-Hamamsy I, Balachandran K, Yacoub MH, Stevens LM, Sarathchandra P, et al. (2009) Endothelium-dependent regulation of the mechanical properties of aortic valve cusps. *J Am Coll Cardiol* 53:1448–55.
18. Bosse K, Hans CP, Zhao N, Koenig SN, Huang N, et al. (2013) Endothelial nitric oxide signaling regulates Notch1 in aortic valve disease. *J Mol Cell Cardiol* 60:27–35.
19. Ciprian AB, Cheng B, Sharma S, Sharma S, Yao L, et al. (2012) Increased Superoxide and eNOS uncoupling in blood vessels of Bmal1-KO mice. *Circ Res* 111:1157–65.

20. Wever RMF, van Dam T, van Rijn HJM, de Groot F, Rabelink TJ. (1997) Tetrahydrobiopterin regulates superoxide and nitric oxide generation by recombinant endothelial nitric oxide synthase. *Biochem Biophys Res Comm* 237:340–4.
21. Kar S, Bhandar B, Kavdia M. (2012) Impact of SOD in eNOS uncoupling: a two-edged sword between hydrogen peroxide and peroxynitrite. *Free Radic Res* 46:1496–513.
22. Li J-M, Shah AM. (2004) Endothelial cell superoxide generation: regulation and relevance for cardiovascular pathophysiology. *Am J Physiol Regul Integr Comp Physiol* 287:R1014–30.
23. Miller JD, Chu Y, Brooks RM, Richenbacher WE, Pena-Silva R, et al. (2008) Dysregulation of antioxidant mechanisms contributes to increased oxidative stress in calcific aortic valvular stenosis in humans. *J Am Coll Cardiol* 52:843–50.
24. Liberman M, Bassi E, Martinatti MK, Lario FC, Wosniak J, et al. (2008) Oxidant generation predominates around calcifying foci and enhances progression of aortic valve calcification. *Arterioscler Thromb Vasc Biol* 28:463–70.
25. Branchetti E, Sainger R, Poggio P, Grau JB. (2013) Antioxidant enzymes reduce DNA damage and early activation of valvular interstitial cells in aortic valve sclerosis. *Arterioscler Thromb Vasc Biol* 33:e66–74.
26. Marchesi C, Ebrahimian T, Angulo O, Paradis P, Schiffrin EL. (2009) Endothelial nitric oxide synthase uncoupling and perivascular adipose oxidative stress and inflammation contribute to vascular dysfunction in a rodent model of metabolic syndrome. *Hypertension* 54:1384–92.
27. Karbach S, Wenzel P, Waisman A, Münzel T, Daiber A. (2014) eNOS uncoupling in cardiovascular diseases – the role of oxidative stress and inflammation. *Curr Pharm Des* 20:3579-94.
28. New SEP, Aikawa E. (2010) Molecular imaging insights into early inflammatory stages of arterial and aortic valve calcification. *Circ Res*. 2011;108:1381–91.

29. Hjortnaes J, Butcher J, Figueiredo JL, Riccio M, Kohler RH, et al. (2010) Arterial and aortic valve calcification inversely correlates with osteoporotic bone remodeling: a role for inflammation. *Eur Heart J* 31:1975–84.
30. Aikawa E, Nahrendorf M, Sosnovik D, Lok VM, Jaffer FA, et al. (2007) Multimodality molecular imaging identifies proteolytic and osteogenic activities in early aortic valve disease. *Circulation* 115:377–86.
31. Kaden JJ, Dempfle C-E, Grobholz R, Fischer CS, Vocke DC, et al. (2005) Inflammatory regulation of extracellular matrix remodeling in calcific aortic valve stenosis. *Cardiovasc Pathol* 14:80–7.
32. Yu Z, Seya K, Daitoku K, Motomura S, Fukuda I, et al. (2011) Tumor necrosis factor- α accelerates the calcification of human aortic valve interstitial cells obtained from patients with calcific aortic valve stenosis via the BMP2-Dlx5 pathway. *J Pharmacol Exp Ther* 337:16–23.
33. Galeone A, Brunetti G, Oranger A, Greco G, Di Benedetto A, et al. (2013) Aortic valvular interstitial cells apoptosis and calcification are mediated by TNF-related apoptosis-inducing ligand. *Int J Cardiol* 169:296-304.
34. Mahler GJ, Farrar EJ, Butcher JT. (2013) Inflammatory cytokines promote mesenchymal transformation in embryonic and adult valve endothelial cells. *Arterioscler Thromb Vasc Biol* 33:121–30.
35. Farrar EJ, Butcher JT. (2013) Heterogeneous susceptibility of valve endothelial cells to mesenchymal transformation in response to TNF α . *Ann Biomed Eng* 42:149–61.
36. Chen JH, Simmons CA. (2011) Cell-matrix interactions in the pathobiology of calcific aortic valve disease: Critical roles for matricellular, matricrine, and matrix mechanics cues. *Circ Res* 108:1510–24.
37. Mahler GJ, Butcher JT. (2011) Inflammatory regulation of valvular remodeling: The good(?), the bad, and the ugly. *Int J Inflam* 2011: 721419.
38. Ghaisas N, Foley J, O'Briain D, Crean P, Kelleher D, et al. (2000) Adhesion molecules in nonrheumatic aortic valve disease: Endothelial expression, serum levels and effects of valve replacement. *J Am Coll Cardiol* 36:2257–62.

39. Bosse Y, Miqdad A, Fournier D, Pepin A, Pibarot P, et al. (2009) Refining Molecular pathways leading to calcific aortic valve stenosis by studying gene expression profile of normal and calcified stenotic human aortic valves. *Circ Cardiovasc Genet* 2:489–98.
40. Miller JD, Weiss RM, Serrano KM, Castaneda LE, Brooks RM, et al. (2010) Evidence for active regulation of pro-osteogenic signaling in advanced aortic valve disease. *Arterioscler Thromb Vasc Biol.* 30:2482–6.
41. Stapleton PA, Goodwill AG, James ME, Brock RW, Frisbee JC. (2010) Hypercholesterolemia and microvascular dysfunction: interventional strategies. *J Inflamm* 7:54.
42. Dasgupta, J, S Subbaram, and K M Connor. (2006) Manganese superoxide dismutase protects from TNF α -induced apoptosis by increasing the steady-state production of H₂O₂. *Antiox Redox Signaling* 8:1295–305.
43. Mele J, Van Remmen H, Vijg J, Richardson A. (2006) Characterization of transgenic mice that overexpress both copper zinc superoxide dismutase and catalase. *Antiox Redox Signaling* 8:628–38.
44. Bai J, Cederbaum AI. (2000) Overexpression of catalase in the mitochondrial or cytosolic compartment increases sensitivity of HepG2 cells to tumor necrosis factor- α -Induced apoptosis. *J Biol Chem* 275:19241–9.
45. Rajamannan NM. (2011) Bicuspid aortic valve disease: the role of oxidative stress in Lrp5 bone formation. *Cardiovasc Pathol* 20:168–76.
46. Rajamannan N. (2013) Role of oxidative stress in calcific aortic valve disease: From bench to bedside - The role of a stem cell niche. In: Morales-Gonzalez JA, ed. *Oxidative Stress and Chronic Degenerative Diseases - A Role for Antioxidants*. Rijeka, Croatia: InTech. pp. 265-87.
47. Heistad DD, Wakisaka Y, Miller J, Chu Y, Pena-Silva R. (2009) Novel aspects of oxidative stress in cardiovascular diseases. *Circ J* 73:201.
48. Sucusky P, Balachandran K, Elhammali A, Jo H, Yoganathan AP. (2009) Altered shear stress stimulates upregulation of endothelial VCAM-1 and

ICAM-1 in a BMP-4–and TGF- β 1–dependent pathway. *Arterioscler Thromb Vasc Biol* 29:254–60.

49. Guerraty MA, Grant GR, Karanian JW, Chiesa OA, Pritchard WF, et al. (2010) Hypercholesterolemia induces side-Specific phenotypic changes and peroxisome proliferator-activated receptor-pathway activation in swine aortic valve endothelium. *Arterioscler Thromb Vasc Biol* 30:225–31.
50. Hess K, Ushmorov A, Fiedler J, Brenner RE, Wirth T. (2009) TNF α promotes osteogenic differentiation of human mesenchymal stem cells by triggering the NF- κ B signaling pathway. *Bone* 45:367–76.
51. Gareus R, Kotsaki E, Xanthoulea S, van der Made I, Gijbels MJJ, et al. (2008) Endothelial cell-specific NF- κ B inhibition protects mice from atherosclerosis. *Cell Metab* 8:372–83.
52. Stephens EH, Saltarrelli JG, Baggett LS, Nandi I, Kuo JJ, et al. (2011) Differential proteoglycan and hyaluronan distribution in calcified aortic valves. *Cardiovasc Pathol* 20:334–42.
53. Hinton RB, Lincoln J, Deutsch GH, Osinska H, Manning PB, et al. (2006) Extracellular matrix remodeling and organization in developing and diseased aortic valves. *Circ Res* 98:1431–8.
54. Acharya A, Hans CP, Koenig SN, Nichols HA, Galindo CL. (2011) Inhibitory role of Notch1 in calcific aortic valve disease. *PLoS ONE* 6:e27743.
55. Fondard O, Detaint D, Lung B, Choqueux C, Adle-Biassette H, et al. (2005) Extracellular matrix remodelling in human aortic valve disease: the role of matrix metalloproteinases and their tissue inhibitors. *Eur Heart J* 26:1333–41.
56. Clark-Greuel JN, Connolly JM, Sorichillo E, Narula NR, Rapoport HS, et al. (2005) Transforming growth factor- β 1 mechanisms in aortic valve calcification: Increased alkaline phosphatase and related events. *Ann Thorac Surg* 83:946–53.
57. Pashkow FJ. (2011) Oxidative stress and inflammation in heart disease: Do antioxidants have a role in treatment and/or prevention? *Int J Inflamm* 2011: 514623.

58. Ruifrok AC, Johnston DA. (2001) Quantification of histochemical staining by color deconvolution. *Anal Quant Cytol Histol* 23:291-9.

CHAPTER 3

INFLAMMATORY CYTOKINES PROMOTE MESENCHYMAL TRANSFORMATION IN EMBRYONIC AND ADULT VALVE ENDOTHELIAL CELLS

This chapter was published in *Arteriosclerosis, Thrombosis, & Vascular Biology*:

Mahler GJ*, Farrar EJ*, Butcher JT (2013) Inflammatory Cytokines Promote
Mesenchymal Transformation in Embryonic and Adult Valve Endothelial Cells.

Arteriosclerosis, Thrombosis, & Vascular Biology 33: 121–130.

*Authors contributed equally to this work.

3.1 Abstract

Inflammatory activation of valve endothelium is an early phase of aortic valve disease pathogenesis, but subsequent mechanisms are poorly understood. Adult valve endothelial cells retain the developmental ability to undergo endothelial to mesenchymal transformation (EndMT), but a biological role has not been established. Here we test whether and how inflammatory cytokines (TNF α and IL-6) regulate EndMT in embryonic and adult valve endothelium.

Using *in vitro* 3D collagen gel culture assays with primary cells, we determined that IL-6 and TNF α induce EndMT and cell invasion in dose dependent manners. Inflammatory-EndMT occurred through an Akt/NF κ B-dependent pathway in both adult and embryonic stages. In embryonic valves, inflammatory-EndMT required canonical TGF β signaling through Alk2/5 to drive EndMT. In adult valve endothelium, however, inflammatory-induced EndMT still occurred when Alk2/5 signaling was blocked. Inflammatory receptor gene expression was significantly upregulated *in vivo* during embryonic valve maturation. Endothelial-derived mesenchymal cells expressing activated NF κ B were found distal to calcific lesions in diseased human aortic valves.

Inflammatory cytokine induced EndMT in valve endothelium is present in both embryonic and adult stages, acting through Akt/NF κ B but differently utilizing TGF β signaling. Molecular signatures of valve EndMT may be important diagnostic and therapeutic targets in early valve disease.

3.2 Introduction

Degenerative heart valve disease (HVD) is a significant contributor to cardiovascular morbidity in the United States. Aortic valve dysfunction affects 2.5% of all Americans and 30% of the elderly [1]. HVD directly claims 20,000 lives annually in the US and sufferers have twice the risk of heart attacks, strokes, and heart failure [1]. In addition, congenital valve abnormalities affect 1%-2% of live births and lead to early structural deterioration [2]. Historically, aortic valve disease (AVD) was thought to be pathogenically similar to vascular atherosclerosis. Both diseases are characterized by loss of endothelial integrity, infiltration of inflammatory cells, accumulation of plasma lipoproteins, release of inflammatory cytokines, mesenchymal proliferation, extracellular matrix remodeling, and the growth of plaque lesions [3]. Unlike atherosclerosis, however, AVD leads to large, obstructive lesions containing significant matrix mineralization [4]. Randomized clinical trials using lipid lowering agents to halt AVD severity or progression have been disappointing [5,6]. These findings underscore the conclusion that mechanisms of aortic valve disease are distinctly different than vascular atherosclerosis. As a consequence, there are currently no established molecular biomarkers specific to AVD progression and no molecular targets for AVD therapy [7].

We previously determined in mice that the degree of inflammation in aortic valves directly correlates with the degree of calcification [8]. Diseased human valve cusps become progressively thickened, with increases in the presence of macrophages and cytokines such as interleukin-6 (IL-6) and tumor necrosis factor-alpha (TNF α) [9-11].

Both IL-6 and TNF α can activate arterial endothelial cells, which is a phenotypic change characterized by upregulation of adhesion molecules such as ICAM-1 and VCAM-1, recruitment of leukocytes, and increased monolayer permeability [10,12,13]. In atherosclerotic plaques, both IL-6 and TNF α drive transcription through nuclear translocation of nuclear factor kappa b (NF κ B), but their role in valve endothelium is unknown [14,15].

Fetal human aortic valve endothelial cells also express ICAM-1 and VCAM-1, which suggests that endothelial activation also occurs during valve development [16]. TNF α , IL-6, and NF κ B expression levels are elevated in the myocardium of children with congenital heart defects affecting valve development [17,18]. NF κ B inhibition during avian heart development leads to valvuloseptal defects and impaired outlet formation [19]. Leptin, a member of the IL-6 superfamily, was shown to induce EndMT in embryonic endocardium, in part through activating TGF β [20]. Akt has also been shown to drive embryonic and adult EndMT [21,22]. Adult ovine aortic valve endothelium has been shown to undergo EndMT *in vitro* and *in vivo* [23-25]. Collectively, these findings motivate the hypothesis that inflammatory signaling toward EndMT may be a developmentally conserved signaling pathway in valve endothelium, but a biological rationale is unclear.

In this study, we determine that both TNF α and IL-6 induce EndMT in embryonic and adult valve endothelium via an Akt/NF κ B dependent pathway. In embryonic valve endocardium, NF κ B acted upstream of TGF β to induce EndMT through Alk2/5. We

found increasing levels of TNF α and IL-6 receptor gene expression in embryonic valve primordia during valve morphogenesis. Interestingly, while TGF β could drive EndMT in adult valve endothelium through Alk2/5, TGF β was not required for NF κ B induced EndMT. Finally, we identify evidence of EndMT in calcified human aortic valves. Taken together, these findings support a developmentally conserved mechanism of valve remodeling via NF κ B induced EndMT that may be a previously unrecognized molecular signature of early AVD.

3.3 Materials and Methods

We employed two well-characterized valve endothelial cell culture systems to test inflammatory signaling on EndMT *in vitro*: Porcine aortic valve endothelial cells (PAVEC) and quail embryonic endocardial explants (QEE) [26-28]. Porcine aortic valve endothelial cells (VEC) are by far the best-characterized and most studied valve endothelial population [1-4]. Non-calcified adult endothelial cells can be obtained from acute traumatic non-cardiac injuries, but are more often acquired from cardiac transplantation surgeries or rejected donor valves. VEC from these sources have a sub-clinical, but likely non-negligible, amount of inflammation and pathology [5-7]. Holliday et al. have shown that human VEC isolated from heart transplant surgeries have elevated α SMA expression, suggesting some pathobiology may be present, including potentially EndMT8. Healthy human VEC have no α -SMA expression *in situ*. Like humans, pigs develop atherosclerotic vascular and valvular lesions without intervention^{9,10}. In addition, pigs fed a high fat and cholesterol diet for up to 6 months develop LDL lipid profiles similar to those in humans and form atherosclerotic lesions, preferentially on the valve fibrosa, with lipid disposition, calcification, cholesterol clefts, signs of continuous inflammation, and prothrombotic tendency [11-15]. No study to date has demonstrated a pure population of cultured valve endothelial cells from small animals such as mice. Collectively, these findings support the use of porcine valve endothelial cells for the adult valve studies.

Porcine aortic valve endothelial cells were isolated using the method shown by Butcher et al. and Gould and Butcher [1,16]. Porcine heart valves were kindly donated

by Shirk Meats of Dundee, NY. Porcine aortic valve endothelial cells (PAVEC) were grown in flasks coated with 50 $\mu\text{g}/\text{mL}$ rat tail collagen I (BD Biosciences, San Jose, CA). Cells were cultured at 37°C and 5% CO_2 in DMEM supplemented with 10% FBS (Invitrogen, Grand Island, NY), 1% penicillin-streptomycin (Invitrogen), and 50 U/mL heparin (Sigma-Aldrich, St. Louis, MO). Culture medium was changed every 48 hours and cells were passaged with 0.05% Trypsin-EDTA (Invitrogen) 1:3 at confluence. Endothelial culture purity was confirmed at the most conservative level via real-time PCR for alpha-smooth muscle actin (not expressed in VEC but expressed in VIC and in cells undergoing EndMT). Cultures with undetectable expression (cycle threshold > 37 cycles) were used in subsequent experiments.

For experiments, 95,000 cells were seeded onto collagen gels at passage 5. After 2 hours 1, 10, or 100 ng/mL of human IL-6 (Sigma-Aldrich) or human TNF α (Sigma-Aldrich) was added to the culture medium for treated cells. For IL-6 inhibitor experiments seeded cells were allowed to attach for 2 hours before the addition of 100 ng/mL IL-6 and 5 μM Akt Inhibitor XI (EMD Chemicals, Gibbstown, New Jersey) or 25 μM STAT3 Inhibitor Peptide (EMD Chemicals). In TNF α inhibitor experiments 100 ng/mL TNF α with 5 μM Akt Inhibitor XI, 25 μM MEK1 inhibitor PD 98059 (EMD Chemicals), or 10 μM SB 431542 ALK5 inhibitor (Sigma-Aldrich) was added to cultures. After 48 hours cell invasion was quantified manually at 60 μm depth into the gel. Immediately after quantifying cell invasion cells were fixed for immunofluorescence in 4% paraformaldehyde or processed for RNA isolation.

Avian endocardial explant culture

The embryonic avian (chick and quail) is a standard animal model for understanding heart and valve development and is ideal for these studies. The avian (quail, chick) embryo does not require a placental circulation and can be cultured outside of the egg for almost all of its gestation [17,18] therefore not requiring death of the mother. Though there are some differences in cardiac anatomy between avians and mammals, the morphogenesis, remodeling, and final anatomy of the clinically important left side of the heart is remarkably similar between chicks and humans [19-22]. Late fetal and postnatal avian aortic and mitral valves exhibit well developed trilaminar matrix striation and fibroblastic cell phenotype similar to humans, whereas matrix stratification is barely detectable in mice [19]. Biological assays with avian and mouse valve progenitors demonstrate identical molecular mechanisms and participants (though specific isoforms may differ) [23,24]. As each assay we perform pools multiple explants per sample, conducting similar experiments with mice would require an impractical number of identically timed pregnant females. The avian is the only embryo model that enables isolation of sufficient numbers of valve explants for 3D *in vitro* experimentation, and therefore suitable for the embryonic experiments. We utilize the chick for its sequenced genome (enabling PCR design), and quail for its QH1 antigen identifying endocardial cells.

Fertile quail eggs were acquired from Lake Cumberland Game Bird Farm (Monticello, KY). Eggs were incubated at 37°C and 60% humidity to stage HH14-. The embryos were placed into sterile Earl's Basic Salt Solution (EBSS, Invitrogen) and staged

according to the criteria of Hamburger and Hamilton [25]. Quail endocardial explant isolation has been previously described [26]. Following endocardial cell isolation, M199 was added to the wells containing 1, 10, or 100 ng/mL of human IL-6 or human TNF α . For inhibitor experiments 100 ng/mL IL-6 was added with 5 μ m Akt Inhibitor XI, 25 μ m STAT3 Inhibitor Peptide, or 10 μ m SB 431542 ALK5 inhibitor or 100 ng/mL TNF α was added with 5 μ m Akt Inhibitor XI, 25 μ m MEKK1 inhibitor PD 98059, or 10 μ m SB 431542 ALK5 inhibitor. Cell invasion was quantified manually at a 60 μ m depth into the gel after 48 hours. The cultures were then fixed in 4% paraformaldehyde for immunofluorescence or processed for RNA isolation.

Three dimensional collagen constructs

Three dimensional collagen gels at a concentration of 1.5 mg/mL collagen were made by combining ice-cold 3X Dulbecco's Modified Eagle's Medium (DMEM, PAVEC; Invitrogen, Carlsbad, CA) or 3X M199 (QEE, Invitrogen), 10% Fetal Bovine Serum (FBS, PAVEC; Invitrogen) or 1% Chick Serum (CS, QEE; Invitrogen), sterile 18 MW water, 0.1 M NaOH, and rat tail collagen I (BD Biosciences, San Jose, CA). A 0.3 mL aliquot of the collagen solution was pipetted into 4 well tissue culture plates (1.9 cm² growth area; Nunc, Rochester, NY) and allowed to gel for at least 1 hour at 37°C and 5% CO₂.

PAVEC were isolated through collagenase digestion as previously described [29], with purity confirmed via non-detection of the mesenchymal ACTA2 gene expression (> 37 cycles via RT-PCR). PAVEC (< passage 5) were cultured as confluent surface

monolayers on the surface of type 1 collagen hydrogels (1.5 mg/ml, 50,000 cells/cm²). Pre-transformed (HH14⁻ staged) quail endocardial explants (QEE) from the atrioventricular (AV) and outflow tract (OFT) valvulogenic regions were cultured as monolayer patches (without myocardium) on 1.5 mg/ml collagen gels as previously described [27].

Collagen gel immunofluorescence

Fixed samples on collagen gels were washed for 15 minutes on a rocker 3 times with PBS, permeabilized with 0.2% Triton-X 100 (VWR International, West Chester, PA) for 10 minutes, and washed another 3 times with PBS. Samples were incubated overnight at 4°C in a 1% BSA (Rockland Immunochemicals, Inc., Gilbertsville, PA) blocking solution followed by another 4°C overnight incubation with mouse anti-porcine PECAM 1:100 (AbD Serotech, Raleigh, NC) or mouse anti-quail QH1 (DSHB, Iowa City, Iowa) and rabbit anti-human α -SMA 1:100 (Spring Bioscience, Pleasanton, CA). For NF- κ B staining, samples were incubated with rabbit anti-human NF- κ B p105 / p50 1:100 (Abcam, Cambridge, MA). After 3 washes for 15 minutes with PBS, samples were exposed to Alexa Fluor[®] 488 or 568 conjugated (Invitrogen), species specific secondary antibodies at 1:100 in 1% BSA for 2 hours at room temperature. Three more washes with PBS for 15 minutes were followed by incubation with DRAQ5 far red nuclear stain (Enzo Life Sciences AG, Lausen, Switzerland) at 1:1000. Samples were washed once more with 18MW water and stored in 18mW water at 4°C. Images were taken with a Leica TCS SP2 laser scanning spectral confocal microscope (Exton, PA). NF κ B nuclear co-localization was

measured with Metamorph 7.1 software (Molecular Devices). Green (NF κ B) and far red (nuclei) channels were each thresholded. Regions were created around each nuclei. The regions were transferred onto the green channel and the thresholded stained area was quantified within the regions.

Human valve section immunofluorescence

Human aortic valves were obtained from adults undergoing planned, non-elective valve replacement surgery by Dr. Sanjay Samy at Robert Packer Hospital in Sayer, PA. Healthy, non-diseased aortic valves were obtained from patients who died from non-valve related illnesses, who had no visible valve pathology, and whose hearts were ineligible for organ donation due to non-valve related defects, provided by Dr. Jonathan Chen, Cornell-Weill Medical School and NY Presbyterian Hospital. Institutional Review Boards at Cornell University, NY Presbyterian Hospital and Robert Packer Hospital approved all procedures. All samples were procured with informed consent from patients. Fixed human valves were paraffin embedded and sectioned at 6 μ m. Sections were placed on slides, de-waxed, hydrated, and antigens were retrieved by placing the slides in 10 mM TRIS base buffer at pH 10.0 at 90°C for 40 minutes. Following antigen retrieval sections were washed with PBS, permeabilized with 0.1% Tween-20, washed again with PBS, and blocked for 1 hour with 5% BSA in PBS. Primary antibodies were added at a concentration of 1:100 and incubated overnight at 4°C. The following primary antibodies were used: human anti-mouse P2B1 (DSHB), rabbit anti-human α -SMA (Spring Bioscience), rabbit anti-human NF κ B p105 / p50 (Abcam), and anti-human Cy5.5-labelled CD45 (generously

provided by Dr. Michael King, Department of Biomedical Engineering, Cornell University, Ithaca, NY). Sections were incubated with species-specific secondary antibodies at 1:100 for 1 hour, washed with PBS, incubated with 1:1000 DRAQ5 (Enzo Life Sciences AG) or 2:10,000 Hoechst 33342 (Invitrogen) for 30 minutes (Enzo Life Sciences AG), washed again with PBS, and mounted with Prolong Gold antifade reagent (Invitrogen).

Western blots

P4 PAVEC and PAEC were grown to 70% confluency in a 6-well plate, treated with CTL media, 100ng/mL TNF α , or 100ng/mL TGF- β 1 for 48 hours at 37C. Cells were then lysed directly on the plate using RIPA buffer supplemented with 25mM NaF, 1mM NaVO $_4$, and 0.5% Protease inhibitor cocktail (Sigma), incubated for 15 min at RT, scraped and homogenized by pipetting up and down, and centrifuged at 15,000 rpm for 10 min. 10ug of protein was loaded into a 10% gel with Laemmli buffer at 1:1 ratio and run for 1 hour at 120V in 25mM Tris, 0.2M Glycine, 1% SDS running buffer. Western blot transfer to nitrocellulose membrane (Thermo Scientific) was performed at 400mA for 1 hour in 25mM Tris, 20% methanol transfer buffer. After rinsing in PBS 0.1% Tween-20, membrane was blocked for 1 hr in Odyssey Blocking Buffer at RT. Mouse anti-pig CD31 (Springer Bioscience) (1:1000), mouse anti-human VE-cadherin (abcam) (1:500), rabbit anti-human alpha-smooth muscle actin (abcam) (1:1000), rabbit anti-human Smad2 and pSmad2 (Cell Signaling) (1:2000), rabbit anti-Snai1 (SCBT) (1:200), mouse anti-human GAPDH (Ambion) (1:2000) were used in Odyssey blocking buffer+0.1%Tween-20 to detect protein expression.

The membrane was washed 4x in PBS-tween, 1x in PBS, and incubated overnight at 4°C with gentle agitation. The same washes were then performed and the membrane was incubated in Odyssey blocking buffer +0.1% Tween-20 +0.2% SDS with 1:20,000 anti-mouse and anti-goat secondary antibodies (Li-Cor IRDye). Blots were imaged using the Odyssey Infrared system (Li-Cor).

Quantitative real-time polymerase chain reaction

Total RNA was extracted using a Norgen total RNA purification kit (Norgen Biotek Corp., Thorold, ON) and RNA was reverse transcribed to cDNA using the SuperScript III RT-PCR kit with oligo(dT) primer (Invitrogen). RT-PCR was performed on all samples using SYBR Green PCR master mix (Applied Biosystems, Foster City, CA) and a MiniOpticon Real-Time PCR Detection System (Biorad, Hercules, CA). Primer sequences are listed in Table 3.1.

Table 3.1 Primer sequences for q-rtPCR on pig or chick mRNA

Primer	Forward sequence	Reverse sequence
Pig 18S	aatgggggttcaacgggttac	tagagggacaagtggcgttc
Pig ACTA2	cagccaggatgtgtgaagaa	tcacccctgatgtctagga
Pig PECAM1	atctgcatctcgtgggaagt	gagctgaagtgtcagcagga
Pig Snail	gcccaactacagcgagctac	ccaggagagagtcccagatg
Pig TGF-B1	ccactctcagcctctctgct	tgggttctcggtatcctacg
Pig VCAM1	ttgttctctgctcacacagc	caatctgcgcaatcatttg
Pig ICAM1	aaaggaggctccatgaaggt	tgccatcgttttccacatta
Pig AKT1	ggcaggaggaagagatgatg	cccagcagcttcaggctactc
Pig MEK1	gagagccgatttgaagcaac	actctgccacttcccaaagt
Pig NFKB1	aggatgggatctgcactgtc	atcagggtgcaccaaagtgc
Chick 18S	cggagagggagcctgagaa	cgccagctcgatcccaaga
Chick ACTA2	cagtttcccttccatcgtg	tggggatttcaaggctcagg
Chick PECAM1	tcactccagtggcatgaaaa	gccaaagatccttctccaca
Chick Slug	cctcctccaaagatcacagc	ccaaccagagaaagtggaa
Chick TGFB3	ggcttgtaaacacgctgaa	tgcaggatttaccaccata
Chick VCAM1	attcctcatgccatttac	ctgaactcgatgggaaaacc
Chick ICAM1	tggccagaaacatatccaca	gcagttccaagattggcttc
Chick AKT1	gatggcacattcattggcta	ggtccactggaggcatctaa
Chick MEK1	aaaccagatcatccgtgagc	tccagccttttcagcactt
Chick NFKB1	atcccaaatgtttgcaatg	tcgaaaaccctctgttttg
Chick IL6RA	ctatggatgaagcgcaggtt	gacaccacgagggtttg
Chick TNFRSF1A	cagtgatgcagttgcaggt	aggtcccattcagctcaga

Apoptosis Assay

Fixed samples on collagen gels were examined for apoptosis using the APO-BrdU TUNEL assay (Invitrogen) according to the instructions provided by the manufacturer.

Briefly, the samples were washed 3 times in the wash buffer and then incubated in DNA labeling solution for 2 hours at 37°C. Samples were washed for 5 minutes on a rocker with rinse buffer, then incubated in Anti-BrdU mouse monoclonal antibody PRB-1, Alexa Fluor 488 conjugate 1:50 (Invitrogen) and Draq5 1:1000 (Enzo Life Sciences AG) for 1 hour at room temperature. 200uL of propidium iodide stain was added to each sample and then incubated for 30 minutes at room temperature. Samples were stored in PBS at 4°C and imaged less than 24 hours later. Images were taken with a Zeiss 710 laser scanning spectral confocal microscope. Custom Matlab code was used to threshold the red (propidium iodide), green (BrdU labeling) and far red (nuclei) channels according to the automated global thresholding level given in analysis of the far red channel. Cell boundaries, nuclei, and BrdU labeling were confirmed visually for each sample. Numbers of apoptotic cells per sample were counted via Matlab using BrdU labeling within a cell boundary as the criteria for identifying an apoptotic cell.

EndMT was quantified via real-time PCR, immunohistochemistry, and Western blotting; while cell invasion was quantified at 60 µm depth with brightfield microscopy (Figure 3.1). NFκB protein nuclear co-localization was quantified for 100 cells for each treatment using Metamorph 7.1 software (Molecular Devices, Sunnyvale, CA). For NFκB transfection, PAVEC cells were trypsinized and electroporated with plasmid encoding the RelA subunit of NFκB (Addgene plasmid 23255) using Neon transfection system (Invitrogen, Carlsbad, CA) and further cultured in 5% serum, antibiotic-free DMEM for 24 hours [30]. The cells were then

trypsinized, re-suspended in normal media (DMEM with 10% fetal bovine serum and 1% penicillin-streptomycin), and seeded onto gels. Invasion assay was performed as described above.

Statistical Analysis

Results are expressed as mean \pm S.E>M., $n \geq 3$ independent cultures per treatment condition, with 5-6 explants pooled for each QEE sample. Data was analyzed with GraphPad Prism version 4 for Windows (GraphPad Software, San Diego, CA). Treatment effects were compared using Analysis of Variance (ANOVA) with Tukey's post hoc paired tests, and data was transformed when necessary to obtain equal sample variances. Differences between means were considered significant at $p \leq 0.05$.

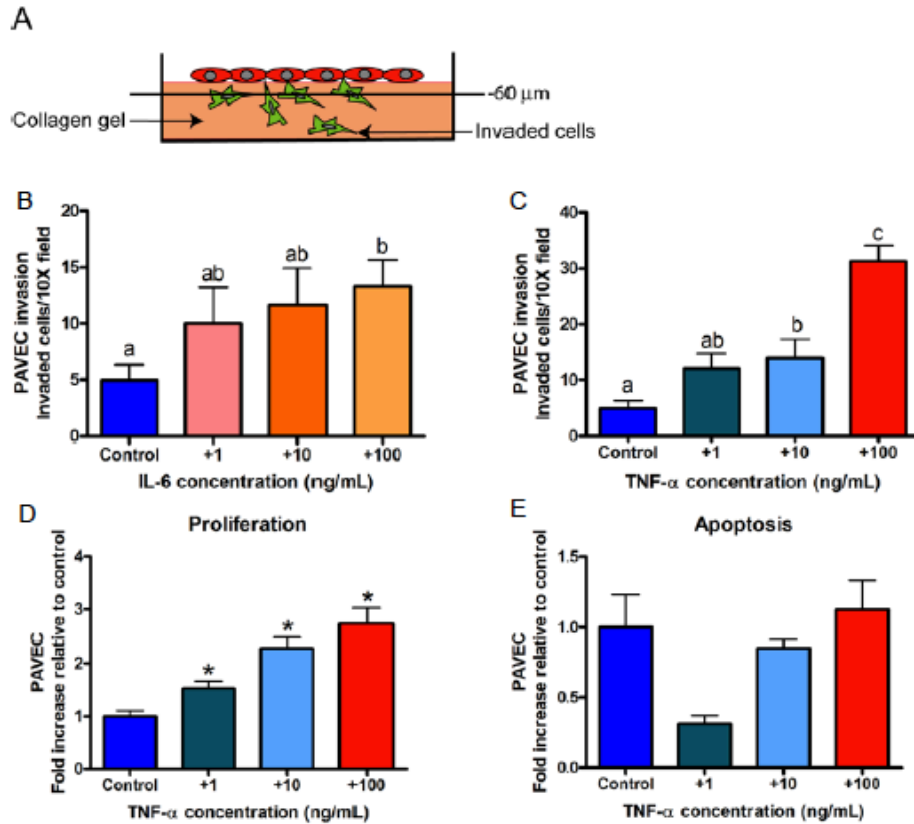


Figure 3.1 TNF α drives EndMT in postnatal VEC.

(A) Cell invasion assay. Embryonic valve endocardial or adult valve endothelial cells are plated onto a 3D collagen gel. After 48 hours, invaded, mesenchymally transformed cells are quantified using a 10X objective and an inverted microscope. First the microscope is focused on the endocardial or endothelial layer on the surface of the gel. Next the microscope is focused 60 μm down into the gel, and the number of in-focus invaded cells is quantified. This process is repeated for all endocardial explants present on the gel, or for four fields in the center of the gel for endothelial monolayers. (B-E) Inflammatory cytokine dose response, proliferation and apoptosis in porcine aortic valve endothelial cells (PAVEC). (B) 100 ng/mL IL-6 treatment for 48 hours significantly increases cell invasion when compared with controls.

(C) A 48 hour 100 ng/mL TNF α treatment significantly increases cell invasion when compared with control, +1 ng/mL, and +10 ng/mL treatments. PAVEC showed a significant increase in proliferation (D), but not apoptosis (E), in response to increasing doses of TNF α for 48 hours. Error bars show \pm SEM, $n \geq 3$ independent monolayers. Bars that do not share any letters are significantly different according to a one-way ANOVA with Tukey's post-test ($p \leq 0.05$).

3.4 Results

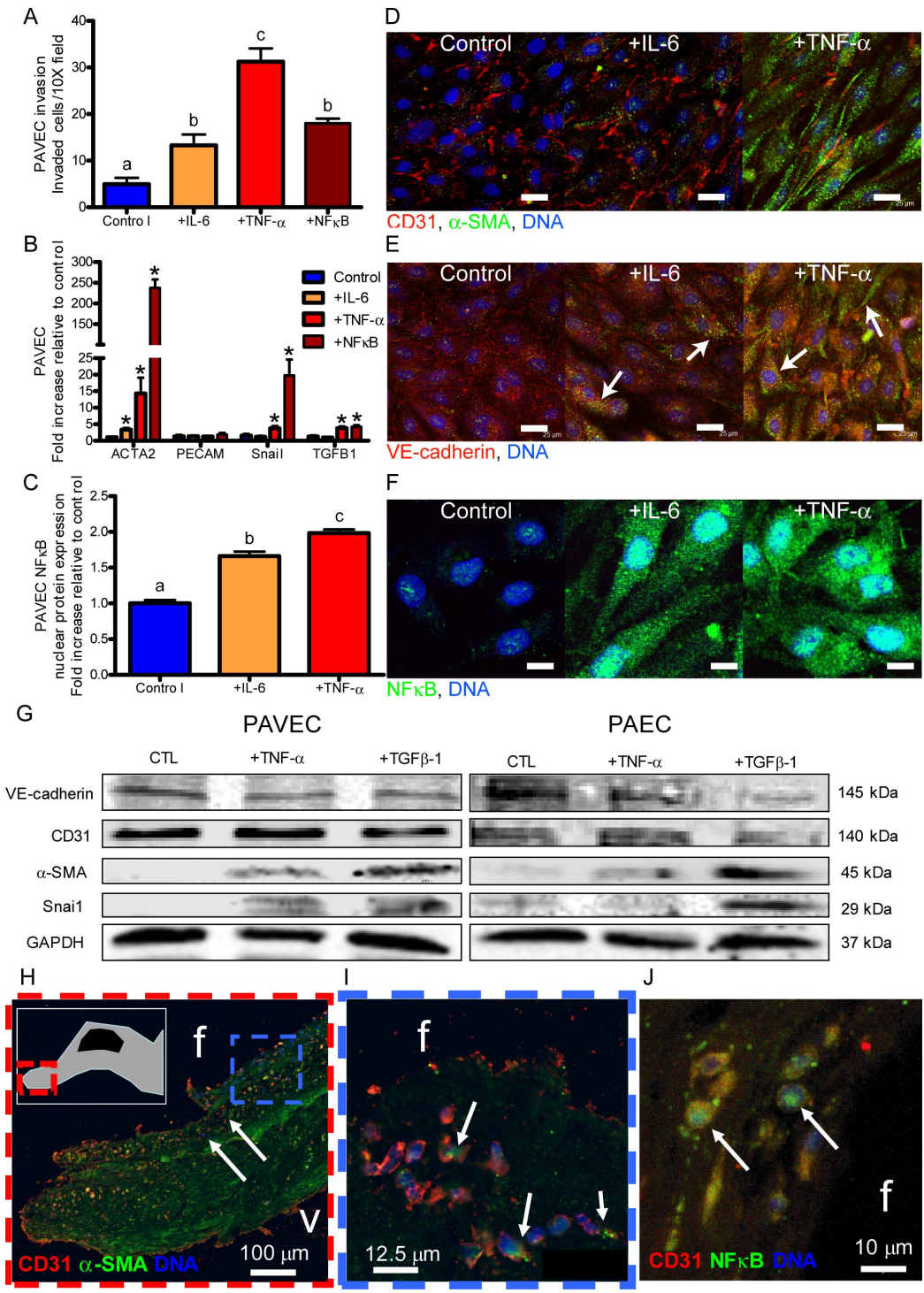
TNF α and IL-6 induce EndMT in adult valve endothelial cells

We first exposed 3D cultured adult PAVEC monolayers to doses of TNF α or IL-6 and quantified changes in EndMT related gene expression, protein expression, and collagen matrix invasion. Both IL-6 and TNF α in 3D culture induced loss of endothelial cell-cell contacts including PECAM-1 and VE-cadherin, acquisition of mesenchymal α -smooth muscle actin (α SMA) and invasion into collagen matrix in a dose-dependent manner (Figure 3.2A,D,E,G; Figures 3.1, 3.3). Genetic overexpression of NF κ B alone was sufficient to cause 3D matrix invasion in PAVEC, supporting an NF κ B-dependent EndMT mechanism (Figure 3.2A). Pro-EndMT related gene expression (ACTA2, Snail, TGF- β 1) was significantly upregulated in response to NF κ B overexpression (238 \pm 20.6, 15.0 \pm 1.1, and 4.2 \pm 0.5 fold respectively), TNF α (14.3 \pm 4.8, 3.8 \pm 0.7, and 3.8 \pm 0.6 fold respectively, p <0.05), but not IL-6 (Figure 3.2B). EndMT-related protein expression (α SMA, Snail increase and VE-cadherin decrease) was shown in PAVEC, but not porcine aortic endothelial cells (PAEC) in response to TNF α (Figure 3.2G). TGF- β 1, however, induced EndMT protein expression in both PAVEC and PAEC (Figure 3.2G). Nuclear translocation of NF κ B was significantly upregulated in response to either IL-6 or TNF α (1.7 \pm 0.1 and 2.0 \pm 0.1 fold increase, p <0.05, Figure 3.1C,F; Figure 3.4). To control for cell number, we quantified PAVEC proliferation (via BrdU incorporation) and apoptosis (via TUNEL) in response to doses of TNF α . PAVEC proliferation increased with TNF α dose (up to 2.7 \pm 0.1 at 100 ng/mL, p <0.05, Figure 3.1D), while apoptosis remained unchanged (Figure 3.1E). Collectively, these results suggest that IL-6 and TNF α induce EndMT and matrix

invasion in adult PAVEC *in vitro* at least in part through NF κ B, with TNF α being a more potent EndMT inducer.

Figure 3.2 Exposure to inflammatory cytokines induces EndMT in PAVEC.

A.) Porcine aortic valve endothelial cell (PAVEC) mesenchymal transformation and invasion of the collagen matrix after 48 hour exposure to 100 ng/mL IL-6, 100 ng/mL TNF α , or genetic overexpression of NF κ B. B.) PAVEC EndMT-related gene expression after 48 hour exposure to 100 ng/mL IL-6 or TNF α , or genetic overexpression of NF κ B C.) PAVEC NF κ B nuclear localization quantification. D.) Confocal images of control, +100 ng/mL IL-6, and +100 ng/mL TNF α PAVEC at a 48 hour time point stained for CD31 (red), α SMA (green), and DNA (blue). E.) Confocal images of control, +100 ng/mL IL-6, and +100 ng/mL TNF α PAVEC at a 48 hour time point stained for VE-cadherin (red), α SMA (green), and DNA (blue). F.) Confocal images of control, +100 ng/mL IL-6, and +100 ng/mL TNF α PAVEC at a 48 hour time point stained for NF κ B (green) and DNA (blue). G.) Western blots for PAVEC and porcine aortic valve endothelial cells (PAEC) exposed to 100 ng/mL TNF α or TGF- β 1 for 48 hours. H.) Diseased human aortic valve endothelial cells co-expressing α SMA and CD31 (on the fibrosa or outflow side and invaded, calcified nodule shown in inset, I.) Expanded frame of Figure 1H. J.) Nuclear translocation of NF κ B in diseased human valve endothelial cells. Error bars show \pm SEM, $n \geq 3$ culture wells. Bars that do not share any letters are significantly different according to a one-way ANOVA with Tukey's post-test ($p \leq 0.05$). For EndMT gene expression (Figure 1B), differences that are significantly different than the control according to an unpaired Student's t-test are indicated with a *. Differences were considered significant at $p \leq 0.05$



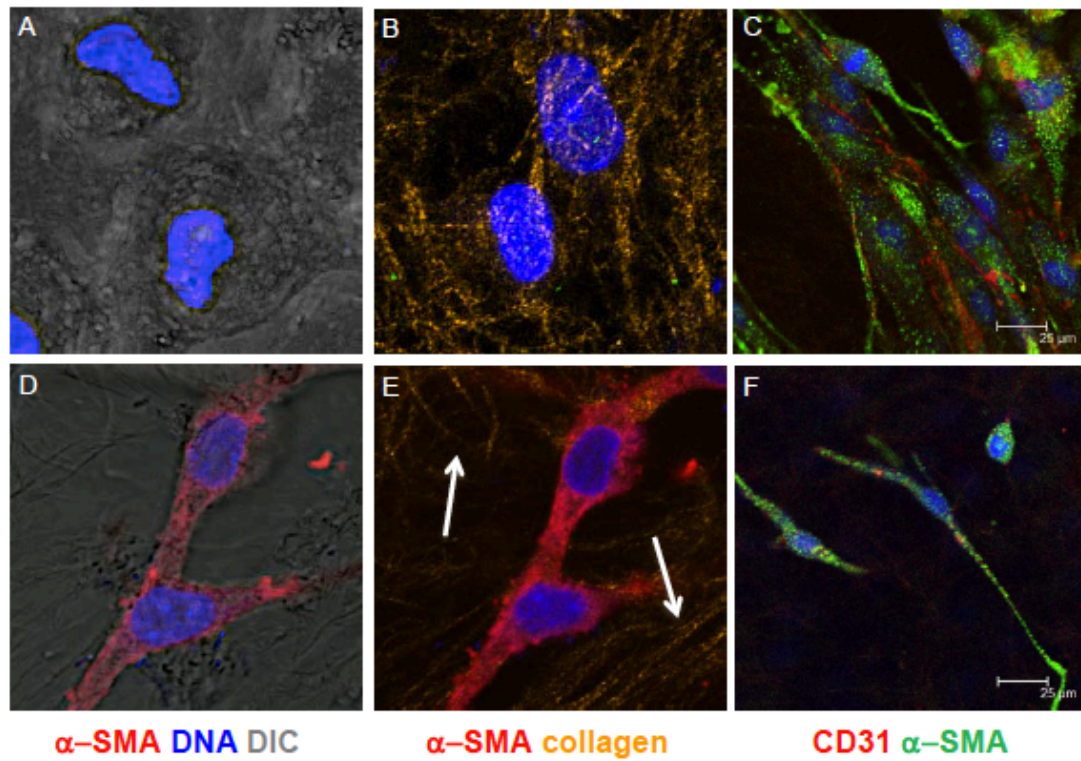


Figure 3.3 Exposure to inflammatory cytokines induces EndMT.

Confocal images of control porcine aortic valve endothelial cells (PAVEC) 48 hours after plating at the surface of the 3D collagen gel (A, B). PAVEC 48 hours following exposure to 100 ng/mL TNF α (D, E). PAVEC 48 hours following exposure to 100 ng/mL TNF α at the surface of the gel (C) and -60 μ m into the gel (F), cells co-express CD31 and α SMA. Arrows show collagen fiber arrangement, invaded cells exposed to TNF α remodel collagen fibers.

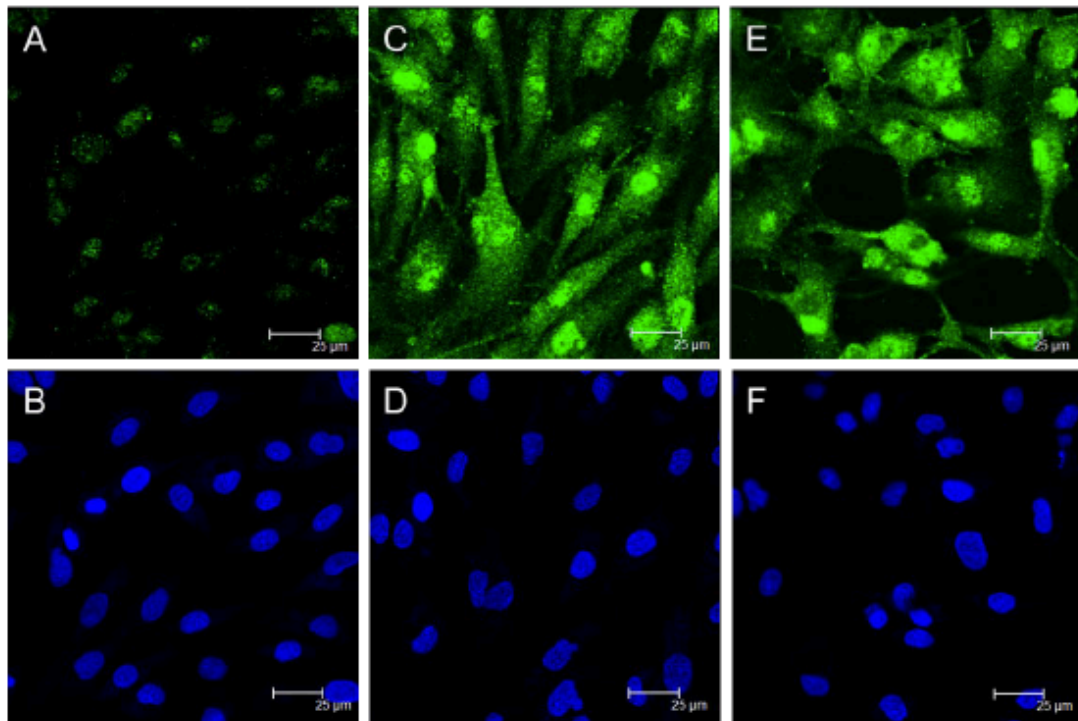


Figure 3.4 NFκB activation in PAVEC exposed to inflammatory cytokines.

Separate green and blue channels for confocal images of control (A, B), +100 ng/mL IL-6 (C, D), and +100 ng/mL TNFα (E, F) PAVEC at a 48 hour time point stained for NFκB (green) and DNA (blue).

EndMT is present in calcified human aortic valves

In explanted human aortic valves with calcific lesions (Figure 3.2G-I) we identified a population of sub-endothelial cells co-expressing αSMA and PECAM1, but not CD45 (Figure 3.5). This suggests the cells were EndMT-derived, but not from an immune origin³¹. The number of invaded fibrosal endothelial cells was 11.13 ± 1.88 cells/40X field (SEM, n = 3 calcified adult valves). Endothelial cells located near the calcified nodule and on the fibrosa side showed decreased VE-cadherin expression (Figure 3.5D). EndMT and potential EndMT-derived cells were only found in the fibrosa layer, distal to sites of calcified lesions. Furthermore, we found that many of these

transformed and invaded cells also co-expressed nuclear NF κ B (Figure 3.2H). Healthy pediatric human valves did not co-express α SMA and VE-cadherin or nuclear NF κ B (Figure 3.6 and 3.7). These findings support that NF κ B-mediated EndMT occurs in human calcific aortic valve disease, but is likely not involved in the mineralization process.

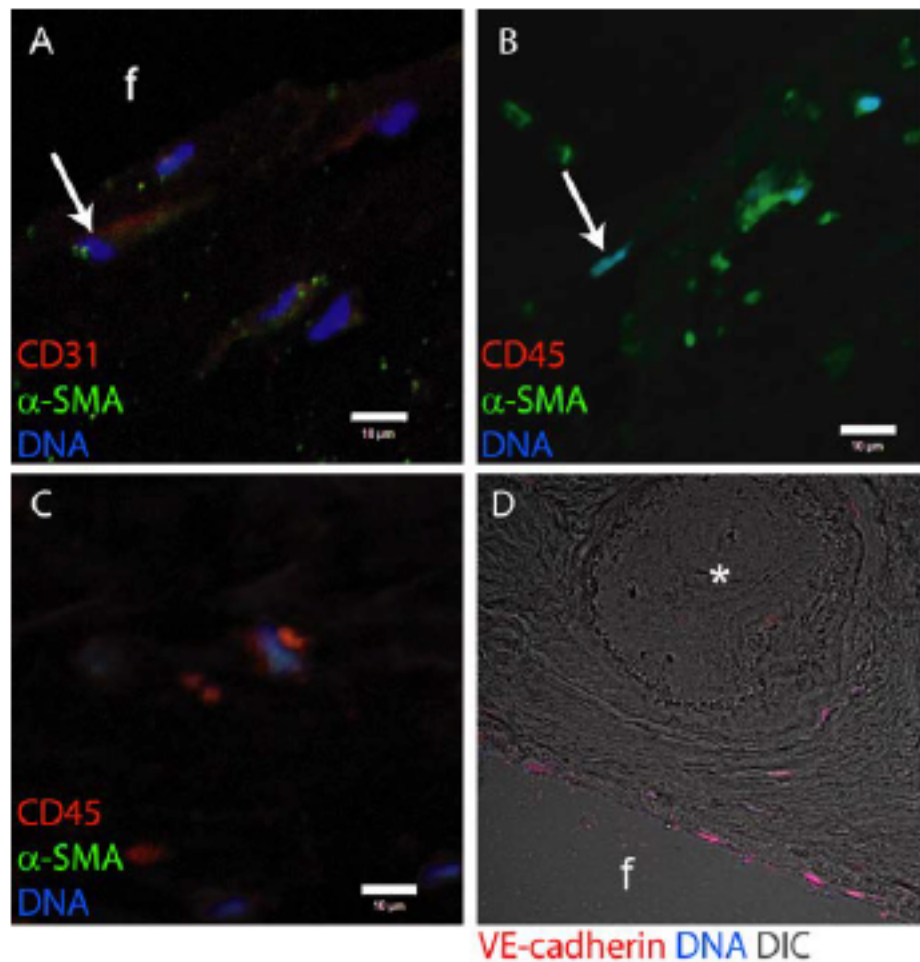


Figure 3.8 Diseased human aortic valve immunohistochemistry.

A, B) Human aortic valve endothelial cells co-expressing CD31 and α SMA do not also express CD45, an immune cell marker. Arrows show the same cell in consecutive sections co-expressing CD31 and α SMA, but not expressing CD45. C) CD45-positive immune cells are present in the diseased human valve. D) The endothelium near the nodule (*) is degraded, and VE-cadherin expression is decreased. Scale bar = 10 μ m.

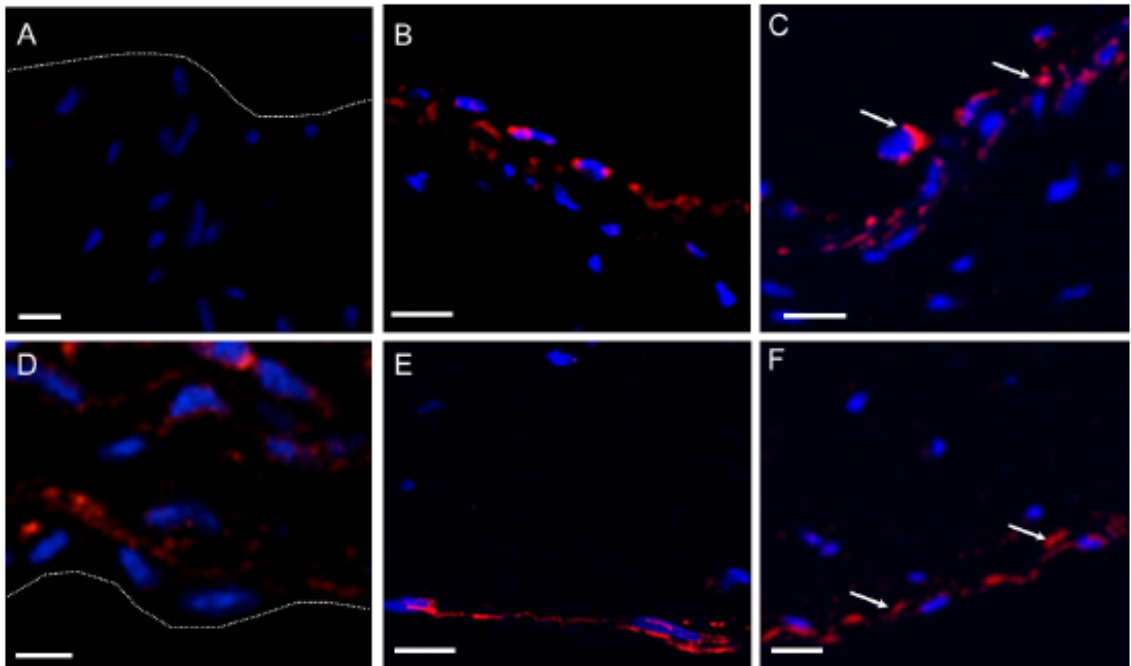


Figure 3.6 Healthy human pediatric valve immunohistochemistry.

Healthy human aortic valve endothelial cells do not co-express VE-cadherin and α SMA and do not express nuclear NF κ B. A-C) fibrosa, D-F) ventricularis. A,D) α SMA. B,E) VE-cadherin. C,F) NF κ B, arrows show lack of nuclear staining in fibrosa and ventricularis endothelial cells. Scale bar = 10 μ m.

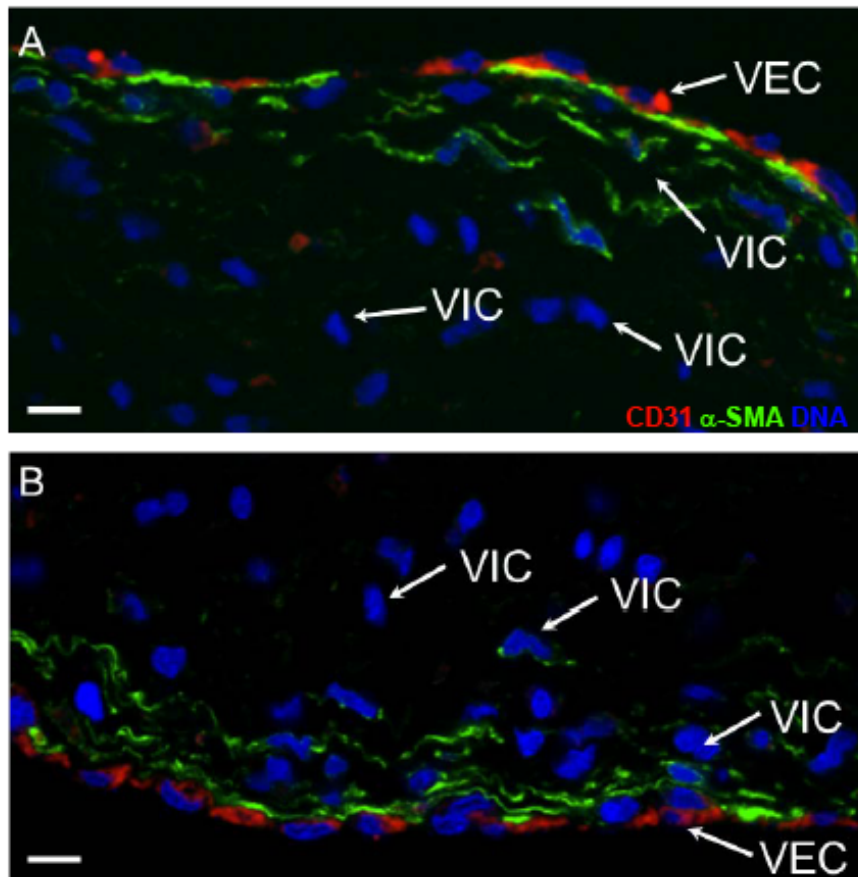


Figure 3.7 Healthy human pediatric valve.

A) fibrosa, B) ventricularis. Green: α SMA, red: CD31, blue: DNA. Scale bar = 10 μ m.

TNF α and IL-6 induce EndMT in embryonic valve endocardium.

Similarly, we quantified the EndMT response characteristics of 3D cultured HH14 pre-transformed QEE monolayers from OFT or AV regions to doses of TNF α and IL-6. As in adult valve endothelium, both IL-6 and TNF α induced loss of QH1, acquisition of α SMA, and collagen matrix invasion (Figure 3.8A, D). Embryonic endocardial EndMT-related genes (ACTA2, Slug, and TGF β 3) were significantly upregulated in valvulogenic endocardium by both IL-6 and TNF α (Figure 3.8B). PECAM1 gene expression was significantly increased in response to inflammatory cytokine (Figure 3.8A). PECAM1 has been shown to be an early marker of cardiovascular development, and the increase in CD31 in culture is likely related to embryonic endocardial differentiation [32]. Downstream NF κ B protein nuclear translocation also occurred in response to either IL-6 or TNF α (Figure 3.8C, E; Figure 3.9). There was no difference in explant area (a control for cell number) with IL-6 or TNF α stimulation in comparison to control (Figure 3.10 C,D). Collectively, these results suggest that both TNF α and IL-6 induce EndMT in embryonic valve endocardial cells *in vitro* with similar potency. We further quantified the expression of inflammatory signaling related genes in the AV and OFT valve forming regions of embryonic hearts across the period of valve morphogenesis (Day 2-Day 10). We determined that ICAM1, NF κ B1, IL6RA (coding for IL-6R α), and TNFRSF1A (coding for TNFR1) gene expression were significantly upregulated in both valve regions as EndMT and valve remodeling progressed (Figure 3.11). These results suggest that inflammatory signaling is active in valves during morphogenesis *in vivo* and directly cause EndMT in valve endocardium *in vitro*.

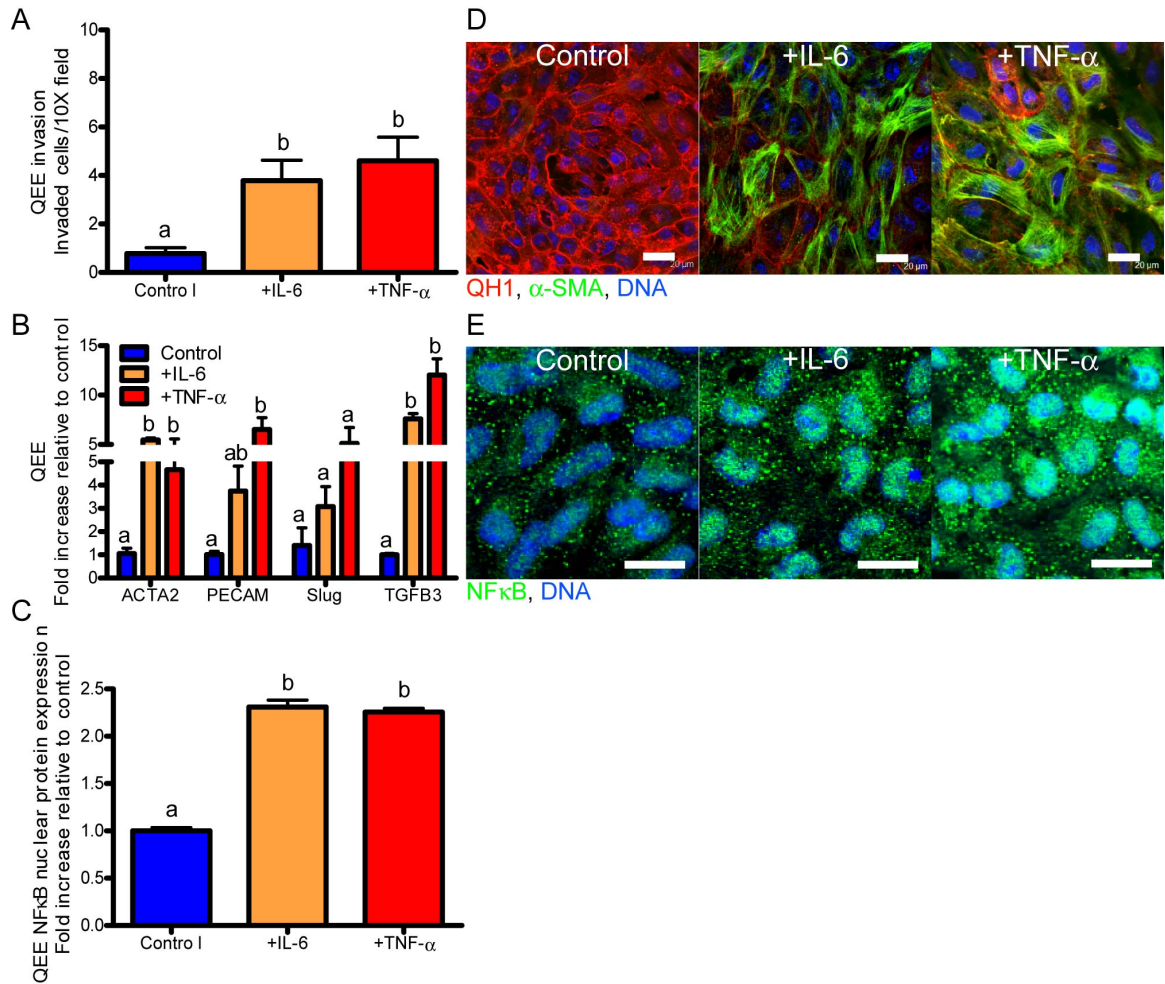


Figure 3.8 Exposure to inflammatory cytokines induces EndMT in embryonic VEC.

A.) Quail endocardial explant (QEE) mesenchymal transformation and invasion of the collagen matrix after 48 hour exposure to 100 ng/mL IL-6 or TNF α . B.) QEE EndMT-related gene expression after 48 hour exposure to 100 ng/mL IL-6 or TNF α . C.) QEE NF κ B nuclear localization quantification. D.) Confocal images of control, +100 ng/mL IL-6, and +100 ng/mL TNF α QEE at a 48 hour time point stained for QH1 (red), α SMA (green), and DNA (blue). E.) Confocal images of control, +100 ng/mL IL-6, and +100 ng/mL TNF α QEE at a 48 hour time point stained for NF κ B (green) and DNA (blue). Error bars show \pm SEM, $n \geq 3$ culture wells with pooled explants. Bars that do not share any letters are significantly different according to a one-way ANOVA with Tukey's post-test ($p \leq 0.05$).

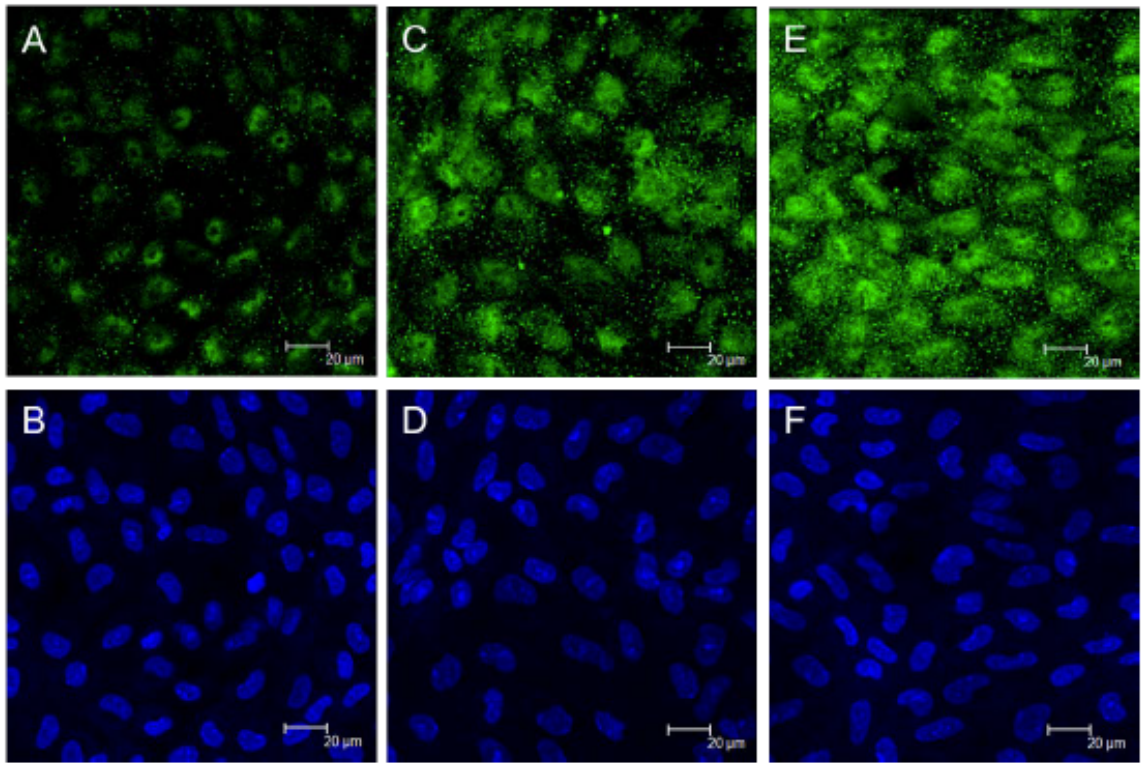


Figure 3.9 NFκB expression in QEE+ TNFα, 48 hours.

Separate green and blue channels for confocal images of control (A, B), +100 ng/mL IL-6 (C, D), and +100 ng/mL TNFα (E, F) QEE at a 48 hour time point stained for NFκB (green) and DNA (blue).

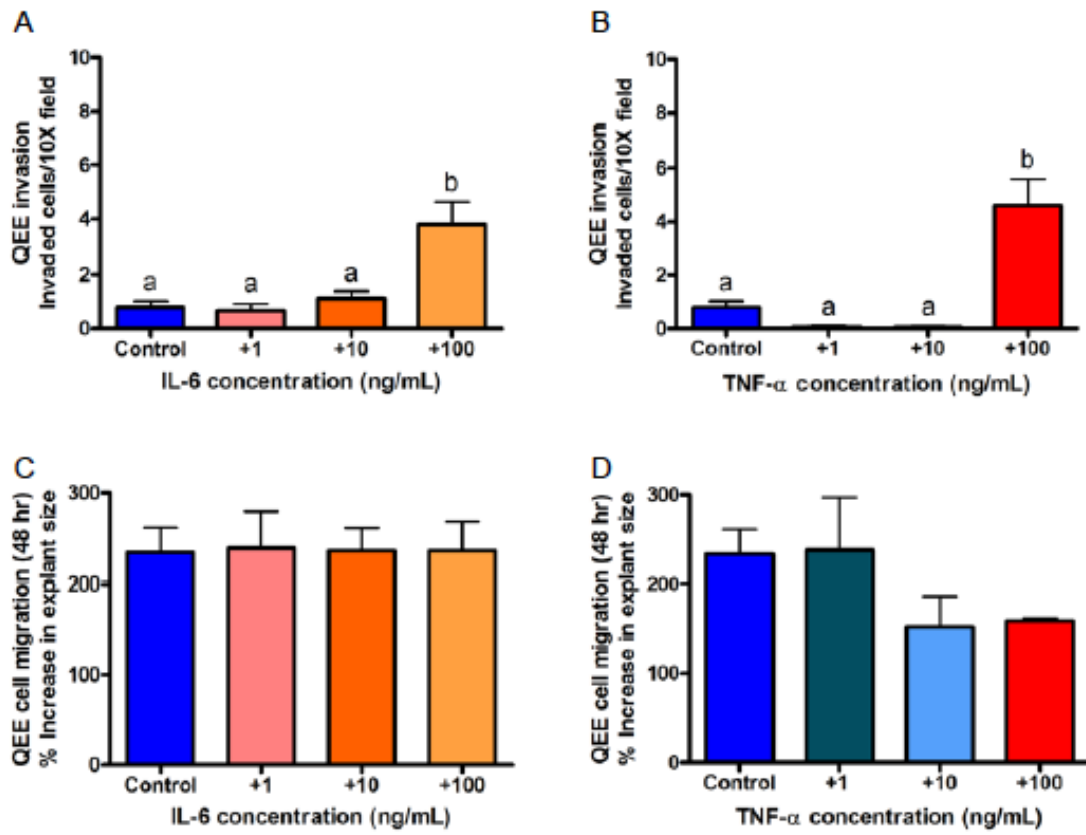


Figure 3.10 Inflammatory cytokine dose response migration and proliferation in QEE.

A, B) A 48 hour exposure to 100 ng/mL IL-6 or TNF α significantly increases cell invasion when compared with control, +1 ng/mL, and +10 ng/mL treatments. C, D) QEE size increased by ~250% after 48 hours, cytokine exposure had no significant effect of QEE proliferation.

Error bars show \pm SEM, $n \geq 3$ batches of pooled explants (QEE). Bars that do not share any letters are significantly different according to a one-way ANOVA with Tukey's post-test ($p \leq 0.05$).

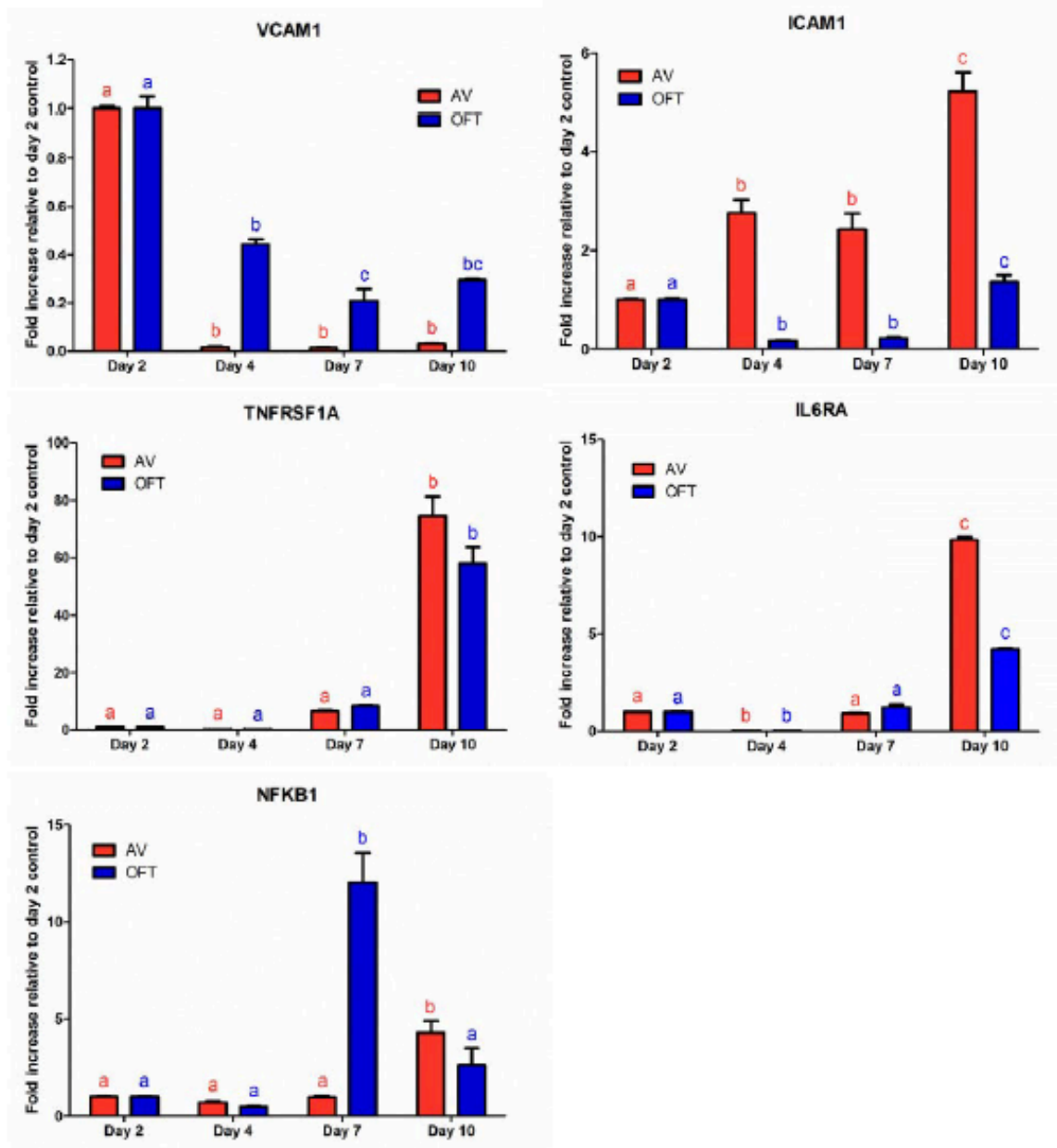


Figure 3.11 Inflammatory gene expression in embryonic valve forming regions.

VCAM1, ICAM1, TNFRSF1A (the gene that codes for TNFR1), IL6RA (the gene that codes for IL-6R α), and NFKB1 in chick day 4, day 7, and day 10 atrioventricular (AV) cushions or valves and outflow tracts (OFT) normalized to day 2 chick AV or OFT. Error bars show \pm SEM, $n \geq 3$. Bars that do not share any letters are significantly different according to a one-way ANOVA with Tukey's post-test ($p \leq 0.05$).

Inflammatory EndMT acts through an Akt/NFκB pathway present in both adult and embryonic valve endothelium.

We next sought to identify the signaling pathway by which inflammatory cytokines induced EndMT through NFκB. Previous studies have shown that TNFα activates NFκB-mediated transcription through Akt and/or MEK1 [33-37]. IL-6 activates STAT3 most potently, but there is also evidence of IL-6-induced NFκB activation through PI3K and Akt [38-41]. Utilizing our 3D culture system, molecular inhibition of either Akt (via 5 μm Akt inhibitor XI) or MEK1 (via 25 μm PD98059) significantly reduced TNFα-induced NFκB expression and nuclear translocation in PAVEC, but only Akt inhibition resulted in complete knockdown (Figures 3.12C,D). Akt inhibition also completely blocked IL-6-induced NFκB gene expression and protein nuclear translocation, while STAT3 inhibition (via 5 μm PpYLKTK STAT3 inhibitor) had no effect (Figure 3.13C,D). Inhibition of Akt completely blocked TNFα induced inflammatory receptor activation (VCAM1, ICAM1), EndMT associated gene expression (ACTA2, Snail, TGF-β1), and subsequent matrix invasion by PAVEC (Figure 3.12A-C). MEK1 blockade also inhibited TNFα-induced inflammatory receptor activation, EndMT gene expression, and subsequent invasion, but to a lesser degree than Akt inhibition. In a similar fashion, Akt inhibition completely blocked IL-6-induced upregulation of inflammatory receptors, EndMT gene expression, and subsequent matrix invasion (Figure 3.13 A-C). STAT3 inhibition, on the other hand, had no effect on any of these responses from IL-6.

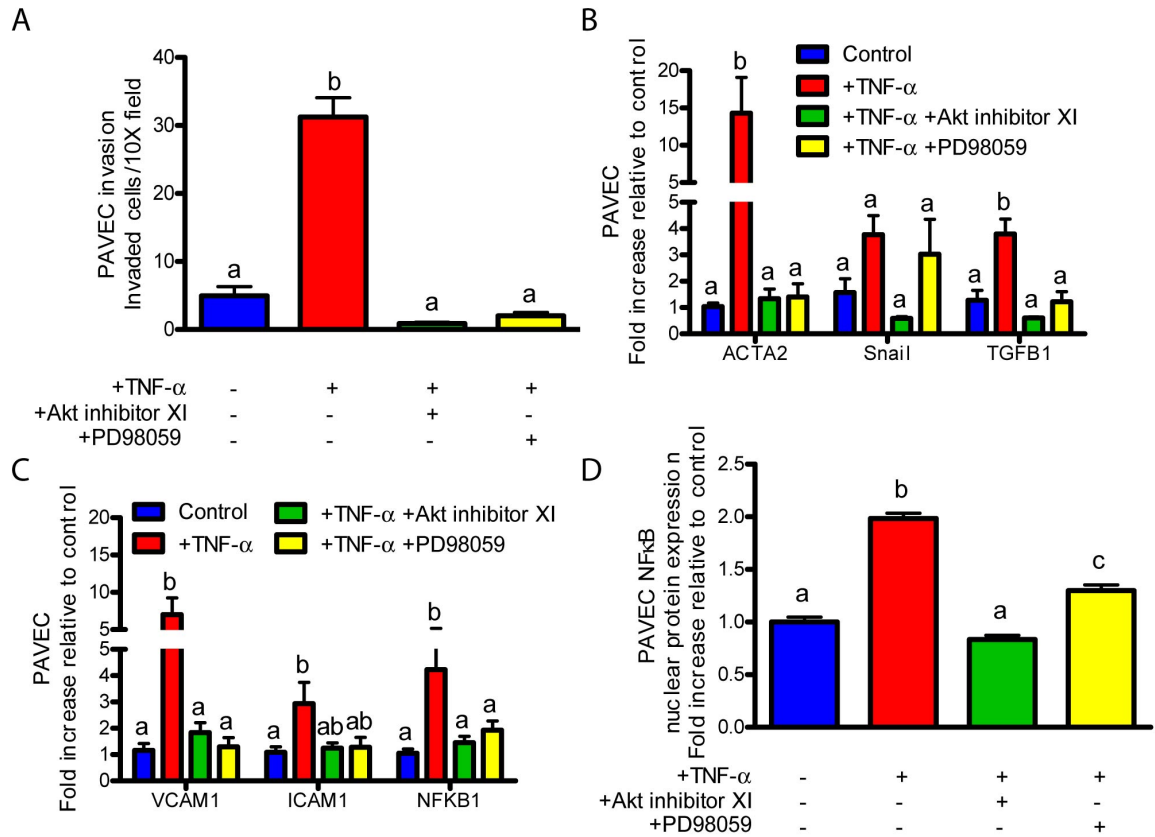


Figure 3.12 TNF α induces EndMT through Akt/MAPK/NF κ B in PAVEC.

A.) Cell invasion after a 48 hour to exposure to 100 ng/mL TNF α or 100 ng/mL TNF α with 5 μ m Akt inhibitor XI or 25 μ m PD98059 MEK1 inhibitor. B.) EndMT-related gene expression after a 48 hour exposure to 100 ng/mL TNF α with inhibitors. C.) Inflammatory activation-related genes after a 48 hour exposure to 100 ng/mL TNF α with inhibitors. D.) PAVEC NF κ B nuclear localization quantification after a 48 hour exposure to 100 ng/mL TNF α with inhibitors. Error bars show \pm SEM, $n \geq 3$ culture wells. Bars that do not share any letters are significantly different according to a one-way ANOVA with Tukey's post-test ($p \leq 0.05$).

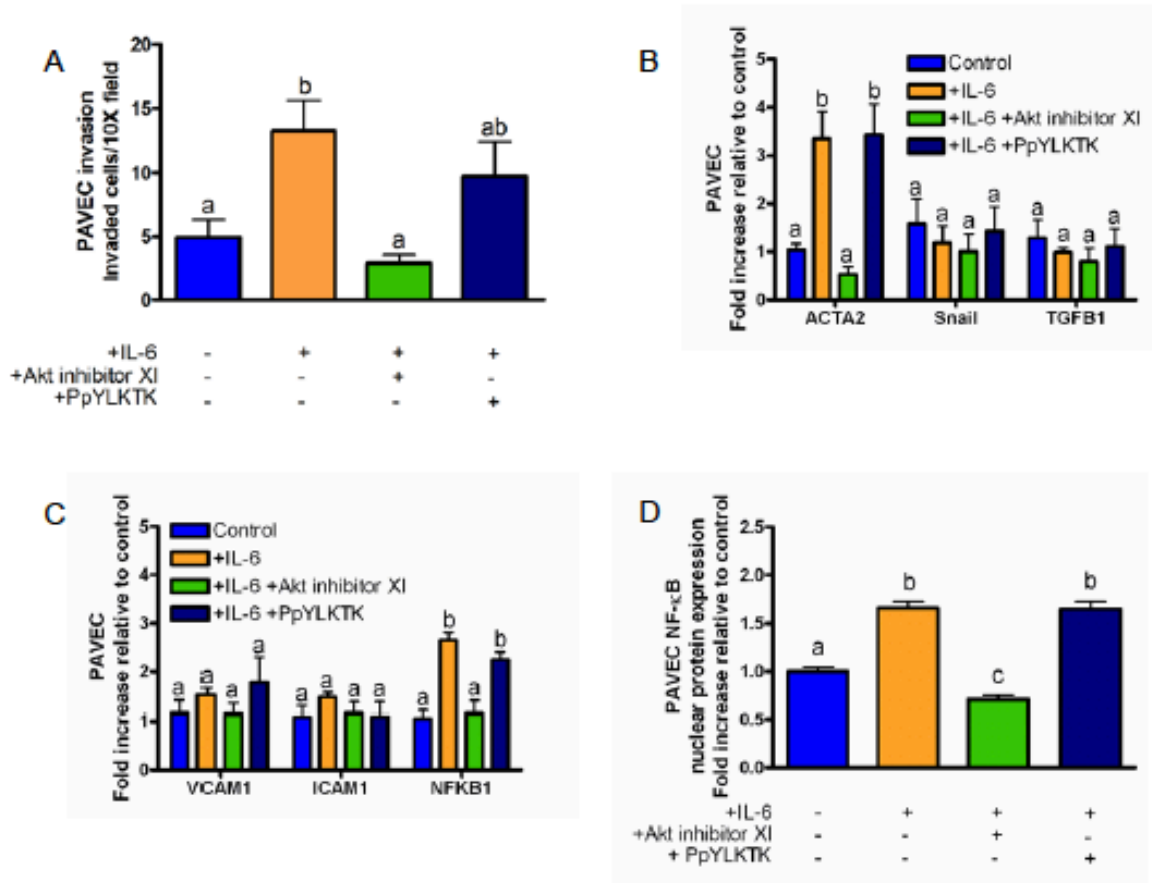


Figure 3.13 IL-6 induces EndMT through Akt/NFκB in PAVEC.

A) Cell invasion after to exposure to 100 ng/mL IL-6 or 100 ng/mL IL-6 with 5 μm Akt inhibitor XI or 5 μm PpYLKTK STAT3 inhibitor. B) ENDMT-related gene expression after exposure to 100 ng/mL IL-6 with inhibitors. C) Inflammatory activation-related genes after exposure to 100 ng/mL IL-6 with inhibitors. D) PAVEC nuclear factor kappa b (NFκB) nuclear localization quantification after exposure to 100 ng/mL IL-6 with inhibitors. Error bars show ±SEM, n ≥ 3 independent monolayers. Bars that do not share any letters are significantly different according to a one-way ANOVA with Tukey's post-test (p ≤ 0.05).

Identical experiments were conducted on avian pre-EndMT valvulogenic endocardial monolayers. As in adult valve endothelium, molecular inhibition of Akt or MEK1 both blocked TNF α -induced NF κ B gene expression and nuclear translocation. Akt inhibition completely blocked NF κ B while MEK1 inhibition only partially blocked NF κ B (Figure 3.14 C,D). IL-6-induced NF κ B gene expression and protein nuclear translocation was also blocked with Akt inhibition, but not STAT3 inhibition (Figure 3.15C,D). Akt or MEK1 inhibition also blocked inflammatory receptor (VCAM1, ICAM1) upregulation, EndMT-related gene expression (ACTA2, Slug, TGF β 3), and collagen invasion by QEE cells (Figure 3.15A-C). As a positive control, Akt1 gene expression was blocked by Akt inhibition in both PAVEC and QEE subjected to TNF α (Figure 3.16, Figure 3.17). Collectively, these results suggest that inflammatory cytokines initiate EndMT at the gene, protein, and function levels through an Akt/NF κ B pathway that is conserved in both adult valve endothelial and embryonic valvulogenic endocardium. TNF α was a more potent inducer of EndMT and resulted in more consistent in pathway responses in both cell types when compared with IL-6. IL-6 may also induce EndMT genes more strongly at an earlier or later time point.

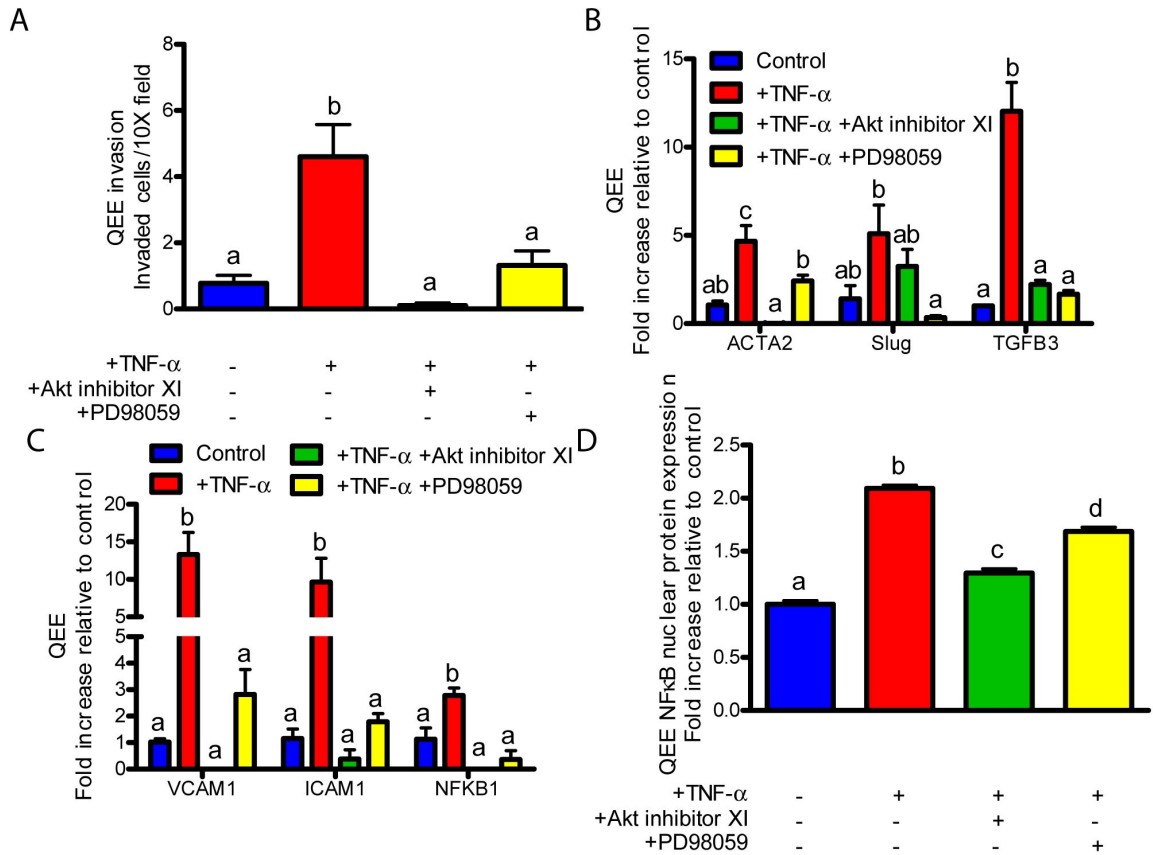


Figure 3.14 TNF α induces EndMT through Akt/MAPK/NF κ B in QEE.

A.) Cell invasion after a 48 hour exposure to 100 ng/mL TNF α or 100 ng/mL TNF α with 5 μ m Akt inhibitor XI or 25 μ m PD98059 MEK1 inhibitor. B.) EndMT-related gene expression after a 48 hour exposure to 100 ng/mL TNF α with inhibitors. C.) Inflammatory activation-related genes after a 48 hour exposure to 100 ng/mL TNF α with inhibitors. D.) QEE NF κ B nuclear localization quantification after a 48 hour exposure to 100 ng/mL TNF α with inhibitors. Error bars show \pm SEM, $n \geq 3$ culture wells with pooled explants. Bars that do not share any letters are significantly different according to a one-way ANOVA with Tukey's post-test ($p \leq 0.05$).

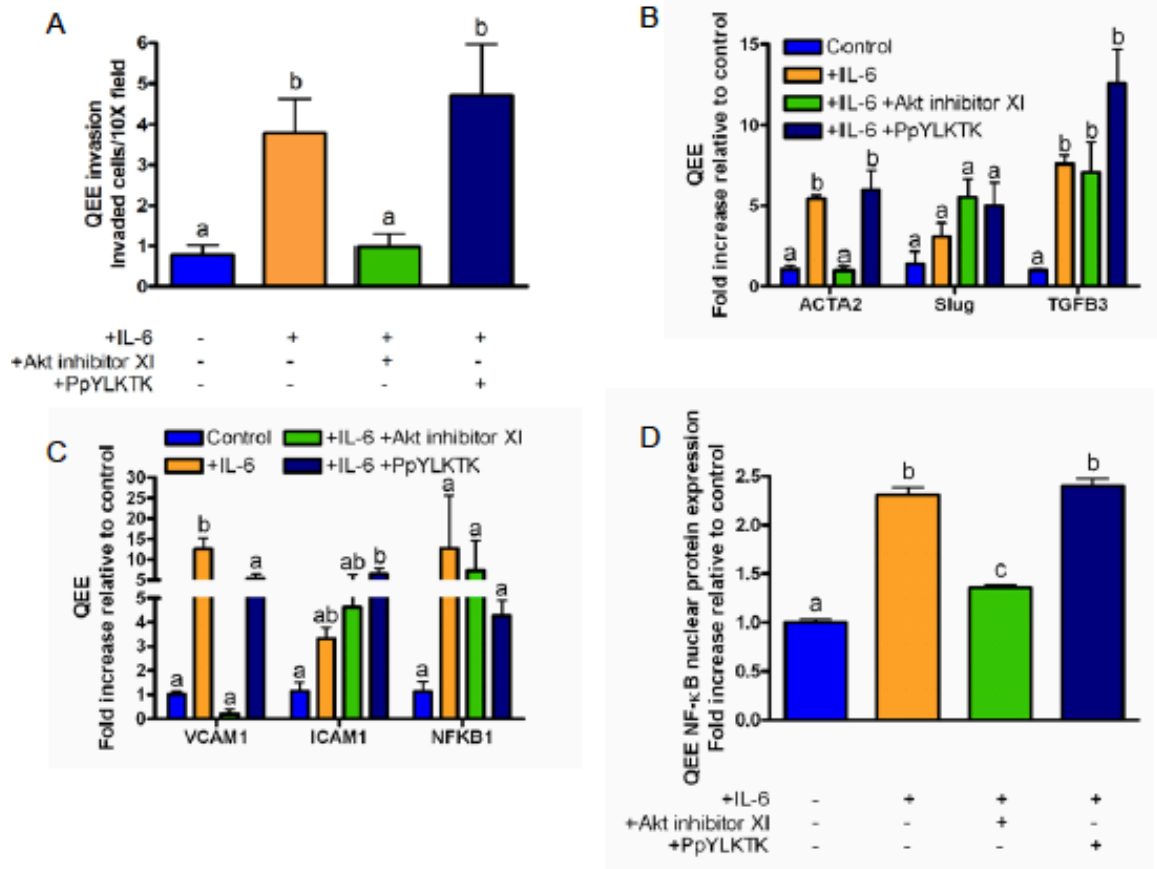


Figure 3.15 IL-6 induces EndMT through Akt/NFκB in QEE.

A) Cell invasion after to exposure to 100 ng/mL IL-6 or 100 ng/mL IL-6 with 5 μm Akt inhibitor XI or 5 μm PpYLKTK STAT3 inhibitor. B) EndMT-related gene expression after exposure to 100 ng/mL IL-6 with inhibitors. C) Inflammatory activation-related genes after exposure to 100 ng/mL IL-6 with inhibitors. D) QEE nuclear factor kappa b (NFκB) nuclear localization quantification after exposure to 100 ng/mL IL-6 with inhibitors. Error bars show ±SEM, n ≥ 3 batches of pooled explants. Bars that do not share any letters are significantly different according to a one-way ANOVA with Tukey's post-test (p ≤ 0.05).

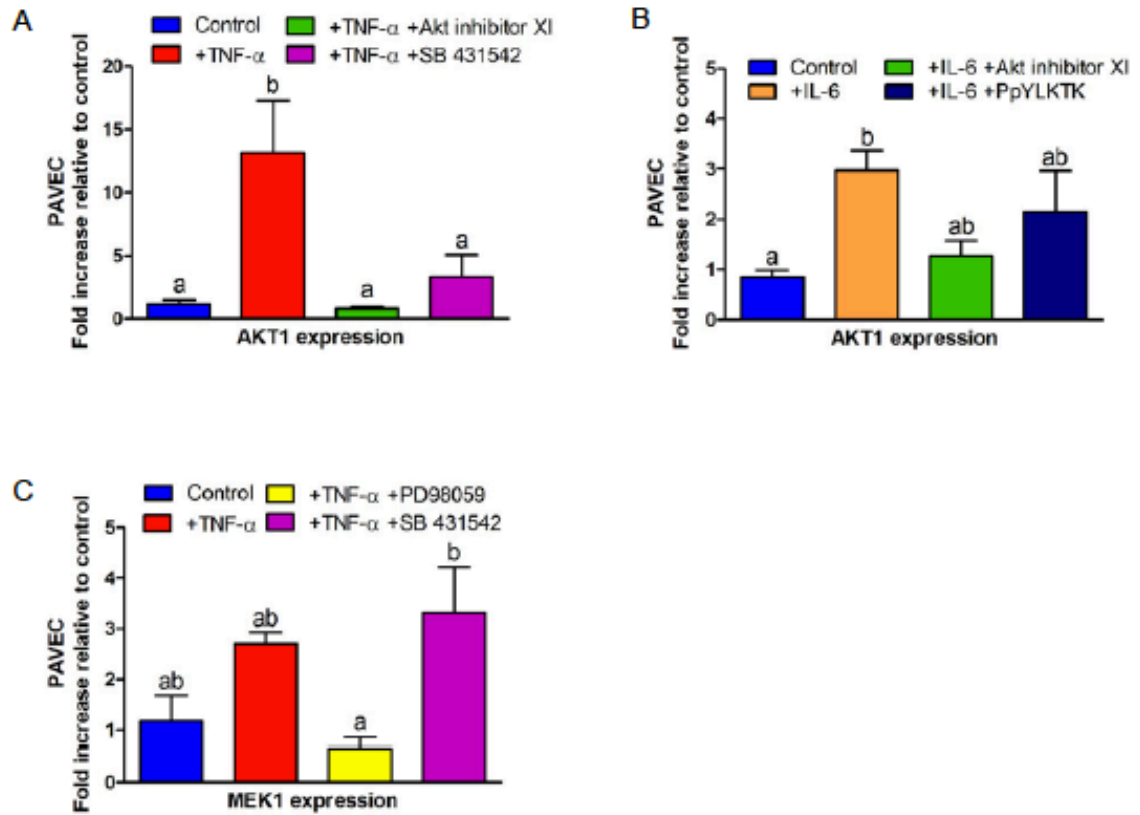


Figure 3.16 Akt and MEK1 inhibitor effects on AKT1 and MEK1 in PAVEC.

A) AKT1 expression was blocked in PAVEC following exposure to 100 ng/mL TNF α and 5 μ m Akt inhibitor XI. B) AKT1 expression was blocked in PAVEC following exposure to 100 ng/mL IL-6 and 5 μ m Akt inhibitor XI. C) MEK1 expression was blocked in PAVEC following exposure to 100 ng/mL TNF α and 25 μ m PD98059 MEK1 inhibitor. Error bars show \pm SEM, $n \geq 3$ independent monolayers. Bars that do not share any letters are significantly different according to a one-way ANOVA with Tukey's post-test ($p \leq 0.05$).

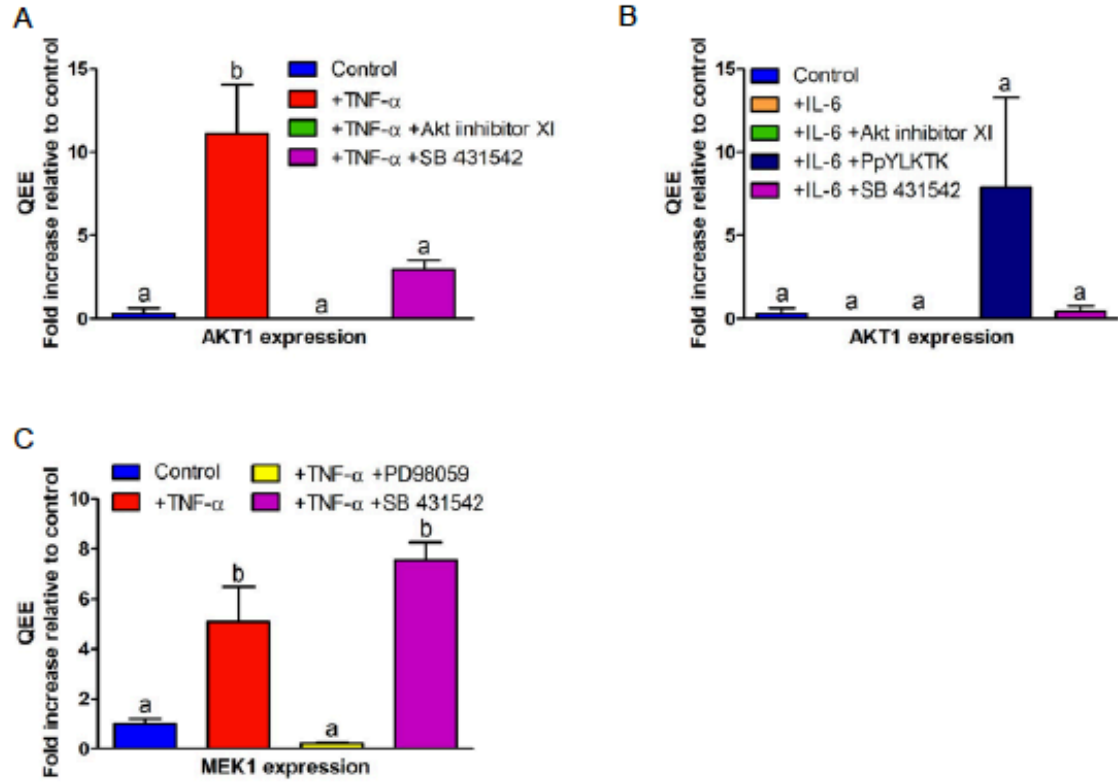


Figure 3.17 Akt and MEK1 inhibitor effects on AKT1 and MEK1 in QEE.

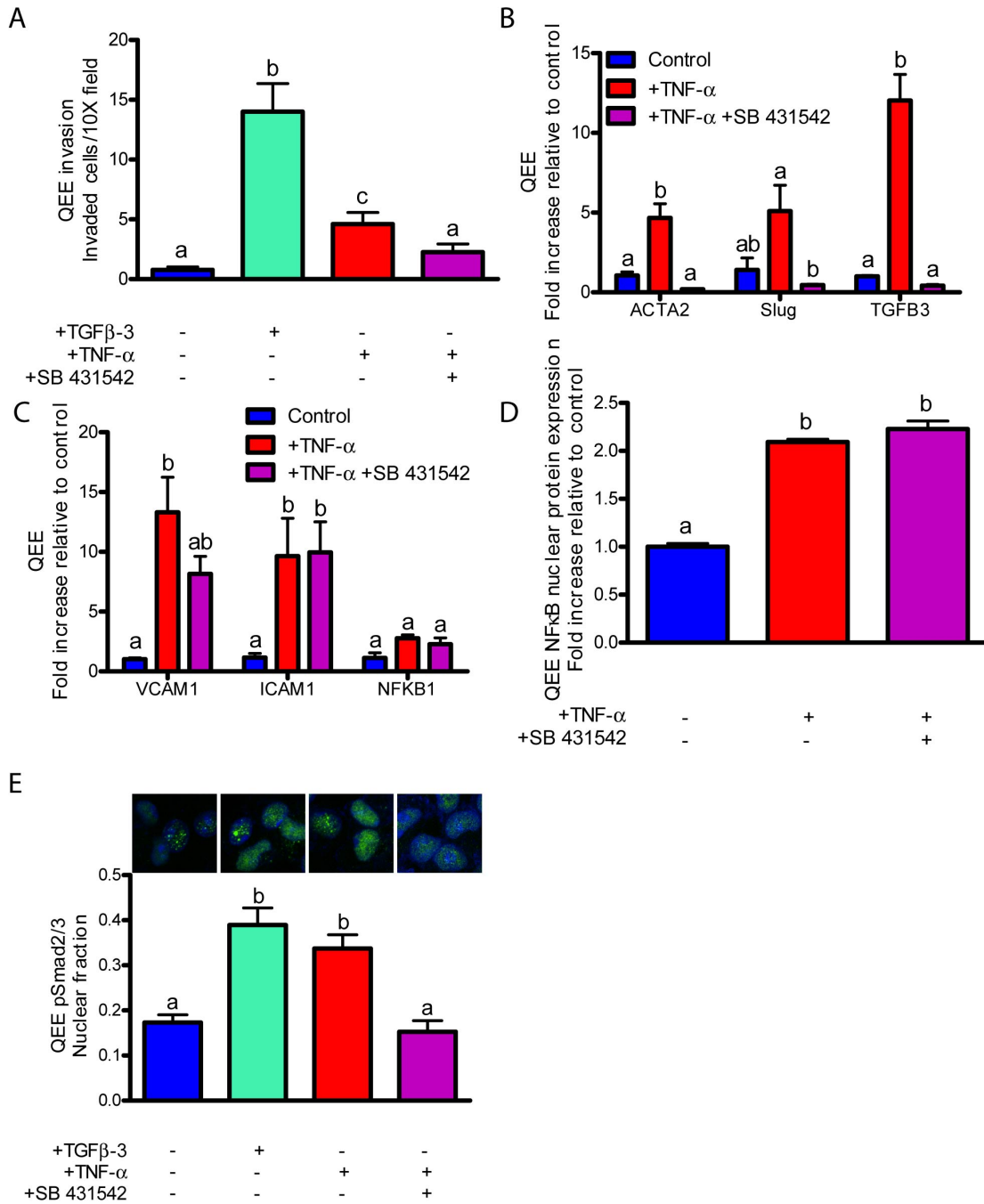
A) AKT1 expression was blocked in QEE following exposure to 100 ng/mL TNF α and 5 μ m Akt inhibitor XI. B) AKT1 expression was blocked in QEE following exposure to 100 ng/mL IL-6 and 5 μ m Akt inhibitor XI. C) MEK1 expression was blocked in QEE following exposure to 100 ng/mL TNF α and 25 μ m PD98059 MEK1 inhibitor. Error bars show \pm SEM, $n \geq 3$ batches of pooled explants. Bars that do not share any letters are significantly different according to a one-way ANOVA with Tukey's post-test ($p \leq 0.05$).

TGFβ signaling through Alk2/5 is required for inflammation-induced embryonic EndMT, but not for adult EndMT.

Previous studies have identified a canonical TGFβ signaling pathway that induces EndMT and is isoform specific: the TGF-β1 isoform in adult VEC, while EndMT invasion is mediated by TGFβ-3 in avian embryonic valve endocardium [23, 42, 43]. We therefore tested whether TGFβ signaling was involved in inflammatory-induced EndMT. As a positive control, exogenous TGFβ-3 (100 ng/ml) induced EndMT matrix invasion in embryonic valve endocardium (Figure 3.18A), while exogenous TGFβ-1 induced EndMT in PAVEC (Figure 6A, Figure 3.19). TNFα induced TGF-β1 gene expression in PAVEC and TGFB3 in QEE (3.79±0.57 and 12.03±1.64, Figures 1B and 2B). IL-6 induced TGFB3 only in QEE (7.61±0.53, Figure 2B). Previous studies demonstrate that TGFβ type I activin receptor-like kinases 2 and 5 (Alk2/5) mediate TGFβ-induced EndMT [44, 45]. Molecular inhibition of Alk2/5 signaling (via 10 μm SB 431542) in QEE reduced EndMT-related gene expression (Figure 3.18B, Figure 3.20B), cell invasion induced by either TNFα or IL-6 (Figure 3.18A, Figure 3.20A), and Smad2/3 phosphorylation and nuclear localization (Figure 3.18E), but did not affect inflammatory activation-related gene expression (Figure 3.18C, Figure 3.20C) or NFκB protein nuclear localization (Figure 3.18D, Figure 3.20D). Together, these results support that inflammatory cytokine-induced EndMT in embryonic valves acts at least in part by canonical TGFβ-Alk-Smad signaling that is downstream of NFκB.

Figure 3.18 Embryonic endocardial monolayers co-opt TGF β in TNF α -EndMT signaling.

A.) Cell invasion after a 48 hour exposure to 100 ng/mL TGF β -3, 100 ng/mL TNF α or 100 ng/mL TNF α with 10 μ m SB 431542 ALK5 inhibitor. B.) EndMT-related gene expression after a 48 hour exposure to 100 ng/mL TNF α with inhibitors. C.) Inflammatory activation-related genes after a 48 hour exposure to 100 ng/mL TNF α with inhibitors. D.) QEE NF κ B nuclear localization quantification after a 48 hour exposure to 100 ng/mL TNF α with inhibitors. E.) pSMAD2/3 nuclear localization following a 48 hour exposure to 100 ng/mL TGF β -3, 100 ng/mL TNF α , or 100 ng/mL TNF α with 10 μ m SB 431542 ALK5 inhibitor. Staining shows p-SMAD2/3 (green) or DNA (blue). Error bars show \pm SEM, $n \geq 3$ culture wells with pooled explants. Bars that do not share any letters are significantly different according to a one-way ANOVA with Tukey's post-test ($p \leq 0.05$).



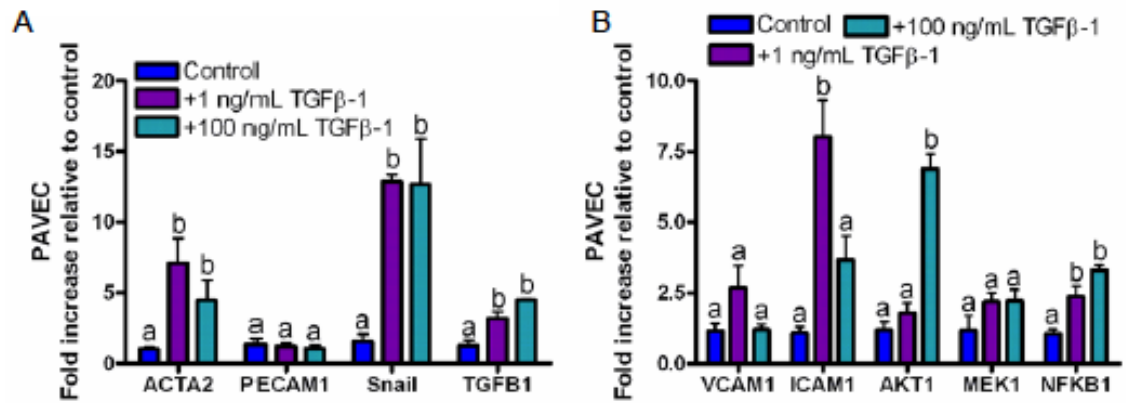


Figure 3.19 Exogenous TGF-β1 induces EndMT in PAVEC.

EndMT-related (A) and inflammatory activation-related (B) gene expression in porcine aortic valve endothelial cells (PAVEC) after exposure to 1 ng/mL or 100 ng/mL TGF-β1. Error bars show ±SEM, n ≥ 3 independent monolayers. Bars that do not share any letters are significantly different according to a one-way ANOVA with Tukey's post-test (p ≤ 0.05).

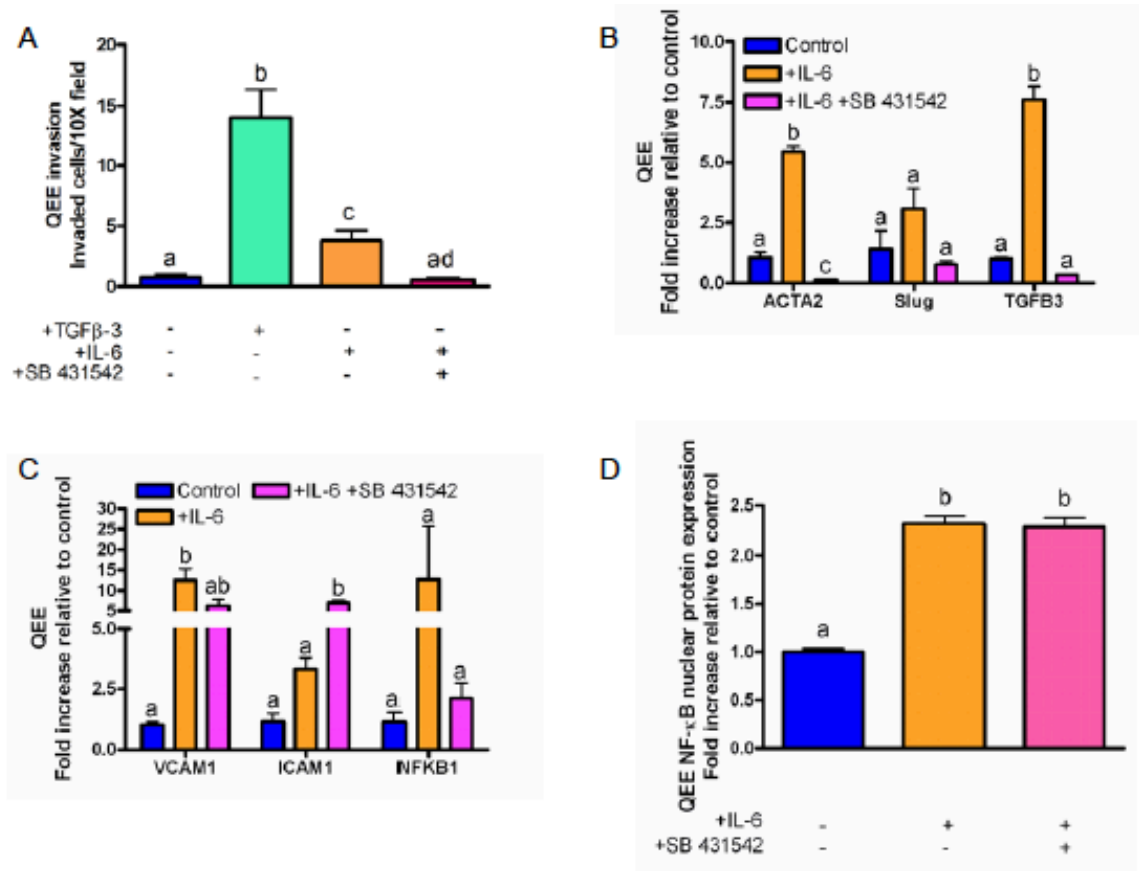


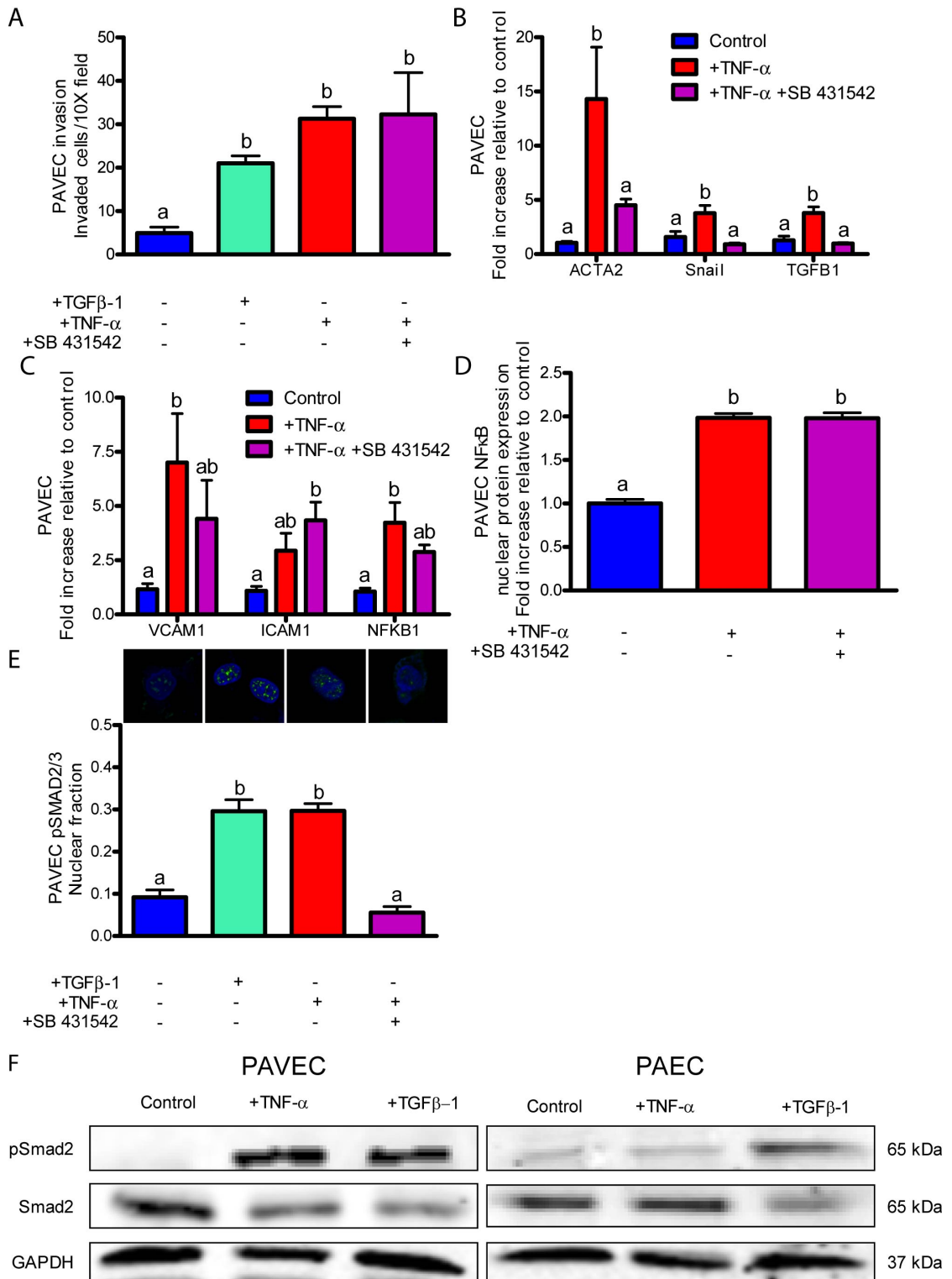
Figure 3.20 Embryonic endocardial monolayers co-opt TGFβ in IL-6-EndMT signaling.

A) Cell invasion after to exposure to 100 ng/mL TGF-β3, 100 ng/mL IL-6, or 100 ng/mL IL-6 with 10 μm SB 431542 ALK5 inhibitor. B) EndMT-related gene expression after exposure to 100 ng/mL IL-6 with inhibitors. C) Inflammatory activation-related genes after exposure to 100 ng/mL IL-6 with inhibitors. D) QEE nuclear factor kappa b (NFκB) nuclear localization quantification after exposure to 100 ng/mL IL-6 with inhibitors. Error bars show ±SEM, n ≥ 3 batches of pooled explants. Bars that do not share any letters are significantly different according to a one-way ANOVA with Tukey's post-test (p ≤ 0.05).

In contrast to embryonic valve endocardium, Alk2/5 inhibition in adult valve endothelial cells (PAVEC) treated with TNF α significantly decreased Smad2/3 phosphorylation and nuclear translocation (Figure 3.21E), but did not result in decreased cell invasion (Figure 3.21A), did not effect EndMT-related or inflammatory activation-related gene expression (Figures 3.21B,C), and did not inhibit NF κ B nuclear localization (Figure 3.21D). Interestingly, endothelial cells from the porcine aorta show increased pSmad2 in response to TGF- β 1, but not to TNF α treatment, suggesting a unique signaling behavior of PAVEC in response to TNF α (Figure 3.21F). These results suggest that Alk2/5 dependent TGF β signaling is not downstream of TNF α -induced EndMT in adult valve endothelium. Therefore, while both embryonic and adult valve endothelium activate an EndMT program in response to TNF α through Akt/NF κ B, TGF β signaling is required and downstream in embryonic, but not required in adult valve endothelium. Adult cells may bypass TGF β signaling because activated NF κ B has been shown to stabilize Snail, an EndMT-regulating transcription factor, in adult cells [46]. In mouse cardiac endothelial cells, treatment with SB431542, but not PD98059 completely blocked TGF β -2-induced EndMT [47].

Figure 3.21 Adult cells do not require TGF β in inflammatory-EndMT signaling.

A.) Cell invasion after a 48 hour exposure to 100 ng/mL TGF- β 1, 100 ng/mL TNF α or 100 ng/mL TNF α with 10 μ m SB 431542 ALK5 inhibitor. B.) EndMT-related gene expression after a 48 hour exposure to 100 ng/mL TNF α with inhibitors. C.) Inflammatory activation-related genes after a 48 hour exposure to 100 ng/mL TNF α with inhibitors. D.) PAVEC NF κ B nuclear localization quantification after a 48 hour exposure to 100 ng/mL TNF α with inhibitors. E.) pSMAD2/3 nuclear localization following a 48 hour exposure to 1 ng/mL TGF- β 1, 100 ng/mL TNF α , or 100 ng/mL TNF α with 10 μ m SB 431542 ALK5 inhibitor. Staining shows pSMAD2/3 (green) or DNA (blue). F.) Western blots for PAVEC or porcine aortic valve endothelial cells (PAEC) exposed to 100 ng/mL TNF α or TGF- β 1 for 48 hours. Error bars show \pm SEM, $n \geq 3$ culture wells with monolayers. Bars that do not share any letters are significantly different according to a one-way ANOVA with Tukey's post-test ($p \leq 0.05$).



3.5 Discussion

The molecular and cellular events that initiate and propagate aortic valve disease are poorly understood and understudied, particularly with the respect to endothelial dysfunction. While the occurrence of EndMT has been previously noted in adult valve endothelium, a biological role remains unclear. EndMT studies in embryonic valves have identified over 100 different regulatory genes, including members of the TGF β , BMP, and VEGF signaling pathways and matrix proteins such as periostin and versican [48-51]. Mis-expression and mutation of many of these genes have been identified in diseased aortic valves [3]. Our results identify a novel, inflammatory cytokine-induced EndMT pathway in aortic valve endothelium through Akt/NF κ B, and further support that this pathway is conserved during embryonic valve development. These findings collectively suggest that an inflammatory reactivation of embryonic-like EndMT may be a mechanism of early aortic valve dysfunction (Figure 3.22).

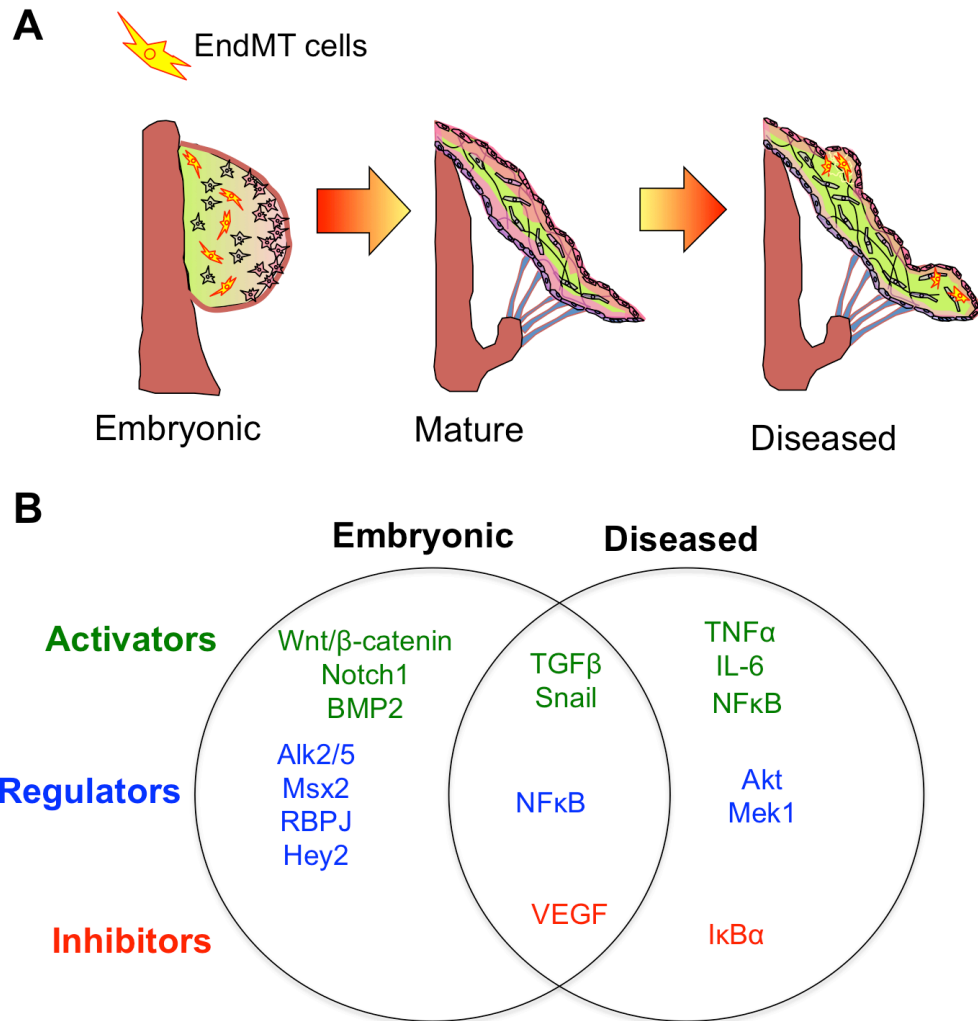


Figure 3.22 EndMT in aortic valve development and disease.

A. EndMT cells are a critical part of valvulogenesis that reappear in an active form in the diseased valve. B. Signaling in embryonic and disease EndMT, including activators, regulators, and inhibitors that are shared between or unique to embryonic and diseased EndMT.

Identifying mechanisms conserved between embryonic and adult valve endothelium remains challenging because there is currently no species for which both embryonic and adult valve endothelial cell cultures have been obtained. Porcine aortic valve endothelial cells are the most characterized and studied adult valve endothelial population, and can be obtained from animals without disease [29, 52-54]. Human aortic valve endothelial cells have been obtained from recipient hearts from cardiac transplantation surgeries or rejected valve donors. While no gross calcification may be present, the valve endothelium exhibits non-negligible inflammatory activation [55-58] Paruchuri et al. identified clonally isolated sub-populations of human pulmonary VEC that were capable of EndMT in response to TGF β , which supports our findings in pure whole VEC populations [59]. Holliday et al. recently showed that *in vitro* cultured human aortic VEC isolated from heart transplant surgeries express endothelial phenotype markers and elevated α SMA, which is in contrast to *in vivo* expression patterns in non-diseased human and porcine aortic valves [16, 60-62]. These co-expression findings suggest that human aortic valve endothelium from these patients may have an increased propensity or capacity for EndMT [60]. Furthermore, several studies demonstrate that inflammatory endothelial activation and calcific degeneration occurs preferentially on the fibrosa side of the valve [4, 63, 64]. Our analysis of calcified human aortic valves found invaded cells co-expressing α SMA and CD31 on the fibrosa surface, suggesting that EndMT correlates with side-specific propagation of AVD [65]. *In situ* mRNA profiling of valve endothelial cells determined hundreds of genes that are differently expressed between sides, with many

further modified in experimental hypercholesteremia [52, 53]. The inflow or ventricularis surface is exposed to pulsatile unidirectional shear stress, while the outflow fibrosa surface experiences nearly oscillatory shear stress [65]. When either endothelial surface is exposed to opposite-sided flow profiles, they similarly upregulate inflammatory receptors [66]. Recently, Wu and colleagues demonstrated that both sides of valve endothelium have the same genetic origin [67]. Our results support and extend these findings to suggest that fibrosa-sided environmental conditions are more conducive to inflammatory activation and EndMT, but additional studies on side-specific endothelial populations are warranted.

Cellular and molecular analysis of embryonic valve formation is almost exclusively conducted with avian and mouse models. Though there are some differences in cardiac anatomy between avians and mammals, the morphogenesis, remodeling, and final anatomy of the clinically important left side of the heart is more similar between chicks and humans than in mice [68-71]. Biological assays with avian and mouse valve progenitors demonstrate identical molecular mechanisms and participants, though which isoforms used may differ [72, 73]. Importantly, chick embryos are inexpensive, can be obtained without additional animal sacrifice, and are very tolerant of experimentation. Our finding of progressive upregulation of inflammatory receptors in valve forming in embryonic chicks is supported by observations in fetal human aortic valves [16]. Our result that EndMT and matrix invasion occurs at least through TGF β -1 in adult porcine cells and TGF β -3 in embryonic quail is supported by several studies [23, 43]. Therefore, we have confidence that the general molecular

regulation we identify is likely conserved across age, but we cannot definitively rule out species differences in the isoforms utilized.

The downstream fate of EndMT-derived mesenchyme in adult valves is of great interest, but was not a focus of this study. Bischoff and Aikawa recently proposed that EndMT creates a type of progenitor-like cell that renews the valve interstitial cell (VIC) population and maintains tissue homeostasis [74]. Both embryonic and adult valvular mesenchymal cells have the potential for osteogenic differentiation [75, 76], but whether these cells are directly EndMT-derived or from subsequent differentiation processes is not yet known. $\text{TNF}\alpha$ and $\text{NF}\kappa\text{B}$ have been linked to the mesenchymal cell molecular and cellular mechanisms that mediate valvular calcification [9, 77]. $\text{TNF}\alpha$ expression and nuclear localization of $\text{NF}\kappa\text{B}$ is present in stenotic human aortic valves [78], and $\text{TNF}\alpha$ treatment of valve interstitial cells in 2D culture induces calcium nodule formation and expression of *runx2* independent of osteogenic media [9, 79, 80]. We found EndMT derived subendothelial cells in calcified human aortic valves, but were always located distal to calcific lesions. This was not unexpected, as valve calcifications are associated with endothelial loss [81]. Taken together, these results support that inflammatory EndMT is a component of early stage AVD, but how these progeny contribute to and/or regulate downstream calcific progression is still unclear.

In conclusion, our results establish an inflammatory mechanism of early aortic valve pathogenesis that is, in part, developmentally conserved. Age dependent use of

canonical TGF β signaling may be an important mode of inflammatory disease pathogenesis distinct from potentially healthy tissue formation and remodeling. Selective molecular inhibition of the AKT/NF κ B pathway in valve endothelium may therefore be a potential strategy for impacting early stage aortic valve disease.

Acknowledgements

We acknowledge Jennifer Richards and Phillip Buskohl for assistance with sample collection. Funding for this work was provided by The Hartwell Foundation, the National Institute of Health (HL110328), the National Science Foundation (CBET-0955712) the American Heart Association Scientist Development Grant (#0830384N), and the LeDucq Foundation (Project MITRAL).

REFERENCES

1. Lloyd-Jones D, Adams R, Carnethon M et al. (2009) Heart disease and stroke statistics--2009 update: A report from the American Heart Association statistics committee and stroke statistics subcommittee. *Circulation* 119: e21-e181.
2. Hoffman JIE, and Kaplan S. (2002) The incidence of congenital heart disease. *J Am Coll Cardiol.* 39: 1890-1900.
3. Hakuno D, Kimura N, Yoshioka M, and Fukuda K. (2009) Molecular mechanisms underlying the onset of degenerative aortic valve disease. *J Mol Med.* 87: 17-24.
4. Mohler ER, III, Gannon F, Reynolds C, Zimmerman R, Keane MG, and Kaplan FS. (2001) Bone formation and inflammation in cardiac valves. *Circulation.* 103: 1522-1528.
5. Chan KL, Teo K, Dumesnil JG, Ni A, and Tam J. (2010) Effect of Lipid lowering with rosuvastatin on progression of aortic stenosis: results of the aortic stenosis progression observation: measuring effects of rosuvastatin (ASTRONOMER) trial. *Circulation.* 121: 306-314.
6. Butcher JT, Mahler GJ, and Hockaday LA. (2011) Aortic valve disease and treatment: The need for naturally engineered solutions. *Adv Drug Deliver Rev.* 63: 242-268.
7. Beckmann E, Grau JB, Sainger R, Poggio Pm and Ferrari G. (2010) Insights into the use of biomarkers in calcific aortic valve disease. *J Heart Valve Dis.* 19: 441-452.
8. Hjortnaes J, Butcher J, Figueiredo J-L, Riccio M, Kohler RH, Kozloff KM, et al. (2010) Arterial and aortic valve calcification inversely correlates with osteoporotic bone remodelling: a role for inflammation. *Eur Heart J.* 31: 1975-1984.
9. Kaden JJ, Kilic R, Sarikoc A, Hagl S, Lang S, Hoffmann U, et al. (2005) Tumor necrosis factor alpha promotes an osteoblast-like phenotype in human aortic valve myofibroblasts: a potential regulatory mechanism of valvular calcification. *Int J Mol Med.* 16: 869-872.

10. Kaden JJ, Dempfle CE, Grobholz R, Fischer CS, Vocke DC, Kilic R, et al. (2005) Inflammatory regulation of extracellular matrix remodeling in calcific aortic valve stenosis. *Cardiovasc Pathol.* 14: 80-87.
11. Davutoglu V, Celik A, and Aksoy M. (2005) Contribution of selected serum inflammatory mediators to the progression of chronic rheumatic valve disease, subsequent valve calcification and NYHA functional class. *J Heart Valve Dis.* 14: 251-256.
12. Alom-Ruiz SP, Anilkumar N, and Shah AM. (2008) Reactive oxygen species and endothelial activation. *Antioxid Redox Signal.* 10: 1089-1100.
13. Von der Thüsen JH, Kuiper J, Van Berkel TJC, and Biessen EAL. (2003) Interleukins in atherosclerosis: Molecular pathways and therapeutic potential. *Pharmacol Rev.* 55: 133-166.
14. Brand K, Page S, Rogler G, Bartsch A, Brandl R, Knuechel R, et al. (1996) Activated transcription factor nuclear factor-kappa B is present in the atherosclerotic lesion. *J Clin Invest.* 97: 1715-1722.
15. Wilson SH, Best PJM, Edwards WD, Holmes DR, Carlson PJ, Celermajer DS, et al. (2002) Nuclear factor-kappa B immunoreactivity is present in human coronary plaque and enhanced in patients with unstable angina pectoris. *Atherosclerosis.* 160: 147-153.
16. Aikawa E, Whittaker P, Farber M, Mendelson K, Padera RF, Aikawa M, et al. (2006) Human semilunar cardiac valve remodeling by activated cells from fetus to adult: Implications for postnatal adaptation, pathology, and tissue engineering. *Circulation.* 113: 1344-1352.
17. Mou SS, Haudek SB, Lequier L, Pena O, Leonard S, Nikaidoh H, et al. (2002) Myocardial inflammatory activation in children with congenital heart disease. *Crit Care Med.* 30: 827-832.
18. Qing M, Schumacher K, Heise R, Wöltje M, Vazquez-Jimenez JF, Richter T, et al. (2003) Intramyocardial synthesis of pro- and anti-inflammatory cytokines in infants with congenital cardiac defects. *J Am Coll Cardiol.* 41: 2266-2274.

19. Hernández-Gutierrez S, García-Peláez I, Zentella-Dehesa A, Ramos-Kuri M, Hernández-Franco P, Hernández-Sánchez F, et al. (2006) NF κ B signaling blockade by Bay 11-7085 during early cardiac morphogenesis induces alterations of the outflow tract in chicken heart. *Apoptosis*. 11: 1101-1109.
20. Nath AK, Brown RM, Michaud M, Sierra-Honigmann MR, Snyder M, and Madri JA. (2008) Leptin affects endocardial cushion formation by modulating EMT and migration via Akt signaling cascades. *J Cell Biol*. 181: 367-380.
21. Meadows K, Iyer S, Stevens M, Wang D, Shechter S, Perruzzi C, et al. (2009) Akt promotes Endocardial-Mesenchyme Transition. *J Angiogenes Res*. 1: 1-9.
22. Kumarswamy R, Volkman I, Jazbutyte V, Dangwal S, Park D-H, and Thum T. (2012) Transforming Growth Factor- β -Induced Endothelial-to-Mesenchymal Transition Is Partly Mediated by MicroRNA-21. *Arterioscler Thromb Vasc Biol*. 32: 361-369.
23. Paranya G, Vineberg S, Dvorin E, Kaushal S, Roth SJ, Rabkin E, et al. (2001) Aortic valve endothelial cells undergo transforming growth factor- β -mediated and non-transforming growth factor- β -mediated transdifferentiation in vitro. *Am J Pathol*. 159: 1335-1343.
24. Yang J-H, Wylie-Sears J, and Bischoff J. (2008) Opposing actions of Notch1 and VEGF in post-natal cardiac valve endothelial cells. *Biochem Biophys Res Commun* 374: 512-516.
25. Wylie-Sears J, Aikawa E, Levine RA, Yang J-H, and Bischoff J. (2011) Mitral Valve Endothelial Cells With Osteogenic Differentiation Potential. *Arterioscler Thromb Vasc Biol*. 31: 598-607.
26. Guerraty M and Mohler ER. (2007) Models of aortic valve calcification. *J Invest Med*. 55: 278-283.
27. Runyan RB and Markwald RR. (1983) Invasion of mesenchyme into three-dimensional collagen gels: A regional and temporal analysis of interaction in embryonic heart tissue. *Dev Biol*. 95: 108-114.
28. Bernanke DH and Markwald RR. (1982) Migratory behavior of cardiac cushion tissue cells in a collagen-lattice culture system. *Dev Biol*. 91: 235-245.

29. Butcher JT, Penrod AM, Garcia AJ, and Nerem RM. (2004) Unique morphology and focal adhesion development of valvular endothelial cells in static and fluid flow environments. *Arterioscler Thromb Vasc Biol.*24: 1429-1434.
30. Chen L, Fischle W, Verdin E, and Greene WC. (2001) Duration of nuclear NF- κ B action regulated by reversible acetylation. *Science.* 293: 1653-1657.
31. Hermiston ML, Xu Z and Weiss A. (2003) CD45: A Critical Regulator of Signaling Thresholds in Immune Cells. *Annu Rev Immunol.* 21: 107-137.
32. Baldwin HS, Shen HM, Yan HC, DeLisser HM, Chung A, Mickanin C, et al. (1994) Platelet endothelial cell adhesion molecule-1 (PECAM-1/CD31): alternatively spliced, functionally distinct isoforms expressed during mammalian cardiovascular development. *Development.* 120: 2539-2553.
33. Devin A, Lin Y, and Liu ZG. (2003) The role of the death-domain kinase RIP in tumour necrosis factor-induced activation of mitogen-activated protein kinases. *EMBO reports.* 4: 623-627.
34. Dhawan P and Richmond A. (2002) A novel NF- κ B-inducing kinase-MAPK signaling pathway up-regulates NF- κ B activity in melanoma cells. *J Biol Chem.* 277: 7920-7928.
35. Vanden Berghe W, Plaisance SP, Boone E, De Bosscher K, Schmitz ML, Fiers W, et al. (1998) p38 and extracellular signal-regulated kinase mitogen-activated protein K-kinase pathways are required for nuclear factor- κ B p65 transactivation mediated by tumor necrosis factor. *J Biol Chem.* 273: 3285-3290.
36. Ozes ON, Mayo LD, Gustin JA, Pfeffer SR, Pfeffer LM, and Donner DB. (1999) NF- κ B activation by tumour necrosis factor requires the Akt serine-threonine kinase. *Nature.* 401: 82 - 85.
37. Pincheira R, Castro AF, Ozes ON, Idumalla PS, and Donner DB. (2008) Type 1 TNF receptor forms a complex with and uses jak2 and c-Src to selectively engage signaling pathways that regulate transcription factor activity. *J Immunol.* 181: 1288-1298.
38. Taga T and Kishimoto T. (2003) gp130 and the interleukin-6 family of cytokines. *Annu Rev of Immunol.* 15: 797-819.

39. Chen RH, Chang MC, Su YH, Tsai YT, and Kuo ML. (1999) Interleukin-6 inhibits transforming growth factor- β -induced apoptosis through the phosphatidylinositol 3-kinase/Akt and signal transducers and activators of transcription 3 pathways. *J Biol Chem.* 274: 23013-23019.
40. Middleton G, Hamanoue M, Enokido Y, Wyatt S, Pennica D, Jaffray E, et al. (2000) Cytokine-induced nuclear factor kappa B activation promotes the survival of developing neurons. *J Cell Biol.* 148: 325-332.
41. Zhang JY, Li Y, and Shen BF. (2003) PI3-K/Akt pathway contributes to IL-6-dependent growth of 7TD1 cells. *Cancer Cell Int.* 3: 1-4.
42. Nakajima Y, Mironov V, Yamagishi T, Nakamura H, and Markwald RR. (1997) Expression of smooth muscle alpha-actin in mesenchymal cells during formation of avian endocardial cushion tissue: A role for transforming growth factor β 3. *Dev Dynam.* 209: 296-309.
43. Ramsdell AF and Markwald RR. (1997) Induction of endocardial cushion tissue in the avian heart is regulated, in part, by TGF β -3-mediated autocrine signaling. *Dev Biol.* 188: 64-74.
44. Mercado-Pimentel ME, Hubbard AD, and Runyan RB. (2007) Endoglin and Alk5 regulate epithelial-mesenchymal transformation during cardiac valve formation. *Dev Biol.* 304: 420-432.
45. Sridurongrit S, Larsson J, Schwartz R, Ruiz-Lozano, and Kaartinen V. (2008) Signaling via the Tgf-beta type I receptor Alk5 in heart development. *Dev Biol.* 322: 208-218.
46. Wu Y, Deng J, Rychahou PG, Qiu S, Evers BM, and Zhou BP. (2009) Stabilization of snail by NF-kappaB is required for inflammation-induced cell migration and invasion. *Cancer Cell.* 15: 416-428.
47. Ghosh AK, Nagpal V, Covington JW, Michaels MA, and Vaughan DE. (2012) Molecular basis of cardiac endothelial-to-mesenchymal transition (EndMT): Differential expression of microRNAs during EndMT. *Cell Signal.* 24: 1031-1036.
48. Armstrong EJ and Bischoff J. (2004) Heart Valve Development: Endothelial Cell Signaling and Differentiation. *Circ Res.* 95: 459-470.

49. Butcher JT and Markwald RR. (2007) Valvulogenesis: the moving target. *Philos Trans R Soc Lond B Biol Sci.* 362: 1489-1503.
50. Person AD, Klewer SE, Runyan RB, and Kwang WJ. (2005) in *International Review of Cytology* Vol. 243;287 (Academic Press).
51. Combs MD and Yutzey KE. (2009) Heart valve development: regulatory networks in development and disease. *Circ Res.* 105: 408-421.
52. Simmons CA, Grant GR, Manduchi E, and Davies PF. (2005) Spatial heterogeneity of endothelial phenotypes correlates with side-specific vulnerability to calcification in normal porcine aortic valves. *Circ Res.* 96: 792-799.
53. Guerraty MA, Grant GR, Karanian JW, Chiesa OA, Pritchard WF, and Davies PF. (2010) Hypercholesterolemia induces side-specific phenotypic changes and peroxisome proliferator-activated receptor- γ pathway activation in swine aortic valve endothelium. *Arterioscler Thromb Vasc Biol.* 30: 225-231.
54. Farivar RS, Cohn LH, Soltesz EG, Mihaljevic T, Rawn JD, and Byrne JG. (2003) Transcriptional profiling and growth kinetics of endothelium reveals differences between cells derived from porcine aorta versus aortic valve. *Eur J Cardio-Thorac.* 24: 527-534
55. Ku C-H, Johnson PH, Batten P, Sarathchandra P, Chambers RC, Taylor PM, et al. (2006) Collagen synthesis by mesenchymal stem cells and aortic valve interstitial cells in response to mechanical stretch. *Cardiovasc Res.* 71: 548-556.
56. Osman L, Yacoub MH, Latif N, Amrani M, and Chester AH. (2006) Role of human valve interstitial cells in valve calcification and their response to atorvastatin. *Circulation.* 114: I-547-552.
57. Hafizi S, Taylor PM, Chester AH, Allen SP, and Yacoub MH. (2000) Mitogenic and secretory responses of human valve interstitial cells to vasoactive agents. *J Heart Valve Dis.* 9: 454-458.
58. Jian B, Narula N, Li Q-y, Mohler ER, III, and Levy RJ. (2003) Progression of aortic valve stenosis: TGF- β 1 is present in calcified aortic valve cusps and promotes aortic valve interstitial cell calcification via apoptosis. *Ann Thorac Surg.* 75: 457-465.

59. Paruchuri S, Yang J-H, Aikawa E, Melero-Martin JM, Khan ZA, Loukogeorgakis S, et al. (2006) Human Pulmonary Valve Progenitor Cells Exhibit Endothelial/Mesenchymal Plasticity in Response to Vascular Endothelial Growth Factor-A and Transforming Growth Factor- β 2. *Circ Res.* 99: 861-869.
60. Holliday CJ, Ankeny RF, Jo H, and Nerem RM. (2011) Discovery of shear- and side-specific mRNAs and miRNAs in human aortic valvular endothelial cells. *Am J Physiol Heart Circ Physiol.* 301: H856-867.
61. Butcher JT, Tressel S, Johnson T, Turner D, Sorescu G, Jo H, et al. (2006) Transcriptional profiles of valvular and vascular endothelial cells reveal phenotypic differences: Influence of shear stress. *Arterioscler Thromb Vasc Biol.* 26: 69-77.
62. Metzler S, Digesu C, Howard J, Filip To S, and Warnock J. (2011) Live en face imaging of aortic valve leaflets under mechanical stress. *Biomech Model Mechan.* 1-7.
63. Mohler III, ER (2000) Are atherosclerotic processes involved in aortic-valve calcification? *Lancet.* 356: 524-525.
64. Mohler III, ER (2004) Mechanisms of aortic valve calcification. *Am J Cardiol.* 94: 1396-1402, A1396.
65. Kilner PJ, Yang G-Z, Wilkes AJ, Mohiaddin RH, Firmin DN, and Yacoub MH. (2000) Asymmetric redirection of flow through the heart. *Nature.* 404: 759-761.
66. Sucaskey P, Balachandran K, Elhammali A, Jo H, and Yoganathan AP. (2009) Altered shear stress stimulates upregulation of endothelial VCAM-1 and ICAM-1 in a BMP-4 and TGF- β 1-dependent pathway. *Arterioscler Thromb Vasc Biol.* 29: 254-260.
67. Wu B, Wang Y, Lui W, Langworthy M, Tompkins KL, Hatzopoulos AK, et al. (2011) *Nfatc1* Coordinates Valve Endocardial Cell Lineage Development Required for Heart Valve Formation. *Circ Res.* 109: 183-192.
68. Hinton RB, Jr., Lincoln J, Deutsch GH, Osinska H, Manning PB, Benson DW, et al. (2006) Extracellular matrix remodeling and organization in developing and diseased aortic valves. *Circ Res.* 98: 1431-1438.

69. Wessels A and Sedmera D. (2003) Developmental anatomy of the heart: a tale of mice and man. *Physiol Genomics*. 15: 165-176.
70. Sedmera D, Cook AC, Shirali G, and McQuinn TC. (2005) Current issues and perspectives in hypoplasia of the left heart. *Cardiol Young*. 15: 56-72.
71. Lincoln J, Alfieri CM, and Yutzey KE. (2004) Development of heart valve leaflets and supporting apparatus in chicken and mouse embryos. *Dev Dyn*. 230: 239-250.
72. Mercado-Pimentel ME, and Runyan RB. (2007) Multiple transforming growth factor-beta isoforms and receptors function during epithelial-mesenchymal cell transformation in the embryonic heart. *Cells Tissues Organs*. 185: 146-156.
73. Boyer AS, Ayerinkas II, Vincent EB, McKinney LA, Weeks DL, and Runyan RB. (1999) TGF- β 2 and TGF- β 3 have separate and sequential activities during epithelial-mesenchymal cell transformation in the embryonic heart. *Dev Biol*. 208: 530-545.
74. Bischoff J and Aikawa E. (2011) Progenitor Cells Confer Plasticity to Cardiac Valve Endothelium. *J Cardiovasc Transl Res*. 4: 710-719.
75. Alfieri CM, Cheek J, Chakraborty S, and Yutzey KE. (2010) Wnt signaling in heart valve development and osteogenic gene induction. *Dev Biol*. 338: 127-135.
76. Chen JH, Yip CY, Sone ED, and Simmons CA. (2009) Identification and characterization of aortic valve mesenchymal progenitor cells with robust osteogenic calcification potential. *Am J Pathol*. 174: 1109-1119.
77. Kaden JJ, Bickelhaupt S, Grobholz R, Haase KK, Sarıkoç A, Kılıç R, et al. (2004) Receptor activator of nuclear factor κ B ligand and osteoprotegerin regulate aortic valve calcification. *J Mol Cell Cardiol*. 36: 57-66.
78. Toli K, Paraskevas KI, Poulakou MV, Agrogiannis G, Kavantzias N, Xanthopoulos V, et al. (2008) Association between plasma levels and immunolocalization of cytokines in heart valve lesions: a possible target for treatment? *Expert Opin Ther Targets*. 12: 1209-1215.

79. Kaden JJ, Dempfle CE, Kilic R, Sarikoc A, Hagl S, Lang S, et al. (2005) Influence of receptor activator of nuclear factor kappa B on human aortic valve myofibroblasts. *Exp Mol Pathol*. 78: 36-40.
80. Yu Z, Seya K, Daitoku K, Motomura S, Fukuda I, and Furukawa K-I. (2011) TNF α accelerates the calcification of human aortic valve interstitial cells obtained from patients with calcific aortic valve stenosis via the BMP2-Dlx5 pathway. *J Pharmacol Exp Ther*. 337: 16-23.
81. Poggianti E, Venneri L, Chubuchny V, Jambrik Z, Baroncini LA, and Picano E. (2003) Aortic valve sclerosis is associated with systemic endothelial dysfunction. *J Am Coll Cardiol*. 41: 136-141.

CHAPTER 4

HETEROGENEOUS SUSCEPTIBILITY OF VALVE ENDOTHELIAL CELLS TO MESENCHYMAL TRANSFORMATION IN RESPONSE TO TNF-ALPHA

This chapter was published in *Annals of Biomedical Engineering*:

Farrar EJ and Butcher JT. Heterogeneous Susceptibility of Valve Endothelial Cells to
Mesenchymal Transformation in Response to TNF α . *Annals of Biomedical
Engineering*. 2013;42(1):149-161.

4.1 Abstract

Lack of understanding of the early mechanisms of aortic valve stenosis and calcification hinders the development of diagnostic and therapeutic intervention strategies. Inflammation is a known component of early aortic valve disease (AVD) and can induce mesenchymal transformation in a subset of aortic valve endothelial cells. Here we present a three-dimensional culture system that allows transforming and non-transforming cells to be independently isolated and analyzed. We have used the system to identify and characterize the dynamic invasion and phenotypic transition of two distinct subsets of endothelial cells: those that invade and transform under TNF α treatment, and those that resist mesenchymal transformation and remain endothelial. We determine that non-transformed cells maintain control levels of endothelial genes VE-cadherin and eNOS, while transformed cells lose these endothelial characteristics and upregulate α -smooth muscle actin. Both subsets of cells have an inflammatory phenotype marked by increased ICAM-1, but transformed cells have increased MMP-9, Notch1, TGF- β , and BMP4, while non-transformed cells do not. Transformed cells also have distinct effects on alignment of collagen fibers as they invade the hydrogel system, which is not found in control endothelial or interstitial valve cells. Understanding the role of transforming and non-transforming endothelial cells in valve disease will provide an important pathological link between early inflammation and later stages of disease. Discovery of the molecular signature of transformation-resistant endothelial cells could inform development of treatment strategies that promote survival of the valve endothelium.

4.2 Introduction

Aortic valve disease (AVD) affects 2.8% of Americans over 75 years of age. Approximately 40% of severe cases undergo cardiothoracic surgery [14] due to the lack of effective pharmaceutical treatments for AVD. Without surgical intervention, the majority of affected patients will die within one year of diagnosis [29]. Inflammation is a hallmark of early aortic valve disease [18] and new molecular imaging techniques have identified endothelial activation and damage to be a key early response [1]. However, limited understanding of the role of inflamed endothelial cells in AVD prohibits development of clinically useful strategies targeting valve endothelial pathobiology.

Recent studies suggest that valve endothelial function is a key regulator of early AVD via recruitment of immune cells [14], dysregulation of protective nitric oxide signaling [27], phenotypic plasticity [32], and through expression of pro-calcific proteins [28]. We recently showed that inflammatory cytokine TNF α drives an endothelial to mesenchymal transition (EndMT) in a subset (5-10%) of adult valve endothelial cells (VEC) [24]. Adult VEC EndMT also occurs in response to pathological levels of mechanical strain [3], elevated TGF- β signaling [26], or activation of cell-signaling ligand Notch1 [33]. These studies used clonal isolations of valve endothelial cells and found, similar to inflammatory-EndMT, that mesenchymal transformation occurred only in a fraction of VEC. This subset of VEC that is uniquely able to transform under EndMT stimuli may have important roles in later AVD. A subset of VEC clonally isolated from MV can undergo EndMT and exhibits

the capacity for osteogenic differentiation, suggesting their potentially unique participation in advanced mitral valve disease [32, 4]. It is unknown how EndMT-VEC in the aortic valve participate in advanced AVD. In addition, the subset of VEC that do not transform may possess unique phenotypic signatures which promote resistance to mesenchymal transformation and potentially an ability to protect against disruption of the protective endothelial layer. These intriguing questions have not been examined due to the difficulty of separating transforming from non-transforming cells during EndMT. Studies are needed which are able to characterize transforming and non-transforming VEC in a controlled manner, elucidating the three-dimensional and time-dependent EndMT response of VEC to pathological conditions.

Here we have designed a system consisting of a porcine aortic valve endothelial cells cultured on a porous membrane combined with a collagen hydrogel. Endothelial cells treated with EndMT stimuli can invade, interact with a collagen gel matrix, and be separately isolated and studied from non-transformed endothelial cells. Aortic valve endothelial cells can maintain an endothelial phenotype on the membrane for up to six days, or undergo a full mesenchymal transformation by invading the underlying matrix. We used the system to characterize time-dependent dynamics of the TNF α -EndMT process, involving distinct stages of endothelial or myofibroblastic protein expression. We identified a unique sub-population of non-transforming cells that maintained endothelial characteristics under TNF α , suggesting resistance to EndMT. We also isolated a subset of transforming endothelial cells, in which we quantified the expression of genes related to aortic valve disease, including MMP-9, TGF- β 1,

Notch1, and BMP4. Finally, we examined the effects of the transforming cells on their surrounding collagen matrix, as an initial investigation of the ability of these cells to contribute to valvular matrix remodeling. These results are an important step forward in characterizing valvular endothelial cells transformed by inflammatory EndMT and understanding their role in the progression of aortic valve disease. Furthermore, the ability to segregate and study a population of non-transforming VEC which are resistant to inflammatory EndMT establishes a foundation for identifying molecular mechanisms which may provide protection against mesenchymal transformation.

4.3 Materials and Methods

Cell isolation and culture

Porcine aortic valve endothelial cells (PAVEC) and porcine valve interstitial cells (PAVIC) were isolated as demonstrated previously¹⁶ from valves donated by Shirk Meats of Dundee, NY. PAVEC were grown in flasks coated with 50 µg/mL rat-tail collagen I (BD Biosciences, San Jose, CA) at 37°C and 5% CO₂ in DMEM supplemented with 10% FBS (Invitrogen, Grand Island, NY), 1% penicillin-streptomycin (Invitrogen, Grand Island, NY), and 50U/mL heparin (Sigma-Aldrich, St Louis, MO). Cells were passaged 1:3 at confluency using 0.25% Trypsin-EDTA (Invitrogen) and media was changed every 48 hours. PAVIC were cultured identically, but without collagen flask coating or heparin in the culture media. Purity of endothelial population was monitored via quantitative real-time PCR, western blot, and immunofluorescent assessment. Only cultures with consistent CD31 and VE-cadherin expression, cobblestone morphology, and non-detectable αSMA expression were used. αSMA levels were measured via real-time PCR (> 37 cycle threshold), western blot, and immunofluorescence. PAVEC and PAVIC cultures were used between passage four and six.

3-D culture system

Tissue-culture treated, sterile, polycarbonate membrane inserts (Corning, Inc., Corning, NY) were obtained in three and eight micron pore sizes and machined to a depth of 0.5mm. Membranes were coated in collagen I, 50 µg/mL (BD Biosciences, San Jose, CA) and filled with collagen gel composed of 10% FBS (Gemini

Biosciences, West Sacramento, CA), 1x Dulbecco's modified eagle medium (D-MEM, Invitrogen, Grand Island, NY), and 2 mg/mL collagen type I (BD Biosciences, San Jose, CA), adjusted to a pH of 7.2. After one hour incubation at 37°C, PAVEC were seeded at 100,000 cells/cm² and allowed to adhere overnight. Membrane system was then carefully submerged in D-MEM+10% FBS and 0.5 g/L heparin (Invitrogen, Grand Island, NY), which served as the control media for all experiments. For experiments, 30 ng/mL TNF α (Sigma Aldrich, St Louis, MO) was added to control media. Membrane system was completely submerged in either control or +TNF α media for two to six days (Figure 4.1). PAVIC gels were made as described previously [6].

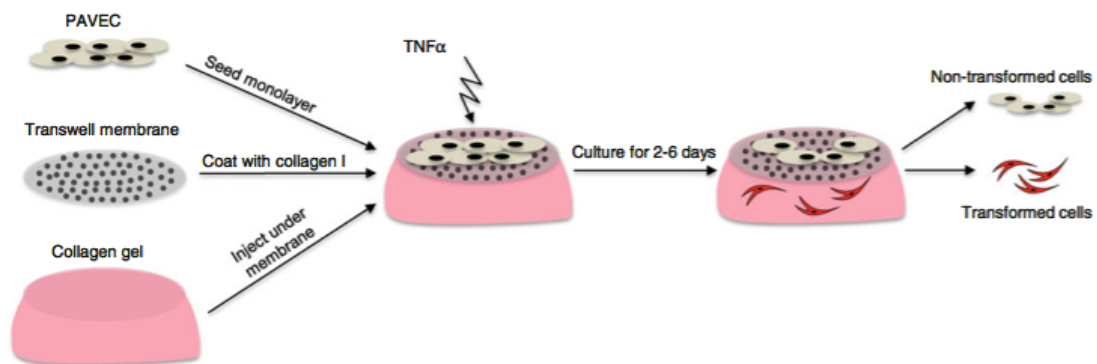


Figure 4.1 Membrane-based platform for VEC culture and evaluation of EndMT.

PAVEC are cultured on a porous membrane that rests on a type I collagen hydrogel. PAVEC are exposed to TNF α treatment for 2-6 days. A subset of PAVEC undergo an endothelial to mesenchymal transformation and a subset remains on the membrane. Cells remaining on membrane are harvested separately from cells that have migrated into the gel.

Western blot

PAVEC were grown to 70% confluency in a 75 cm² tissue culture flasks, then lysed directly on the plate using RIPA buffer supplemented with 25mM NaF, 1mM NaVO₄, and 0.5% Protease inhibitor cocktail (Sigma), incubated for 15 min at RT, scraped and homogenized by pipetting up and down, and centrifuged at 15,000 rpm for ten minutes. 10ug of protein was loaded into a 4-15% gradient gel (Bio-Rad, Hercules, CA) with 2x Laemmli buffer (Bio-Rad, Hercules, CA) at 1:1 ratio and run for one hour at 120V in 25mM Tris, 0.2M Glycine, 1% SDS running buffer. Western blot transfer to nitrocellulose membrane (Thermo Scientific, Rockford, IL) was performed at 400mA for one hour in 25mM Tris, 20% methanol transfer buffer. After rinsing in PBS 0.1% Tween-20, membrane was blocked for one hour in Odyssey Blocking Buffer (Li-Cor, Lincoln, NE) at RT. Mouse anti-human VE-cadherin (Abcam, Cambridge, MA) (1:1000), rabbit anti-human alpha-smooth muscle actin (Abcam, Cambridge, MA) (1:1000), and mouse anti-human GAPDH (Invitrogen, Grand Island, NY) (1:10,000) were used in Odyssey blocking buffer+0.1%Tween-20 to detect protein expression. The membrane was washed 4x in PBS-tween, 1x in PBS, and incubated overnight at 4°C with gentle agitation. The same washes were then performed and the membrane was incubated in Odyssey blocking buffer +0.1% Tween-20 +0.2% SDS with 1:20,000 anti-mouse and anti-goat secondary antibodies (Li-Cor IRDye, Lincoln, NE). Blots were imaged using the Odyssey Infrared system (Li-Cor, Lincoln, NE). After purity of endothelial population was confirmed, PAVEC from the same cell isolation were used in membrane system experiments.

Immunofluorescence

Intact membrane system (with cells on membrane and/or within collagen gel) was rinsed twice in PBS and fixed in 4% paraformaldehyde for one hour at 37°C. Samples were rinsed three times on a rocker with PBS for 15 minutes each, permeabilized with 0.2% Triton-X (VWR International, West Chester, PA) for ten minutes on rocker, and blocked in 10% goat serum for one hour at 37°C. Samples were rinsed briefly in PBS and primary antibodies were added: mouse anti-pig CD31 (AbD Serotec, Kidlington, UK, 1:100), rabbit anti-human α SMA (Abcam, Cambridge, MA, 1:100), rabbit anti-human Snail (Santa Cruz Biotechnology, Dallas, TX, 1:50) and AlexaFluor 488® phalloidin (Invitrogen, Grand Island, NY, 1:100). Samples were incubated overnight at 4°C, rinsed three times in PBS on rocker for 15 minutes each, and species-specific secondary antibodies raised in goat conjugated to Alexa Fluor® 488 or 568 fluorophores were added (Invitrogen, Grand Island, NY 1:100). Samples were incubated for two hours at room temperature, rinsed, then incubated for an additional 30 minutes with Draq5 nuclear stain (Enzo Life Sciences AG, Lausen, Switzerland, 1:1000). Samples were rinsed thoroughly in PBS three times on rocker for 15 minutes each, then imaged using a Zeiss 710 (Thornwood, NY) laser scanning confocal microscope. Confocal reflectance was used to image collagen fibers within the gel, collected as a separate stack but with identical spatial-resolution settings as the immunofluorescence imaging.

Quantitative real-time polymerase chain reaction

To separately isolate PAVEC remaining on the membrane from PAVEC within the collagen gel, the collagen gel was first removed from the membrane system and vortexed in RLT buffer plus 1% beta-mercaptoethanol (Qiagen, Valencia, CA) until dissolved and frozen at -80°C. The membrane was then submerged in 0.25% trypsin-EDTA for five minutes at 37°C. Three times the volume of media was added to the membrane unit to stop the trypsin reaction and any remaining cells were scraped gently from the membrane. The cell, trypsin, and media solution was then spun down at 1000rpm for five minutes at room temperature. The cell pellet was rinsed in 1x PBS, resuspended in RLT buffer plus 1% beta-mercaptoethanol, and frozen at -80°C.

Total RNA was extracted using a RNeasy total RNA purification kit (Qiagen, Valencia, CA) and RNA was reverse transcribed to cDNA using the iScript™ cDNA synthesis kit (Biorad, Hercules, CA). Quantitative real-time PCR was performed on all samples using SYBR Green PCR master mix (Applied Biosystems, Foster City, CA), and a CFX96 or MiniOpticon Real-Time PCR Detection System (Bio-Rad, Hercules, CA) (Table 4.1).

Table 4.1 Quantitative rt-PCR primers used in membrane-EndMT assays

Gene	Forward primer	Reverse primer
18S	TAGAGGGACAAGTGGCGT	AATGGGGTTCAACGGGTT
ACTA2	CAGCCAGGATGTGTGAAGAA	TCACCCCCTGATGTCTAGGA
CD31	ATCTGCATCTCGTGGGAAGT	GAGCTGAAGTGTCAGCAGGA
Snai1	GCCCAACTACAGCGAGCTAC	CCAGGAGAGACTCCCAGATG
VE-cadherin	CGTGGTGGAAACACAAGATG	TGTGTACCTGGTCTGGGTGA
MMP-9	TGGGAGTACTGGCGACTCT	ACTTGGCGTCCAGAGAAGAA
TGF- β 1	TTTCTGGTGGGGAGACAGAC	CTCCCCTAGGCTGCTTTCTT
Notch1	TGGATGGCATCAATTCCTTT	GGGCAGGTACACTTGTAGGC
BMP-4	AAAAAGTCGCCGAGATTCAG	CCGCATGTAATCTGGGATG
ICAM-1	AAAGGAGGCTCCATGAAGGT	TGCCATCGTTTTCCACATTA
VCAM-1	TTGTTGCCTCGTCACACAGC	CAATCTGCGCAATCATTTTG
NOS3	TGCATGACATTGAGAGCAAAGG	GATGGTCGAGTTGGGAGCAT

Data analysis

All experiments were performed with $n \geq 3$. Data is expressed as mean \pm standard error of the mean (SEM). All comparisons between two groups were made using two-tailed, unpaired t-tests assuming unequal variance. Comparisons between multiple groups were made using ANOVA. Differences between means were considered significant when $p < 0.05$.

4.4 Results

Culture system supports maintenance of PAVEC monolayers and collagen invasion.

Pure populations of healthy PAVEC, with confirmed expression of VE-cadherin and no α SMA (Figure 4.2A), were cultured for up to six days on either the 3mm membrane (Figure 4.2B) or the 8mm membrane (Figure 4.2C). PAVEC cultured on membranes form confluent monolayers with strong CD31 expression and cobblestone morphology (Figure 4.2D). PAVEC have no α SMA expression and do not invade the underlying gel (Figure 4.2E,F). When treated with $\text{TNF}\alpha$, a subset of PAVEC passes through the membrane and invades the underlying gel (Figure 4.2G).

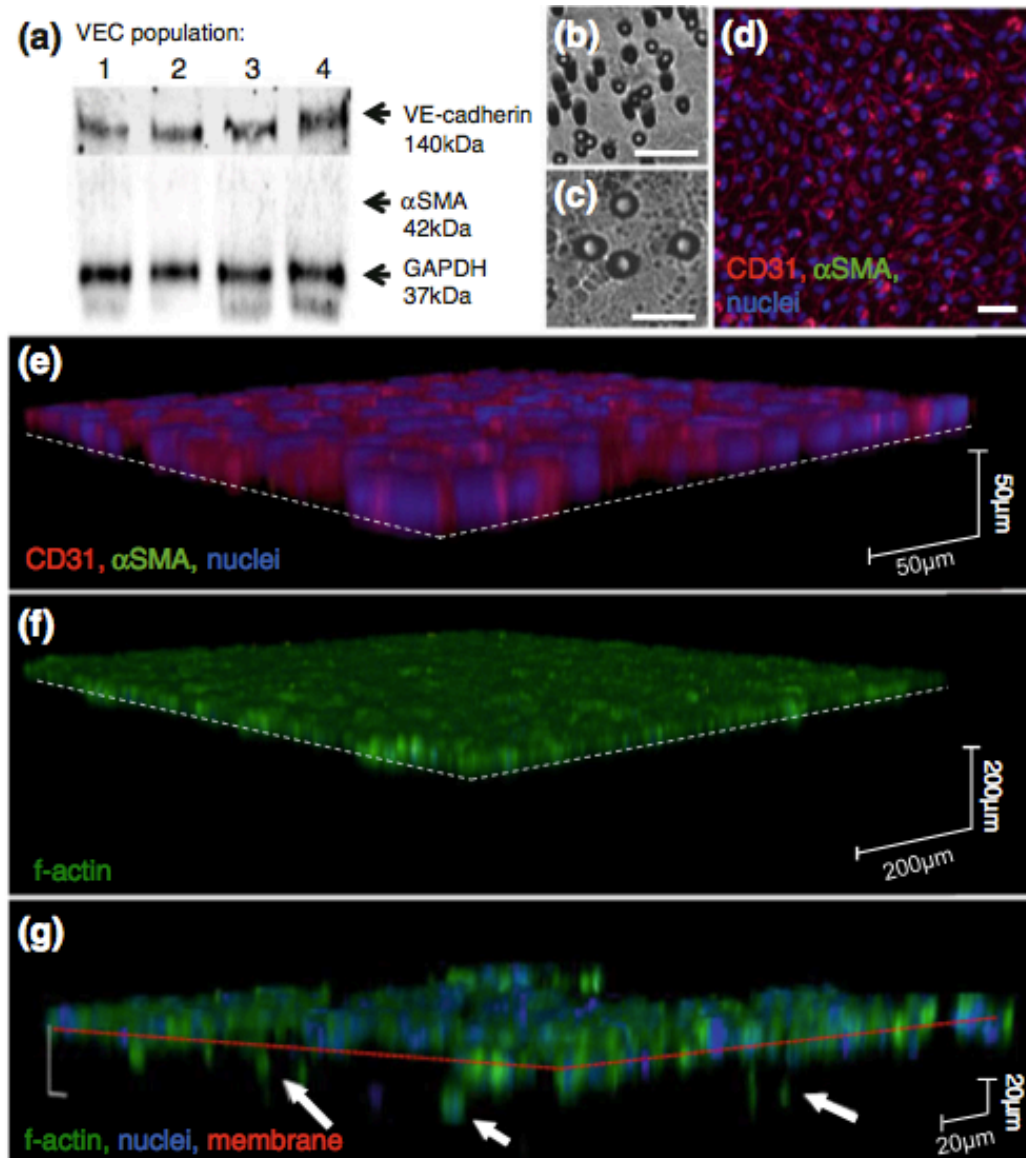


Figure 4.2 Characterization of membrane culture system and EndMT response to TNF α .

A. Western blot analysis of a random sampling of four of the populations of PAVEC used in the study. Populations of PAVEC were sampled for western blot analysis of protein content at passage three and used in experiments at passages four to six. All populations showed strong VE-cadherin expression and no α SMA expression. B, C. 3 μ m and 8 μ m membrane pores, scale bar is 20 μ m. D. PAVEC cultured on the membrane system for six days retain strong CD31 expression, no α SMA expression, and cobblestone morphology. Scale bar is 20 μ m. E, F. PAVEC cultured on the membrane system in control conditions for six days do not express α SMA and do not pass through the membrane into the hydrogel. G. After 48 hours of TNF α treatment, a subset of PAVEC invade through the membrane into the hydrogel (arrows) and a subset remains on the membrane.

We then used confocal microscopy to image PAVEC undergoing EndMT on the membrane system (Figure 4.3). Viewed from above, *en face* to the membrane surface, we observed heterogeneity in the expression of α SMA within PAVEC remaining on the membrane. All PAVEC expressed CD31 (red), but only a subset had increased α SMA expression (green, arrows) (Figure 4.3A). Using a three-dimensional reconstruction to view the system from the side, we imaged a single PAVEC passing through a membrane pore (Figure 4.3A, arrowheads; Figure 4.3B, dashed lines). The invading cell had increased α SMA (green) and decreased CD31 (red, arrow), consistent with an EndMT phenotypic shift. When the same cell field was reconstructed as a three-dimensional image (Figure 4.3C), the same invading cell was seen to be protruding into the collagen gel (arrow). Other PAVEC were also observed to be invading the gel (asterisks). A subset of PAVEC remained on the surface of the membrane (Figure 4.3B, 4.3C). These cells were variably distributed across the membrane pores (Figure 4.3A), suggesting that proximity to a pore was not the primary factor in deciding whether a cell would invade. This variation in invasion suggested that the initial population of VEC possessed variation in ability or propensity to undergo EndMT with TNF α stimulus.

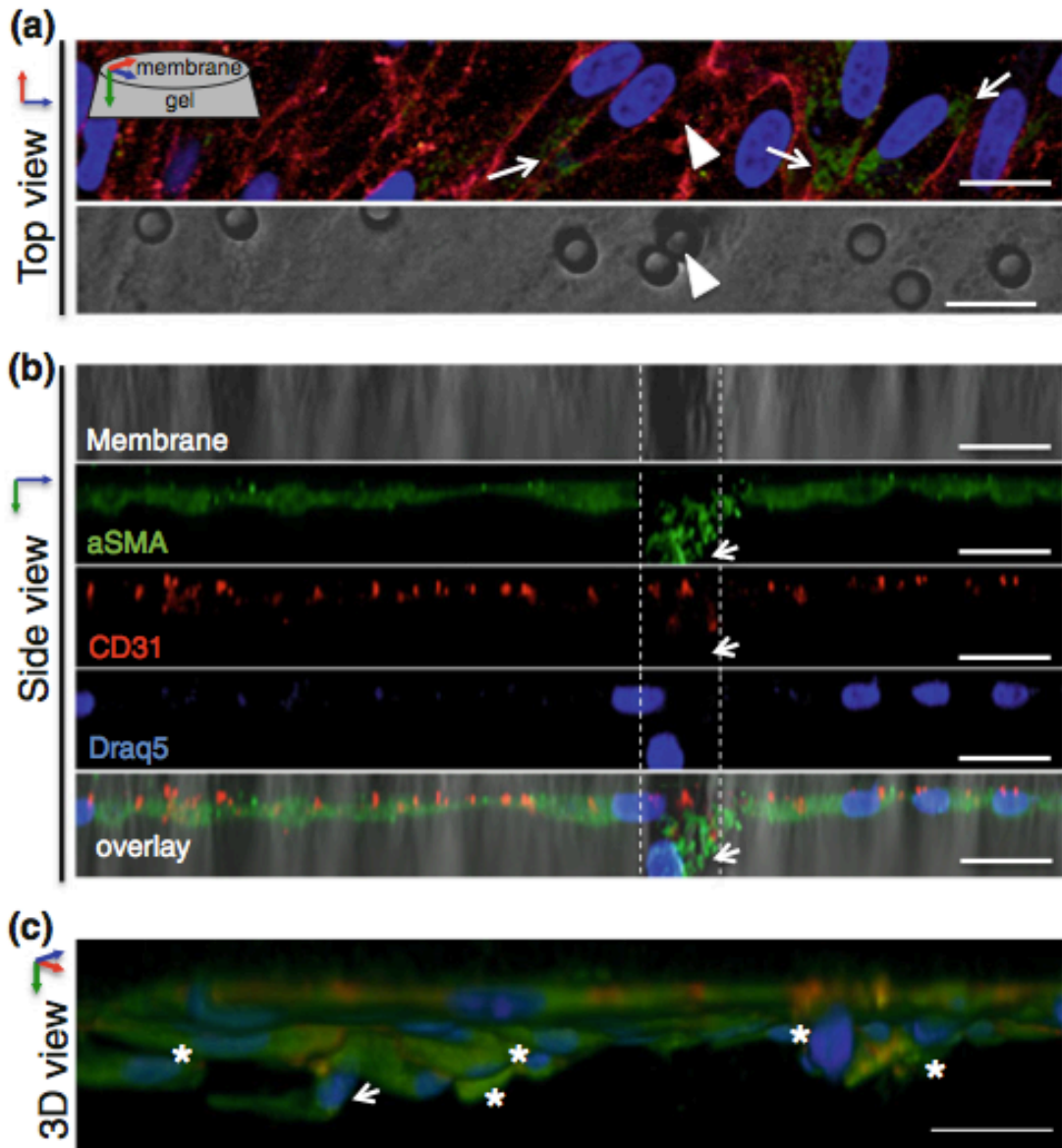


Figure 4.3 Imaging of TNF α -EndMT process.

A. Top view. After 48 hours of TNF α treatment, a subset of VEC have increased α SMA expression (arrows). In this image, a single VEC has begun to pass through a pore in the membrane (arrowhead). Lower panel shows 3 μ m membrane, arrowhead indicates the pore associated with the invading VEC. B. Side view of same cell field. Reconstruction of a high-resolution image stack of the same cell field as in A shows invasion of VEC through the pore (dashed lines). The migrating VEC has reduced CD31 and increased α SMA (arrow). C. Three-dimensional reconstruction of the same cell field as in A, B shows the same invading VEC (arrow), as well as other VEC in the same region invading through the membrane into the hydrogel (asterisks). The invading cells have increased α SMA and express CD31. Scale bar is 20 μ m.

Time-dependent dynamics of TNF α -EndMT

Using the membrane system to separate transformed PAVEC (T-VEC) from non-transformed PAVEC (NT-VEC), we characterized the EndMT phenotype of both cell populations after two, four, or six days of TNF α treatment. All treatment groups (T-VEC and NT-VEC) were compared to PAVEC cultured on the membrane for equal lengths of time in control media. There was no invasion in control groups. Using the 3 μ m pore membrane, we found that endothelial cell-cell adhesion protein VE-cadherin was increased in NT-VEC at day two (2.08 ± 0.19 fold, $p=0.01$) and remains similar to control levels through day four (0.68 ± 0.1 fold, $p=0.23$) and day six (0.82 ± 0.1 fold, $p=0.32$) (Figure 4.4A). The initial increase in VE-cadherin expression may be due to the re-organization of cell-cell contacts as subsets of PAVEC invade and NT-VEC form new attachments. The gene encoding transcription factor Snail (*Snai1*), which is associated with EMT⁷, was increased in both NT-VEC (7.6 ± 2.8 fold, $p=0.008$) and T-VEC (4.4 ± 0.2 fold, $p=0.05$) after two days of treatment, when compared to PAVEC treated with control media (Figure 4.4B). At four days, *Snai1* was decreased in NT-VEC (0.36 ± 0.04 fold, $p=0.09$) and increased in T-VEC (7.81 ± 1.5 fold, $p=0.02$). At six days, *Snai1* was decreased in NT-VEC (0.13 ± 0.01 fold) and increased in T-VEC (2.4 ± 0.9 fold, $p=0.02$). NT-VEC maintained low expression of α SMA through day two (1.05 ± 0.4 , $p=0.3$), four (0.23 ± 0.09 , $p=0.02$), and six (not detectable). However, T-VEC increased in α SMA over time, through day two (3.1 ± 1.0 fold, $p=0.1$), day four (2.13 ± 0.2 fold, $p=0.1$), and day six (15.6 ± 1.1 fold, $p=0.006$) (Figure 4.4C).

To understand the effects of pore size on the time dynamics of PAVEC TNF α -EndMT, we repeated the EndMT time-course experiments with an 8 μ m pore-size membrane. We found that the stages of EndMT were the same with the larger pores, but occurred more rapidly. NT-VEC had decreased VE-cadherin at day two (0.18 \pm 0.01 fold, p=0.0001) which could be due to re-organization of cell-cell contacts during the first phase of invasion. NT-VEC had VE-cadherin levels similar to control samples at day three (0.8 \pm 0.2 fold, p=0.3) and day four (0.8 \pm 0.06 fold, p=.07). T-VEC had increased expression of VE-cadherin at day three (5.0 \pm 1.9 fold, p=0.4), suggesting that transformed cells maintain some of their endothelial characteristics as they invade. T-VEC had decreased VE-cadherin by day four (0.1 \pm 0.1 fold, p>10⁻⁶), indicating progressive mesenchymal transformation (Figure 4.4D). NT-VEC had levels of Snai1 lower than control at day two (0.5 \pm 0.02 fold, p=0.02), and similar to control at day three (2.0 \pm 0.5 fold, p=0.15) and day four (1.1 \pm 0.01 fold, p=0.3). Snai1 expression was increased in T-VEC at day three (22.5 \pm 3.2 fold, p< 10⁻³) and returned to control levels by day four (Figure 4.4E). Absence of an upregulation in Snai1 in NT-VEC could be attributed to the larger pore size, which allows EndMT cells to undergo full mesenchymal transformation more rapidly. Thus, Snai1 increase may occur prior to the two-day time-point. NT-VEC had α SMA levels similar to control. T-VEC had low levels of α SMA at day two (0.01 \pm 0.003 fold, p=0.4) and day three (0.8 \pm 0.5 fold, p=0.03). T-VEC had increased α SMA at four days after treatment (14.8 \pm 2.5 fold, p< 10⁻⁴), rather than the six days required for increased α SMA in the 3 μ m system (Figure 4.4F). These results suggest that a larger pore size does not affect

the mechanism of progression of TNF α -EndMT in PAVEC, but allows the process to occur more rapidly.

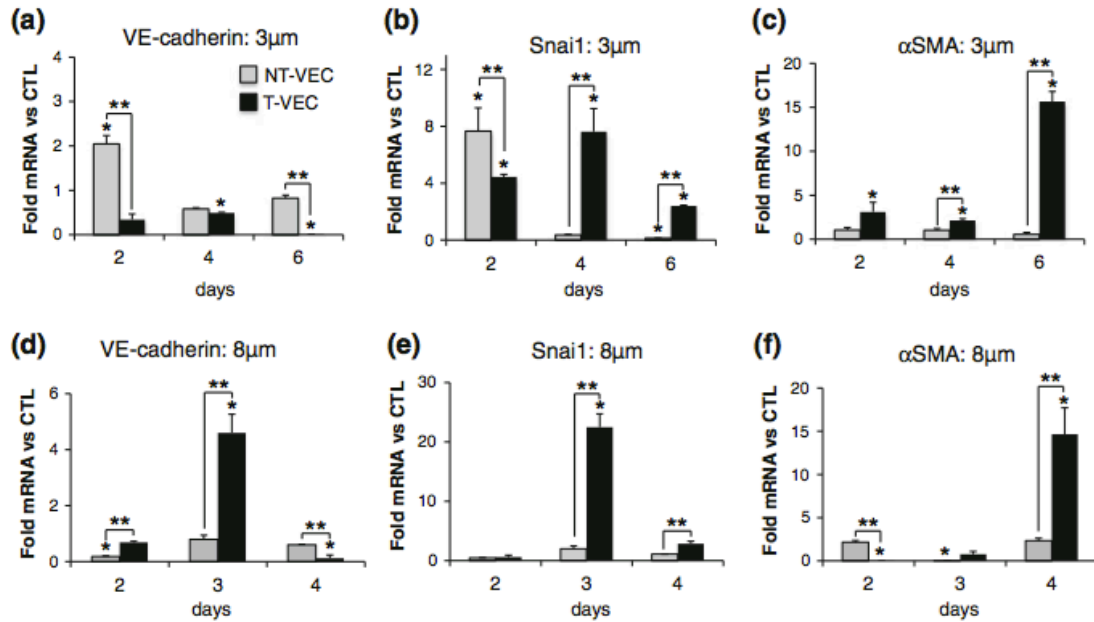


Figure 4.4 Time-dependent expression of EndMT genes in VEC treated with TNF α .

A-C, 3 μ m pore membrane. A. VE-cadherin expression was initially increased in NT-VEC and returned to control levels at day four and six. VE-cadherin decreased in the T-VEC population over time. B. Snai1 expression was elevated initially in both VEC populations. At day four, Snai1 decreased in NT-VEC to less than control and remained elevated in T-VEC until day six. C. α SMA expression was low in NT-VEC and increased in T-VEC. D-F, 8 μ m pore membrane. D. VE-cadherin expression was decreased in VEC remaining on membrane. Transformed VEC had elevated VE-cadherin expression on day three of treatment that is decreased by day four. E. Transformed VEC had elevated Snai1 expression after three days of treatment. F. Transformed VEC had highly elevated α SMA expression after four days of TNF α treatment. VEC remaining on membrane maintained α SMA levels similar to control (> 37 cycles). All experiments performed with n > 3. Errors bars indicate SEM. * indicates p < 0.05 versus control VEC at same time point; ** indicates p < 0.05 versus indicated group, according to ANOVA followed by Student's t-test.

EndMT protein expression in transforming valve endothelial cells

To confirm the changes in gene expression and time dynamics of EndMT observed in the membrane system, we analyzed expression and localization of CD31, Snail, and

α SMA proteins in NT-VEC and T-VEC across two, four, and six days of treatment on the 3 μ m pore membrane. NT-VEC had initial increases in Snail expression and nuclear localization at day two, which was decreased at day four and six. NT-VEC consistently expressed membranous CD31, an endothelial marker (Figure 4.5A). T-VEC co-expressed CD31 and α SMA at day two, with increasing α SMA at day four and day six (Figure 4.5B). CD31 expression decreased at day six, but was still observable at some cell-cell junctions.

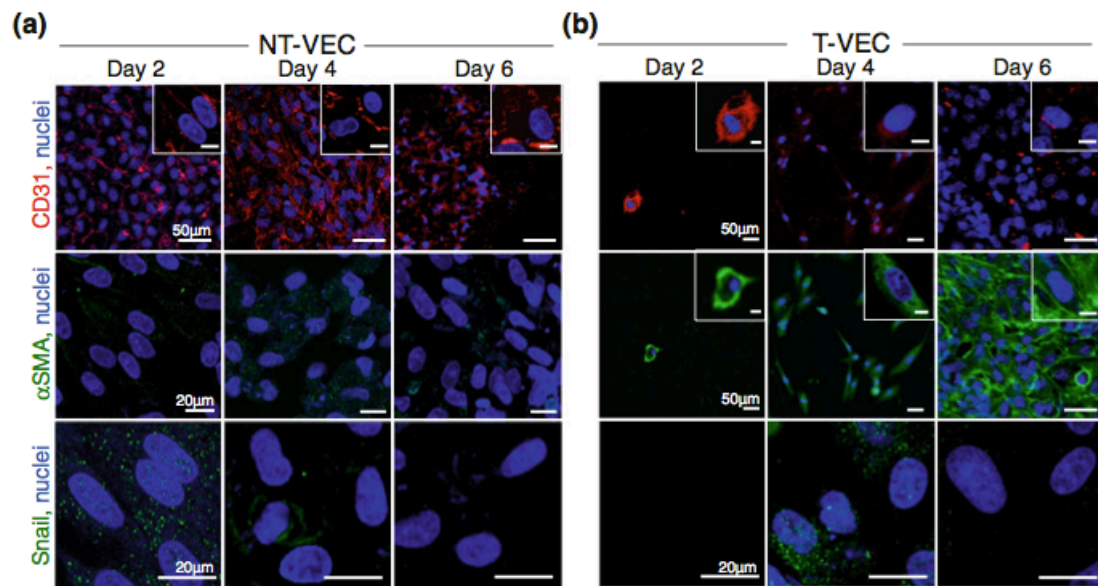


Figure 4.5 Expression of EndMT proteins in non-transformed and transformed cells.

A. CD31, Snail, and α SMA expression in non-transformed VEC (NT-VEC) after 2, 4, and 6 days of TNF α treatment. B. CD31, Snail, and α SMA expression in transformed VEC (T-VEC) after 2, 4, and 6 days of TNF α treatment. Images are representative of > 3 independent experiments. Scale bar length is indicated in leftmost panel of each row. Scale bar of inset images is 10 μ m.

Characterization of transformed valve endothelial cells

We then used the membrane system to characterize expression of genes related to valve disease in both NT-VEC and T-VEC. We compared NT-VEC and T-VEC with

untreated VEC controls, with porcine aortic valve interstitial cells (VIC) embedded in the collagen gel with no treatment, and with embedded VIC treated with TNF α . Control VEC (0.05 \pm 0.02 fold, p=0.03) and NT-VEC (not detected) had very low levels of MMP-9 compared to control VIC. T-VEC, however, had very high levels of MMP-9 (250 \pm 43 fold, p=0.0002) compared to control VIC (Figure 4.6A). VIC+TNF α also had elevated MMP-9 (3.0 \pm 0.24 fold, p=0.043) compared to control VIC. TGF- β 1 was increased in T-VEC (6.9 \pm 1.5 fold, p=0.009) and VIC+TNF α (6.1 \pm 1.0 fold, p=0.002) compared to control VIC (Figure 4.6B). Notch1 was increased in control VEC (3.78 \pm 0.24 fold, p=0.002), T-VEC (75.8 \pm 4.7 fold, p=0.003), and VIC+TNF α (4.1 \pm 0.4 fold, p=0.0009) compared to control VIC. NT-VEC (1.39 \pm 0.04 fold, p=0.09) had similar levels of Notch1 as control VIC (Figure 4.6C). BMP-4 was increased in control VEC (6.98 \pm 0.6 fold, p=0.002), T-VEC (38.84 \pm 0.4 fold, p=0.006), and VIC+TNF α (3.63 \pm 1.1 fold, p=0.05) compared to control VIC (Figure 4.6D). NT-VEC (0.78 \pm 0.13, p=0.34) had similar levels of BMP-4 as control VIC.

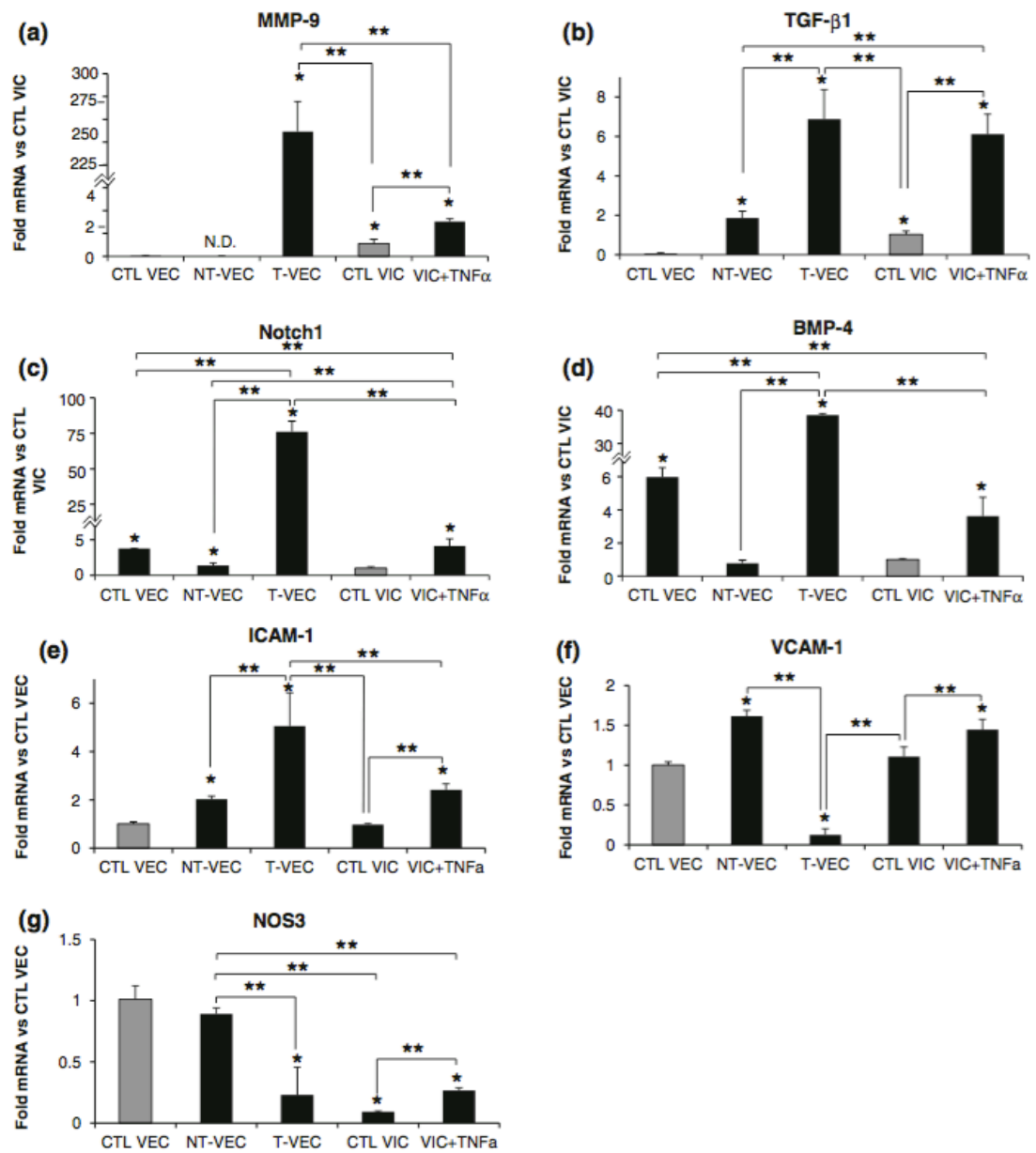
We also examined expression of inflammatory adhesion molecules ICAM-1 and VCAM-1 in all groups compared to control VEC. ICAM-1 was increased in NT-VEC (2.0 \pm 0.2 fold, p=0.009), T-VEC (5.05 \pm 1.9 fold, p=0.05), and VIC+TNF α (2.4 \pm 0.4 fold, p=0.004) compared to control VEC (Figure 4.6E). Control VIC had similar levels of ICAM-1 as control VEC (0.97 \pm 0.04 fold, p=0.79). VCAM-1 was increased in NT-VEC (1.6 \pm 0.1 fold, p=0.009) and VIC+TNF α (1.4 \pm 0.2 fold, p=0.047) compared to control VEC. Control VIC had similar levels of VCAM-1 as control VEC (1.1 \pm 0.12, p=0.49)(Figure 4.6F). Finally, we quantified levels of the gene encoding endothelial

nitric oxide synthase (eNOS), NOS3, across groups compared to control VEC as a further examination of endothelial phenotype. NT-VEC had similar levels of NOS3 as control VEC (0.9 ± 0.09 fold, $p=0.42$), while T-VEC (0.23 ± 0.4 , $p=0.16$), control VIC (0.09 ± 0.01 fold, $p < 10^{-3}$), and VIC+TNF α (0.27 ± 0.04 fold, $p=10^{-3}$) had decreased levels of NOS3 compared to control VEC (Figure 4.6G).

Figure 4.6 Comparison of genes in transformed and non-transformed VEC.

A-D. All samples normalized to control VIC, isolated from membrane system or VIC hydrogels after two days of treatment. A. MMP-9 was elevated in T-VEC and VIC+TNF α but not in control VEC or NT-VEC. B. TGF- β 1 was elevated in T-VEC and VIC+TNF α , at control levels in NT-VEC and decreased in control VEC, compared to control VIC. C. Notch1 was higher in control VEC, T-VEC, and VIC+TNF α compared to control VIC. NT-VEC had Notch1 levels similar to control VIC. D. BMP4 expression was higher in control VEC, T-VEC, and VIC+TNF α than in control VIC. NT-VEC had BMP4 levels similar to control VIC.

E-G. All samples normalized to control VEC, isolated from membrane system or VIC hydrogel after two days of treatment. E. ICAM-1 levels were similar in control VEC and control VIC. NT-VEC, T-VEC, and VIC+TNF α had elevated ICAM-1 levels, with T-VEC having the highest expression. F. VCAM-1 levels were similar in control VEC and control VIC. NT-VEC and VIC+TNF α had elevated VCAM-1 levels and T-VEC had decreased VCAM-1 compared to control VEC. G. NOS3 levels were similar in control VEC and NT-VEC. NOS3 levels were lower in T-VEC, control VIC, and VIC+TNF α compared to control VEC. All experiments performed with $n > 3$. Errors bars indicate SEM. * indicates $p < 0.05$ versus control; ** indicates $p < 0.05$ versus indicated group, according to ANOVA followed by Student's t-test. VCAM-1 indicates vascular cell adhesion protein 1; ICAM-1, intercellular adhesion molecule 1.



Transformed valve endothelial cells rearrange collagen extracellular matrix.

Lastly, we further characterized the phenotype of T-VEC by assessing the arrangement of collagen fibers in gels containing T-VEC versus gels with control VEC or VIC. Control VEC cultured directly on collagen gels did not affect the arrangement of collagen fibers (Figure 4.7A). In contrast, collagen fibers in the region of T-VEC were elongated and aligned with the long axes of the transformed cells (Figure 4.7B, dashed double arrows). VIC embedded in an identical collagen gel did not affect collagen fiber alignment (Figure 4.7C). Similar to the control VEC condition, the fibers in the VIC gels were short and randomly oriented. The ability of T-VEC to interact with the collagen gel suggests that T-VEC may be able to play a role in affecting the changes in extracellular matrix seen in AVD [10].

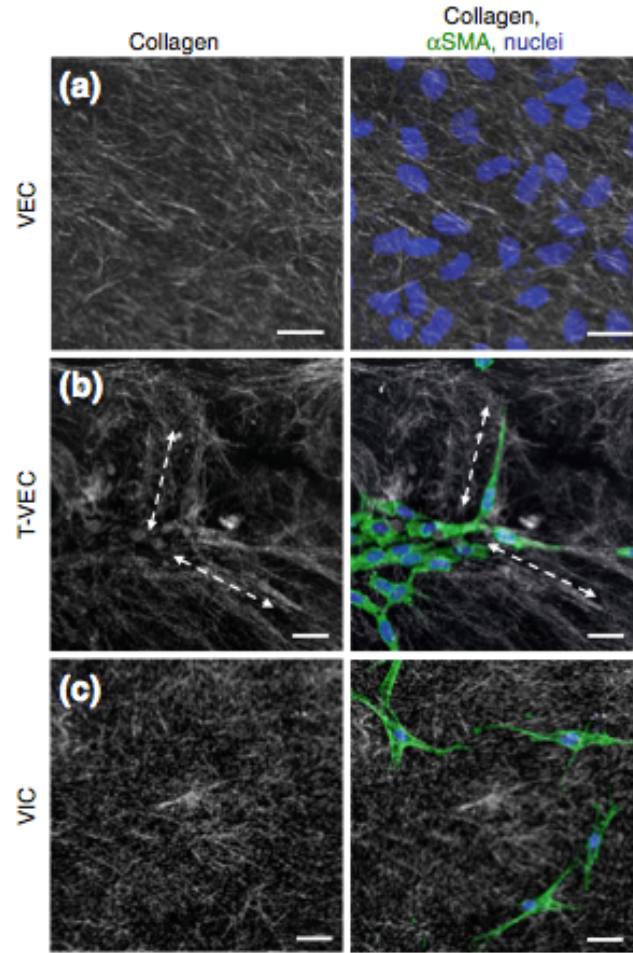


Figure 4.7 Collagen fibers surrounding transformed and non-transformed VEC.

A. Collagen fibers in control gels (left panel) have random alignment and length. Control VEC seeded on the surface of a control gel did not change the alignment of collagen fibers (right). B. Collagen gels with invaded T-VEC, isolated as a whole gel from the membrane system and fixed immediately, had long collagen fibers (dashed lines) that were aligned with the long axis of T-VEC. C. Collagen gels with embedded valve interstitial cells had random alignment and length (left), not aligned with embedded VIC (right). Green = f-actin; representative images of n=4 experiments.

4.5 Discussion

A greater understanding of the heterogeneity, time-dependence and pathogenic role of valve endothelial cells undergoing mesenchymal transformation is necessary to connect EndMT pathophysiology with the treatment of aortic valve disease. Here we

have utilized a novel *in vitro* system to characterize TNF α -induced EndMT in aortic valve endothelial cells. We identified a population of non-transforming aortic valve endothelial cells that resists TNF α -EndMT and retains an endothelial phenotype, and a population of transformed cells that acquires a mesenchymal and pro-disease phenotype with TNF α treatment.

Previous studies have employed clonal isolation systems to study and assess the ability of certain subgroups of VEC to undergo EndMT [3, 4, 26, 32, 33]. The use of primary cells cultured together on the membrane system described here is advantageous because it allows cell-cell communication between transforming and non-transforming cells, as would occur *in vivo*. Additionally, it is possible to separate transforming from non-transforming cells, post-EndMT. The advantages of the cell-cell communication allowed in this system can be expanded by using a location-specific isolation of VEC such as those near the valve commissures that have shown increased inflammation in early disease [1], or a side-specific isolation. These further studies would capitalize on the ability to culture a heterogeneous population of cells while narrowing the window of examination.

The three-dimensional nature of this system has the advantage of allowing a more physiological mesenchymal transformation than traditional two-dimensional EndMT assays. An endothelial cell that has undergone full mesenchymal transformation will not only change morphology and phenotype, but will invade its underlying substrate and develop complex mechanisms of interaction with its three-dimensional

extracellular environment [22]. This system allows full invasion of VEC undergoing EndMT into a more physiological environment of collagen hydrogel. Allowing matrix invasion makes assessment of traits such as matrix interactions and matrix metalloproteinase expression in transformed and non-transformed VEC possible. The results of this study suggest that VEC cultured on the membrane undergoing TNF α -stimulated EndMT invade the matrix to the same extent as VEC cultured directly on the hydrogel [24] (data not shown), despite the difference in stiffness between each surface. An assessment of the effect of the difference in stiffness between membrane and hydrogel could be easily conducted using membranes of different materials with different mechanical properties. The membrane used here can be adjusted via modulation of pore size, hydrogel composition, and membrane coating substrate.

Beyond developing a system for assessment of transforming and non-transforming VEC undergoing EndMT, we have evaluated the dynamics of this process in the initial response of VEC to TNF α . Our results show that inflammatory EndMT is a complex phenomenon with the potential to contribute to various elements of early valve disease. Mesenchymal transformation could contribute to a fraction of the endothelial denudation observed in diseased valves, linking inflammatory activation of the endothelium [17] to endothelial loss during the calcification stage [15].

Unraveling the time dynamics of EndMT in the valve is key in understanding the role of certain biological actors known to play complex parts in the progression of valve disease. For example, TGF- β is known to have both protective [23] and detrimental

effects [31] in the aortic valve. These complex and seemingly opposing responses can be elucidated via this membrane system, which separates VEC as they transform or resist transformation, elucidating the time-dependency of each event. Further complexity could be assessed via addition of co-cultured valvular interstitial cells to the hydrogel component. Finally, the system can be used to screen anti-EndMT therapies (such as in the context of cancer or fibrosis) [11, 19] in a stage-dependent manner.

The fate of adult VEC undergoing EndMT is unclear. This study provides initial evidence that T-VEC may be participants in some of the early mechanisms of AVD, through increased expression of MMP-9, TGF- β 1, Notch1, and BMP4, as well as via collagen remodeling (Figure 4.8). MMP-9 is expressed in stenotic but not healthy aortic valves [9], linking increased MMP-9 and T-VEC collagen remodeling to the changes in extracellular matrix organization observed in early valve disease. We note that remodeling of a collagen hydrogel is not the same as T-VEC affecting the complex ECM composition of a native valve, but their aggressive invasive phenotype and distinct effects on collagen fiber alignment suggest that they have increased ability to affect their extracellular environment. TGF- β 1 is known to be regulated by TNF α and is implicated in accelerating calcification of aortic valve interstitial cells [21, 25]. T-VEC in this study had increased TGF- β 1 mRNA, whereas NT-VEC had levels comparable to quiescent VIC. T-VEC may contribute to levels of TGF- β 1 in the diseased aortic valve, accelerating calcification of native VIC. Notch1 initiates EndMT in the developing valve [8] and in postnatal aortic VEC [33]. Notch1 was

increased in T-VEC, agreeing with a link to valve EndMT. Interestingly, levels of Notch1 in NT-VEC were comparable to VIC controls and lower than control VEC, suggesting that they may have a decreased EndMT potential or a native predisposition against EndMT. Future studies are needed to assess whether Notch1 levels in T-VEC could be repressed over longer time-scales, as has been shown in animal models of aortic valve calcification. BMP-4 mediates endothelial inflammatory activation [30], promotes vascular calcification [5], and initiates EndMT in valvulogenesis [20]. BMP4 antagonists are repressed in CAVD [2]. BMP-4 was decreased in NT-VEC, agreeing with a quiescent or protective role for these cells in valve disease. BMP-4 was increased in T-VEC, which could contribute both to a continued EndMT-activation paradigm and to acceleration of calcification. Sustained activation of inflammatory adhesion molecules ICAM-1 and VCAM-1 in NT-VEC suggests that the population of VEC that resists transformation under TNF α treatment is able to maintain an inflammatory phenotype while not undergoing an EndMT response. This result, coupled with the sustained endothelial phenotype of these cells as evidenced by maintaining control levels of VE-cadherin and endothelial nitric oxide synthase, suggest that this population of cells may possess a distinct molecular signature which protects against some of the detrimental effects of inflammation.

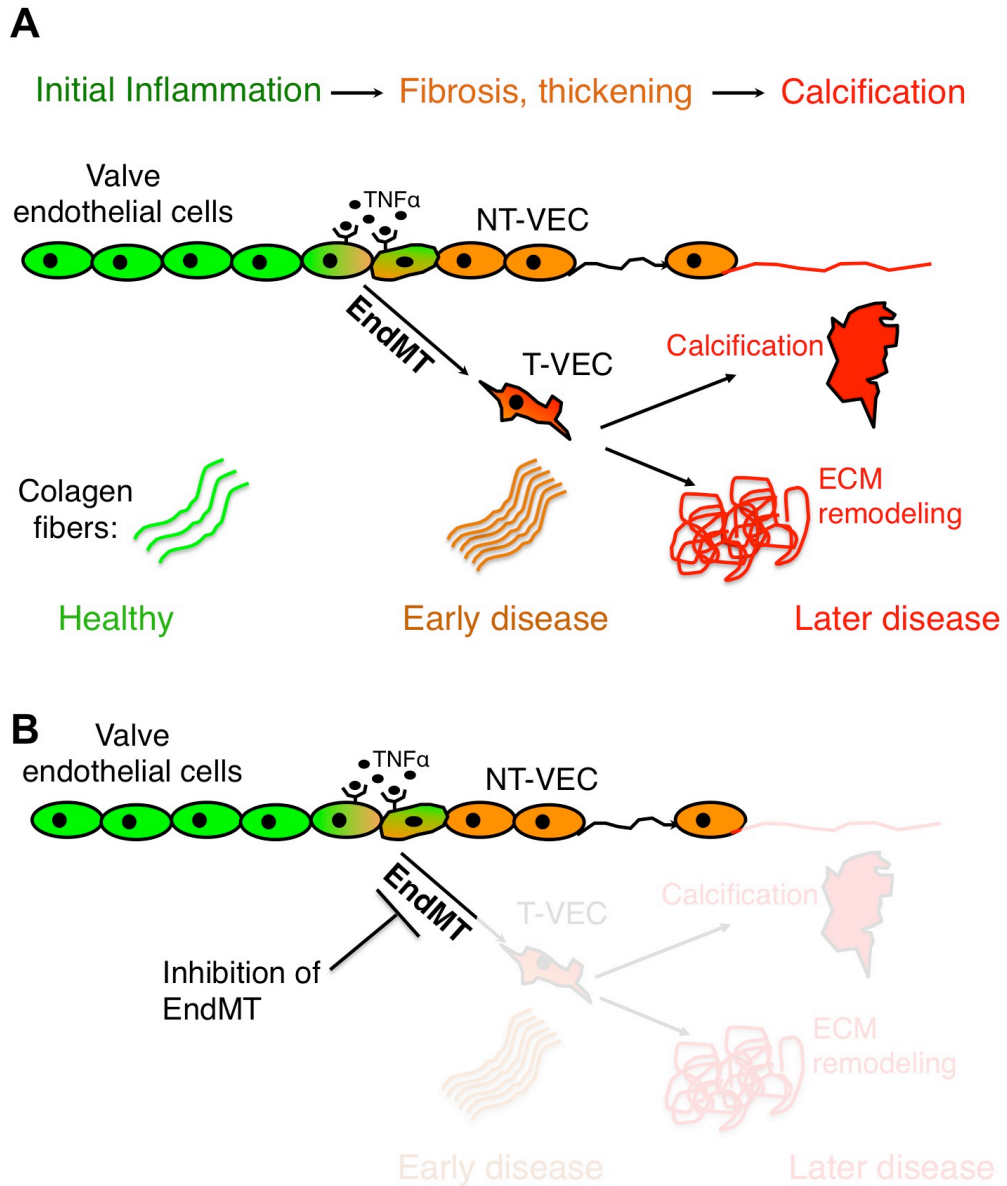


Figure 4.8. Transformed (T-VEC) and non-transformed (NT-VEC) endothelial cells in aortic valve disease.

A. T-VEC that have undergone EndMT as a result of TNF α contribute to valve disease via gain of a pro-calcific phenotype and by their disorganization of their collagen fiber environment. B. Inhibition of EndMT would result in preservation of the NT-VEC population, which could preserve the valve against degeneration by secretion of nitric oxide, barrier against invading cells, and regulation of mechanical function.

This study is an initial investigation of the differences in aortic valve endothelial response to TNF α , specifically regarding the EndMT response mechanism. The *in vitro* nature of the study makes it well suited for separating distinct cell populations and characterizing their time-dependent response to treatment. We recognize that TNF α treatment represents one facet of early aortic valve disease and the EndMT response is a single component of a complex pathological phenomenon. In addition, our method of harvesting cells from across the entire surface of the porcine aortic valve, rather than in a side-specific manner, does offer continuing avenues of exploration in terms of identifying whether transforming VEC come preferentially from certain regions of the aortic valve surface or whether tendency to transform is effected from extracellular phenomenon such as shear stress or strain. These elements could easily be incorporated into the system described in this study, with the same benefits of ability to separate distinct populations and allow fully three-dimensional invasion and matrix interactions. Overall, the three-dimensional nature of the system, the molecular signatures identified between transforming and non-transforming populations, and the amenability of the technique to increasing levels of complexity across time, cell type, and endpoint analysis lays an important foundation for understanding the role of EndMT in valve disease progression.

4.6 Conclusion

In the present study, we have designed a system that allows for highly specified characterization of EndMT dynamics. We have built upon previous studies to validate

the ability of the system to allow healthy endothelial cells treated with TNF α to undergo the full phenotypic shift characteristic of EndMT, including repression of endothelial proteins, upregulation of mesenchymal proteins, and invasion into a three-dimensional collagen hydrogel environment. We have shown that the subset of VEC which undergo TNF α -EndMT may have unique abilities to contribute to the earliest stages of AVD via collagen remodeling and increased MMP-9, TGF- β 1, Notch1, and BMP-4 expression. The subset of VEC which resists TNF α -EndMT is shown to express inflammatory adhesion proteins, yet retain endothelial characteristics such as VE-cadherin, CD31, and endothelial nitric oxide synthase expression. The results of this study provide an important baseline for isolation and characterization of VEC, which have undergone postnatal EndMT. We have shown for the first time that transformed valve endothelial cells have a phenotype which suggests they could contribute to advanced AVD, that there exists a subpopulation of valve endothelial cells with resistance to TNF α -EndMT, and designed a system which can be used for investigation of EndMT dynamics across physiological contexts.

REFERENCES

1. Aikawa E, Nahrendorf M, Sosnovik D, Lok VM, Jaffer FA, et al. (2007) Multimodality molecular imaging identifies proteolytic and osteogenic activities in early aortic valve disease. *Circulation* 115:377–386.
2. Ankeny RF, Thourani VH, Weiss D, Vega JD, Taylor WR, Nerem RM, et al. (2011) Preferential activation of SMAD1/5/8 on the fibrosa endothelium in calcified human aortic valves: association with low BMP antagonists and SMAD6. *PLoS ONE* 6:e20969.
3. Balachandran KP, Alford P, Wylie-Sears J, Goss JA, Grosberg A, Bischoff J, et al. (2011) Cyclic strain induces dual-mode endothelial- mesenchymal transformation of the cardiac valve. *Proc Natl Acad Sci USA* 108:19943–8.
4. Bischoff J, and Aikawa E. (2011) Progenitor cells confer plasticity to cardiac valve endothelium. *J Cardiovasc Trans Res* 4:710–719.
5. Boström K, Watson KE, Horn S, Wortham C, Herman IM, and Demer LL. (1993) Bone morphogenetic protein expression in human atherosclerotic lesions. *J Clin Invest* 91:1800–1809.
6. Butcher JT and Nerem RM. (2006) Valvular endothelial cells regulate the phenotype of interstitial cells in co-culture: Effects of steady shear stress. *Tissue Eng.* 12:905–915.
7. Cano A, Pérez-Moreno MA, Rodrigo I, Locascio A, Blanco MJ, del Barrio MG, et al. (2000) The transcription factor Snail controls epithelial–mesenchymal transitions by repressing E-cadherin expression. *Nat Cell Biol* 2:76–83.
8. Chang ACY, Fu Y, Garside VC, Niessen K, Chang L, Fuller M, et al. (2011) Notch initiates the endothelial-to-mesenchymal transition in the atrioventricular canal through autocrine activation of soluble guanylyl cyclase. *Dev Cell* 21:288–300.
9. Edep ME, Shirani J, Wolf P, and Brown DL. (2000) Matrix metalloproteinase expression in nonrheumatic aortic stenosis. *Cardiovasc Pathol* 9:281–286.

10. Fondard O, Detaint D, Lung B, Choqueux C, Adle-Biassette H, Jarraya M, et al. (2005) Extracellular matrix remodeling in human aortic valve disease: The role of matrix metalloproteinases and their tissue inhibitors. *Eur Heart J* 26:1333–1341.
11. Galichon P and Hertig A. (2011) Epithelial to mesenchymal transition as a biomarker in renal fibrosis: are we ready for the bedside? *Fibrog Tissue Repair* 4:11.
12. Garg V, Muth AN, Ransom JF, Schluterman MK, Barnes R, King IN, et al. (2005) Mutations in NOTCH1 Cause Aortic Valve Disease. *Nature* 437:270-274.
13. Ghaisas N, Foley J, O'Briain D, Crean P, Kelleher D, and Walsh M. (2000) Adhesion molecules in nonrheumatic aortic valve disease: Endothelial expression, serum levels and effects of valve replacement. *J Am Coll Cardiol* 36:2257–2262.
14. Go AS, Mozaffarian D, Roger VL, Benjamin EJ, Berry JD, Borden WB, et al. (2013) Heart disease and stroke statistics--2013 Update: A report from the American Heart Association. *Circulation* 127:e6–e245.
15. Goldberg SH, Elmariah S, Miller MA, and Fuster V. (2007) Insights into degenerative aortic valve disease. *J Am Coll Cardiol* 50:1205-1230.
16. Gould RA and Butcher JT. (2010) Isolation of Valvular Endothelial Cells. *J Visualized Exp* 46:1–5.
17. Guerraty MA, Grant GR, Karanian JW, Chiesa OA, Pritchard WF, and Davies PF. (2010) Hypercholesterolemia induces side-specific phenotypic changes and peroxisome proliferator-activated receptor- pathway activation in swine aortic valve endothelium. *Arterioscler Thromb Vasc Biol* 30:225–231.
18. Hjortnaes JJ, Butcher JT, Figueiredo JL, Riccio M, Kohler RH, Kozloff KM, et al. (2010) Arterial and aortic valve calcification inversely correlates with osteoporotic bone remodelling: a role for inflammation. *Eur Heart J* 31:1975–1984.
19. Hollier BG, Tinnirello AA, Werden SJ, Evans SW, Taube JH, Sarkar TR, et al. (2013) FOXC2 expression links epithelial-mesenchymal transition and stem cell properties in breast cancer. *Cancer Res* 73:1981–1992.

20. Jia Q, McDill BW, Li SZ, Deng C, Chang CP, and Chen F. (2007) Smad signaling in the neural crest regulates cardiac outflow tract remodeling through cell autonomous and non-cell autonomous effects. *Dev Biol* 311:172–184.
21. Jian B, Narula N, Li Q, Mohler E, and Levy R. (2003) Progression of aortic valve stenosis: TGF-beta 1 is present in calcified aortic valve cusps and promotes aortic valve interstitial cell calcification via apoptosis. *Ann Thorac Surg* 75:457–465.
22. Kalluri R and Weinberg RA (2009) The basics of epithelial-mesenchymal transition. *J Clin Invest* 119:1420–1428.
23. Liu AC and Gotlieb AI. (2008) Transforming growth factor- β regulates in vitro heart valve repair by activated valve interstitial cells. *Am J Pathol* 173:1275–1285.
24. Mahler GJ, Farrar EJ, and Butcher JT. (2013) Inflammatory Cytokines Promote Mesenchymal Transformation in Embryonic and Adult Valve Endothelial Cells. *Arterioscler Thromb Vasc Biol* 33:121–130.
25. Mohler ER, Chawla Mk, Chang AW, Vyavahare N, Levy RJ, Graham L, et al. (1999) Identification and characterization of calcifying valve cells from human and canine aortic valves. *J Heart Valve Dis* 8:254–260.
26. Paranya G, Vineberg S, Dvorin E, Kaushal S, Roth SJ, Rabkin E, et al. (2001) Aortic valve endothelial cells undergo transforming growth factor-beta-mediated and non-transforming growth factor-beta-mediated transdifferentiation in vitro. *Am J Pathol* 159:1335–1343.
27. Richards J, El-Hamamsy I, Chen S, Sarang Z, Sarathchandra P, Yacoub MH, et al. (2013) Side-specific endothelial-dependent regulation of aortic valve calcification: Interplay of hemodynamics and nitric oxide signaling. *Am J Pathol* 182:1922-1931.
28. Simmons CA, Grant GR, Manduchi E, and Davies PF. (2005) Spatial heterogeneity of endothelial phenotypes correlates with side-specific vulnerability to calcification in normal porcine aortic valves. *Circulation Res* 96:792–799.
29. Stewart WJ and Carabello BA. (2006) Aortic Valve Disease. In: *Textbook of Cardiovascular Medicine*, edited by Topol EJ, Califf RM, Prystowsky EN, Thomas

JD, and Thompson PD. Philadelphia, PA: Lippincott Williams, & Wilkins, pp. 366–388.

30. Sucaskey P, Balachandran K, Elhammali A, Jo H, and Yoganathan AP. (2009) Altered shear stress stimulates upregulation of endothelial VCAM-1 and ICAM-1 in a BMP-4–and TGF- β 1–dependent pathway. *Arterioscler Thromb Vasc Biol* 29:254–260.

31. Walker GA, Masters KS, Shah DN, Anseth KS, and Leinwand LA. (2004) Valvular myofibroblast activation by transforming growth factor-beta: Implications for pathological extracellular matrix remodeling in heart valve disease. *Circulation Res* 95:253–260.

32. Wylie-Sears J, Aikawa E, Levine RA, Yang JH, and Bischoff J. (2011) Mitral valve endothelial cells with osteogenic differentiation potential. *Arterioscler Thromb Vasc Biol* 31:598–607.

33. Yang JH, Wylie-Sears J, and Bischoff J. (2008) Opposing actions of Notch1 and VEGF in post-natal cardiac valve endothelial cells. *Biochem Biophys Res Commun* 374:512–516.

CHAPTER 5

NFKB REGULATES ENDOTHELIAL TO MESENCHYMAL TRANSFORMATION AND SUSCEPTIBILITY TO CALCIFICATION IN THE AORTIC VALVE

The data in Figure 5.4C, D and Figure 5.5B were collected by Kevin S. Hsu

5.1 Abstract

Aims

Inflammation is a known feature of aortic valve disease, but its role in driving valve degeneration is not well understood. NF κ B (p65) signaling governs many inflammatory and osteogenic pathways and may link inflammation with aortic valve calcification.

Methods & Results

We used valve-specific deletion of IKK β and LDL receptor knock-out to create a mouse model of aortic valve degeneration with NF κ B inactivation in the aortic valve. These mice were protected against aortic valve endothelial inflammatory activation, leaflet thickening, transvalvular velocity increase, calcification, and collagen accumulation compared to age-matched LDLR^{-/-} mice. Three-dimensional porcine aortic valve cell culture with p65-specific over-expression and inhibition experiments were used to show that NF κ B p65 regulates endothelial to mesenchymal transformation and calcification of both endothelial and interstitial cells.

Conclusions

NF κ B signaling regulates key inflammatory and calcification mechanisms in aortic valve disease, both *in vitro* and *in vivo*. Targeting NF κ B presents a new option for therapeutic intervention in valve degeneration.

5.2 Introduction

Nuclear factor kappa-light-chain-enhancer of activated B cells (NF κ B) is a family of transcription factors that is present in most animal cell types. It can regulate cell response to stress, inflammation, DNA damage, viral attack, and free radicals by triggering transcription of a wide range of genes controlling cell proliferation, survival, immune response, and differentiation. It belongs to a specific family of “rapid-acting” transcription factors because it is continually present in the cytoplasm in its inactive state and therefore is readily activated and translocated to the nucleus upon stimuli.

There are five NF κ B proteins, each with a different subset of transcriptional targets: RelA, RelB, c-Rel, NF κ B1 (p105/p50), and NF κ B2 (p100/p52). All five share a Rel homology domain; only NF κ B1 and NF κ B2 have an additional region of ankyrin repeats which mediate protein-protein interactions, including cytoplasmic binding of I κ B's (rev: [1]). NF κ B levels are tightly regulated by an auto-feedback mechanism in which NF κ B triggers transcription of I κ B α , which then acts to sequester NF κ B in the cytoplasm. This results in a characteristic oscillatory activation as NF κ B is released and sequestered [2]. IKK β is a kinase that phosphorylates the inhibitor of kappa B (I κ B). I κ B binds NF κ B in its inactive state; phosphorylation of I κ B causes it to degrade, allowing freed NF κ B to enter the nucleus and transcribe various downstream targets. This pathway is the canonical NF κ B activation pathway (Figure 5.1).

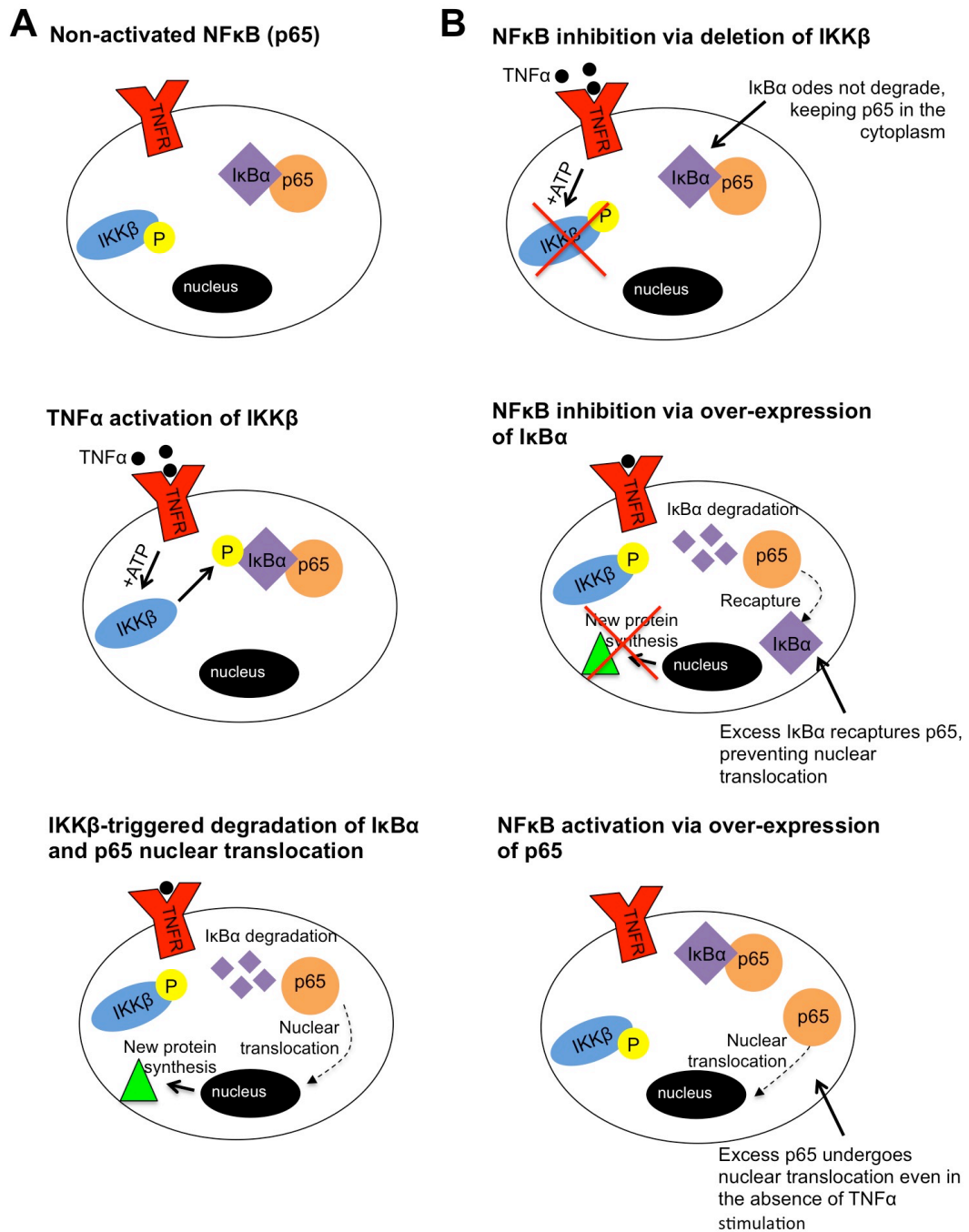


Figure 5.1 Canonical NFκB signaling and methods of modulation.

- A. TNFα activates the p65 subunit of NFκB by triggering IKKβ to phosphorylate IκBα. IκBα undergoes ubiquitin-mediated protein degradation, releasing p65 to enter the nucleus and stimulate new protein synthesis. B. NFκB can be inhibited by deletion of IKKβ or over-expression of IκBα. Over-expression of p65 stimulates constitutive NFκB activity, as excess p65 proteins are not trapped in the cytoplasm by IκBα.

NF κ B signaling regulates a wide range of cardiovascular diseases, including atherosclerosis, myocardial ischaemia/reperfusion injury, ischaemic preconditioning, vein graft disease, cardiac hypertrophy and heart failure (review: [3]). A transgenic mouse model with a dominant negative form of the NF κ B inhibitor I κ B (DN I κ B) was protective against vascular remodeling and aneurysm [4]. Endothelial cell-specific expression of DN I κ B or knock-out of NF κ B essential modulator (NEMO) was sufficient to protect against development of atherosclerosis in a hypercholesterolemic mouse model. Early lesions of aortic valve disease (AVD) are similar to atherosclerotic plaques [5], but the role of NF κ B in regulating the development of AVD has not been investigated.

NF κ B is a likely candidate for governance of AVD due to the power and breadth of its transcriptional targets, many of which are known to feature in AVD. It is known to regulate inflammation [6] and cell survival [1,7], which drive early valve endothelial activation [2,8] and dystrophic calcification [3,9], respectively. The canonical NF κ B pathway is an essential mediator of TNF α signaling [4,10], known to drive valve endothelial cell pathology [5,11] and valve interstitial cell phenotype [6,12]. NF κ B is also a first responder to changes in hemodynamics [13,14], which are thought to accelerate AVD in patients with bicuspid aortic valve [15]. Further, NF κ B regulates oxidative stress signaling [16], a known feature of calcified human aortic valve lesions [17,18]. eNOS uncoupling, a recently demonstrated feature of early AVD [40], has been shown to trigger NF κ B in vascular endothelial cells [19]. NF κ B also regulates

bone-forming processes that are likely involved in the mineralization of the valve in advanced AVD [20,21], specifically through activation of the kinase IKK β [22]. Adult aortic valve cells are more aggressive in activation of canonical NF κ B signaling than pediatric cells [23], inducing downstream targets such as BMP-2, ICAM-1, and IL-6 that are implicated in osteoblastic differentiation of valve interstitial cells [24-26].

Nuclear factor of activated T-cells-c1 (Nfatc1) is a transcription factor that is highly expressed in the developing valve endocardium and is required for formation of healthy valves [27,28]. LDLR^{-/-} that are fed a 16-week western diet have thickened AV leaflets, reduced endothelial cell coverage, increased α SMA, increased ALP, more mineralization, increased prevalence of cells with ALP-positive pro-osteoblast phenotype, increased mRNA of BMP2, Runx2, ALP, and increased AV velocity [29,30]. We hypothesized that the inactivation of NF κ B in the aortic valve via floxing of IKK β [31] would improve aortic valve function in the high-fat, LDLR^{-/-} model of AVD.

5.3 Materials and Methods

Transgenic mouse model

The Zhou Lab (Einstein University) kindly provided a mouse that expresses the Cre recombinase enzyme specifically in the cells of the cardiac outflow tract and atrioventricular canal, driven by the *Nfatc1* P1 promoter, as described in [28]. The Karin lab (University of California, San Diego) kindly provided a mouse with IKK β -floxed allele [32]. The mice were crossed with LDLR^{-/-} mice from Jackson Labs (#2270), given to us by the Qi Lab (Cornell University), and with ROSA26 reporter mice (Jax #003474), given to us by the Kotlikoff lab (Cornell University). All mice were on a C57/Bl6 background, backcrossed for genetic homogeneity for > 5 generations. We utilized these lines to establish three mouse groups: wild type, AVD, and AVD+IKK β ^{ff} (Figure 5.2, Table 5.2). AVD and AVD+IKK β ^{ff} mice were fed a high fat diet (Harlan Teklad #TD88137, 42% of calories from fat, 0.25% cholesterol) from 4-20 weeks of age in order to establish aortic valve disease, as described previously [33].

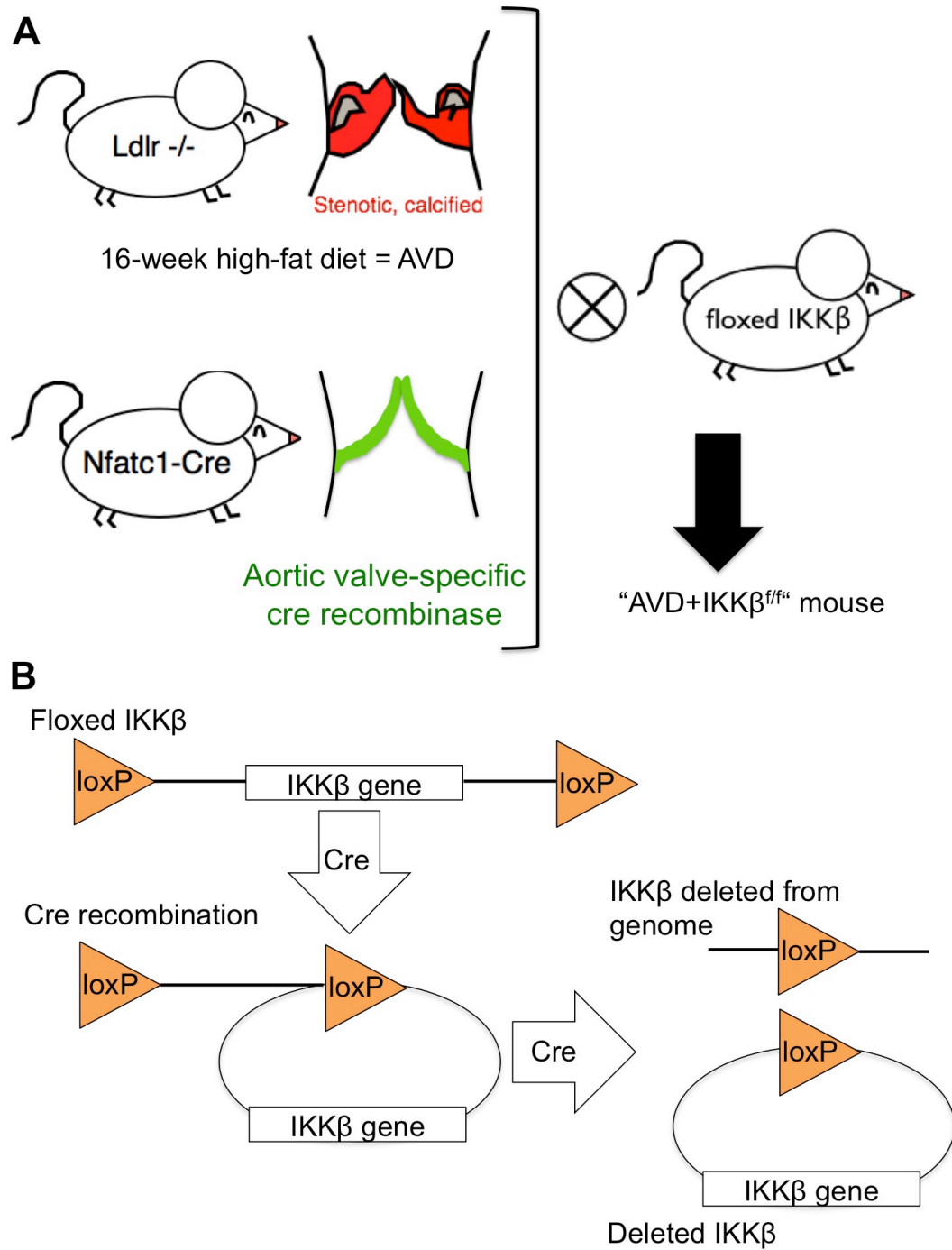


Figure 5.2 Creation of control, AVD, and AVD+IKK β^{ff} mice.

A. LDLR $^{-/-}$ with 16-week high fat diet was used as our model of aortic valve disease. An Nfatc1 Cre mouse from the Zhou lab was used for valve-specific expression of cre recombinase. Crossing these mice with an IKK β^{ff} mouse resulted in a mouse with AVD and lacking the ability to activate NF κ B. B. Mechanism of Cre-mediated deletion of IKK β in the valve.

Table 5.1 Mouse groups, genotypes, and diet conditions

	LDLR	Nfatc1 Cre	IKKβ	High fat diet
Control	+/+	+	+/+	None
AVD	-/-	+	+/+	4 months
AVD+IKK$\beta^{fl/fl}$	-/-	Cre	fl/fl	4 months

The AVD+IKK $\beta^{fl/fl}$ group had expression of the lacZ reporter in areas of Cre activity (Figure 5.3), generalized deletion of the LDL receptor, and valve-specific deletion of the IKK β gene.

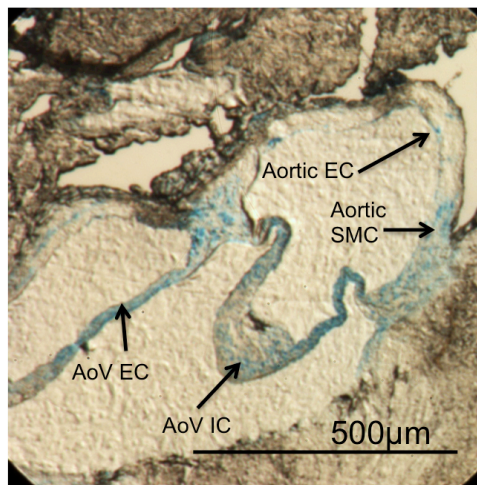


Figure 5.3. LacZ staining of 5 month-old *Nfatc1^{Cre}*;ROSA mice.

Cre expression is restricted to the aorta and aortic valve.

Mendelian ratios of AVD+IKK $\beta^{fl/fl}$ offspring indicated no embryonic lethality (Table 5.2). Mean litter size was seven pups and the male:female ratio was 1.23 +/- 0.53.

Table 5.2 Offspring ratios of Nfatc1^{Cre};IKK β ^{flox};LDLR^{KO} mice

N= 70 mice, all mice Nfatc1^{Cre} positive and homozygous LDLR^{-/-}.

	IKK β ^{+/+}	IKK β ^{flox/+}	IKK β ^{flox/flox}
Expected	25%	50%	25%
Actual	31%	46%	23%

Echocardiography

AV function was assessed at five months of age using echocardiography according to established procedures [33]. Briefly, mice were anesthetized using inhaled 1.8% isoflurane and cradled in the left lateral recumbent position. Abdominal hair was removed using a chemical depilatory cream and warmed ultrasound transmission gel was applied to the anterior thorax. An ultra-high frequency linear array probe (MS550D 22–55 MHz transducer, Vevo[®]) was applied in the long-axis position to the chest. The imaging probe was coupled to the Vevo[®] 2100 system (VisualSonics). Aortic valve leaflet dynamics and ventricular dilation were imaged using the ECG-Gated KiloHertz Visualization (EKV) software (VisualSonics), which captures 5,000 fps in order to create high-resolution videos of cardiac movement. M-mode was used to measure diameter of the aortic root, just above the aortic sinus. Transvalvular velocity and pressure gradients were captured using the pulsed-wave Doppler mode and manual tracing of > 3 velocity time intervals on the resulting plots.

Histology

Mouse hearts were isolated, perfused, fixed, embedded in paraffin, sectioned, and mounted as previously described (Ch 6). Slides were deparaffinized through xylene and graded ethanol and rinsed in deionized water.

For Alizarin Red S, sections were stained with freshly made 1% Alizarin Red S solution, pH 4.7, for 30 seconds. They were then dipped 20x in 100% acetone, followed by 20 dips in 50% acetone, 50% xylene. Sections were cleared in three changes of xylene and mounted with PermountTM mounting media.

For von Kossa, slides were rinsed in three changes of distilled water, and then incubated in a 1% silver nitrate solution under UV light for 20 minutes. Excess silver nitrate was removed by a five-minute incubation in 5% sodium thiosulfate and sections were counterstained with nuclear fast red for five minutes. Sections were cleared and mounted as above.

Russell-Movat stain was done according to Appendix C.

In vitro genetic modulation

The p65 (RelA) sub-unit of NF κ B was over-expressed *in vitro* via transfection of RelA. GFP-RelA was a gift from Warner Greene (Addgene plasmid # 23255), as described in [34]. Inhibition of NF κ B p65 was achieved by transfection of dominant-negative I κ B α . pBabe-GFP-IKBalphamut (super repressor) was a gift from William Hahn (Addgene plasmid # 15264), as described in [35]. Electroporation delivery was used as described previously (Chapter 6).

5.4 Results

Inactivation of p65 signaling in the AoV does not affect valve development

Deletion of IKK $\beta^{f/f}$ in the valve did not affect heart morphology (Figure 5.4A). Aortic valve and aortic root were similar between WT and IKK $\beta^{f/f}$ hearts (Figure 5.4B). Distensibility, peak velocity, leaflet thickness, and peak transvalular gradient were not affected in IKK $\beta^{f/f}$ hearts (Figure 5.4C-F).

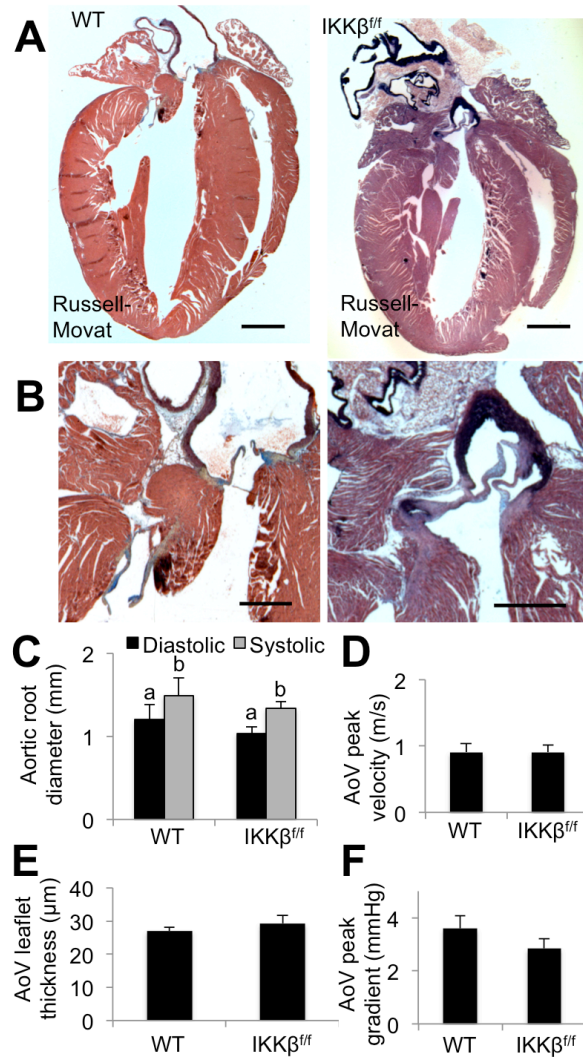


Figure 5.4 Characterization of the effect of IKK β deletion on valve function.

A. Russell-Movat staining of 5 month-old WT and IKK $\beta^{fl/fl}$ mouse hearts. Scale bar is 1mm. B. Magnification of aortic valve region of A. Scale bar is 500 μ m. C. Measurement of aortic root diameter from echocardiographic M-mode with comparison between systole and diastole. Groups with different letters are statistically significant. D. Peak velocity through aortic valve, no difference between groups. E. Thickness of the AoV leaflet, measured from EKV. No difference between groups. F. Peak pressure gradient across AoV, no difference between groups.

Inactivation of p65 signaling in the AoV prevents AVD in LDLR^{-/-} mice

Cytosolic p65 was expressed primarily in the endothelium of both control and AVD groups, with lower levels across both endothelial and interstitial cells in the AVD+IKK β^{ff} (LDLR^{-/-};IKK β^{ff}). In AVD, nuclear localization of p65 was increased primarily in valve endothelial cells (VEC), but also in a small population of valve interstitial cells (VIC) (Figure 5.5A, arrows). Floxing IKK β prevented nuclear translocation of p65. Inactivation of p65 activity was confirmed via immunofluorescence for VCAM-1, a direct transcriptional target of p65. VCAM-1 was elevated in AVD and not in the AVD+IKK β^{ff} (Figure 5.5B). Both apoptosis (Figure 5.5C) and proliferation (Figure 5.5D) were elevated in AVD mice, but not in AVD+IKK β^{ff} .

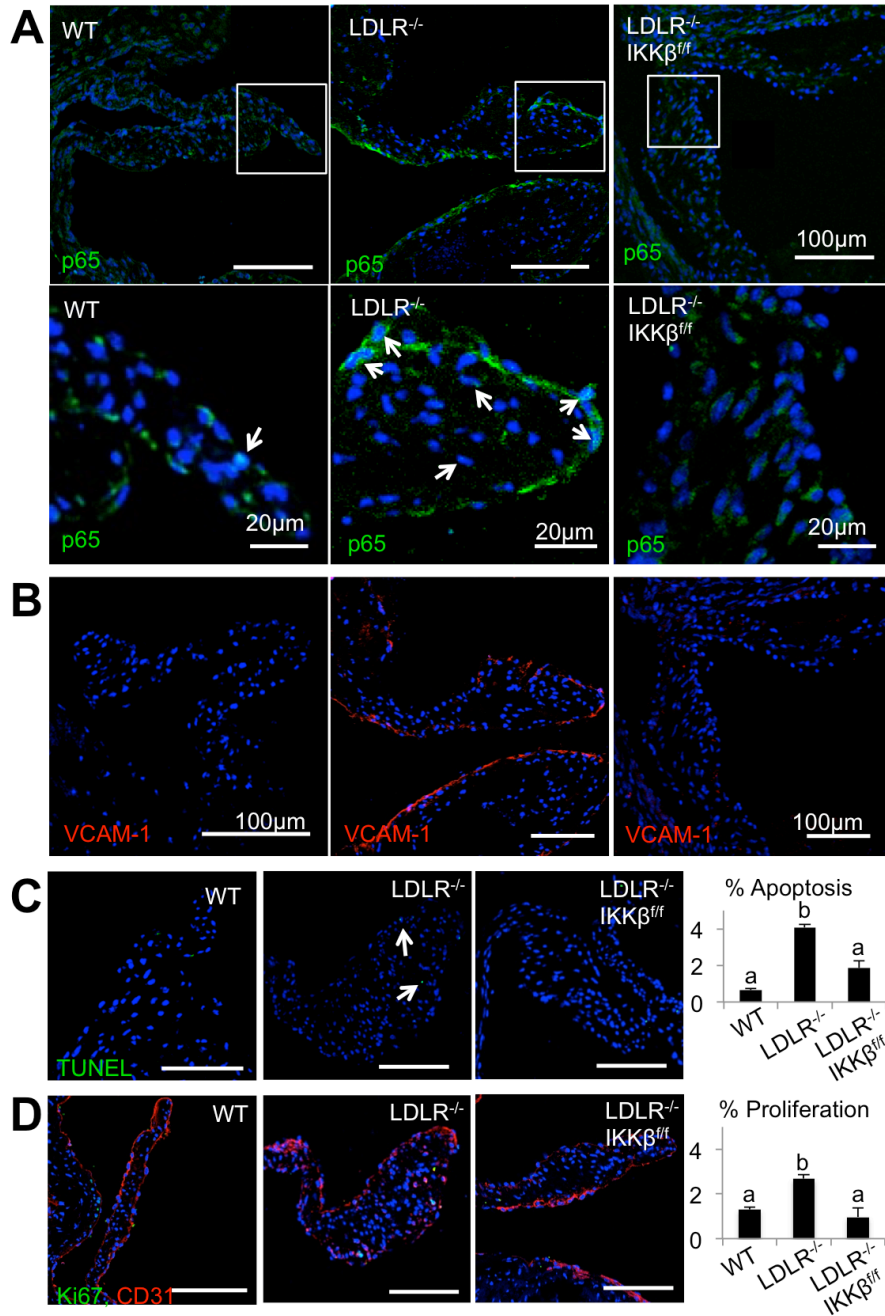


Figure 5.5 p65 and VCAM-1 expression in AVD and AVD+IKKβ^{fl/fl} mice.

A. Representative images of p65 (green) protein expression and nuclear localization (arrows) in aortic valve leaflets of 5 month-old WT, AVD, and AVD+IKKβ^{fl/fl} mice. Scale bar is 20μm.
 B. Representative images of VCAM-1 (red) protein expression in same groups. Scale bar is 100μm.
 C. TUNEL assay for apoptosis in AoV of same groups, quantification of the percent of cells in the AoV positive for TUNEL staining.
 D. Analysis of proliferation in AoV of same groups via Ki67 staining. Ki 67 (green) and CD31 (red). Quantification of percent of cells in the AoV positive for nuclear Ki67.

Echocardiographic analysis revealed statistically significant increase in thickness of the AoV leaflets, aortic velocity, and peak AoV gradient in AVD mice, but not in AVD+IKK $\beta^{f/f}$ (Figure 5.6A, B, Figure 5.7A). Serum cholesterol was elevated in AVD mice and further elevated in AVD+IKK $\beta^{f/f}$ (Figure 5.7B). Histological analysis showed increased calcium deposition, mineralization, and collagen content in AVD mice, but not in AVD+IKK $\beta^{f/f}$ (Figure 5.6C, D, and E). AVD+IKK $\beta^{f/f}$ had increased GAG content compared to control and AVD groups (Figure 5.7C). Valve area was not different between groups (Figure 5.7D).

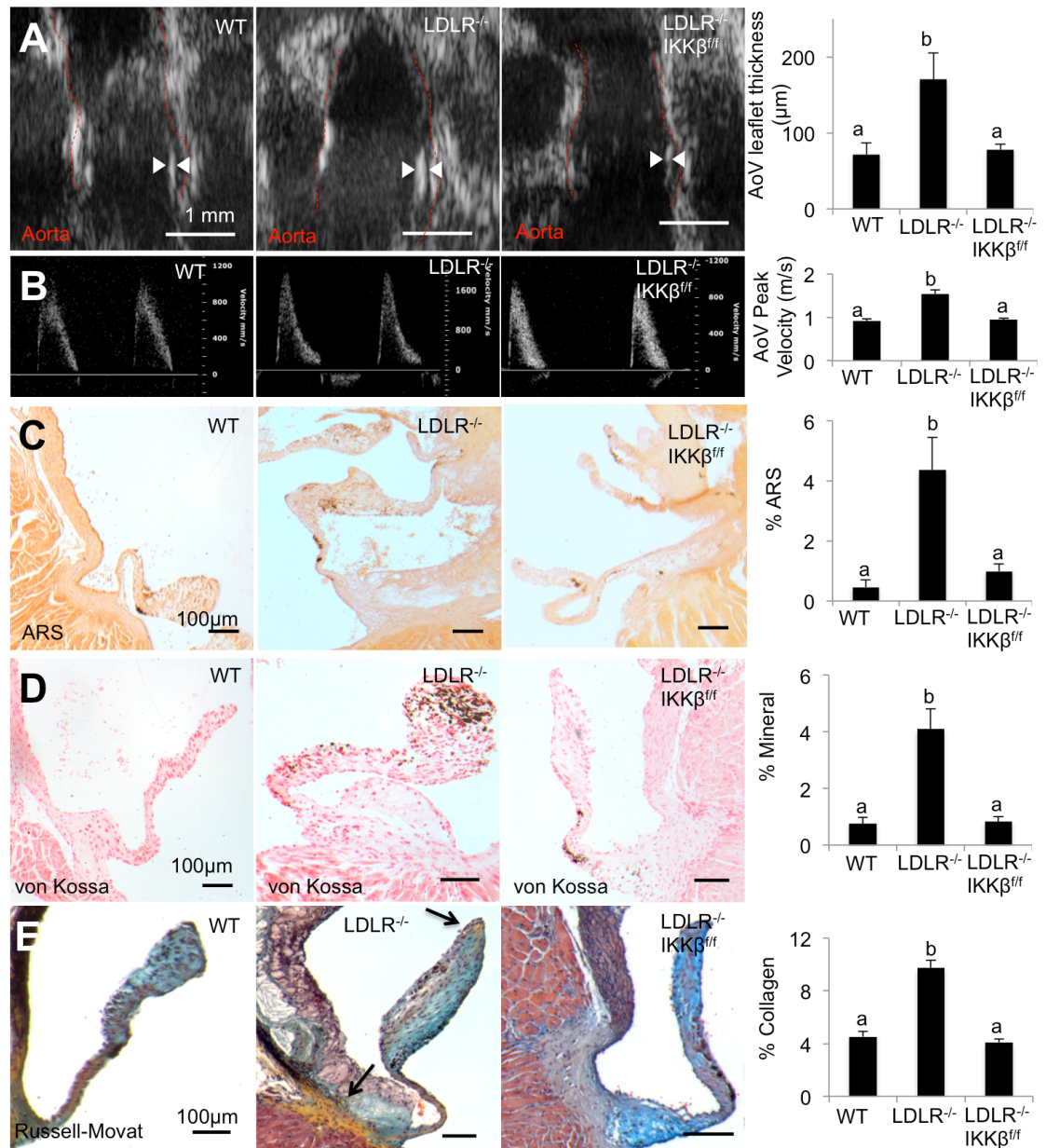


Figure 5.6 Inactivation of NFκB prevents development of aortic valve calcification.

A. Echocardiographic imaging of AoV at peak systole (arrowheads indicate max thickness), Scale bar is 1 mm. B. Pulsed-wave Doppler imaging of maximum flow through AoV. Scale is indicated on side-bar of each panel, units of mm/s. Mean peak velocity for each group was calculated using the average peak from > three cardiac cycles for each mouse. C. Alizarin Red S stain for calcium in AoV. D. von Kossa staining for mineral deposition in AoV. E. Russell-Movat stain for collagen (yellow), glycosaminoglycans (blue), elastin (black), and mucins (red) in AoV. Quantification indicates percent of the total valve area that was positive for indicated stain. Groups that do not share letters are statistically significant. P < 0.05.

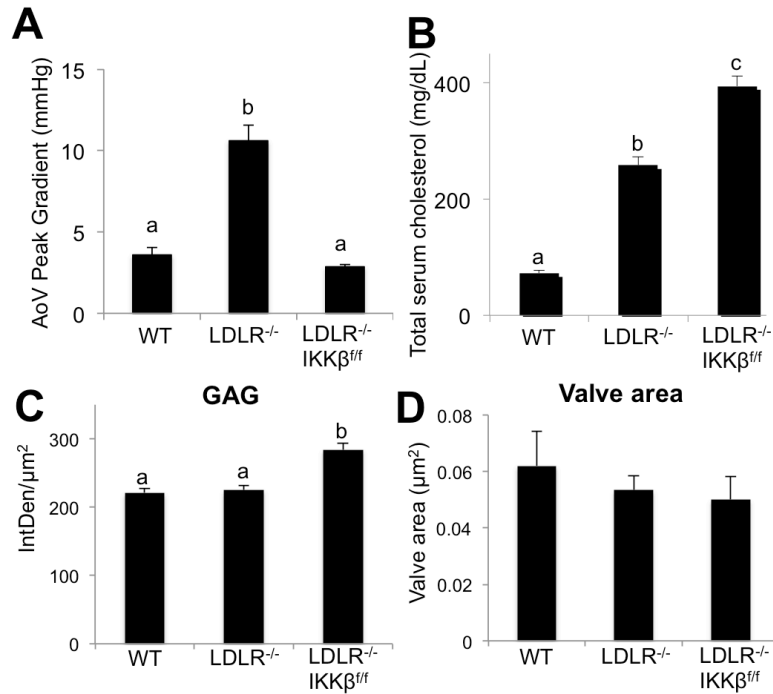


Figure 5.7 Valve function changes with AVD or AVD+IKK $\beta^{f/f}$.

A. AoV peak gradient from average of three velocity time interval traces. B. Total serum cholesterol in each group, collected at 5 months of age. C. GAG content according to Russell-Movat stain (blue). D. Valve area, calculated from the maximum valve area observed in each sample and averaged across all animals in each group (no significant differences). Groups that do not share letters are statistically significant, $P < 0.05$.

Echocardiography also revealed improved left ventricular (LV) function by inactivation of valve NF κ B. Overlay of minimum systolic ventricular volume (red) over maximum diastolic volume (blue) showed reduced LV contraction in AVD that was prevented in AVD+IKK $\beta^{f/f}$ (Figure 5.8A). The AVD group had a 12% reduction in LV contraction (Systolic volume/diastolic volume) that was not present in AVD+IKK $\beta^{f/f}$ (Figure 5.8B). In addition to improved valve function, reduced aortic plaque formation also contributed to improved cardiac function in AVD+IKK $\beta^{f/f}$ (Figure 5.8C). The mean plaque area in AVD+IKK $\beta^{f/f}$ hearts was higher than control mice, but less than the AVD group (Figure 5.8D). Further analysis of LV function

revealed increased end-diastolic volume, decreased stroke volume, and decreased ejection fraction in AVD mice that was prevented by inactivation of NF κ B in AVD+IKK β^{ff} mice (Figure 5.8E). Interestingly, measurement of the aortic root during peak systole and peak diastole revealed a loss of aortic distensibility in AVD that was not prevented by AVD+IKK β^{ff} (Figure 5.9).

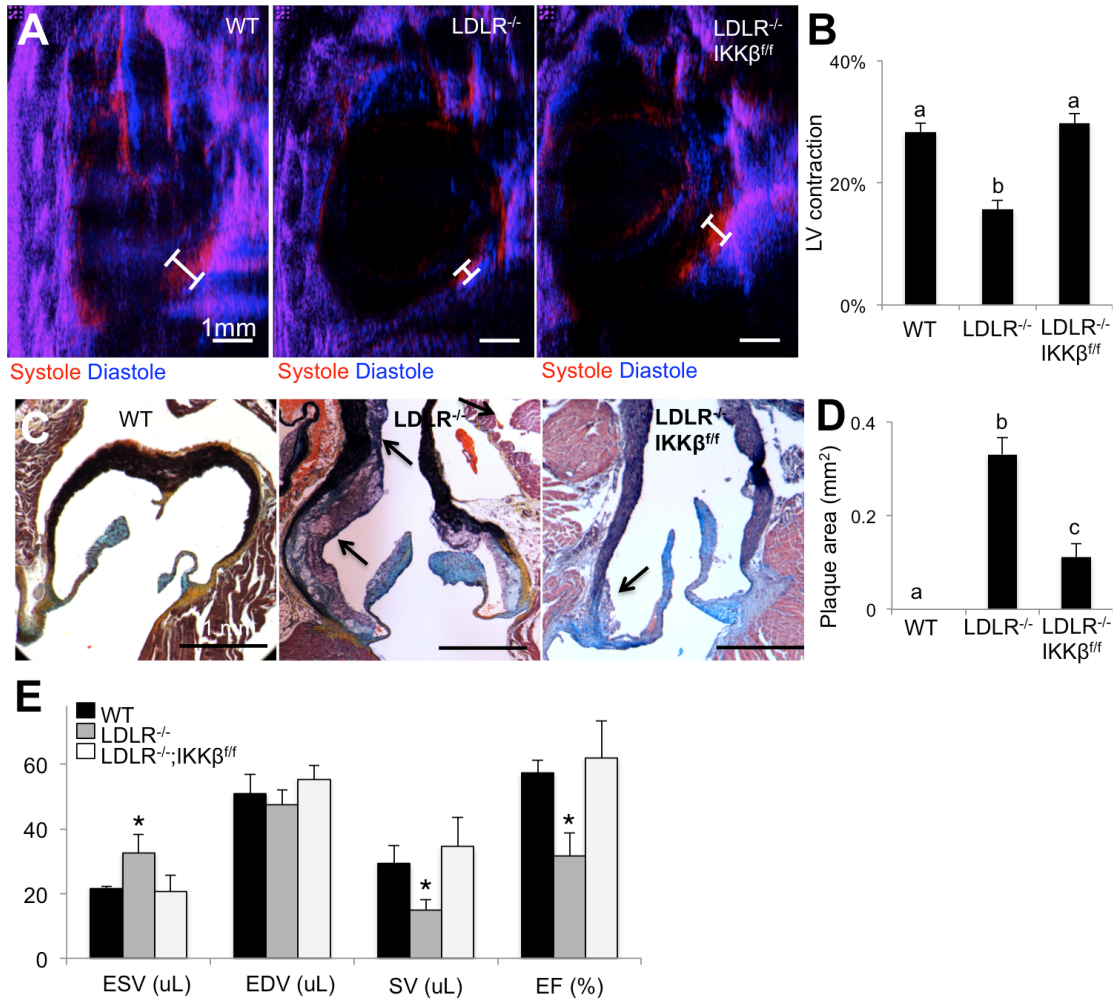


Figure 5.8 Cardiac function and aortic plaques are improved by NFκB inactivation.

A. Long-axis echocardiographic imaging of left ventricle during peak systole (red) and peak diastole (blue). Images were made 50% transparent and overlaid. Red areas show contraction of the left ventricle. White bars indicate contraction of ventricular wall. Scale bar is 1mm. B. Quantification of LV contraction using systolic volume/diastolic volume. 0% indicates no change in ventricular volume over the cardiac cycle. C. Russell-Movat staining of the aortic root and AoV. Arrows indicate plaques. Scale bar is 1mm. D. Mean plaque area across groups, calculated from the maximum plaque area observed in each sample. Groups that do not share letters are statistically significant, $p < 0.05$. E. Left ventricular function, calculated from systolic and diastolic volumes. * indicates $p < 0.05$ versus WT. Unit for each group of bars is noted in parentheses.

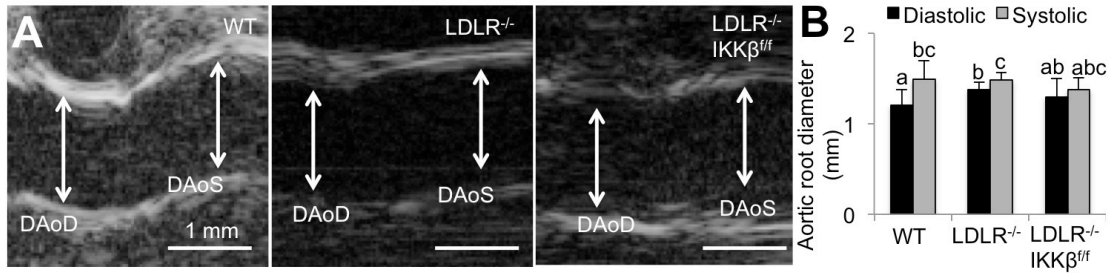


Figure 5.9 Aortic root diameter and distensibility.

A. M-mode echocardiographic measurements of aortic root diameter during peak diastole (DAoD) and peak systole (DAoS). Scale bar is 1 mm. B. Comparison of change in aortic diameter between diastole and systole across groups. Groups that do not share letters are statistically significant.

p65 is necessary and sufficient for inflammatory-EndMT in VEC

We used porcine aortic valve endothelial cells (VEC) cultured on physiologically relevant 3-D collagen hydrogels to examine p65 activity in VEC under disease conditions at an early (48 hour) stage of response. Control VEC had minimal nuclear expression of p65. TNF α treatment induced a statistically significant increase in p65 nuclear expression, but OGM did not (Figure 5.10A, B).

We then examined the effect of p65 modulation on TNF α -driven EndMT in VEC. Transfection of empty vector (+CTL) did not affect TNF α -driven EndMT, which was characterized by loss of VE-cadherin (Figure 5.10C, D) and increase in α SMA (Figure 5.10E, F). Transfection of p65 (+p65) induced EndMT even without TNF α , indicating that p65 over-activation is sufficient for TNF α -driven EndMT. Transfection of p65 inhibitor (+I κ B α) prevented TNF α -driven EndMT. Interestingly, VEC+I κ B α did have a slight increase in ACTA2 mRNA under both CTL and TNF α conditions (Figure 5.10F), but no α SMA protein expression was observed in these cells (Figure 5.10E).

Inactivation of p65 signaling prevents disease-associated EndMT in LDLR^{-/-} mice

In vivo, EndMT of the postnatal AoV is characterized by co-expression of endothelial (CD31) and mesenchymal (α SMA) proteins in the same cell. In our mouse model, we observed little to no expression of α SMA and a robust, intact endothelial layer positive for CD31. In AVD mice (LDLR^{-/-}), overall α SMA expression was higher and there were many observable cells with co-expression of CD31 and α SMA (Figure 5.10G, arrows). AVD+IKK β ^{f/f} mice had α SMA expression levels comparable to control and no observable cells with co-expression of CD31 and α SMA.

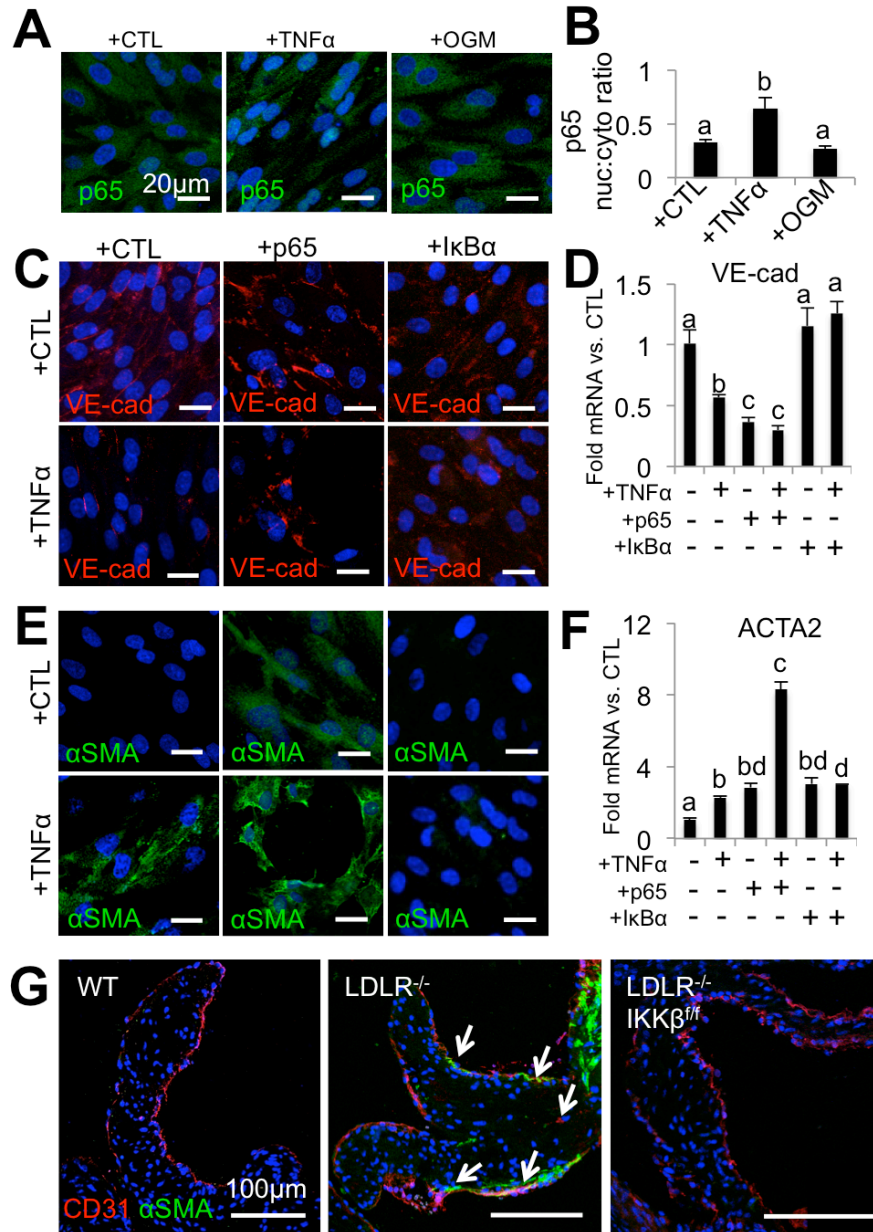


Figure 5.10 NF κ B activation is necessary and sufficient for aortic valve EndMT.

A. Representative images of p65 expression in 48 hour VEC on 3D hydrogels treated with TNF α or OGM. Scale bar is 20 μ m. B. Quantification of p65 nuclear translocation in VEC using the ratio of nuclear to cytosolic p65 protein (nuc:cyto ratio). C. VE-cad protein expression in VEC with p65 over-expression or inhibition (+IkB α), with 48 hour control or TNF α treatment. Scale bar is 20 μ m. D. VE-cad mRNA in VEC, same conditions as C. E. α SMA protein expression in VEC, same conditions as C. F. ACTA2 (α SMA gene) mRNA in VEC, same conditions as C. Groups that do not share letters are statistically significant, $p < 0.05$. G. CD31 and α SMA expression in 5 month-old mouse AoV. Arrows indicate cells co-expressing CD31 and α SMA. Scale bar is 100 μ m.

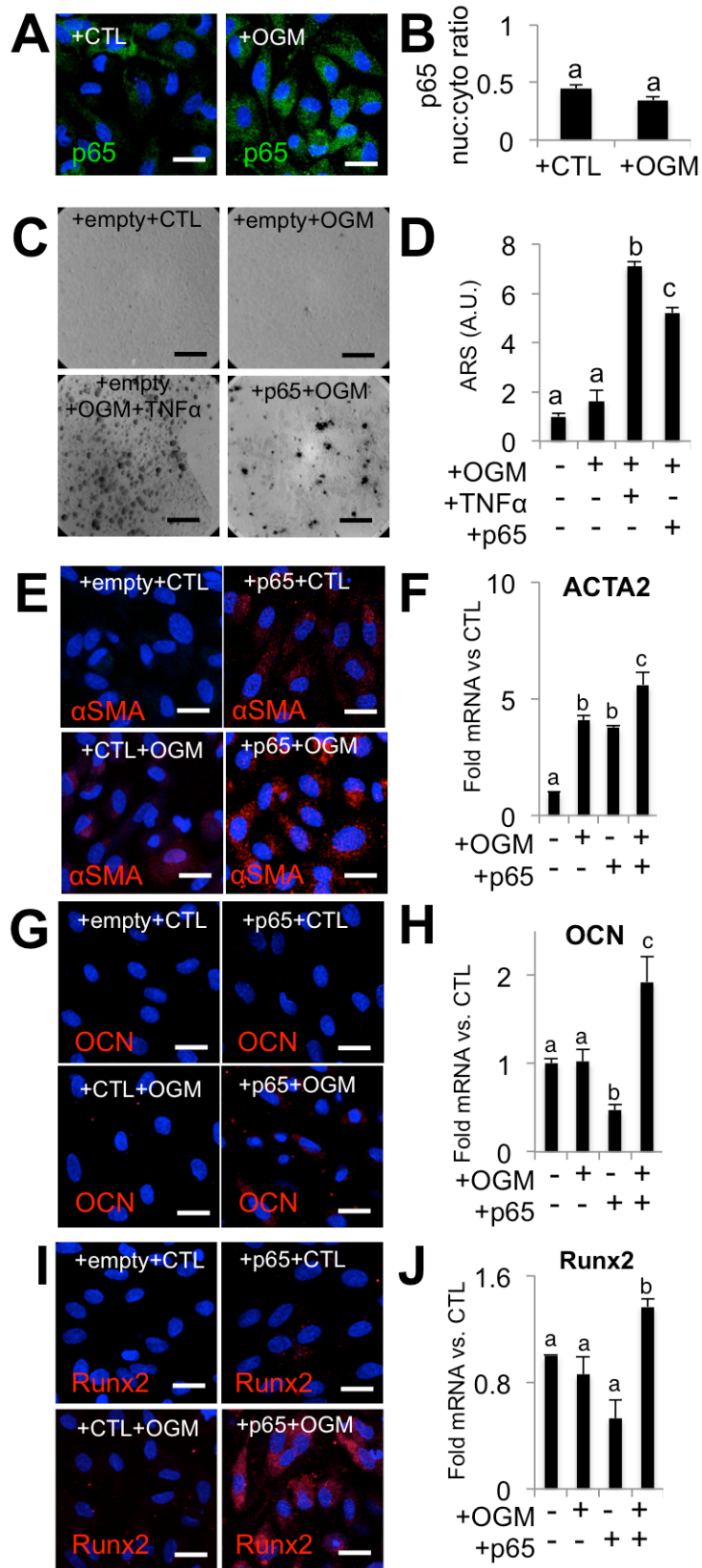
p65 over-expression makes VEC active participants in calcification under OGM stimulus

We then examined the effect of p65 on the participation of VEC in valve calcification. Treatment of VEC for 14 days with osteogenic media (OGM) did not increase p65 nuclear expression (Figure 5.11A, B) or VEC calcification (Figure 5.11C). However, co-treatment with OGM and TNF α drove VEC calcification. Interestingly, over-expression of p65 and OGM treatment also drove VEC calcification. Quantification of Alizarin Red S (ARS) dye uptake confirmed the similar increases in calcium deposition by VEC+OGM+TNF α and VEC+p65+OGM.

In the same way, VEC with OGM treatment did not show increased α SMA, osteocalcin (OCN), or Runx2 protein expression. However, over-expression of p65 in VEC with OGM treatment showed increased α SMA, OCN, and Runx2 expression (Figure 5.11E, G, I). Runx2 increase was both cytosolic and nuclear. ACTA2 mRNA was increased in VEC+OGM, +p65, and +p65+OGM (Figure 5.11F). OCN mRNA was decreased in VEC+p65, but significantly increased in +p65+OGM (Figure 5.10H). Runx2 showed a similar trend (Figure 5.11J).

Figure 5.11 NFκB activation enables endothelial osteogenic differentiation.

A. Representative images of p65 expression in 14-day VEC on 3D hydrogels treated with CTL or OGM. B. Quantification of p65 nuclear translocation in VEC using the ratio of nuclear to cytosolic p65 protein (nuc:cyto ratio). C. Alizarin Red S staining for calcium in 14 day VEC treated with CTL, OGM, OGM+TNF α , or +p65+OGM. D. Quantification of calcium deposition using ARS stain. E. α SMA protein expression in VEC with or without p65 over-expression with 14-day control or OGM treatment. F. ACTA2 mRNA in VEC, same conditions as E. G. Osteocalcin protein expression in VEC, same conditions as E. H. Osteocalcin mRNA in VEC, same conditions as E. I. Runx2 protein expression in VEC, same conditions as C. J. Runx2 mRNA in VEC, same conditions as E. Groups that do not share letters are statistically significant, $p < 0.05$. Scale bar is 20 μ m.



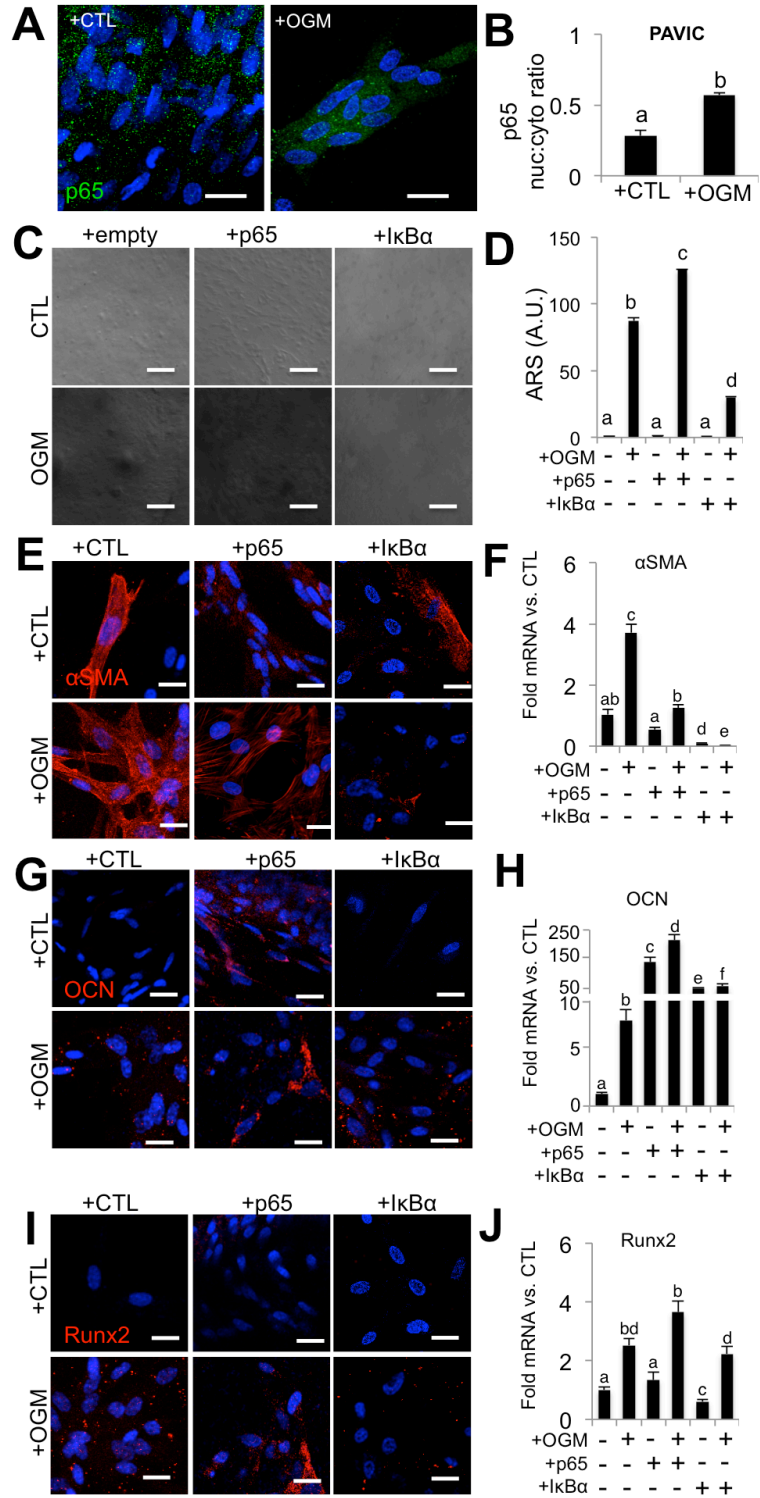
p65 signaling is active in pro-osteogenic VIC, blocking p65 signaling prevents VIC calcification

Considering the whole-valve protective effect of p65 inhibition *in vivo*, we sought to understand the effect of p65 modulation on valve interstitial cells in addition to valve endothelial cells. We transfected porcine aortic valve interstitial cells (VIC) with empty, p65, or I κ B α vectors and then cultured them in 3-D collagen hydrogels for 14 days with or without OGM treatment. We found that OGM induced a significant increase in VIC p65 nuclear expression after 14 days of culture (Figure 5.12A, B).

Over-expression of p65 exacerbated VIC calcification response to OGM and inhibition of p65 (+I κ B α) mitigated VIC calcification response (Figure 5.12C, D). Similarly, inhibition of p65 lowered VIC α SMA expression in both control and OGM conditions compared to control VIC (Figure 5.12E, F). Runx2 protein expression was exacerbated in VIC+p65+OGM compared to control VIC in OGM. Over-expression of p65 increased OCN expression in both control and OGM. Inhibition of p65 did not mitigate increases in OCN (Figure 5.12G, H). Inhibition of p65 mitigated increases in Runx2 in OGM condition (Figure 5.12I, J).

Figure 5.12 NFκB modulates interstitial cell calcification.

A. p65 expression in 14-day VIC in 3D hydrogels treated with CTL or OGM. Scale bar is 20μm. B. Quantification of p65 nuclear translocation in VIC using the ratio of nuclear to cytosolic p65 protein (nuc:cyto ratio). C. Alizarin Red S staining for calcium in 14 day VIC with p65 over-expression (+p65) or inhibition (+IκBα) treated with CTL or OGM. Scale bar is 100μm. D. Quantification of calcium deposition using ARS stain. E. αSMA protein expression in VIC, F. ACTA2 mRNA in VIC, G. Osteocalcin protein expression in VEC, same conditions as E. H. Osteocalcin mRNA in VEC, same conditions as E. I. Runx2 protein expression in VEC, same conditions as C. J. Runx2 mRNA in VEC, same conditions as E. Groups that do not share letters are statistically significant, $p < 0.05$. Scale bar is 20μm.



5.5 Discussion

The importance of inflammatory pathway management in AVD treatment design

The results of this study present new evidence for the importance of the canonical NF κ B pathway in AVD pathology and treatment. We found that inactivation of the canonical NF κ B pathway via deletion of IKK β reduced valve endothelial inflammation *in vivo*. Inflammation is a known feature of both early and late stages of AVD [36-38], with important repercussions for both endothelial [39,40] and interstitial [41] cell participation in disease. The observed mitigation of inflammation (VCAM-1) was not related to lowered serum cholesterol, so the downstream improvements in valve function can not be attributed to serum cholesterol effects, as demonstrated elsewhere [42]. This demonstrated connection between reduction of inflammatory activation of the endothelium and improved valve function emphasizes the need for early diagnosis, affirming studies that demonstrate positive effects of early intervention and mitigation of inflammation in AVD management [43].

New evidence for VEC active contribution to AVD

Our results provide further *in vitro* and *in vivo* evidence for NF κ B stimulation of postnatal EndMT in the aortic valve. This phenomenon could share mechanisms with oncology, as NF κ B is known to be essential for epithelial to mesenchymal transformation (EMT) in breast cancer [44], particularly due to TNF α signaling via IKK β and p65 in breast cancer [45]. In postnatal epithelial cells, a recent study demonstrated that p65 and Snail1 co-regulate EMT, possibly through p65 nuclear recruitment of Snail1 [46]. A similar mechanism may be at play in postnatal aortic

valve EndMT, which has been demonstrated in multiple contexts including aberrant mechanical environment [47], as a consequence of inflammation [11,39], and in response to TGF β . These findings underline an active role for VEC in aortic valve disease that has been demonstrated previously [36,48-50] and identify a new p65-dependent mechanism for VEC involvement in valve degeneration.

NF κ B is a “gatekeeper” to VEC participation in calcification – connects inflammation to calcification, potentially via differentiation of EC to OPC

These results demonstrate a role for p65 as a “gatekeeper” for VEC participation in valve calcification by connecting inflammatory activation to a downstream osteogenic phenotype. Activation of p65 could be controlling a phenotypic shift from quiescent to EndMT-activated to osteogenic VEC, as in a recent study where TNF α promoted osteogenic differentiation of mesenchymal stem cells via IKK β activation [51]. One way in which this could occur in AVD is through TNF α -driven differentiation of an endothelial progenitor population that has previously been identified in postnatal valves [52]. Such a transition occurs in atherosclerosis, as the vascular endothelium contributes osteoprogenitor cells during lesion formation [53]. Finally, a recent study showed co-localization of nuclear NF κ B with osteocalcin in the interstitium of both healthy and calcified human aortic valves [54]. However, this co-localization occurred in the valve endothelium only in calcified valves, supporting a role for endothelial p65 signaling as a gatekeeper for VEC calcification.

NFκB enhances VIC-driven calcification, blocking NFκB mitigates VIC calcification

We also found that p65 enhances interstitial cell participation in valve calcification and that inhibition of p65 signaling mitigates that participation. This may be the mechanism behind a recent finding that tissue stiffness activates VIC calcification [55], as tissue stiffness is known to activate NFκB in certain cancer cell types [56]. NFκB could be mechanotransductive signaling bridge between ECM and calcification in VIC, participating in positive feedback loop via RhoA-p65 interaction, as demonstrated in renal cells [57]. Further evidence for a role for p65 in calcification comes from the vasculature, where p65 is known to promote calcification via ANKH signaling [58]. NFκB clearly triggers different signaling pathways in VIC than in VEC, likely through transcriptional binding targets that should be further investigated.

NFκB signaling as novel therapeutic target

The results of this study present p65 as a novel therapeutic target for AVD. Supporting this approach are recent findings that osteoprotegerin mitigates AVD calcification [59]. Osteoprotegerin is a decoy receptor for receptor activator of nuclear factor-κB ligand (RANKL) [60], which activates the canonical NFκB pathway [61]. RANKL is necessary for bone formation and is upregulated in calcified aortic valves [62], pointing to NFκB signaling as an important driver of valve calcification that could be the mechanism behind the efficacy of osteoprotegerin treatment. There are a number of other drugs that target NFκB signaling, such as pyrrolidine-dithiocarbamate (PDTC) [63]. PDTC has been shown to be effective in mouse models of

cardiovascular disease [64] and may be able to capitalize on the novel NF κ B mechanisms of AVD shown here.

Strategy	Mechanism	Agent	FDA status
Proteasome inhibitor	Blocks degradation of I κ B α	Bortezomib [65], Carfilzomib [66]	Approved (2003, 2012) for multiple myeloma
Nutraceuticals	Generic anti-inflammatory effects	Curcumin (component of tumeric) [67]	Phase II clinical trials for pancreatic & breast cancer
IKK inhibitor	Irreversibly blocks IKK phosphorylation	BAY 11-7082 [68]	Preclinical testing
Gene therapy	regulation of NF κ B transcription/activity	RelA antisense oligonucleotides [69]	Preclinical testing
		miRNA mimetics [70]	Phase I clinical trials (2013) for liver cancer
RANKL inhibitor	Binds RANKL (receptor activator of NF κ B ligand)	Denosumab [71]	Approved (2010) for osteoporosis, preclinical trials
	RANKL decoy receptor	Recombinant osteoprotegerin [72]	Preclinical testing

REFERENCES

1. Ghosh S, May MJ, Kopp EB (1998) NF κ B and Rel Proteins: Evolutionarily Conserved Mediators of Immune Responses. *Annual Review of Immunology* 16: 225–260.
2. Sun S, Ganchi P, Ballard D, Greene W (1993) NF-kappa B controls expression of inhibitor I kappa B alpha: evidence for an inducible autoregulatory pathway. *Science* 259: 1912–1915.
3. Van der Heiden K, Cuhlmann S, Luong LA, Zakkar M, Evans PC (2010) Role of nuclear factor κ B in cardiovascular health and disease. *Clinical Science* 118: 593–605.
4. Saito T, Hasegawa Y, Ishigaki Y, Yamada T, Gao J, et al. (2013) Importance of endothelial NF- κ B signalling in vascular remodelling and aortic aneurysm formation. *Cardiovascular Research* 97: 106–114.
5. Otto CM, Kuusisto J, Reichenbach DD, Gown AM, O'Brien KD (1994) Characterization of the early lesion of “degenerative” valvular aortic stenosis. Histological and immunohistochemical studies. *Circulation* 90: 844–853.
6. Chen LW, Egan L, Li ZW, Greten FR, Kagnoff MF, et al. (2003) The two faces of IKK and NF-kappaB inhibition: prevention of systemic inflammation but increased local injury following intestinal ischemia-reperfusion. *Nat Med* 9: 575–581.
7. Maeda S, Chang L, Li ZW, Luo JL, Leffert H, et al. (2003) IKK β Is Required for Prevention of Apoptosis Mediated by Cell-Bound but Not by Circulating TNF α . *Immunity* 19: 725–737.
8. Ghaisas N, Foley J, O'Briain D, Crean P, Kelleher D, et al. (2000) Adhesion molecules in nonrheumatic aortic valve disease: Endothelial expression, serum levels and effects of valve replacement. *Journal of the American College of Cardiology* 36: 2257–2262.
9. Mohler ER III (2000) Are atherosclerotic processes involved in aortic-valve calcification? *The Lancet* 356: 524–525.

10. MacKenzie CJ, Ritchie E, Paul A, Plevin R (2007) IKK α and IKK β function in TNF α -stimulated adhesion molecule expression in human aortic smooth muscle cells. *Cellular Signalling* 19: 75–80.
11. Farrar EJ, Butcher JT (2013) Heterogeneous Susceptibility of Valve Endothelial Cells to Mesenchymal Transformation in Response to TNF α . *Annals of Biomedical Engineering* 42: 149–161.
12. Venardos N, Nadlonek NA, Zhan Q, Weyant MJ, Reece TB, et al. (2014) Aortic valve calcification is mediated by a differential response of aortic valve interstitial cells to inflammation. *Journal of Surgical Research* 190: 1–8.
13. Hajra L, Evans A, Chen M, Hyduk S, Collins T, et al. (2000) The NF-kappa B signal transduction pathway in aortic endothelial cells is primed for activation in regions predisposed to atherosclerotic lesion formation. *Proceedings of the National Academy of Sciences* 97: 9052–9057.
14. Mohan S, Mohan N, Sprague EA (1997) Differential activation of NF- κ B in human aortic endothelial cells conditioned to specific flow environments. *American Journal of Physiology-Cell Physiology* 42: C572.
15. Chandra S, Rajamannan NM, Sucosky P (2012) Computational assessment of bicuspid aortic valve wall-shear stress: implications for calcific aortic valve disease. *Biomech Model Mechanobiol* 11: 1085–1096.
16. True AL, Rahman A, Malik AB (2000) Activation of NF- κ B induced by H₂O₂ and TNF α and its effects on ICAM-1 expression in endothelial cells. *American Journal of Physiology-Lung Cellular and Molecular Physiology* 279: L302–L311.
17. Miller JD, Chu Y, Brooks RM, Richenbacher WE, Pena-Silva R, et al. (2008) Dysregulation of Antioxidant Mechanisms Contributes to Increased Oxidative Stress in Calcific Aortic Valvular Stenosis in Humans. *Journal of the American College of Cardiology* 52: 843–850.
18. Liberman M, Bassi E, Martinatti MK, Lario FC, Wosniak J, et al. (2008) Oxidant generation predominates around calcifying foci and enhances progression of aortic valve calcification. *Arteriosclerosis, Thrombosis, & Vascular Biology* 28: 463–470.

19. Khan BV, Harrison DG, Olbrych MT, Alexander RW, Medford RM (1996) Nitric oxide regulates vascular cell adhesion molecule 1 gene expression and redox-sensitive transcriptional events in human vascular endothelial cells. *Proc Natl Acad Sci U S A* 93: 9114–9119.
20. Crotti TN, Smith MD, Findlay DM, Zreiqat H, Ahern MJ, et al. (2004) Factors regulating osteoclast formation in human tissues adjacent to peri-implant bone loss: expression of receptor activator NF κ B, RANK ligand and osteoprotegerin. *Biomaterials* 25: 565–573.
21. Boyce BF, Yao Z, Xing L (2010) Functions of nuclear factor κ B in bone. *Annals of the New York Academy of Sciences* 1192: 367–375.
22. Ruocco MG, Maeda S, Park JM, Lawrence T, Hsu L-C, et al. (2005) I κ B kinase (IKK) β , but not IKK α , is a critical mediator of osteoclast survival and is required for inflammation-induced bone loss. *Journal of Experimental Medicine* 201: 1677–1687.
23. Deng X-S, Meng X, Zeng Q, Fullerton D, Mitchell M, et al. (2015) Adult Aortic Valve Interstitial Cells Have Greater Responses to Toll-Like Receptor 4 Stimulation. *The Annals of Thoracic Surgery* 99: 62–71.
24. Wang D, Zeng Q, Song R, Ao L, Fullerton DA, et al. (2014) Ligation of ICAM-1 on human aortic valve interstitial cells induces the osteogenic response: A critical role of the Notch1-NF- κ B pathway in BMP-2 expression. *BBA - Molecular Cell Research* 1843: 2744–2753.
25. Hussein El D, Boulanger M-C, Mahmut A, Bouchareb R, Laflamme M-H, et al. (2014) P2Y2 receptor represses IL-6 expression by valve interstitial cells through Akt: Implication for calcific aortic valve disease. *Journal of Molecular and Cellular Cardiology* 72: 146–156.
26. Zeng Q, Song R, Ao L, Xu D, Venardos N, et al. (2014) Augmented Osteogenic Responses in Human Aortic Valve Cells Exposed to oxLDL and TLR4 Agonist: A Mechanistic Role of Notch1 and NF- κ B Interaction. *PLoS ONE* 9: e95400.
27. Chang CP, Neilson JR, Bayle JH, Gestwicki JE, Kuo A (2004) A field of myocardial-endocardial NFAT signaling underlies heart valve morphogenesis. *Cell* 118: 649–663.

28. Zhou B, Wu B, Tompkins KL, Boyer KL, Grindley JC, et al. (2005) Characterization of Nfatc1 regulation identifies an enhancer required for gene expression that is specific to pro-valve endocardial cells in the developing heart. *Development* 132: 1137–1146.
29. Matsumoto Y, Adams V, Jacob S, Mangner N, Schuler G, et al. (2010) Regular Exercise Training Prevents Aortic Valve Disease in Low-Density Lipoprotein-Receptor-Deficient Mice. *Circulation* 121: 759–767.
30. Schlotter F, Matsumoto Y, Mangner N, Schuler G, Linke A, et al. (2012) Regular Exercise or Changing Diet Does Not Influence Aortic Valve Disease Progression in LDLR Deficient Mice. *PLoS ONE* 7: e37298.
31. Greten FR, Eckmann L, Greten TF, Park JM, Li ZW, et al. (2004) IKK β links inflammation and tumorigenesis in a mouse model of colitis-associated cancer. *Cell* 118: 285–296.
32. Egan LJ, Eckmann L, Greten FR, Chae S, Li Z-W, et al. (2004) IkappaB-kinasebeta-dependent NF-kappaB activation provides radioprotection to the intestinal epithelium. *Proc Natl Acad Sci U S A* 101: 2452–2457.
33. Drolet M-C, Roussel E, Deshaies Y, Couet J, Arsenault M (2006) A High Fat/High Carbohydrate Diet Induces Aortic Valve Disease in C57BL/6J Mice. *Journal of the American College of Cardiology* 47: 850–855.
34. Chen L-F, Fischle W, Verdin E, Greene WC (2001) Duration of Nuclear NF- κ B action regulated by reversible acetylation. *Science* 293:1653-1657.
35. Boehm JS, Zhao JJ, Yao J, Kim SY, Firestein R, et al. (2007) Integrative Genomic Approaches Identify IKBKE as a Breast Cancer Oncogene. *Cell* 129: 1065–1079.
36. Coté N, Mahmut A, Bosse Y, Couture C, Pagé S, et al. (2013) Inflammation Is Associated with the Remodeling of Calcific Aortic Valve Disease. *Inflammation* 36: 573–581.
37. Pashkow FJ (2011) Oxidative Stress and Inflammation in Heart Disease: Do Antioxidants Have a Role in Treatment and/or Prevention? *International Journal of Inflammation* 2011: 1–9.

38. New SEP, Aikawa E (2011) Molecular Imaging Insights Into Early Inflammatory Stages of Arterial and Aortic Valve Calcification. *Circulation Research* 108: 1381–1391.
39. Mahler GJ, Farrar EJ, Butcher JT (2013) Inflammatory Cytokines Promote Mesenchymal Transformation in Embryonic and Adult Valve Endothelial Cells. *Arteriosclerosis, Thrombosis, & Vascular Biology* 33: 121–130.
40. Farrar EJ, Huntley GD, Butcher JT (2015) Endothelial-Derived Oxidative Stress Drives Myofibroblastic Activation and Calcification of the Aortic Valve. *PLoS ONE*: 1–19.
41. Yu Z, Seya K, Daitoku K, Motomura S, Fukuda I, et al. (2011) Tumor necrosis factor- α accelerates the calcification of human aortic valve interstitial cells obtained from patients with calcific aortic valve stenosis via the BMP2-Dlx5 pathway. *Journal of Pharmacology and Experimental Therapeutics* 337: 16–23.
42. Miller JD, Weiss RM, Serrano KM, Brooks RM, Berry CJ, et al. (2009) Lowering Plasma Cholesterol Levels Halts Progression of Aortic Valve Disease in Mice. *Circulation* 119: 2693–2701.
43. Antonini-Canterin F, Hîrșu M, Popescu BA, Leiballi E, Piazza R, et al. (2008) Stage-Related Effect of Statin Treatment on the Progression of Aortic Valve Sclerosis and Stenosis. *The American Journal of Cardiology* 102: 738–742.
44. Huber MA, Aoitei N, Baumann B, Grunert S, Sommer A, et al. (2004) NF- κ B is essential for epithelial-mesenchymal transition and metastasis in a model of breast cancer progression. *Journal of Clinical Investigation* 114: 569–581.
45. Li CW, Xia W, Huo L, Lim SO, Wu Y, et al. (2012) Epithelial-Mesenchymal Transition Induced by TNF α Requires NF- κ B-Mediated Transcriptional Upregulation of Twist1. *Cancer Research* 72: 1290–1300.
46. Stanisavljevic J, Porta-de-la-Riva M, Batlle R, de Herreros AG, Baulida J (2012) The p65 subunit of NF- κ B and PARP1 assist Snail1 in activating fibronectin transcription. *Journal of Cell Science* 124: 4161–4171.

47. Balachandran K, Alford P, Wylie-Sears J, Goss JA, Grosberg A, et al. (2011) Cyclic strain induces dual-mode endothelial- mesenchymal transformation of the cardiac valve. *Proceedings of the National Academy of Sciences* 108:19943-19948.
48. El-Hamamsy I, Balachandran K, Yacoub MH, Stevens LM, Sarathchandra P, et al. (2009) Endothelium-Dependent Regulation of the Mechanical Properties of Aortic Valve Cusps. *Journal of the American College of Cardiology* 53: 1448–1455.
49. Bosse K, Hans CP, Zhao N, Koenig SN, Huang N, et al. (2013) Endothelial nitric oxide signaling regulates Notch1 in aortic valve disease. *Journal of Molecular and Cellular Cardiology* 60: 27–35.
50. Richards J, El-Hamamsy I, Chen S, Sarang Z, Sarathchandra P, et al. (2013) Side-Specific Endothelial-Dependent Regulation of Aortic Valve Calcification. *The American Journal of Pathology*: 1–11.
51. Hess K, Ushmorov A, Fiedler J, Brenner RE, Wirth T (2009) TNF α promotes osteogenic differentiation of human mesenchymal stem cells by triggering the NF- κ B signaling pathway. *Bone* 45: 367–376.
52. Bischoff J, Aikawa E (2011) Progenitor Cells Confer Plasticity to Cardiac Valve Endothelium. *J of Cardiovasc Trans Res* 4: 710–719.
53. Yao Y, Jumabay M, Ly A, Radparvar M, Cubberly MR, et al. (2013) A Role for the Endothelium in Vascular Calcification. *Circulation Research* 113: 495–504.
54. Gössl M, Khosla S, Zhang X, Higano N, Jordan KL, et al. (2012) Role of Circulating Osteogenic Progenitor Cells in Calcific Aortic Stenosis. *Journal of the American College of Cardiology* 60: 1945–1953.
55. Yip CYY, Chen JH, Zhao R, Simmons CA (2009) Calcification by Valve Interstitial Cells Is Regulated by the Stiffness of the Extracellular Matrix. *Arteriosclerosis, Thrombosis, & Vascular Biology* 29: 936–942.
56. Ishihara S, Yasuda M, Harada I, Mizutani T, Kawabata K, et al. (2013) Substrate stiffness regulates temporary NF- κ B activation via actomyosin contractions. *Experimental Cell Research* 319: 2916–2927.

57. Wu X, Guo R, Chen P, Wang Q, Cunningham PN (2009) TNF induces caspase-dependent inflammation in renal endothelial cells through a Rho- and myosin light chain kinase-dependent mechanism. *American Journal of Physiology-Renal Physiology* 297: F316–F326.
58. Zhao G, Xu M-J, Zhao M-M, Dai X-Y, Kong W, et al. (2012) Activation of nuclear factor-kappa B accelerates vascular calcification by inhibiting ankylosis protein homolog expression. *Kidney Int* 82: 34–44.
59. Weiss RM, Lund DD, Chu Y, Brooks RM, Zimmerman KA, et al. (2013) Osteoprotegerin Inhibits Aortic Valve Calcification and Preserves Valve Function in Hypercholesterolemic Mice. *PLoS ONE* 8: e65201.
60. Boyce BF, Xing L (2007) Biology of RANK, RANKL, and osteoprotegerin. *Arthritis Res Ther* 9: S1.
61. Hoffman A, Baltimore D (2006) Circuitry of nuclear factor kB signaling. *Immunological Reviews* 210: 171–186.
62. Kaden J, Bickelhaupt S, Grobholz R, Haase KK, Sarikoç A, et al. (2004) Receptor activator of nuclear factor κ B ligand and osteoprotegerin regulate aortic valve calcification. *Journal of Molecular and Cellular Cardiology* 36: 57–66.
63. Liu SF, Ye XB, Malik, AB (1999) Inhibition of NF-kappa B activation by pyrrolidine dithiocarbamate prevents in vivo expression of proinflammatory genes. *Circulation* 100: 1330–1337.
64. Lim JJ, Li X, Lu J, Pedego TM, Demer L, et al. (2015) Protective Role of Smad6 in Inflammation-Induced Valvular Cell Calcification. *J Cell Biochem*. Epub ahead of print.
65. Orlowski RZ, Voorhees PA, Garcia RA, Hall MD, Kudrik FJ, Allred T, et al. (2015) Phase 1 Trial of the Proteasome Inhibitor Bortezomib and Pegylated Liposomal Doxorubicin in Patients with Advanced Hematologic Malignancies. *Blood* 105: 3058–65.
66. Vij R, Siegel DS, Jagannath S, Jakubowiak AJ, Stewart AK, McDonagh K, et al. (2012) An Open-Label, Single-Arm, Phase 2 Study of Single-Agent Carfilzomib in

Patients with Relapsed and/or Refractory Multiple Myeloma Who Have Been Previously Treated with Bortezomib. *British Journal of Haematology* 158: 739–48.

67. Prasad S, Gupta SC, Tyagi AK, Aggarwal BB. (2014) Curcumin, a component of golden spice: From bedside to bench and back. *Biotechnology Advances* 32: 1053–64.

68. Pierce JW, Schoenleber R, Jesmok G, Best J, Moore SA, Collins T, et al. (1997) Novel Inhibitors of Cytokine-Induced I κ B α Phosphorylation and Endothelial Cell Adhesion Molecule Expression Show Anti-Inflammatory Effects in Vivo. *Journal of Biological Chemistry* 272: 21096–103.

69. Greten FR, Eckmann L, Greten TF, Park JM, Li ZW, Egan LJ, et al. (2004) IKK β Links Inflammation and Tumorigenesis in a Mouse Model of Colitis-Associated Cancer. *Cell* 118: 285–96.

70. Kasinski AL, Slack FJ (2011) MicroRNAs en route to the clinic: progress in validating and targeting microRNAs for cancer therapy. *Nature Reviews Cancer* 11: 849-864.

71. McClung MR, Lewiecki EM, Cohen SB, Bolognese MA, Woodson GC, Moffett AH (2006) Denosumab in Postmenopausal Women with Low Bone Mineral Density. *New England Journal of Medicine* 354:821-831.

72. Schwarz EM, Ritchlin CT (2007) Clinical Development of ant-RANKL therapy. *Arthritis Research & Therapy* 9(Suppl 1): S7.

CHAPTER 6

CHARACTERIZATION OF THE ROLE OF OCT4 IN ADULT AORTIC VALVE DISEASE

6.1 Abstract

Aims

There is significant overlap between the mechanisms active in aortic valve development and disease, but thus far no targetable factors have been identified. Here we investigate the role of Oct4, a transcription factor known to direct heart formation, in inflammatory and calcific pathogenesis of the adult valve.

Methods and Results

Healthy and diseased human valve tissue, 3-D *in vitro* co-culture models, and an *in vivo* model of valve calcification was used to characterize the role of Oct4 in normal and calcifying aortic valves. We found that Oct4 is nuclear localized in the calcified human aortic valve, in both endothelial and interstitial cells. *In vitro*, modulation of Oct4 regulated features of TNF α -driven EndMT. In long-term studies, over-expression of Oct4 drove endothelial participation in calcification. Inhibition of Oct4 mitigated valve interstitial cell calcification via repression of Runx2 and osteocalcin. A hypercholesterolemic mouse model of early aortic valve disease showed increased Oct4 expression specific to the valve endothelium.

Conclusions

Oct4 regulates inflammatory and calcific elements of aortic valve disease in a cell-specific manner. Inhibition of Oct4 activation, particularly in valve interstitial cells, could form the basis of a novel therapeutic intervention strategy.

6.2 Introduction

Aortic valve disease (AVD) is a significant contributor to cardiovascular death in the U.S.A., occurring in 2.8% of Americans over the age of 75 [1]. The causes of AVD are unknown, but recent studies suggest significant overlap between AVD mechanisms and the mechanisms of valvulogenesis. One such mechanism is the endothelial to mesenchymal transformation (EndMT), in which endocardial cells of the developing heart outflow tract become mesenchymal, populating and remodeling the aortic valve leaflet [2]. EndMT is necessary for healthy cell migration, matrix digestion, cell separation, and growth in the developing valve. Many of these same events occur in AVD, including activation of endothelial cells, matrix disorganization, proliferation, and cell migration [3].

Recently, we have shown that EndMT occurs in postnatal valve disease due to inflammatory stimulus, via similar pathways as in the developing heart [4,5]. Other groups have shown postnatal valve EndMT as a consequence of strain [38], altered shear stress [6], and elevated Notch signaling [7]. Similarities between postnatal and developmental EndMT (rev: [8,9]) suggests that EndMT may provide a source of valve cells in the interstitium with increased differentiation potential in the beginning stages of valve disease. Indeed, a recent study from our lab indicates that a sub-population of adult VEC that undergo inflammatory EndMT and have a pro-AVD phenotype and ability to remodel their extracellular matrix environment [10]. It is not known whether this particular type of postnatal, inflammation-driven EndMT is a robust transdifferentiation event, as shown in other tissues [11].

Recent studies have shown that adult aortic valves contain a subpopulation of cells with phenotypic plasticity, collectively known as “mesenchymal progenitors”. These valve interstitial cells (VIC) can differentiate into osteogenic, adipogenic, chondrogenic, and myofibroblastic lineages [12]. The origin of these cells is currently unknown. One source is circulating endothelial progenitor cells, but these account for only 4% of cells with demonstrated phenotypic plasticity in sclerotic valves [13,14]. We hypothesize that these mesenchymal progenitors in adult valves are transdifferentiated valve endothelial cells, populating the valve mesenchyme due to inflammatory EndMT. Pro-EndMT stimulation initiates valve endothelial cell transdifferentiation, whereby VEC become activated mesenchymal cells and participate in valve pathology by taking on an osteogenic or myofibroblastic phenotype.

One mechanism by which this transdifferentiation may occur is through upregulation of stem-cell regulating transcription factors in valve endothelial cells involved in AVD EndMT. Octamer binding transcription factor 4 (Oct4), also known as POU5F1, is a critical regulator of self-renewal and differentiation in stem cells [15]. It is strongly expressed in the inner cell mass (ICM) and repressed in the trophoectoderm [39]. Oct4 is one of four governing transcription factors in induced pluripotent stem cells (iPS) [16-18] and one of two necessary factors in porcine iPS [19]. Tight regulation of Oct4 is essential in directing embryonic stem cells towards a cardiac lineage [20]. Oct4 is

persistently expressed in cardiac progenitors that have been used in regeneration post-myocardial infarction [21].

In this study, we characterize the expression of Oct4 in healthy and calcified human aortic valve leaflets. We use a transwell assay to identify Oct4 levels in VEC involved in different stages of inflammatory EndMT. We characterize the role of Oct4 in TNF α -driven EndMT by utilizing over-expression and antisense Oct4 plasmids. We further analyze the role of Oct4 in cell-specific contributions to valve calcification, utilizing long-term studies and 3-D *in vitro* co-culture models in combination with genetic manipulation. Finally, we identify Oct4 as a feature of hypercholesterolemic valve disease in an *in vivo* model of aortic valve degeneration.

6.3 Materials and Methods

Porcine aortic valve cell co-culture model

3-D collagen hydrogels with porcine aortic valve interstitial, endothelial, or interstitial/endothelial cell co-culture were created as described previously [22]. Briefly, valve interstitial cells (VIC) were trypsinized and resuspended at a concentration of 1 million cells/mL in a 2 mg/mL collagen solution supplemented with 10% FBS and neutralized with NaOH. 200 μ L of this VIC gel solution was pipetted into individual wells of a 24-well plate, each well having been previously lined with a barrier of hydrophobic pen (ImmEdge, Vector Labs) in order to create a gel bolus in the center of the well. The VIC gel was allowed to polymerize in the incubator at 37°C for > 20 minutes, or until set. For co-culture, VEC were seeded on the surface of the VIC gel at a density of 100,000 cells/cm². VEC-only gels were made as described in previous chapters. Transwell migration assay was carried out as described in [10].

Immunofluorescence

Immunofluorescent staining of cells on hydrogels was completed as described in previous chapters. Primary antibodies used were Oct4 (Cell Signaling Technology, #2750), Runx2 (Abcam, ab76956), α SMA (Abcam, ab5694), and osteocalcin (Abcam, ab13418). Secondary antibodies were Alexa FluorTM 568 and 488 (Life Technologies). Nuclear staining was done with Draq5 (Cell Signaling Technology, #4084).

Alizarin Red S Staining for calcium

The Alizarin Red S (ARS) stain was used to visualize calcium deposition in our gels. Gels were fixed overnight in 4% PFA and rinsed thoroughly in 1x PBS. A 2% solution of ARS in distilled water was applied to cover each gel and allowed to incubate at room temperature for 20 minutes. Gels were then rinsed in plenty of 1x PBS until a negative control gel (no cells) was completely cleared of dye. Stained gels were imaged on a Zeiss widefield microscope with a Lumenera INFINITY microscope camera.

Mouse aortic valve analysis

Five month-old C57/Bl6J wild type mice were sacrificed and perfused with 1x PBS via the left ventricle in order to clear the heart of blood. The heart was removed, rinsed in 1x PBS, and fixed in 4% PFA at 4°C overnight. The heart was then moved to 70% EtOH for > 24 hours, then embedded *en face* in a paraffin block according to standard procedure by the Cornell University Veterinary Histology Laboratory. Microtome was used to cut 6µm sections of the heart, which were mounted on slides and allowed to dry overnight. Immunofluorescence was carried out in the same manner as human valve paraffin sections, as described in chapter four.

Quantitative real-time PCR

Q-rtPCR for mRNA in porcine cells was carried out as described previously, with the addition of Oct4 forward primer GCAGTGA CTATTCGCAACGA and reverse primer TAGCCTGGGGTACCAAATG (5' to 3').

Electroporation of Oct4 and Antisense Oct4

Plasmids expressing Oct4 and an antisense sequence for inhibition of Oct4 activity were kindly provided to us by the Puceat Lab, INSERM, Marseille, France, as described in [20]. An empty vector was used as control. The empty vector was not observed to have any effect across conditions and cell types. Plasmids were delivered to VEC or VIC using the 100 μ L Neon[®] Transfection System (Life Technologies), according to the manufacturer's instructions. Electroporation conditions were 1600V, 20ms, 1 pulse.

6.4 Results

Oct4 expression in healthy and calcified human aortic valves

In healthy valves from patients with no other cardiovascular disease or valve pathology, Oct4 was present in the cytoplasm (but not nuclei) of cells. Cytoplasmic Oct4 was more highly expressed in VEC than in VIC. There was more Oct4 in VEC on the ventricularis side of the AoV than on the fibrosa side. At the free edge of the AoV, Oct4 was present in approximately 10% of VIC. There was less Oct4 in VEC near the free edge than at the root of the valve (Figure 6.1).

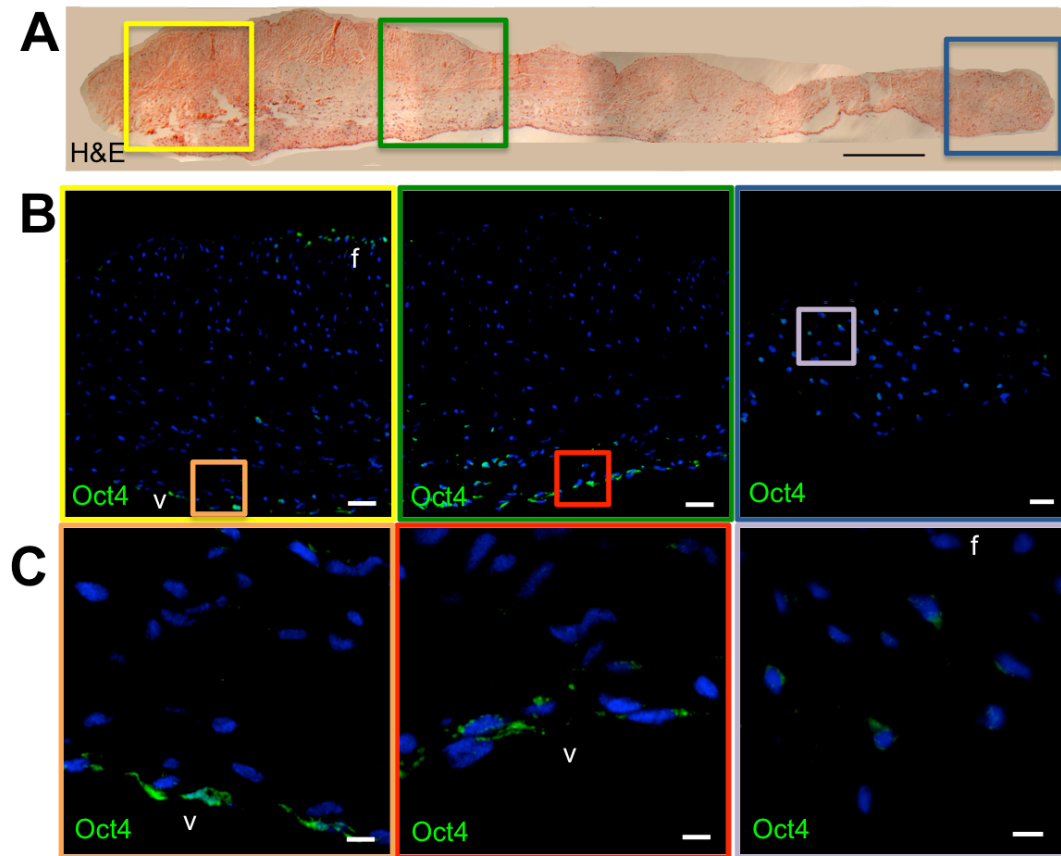


Figure 6.1 Oct4 in healthy human aortic valve leaflets.

A. H&E staining of representative healthy human aortic valve leaflet. Colored boxes correspond to the magnified regions shown in lower panels. B. Oct4 (green) and nuclei (blue) in different regions of healthy human aortic valve leaflet. Colored boxes correspond to magnified regions shown in lower panels. Scale bar is 100 μ m. C. Magnified views of boxed areas from panel B. Scale bar = 10 μ m.

In calcified human aortic valves, Oct4+ positive nuclei are found throughout the valve leaflet (Figure 6.2). We observed nuclear Oct4 in cells proximal to regions of mature calcification (green box). We also observed nuclear Oct4 in VEC in both heavily diseased regions (yellow box) and in regions distal to observable calcification (blue box). Interestingly, VEC with nuclear Oct4 were only observed on the fibrosa side of

the valve. VIC with nuclear Oct4 were observed throughout the valve leaflet, in approximately 10% of VIC.

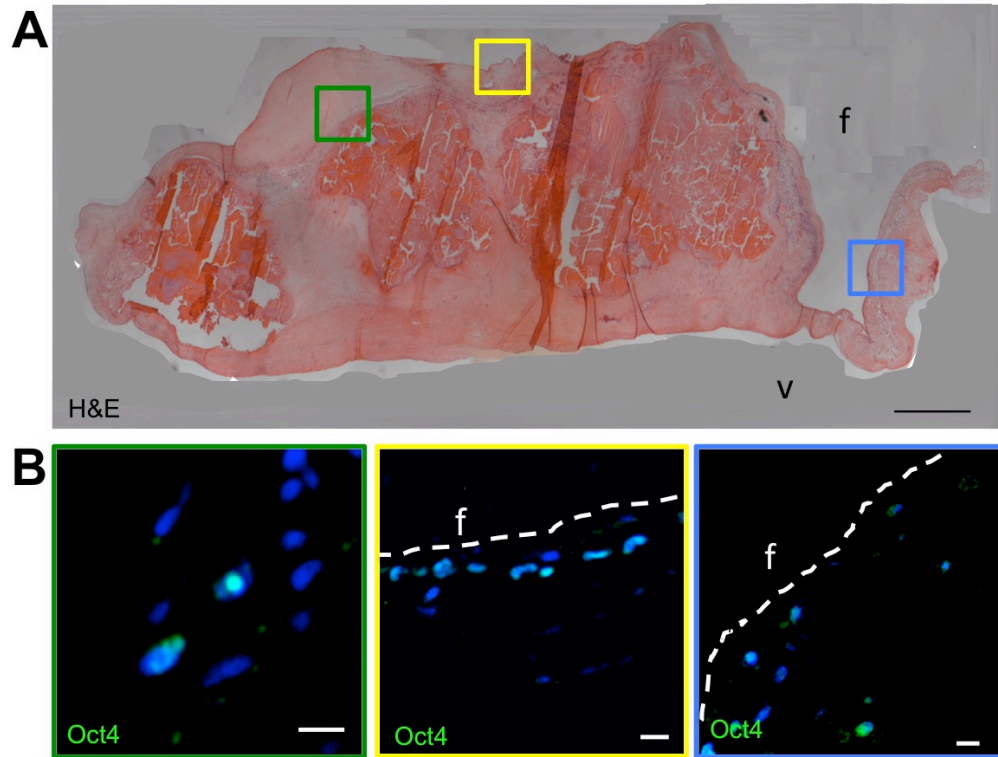


Figure 6.2 Oct4 in calcified human aortic valve leaflets.

A. H&E staining of representative calcified human aortic valve leaflet. (N = 11) Colored boxes correspond to the magnified regions shown in lower panels. Scale bar is 1 mm. B. Oct4 (green) and nuclei (blue) in different regions of calcified human aortic valve leaflet. Colored boxes correspond to magnified regions shown in lower panels. Scale bar is 10 μ m.

Role of Oct4 in regulation of inflammatory endothelial to mesenchymal transformation in valve endothelial cells

We then over-expressed (+Oct4) or inhibited (+ASOct4) Oct4 in VEC (Figure 6.3) and VIC. Vectors maintained over-expression or inhibition out to 14 days of culture in control or osteogenic conditions (Figure 6.4). VEC+Oct4 or +ASOct4 were then cultured for 48 hours on 3D collagen hydrogels (Figure 6.5A). VEC transfected with

the control vector (+empty) had low Oct4 that was localized to the nucleus, robust expression of the endothelial protein CD31, and no α SMA. Over-expression of Oct4 showed good increase in Oct4 expression in both the nucleus and cytosol, maintained CD31 comparable to control, and had no α SMA. Transfection of ASOct4 blocked Oct4 expression, decreased CD31 and increased α SMA.

Transwell migration experiment revealed decreased Oct4 in VEC undergoing EndMT due to the stimulus of TNF α . Oct4 was increased in VEC that resisted TNF α -EndMT, which remained on the surface of the transwell as an intact endothelial layer (Figure 6.4B). VEC cultured on collagen hydrogels and treated with TNF α had significant upregulation of Snai1 mRNA after 48 hours. Over-expression of Oct4 in VEC increased the basal level of Snai1 mRNA, but did not affect VEC Snai1 response to TNF α treatment. Inhibition of Oct4 by transfection of an Oct4 antisense vector (ASOct4) lowered basal levels of Snai1 and blocked VEC upregulation of Snai1 in response to TNF α (Figure 6.5B).

VEC cultured on collagen hydrogels and treated with TNF α had significant upregulation of ACTA2 mRNA after 48 hours. Over-expression of Oct4 increased the basal level of ACTA2 expression, but inhibition of Oct4 did not block ACTA2 increase. Inhibition of Oct4 with the antisense plasmid increased basal level of ACTA2 with and without TNF α treatment (Figure 6.5C). VEC cultured on collagen hydrogels and treated with TNF α had significant downregulation of VE-cadherin

mRNA after 48 hours. This decrease was unaffected by over-expression or inhibition of Oct4 (Figure 6.5D).

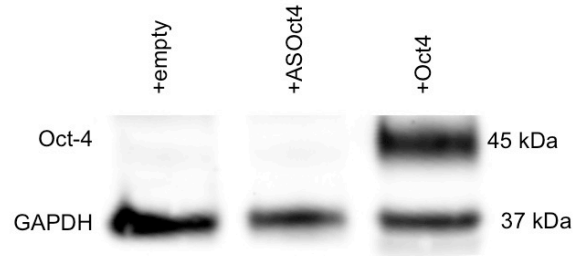


Figure 6.3 Delivery of ASOct4 and Oct4 plasmids to PAVEC.

Western blot, 2D culture, 48 hours post-transfection. Representative image of N=3 independent experiments.

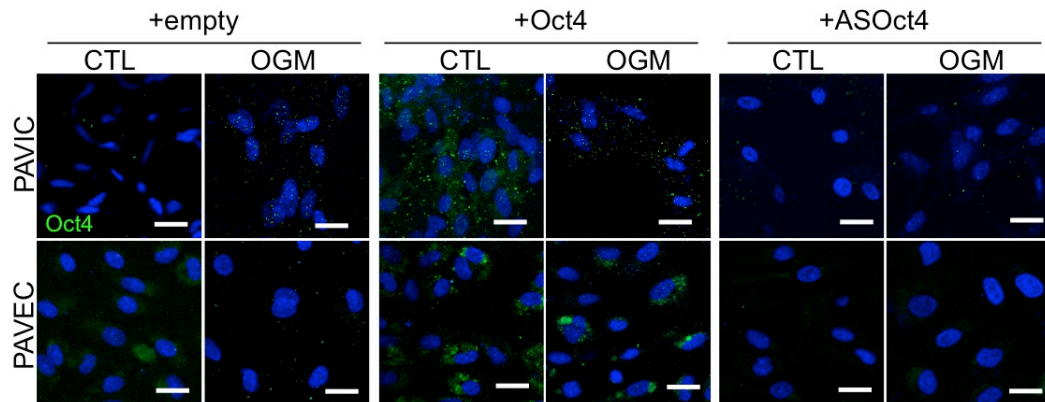


Figure 6.4 Oct4 protein expression in PAVIC and PAVEC after 14 days.

Cells were transfected with empty vector, Oct4, or ASOct4 and cultured in CTL or OGM condition. Representative images of N=4 independent experiments. Scale bar is 20µm.

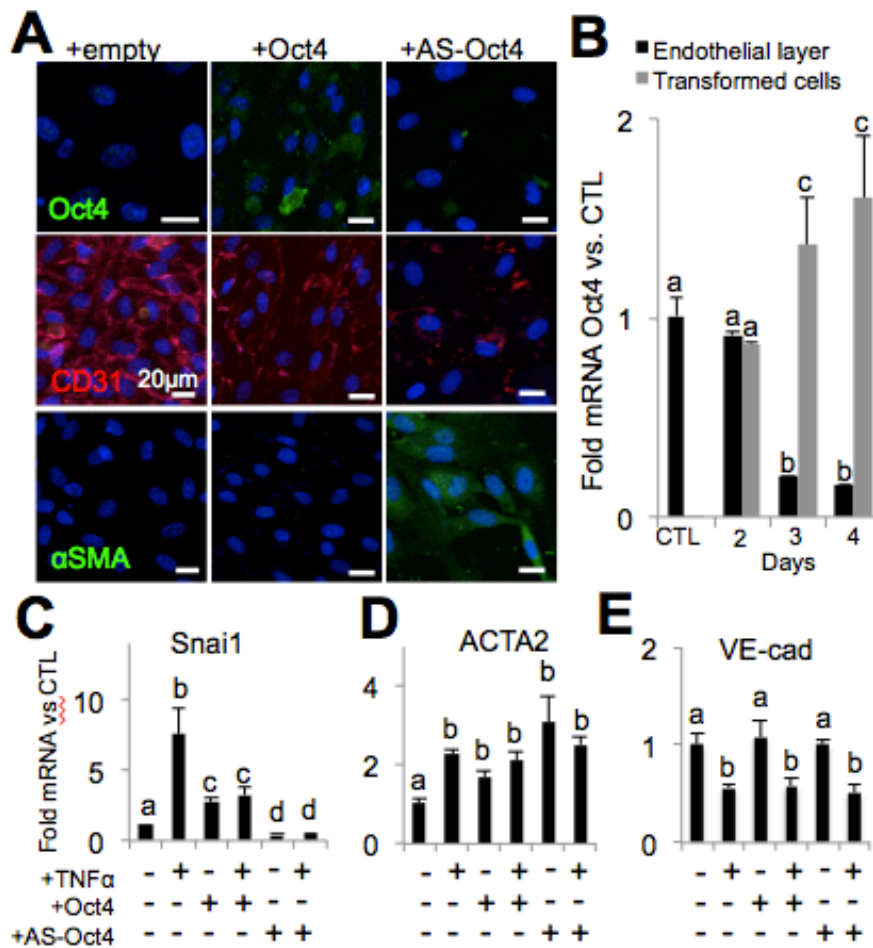


Figure 6.5 Effect of Oct-4 modulation on VEC inflammatory EndMT.

A. Immunofluorescent staining of Oct4, CD31, and VE-cadherin protein expression in VEC on hydrogels in control media for 48 hours, with indicated transfections. B. Separation and analysis of Oct-4 mRNA in non-transformed and transformed VEC after 2-4 days of TNF α treatment. C. Snai1 mRNA in VEC with over-expression or inhibition of Oct-4, treated with control or TNF α for 48 hours. D. ACTA2 mRNA, same conditions as C. E. VE-cad mRNA, same conditions as C. N \geq 3 for all experiments. Bars with different letters are statistically different (p < 0.05), error bars indicate SEM.

Cell-specific changes in Oct4 expression in pro-osteogenic and/or inflammatory environments

We then examined the expression of Oct4 in pathologically relevant culture conditions, namely in osteogenic (+OGM) or osteogenic and inflammatory (OGM+TNF α) treatment media for 14 days. When cultured alone, VIC upregulated Oct4 in response to OGM and, to a lesser degree, in response to OGM+TNF α (Figure 6.6A). VEC showed lower basal levels of Oct4 mRNA after 14 days than VIC. Interestingly, VEC upregulated Oct4 in response to OGM, but not in response to OGM+TNF α (Figure 6.6B). This may be due to a shift in phenotype of VEC undergoing EndMT in response to TNF α . Co-culturing VIC+VEC increased overall Oct4 levels. The co-culture showed decreased Oct4 in response to OGM, possibly due to a synergistic/protective effect of VEC when cultured with VIC. VIC+VEC cultured had increased Oct4 in response to TNF α (Figure 6.6C).

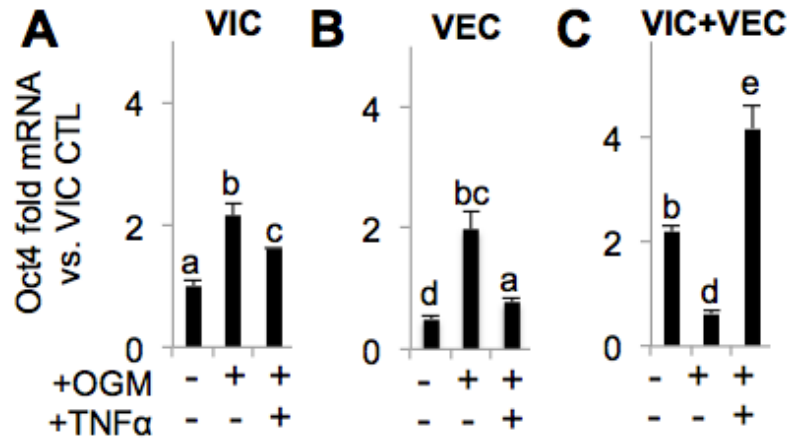


Figure 6.6 Oct4 mRNA in 14 day valve cell co-culture (+OGM, + TNF α).

A. 14 day culture of VIC embedded in hydrogels with OGM and TNF α treatment. B. 14 day culture of VEC on surface of hydrogel with OGM and TNF α treatment. C. 14 day co-culture of embedded VIC with VEC seeded on surface of hydrogels with OGM and TNF α treatment.

N \geq 3 for all experiments. Bars with different letters are statistically different (p < 0.05) compared to VIC only control, error bars indicate SEM.

Over-expression of Oct4 permits VEC to undergo calcification and upregulate pro-osteogenic signaling.

This study and others from our lab [22] have shown that VEC cultured on 3D hydrogels do not calcify in response to osteogenic stimulus. However, when Oct4 was over-expressed in VEC, VEC calcified in response to osteogenic media (Figure 6.7A). Oct4 over-expression plasmid increased basal Oct4 by 1.64 fold in CTL condition and increased to 29.4 fold with OGM treatment (Figure 6.7B). VEC+Oct4 had significantly higher expression of ACTA2/ α SMA and osteocalcin in response to OGM (Figure 6.7C,D). Osteocalcin is produced by osteoblasts and is an indicator of bone formation. Interestingly, VEC+Oct4 had less of the pro-osteogenic transcription factor Runx2 mRNA than non-transfected VEC. However, examination of protein expression showed highest levels of both nuclear and cytosolic Runx2 protein in

VEC+Oct4+OGM (Figure 6.7E). Runx2 signaling in VEC+Oct4 may drive pro-osteogenic differentiation.

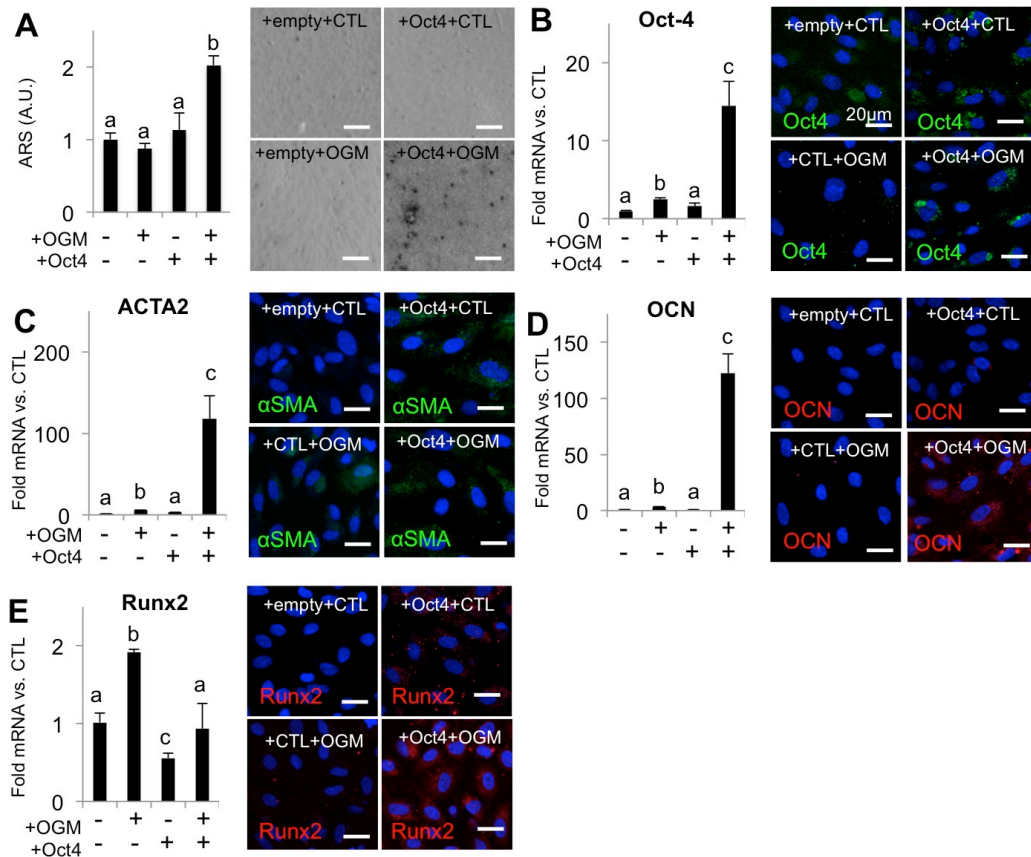


Figure 6.7 Oct4 over-expression enables VEC calcification and pro-osteogenic signaling.

A. Alizarin Red S staining and quantification of 14 day VEC. Scale bar is 100 μ m. B. Oct4 mRNA levels and protein expression. C. ACTA2 mRNA and α SMA protein expression. D. Osteocalcin mRNA levels and protein expression. E. Runx2 mRNA levels and protein expression. Scale bars for immunofluorescence images are 20 μ m. Images are representative of N > 3 independent experiments. For q-rtPCR data, N \geq 3 for all experiments. Bars with different letters are statistically different (p < 0.05), error bars indicate SEM.

Oct4 regulates calcification and development of osteoblast-like phenotype in valve interstitial cells.

In VIC, over-expression of Oct4 increased calcification, though calcium deposition appeared diffuse and not nodular. Inhibition of Oct4 with the antisense plasmid (ASOct4) reduced VIC calcification (Figure 6.8A). VIC+Oct4 showed an increased upregulation of Oct4 mRNA in response to OGM that was blocked by ASOct4. (Figure 6.8B). Over-expression of Oct4 slightly reduced VIC myofibroblastic response to OGM, as indicated by ACTA2 mRNA levels and α SMA protein expression. VIC+ASOct4 showed decreased ACTA2 mRNA in both CTL and OGM groups, but similar α SMA protein changes. VIC+Oct4 had elevated osteocalcin mRNA in both CTL and OGM conditions. Oct4 and ASOct4 did not affect osteocalcin protein expression (Fig 6.8C). VIC+Oct4 had highly elevated Runx2 mRNA in both control and OGM conditions. VIC+ASOct4 had slightly elevated Runx2 mRNA in both control and OGM conditions. Runx2 protein was elevated in VIC+OGM and VIC+ASOct4+OGM conditions (Figure 6.8D).

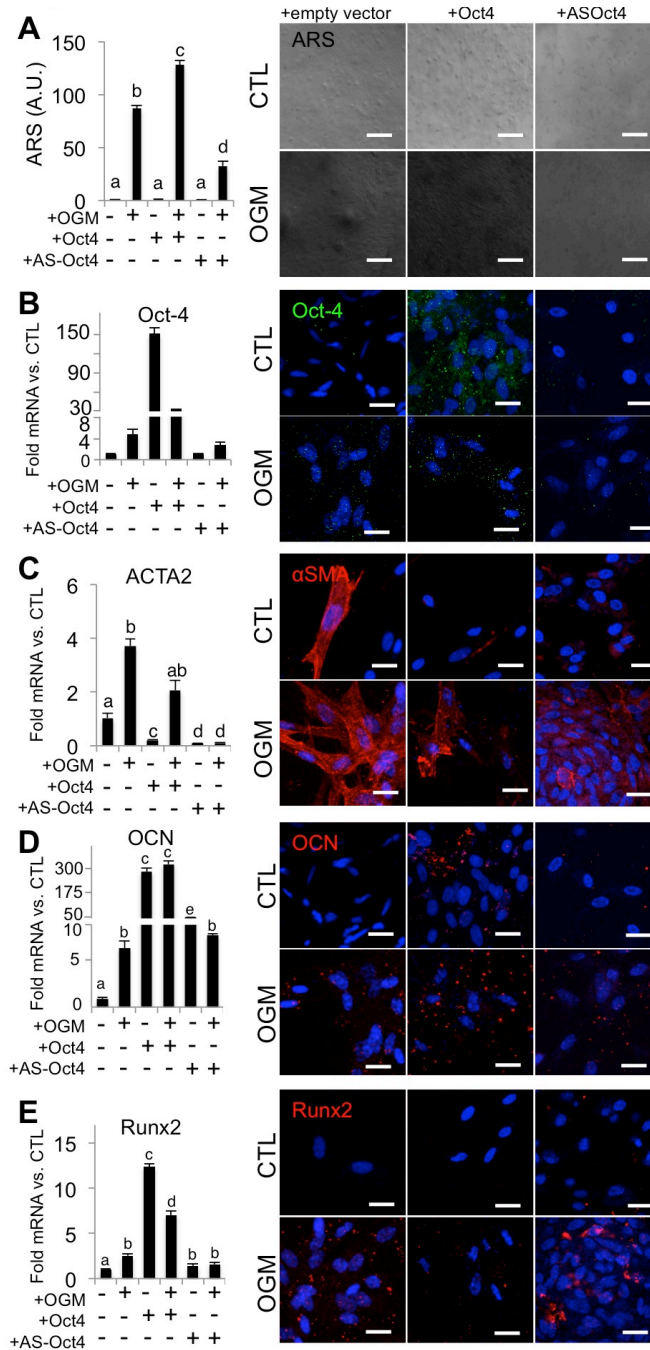


Figure 6.8 Effect of Oct4 over-expression or inhibition on VIC calcification.

14 day VIC+CTL or OGM, with Oct4 over-expression or inhibition (antisense Oct4 transfection). A. Alizarin Red S staining and quantification. Scale bar is 100 μ m. B. Oct4 mRNA levels and protein expression. C. ACTA2 mRNA and α SMA protein expression. D. Osteocalcin mRNA levels and protein expression. E. Runx2 mRNA levels and protein expression. Scale bars for immunofluorescence images are 20 μ m. Images are representative of N > 3 independent experiments. For q-rtPCR data, N \geq 3 for all experiments. Bars with different letters are statistically different ($p < 0.05$), error bars indicate SEM.

Upregulation of Oct4 in stenotic LDLR^{-/-} mouse aortic valves

Healthy adult mice showed no expression of Oct4 protein in the aortic valve. LDLR^{-/-} mice were fed a high fat (Western) diet from 4-20 weeks of age and used as a model of aortic valve sclerosis. Elsewhere, we show increased aortic blood flow velocity and calcific deposition in the valves of these mice (Chapter 7). LDLR^{-/-} mice with the high fat diet showed increased Oct4 expression in aortic valve endothelial cells on both sides of the valve (Figure 6.9).

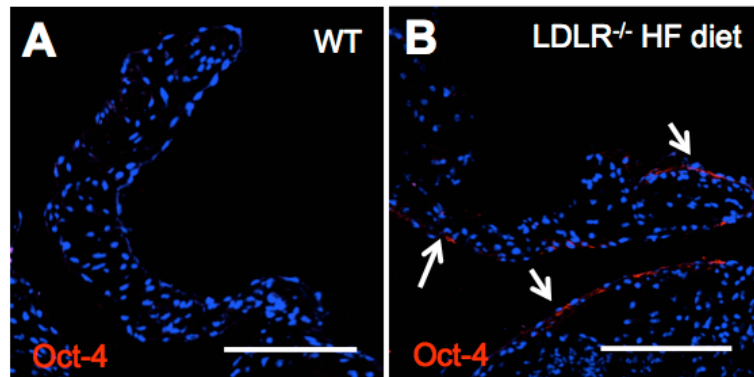


Figure 6.9 Oct4 expression in healthy and diseased adult mouse aortic valves.

A. Oct4 protein expression in 20 week-old wild type C57 Bl6 mice fed a control diet. B. Oct4 protein expression in 20 week-old LDLR^{-/-} mice fed a high fat diet (Western diet) for 16 weeks. N = 4. Scale bar is 100 μ m.

6.5 Discussion

These findings present Oct4 as a new addition to the growing list of transcriptional factors that are active in both valve development and disease (review: [9]). These factors, including Notch1 [23], Sox9 [24,25], and Msx2 [26], often lend insight to the design of diagnostic and therapeutic strategies for AVD. The overlap between valve development and disease can also elucidate how these factors govern pathology.

The results shown here demonstrate an active role for Oct4 in regulation of postnatal aortic valve EndMT. Understanding postnatal valve cell transdifferentiation events such as EndMT can improve tissue engineering, potentially through controlling VEC phenotype by tuning controlling factors like Oct4. A recent review suggests that inducing EndMT in postnatal cells on tissue engineered valves could promote healthy matrix remodeling and condensation, like that which occurs in valvulogenesis [27]. However, the results shown here demonstrate the complex nature of EndMT in postnatal cells. We observed upregulation of Oct4 in VEC undergoing EndMT, indicating that extreme caution is recommended when using EndMT to populate tissue-engineered constructs. High levels of Oct4 may make EndMT-VEC prone to aberrant transdifferentiation, making these cells particularly challenging to direct towards a desired and permanent phenotype.

Here, we found that over-expression of Oct-4 upregulated Snai1 and ACTA2, suggesting it is an EndMT inducer. Snai1 is regulated by Notch in development and is critical to valve EMT [28]. ASOct4 blocked Snai1 signaling, similar to how Oct4

inhibition has been observed to prevent EMT in cancer cells [29] and in circulating stem cells [30]. Oct4-EndMT mechanisms may also have overlap with postnatal inflammatory-EndMT. Smad2 signaling features in both TNF α -EndMT of adult valve endothelial cells [4] and in regulation of Oct4 levels in the embryo [31].

We also used the transwell assay to divide valve endothelial cells into transforming and non-transforming populations, as demonstrated previously [10]. The assay showed that non-transforming cells have less Oct4 expression than transforming cells, suggesting that Oct4 levels dictate the final differentiation fate of endothelial cells, similar to in the embryo [32]. This also suggests that there is heterogeneity in the ability of postnatal valve endothelial cells to undergo EndMT transdifferentiation. The ability to upregulate Oct4 may be a prerequisite for valve endothelial cells to undergo EndMT.

Over-expression of Oct4 did not change the basal phenotype of valve endothelial cells, but it did make a pro-myofibroblastic and osteogenic shift possible in VEC exposed to osteogenic stimuli. This points to a VEC population with osteogenic potential given an increase in Oct4 expression. Progenitor cells have been described in the postnatal valve endothelium previously [33], but their mechanism in disease had not been elucidated. Oct4 may be a key factor in VEC participation in late-stage valve calcification.

Transfection of Oct4 changed valve interstitial cells from a quiescent to a pro-osteogenic phenotype via upregulation of OCN and Runx2, but not α SMA. Oct4 transfection also increased calcium deposition of VIC. ASOct4 mitigated calcium deposition and α SMA in VIC with osteogenic stimulus. This modulation of VIC calcification by Oct4 may be explained by interaction between Oct4 and the growth factor BMP-2. BMP-2 is elevated in human AVIC from calcified valves [34] and is known to accelerate the calcification of aortic valve interstitial cells [35]. In development, Oct4 is upregulated by BMP-2 [20] and may be similarly controlled in the calcifying valve. Therefore, an increase in BMP-2 during the calcification process may upregulate Oct4 expression in the valve, driving the increased calcification demonstrated here.

These findings should be examined *in vivo* in order to understand the overlap between native valve cells that gain Oct4-mediated transdifferentiation potential and extravalvular progenitor cells such as circulating osteoprogenitor cells [36]. Specifically, mice with valve-specific and valve endothelium-specific cre recombinase should be used to delete Oct4 in the aortic valve. This experiment combined with a model of AVD would elucidate the role of Oct4-mediated transdifferentiation as a homeostatic or disease-associated event. In addition, the necessity of Oct4 for valve cell transdifferentiation in the form of EndMT and pro-osteogenic differentiation should be closely investigated, given recent findings regarding the dispensability of Oct4 in somatic stem cell populations [37]. Overall, Oct4 activity in calcific aortic

valve disease represents a novel mechanism for valve cell transdifferentiation and a new area of investigation regarding valve progenitor cell populations.

REFERENCES

1. Mozaffarian D, DrPH, Benjamin FEJ, Go FAS, Arnett MDK, et al. (2015) Heart Disease and Stroke Statistics - 2015 Update. *Circulation* 131: e29–e322.
2. Butcher JT, Markwald RR (2007) Valvulogenesis: the moving target. *Philosophical Transactions of the Royal Society B* 362: 1489–1503.
3. Rajamannan NM, Evans FJ, Aikawa E, Grande-Allen KJ, Demer LL, et al. (2011) Calcific Aortic Valve Disease: Not Simply a Degenerative Process. *Circulation* 124: 1783–1791.
4. Mahler GJ, Farrar EJ, Butcher JT (2013) Inflammatory Cytokines Promote Mesenchymal Transformation in Embryonic and Adult Valve Endothelial Cells. *Arteriosclerosis, Thrombosis, & Vascular Biology* 33: 121–130.
5. Mahler GJ, Butcher JT (2011) Inflammatory Regulation of Valvular Remodeling: The Good(?), the Bad, and the Ugly. *International Journal of Inflammation* 2011: 1–13.
6. Mahler GJ, Frenzl CM, Cao Q, Butcher JT (2014) Effects of shear stress pattern and magnitude on mesenchymal transformation and invasion of aortic valve endothelial cells. *Biotechnol Bioeng* 111: 2326–2337.
7. Yang J-H, Wylie-Sears J, Bischoff J (2008) Opposing actions of Notch1 and VEGF in post-natal cardiac valve endothelial cells. *Biochemical and Biophysical Research Communications* 374: 512–516.
8. Combs MD, Yutzey KE (2009) Heart valve development regulatory networks in development and disease. *Circulation Research* 105: 408–421.
9. Wirrig EE, Yutzey KE (2014) Conserved Transcriptional Regulatory Mechanisms in Aortic Valve Development and Disease. *Arteriosclerosis, Thrombosis, & Vascular Biology* 34: 737–741.

10. Farrar EJ, Butcher JT (2013) Heterogeneous Susceptibility of Valve Endothelial Cells to Mesenchymal Transformation in Response to TNF α . *Annals of Biomedical Engineering* 42: 149–161.
11. Kalluri R (2009) EMT: When epithelial cells decide to become mesenchymal-like cells. *The Journal of Clinical Investigation* 119: 1417–1419.
12. Chen J-H, Yip CYY, Sone ED, Simmons CA (2009) Identification and Characterization of Aortic Valve Mesenchymal Progenitor Cells with Robust Osteogenic Calcification Potential. *The American Journal of Pathology* 174: 1109–1119.
13. Visconti RP, Ebihara Y, LaRue AC, Fleming PA, McQuinn TC, et al. (2006) An in vivo analysis of hematopoietic stem cell potential. *Circulation Research* 98: 690–696.
14. Skowasch D, Schrempf S, Wernert N, Steinmetz M, Jabs A, et al. (2005) Cells of primarily extravalvular origin in degenerative aortic valves and bioprostheses. *European Heart Journal* 26: 2576–2580.
15. Nichols J, Zevnik B, Anastassiadis K, Niwa H (1998) Formation of pluripotent stem cells in the mammalian embryo depends on the POU transcription factor Oct4. *Cell* 95: 379–391.
16. Takahashi K, Yamanaka S (2006) Induction of pluripotent stem cells from mouse embryonic and adult fibroblast cultures by defined factors. *Cell* 126: 663–676.
17. Shi G, Jin Y (2010) Role of Oct4 in maintaining and regaining stem cell pluripotency. *Stem Cell Research Therapy* 1: 39.
18. Sternecker J, Höing S, Schöler HR (2011) Concise Review: Oct4 and More: The Reprogramming Expressway. *Stem Cells* 30: 15–21.
19. Liu K, Ji G, Mao J, Liu M, WANG L, et al. (2012) Generation of Porcine-Induced Pluripotent Stem Cells by Using OCT4 and KLF4 Porcine Factors. *Cellular Reprogramming* 14: 505–513.

20. Zeineddine D, Papadimou E, Chebli K, Gineste M, Liu J, et al. (2006) Oct-3/4 Dose Dependently Regulates Specification of Embryonic Stem Cells toward a Cardiac Lineage and Early Heart Development. *Developmental Cell* 11: 535–546.
21. Blin G, Nury D, Stefanovic S, Neri T, Guillevic O, et al. (2010) A purified population of multipotent cardiovascular progenitors derived from primate pluripotent stem cells engrafts in postmyocardial infarcted nonhuman primates. *The Journal of Clinical Investigation* 120: 1125.
22. Richards J, El-Hamamsy I, Chen S, Sarang Z, Sarathchandra P, et al. (2013) Side-Specific Endothelial-Dependent Regulation of Aortic Valve Calcification. *The American Journal of Pathology*: 1–11.
23. Garg V, Muth AN, Ransom JF, Schluterman MK, Barnes R, et al. (2005) Mutations in NOTCH1 cause aortic valve disease. *Nature* 437: 270–274.
24. Lincoln J, Kist R, Scherer G, Yutzey KE (2007) Sox9 is required for precursor cell expansion and extracellular matrix organization during mouse heart valve development. *Developmental Biology* 305: 120–132.
25. Peacock JD, Levay AK, Gillaspie DB, Tao G, Lincoln J (2010) Reduced Sox9 Function Promotes Heart Valve Calcification Phenotypes In Vivo. *Circulation Research* 106: 712–719.
26. Chakraborty S, Wirrig EE, Hinton RB, Merrill WH, Spicer DB, et al. (2010) Twist1 promotes heart valve cell proliferation and extracellular matrix gene expression during development in vivo and is expressed in human diseased aortic valves. *Developmental Biology*: 1–46.
27. Sewell-Loftin MK, Chun YW, Khademhosseini A, Merryman WD (2011) EMT-Inducing Biomaterials for Heart Valve Engineering: Taking Cues from Developmental Biology. *J of Cardiovasc Trans Res* 4: 658–671.
28. Timmerman LA, Grego-Bessa J, Raya A, Bertan E, Perez-Pomares JM (2004) Notch promotes epithelial-mesenchymal transition during cardiac development and oncogenic transformation. *Genes & Development* 18: 99–115.

29. Dai X, Ge J, Wang X, Qizn X, Zhang C, et al. (2012) OCT4 regulates epithelial-mesenchymal transition and its knockdown inhibits colorectal cancer cell migration and invasion. *Oncol Rep* 29: 155–160.
30. Wang W, Vootukuri S, Meyer A, Ahamed J, Collier BS (2014) Association Between Shear Stress and Platelet-Derived Transforming Growth Factor- β 1 Release and Activation in Animal Models of Aortic Valve Stenosis. *Arteriosclerosis, Thrombosis, & Vascular Biology* 34: 1924–1932.
31. Waldrip WR, Bikoff EK, Hoodless PA, Wrana JL, Robertson EJ (1998) Smad2 Signaling in Extraembryonic Tissues Determines Anterior-Posterior Polarity of the Early Mouse Embryo. *Cell* 92: 797–808.
32. Wang ZZ, Au P, Chen T, Shao Y, Daheron LM, et al. (2007) Endothelial cells derived from human embryonic stem cells form durable blood vessels in vivo. *Nature Biotechnology* 25: 317–318.
33. Bischoff J, Aikawa E (2011) Progenitor Cells Confer Plasticity to Cardiac Valve Endothelium. *J of Cardiovasc Trans Res* 4: 710–719.
34. Yang X, Fullerton DA, Su X, Ao L, Cleveland JC, et al. (2009) Pro-Osteogenic Phenotype of Human Aortic Valve Interstitial Cells Is Associated With Higher Levels of Toll-Like Receptors 2 and 4 and Enhanced Expression of Bone Morphogenetic Protein 2. *Journal of the American College of Cardiology* 53: 491–500.
35. Seya K, Yu Z, Kanemaru K, Daitoku K, Akemoto Y, et al. (2011) Contribution of Bone Morphogenetic Protein-2 to Aortic Valve Calcification in Aged Rat. *J Pharmacol Sci* 115: 8–14.
36. Bostrom KI, Rajamannan NM, Towler DA (2011) The Regulation of Valvular and Vascular Sclerosis by Osteogenic Morphogens. *Circulation Research* 109: 564–577.
37. Lengner CJ, Camargo FD, Hochedlinger K, Welstead GG, Zaidi S, et al. (2007) Oct4 Expression Is Not Required for Mouse Somatic Stem Cell Self-Renewal. *Cell Stem Cell* 1: 403–415.

38. Balachandran, K., P. Alford, J. Wylie-Sears, J. A. Goss, A. Grosberg, et al. (2011) Cyclic strain induces dual-mode endothelial- mesenchymal transformation of the cardiac valve. *Proc. Natl. Acad. Sci. U. S. A.* 108: 19943-19948.

39. Pesce, Maurizio, and Hans R Schöler. (2001) Oct-4: Gatekeeper in the Beginnings of Mammalian Development. *Stem Cells* 19: 271–278.

CHAPTER 7

VALVE INTERSTITIAL CELL CONTRACTILITY DIRECTS CALCIFICATION AND EXTRACELLULAR MATRIX REMODELING PROCESSES VIA RHOA SIGNALING

Portions of the “Methods” section of this chapter were authored by Varsha Pramil.

Jennifer Richards created Figure 7.1 and took the photos in Figure 7.2

7.1 Abstract

Aims

Valve interstitial cells are dynamic and aggressive players in aortic valve calcification, but their role in modulating the changing mechanical environment of the calcifying aortic valve is not well understood. The goal of this study was to characterize the contractility of valve interstitial cells in long-term (14 day) pro-osteogenic conditions and to understand how valve interstitial cell contractility contributes to calcific degeneration of the aortic valve.

Methods & Results

A novel bioreactor system for quantifying aortic valve interstitial cell contractility in 3-D hydrogels was designed and characterized in control and osteogenic conditions over 14 days. Interstitial cells demonstrated a powerful ability to exert contractile force on their environment and to align collagen fibers with the direction of tension. Osteogenic environment disrupted interstitial cell contractility and led to disorganization of the collagen matrix, concurrent with increased RhoA, α SMA, TGF- β , Runx2 and calcific nodule formation. Inhibition of RhoA blocked pro-osteogenic signaling and calcific nodule formation, but not pro-chondrogenic signaling. Time-course correlation analysis indicated a significant correlation between interstitial cell remodeling of collagen fibers and calcification events.

Conclusions

Interstitial cell contractility mediates internal stress state and organization of the aortic valve extracellular matrix. Osteogenesis disrupts interstitial cell mechanical phenotype

and drives disorganization, nodule formation, and pro-calcific signaling via a RhoA-dependent mechanism.

7.2 Introduction

Aortic valve disease is a leading cause of cardiovascular morbidity resulting in approximately 15,000 deaths per year in the USA. It is primarily a disease of the elderly, occurring in 2.8% of Americans over the age of 75 [1]. It is an active degenerative process driven by complex cell-cell and cell-matrix interactions [2]. Despite sharing risk factors with atherosclerosis [3], it is a pathobiologically unique disease that has no clinically proven intervention strategies outside of cardiothoracic surgery [4].

Valve interstitial cells (VIC) are the predominant cell type in the aortic valve, residing within the valve tissue mesenchyme. VIC interact with the extracellular matrix, the endothelial cell lining, and invaded extravalvular cells [5]. VIC can have quiescent or active phenotype, with the latter involved in valve disease [6]. VIC can also become activated in response to changes in their mechanical [7] or biochemical [8] situation, initiating a complex feedback loop between cell and environment. Elucidation of the factors governing this feedback loop is critical to the design of therapeutics that could slow valve degeneration.

As the aortic valve becomes diseased, its mechanics change in a number of ways. The leaflets stiffen as calcific nodules form [9], the extracellular matrix becomes disorganized [10] and altered in composition [11], and the strain experienced by VIC increases [12]. These changes influence VIC phenotype. Strain state regulates VIC cytokine secretion [13,14], calcification [15], collagen synthesis [16], alignment [17],

and proliferation [18]. Extracellular matrix composition influences VIC homeostasis [19,20], in part through modulation of leaflet [21] and cellular [22] stiffness. However, little is known about how these phenotypic changes feed back onto the mechanical state and pathological degeneration of the valve tissue. It is difficult to uncouple changes in the environment from changes in cellular mechanical activity.

In this study, we have designed a novel system to culture VIC in 3D hydrogels with a controlled and sustained level of tension. The system allows measurement of contractile force VIC exert on their surroundings, as well as imaging of changes to collagen and cell morphology via longitudinal confocal imaging. We have characterized the interplay between VIC contractility, cytoskeletal arrangement, collagen fiber dynamics, and mechanotransductive cell signaling in control and osteogenic conditions

7.3 Materials and Methods

System manufacturing

To create the systems, the Sylgard 184 silicone elastomer kit (Dow Coming, 3097358-1004) was used. From the kit, 56 grams of elastomer and 4 grams of elastomer curing agent were thoroughly mixed until mixture is white and bubbly. This mixture was degased in a vacuum chamber for 30-45 minutes, until clear. The PDMS mixture was poured into plastic molds (Figure 7.1A) and heated in an oven overnight at 65 degrees Celsius. Next, the cured PDMS was removed from the molds. The squares were then cut and inserted into slots in the PDMS spring system (Figure 7.1B) and sealed with more of the PDMS mixture. Next, 1-inch springs (Lee Spring Co., CI 010B 13 S316) were washed with soap, grease remover and DI water. They were then cut to fit into the spring systems as shown in Figure 1 and sealed with PDMS mixture. Next, plugs for the bottom of the spring system were made to ensure the seeded gel is confined to the top of the spring system.

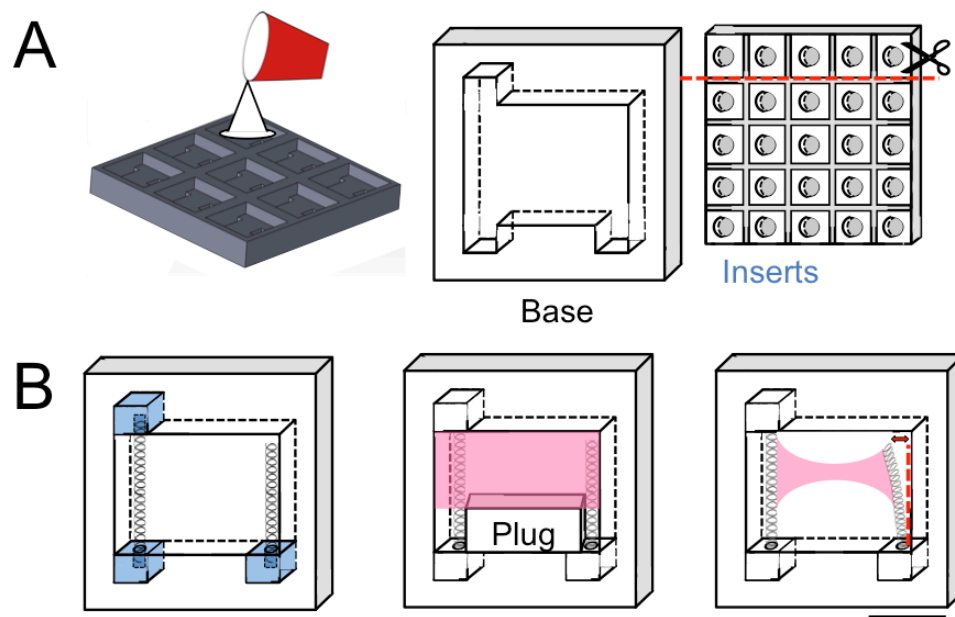


Figure 7.1 Design and manufacturing of system to measure VIC contractility.

A. Custom molds machined from polycarbonate. B. Inserts and springs were inserted into device base to form complete system (left). Temporary plug prevented downward flow of collagen hydrogel (pink) as VIC gels were applied to upper region of device (center). The plug was removed once the gel polymerized. Over 14 days, hydrogel+VIC contracted, deflecting cantilevered spring (right) by a measurable amount. Scale bar is 1 cm.

Spring Force Device Calibration

The spring system was cut on the right side so that the deflected spring is free to be pushed by a balance (Figure 7.2). A pair of forceps is pushed through the left side of the PDMS and the end of the forceps is attached to the finest-moving arm of the micro injector. The spring was lowered so that it was perpendicular to the balance scale plate. The spring was positioned so that only the very end of the spring will be moved as the micro injector lowers the spring onto the scale. The point just before the spring will register force on the scale was determined and the scale was set to “0.000 g.” Next, using the fine adjustment knob, the spring system was lowered in increments of

50 microns. The spring system was lowered a total of 1000 microns. The total force (in grams) exerted by the spring at each increment of 50 microns was recorded for each lowering of the spring system. This was repeated three times and three plots of grams vs. microns were created and a calibration curve relating force to deflection was determined using the average of these plots (Figure 7.2B). Calculation of effective modulus (EI) for the system was determined using beam theory and the average force vs. deflection curve for three springs (Figure 7.2C).

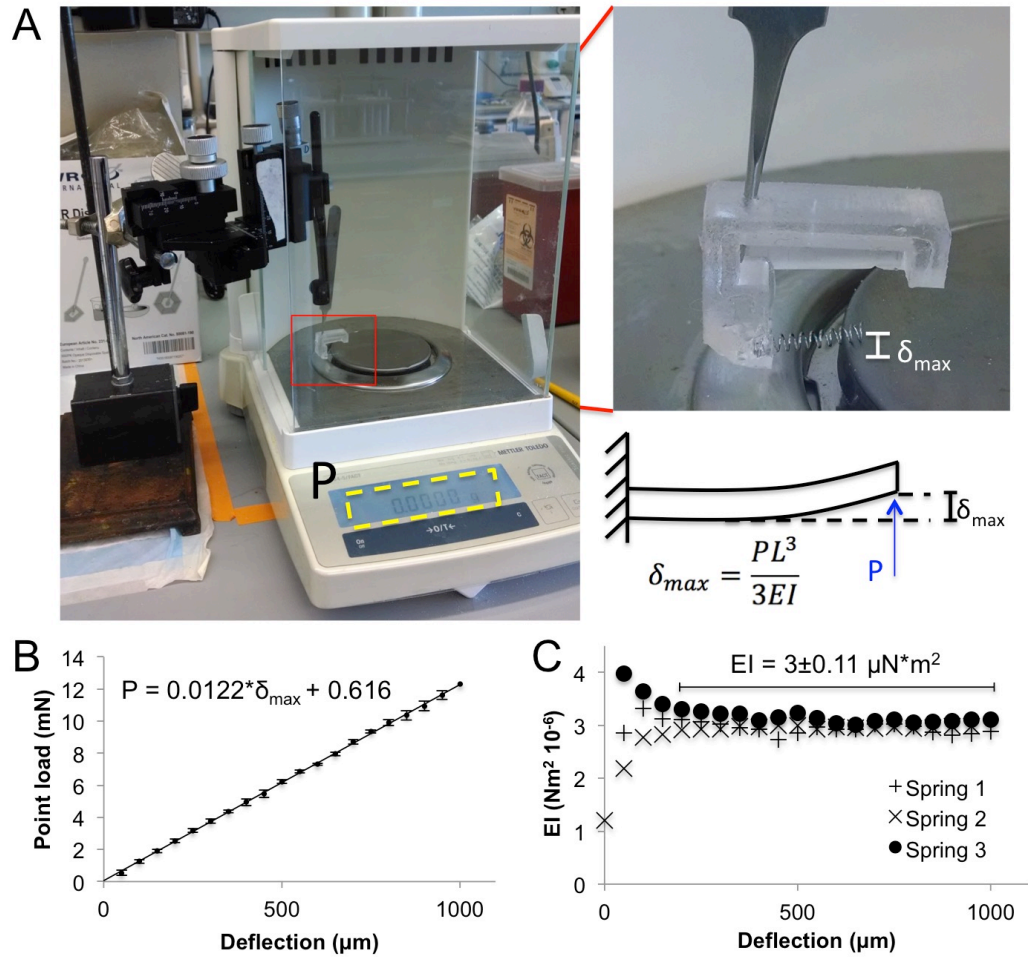


Figure 7.2 Calibration of system to measure VIC contractility.

A. Set-up for empirical calibration of spring in manufactured system. B. Load versus deflection curve for representative spring. C. Effective modulus (EI) for the system, calculated based on calibration curves for three different systems (Spring 1-3).

Cleaning and Prepping Spring Systems

In order to clean the spring systems, they were scrubbed gently with Alconox solution and then rinsed with DI water. The PDMS plug was then inserted into the base of the system, between the two springs, and the spring systems were autoclaved with a 30:00 min sterilize, 25:00 min dry solids cycle. After being autoclaved, the spring systems were placed in the incubator for at least one hour before being seeded.

Imaging Gels

The gels were imaged in a laminar flow hood using an inverted dissection microscope with a Lumenera INFINITY 1-5 5.0 megapixel CMOS digital camera for microscopes attached, using the smallest zoom size (0.67x). The images were then imported into ImageJ. A picture of a hemacytometer at the same zoom size was taken to set a scale for the pictures of the gels.

Measuring Deflection and Contractile Force

From the pictures of the spring systems, the deflection of the springs was measured. A straight line was drawn from the bottom edge of the left spring to the top edge of the right spring and measured. Next, the length of the left spring was measured and then, using the Pythagorean theorem, the deflection of the right spring was calculated. This method controlled for minute differences in the placement and angle of the right-hand spring within each system. Force was calculated from spring deflection using the empirical calibration curve (Figure 7.2B).

$$P_{VIC} = 0.0122 * \delta_{max} + 0.616$$

Where P_{VIC} is contractile force in mN and δ_{max} is the maximum deflection of the spring. The thickness of each gel was also measured at the thinnest point at the middle of each gel. The gels were assumed to be perfectly cylindrical at the center, thus the area was assumed to be:

$$Area_{gel} = \pi * thickness^2$$

Force and gel thickness were used to calculate contractile stress (σ) in the gel at the thinnest point, using:

$$\sigma = \frac{F_{VIC}}{Area_{gel}}$$

Cell isolation & culture

Porcine aortic valve leaflets were obtained locally. A 600U/mL collagenase solution with Dulbecco's Modified Eagle Medium (DMEM) was used to digest the leaflet surfaces for three minutes. Valve endothelial cells were then removed by scraping. The remaining leaflet tissue was incubated for 12-18 hours in fresh collagenase solution and then homogenized. The homogenized solution was spun down, resuspended in fresh media, and grown to confluency. Cell growth media was DMEM supplemented with 10% fetal bovine serum and 1% penicillin. To passage, the cells were trypsinized and then centrifuged at 1500 rpm for 5 minutes. The supernatant was aspirated, and the cell pellet was mixed with 15 mL of DMEM media and then added to a T-75 flask. The media for the cells were changed every two days, and the cells were passaged at confluency.

Hydrogel synthesis & culture

Porcine aortic valve interstitial cells at passage 4-7 from a T-175 (Falcon) flask were rinsed with PBS (1X Phosphate buffered saline). 7 mL of Trypsin (0.25% Trypsin-EDTA) was then added to the flask and the flask was then placed in an incubator at 37 degrees Celsius for 5 minutes. Next, 21 mL of DMEM (Dulbecco's modified eagle's

medium) was added to the T-175 flask to deactivate the trypsin, and the solution was transferred to a 50 mL tube. Next, the cells were counted using a hemocytometer. The desired cell suspension volume was 2,000,000 cells/mL (800,000 cells/gel). The cell suspension was centrifuged at 1000 rpm for 5 minutes. Afterwards, the supernatant was aspirated and in this order, 3X DMEM, 18 MΩ H₂O, 10% FBS, Collagen type I (rat tail), and 0.1 M NaOH were added to the cell pellet and the resulting gel solution was mixed well. Next, 400 μL of the gel solution was pipetted into the hollow between the two springs above the PDMS plug, making sure that the gel solution is within the coils of the two springs (Figure 7.1B). Then, the spring system with the seeded gel was placed into incubator for 30 minutes. Next, the PDMS plug was removed, and 800 μL of DMEM was added to the gels, and the spring systems were then placed in the incubator. Gels were cultured in either control medium (DMEM+10% FBS+1% Penicillin-Streptomycin) or osteogenic medium (control media supplemented with 10 mmol/L β-glycerophosphate, 50 mg/mL ascorbic acid, and 10 nmol/L dexamethasone, OGM) for 14 days with media changed every 48 hours.

Quantitative RT-PCR

After 1, 5, or 14 days, cellular RNA was isolated and purified with RNeasy Mini Kit (Qiagen), according to the manufacturer's instructions. cDNA was then synthesized from the isolated RNA with an iScript cDNA Synthesis Kit. Quantitative real-time PCR was performed with SYBR Green PCR master mix (Applied Biosystems) according to the manufacturer's instructions, and the CFX96 system (Bio-Rad).

Primers able to detect 18S, RhoA, Sox9, TGF- β 1, RunX2, α SMA and MMP-9 were used to quantify the expression of these genes in PAVIC under healthy and osteogenic conditions. The results were then statistically analyzed with a t-test. $P < 0.05$ was considered statistically significant.

Table 7.1 Quantitative rt-PCR primers

Gene	Forward	Reverse
18S	AATGGGGTTCAACGGGTTAC	TAGAGGGACAAGTGGCGTTC
RhoA	AACAGGATTGGTGCTTTTGG	CAGCAGGGTTTCACAAGACA
ACTA2	CAGCCAGGATGTGTGAAGAA	TCACCCCCTGATGTCTAGGA
COL1A1	AGAAGACATCCCACCAGTCA	CGTCATCGCACAACACATTG
COL2A1	GTCTACCCCAATCCAGCAAA	GTCTACCCCAATCCAGCAAA
COL3A1	TTGGCCCTGTTTGCTTTTAA	TGGTTGACAAGATGAGAACAAAA
MMP-9	ACACACACGACATCTTCC	AAGGTCACGTAGCCCACAA
Sox9	GGAGACTGCTGAATGAGAGC	CGTTCTTCACCGACTTTCTC
TGF-β1	CCACTCTCAGCCTCTCTGCT	TGGGTTCTCGGTATCCTACG
Runx2	GCACTACCAGCCACCTTAA	TATGGAGTGCTGCTGGTCTG
ALP	ATGAGCTCAACCGGAACA	GTGCCCATGGTCAATCCT

Collagen Gel Immunofluorescence

The hydrogels+VIC were kept in the spring systems for fixation and staining, in order to maintain cell and collagen morphology. Gels were fixed with 4% PFA and incubated for 4 hours at 4° Celsius. The gels were then washed 3 times for 15 minutes each with 1X PBS and then permeabilized and rocked with 0.2% Triton-X 100 for 10 minutes. The gels were again washed 3 times for 15 minutes each with 1X PBS. Next, blocking solution (10% goat serum, 1% BSA in 1X PBS) was added to the gels and was incubated overnight at 4 degrees Celsius. This was followed by an overnight incubation with primary antibody (α SMA goat anti-rabbit (Abcam)) and phalloidin stain for f-actin (Alexa Fluor 488 conjugated, Life Technologies) at 4 degrees Celsius. After another 3 washes for 15 minutes each with 1X PBS, the gels were incubated with a secondary antibody (goat anti-rabbit Alexa Fluor 568, Life Technologies) at 1:200 dilution in PBS for two hours. Next, the gels were washed another 3 times for 15 minutes each with PBS. This is followed by incubation with a 1:1000 dilution of DRAQ5 far-red nuclear stain (Cell Signaling Technology) in 1X PBS for 30 minutes. The gels were then again washed 3 times for 15 minutes each with 1X PBS. The gels were then imaged using a Zeiss 710 or 780 laser scanning confocal microscope. Collagen reflectance microscopy was used to simultaneously collect collagen fiber images.

Live-Dead Assay

A live-dead assay was done on the gels every 48 hours to check for cell viability (LIVE/DEAD® Viability/Cytotoxicity Kit, for mammalian cells, Life Technologies).

The gels were first washed with 1X PBS, then incubated with a 4 μ M EthD and 2 μ M Calcein 1X PBS solution for 30 minutes. Next, the gels were again washed with 1X PBS and DMEM was added to the gels. The gels were then imaged with a Zeiss microscope. Green cells signified live cells, and red cells signified dead cells. Proportion of live/dead cells was quantified using ImageJ.

DN-RhoA Transfection

Cells were first cultured in 6-well plates for 24 hours in antimicrobial-free media. Roche X-tremeGene 9 was mixed with 1X DMEM in a sterile tube at a 3 μ L reagent/100 μ L medium dilution. Next, 1 μ g of dominant-negative RhoA plasmid (DN-RhoA) was added to this solution, and the resulting solution was incubated at room temperature for 30 minutes. Then, 100 μ L of the solution was added to each well and the 6 well plate was incubated for 18-72 hours. The cells were then washed with 1 X PBS and incubated with normal DMEM. The cells were split at confluency and used within one passage/48 hours of initial transfection.

Cell and collagen fiber alignment analysis

Interstitial cell f-actin fiber and collagen fibril alignment angle distributions were analyzed as previously described [17]. Briefly, z-stack images of gels were collected via confocal and collagen reflectance microscopy, at a resolution of 2 μ m per slice, for at least 200 μ m of the total depth of the gel and up to 400 μ m. Maximum intensity projections of 20 μ m stacks for cells and fibers at the central region of each

gel were compiled using ImageJ. The average of three representative 20 μ m stacks was used to calculate alignment for each gel. Regions of distinct nodule formation in OGM condition were avoided, unless otherwise noted in text. F-actin and collagen fiber alignment was quantified using a MATLAB algorithm adapted from [17] and [23].

7.4 Results

Design of system to culture VIC in 3D while measuring contractile force

We designed the system so that a physiologically relevant density of VIC could be cultured within a collagen hydrogel of substantial thickness (approximately 1mm in the central region), recapitulating the native valve tissue as closely as possible. The systems were made from PDMS poured into polycarbonate molds in order to achieve low costs and high reproducibility. The VIC seeded in the gels within the system are well spread and quiescent (no α SMA) (Figure 7.3A). Live/dead analysis indicated good viability over 14 days, with only a slight decrease in live cells at day 14 in both CTL and OGM conditions (Figure 7.3B). Cell density was consistent over 14 days, with a slight increase in CTL condition due to compaction of the hydrogel (Figure 7.3C).

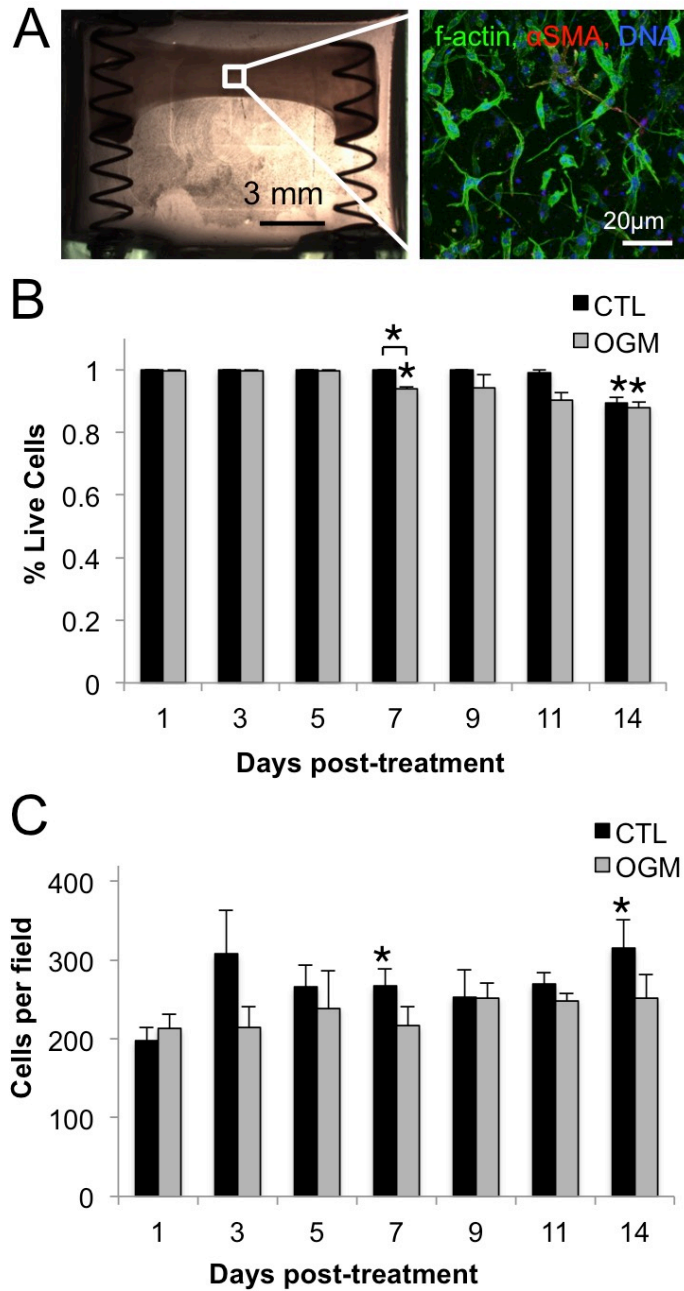


Figure 7.3 Characterization of system to measure VIC contractility.

A. Completed system at day 0, with hydrogel+VIC (left). F-actin (green), α SMA (red), and nuclei (blue) of hydrogel+VIC after 24 hours of culture in control media (right). B. Cell viability in CTL and OGM conditions over 14 days of culture in the system. C. Cell density in CTL and OGM conditions over 14 days of culture in the system. $N \geq 3$. * indicates $p < 0.05$ versus CTL at same time point. Error bars indicate SEM.

Pro-osteogenic environment dysregulates the native ability of VIC to organize and maintain their mechanical environment.

VIC in control condition were classified as normal VIC (nVIC) and VIC in osteogenic condition were classified as osteoblast-like VIC (obVIC), due to their ability to deposit calcium and form nodules. We found that nVIC compact the hydrogel over 14 days, decreasing its thickness. obVIC stop compacting the gel after only 5 days and are significantly thicker than control gels after day 11 ($p < 0.001$ for both) (Figure 7.4A). At day 1, obVIC exert higher contractile force and create higher internal stress in the hydrogel than nVIC. This trend reverses at day 5, after which nVIC exert increasing stress but obVIC stress decreases up to day 14 (Figure 7.4B).

At day 1, obVIC gels show higher alignment of collagen fibers respective to the direction of tension in the hydrogel compared to nVIC gels. However, by day 5 the fiber alignment is similar in obVIC and nVIC gels. After day 5, the trend reverses. obVIC gels show decreased fiber alignment compared to nVIC gels from day 7-14 (Figure 7.4C).

Fiber density analysis showed a similar trend. At day 1, obVIC gels have a higher density of collagen fibers than nVIC. Both types of gels show equivalent fiber density until day 14, when obVIC gels have significantly lower collagen fiber density than nVIC gels (Figure 7.4D).

Therefore, we found that VIC in our system show 3 distinct phases of mechanical response to OGM condition. At day 1, there is an acute response phase in which obVIC are more mechanically activated than nVIC. At day 5, VIC move into the transition phase, in which obVIC and nVIC mechanical activity appears equal. At day 14, we find a mature pathological response phase. ObVIC show a signature mechanical response, in which the gels are thicker, lower stress, less aligned, and have less dense collagen than nVIC.

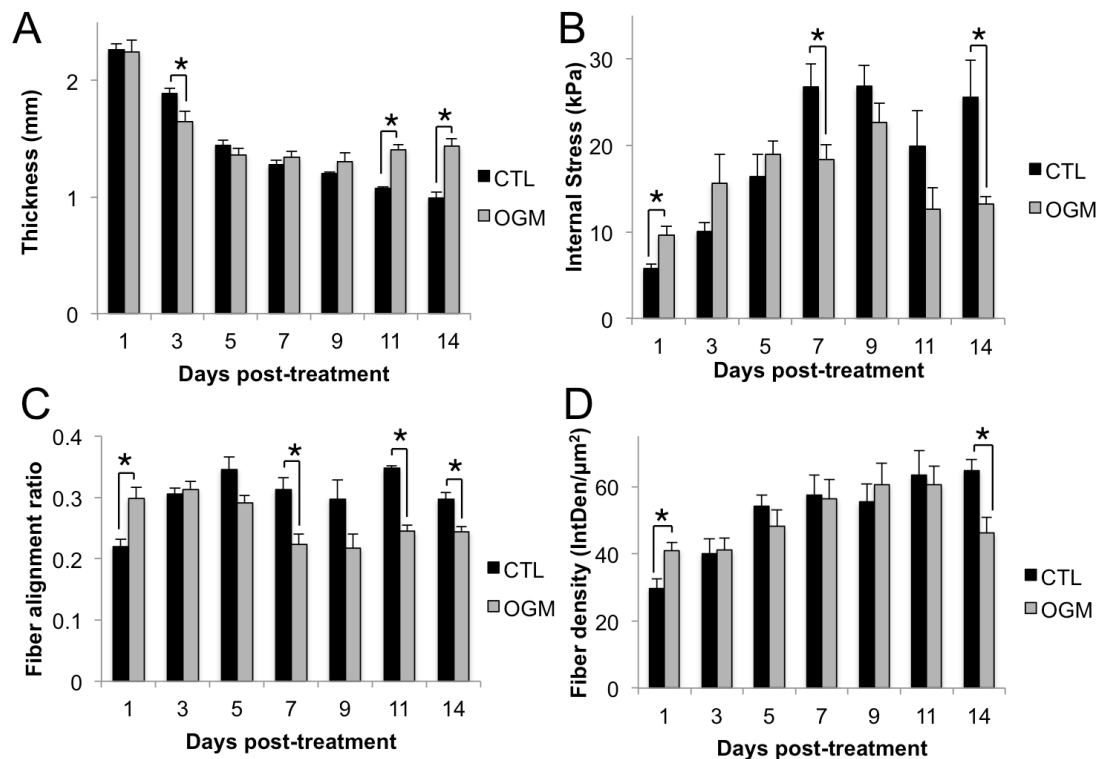


Figure 7.4 Pro-osteogenic environment disrupts native mechanical activity of VIC.

A. Thickness of the hydrogels. Thickness was measured every 48 hours over 14 days in control and osteogenic conditions. B. Internal stress in hydrogels. Stress was calculated from force exerted by VIC on the spring divided by the cross-sectional area of the gel at the thinnest point. C. Alignment of collagen fibers in the hydrogels. Alignment ratio of 1 indicates perfect alignment with direction of tension in hydrogel, alignment of 0 indicates fibers perpendicular to direction of tension. D. Density of collagen fibers in the hydrogels, calculated using ImageJ. N > 3 for all experiments, * indicates $p < 0.05$, error bars indicate SEM.

Dysregulation of VIC morphology and myofibroblastic signaling correlates with phases of mechano-osteogenic response.

We assessed cell morphology, f-actin fiber dynamics, and α SMA expression at each phase of VIC response. We found that nVIC have consistent alignment of cell cytoskeleton with direction of tension and only slight increase in α SMA over 14 days. In contrast, obVIC have f-actin fibers aligned with the direction of tension at day 1, but increasing disorganization and expression of α SMA at day 5 and even more so at day 14 (Figure 7.5A). Quantification of f-actin fiber directionality showed decreasing alignment of obVIC cytoskeleton over time relative to nVIC (Figure 7.5B). We then analyzed mRNA levels of mechanotransductive protein RhoA and myofibroblastic marker α SMA (ACTA2 gene) at each phase of response. ObVIC had higher levels of RhoA mRNA than nVIC at day 1, indicating an aggressive initial mechanotransductive response. RhoA mRNA decreased over time in both obVIC and nVIC. α SMA increased similarly over the first two phases (day 1 and 5) in both nVIC and obVIC. However, at the third phase (day 14), obVIC had significantly higher expression of α SMA (Figure 7.5C).

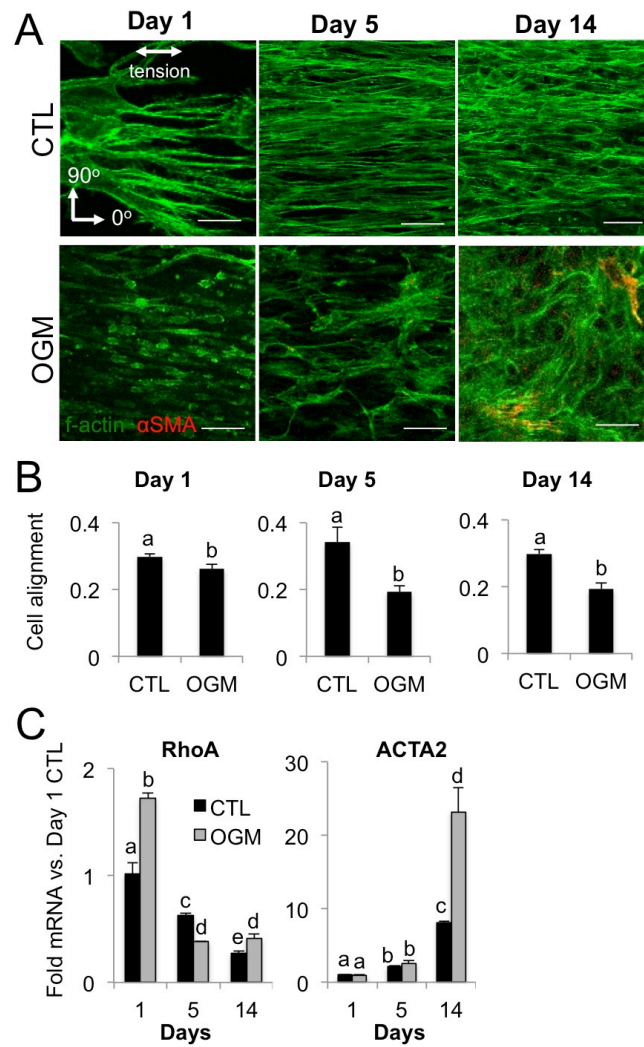


Figure 7.5 Pro-osteogenic environment increases VIC myofibroblastic signaling.

A. F-actin (green) and α SMA (red) in CTL or OGM condition at day 1, 5, and 14. Scale bar is 50 μ m. B. Alignment of VIC in CTL or OGM condition at day 1, 5, and 14, where a value of 1 indicates cells are perfectly aligned with the direction of tension. C. RhoA and ACTA2 mRNA in CTL or OGM condition at day 1, 5, and 14. $N \geq 3$ for all experiments. Bars with different letters are statistically different ($p < 0.05$), error bars indicate SEM.

Pro-osteogenic environment disrupts ability of VIC to organize collagen matrix

Collagen fiber imaging revealed significant changes in the collagen hydrogel environment at each phase of VIC response to OGM. In the acute phase (day 1), obVIC drove increased alignment of collagen fibers in the direction of gel tension compared to nVIC. In the transition phase (day 5), fiber alignment is similar in both nVIC and obVIC gels. However, as VIC reached the mature pathological phase (day 14), nVIC gels had fiber alignment similar to day 5, but obVIC gel fibers are highly disorganized (Figure 7.6A).

Analysis of collagen isoform mRNA showed a corresponding switch from the acute to the transition phase, with exaggerated response at the mature phase. Specifically, Collagen I was lower in obVIC at day 1, but increased over time and was higher than nVIC at all later stages. nVIC synthesized increasing amounts of collagen II over time, whereas obVIC plateaued in their level of collagen II mRNA synthesis across days 1-14. Collagen III was similar in nVIC and obVIC at day 1, but was significantly higher in obVIC from day 5 onwards (Figure 7.6B).

We then examined MMP-9 mRNA for an indication of matrix remodeling activity and Sox-9 as a marker of chondrogenic differentiation. In the acute phase, MMP-9 was lower in obVIC, but in the transition phase obVIC had significantly higher MMP-9 than nVIC. Both nVIC and obVIC had almost undetectable MMP-9 mRNA at the mature phase. Sox9, a transcriptional driver of chondrogenic differentiation that is regulated by RhoA and repressed in calcifying valves, was repressed in obVIC at the

transition and mature phases compared to nVIC. nVIC showed increased Sox9 mRNA at the mature phase compared to earlier phases (Figure 7.6C).

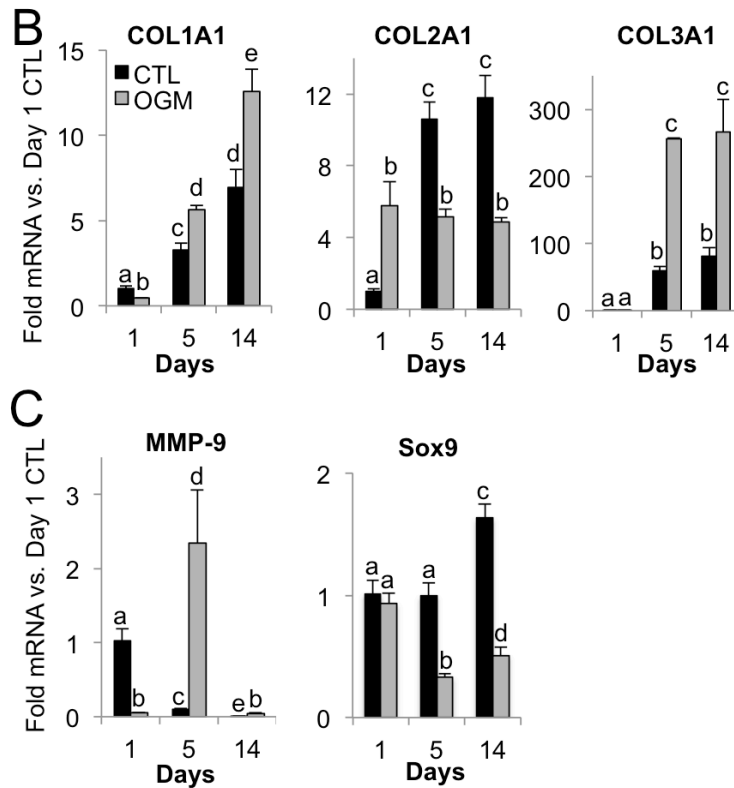
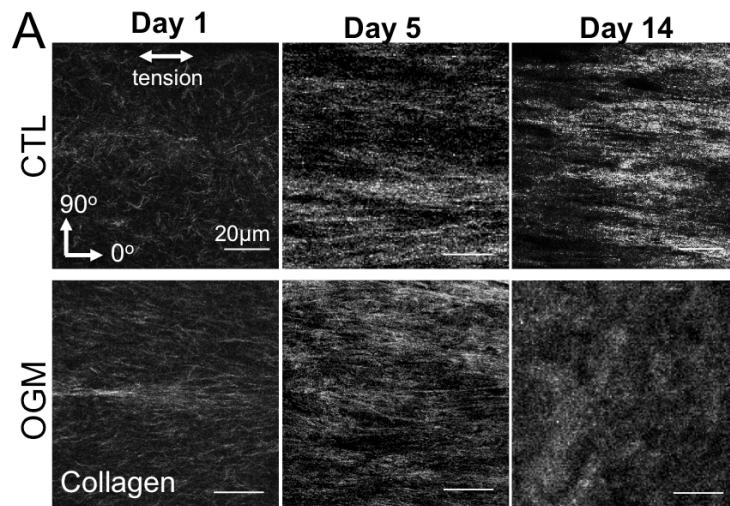


Figure 7.6 Pro-osteogenic environment disrupts VIC organization of collagen matrix.

A. Representative images of collagen fibers in CTL and OGM hydrogels at day 1, 5, and 14. B. Collagen isoform mRNA in CTL and OGM hydrogels at day 1, 5, and 14. C. MMP-9 and Sox9 mRNA in CTL and OGM hydrogels at day 1, 5, and 14. $N \geq 3$ for all experiments. Bars with different letters are statistically different ($p < 0.05$), error bars indicate SEM.

Early increase in TGF- β 1 drives progressive calcification of osteogenic VIC gels

Low-magnification bright field images revealed increasing nodule formation in obVIC gels over time (Figure 7.7A, arrows). Confocal microscopy of nodules at the transition (day 5) and mature (day 14) phases showed increased α SMA, cell aggregation, and significant disruption of collagen architecture near nodules. Quantification of nodules over time indicated significantly higher nodule formation in obVIC gels versus nVIC at transition and mature phases (Figure 7.7B). Pro-calcific cytokine TGF- β 1 was increased in obVIC compared to nVIC at the initial phase, but not at transition or mature phases (Figure 7.7C). Pro-osteogenic transcription factor Runx2 was higher in obVIC at all time points. ALP mRNA was the most drastically increased pro-osteogenic signaling factor we observed in obVIC, reaching over 1000-fold versus nVIC the by the transition phase time point and maintaining highly upregulated levels through the mature phase.

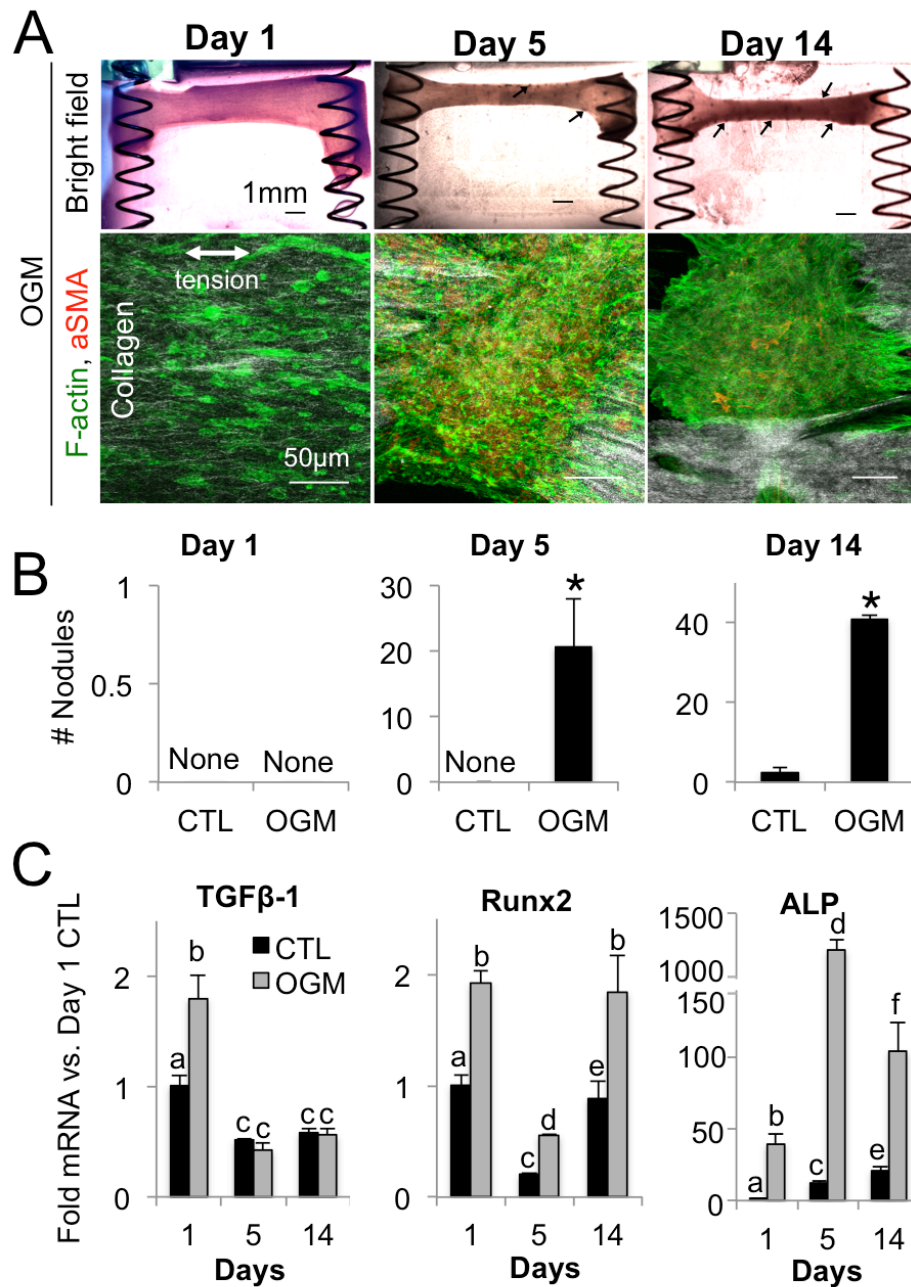


Figure 7.7 Nodules and osteogenic signaling in mechanically active VIC hydrogels.

A. Bright-field images of OGM hydrogels at day 1, 5, and 14. Arrows indicate nodules. B. Number of nodules formed in CTL and OGM hydrogels at day 1, 5, and 14. * indicates $p < 0.05$ versus CTL. C. TGF- β 1, Runx2, and ALP mRNA in CTL and OGM hydrogels at day 1, 5, and 14. $N \geq 3$ for all experiments. Bars with different letters are statistically different ($p < 0.05$), error bars indicate SEM.

Inhibition of RhoA suppresses osteogenic and promotes chondrogenic VIC phenotype

In order to investigate the role of RhoA in VIC osteogenic response over time, we transfected VIC with a dominant-negative form of RhoA prior to seeding in the hydrogels within the spring system. We found that DN-RhoA significantly decreased the number of nodules formed by VIC in the osteogenic environment, compared to VIC transfected with a control vector (Figure 7.8A, B). In the mature phase, DN-RhoA decreased fiber alignment and density in both control and OGM conditions compared to empty vector controls (Figure 8C, D). DN-RhoA also led to increased gel thickness in both control and OGM conditions (Figure 7.8E).

We then examined cellular mRNA signaling profiles in VIC+DN-RhoA at the mature pathological phase. ACTA2 levels were the same, but MMP-9 increases were blocked by DN-RhoA transfection. Sox9 transcription was highly increased in the OGM condition. Collagen I and III mRNA were significantly decreased and collagen II was increased in DN-RhoA compared to controls. Pro-calcific signaling genes ALP, TGF- β 1, and Runx2 were uniformly downregulated in VIC+DN-RhoA, in both control and OGM environments.

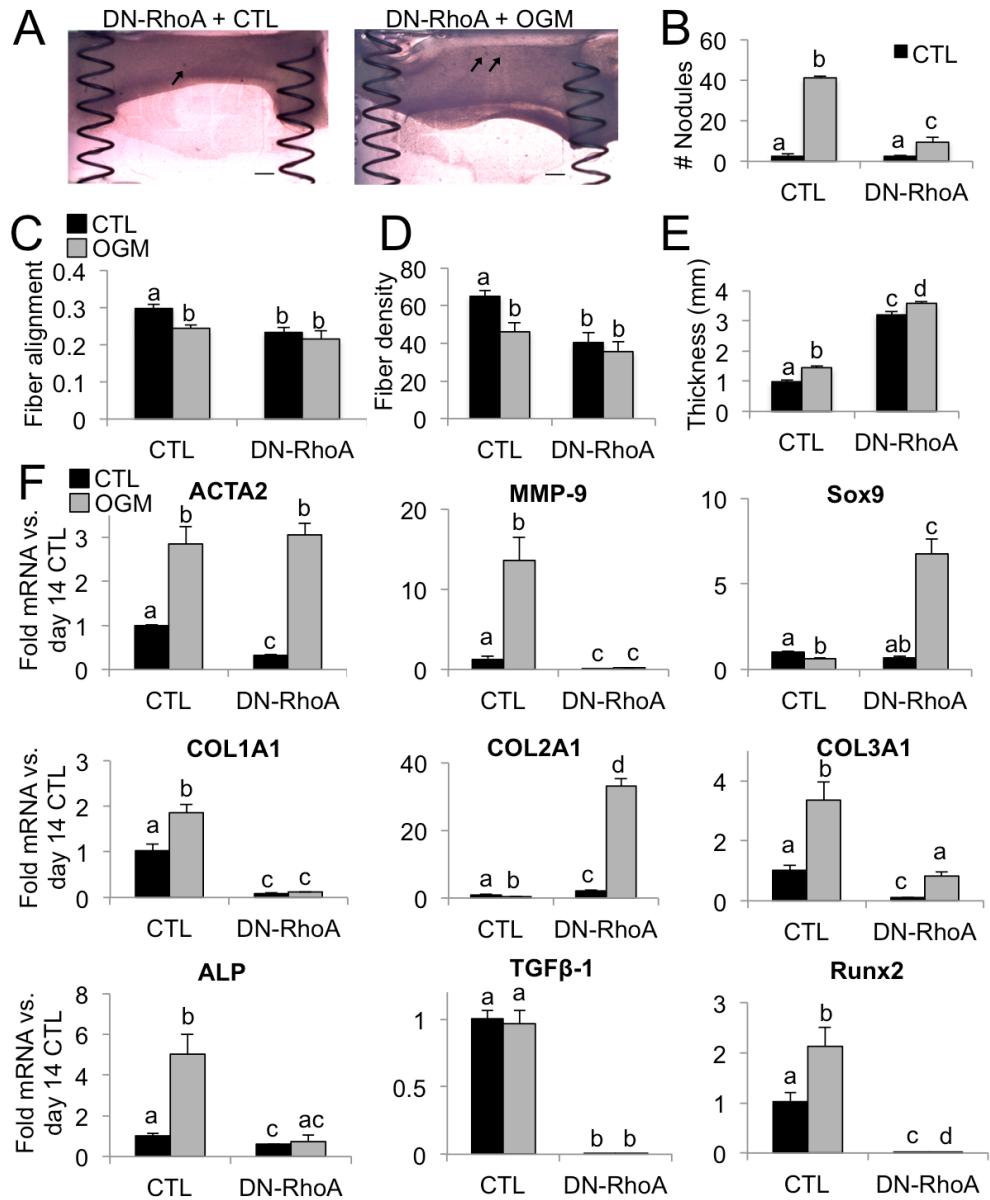


Figure 7.8 RhoA inhibition blocks osteogenic response of VIC.

A. Brightfield images of VIC+DN-RhoA, CTL or OGM condition at day 14, showing reduction in nodule formation (arrows). B. Number of nodules per gel at day 14. N = 4. C. Quantification of fiber alignment at day 14. A value of 1 indicates cells are perfectly aligned with the direction of tension. D. Quantification of fiber density. E. Quantification of gel thickness. F. Analysis of mRNA for matrix remodeling, collagen isoforms, and pro-osteogenic genes in VIC+DN-RhoA, CTL or OGM condition at day 14. N ≥ 3 for all experiments. Bars with different letters are statistically different (p < 0.05), error bars indicate SEM.

Collagen fiber dynamics correlate with VIC mechanobiological activity

We then analyzed the mechanical and pathological changes in VIC systems over time to assess correlations between different variables. In nVIC gels, collagen fiber density increased as fiber alignment increased ($p=0.03$). This correlation was lost in obVIC gels ($p=0.14$) (Figure 7.9A). In nVIC gels, gel thickness decreased as fiber alignment increased ($p=0.05$). Loss of organized collagen structure and nodule formation degraded this correlation in obVIC gels (OGM, $p=0.14$) (Figure 7.9B).

In nVIC gels, gel thickness decreased as fiber density increased ($p=1.6E-5$). In obVIC gels, gels did not undergo thinning as density increased because of the increasing disorganization of collagen fibers over time (OGM, $p=0.16$) (Figure 7.9C). In nVIC gels, internal stress increased as fiber density increased (CTL, $p=0.01$). In obVIC gels, relationship between stress and density was not as strong due to loss of collagen organization and nodule formation (OGM, $p=0.22$) (Figure 7.9D).

In obVIC gels, there was increased nodule formation as collagen fiber alignment decreased and thickness of the gels decreased ($p=0.01$, $p=0.02$ respectively). nVIC gels did not show any trends with respect to nodule formation, as there were no observable nodules (figure 7.9E, F).

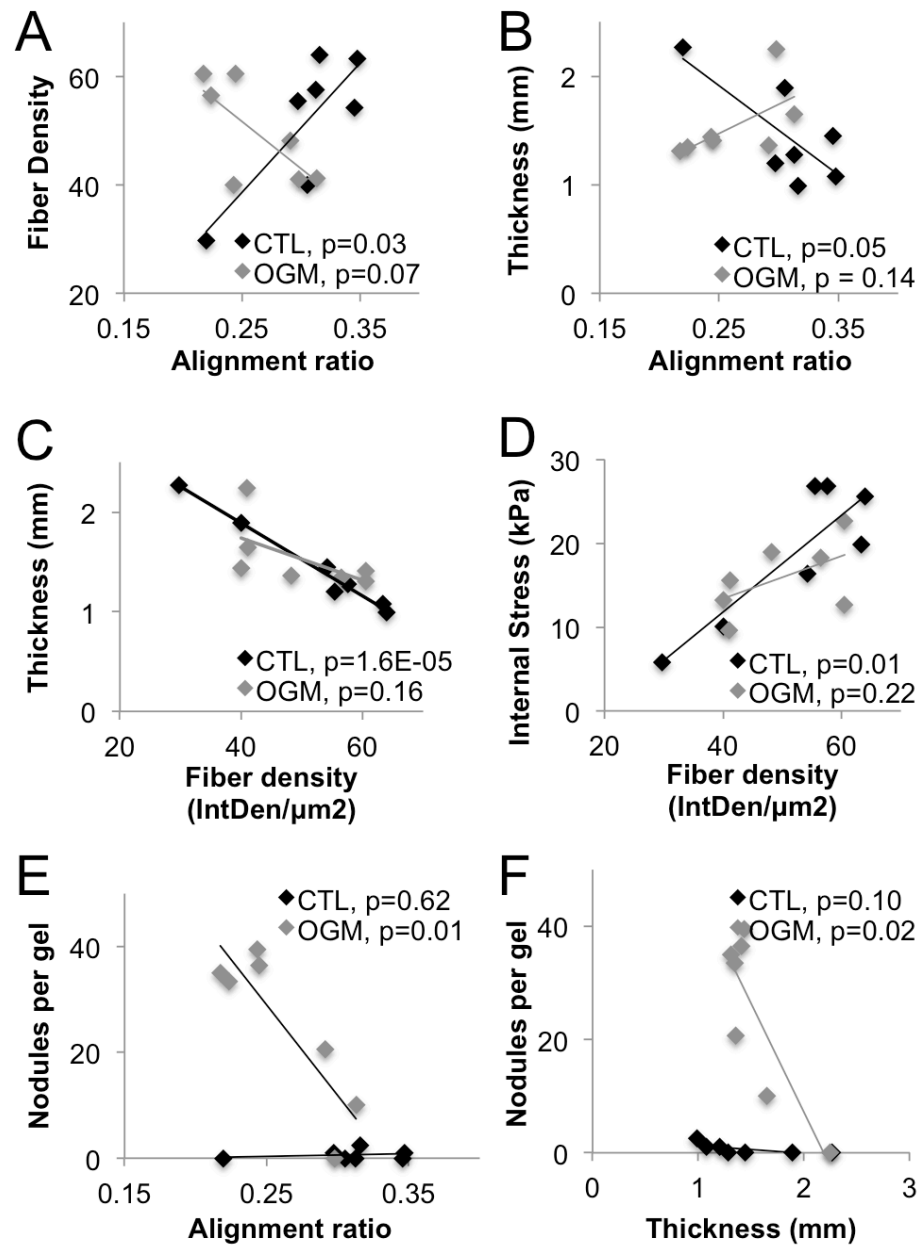


Figure 7.9 Collagen fiber dynamics correlate with VIC mechanical activation.

Analysis of Pearson's linear correlation coefficient between different sets of mechanical, biological, and pathological outputs in the VIC+hydrogel spring systems. All data sets include days 1 through 14. Only comparisons with at least one statistically significant correlation ($p < 0.05$) are shown, all other comparisons were not significant.

7.5 Discussion

Importance of our novel system design

This is the first system that combines a tensioned but flexible boundary condition with a 3-D hydrogel that recapitulates physiological cell number and density. Others have utilized a fixed-boundary condition system that applies tension through a gel, (ex. [13], [16,24]), or examined single-cell level mechanobiology with microfabricated flexible-boundary condition systems [25]. Contractile force generation has been measured using *ex vivo* valve tissue [26], but these results can be hard to interpret due to the complexity of the valve microenvironment. Our system is tunable; different cell types and extracellular matrix components can be added and adjusted in order to assess their differing effects.

The system also has the advantage of being inexpensive, easily manufactured, and amenable to a variety of sterilization techniques including autoclaving. As shown here, the system can be live-imaged without disassembly, allowing for dynamic longitudinal studies. Only one type of spring was characterized within the system for use in this study; however, springs with different pitch and wire thickness could be inserted to investigate the effect of stiffer or more flexible boundary conditions.

Identification of acute, transition, and mature phases of VIC mechano-pathological response

Previous studies examining the dynamics of VIC mechanics in valve pathology have been conducted over very short time periods (less than 72 hours) [11,16,18,21].

However, degeneration of the aortic valve occurs over much longer time scales *in vivo*, and *in vitro* calcification has been shown to take at least 14 days to develop [27]. Studies that have examined longer time periods, 21 days [24] and 14 days [28], have only focused on the end time point. This study presents 14-day data and also reveals important intermediate phases (day 1 and day 5) that have not been shown previously (Figure 7.10). We found that at day one, obVIC exert more stress, have higher fiber alignment, and higher fiber density. We characterize this as the acute phase of VIC mechanoreactive response to the osteogenic, pathological environment. Interestingly, by day five, we observed that nVIC and obVIC exert similar stress and have similar fiber alignment and density. We characterize this as the transition phase in which obVIC have begun nodule formation, have increased osteogenic signaling, and significant disruption of cell alignment, but have not yet significantly remodeled their collagen environment. Finally, at day 14, we saw mature nodule formation and calcific signaling and significant changes in collagen fiber alignment and density. We characterize this as the mature pathological phase of VIC mechanopathological response.

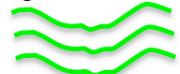
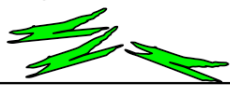
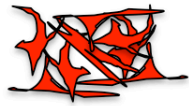
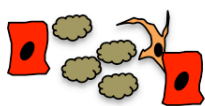
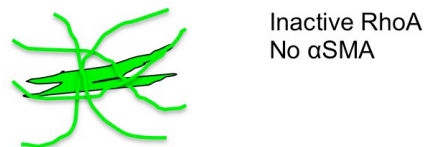
	Day	1	5	14
Collagen	CTL	Moderately dense, somewhat aligned 	More dense, somewhat aligned 	Most dense, very aligned 
	OGM	Moderately dense, aligned 	More dense, somewhat aligned 	Most dense, misaligned 
Cells Quiescent VIC:  Myofibroblastic VIC: 	CTL	Moderately dense, somewhat aligned 	More dense, aligned 	Most dense, very aligned 
	OGM	Moderately dense, somewhat aligned 	Moderately dense, misaligned 	Most dense, misaligned 
Calcification Osteoblast-like cell:  Myofibroblastic cell:  Calcium: 	CTL	No nodules	No nodules	Very few nodules
	OGM	No nodules	> 15 nodules 	> 35 nodules 

Figure 7.9 Dynamics of collagen, cells, and calcification in VIC in tensioned hydrogels.

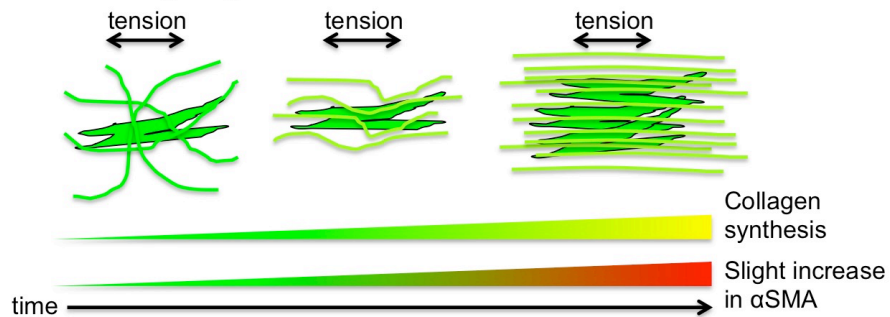
TGF-β1 is an important mediator of VIC mechanopathology in the acute phase

TGF-β1 increase is likely connected to the increase in RhoA in the acute phase (day 1), increasing cell tension and prompting the early contractile response of VIC to OGM, as has been shown in fibroblasts [29]. Early TGF-β1 activity also underpins the observed pro-fibrotic response of VIC [30], increased collagen synthesis [31], and the beginnings of the calcification response [32] (Figure 7.11).

VIC in non-tensioned hydrogel environment



VIC in tensioned hydrogel environment



VIC in tensioned hydrogel environment + osteogenic stimulus

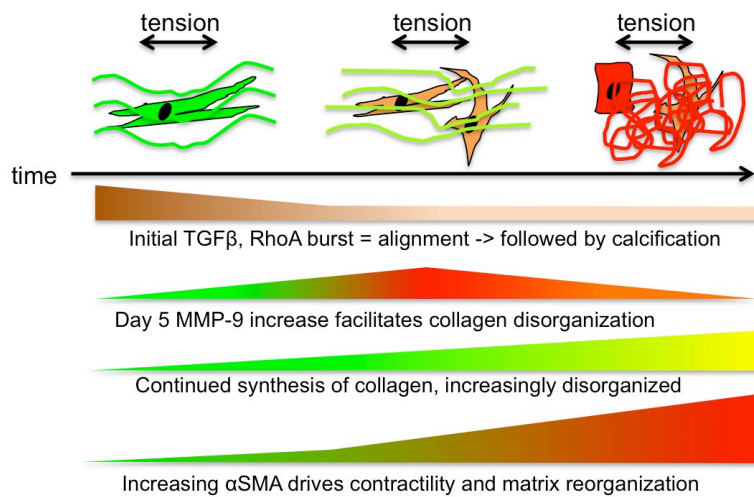


Figure 7.10 Interactions between cells, collagen, signaling molecules, and tension.

Many VIC calcification studies supplement osteogenic media with TGF- β 1 [28], despite TGF- β 1 being an important autocrine and paracrine signal that develops throughout valve calcification [33]. In this study, TGF- β 1 is not added to the osteogenic media, allowing VIC to produce their own TGF- β 1 at the acute phase. Our longitudinal results indicate that TGF- β 1 is an important early responder to osteogenic conditions. This agrees with studies in osteoprecursor cells that indicate that endogenous TGF- β 1 production is increased by both ascorbic acid and β -glycerophosphate [34], components of our osteogenic media. TGF- β 1 also induces rapid ALP expression in osteoblastic differentiation[35] and targets Runx2 transcriptional activity[36].

Changes in collagen organization dominate the transition phase

A recent study showed that collagen disruption or deficiency is sufficient to induce calcification in aortic valve leaflets [20]. Our results showed increased organization and elevated density of collagen in OGM condition in the acute phase, but this trend had leveled out by the transition phase (day 5) and was reversed by the mature phase (day 14). This suggests that VIC induce an early, pro-fibrotic increase in collagen in response to osteogenic stimuli that changes to a pro-calcific decrease in collagen synthesis [37] through the transition (day 5) and mature pathological (day 14) phases. Our mRNA results indicate that this phenomenon is dominated by changes in collagen II synthesis, which is lower than control at both day 5 and day 14, as opposed to collagen I or III.

Tension promotes early and aggressive calcification, dependent on RhoA activity

Both Runx2 and ALP are upregulated in the acute phase of OGM stimulation (day 1). Dominant response then switches to ALP in the transition phase (day 5). By the mature phase (day 14), both factors are again in effect. This early and sustained pro-osteogenic cell signaling demonstrates the importance of a physiologically-relevant tensioned environment in stimulating VIC response to pro-calcific stimuli. OGM also inhibited the ability of VIC to generate contractile force, which changes the ability of VIC to regulate valve leaflet stiffness [38] and response to vasoactive agents [26].

The aggressive early mechanopathological calcification response is likely mediated by TGF- β 1 via RhoA signaling, as suppression of RhoA activation via transfection with DN-RhoA decreased both fiber alignment and density, suppressing collagen I and III synthesis and increasing expression of collagen II. DN-RhoA also decreased expression of ALP and Runx2 and increased expression of Sox9, suggesting a switch from pro-calcific to pro-chondrogenic phenotype [39]. Inhibition of RhoA may also block the trafficking of molecules involved in VIC mineralization. For example, a recent study showed that mechanical strain promoted calcification by stimulating localization of ENPP1 to the cell membrane via RhoA/ROCK signaling [40]. Our results provide strong evidence that RhoA is a major regulator of the phenotype and mechanical activity of VIC under osteogenic stimuli.

Interestingly, our system showed that obVIC actively remodel their environment and compact the gel as a whole, but to a lesser overall extent than nVIC. Although nVIC gels are thinner than obVIC gels from day 11-14, obVIC nodule formation correlates with progressive thinning of the obVIC gels. This is likely due to the overall increased mechanical activity of obVIC over time, despite the disorganization of their mechanical response. Decreased collagen II synthesis and decreased fiber density also contribute to the thickness of obVIC gels in the mature pathological phase.

VIC have an active role to play in regulating their mechanical environment –this role is disrupted by pathological osteogenic differentiation

Our results provide evidence for an active role of VIC in maintaining the collagen environment of a healthy valve via increasing collagen fiber alignment and density over time, continuing synthesis and regulation of collagen isoforms, and generation of contractile force. These activities are disrupted as VIC undergo pathological response to osteogenic stimulation. OGM environment disrupted cell and collagen fiber alignment, inhibiting the ability of VIC to compact and organize their extracellular matrix environment as they would in a healthy gel.

This study affirms the importance of VIC regulation of the extracellular matrix, which is actively involved in the pathogenesis of CAVD through the modulation of biochemical and biomechanical signals [41]. ECM disruption also creates a negative feedback loop between cell and matrix mechanics, changes surface receptor binding, disrupts paracrine signaling, and changes transduction of force through the

extracellular environment [19]. Analysis of collagen isoforms and MMP-9 mRNA indicated VIC ECM changes are mediated by both synthesis of new collagen and by reorganization of the existing matrix. In particular, in the acute phase, obVIC showed increased collagen II mRNA and decreased MMP-9, indicating that the initial ECM response is mediated primarily by new collagen synthesis and not by matrix reorganization. In the transition phase, collagen II was decreased and MMP-9 was increased, pointing to a shift from synthesis to reorganization of collagen fibers. This is an important feature of dynamic VIC-matrix interaction that agrees with previous observations of valve thickening and fibrosis [42] followed by matrix disorganization [43,44].

REFERENCES

1. Mozaffarian D, DrPH, Benjamin FEJ, Go FAS, Arnett MDK, et al. (2015) Heart Disease and Stroke Statistics - 2015 Update. *Circulation* 131: e29–e322.
2. Rajamannan NM, Evans FJ, Aikawa E, Grande-Allen KJ, Demer LL, et al. (2011) Calcific Aortic Valve Disease: Not Simply a Degenerative Process. *Circulation* 124: 1783–1791.
3. Stewart BF, Siscovick D, Lind BK, Gardin JM, Gottdiener JS, et al. (1997) Clinical Factors Associated With Calcific Aortic Valve Disease. *Journal of the American College of Cardiology* 29: 630–634.
4. Cawley PJ, Otto CM (2009) Prevention of calcific aortic valve stenosis—fact or fiction? *Ann Med* 41: 100–108.
5. Taylor PM, Batten P, Brand NJ, Thomas PS, Yacoub MH (2003) The cardiac valve interstitial cell. *The International Journal of Biochemistry & Cell Biology* 35: 113–118.
6. Liu AC, Joag VR, Gotlieb AI (2007) The Emerging Role of Valve Interstitial Cell Phenotypes in Regulating Heart Valve Pathobiology. *The American Journal of Pathology* 171: 1407–1418.
7. Honda S, Miyamoto T, Watanabe T, Narumi T, Kadowaki S, et al. (2014) A novel mouse model of aortic valve stenosis induced by direct wire injury. *Arteriosclerosis, Thrombosis, & Vascular Biology* 34: 270–278.
8. Yu Z, Seya K, Daitoku K, Motomura S, Fukuda I, et al. (2011) Tumor necrosis factor- α accelerates the calcification of human aortic valve interstitial cells obtained from patients with calcific aortic valve stenosis via the BMP2-Dlx5 pathway. *Journal of Pharmacology and Experimental Therapeutics* 337: 16–23.
9. Freeman RV, Otto CM (2005) Spectrum of Calcific Aortic Valve Disease: Pathogenesis, Disease Progression, and Treatment Strategies. *Circulation* 111: 3316–3326.

10. Latif N, Sarathchandra P, Taylor PM, Antoniw J, Yacoub MH (2005) Localization and pattern of expression of extracellular matrix components in human heart valves. *The Journal of Heart Valve Disease* 14: 218–227.
11. Chen JH, Simmons CA (2011) Cell-Matrix Interactions in the Pathobiology of Calcific Aortic Valve Disease: Critical Roles for Matricellular, Matricrine, and Matrix Mechanics Cues. *Circulation Research* 108: 1510–1524.
12. Butcher JT, Simmons CA, Warnock JN (2007) Mechanobiology of the Aortic Heart Valve. *Journal of Heart Valve Disease* 17: 62–73.
13. Merryman WD, Lukoff HD, Long RA, Engelmayer GC Jr, Hopkins RA, et al. (2007) Synergistic effects of cyclic tension and transforming growth factor- β 1 on the aortic valve myofibroblast. *Cardiovascular Pathology* 16: 268–276.
14. Walker GA, Masters KS, Shah DN, Anseth KS, Leinwand LA (2004) Valvular myofibroblast activation by transforming growth factor-beta: implications for pathological extracellular matrix remodeling in heart valve disease. *Circulation Research* 95: 253–260.
15. Fisher CI, Chen J, Merryman WD (2012) Calcific nodule morphogenesis by heart valve interstitial cells is strain dependent. *Biomech Model Mechanobiol* 12: 5–17.
16. Balachandran K, Bakay MA, Connolly JM, Zhang X, Yoganathan AP, et al. (2011) Aortic valve cyclic stretch causes increased remodeling activity and enhanced serotonin receptor responsiveness. *The Annals of Thoracic Surgery* 92: 147–153.
17. Gould RA, Chin K, Santisakultarm TP, Dropkin A, Richards JM, et al. (2012) Cyclic strain anisotropy regulates valvular interstitial cell phenotype and tissue remodeling in three-dimensional culture. *Acta Biomaterialia* 8: 1710–1719.
18. Balachandran K, Sucusky P, Jo H, Yoganathan AP (2009) Elevated cyclic stretch alters matrix remodeling in aortic valve cusps: implications for degenerative aortic valve disease. *AJP: Heart and Circulatory Physiology* 296: H756–H764.
19. Li C, Xu S, Gotlieb AI (2013) The progression of calcific aortic valve disease through injury, cell dysfunction, and disruptive biologic and physical force feedback loops. *Cardiovascular Pathology* 22: 1–8.

20. Rodriguez KJ, Piechura LM, Porras AM, Masters KS (2014) Manipulation of valve composition to elucidate the role of collagen in aortic valve calcification. *BMC Cardiovascular Disorders* 14: 1–10.
21. Merryman WD, Youn I, Lukoff HD (2006) Correlation between heart valve interstitial cell stiffness and transvalvular pressure: implications for collagen biosynthesis. *Am J Physiol Heart Circ Physiol* 290: H224–H231.
22. Liu H, Sun Y, Simmons CA (2013) Determination of local and global elastic moduli of valve interstitial cells cultured on soft substrates. *Journal of Biomechanics* 46: 1967–1971.
23. Bowles RD, Williams RM, Zipfel WR, Bonassar LJ (2010) Self-assembly of aligned tissue-engineered annulus fibrosus and intervertebral disc composite via collagen gel contraction. *Tissue Eng Part A* 16: 1339–1348.
24. Ferdous Z, Jo H, Nerem RM (2011) Differences in valvular and vascular cell responses to strain in osteogenic media. *Biomaterials* 32: 2885–2893.
25. Yang MT, Fu J, Wang Y-K, Desai RA, Chen CS (2011) Assaying stem cell mechanobiology on microfabricated elastomeric substrates with geometrically modulated rigidity. *Nat Protoc* 6: 187–213.
26. Kershaw JD, M M, HH S, MH Y, AH C (2004) Specific regional and directional contractile responses of aortic cusp tissue. *Journal of Heart Valve Disease* 13: 798–803.
27. Cloyd KL, El-Hamamsy I, Boonrungsiman S, Hedegaard M, Gentleman E, et al. (2012) Characterization of Porcine Aortic Valvular Interstitial Cell “Calcified” Nodules. *PLoS ONE* 7: e48154.
28. Balachandran K, Sucusky P, Jo H, Yoganathan AP (2010) Elevated Cyclic Stretch Induces Aortic Valve Calcification in a Bone Morphogenic Protein-Dependent Manner. *The American Journal of Pathology* 177: 49–57.
29. Meyer-ter-Vehn T, Sieprath S, Katzenberger B, Gebhardt S, Grehn F, et al. (2006) Contractility as a Prerequisite for TGF- β -Induced Myofibroblast Transdifferentiation in Human Tenon Fibroblasts. *Investigative Ophthalmology & Visual Science* 47: 4895–4904.

30. Leask A, Abraham DJ (2004) TGF- β signaling and the fibrotic response. *The FASEB Journal* 18: 816–827.
31. Syedain ZH, Tranquillo RT (2011) TGF- β 1 diminishes collagen production during long-term cyclic stretching of engineered connective tissue Implication of decreased ERK signaling. *Journal of Biomechanics* 44: 848–855.
32. Clark-Greuel JN, Connolly JM, Sorichillo E, Narula NR, Rapoport HS, et al. (2007) Transforming Growth Factor- β 1 Mechanisms in Aortic Valve Calcification: Increased Alkaline Phosphatase and Related Events. *The Annals of Thoracic Surgery* 83: 946–953.
33. Jian B, Narula N, Li Q-Y, Mohler ER III, Levy RJ (2003) Progression of aortic valve stenosis: TGF- β 1 is present in calcified aortic valve cusps and promotes aortic valve interstitial cell calcification via apoptosis. *The Annals of Thoracic Surgery* 75: 457–465.
34. Park J-B (2012) The Effects of Dexamethasone, Ascorbic Acid, and β -Glycerophosphate on Osteoblastic Differentiation by Regulating Estrogen Receptor and Osteopontin Expression. *Journal of Surgical Research* 173: 99–104.
35. de Gorter DJ, van Dinther M, Korchynskiy O, Dijke ten P (2011) Biphasic effects of transforming growth factor β on bone morphogenetic protein-induced osteoblast differentiation. *J Bone Miner Res* 26: 1178–1187.
36. Lee K-S, Kim H-J, Li Q-L, Chi X-Z, Ueta C, et al. (2000) Runx2 is a common target of transforming growth factor β 1 and bone morphogenetic protein 2, and cooperation between Runx2 and Smad5 induces osteoblast-specific gene expression in the pluripotent mesenchymal precursor cell line C2C12. *Molecular and Cellular Biology* 20: 8783–8792.
37. Acharya A, Hans CP, Koenig SN, Nichols HA, Galindo CL, et al. (2011) Inhibitory Role of Notch1 in Calcific Aortic Valve Disease. *PLoS ONE* 6: e27743.
38. David Merryman W, Shadow Huang H-Y, Schoen FJ, Sacks MS (2006) The effects of cellular contraction on aortic valve leaflet flexural stiffness. *Journal of Biomechanics* 39: 88–96.

39. Peacock JD, Levay AK, Gillaspie DB, Tao G, Lincoln J (2010) Reduced Sox9 Function Promotes Heart Valve Calcification Phenotypes In Vivo. *Circulation Research* 106: 712–719.
40. Bouchareb R, Boulanger M-C, Fournier D, Pibarot P, Messaddeq Y, et al. (2014) Mechanical strain induces the production of spheroid mineralized microparticles in the aortic valve through a RhoA/ROCK-dependent mechanism. *Journal of Molecular and Cellular Cardiology* 67: 49–59.
41. Fondard O, Detaint D, Lung B, Choqueux C, Adle-Biassette H, et al. (2005) Extracellular matrix remodelling in human aortic valve disease: the role of matrix metalloproteinases and their tissue inhibitors. *European Heart Journal* 26: 1333–1341.
42. Leopold JA (2012) Cellular Mechanisms of Aortic Valve Calcification. *Circulation: Cardiovascular Interventions* 5: 605–614.
43. Hinton RB, Lincoln J, Deutsch GH, Osinska H, Manning PB, et al. (2006) Extracellular matrix remodeling and organization in developing and diseased aortic valves. *Circulation Research* 98: 1431–1438.
44. Yip CYY, Chen JH, Zhao R, Simmons CA (2009) Calcification by Valve Interstitial Cells Is Regulated by the Stiffness of the Extracellular Matrix. *Arteriosclerosis, Thrombosis, & Vascular Biology* 29: 936–942.

CHAPTER 8

FUTURE DIRECTIONS & CONCLUSIONS

The echocardiography data for Figure 8.6 were collected by Kevin S. Hsu.

Table 8.1 and Figures 8.9-11 were created by Ian J. Forsythe.

The ChIP data for Table 8.2 were collected by the Puc at Lab, INSERM, France.

8.1 Future Directions

The role of oxidative stress in aortic valve disease

In chapter 2 of this thesis, we found that TNF α -driven endothelial oxidative stress (OxS) is an initiating mechanism for the dysregulation of OxS that has been described as a feature of late-stage AVD [1,2]. We further showed robust in vitro and ex vivo evidence for the benefits of BH₄ and superoxide dismutase (SOD) in OxS management. In order to further investigate this mechanism, in vivo studies of pharmaceutical OxS management should be designed.

To translate our findings in vivo, it would be highly feasible for our lab to combine our existing mouse model of AVD, the LDLR^{-/-} high fat diet model, with different OxS management drugs. eNOS uncoupling could be directly targeted via administration of the BH₄ precursor sapropterin, in the form of FDA-approved drug KuvanTM (sapropterin-dihydrochloride). Downstream of eNOS uncoupling, excess superoxide could be targeted via administration of Tempol, an SOD mimetic (Figure 1). We also showed in vitro the benefits of targeting mitochondrial reactive oxygen species with Apocynin (acetovanillone), a general preventor of OxS increase. Apocynin is also already FDA-approved and is very inexpensive. We calculate that Apocynin administration for OxS measurement could be tested in vivo for approximately \$0.01/day/mouse.

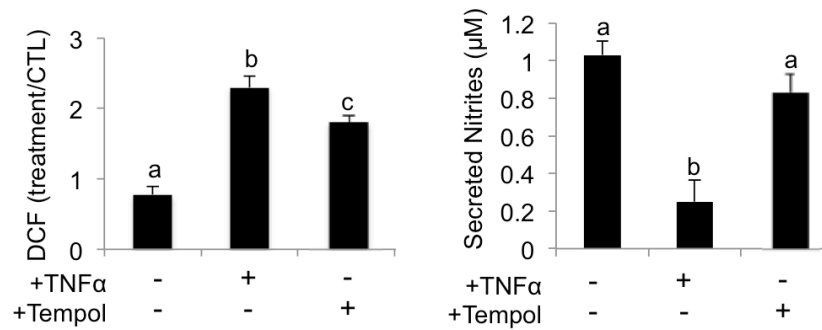


Figure 8.1 Effect of SOD-mimetic Tempol on 30 minute TNF α -VEC oxidative stress.

N > 3, bars with different letters are statistically different (p < 0.05), error bars indicate SEM.

It is also important to understand the role of TGF β signaling in the preservation of endothelial function. We have done preliminary testing of an Akt inhibitor on TNF α -driven OxS. Akt modulates TGF β signaling by the recruitment of Smad3 to the nucleus [3] and has a role in TGF β -driven EndMT [4], so Akt inhibition is a first step towards understanding the contribution of TGF β to VEC dysfunction. We found that the inhibitor Akt XI (5 μ M) mitigated short-term (30 minute) increases in valve endothelial OxS (Figure 2). We also used Alk2/5 inhibitor SB431542 (10 μ M on porcine aortic VEC) in chapter 3 of this work, showing that Alk2/5 TGF β signaling was not necessary for inflammatory EndMT in postnatal VEC. This experiment could be extended to assess the role of Alk2/5 receptor signaling in TNF α -driven endothelial OxS.

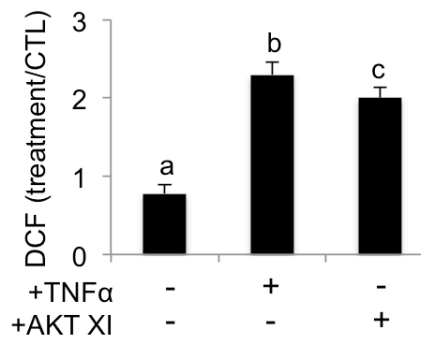


Figure 8.2 Effect of Akt inhibition on 30 minute TNF α -VEC oxidative stress.

N > 3, bars with different letters are statistically different (p < 0.05), error bars indicate SEM.

We also suggest considering the acute (30 minute) OxS effect of TNF α and TGF β -Akt signaling in VEC. We have preliminary evidence that TNF α drives an increase in eNOS activity at 30 minutes after treatment that is blocked by L-NAME or Akt XI. Increased eNOS activity is indicated by increased nitric oxide secretion (Figure 3A), increased expression of phosphorylated eNOS protein (Figure 3B-D), and increased immunofluorescent staining for phosphorylated eNOS (Figure 3E). This points to an initial ability of the VEC to protect themselves against TNF α by secreting nitric oxide. This protective effect degrades over time as the VEC undergo longer-term TNF α effects, such as EndMT. Significant (> 5% of VEC) EndMT is observed at 48 hours after TNF α treatment and corresponds with reduced eNOS activity.

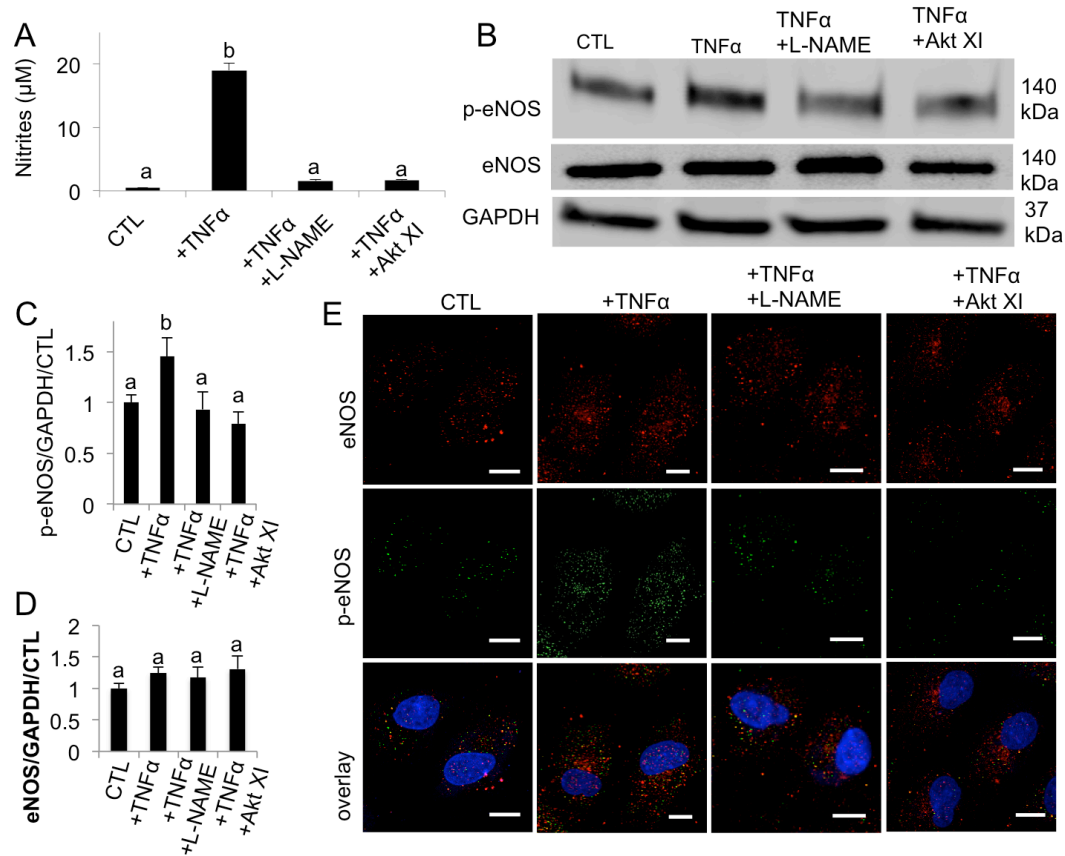


Figure 8.3 Acute eNOS response of adult valve endothelial cells to TNF α .

A. Quantification of nitric oxide secretion by VEC 30 minutes after treatment using the Griess assay. B. Western blot analysis of phosphorylated (p-eNOS) and unphosphorylated eNOS in VEC 30 minutes after treatment. Scale bar is 10 μ m.

Acute increase in nitric oxide in response to TNF α has been described in other endothelial cell populations as an apoptotic regulatory response [5]. We did indeed find that blocking eNOS (+L-NAME) in 30 minute VEC+TNF α led to an increase in apoptosis (Figure 8.4A, B). This appears to be mediated both by Akt and NF κ B signaling (Figure 8.4C, D). Understanding the degradation of eNOS function due to

TNF α , from a 30-minute increase to a 48-hour decrease, is important to using eNOS as an effective target for AVD therapy.

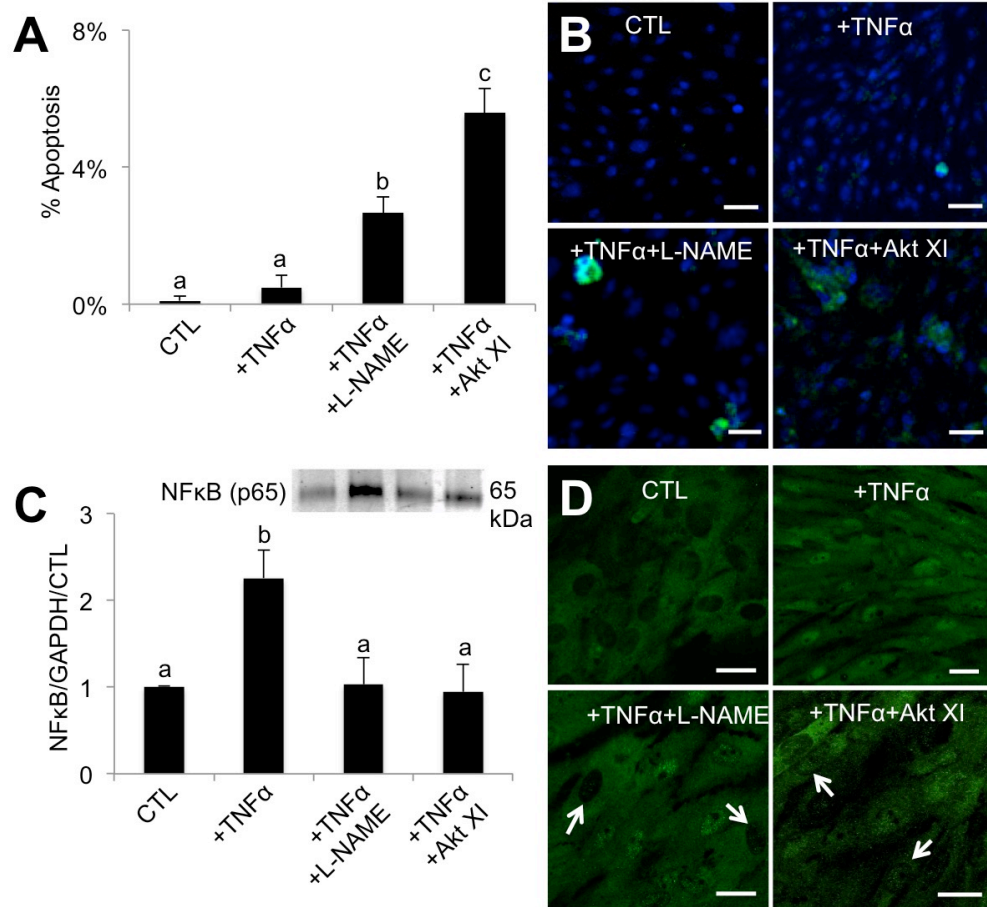


Figure 8.4 Apoptotic and NF κ B signaling response of VEC to TNF α .

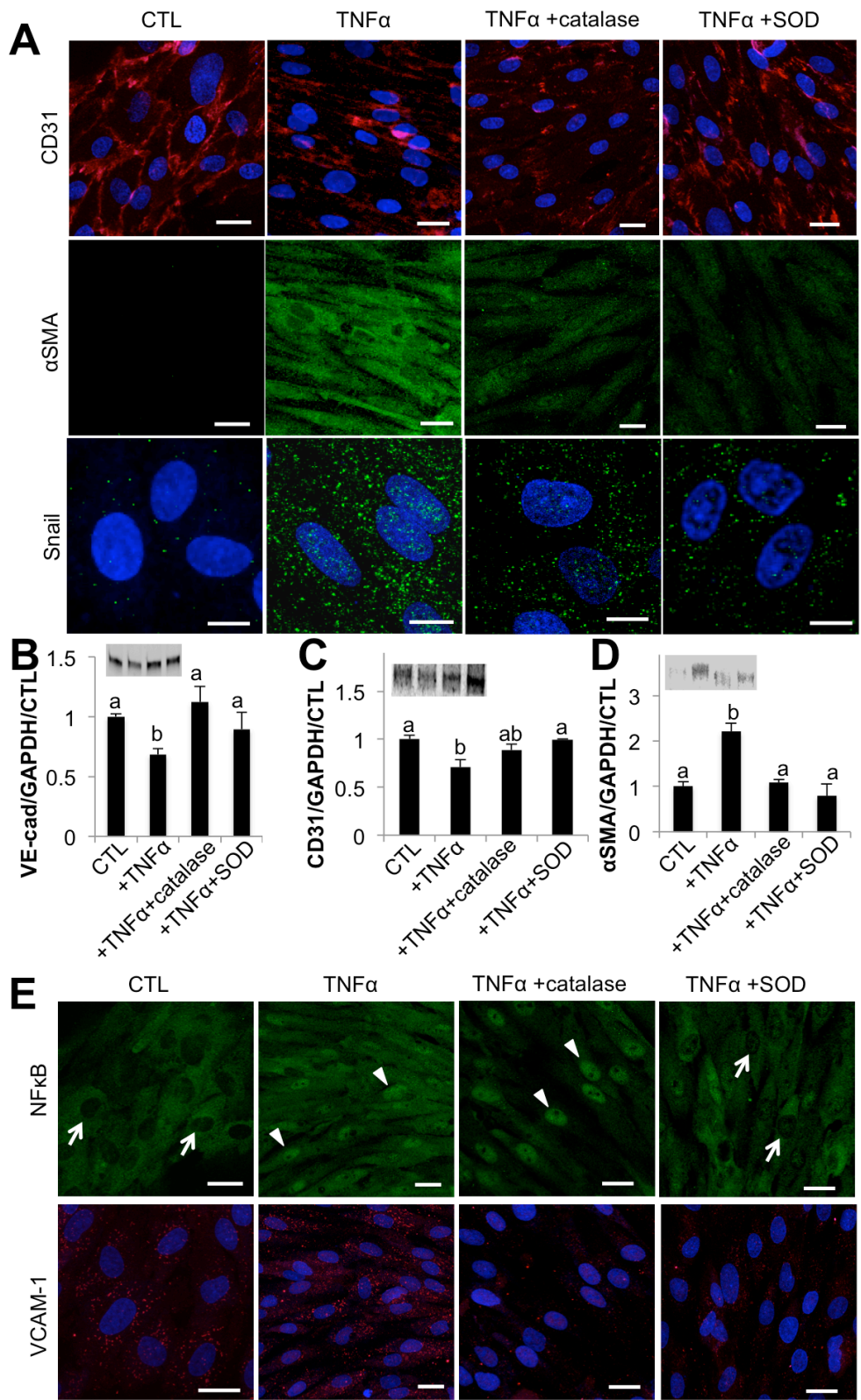
A. Quantification of apoptosis in VEC 30 minutes after treatment. B. TUNEL stain for apoptosis in 30 minute VEC. C. Quantification of NF κ B p65 protein expression in VEC via western blot. Inset is representative blot with treatments indicated on x-axis, in same order. D. Immunofluorescent staining for NF κ B. Arrows indicate nuclei negative for NF κ B in lower panels. Scale bar is 20 μ m.

Finally, we did also observe some interplay between the OxS and EndMT effects of TNF α on VEC. Treatments that blocked eNOS (L-NAME) or Akt (Akt XI) also blocked NF κ B protein synthesis (Figure 8.4C) and nuclear translocation (Figure 8.4D), which we have shown to be necessary for TNF α EndMT.

TNF α also drives endothelial dysfunction through increases in hydrogen peroxide and superoxide, so we wondered whether blocking increases in OxS could block TNF α EndMT. We found that both catalase, which reduces hydrogen peroxide, and superoxide dismutase mitigated TNF α EndMT effects (Figure 8.5A-D). Interestingly, catalase appeared to increase TNF α -driven NF κ B activity, but decreased VCAM-1 expression, which is a direct target of NF κ B. Superoxide dismutase mitigated both NF κ B and VCAM-1 (Figure 8.5E). This suggests that using catalase to mitigate TNF α effects by reducing hydrogen peroxide may not be as efficacious as targeting superoxide. Some reports even suggest that catalase can even increase cell sensitivity to TNF α [6], which would be detrimental to our objective of mitigating TNF α as an initiating mechanism of AVD.

Figure 8.5 Interplay between EndMT and OxS signaling in VEC+TNF α .

A. Immunofluorescent staining of EndMT proteins in 48 hour VEC with TNF α and different antioxidants. Scale bar is 20 μ m. B. Quantification of western blot of VE-cadherin, inset is representative of N=3 blots, 140kDa band. C. Quantification of western blot of CD31, inset is 130kDa band. D. Quantification of western blot of α SMA, inset is 42kDa band. E. Immunofluorescent staining of NF κ B and VCAM-1 in 48 hour VEC. Arrows indicate cell nuclei that are negative for NF κ B. Arrowheads indicate cell nuclei positive for NF κ B.



Capitalizing on the heterogeneous ability of postnatal valve endothelial cells to undergo EndMT

In chapter four, we used a novel transwell assay to demonstrate the heterogeneous ability of adult porcine aortic valve endothelial cells (VEC) to undergo mesenchymal transformation in response to TNF α . The question remains: why do some VEC undergo EndMT in response to TNF α and some do not? Is the population that remains endothelial protected against mesenchymal transformation, or does the transforming population have special transdifferentiation ability? These options are not mutually exclusive. Other studies have shown spatially distinct VEC phenotypes in the adult aortic valve [7,8], which supports a role for differential EndMT-protective mechanisms across VEC. We have shown that transformed VEC have a pro-disease phenotype, suggesting that they participate in downstream pathogenic events. Thus, identification of EndMT-protective mechanisms in non-transforming VEC could have powerful benefits for preservation of the valve endothelium and protection against disease.

Some studies suggest that EndMT is a homeostatic mechanism that replenishes the valve interstitial cell population over time [9], so an anti-EndMT intervention would need to be carefully tuned to avoid off-target negative effects. Our *in vivo* work with the inactivation of NF κ B in mice suggests that NF κ B inhibition may be a way to block disease-associated EndMT without detriment to the healthy valve.

A large-scale mRNA screen of non-transforming versus transforming VEC from the transwell assay could reveal other potential anti-EndMT phenotypes unique to VEC that resist inflammatory mesenchymal transformation. The existing challenge with this is the small number of transforming cells obtained from the transwell assay (< 15,000 total), which limits the concentrations of mRNA that can be obtained (currently ~ 1ng/uL). However, recent advances in RNA-sequencing, particularly the Ovation® System, suggest that sequencing from minute quantities (~100pg) of RNA may be possible [10]. In our system, these new techniques combined with the use of larger transwell plates (6-well size) for culture of higher cell numbers (~1-2 million cells/well) could provide greater quantities of cells for analysis of in both transforming and non-transforming populations.

In vivo BAY 11-782 inhibition of NFκB

In chapter five of this work, we demonstrated a role for NFκB in governing valve EndMT and calcification, but it needs to be shown whether NFκB could work *in vivo* as an anti-EndMT target. One option for *in vivo* NFκB inhibition is the inhibitor of IKKβ activity, BAY 11-7082 [11]. BAY has been shown to block NFκB p65 activity in mice when administered via intraperitoneal injection [12]. NFκB has been the focus of many studies regarding inflammation in cancer development, thus there have been many attempts to modulate its function *in vivo* [13]. Cross-talk between oncology and AVD may lead to future avenues for AVD treatment via NFκB modulation.

In vivo over-activation of NFκB

In chapter five, we present the results of NFκB inactivation on AVD. We would also suggest exploration of the valve-specific effects of NFκB over-activation on the valve. One way to induce constitutive activation of NFκB would be to knock out IκBα, the molecule that binds NFκB in the cell cytoplasm, preventing nuclear translocation and transcriptional activity. Full IκBα^{-/-} mice die within eight days of birth, but show robust constitutive NFκB activation throughout the mouse [14]. Combination of our spatially-restricted, valve-specific Cre (Nfatc1^{Cre}) with an IκBα^{lox/lox} mouse would create a new line with constitutive activation of NFκB only in the valve. We could then examine these mice for valve phenotype and assess the effects of NFκB on valve formation.

Valve endothelial cell specific inhibition of NFκB

We would also like to characterize the endothelial-specific effects of NFκB inhibition *in vivo*. We showed in chapter five that whole-valve inactivation of NFκB led to protection against AVD, but our *in vitro* work points to a specific role for endothelial NFκB in AVD degeneration that needs to be further elucidated. Our collaborators at Einstein University have created a mouse with an enhancer element added to the Nfatc1 promoter that “turns on” the promoter only after the EndMT events of valvulogenesis, resulting in expression only in the valve endocardium, rather than the whole valve [15,16]. They have added cre recombinase to this promoter element (VEC^{Cre}), which we have combined with our IKKβ floxed mouse to selectively delete IKKβ in the aortic valve endothelium (VEC^{Cre};IKKβ^{f/f}). We then combined this

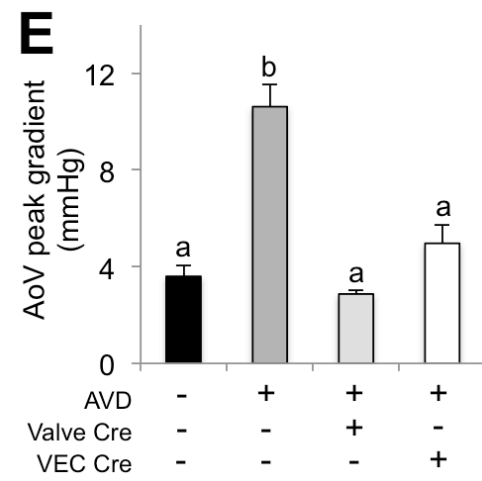
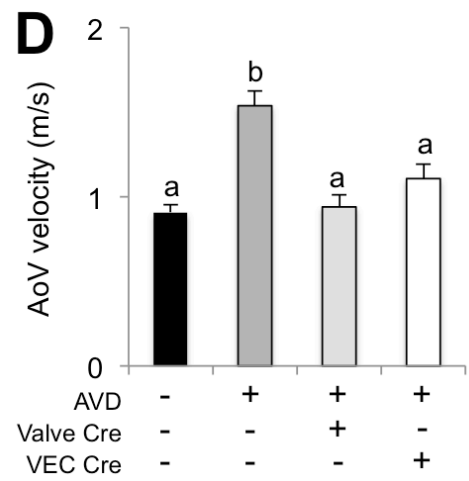
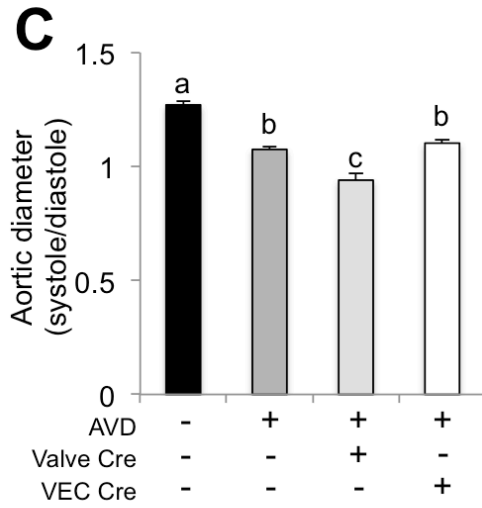
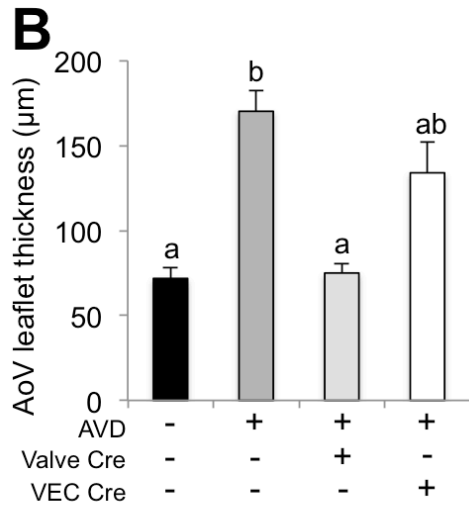
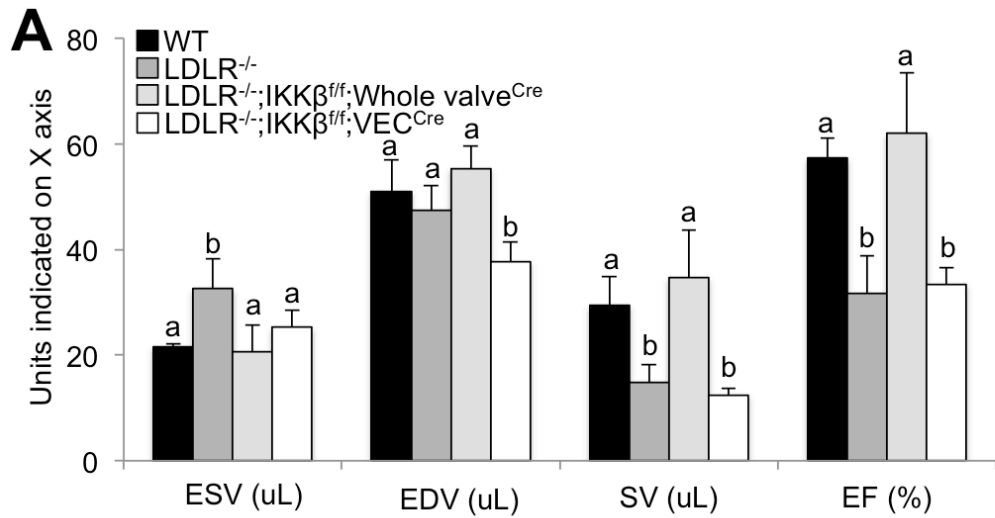
VEC^{Cre};IKK β ^{f/f} mouse with our LDLR^{-/-} high fat diet AVD model to investigate the effects of endothelial inactivation of NF κ B on AVD.

Valve endothelial cell specific inhibition of NF κ B: Preliminary results

Our preliminary results show a moderate improvement of AVD in the VEC^{Cre};IKK β ^{f/f} mouse (Figure 6). End systolic volume was improved, indicating improved left ventricular contractility; however, end diastolic volume, stroke volume, and ejection fraction were not improved versus LDLR^{-/-} (Figure 8.6A). Aortic valve (AoV) leaflet thickness was not statistically different than either wild type or AVD mice (Figure 8.6B), indicating a need for more samples to confirm effect of VEC^{Cre};IKK β ^{f/f}. Aortic root distensibility was similar to AVD but higher than the Valve^{Cre}, again suggesting an intermediate effect (Figure 8.6C). Aortic velocity and AoV peak gradient were improved in the VEC^{Cre} to a similar extent as in the Valve^{Cre}, (Figure 8.6D, E) indicating that endothelial inactivation of NF κ B is sufficient to rescue valve hemodynamic function. It remains to be seen what endothelial NF κ B mechanisms are behind this rescue effect. We would like to perform the same histological and protein analyses on the VEC^{Cre} mice as we performed in chapter five and also assess the model for oxidative stress effects.

Figure 8.6 Effect of VEC-specific NFκB inactivation on aortic valve disease *in vivo*.

A. Left ventricular function analysis of control (WT), AVD (LDLR^{-/-}), whole-valve NFκB inactivation (LDLR^{-/-};IKKβ^{fl/fl};whole valve^{Cre}), and valve endothelial cell only NFκB inactivation (LDLR^{-/-};IKKβ^{fl/fl};VEC^{Cre}). B. AoV leaflet thickness analysis from echocardiographic EKV images of the aortic valve, at maximum systole. C. Aortic root distensibility, calculated from ratio of aortic diameter in systole over diastole. D. Peak AoV velocity, from pulsed wave Doppler echocardiography. E. AoV peak gradient, from average of three velocity time intervals and echocardiographic analysis of AoV flow dynamics. 5 month-old mice, 4 months of high fat diet in all models except WT control. N > 5 for each group. Bars with different letters are statistically different (p < 0.05), error bars indicate SEM.



Valve endothelial cell lineage tracing in AVD

Finally, we would like to use the VEC^{Cre} mouse in combination with the ROSA26 lacZ reporter in order to trace the fate of valve endothelial cells in healthy and AVD adult mice. This is an important experiment that will show the role of EndMT in postnatal valves. Our system has an important advantage over other endothelial-cre mouse lines, such as the Tie2Cre [17], the flk-1^{Cre} [18], and the VE-cadherin^{Cre} [19]. In these other lines, the endothelial cre is “turned on” from the earliest stages of development. An essential step in valve formation is endothelial to mesenchymal transformation of the endothelial/endocardial cells of the developing outflow tract. Thus, Cre+ endothelial cells become the mesenchymal cells of the valve, making the whole valve positive for Cre expression, rather than just the endothelium. In contrast, our VEC^{Cre} mouse utilizes the promoter-enhancer region to ensure that the Cre is “turned on” only after valve EndMT occurs. In this way, the Cre is expressed only in the endothelial cells of the mature valve, rather than both the endothelial and mesenchymal populations. A Cre that is restricted to the postnatal valve endothelial cells and not the whole valve is critical to tracing the fate of VEC in adult valve disease.

Crossing our VEC^{Cre} mouse with a ROSA26 mouse will allow for lineage tracing of valve endothelial cells via lacZ staining of tissue in both healthy and AVD adult mice. This would make it possible for the first time to evaluate the fate of valve endothelial cells in valve disease. LacZ staining would color VEC blue, allowing for quantification of the number of VEC that undergo EndMT and invade the valve mesenchyme in both healthy and AVD mice. This should be performed in five month

old wild type mice, LDLR^{-/-};VEC^{Cre};ROSA26 mice with the high fat diet, and in LDLR^{-/-};VEC^{Cre};ROSA26 mice with IKK β floxed. Thus, we would be able to visualize the fate of VEC in control adult mice, mice with valve disease, and mice with valve disease with NF κ B inactivated in VEC. This experiment would allow for a complete *in vivo* understanding of the role of EndMT and VEC NF κ B signaling in LDLR^{-/-} valve disease.

Microarray analysis of downstream effects of NFκB in VEC (Preliminary data)

We transfected porcine aortic VEC with our GFP-NFκB p65 plasmid and cultured them over night. Fluorescence-activated cell sorting was used to select for GFP- NFκB p65+ cells. These cells were re-plated and grown overnight. RNA was isolated from the sorted, NFκB transfected cells and used to run an Agilent-026440 Sus scrofa (Pig) Oligo Microarray v2. The Cornell Genomics core ran the microarray for us. A master's of biomedical engineering student, Ian Forsythe, analyzed the results in Genespring and Ingenuity Pathway Analysis software.

We interrogated the microarray results for genes related to EndMT or valve calcification that were significantly affected (up-regulated or down-regulated > 2-fold) by NFκB p65 over-activation (Figure 8.7). We found a robust EndMT effect, with many endothelial-associated genes downregulated and mesenchymal/invasive genes upregulated. We also interrogated the microarray for genes related to aortic valve disease (Figure 8.8A) and related to somatic cell reprogramming (Figure 8.8B).

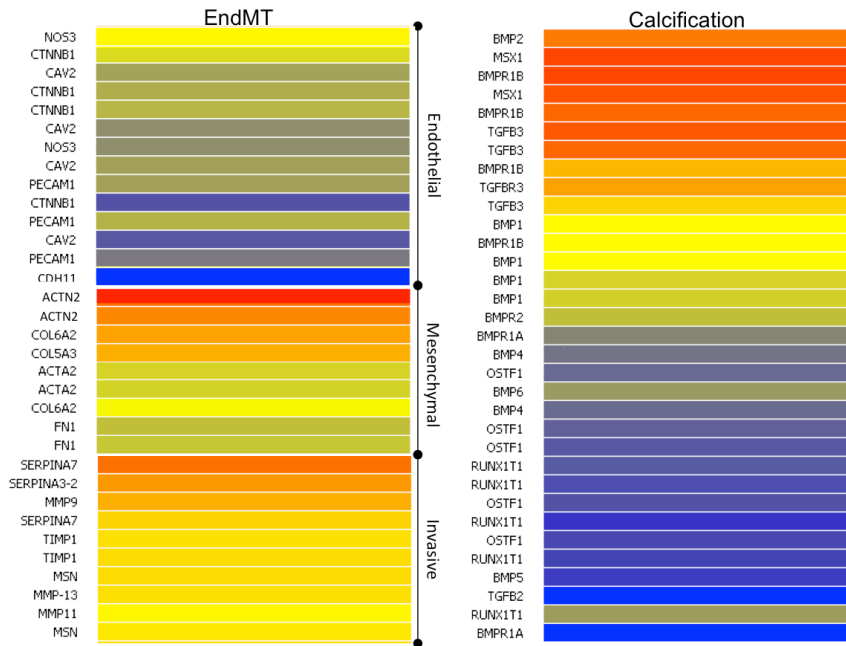


Figure 8.7 VEC+NFκB microarray results for EndMT and calcification genes.

Red indicates upregulation, blue indicates downregulation. Data is the mean fold change of N = 3 replicates of microarray.

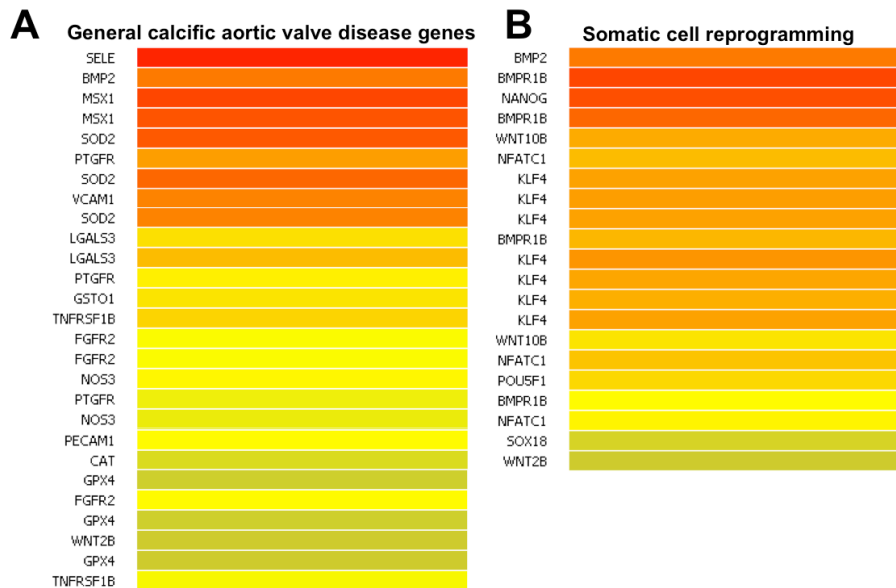


Figure 8.8 VEC+NFκB microarray results for AVD and reprogramming genes.

Red indicates upregulation, blue indicates downregulation. Data is the mean fold change of N = 3 replicates of microarray. Klf4 replicates in panel B are different isoforms of the Klf4 gene.

Finally, we used Ingenuity Pathway Analysis (IPA) to link some of the RNA changes we observed into signaling networks. Ian Forsythe describes his analysis of the VEC+NF κ B data:

“25 different networks were represented by the data, displayed in [Table 8.1]. A number of the represented networks were associated with system development and morphology. The highest rated network for NF κ B is related to skeletal and muscular development as well as organ morphology and is displayed in [Figure 8.9]. An inspection of the network shows a central downregulation predicted for Jnk, a kinase that plays a role in cellular proliferation and differentiation. The second highest rated network of the system shows an upregulation in G-Protein coupled signaling. Network 18, shown in [Figure 8.10], displays a downregulation of BMP4/6/7 while BMP2 is increased. A heightened expression of IL-10 is also shown to be central to network 18, again associated with system development and function. Network 25, [Figure 8.11], indicates that VEGFA, vascular endothelial growth factor A, is at the center of the network and activated by a number of factors within the network. A number of canonical pathways were also represented by the data with the largest changes observed in the largest representation in the Hepatic Fibrosis/Hepatic Stellate Cell Activation pathway, with significant changes to pathways associated with Interleukin signaling and Glucocorticoid Receptor Signaling. An analysis of these pathways as well as inspection of upstream regulators shows an increase in positive inflammatory feedback. The Hepatic Fibrosis pathway highlights the activity of VEGF in cell proliferation as well as other activities including collagen synthesis from

IL-4R. Upstream analysis showed elevated levels of TNF, STAT, and other transcription factors.”

Ian Forsythe, M.Eng. Report II, May 2013. Butcher Lab, Cornell University

Table 8.1 NFκB Networks

ID	Score	Top Functions
1	38	Skeletal and Muscular System Development and Function, RNA Post-Transcriptional Modification, Organ Morphology
2	31	Cell Signaling, Behavior, Digestive System Development and Function
3	31	Cell Morphology, Amino Acid Metabolism, Post-Translational Modification
4	31	Cell-To-Cell Signaling and Interaction, Cellular Movement, Hematological System Development and Function
5	30	Carbohydrate Metabolism, Energy Production, Small Molecule Biochemistry
6	30	Cellular Assembly and Organization, DNA Replication, Recombination, and Repair, Gene Expression
7	30	Embryonic Development, Lymphoid Tissue Structure and Development, Organ Development
8	28	Cardiovascular Disease, Developmental Disorder, Hereditary Disorder
9	28	DNA Replication, Recombination, and Repair, Nucleic Acid Metabolism, Small Molecule Biochemistry
10	27	DNA Replication, Recombination, and Repair, Energy Production, Nucleic Acid Metabolism
11	26	Cell Death and Survival, Infectious Disease, Respiratory Disease
12	26	Cell Death and Survival, Cell Morphology, Cellular Function and Maintenance
13	26	Cellular Development, Cellular Growth and Proliferation, Hematological System Development and Function
14	26	Post-Translational Modification, Cell Signaling, Vitamin and Mineral Metabolism
15	25	Cellular Movement, Cell Morphology, Cellular Development
16	25	Free Radical Scavenging, Small Molecule Biochemistry, Cell Cycle
17	24	Endocrine System Development and Function, Lipid Metabolism, Small Molecule Biochemistry
18	24	Endocrine System Development and Function, Lipid Metabolism, Molecular Transport
19	24	RNA Post-Transcriptional Modification, Antimicrobial Response, Inflammatory Response
20	24	Cell Death and Survival, Cellular Development, Cellular Growth and Proliferation

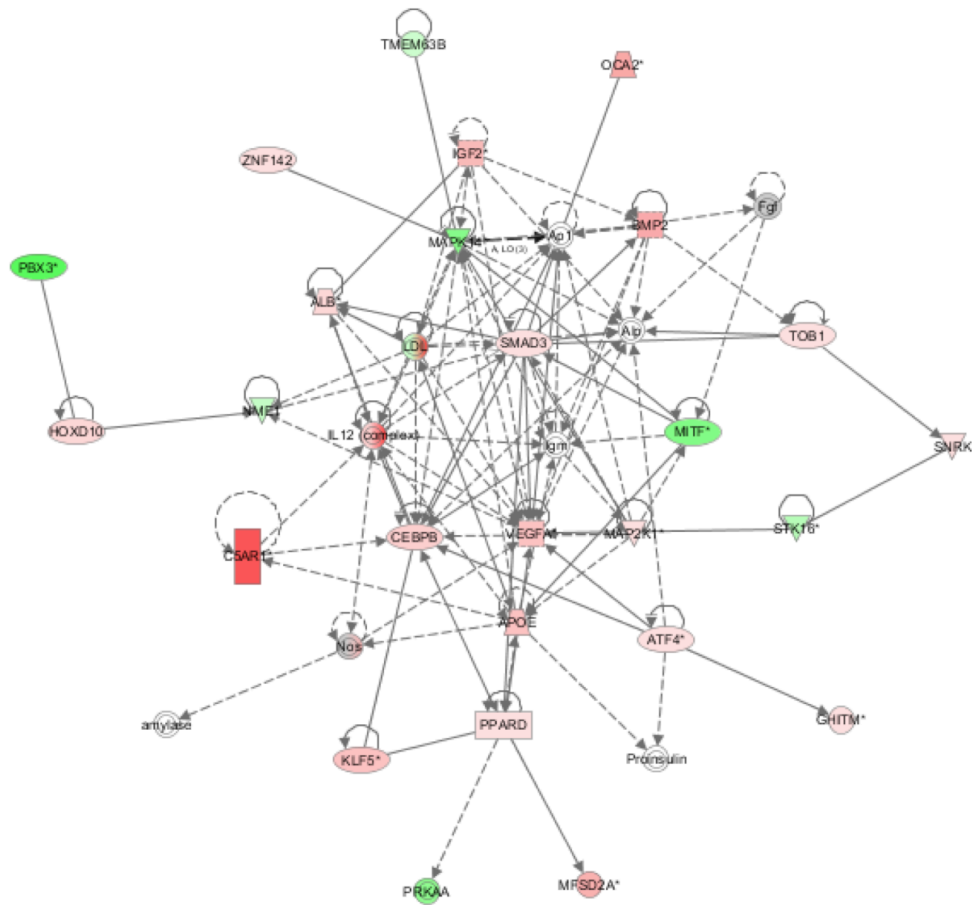


Figure 8.11 Network 25 for NFκB Data

Further elucidation of the role of Oct4 in aortic valve disease

In the microarray results noted above, POU5F1 (Oct4) is significantly upregulated in VEC+NFκB. This leads us to hypothesize that NFκB and Oct4 signaling are regulated in AVD. In order to test this hypothesis, we performed immunofluorescent staining for Oct4 protein in control, AVD, and AVD+NFκB inactivation mouse valves. We found no observable expression of Oct4 in 5-month-old control mouse valves (Figure 8.12A). Oct4 was increased in AVD (LDLR^{-/-}) aortic valves, particularly in the VEC (Figure 8.12B, arrows). Oct4 expression was not decreased in AVD+NFκB inactivation mouse valves (LDLR^{-/-};IKKβ^{fl/fl};whole valve^{Cre}), compared to AVD valves (Figure 8.12C). There was, however, more Oct4 expression in the interstitial cells of AVD+NFκB inactivation, compared to AVD.

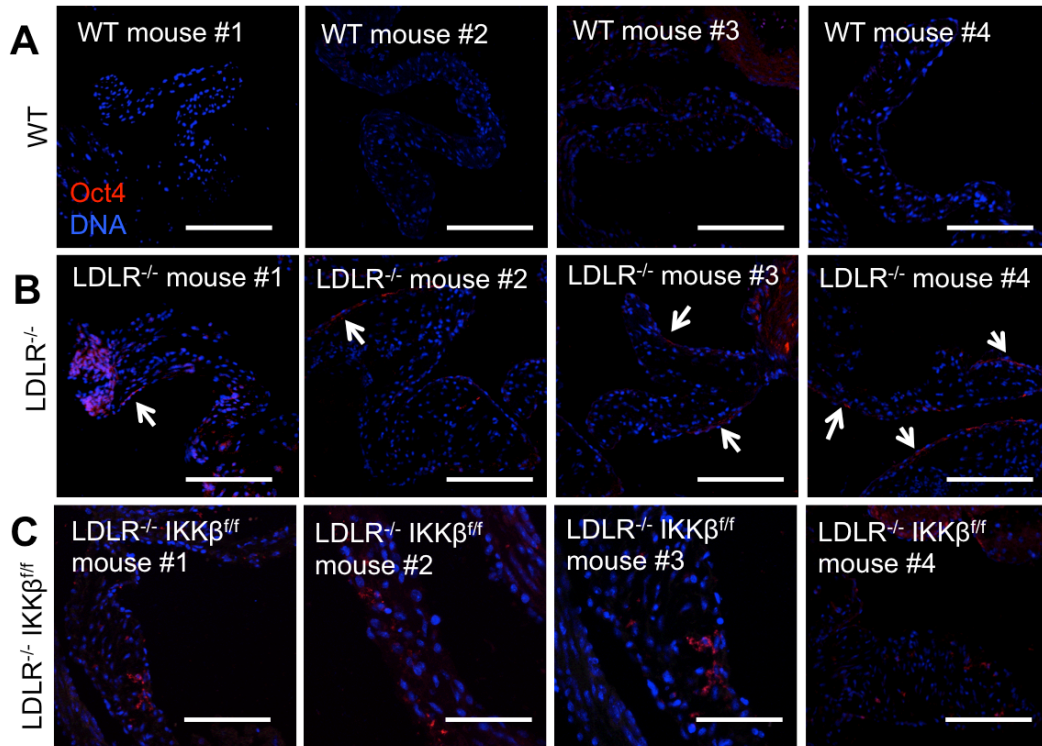


Figure 8.12 Oct4 expression in adult mouse aortic valves.

A. Oct4 (red) expression in four different aortic valves from wild type (C57/Bl6 J) mice. B. Oct4 expression in the aortic valves of mice with $LDLR^{-/-}$ +high fat diet AVD. Arrows indicate elevated Oct4 in valve endothelium. C. Oct4 expression in the aortic valves of mice with AVD and whole-valve NF κ B inactivation. Mice are all 5 months old. Scale bar is 100 μ m. Fibrosa side of valve is nearer to top of page in all images.

We would also like to functionalize the role of Oct4-mediated reprogramming in the postnatal valve by creating a valve-specific Oct4 knock-out mouse. *Oct4* null homozygous embryos die *in utero* [20], and Oct4 is necessary for direction of stem cells to a cardiac lineage [21], thus the deletion of Oct4 would need to be both spatially and temporally regulated. A tetracycline-activated valve-specific cre recombinase system could induce deletion of a floxed Oct4 only in the valves of the adult mouse. This system could be used to investigate the role of Oct4 in reprogramming, EndMT, and transdifferentiation of adult valve cells. Our

collaborators at Einstein University in the Zhou lab have a tet-inducible *Nfatc1*^{Cre} mouse that could be crossed with an Oct4 floxed mouse [22] in order to delete Oct4 at different points of valve formation, postnatal development, and disease. It would be interesting to attempt a rescue of valve disease at different points along the timeline of disease development. We currently use four months of high fat diet to induce disease, so the tet-induction could be done after 0, 1, 2, 3 or 4 months of diet to assess affect on valve function. It would also be interesting to perform this study with the tet-inducible cre and the floxed *IKK β* mouse, in order to assess time-dependent effects of NF κ B inactivation.

Interactions of NF κ B and Oct4 signaling in vitro

To further elucidate the interplay between NF κ B and Oct4 signaling, we performed double transfections of NF κ B p65 with antisense Oct4 (ASOct4) and of Oct4 with dominant-negative I κ B α . We examined the effect of these transfections on 14 day PAVEC or PAVIC with control or osteogenic media.

There appears to be interplay between NF κ B and Oct4 signaling in both cell types that needs to be further elucidated, but we have made some preliminary observations. In PAVEC, p65 over-expression was not reduced by co-transfection with ASOct4. Oct4 over-expression was not reduced by I κ B α . The pro-osteogenic phenotype observed in chapter six of VEC+p65+OGM was not affected by co-transfection of p65+ASOct4. Oct4 over-expression promoted NF κ B expression in VEC+I κ B α (Figure 8.13). All this

leads us to conclude that in VEC, Oct4 is upstream of NFκB, but Oct4 signaling is not necessary for NFκB-mediated osteogenic shift in VEC.

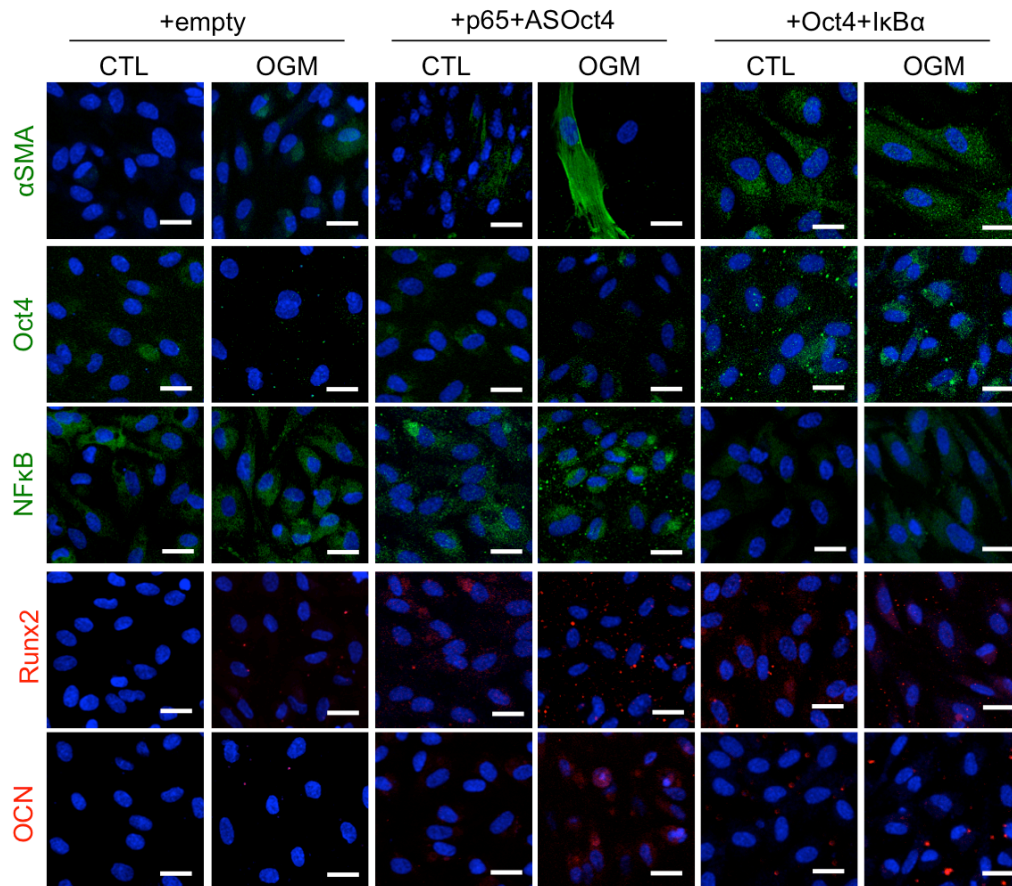


Figure 8.13 Interplay between NFκB and Oct4 signaling in PAVEC.

Immunofluorescent staining for proteins related to AVD progression, 14-day culture in control or osteogenic media. Images representative of N=3 independent experiments.

In PAVIC, p65+ASOct4 or Oct4+IκBα repressed αSMA in both control and OGM conditions. P65 co-transfection did not rescue Oct4 expression in VIC+p65+ASOct4. Oct4 expression did not rescue p65 nuclear translocation in VIC+Oct4+IκBα. Neither co-transfection affected Runx2 expression. Co-transfections appeared to increase osteocalcin expression in both control and OGM conditions (Figure 8.14). These

changes suggest that NF κ B and Oct4 signaling in VIC modulate myofibroblastic phenotype (α SMA) and osteoblastic phenotype (Osteocalcin).

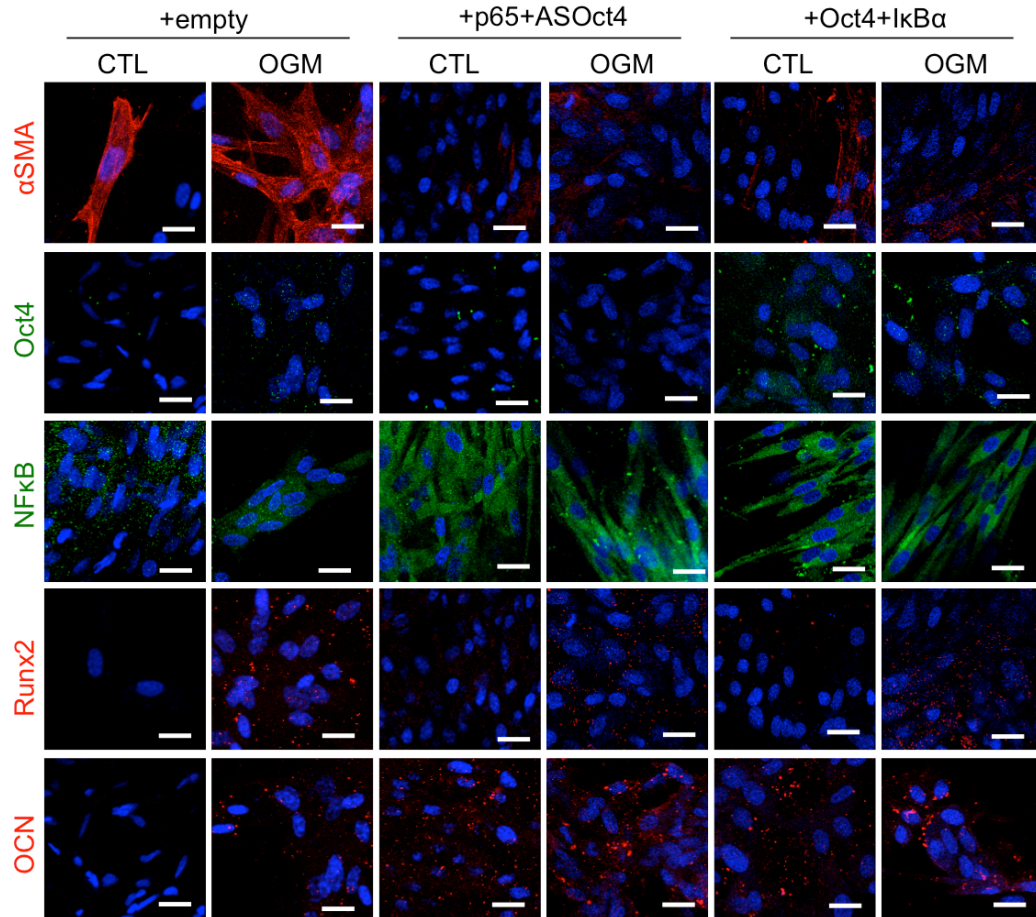


Figure 8.14 Interplay between NF κ B and Oct4 signaling in PAVIC.

Immunofluorescent staining for proteins related to AVD progression, 14-day culture in control or osteogenic media. Images representative of N=3 independent experiments.

ChIP sequencing of Oct4 binding targets in PAVIC

In order to understand the function of Oct4 in valve cells, we collaborated with the Puceat Lab (INSERM, Marseille, France) to perform chromatin immunoprecipitation (ChIP) on porcine aortic valve interstitial cells transfected with Oct4. We found that in porcine aortic VIC, Oct4 binds a number of DNA targets that are associated with AVD (Table 8.2). These targets may explain how ASOct4 inhibits VIC participation in calcification.

Table 8.2 DNA binding targets of Oct4 in aortic valve interstitial cells

DNA target	Function in AV	Reference
BMPRI	Required for BMP signaling in valvulogenesis	[23]
Cadherin 11	required for valvulogenesis, involved in calcification	[24, 25]
Mef2C	upregulated in pediatric and adult diseased AV	[26]
Nanog	upregulated in VEC by NFκB	Unpublished data, Figure 8.8
Nkx2.5	loss of function associated with BAV	[27]
Osteonectin	detected at sites of valve mineralization	[28]
P53	regulates cell response to DNA damage, possibly connects apoptosis with Smad1/BMP2 signaling	[29]
Periostin	protective against AVD	[30]
Tbx18	expressed in the developing valves	[31]
Thrombospondin	elevated thrombospondin-2 found in human sclerotic valves	[32]
VEGFC	associated with Lymphangiogenesis in human stenotic valves	[33]

Effect of changing boundary conditions on valve interstitial cell contractility and osteogenic mechanoregulation

In chapter seven, we designed a novel system to culture VIC in three dimensions while simultaneously measuring contractility. We measured contractility by analyzing deflection of a cantilevered spring. As a future direction for this project, we would like to understand the effect of changing the stiffness of the cantilevered spring. A stiffer spring would raise the perceived stiffness of the cell's environment and a more flexible spring would lower it.

We have preliminary data showing that a stiffer spring promotes a myofibroblastic phenotype (higher α SMA) and a more compliant spring promotes an osteoblastic phenotype (higher Runx2) (Figure 8.15). This agrees with a previous study showing control of VIC phenotype by matrix stiffness and cytoskeletal tension [34]. This study also showed that apoptosis and Akt signaling were involved in VIC sensing of their mechanical environment, which would need to be investigated in our system.

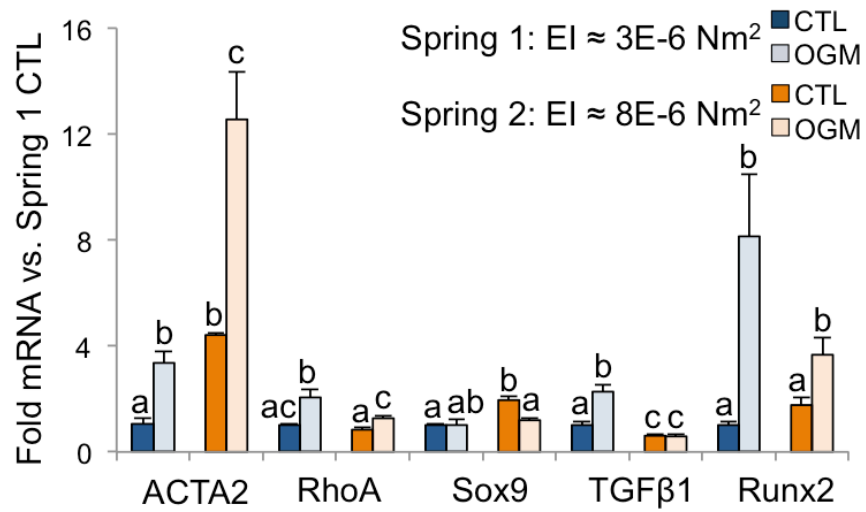


Figure 8.15 Effect of changing cantilevered spring stiffness on VIC phenotype.

Fold mRNA for each gene is compared to that gene's Spring 1 control. Letters indicate statistical significance within the different groups of a single gene. Bars with different letters are statistically significant. Effective modulus (EI) for the two springs was calculated from empirical testing of the springs as described in chapter seven.

REFERENCES

1. Miller JD, Chu Y, Brooks RM, Richenbacher WE, Pena-Silva R, et al. (2008) Dysregulation of Antioxidant Mechanisms Contributes to Increased Oxidative Stress in Calcific Aortic Valvular Stenosis in Humans. *Journal of the American College of Cardiology* 52: 843–850.
2. Liberman M, Bassi E, Martinatti MK, Lario FC, Wosniak J, et al. (2008) Oxidant generation predominates around calcifying foci and enhances progression of aortic valve calcification. *Arteriosclerosis, Thrombosis, & Vascular Biology* 28: 463–470.
3. Conery AR, Cao Y, Thompson EA, Townsend CM, Ko TC, et al. (2004) Akt interacts directly with Smad3 to regulate the sensitivity to TGF-beta induced apoptosis. *Nature Cell Biology* 6: 366–372.
4. Medici D, Potenta S, Kalluri R (2011) Transforming growth factor- β 2 promotes Snail-mediated endothelial–mesenchymal transition through convergence of Smad-dependent and Smad-independent signalling. *Biochem J* 438: 515–520.
5. Bulotta S, Barsacchi R, Rotiroti D, Borgese N, Clementi E (2000) Activation of the Endothelial Nitric-oxide Synthase by Tumor Necrosis Factor-alpha. *Journal of Biological Chemistry* 276: 6529–6536.
6. Bai J, Cederbaum AI (2000) Overexpression of Catalase in the Mitochondrial or Cytosolic Compartment Increases Sensitivity of HepG2 Cells to Tumor Necrosis Factor-alpha -induced Apoptosis. *Journal of Biological Chemistry* 275: 19241–19249.
7. Simmons CA, Grant GR, Manduchi E, Davies PF (2005) Spatial heterogeneity of endothelial phenotypes correlates with side-specific vulnerability to calcification in normal porcine aortic valves. *Circulation Research* 96: 792–799.
8. Paranya G, Vineberg S, Dvorin E, Kaushal S, Roth SJ, et al. (2001) Aortic Valve Endothelial Cells Undergo Transforming Growth Factor-beta-Mediated and Non-Transforming Growth Factor-beta-Mediated Transdifferentiation in Vitro. *The American Journal of Pathology* 159: 1335–1343.
9. Bischoff J, Aikawa E (2011) Progenitor Cells Confer Plasticity to Cardiac Valve Endothelium. *J of Cardiovasc Trans Res* 4: 710–719.

10. Tariq MA, Kim HJ, Jejelowo O, Pourmand N (2011) Whole-transcriptome RNAseq analysis from minute amount of total RNA. *Nucleic Acids Research* 39: e120–e120.]
11. Lee J, Rhee MH, Kim E, Cho JY (2012) BAY 11-7082 Is a Broad-Spectrum Inhibitor with Anti-Inflammatory Activity against Multiple Targets. *Mediators of Inflammation* 2012: 1–11.
12. Miyamoto R, Ito T, Nomura S, Amakawa R, Amuro H, et al. (2010) Inhibitor of I κ B kinase activity, BAY 11-7082, interferes with interferon regulatory factor 7 nuclear translocation and type I interferon production by plasmacytoid dendritic cells. *Arthritis Res Ther* 12: R87.
13. Lin Y, Bai L, Chen W, Xu S (2010) The NF- κ B activation pathways, emerging molecular targets for cancer prevention and therapy. *Expert Opin Ther Targets* 14: 45–55.
14. Beg AA, Sha WC, Bronson RT, Baltimore D (1995) Constitutive NF- κ B activation, enhanced granulopoiesis, and neonatal lethality in I κ B α -deficient mice. *Genes & Development* 9: 2736–2746.
15. Wu B, Wang Y, Lui W, Langworthy M, Tompkins KL, et al. (2011) *Nfatc1* Coordinates Valve Endocardial Cell Lineage Development Required for Heart Valve Formation. *Circulation Research* 109: 183–192.
16. Zhou B, Wu B, Tompkins KL, Boyer KL, Grindley JC, et al. (2005) Characterization of *Nfatc1* regulation identifies an enhancer required for gene expression that is specific to pro-valve endocardial cells in the developing heart. *Development* 132: 1137–1146.
17. Kisanuki YY, Hammer RE, Miyazaki J-I, Williams SC, Richardson JA, et al. (2001) Tie2-Cre Transgenic Mice: A New Model for Endothelial Cell-Lineage Analysis in Vivo. *Developmental Biology* 230: 230–242.
18. Licht AH, Raab S, Hofmann U, Breier G (2004) Endothelium-specific Cre recombinase activity in flk-1-Cre transgenic mice. *Developmental Dynamics* 229: 312–318.

19. Hendrix M, Seftor E, Meltzer P, Gardner L, Hess A, et al. (2001) Expression and functional significance of VE-cadherin in aggressive human melanoma cells: Role in vasculogenic mimicry. *P Natl Acad Sci Usa* 98: 8018–8023.
20. Nichols J, Zevnik B, Anastassiadis K, Niwa H (1998) Formation of pluripotent stem cells in the mammalian embryo depends on the POU transcription factor Oct4. *Cell* 95: 397–391.
21. Zeineddine D, Papadimou E, Chebli K, Gineste M, Liu J, et al. (2006) Oct-3/4 Dose Dependently Regulates Specification of Embryonic Stem Cells toward a Cardiac Lineage and Early Heart Development. *Developmental Cell* 11: 535–546.
22. Kehler J, Tolkunova E, Koschorz B, Pesce M, Gentile L, et al. (2004) Oct4 is required for primordial germ cell survival. *EMBO Rep* 5: 1078–1083.
23. Chester AH, El-Hamamsy I, Butcher JT, Latif N, Bertazzo S, et al. (2014) The living aortic valve: From molecules to function. *Global Cardiology Science and Practice* 2014: 11. doi:10.1007/s11886-009-0015-y.
24. Zhou J, Bowen C, Lu G, Knapp C III, Recknagel A, et al. (2013) Cadherin-11 Expression Patterns in Heart Valves Associate with Key Functions during Embryonic Cushion Formation, Valve Maturation and Calcification. *Cells Tissues Organs* 198: 300–310. doi:10.1159/000356762.
25. Hutcheson JD, Chen J, Sewell-Loftin MK, Ryzhova LM, Fisher CI, et al. (2012) Cadherin-11 Regulates Cell–Cell Tension Necessary for Calcific Nodule Formation by Valvular Myofibroblasts. *Arteriosclerosis, Thrombosis, & Vascular Biology* 33: 1–10. doi:10.1161/ATVBAHA.112.300278/-/DCI.
26. Wirrig EE, Hinton RB, Yutzey KE (2011) Differential expression of cartilage and bone-related proteins in pediatric and adult diseased aortic valves. *Journal of Molecular and Cellular Cardiology* 50: 561–569. doi:10.1016/j.yjmcc.2010.12.005.
27. Qu X-K, Qiu X-B, Yuan F, Wang J, Zhao C-M, et al. (2014) A Novel NKX2.5 Loss-of-Function Mutation Associated With Congenital Bicuspid Aortic Valve. *The American Journal of Cardiology* 114: 1891–1895. doi:10.1016/j.amjcard.2014.09.028.
28. Perrotta I, Russo E, Camastra C, Filice G, Di Mizio G, et al. (2011) New evidence for a critical role of elastin in calcification of native heart valves:

immunohistochemical and ultrastructural study with literature review. *Histopathology* 59: 504–513. doi:10.1111/j.1365-2559.2011.03977.x.

29. Towler DA (2013) Molecular and Cellular Aspects of Calcific Aortic Valve Disease. *Circulation Research* 113: 198–208. doi:10.1161/CIRCRESAHA.113.300155.

30. Tkatchenko TV, Moreno-Rodriguez RA, Conway SJ, Molkentin JD, Markwald RR, et al. (2009) Lack of periostin leads to suppression of Notch1 signaling and calcific aortic valve disease. *Physiological Genomics* 39: 160–168. doi:10.1152/physiolgenomics.00078.2009.

31. Combs MD, Yutzey KE (2009) Heart valve development regulatory networks in development and disease. *Circulation Research* 105: 408–421.

32. Pohjolainen V, Mustonen E, Taskinen P, Näpänkangas J, Leskinen H, et al. (2012) Atherosclerosis. *Atherosclerosis* 220: 66–71. doi:10.1016/j.atherosclerosis.2011.10.003.

33. Syväranta S, Helske S, Lappalainen J, Kupari M, Kovanen PT (2012) Atherosclerosis. *Atherosclerosis* 221: 366–374. doi:10.1016/j.atherosclerosis.2011.12.034.

34. Yip CYY, Chen JH, Zhao R, Simmons CA (2009) Calcification by Valve Interstitial Cells Is Regulated by the Stiffness of the Extracellular Matrix. *Arteriosclerosis, Thrombosis, & Vascular Biology* 29: 936–942.

8.2 Conclusions

This thesis demonstrates the significance of active endothelial contribution to the early stages of aortic valve disease. The endothelium has been shown to protect valve health, but this is the first comprehensive study demonstrating robust endothelial participation in valve calcification. We have primarily examined how the cytokine TNF α drives this shift in phenotype from protective to aggressive. We have elucidated two novel roles for TNF α in driving endothelial dysfunction: via dysregulation of oxidative stress and via stimulation of an endothelial to mesenchymal transformation (EndMT) (Figure 8.16). Endothelial oxidative stress drives whole-valve degeneration (chapter 2) via eNOS uncoupling and elevation of superoxide. Endothelial cells that undergo EndMT have a pro-disease phenotype, matrix remodeling capabilities, and participate in calcification (chapters 3-4). We have demonstrated that NF κ B is necessary and sufficient for EndMT and that it controls both endothelial and interstitial cell participation in valve disease (chapter 5). We have also demonstrated important roles for reprogramming factor Oct4 and VIC contractility in degeneration of the aortic valve (chapter 6-7). Overall, this work represents a significant step forward in the understanding of what initiates and drives aortic valve calcification, especially enlightening the active role of valve endothelial cells.

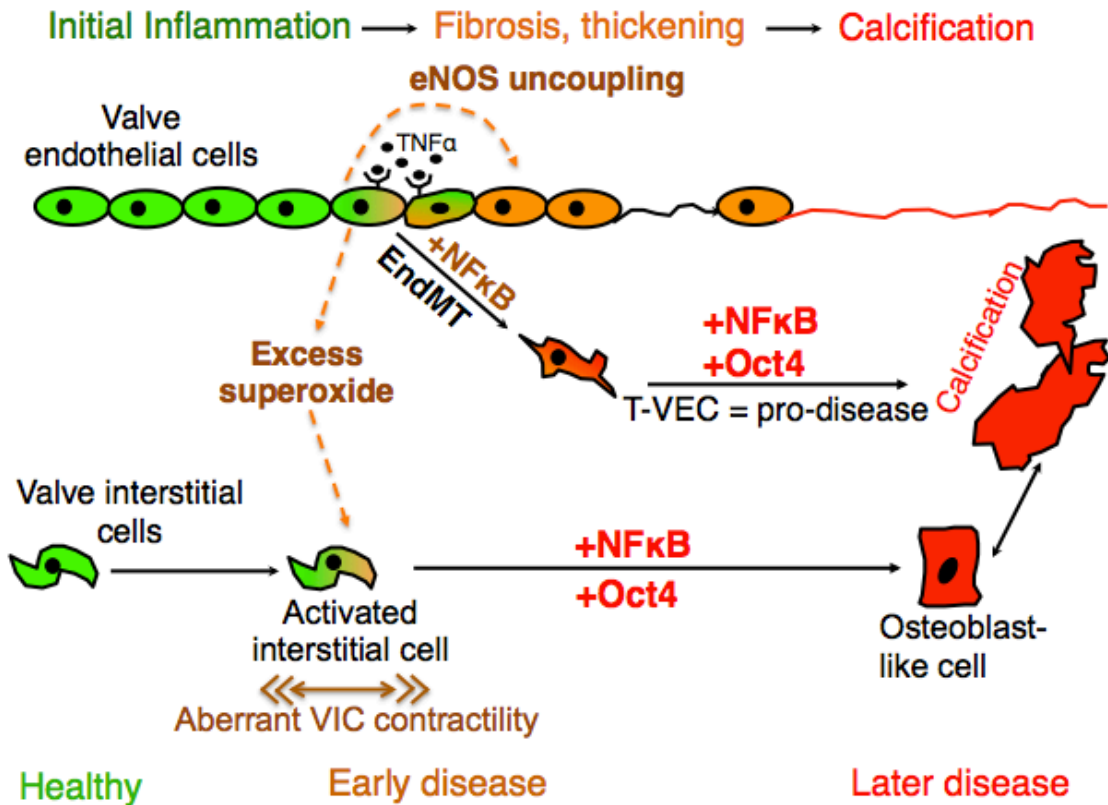


Figure 8.16. Conclusion of findings contained in this thesis.

In this thesis, we present findings that show the source and significance of endothelial oxidative stress (chapter 2), a role for EndMT (chapter 3 and 4), the governing influence of NFκB (chapter 5), reprogramming effects of Oct4 (chapter 6), and characterization of changes in interstitial cell contractility during disease (chapter 7).

CHAPTER 9

LEARNING SPATIAL VISUALIZATION: BEYOND DRILLS AND INTO EARLY MASTERY

This chapter was published as a conference proceeding, for the European Society for
Engineering Education:

E. Farrar, O.O. Adebayo, T. J. McCray, R. Evans, and T. Nathans-Kelly, “Learning
Spatial Visualization: Beyond Drills and Into Early Mastery.” SEFI 2014.

9.1 Abstract

Students entering university-level engineering programs must be adept at spatial visualization and reasoning. To raise performance in first-year students who tested poorly on spatial visualization skills, the Cornell University Engineering Success program used the National Science Foundation's ENGAGE curriculum to introduce spatial visualization basics. Results were strong, with an overall 13% improvement in tested skills. However, our aims were more ambitious. Our team believed that authentic skills application could provide deeper learning, applicable toward school and engineering work. Student teams worked with biomedical researchers who asked for professional-level visualizations. We employed an action-research methodology (observations, journals, expert responses, and e-portfolios), tracking their acquisition of spatial concepts, representations, and critical stances. Students evidenced knowledge through their innovative use of support technologies to create insightful visualizations of complex engineering data and reliably model biomedical mechanisms relevant to human disease. They also demonstrated critical stances by utilizing appropriate, specific and relevant spatial visualization skills to most effectively communicate each engineering concept. Through peer evaluations, students were also able to identify and critique the use of specific spatial skills by other student teams during project presentations. In this work, we describe our innovative project-based approach to teaching spatial visualization and we will suggest how this approach could inform the transformation of "drill-and-demonstrate" approaches, serving a model for similar courses at other institutions.

9.2 Introduction

In the College of Engineering at Cornell University, the goal of the Office of Diversity Programs in Engineering (DPE) is to support students, especially those from backgrounds traditionally underrepresented in engineering, and to provide the programming necessary to assist them in being successful. Consequently, we created a new spatial visualization course, entitled Spatial Visualization/Thinking for Engineers. This course was one of three interventions outlined in a grant awarded by the National Science Foundation (NSF) and the Science, Technology, Engineering, and Mathematics Talent Expansion Program (STEP) (award: DUE #1317501).

During our course preparation and development, we noticed that the range of definitions for “spatial visualization” (SV) is wide and varied. Perhaps the simplest definition is “the ability to mentally manipulate, rotate, twist, or invert pictorially presented stimuli” [1]. Others define it as “the ability to manipulate complex spatial information when several stages are needed to produce the correct solution” [2]. The first definition represents spatial visualization as a kind of mental exercise; the second as a response to a particular problem or project. Other schools of thought refer to “spatial ability” or “representing, transforming, generating and recalling symbolic, nonlinguistic information” [3], and that relation to “spatial thinking” or “a constructive amalgam of three elements: concepts of space, tools of representation and processes of reasoning” [4]. These different terms are often used interchangeably,

For the purposes of this paper, our team defines SV skills more generally as *spatial intelligence*, a term that contains for us the ideas of spatial visualization and spatial perception, including the activities of mental rotation of objects, spatial relation between objects, and overall spatial orientation [5]. As with mastery of any set of complex skills, doing one type of activity repeatedly does not develop that mastery; instead, a variety of sub-tasks or related tasks will move practitioners towards mastery [5].

Three groupings of research have emerged regarding the development of SV skills in students. First, some studies record group differences, often related to gender; these studies document findings related to particular kinds of SV skills, e.g., 3D mental rotations. The strongest explanation for these differences is dissimilar socialization processes [3, 4, 5]. Second, other findings report that it is possible to reduce or even eliminate these differences through direct instruction [6, 7, 8, 9]. Third, reducing or eliminating these differences or simply enhancing SV skills generally seems to be predictive of student success, typically defined as retention in the STEM fields [6, 8, 10, 11]. There is an important caveat related to the third of these understandings. We did not find in the literature empirical evidence or investigations that describe how students actually use or apply their newly-won SV skills in authentic engineering projects or to solve real engineering problems. While there may be some suggestive correlations that SV skills vary according to socialization, and that these variances can be reduced or eliminated, there is little if any evidence of what that “success” actually entails other than retention at the academic organization.

It was with all three of these understandings and this final important caveat in mind that the Engineering Communications Program (ECP), DPE, the Cornell University Engineering Success (CUES) program, and two Ph.D. graduate students from Biomedical Engineering designed and implemented an innovative active-learning, project-based course to teach Under Represented Minority (URM) and First Generation at College (FGC) students SV skills. Along with improving their SV skills, we were equally (actually more) interested in developing their spatial intelligence as applied to authentic engineering projects.

9.3 Course description and research methodologies

The cohort of students involved in this first iteration of our SV course were pre-registered based on their invitation to and voluntary enrollment in the Robert L. Ryan Scholars Program (first-year students who have demonstrated potential despite a variety of educational risk factors). These factors include low resourced high school, low socioeconomic status (SES), FGC student, English as a second language, single parent household, and limited access to rigorous advanced placement math and science coursework. In the fall semester, all of the Ryan Scholars (31 students) were pre-registered for the spatial visualization course regardless of their score on the Purdue Spatial Visualization Test (PSVT).

Our SV course was taught weekly for 14 weeks in the fall semester of 2013 at Cornell University. Following the NSF ENGAGE curriculum [13], the first six lectures instilled SV skills, including rotations, reflections, flat-patterns, cutting planes, combining objects, and isometric/orthographic sketching. We used the PSVT to conduct pre- and post-testing of spatial visualization tasks. The pre-test was administered prior to the beginning of the course; the post-test was administered in week 6. Then, the course's second phase consisted of team projects, each with a *client* from Cornell biomedical engineering faculty. Instructors had worked prior to the course with those faculty to frame a visualization request that would extend students' SV skills using the faculty's own cutting-edge engineering research data. These projects were to challenge the students' ability to understand, manipulate, and communicate complex SV concepts by requiring them to create clear and accurate

visuals. Final deliverables to faculty included formal team presentations where they were evaluated by their peers, the instructors, and the faculty clients.

As we developed the course, we became very aware of how the term *project-based learning* (PjBL) was typically used and that it held a decidedly different meaning than problem-based learning (PBL), which often includes project-based learning within its framework. Both are, like spatial intelligence, complex: they provide a focus for intellectual inquiry; they eschew a tidy problem statement or any predetermined outcome; they encourage application of knowledge rather than rote learning; they rely on student action and critical thinking; functioning in teams; they encourage hands-on work; and they facilitate learning guided by faculty serving as mentors or guides [14-22].

From the start, we deployed PjBL purposefully, incorporating faculty clients who provided the projects for student teams. Our reasoning and research lead us to believe that having a concrete deliverable was a powerful tool for student engagement at a deep learning level. As such, we purposefully included client meetings and assessment as 2.5% and 5% of the final grade, respectively. We understood well that, while PBL may have some expected or predictable outcomes, PjBLs have no such comforts. Client interaction can bring new and fresh constraints, freedoms, or regulating factors on a team's project. The instructor often will not be able to anticipate a client simply saying "I don't like this team's approach at all," or "Can you do this all again, but this time aim for an audience of 8th graders?" In a sense, the instructors deploying PjBL have to be as agile (or more so) than the student teams working with the client. As

PjBL work often does not have a pre-determined outcome or deliverable, clients can (and did) frame the deliverable with their teams variously. Projects were contingent on the client's specific need, and the projects were "real" and "authentic" because the deliverables/artifacts were going to be put into immediate use for biomedical engineering research purposes, in our case. The deliverables were to be a technical report (for academic assessment), a formal presentation where all clients and other stakeholders were present (assessed by clients and instructors alike), and the delivery of the client's requested artifact (poster, demo model, visual, etc.). The artifact needed to meet the specific stated needs of the client (which may differ from the expectations of the instructors) while also meeting the requirements of the academic unit.

We believed that this project-based course design would not only teach students SV skills, but empower them to apply these skills in real engineering contexts, thus enhancing and deepening their knowledge of spatial visualization. Furthermore, we believed that such early application of spatial visualization skills would provide relevant practice for engineering students for future school and engineering work. In addition, immediate examination of the process of applying spatial visualization skills to engineering project work would enable us to understand if and how SV skills specifically and spatial intelligence more generally enhances success in engineering.

In order to study students' development or what "success" might actually entail, we employed two research methodologies. The first was an action research methodology, intentionally creating a new course design that went beyond drill-and-demonstrate. We

wanted to deploy active-learning with a project-based pedagogy. We adhered to the standard approach for such action research, i.e., plan, act, observe, and reflect, collecting both quantitative and qualitative in nature. Inputs included PSVT pre- and post-test results, in-class instructor observations, journals, expert feedback on project results, student progress reports, project evaluations, and e-portfolios. We then used our second research methodology, “grounded theory” to code and analyze the data. Combining these two methodologies enabled us to track and learn about students’ acquisition of SV skills, the development of spatial intelligence, their application of those skills, and their ability to critically evaluate their own and others’ use of spatial intelligence.

9.4 Results

Students showed enhanced spatial visualization knowledge after ENGAGE lectures

As noted above, the PSVT was twice administered. Students showed overall improvement after attending the prescribed six one-hour lectures. The mean score increased by 13% in the post-test as compared to the pre-test mean score of 75% (student's t-test, $p < 0.05$). Furthermore, the spread in scores decreased, from a range of 35-100% on the pre-test to a range of 53-100% on the post-test, with 26 out of 31 students scoring higher on the post-test than the pre-test, two students with no change, and three students with a 1-question reduction in score.

Phase 1 of SV Project-Based Learning: Bridging the gap between SV skills and the engineering project

In partnership with Cornell Biomedical Engineering faculty, the graduate student instructors designed four eight-week projects that would deploy student SV skills in a meaningful engineering context. Each faculty "client" provided a set of images and/or data from his or her laboratory's research where a visualization was needed. Clients framed the basics: the information to be communicated via the visual, the target audience, and the nature of the final product (2-D, 3-D, animated, or unspecified). Here, we will present one client project, "Nuclear Squeeze," to show the stages of student team work

"Nuclear Squeeze" was completed for Dr. Jan Lammerding, whose lab studies the mechanical properties of cell nuclei and how those properties are modified in diseased

cells. . The Lammerding lab uses high-resolution confocal microscopy, a custom-nanofabricated cellular-level “obstacle course,” and fluorescently labeled cells to take images of single cells passing through a constriction, which allows them to observe and quantify the forces that cause a cell’s nucleus to deform. Dr. Lammerding requested a visual of the three-dimensional cell moving and changing shape over time, as it progressed through the obstacle course. The visual must explain to a layperson the movement of the cell and to answer one question, “Does the cell’s nucleus change in *volume* as it moves through the obstacle course?”

Nuclear Squeeze project teams were given a set of two-dimensional, multi-channel confocal microscopy images of the cell in the obstacle course with three distinct components: images of the cell body (green), images of the cell nucleus (blue), and images of the obstacle course (gray) (Figure 9.1A). The images were taken in “stacks” that could be compiled to create a 3-D picture of the cell (Figure 9.1B). These stacks were collected at regular intervals to create a full data set describing the 3-D cell’s movement in time (Figure 9.1C).

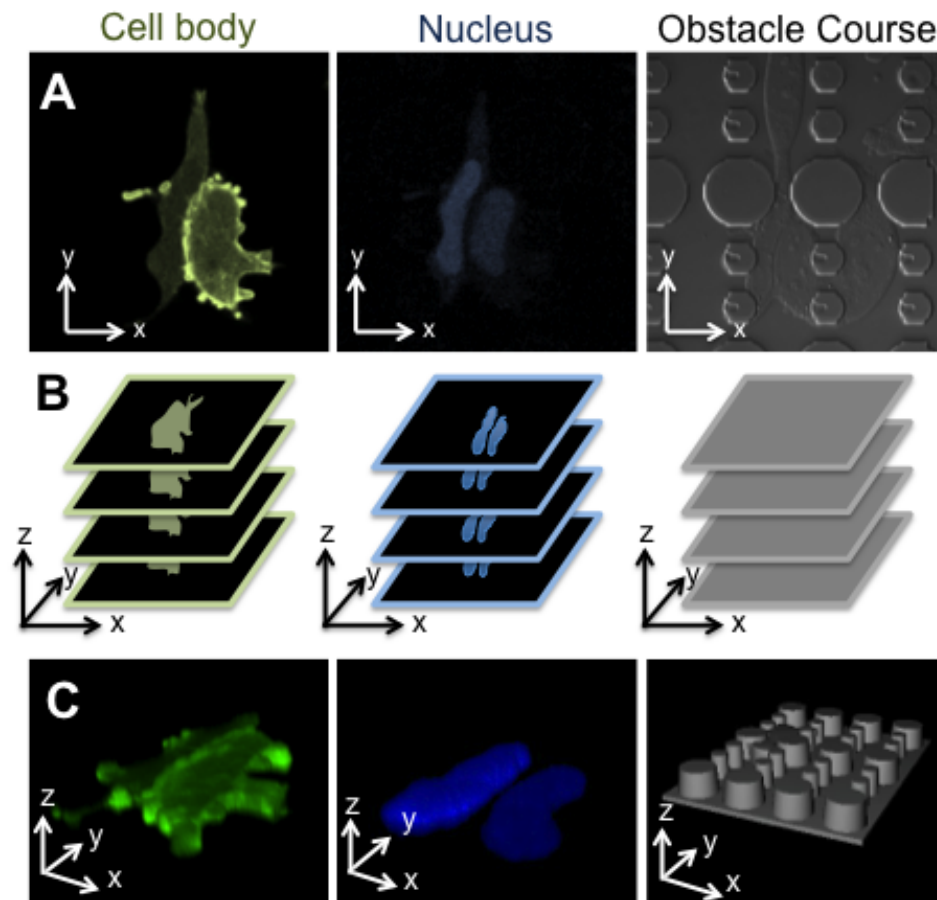


Figure 9.1 SV Project “Nuclear Squeeze” data from faculty client.

A. “Top-view” confocal microscopy images were taken of cells moving through a nano-fabricated obstacle course (green: cell body, blue: cell nucleus, gray: obstacle course). B. Sets of images had to be compiled by students into vertical “stacks” of 2-D images that could be rendered into 3-D by using image analysis software. C. These are 3-D renderings of image stacks, visualizing cell body, cell nucleus, and obstacle course.

To facilitate cognitive connections between lectures and the client project, instructors created a worksheet for each project that connected students' SV skills to the client requests (see Figure 9.2). These activities connected the SV skills learned in the course to the Nuclear Squeeze project, initiating students' application of spatial intelligence/reasoning.

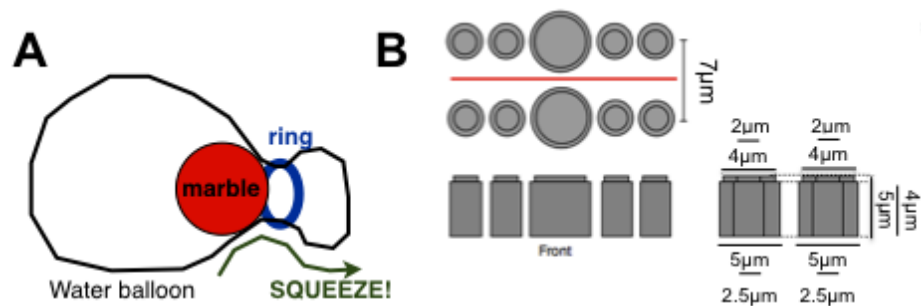


Figure 9.2 Partial worksheet for the Nuclear Squeeze project.

Worksheet was designed by instructors to bridge the gap between SV lectures and projects. A. Analogy of cell moving through an obstacle course to a water balloon with a marble inside being passed through a ring. B. Orthographic projections of the “obstacle course” used by the Lammerding lab to apply forces to cells. Students had to create isometric drawings of the system and identify axes of symmetry.

An early launch in the fifth week of the course included teams receiving their client's request and preparing for an initial client meeting. Teams created lists of three clarifying and/or extending questions for clients. During this client meeting, students and clients alike gained their footing:

- Student: *What do you think you could get out of looking at this in 3D?*
- Client: *Let me turn that back to you...Do you gain much by looking at this data in 3-D? Or do you not really gain much by doing this in 3-D versus using the best plane in 2-D?*

Such interactions reveal the hesitancy of students to claim SV proficiencies. Still, they lacked the confidence to deploy their SV skills in a real-world context. Thus, clients

played an important role in maintaining the status of the students as SV consultants, by encouraging the students to act as SV experts.

Phase 2 of SV Project-Based Learning: Students iteratively apply SV knowledge to complete project tasks.

Student teams progressed through three general stages of project work (Figure 9.3), as documented inside their e-portfolios and teacher interactions. First, students strove to understand the data set given to them by their client. Second, students iteratively applied SV skills and technology to develop an appropriate visual. Third, students revealed that visual to their clients and others.

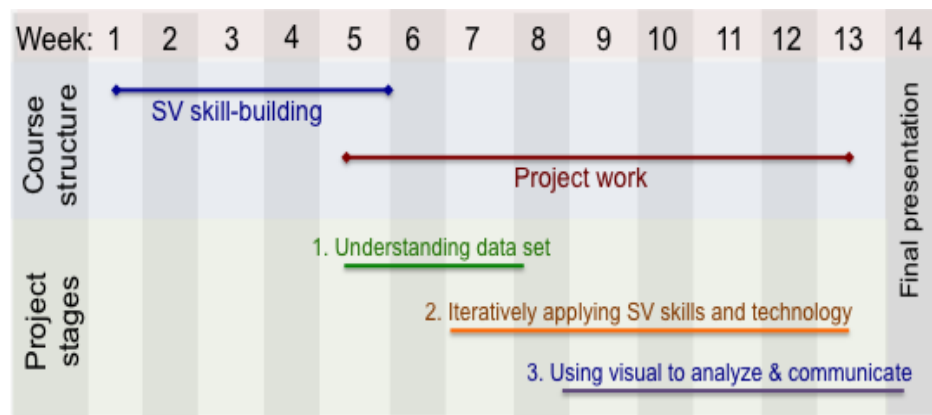


Figure 9.3 Structure and components of spatial visualization course.

Skill-building and project-based structure of the course over 14 weeks of instruction (upper).
Project work proceeded in three overlapping stages (lower).

In Stage One, students attempted to grasp the client's data and to create a thorough understanding of the problem at hand. This stage was characterized by student e-portfolio entries such as these:

- *[I] Was unfamiliar with the structure of a cell, so I researched info online.*
- *By attending the client meeting, now I know what the main goal of the project is as well as a more concrete idea of what to do. [sic]*

Stage Two could happen only once they understood the context of their data set. Then, they iteratively applied SV skills to begin creating visuals. The instructors encouraged and mentored the use of technology, including MATLAB®, ImageJ®, SolidWorks®, and PowerPoint®. Students then connected SV lecture content to real-world applications. For example, students described challenges they overcame in using SV within the image processing software, ImageJ:

- *Had problems with orthogontal [sic] views in ImageJ. Solved it by changing resolution of image.*
- *Played with imageJ and figured out how to do an animated 3d gif. Also made orthographic images of our data. [sic]*

Armed with their developing language and skills, students easily manipulated SV technologies to create 3-D models, 2-D representations, cutting planes, and isometric views of the concepts integral to their client's project. For instance, it was only after the Nuclear Squeeze team had created an isometric view of the images that students began to truly understand the challenge of quantifying a 3-D quantity such as *volume* from a set of 2-D images. Such understanding arose from the authentic SV interaction.

In Stage Three, analysis and communication, students cycled between visual creation, visual analysis, and visual communication, with clarity as the goal. For example, the Nuclear Squeeze students created a beautiful isometric 3-D rendering of the cell moving through the obstacle course over time. However, they found that the isometric view of the whole cell was not sufficient in answering their client's question: "Does the nucleus change in volume over time?" The team revised the visual to answer the question, eventually deciding to employ multiple orthographic views. They wrote:

-- [We] Calculated an estimated volume of cell based on pixel area of top and side view pictures... Figuring out how to find pixel area of irregular shape in photoshop. Found out through online researching. (emphasis added)

Finally, this group used a subset of their different visuals to communicate details of the data set, their approach, and their conclusion. Students made a 3-D CAD of the cell within the obstacle course to facilitate their own understanding and to print a hand-held replica of the obstacle course for their final presentation (Figure 9.4A). They also used multiple image-rendering functionalities within ImageJ to visualize and assess the data set, including a surface plot of the cell's shape (Figure 9.4B). Furthermore, the students presented the orthographic views (top and side) of the cell at different time points of its migration through the obstacle course to communicate to their audience how they calculated change in nuclear volume (Figure 9.4C).

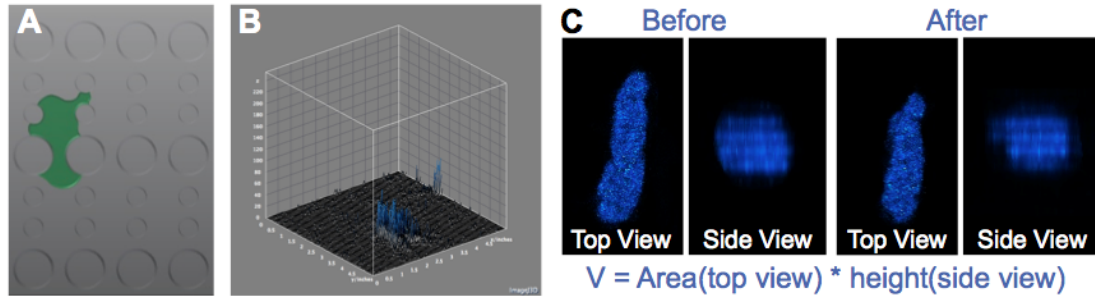


Figure 9.4 Visuals created by students working on the Nuclear Squeeze project.

A. CAD drawings of the cell (green) within the obstacle course (gray). B. Surface plot of the cell nucleus (blue). C. Orthographic projections of the cell nucleus viewed from the top and side, with volume calculations.

Phase 3 of SV Project-Based Learning: Students act as SV experts, examining and critiquing use of SV in the final projects

Throughout the project, students were able to use their mastery of SV to critically evaluate their own use of visuals in representing and evaluating an engineering concept, documenting progress in e-portfolios. Students commented:

-- I tried to observe a change in the nucleus by overlaying 3 channels of images, but realized it was too cluttered.

-- [The challenge is] deciding which software would be best suited to our desired task and whether our approach to using the software will be viable throughout all stages of the project. The way to solve this is to keep experimenting.

Their demonstrated insight into the effectiveness of different visualization strategies points to translation of SV skills learned in lecture to the ability to create, interpret, assess, evaluate, and improve visuals of their own creation in real-world engineering contexts.

The course culminated with a formal presentation for peers, instructors, and faculty clients. At the same, students evaluated their peers' projects, specifically for SV prowess (Figure 9.5). Students identified use of simulations" as praise-worthy SV, indicating that the videos or animations used by their peers facilitated understanding. Students also praised "scaling" to zoom in or out on a feature and the use of vectors to indicate direction, among others. The ability of students to not only use, but to identify and critique the use of these complex strategies in others, is evidence of their ability to deploy SV skills successfully and act as subject matter experts in the use of SV in real-world engineering contexts.

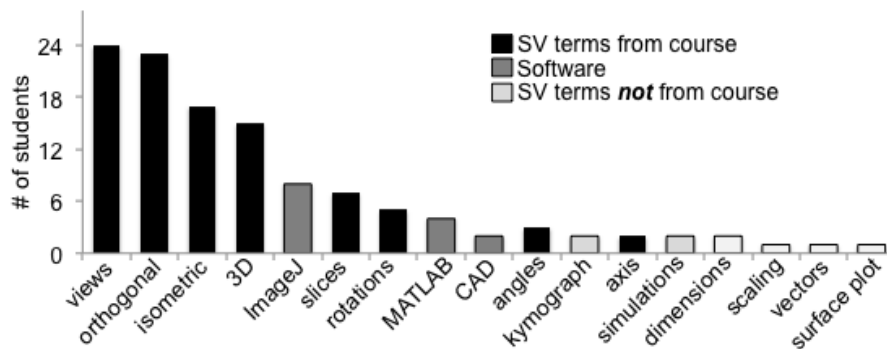


Figure 9.5 Frequency of student use of different terms in peer evaluation of SV projects.

Note the range of terms not specifically taught but gained.

9.5 Discussion

This spatial visualization course went beyond drill-and-demonstrate methods. Faced with complex research-based data sets, they deployed knowledge of SV to understand the data, examine it, manipulate it and communicate it. Students not only gained basic spatial skills, but they were then able to use those skills successfully and authentically. Unlike many first-year courses, this course did not simply assume students were novices, but instead afforded them with an opportunity to become early experts.

Faculty clients were at the core of the course's success, critically examining and assessing students' ability. An innovation in this course is the direct interaction between first-year students and with high-level engineering researchers (all too rare). This course enabled and encouraged first-year students to work directly with faculty and the community of practice. Faculty provided feedback throughout the course and students gained confidence in their abilities to understand and in turn, engage in intellectual dialogues about current research projects. As a result, students were exposed to engineering beyond the usual first-year mathematics and science courses, and this exposure deepened their interest in engineering, as students sought to learn more and communicated frequently with their faculty clients.

Using e-portfolios, students were encouraged to self-reflect on their progress and challenges throughout the duration of the course. This generative knowledge began to build a mastery of spatial techniques, thus enhancing spatial intelligence. Indeed we might argue that in a preliminary way the above results represent important empirical

evidence concerning what spatial intelligence actually involves. Through the acquisition of generative knowledge, students were not only able to understand the data presented to them, but were able to manipulate it, synthesize information and critically examine their use of learned skills in communicating the data. E-portfolio provided instructors with a direct lens to not only examine student progress and challenges, but to also understand the process by which students acquired generative knowledge in the course.

Unlike typical first-year classes, this course empowered spatial mastery through the use of several innovative methods. First, this course went beyond the usual drill-and-demonstrate method by implementing the application of visual skills in current engineering projects. Furthermore, students were not only assumed to be proficient at SV, but they were treated as experienced consultants in their interactions with current engineering faculty clients. Engagement with faculty in discussions about current research built student confidence and deepened the knowledge of engineering and its applications. Throughout the course, students were also able to acquire generative knowledge through self-reflection and the use of E-portfolios, further building a mastery of spatial skills and enhanced spatial intelligence.

Acknowledgements

Our team thanks NSF (award: DUE #1317501), and its continued support through its ENGAGE programs. As well, we thank Dr. Jan Lammerding and Greg Fedorchek for assisting with the “Nuclear Squeeze” project, Cornell University and the Office of Diversity Programs in Engineering.

REFERENCES

1. McGee MG. (1979) Human spatial abilities: Psychometric studies and environmental, genetic, hormonal, and neurological influences. *Psychological Bulletin* 86: 889-918.
2. Voyer D, Voyer S, and Bryden MP. (1995) Magnitude of sex differences in spatial abilities: A meta-analysis and consideration of critical variables. *Psychological Bulletin* 117: 250-270.
3. Linn MC and Petersen AC. (1985) Emergence and characterization of gender differences in spatial abilities: A meta-analysis. *Child Development* 56: 1479-1498, 1985.
4. National Research Council (2006) *Learning to think spatially*. Washington, D.C.: The National Academies Press.
5. Lieu D and Sorby SA. (2009) *The fundamentals of visualization, modeling, and graphics for engineering design*. Delmar, Cengage Learning, Clifton Park, NY.
6. Sorby SA and Baartmans BJ. (2000) The development and assessment of a course for 3-D spatial visualization skills of first year engineering students. *Journal of Engineering Education* 89: 301-307.
7. Martin-Dorta N, Saorin JL, and Contero M. (2008) Development of a fast remedial course to improve the spatial abilities of engineering students. *Journal of Engineering Education* 97:505-513.
8. Sorby SA. (2009) Educational research in developing 3-D spatial skills for engineering students. *International Journal of Science Education* 31: 459-480.
9. Newcombe NS and Stieff M. (2011) Six Myths about Spatial Thinking. *International Journal of Science Education* 34: 955-971.
10. His S, Linn MC and Bell JE. (1997) The role of spatial reasoning in engineering and the design of spatial instruction. *Journal of Engineering Education* 86: 151-158.

11. Sorby SA. (1999) Developing 3-D spatial visualization skills. *Engineering Design Graphics Journal* 63: 21-32.
12. Strong S and Smith R. (2001) Spatial visualization: Fundamentals and trends in engineering graphics. *Journal of Industrial Technology* 18: 1-6.
13. ENGAGE Learning, National Science Foundation. Retrieved from <http://www.engageengineering.org/>, 2014.
14. Donnelly R and Fitzmaurice M. (2005) Collaborative project-based learning and problem-based learning in higher education: A consideration of tutor and student roles in learner-focused strategies. *Emerging Issues in the Practice of University Learning and Teaching*: 87-98.
15. Savery JR (2006) Overview of problem-based learning; Definitions and Distinctions. *The Interdisciplinary J of Problem-based Learning* 1: 9-20.
16. Zastavker YV, Ong M, and Page L. (2006) Women in Engineering: Exploring the effects of project-based learning in a first-year undergraduate engineering program. 36th ASEE/IEEE Frontiers in Education Conference, session S3G-1.
17. Swan CW, Paterson KG, and Bielefeldt AR. (2009) Measuring the impacts of project-based service learning in engineering education. 39th ASEE/IEEE Frontiers in Education Conference, session M3B-1.
18. Barge S, Principles of Problem and Project Based Learning: The Aalborg PBL Model (Aalborg University), <http://www.en.aau.dk/>.
19. Bedard D, Lison C, Dalle D, Cote D, and Boutin N. (2012) Problem-based and project-based learning in engineering and medicine: Determinants of students' engagement and persistence. *Interdisciplinary J of Problem-based Learning* 6: 7-30.
20. Pleiss G, Perry M, Zastavker YV (2012) Student self-efficacy in introductory project-based learning courses. 2012 Frontiers in Education Conference, pp. 1-6.
21. Galand B, Frenay M, and Raucant B. (2012) Effectiveness of problem-based learning in engineering education: A comparative study on three levels of knowledge structure. *International J of Engineering Education* 28: 939-947.

22. Tseng KH, Chang CC, Lou SJ, Chen WP. (2013) Attitudes towards science technology, engineering, and mathematics (STEM) in a project-based learning (PjBL) environment. *Int J Technol Des Edu* 23: 87-102.

CHAPTER 10

VALVULAR HEART DISEASES IN THE DEVELOPING WORLD: DEVELOPMENTAL BIOLOGY TAKES CENTER STAGE

This chapter was published in the *Journal of Heart Valve Disease*:

Farrar EJ and Butcher JT. Valvular Heart Disease in the Developing World:

Developmental Biology Takes Center Stage. *J Heart Valve Disease*;2012(2):234-40.

10.1 Abstract

Heart valve disease is a significant and increasing global problem. In the developing world, the primary sufferers are children and young adults, the critical engine of future economic growth. Up to 10 times the current number of known sufferers are undiagnosed in these countries. Among the most prevalent and neglected diseases are rheumatic heart disease and endomyocardial fibrosis. The etiologies of these diseases can be described in part as a dysregulation or reactivation of developmental biology pathways. Connecting mechanisms of valvulogenesis and disease etiology may therefore be an excellent strategy to identify therapeutic targets. These local diseases require local solutions tailored to local resources. Collaboration with experienced researchers should be an encouraged way forward to accelerate knowledge creation and clinical translation.

10.2 Introduction

Cardiovascular disease (CVD) is the leading killer worldwide. 80% of all CVD cases occur in developing countries [1], causing more than 19% of deaths –more than war and malaria combined [2]. These rates are compounded by a lack of progress in applicable therapies because the cardiovascular needs of developing countries are inherently different from the degenerative pathologies of the Western world. Non-ischemic diseases characterized by fibrosis and inflammation that affect young people are of serious concern in impoverished regions such as sub-Saharan Africa, requiring different treatment strategies than those that are effective in the ischemic afflictions of the elderly common in the developed world [3].

The pathological disparity arises from causal factors linked to economic conditions such as poor hygiene, inadequate nutrition, and lack of proper health care [3]. Without medical intervention, relatively benign childhood diseases quickly become degenerative, compounded by the effects of hunger and harsh environmental conditions on immune response. In consequence, CVD manifests at a much earlier age, creating a demographic in which young adults and children are the predominantly affected populations rather than the elderly [3-7]. This troubling trend has serious consequences for countries still progressing towards economic stability because it directly undermines both the foundational workforce and the ability of these societies to progress technologically and socially.

Two of the most prevalent CVDs in the young people of sub-Saharan Africa are endomyocardial fibrosis (EMF) and rheumatic heart disease (RHD) [8]. However, these pathologies represent an enormous burden of disease that is generally overlooked in the research priorities of developed nations; for example, less than 0.4% of global funding is allocated to rheumatic fever research despite the 68 million people currently affected by this disease [6,9-11]. Charitable initiatives for global health often skip over RHD, perhaps because of its non-infectious epidemiology, in their mission to eradicate infectious diseases such as malaria and HIV. Nor is it confronted in developed nations, which have succeeded in diminishing its influence through improved hygiene and access to antibiotics in the initial febrile stages. However, as long as poor sanitation and limited health care dominate the conditions of the third world, designing a therapeutic approach to diseases such as RHD that is amenable to the resources and environment of developing countries should be paramount.

The purpose of this review is to summarize the state of EMF and RHD in sub-Saharan Africa and to conclude with a discussion of future avenues for advancing both understanding and clinical effectiveness in treating these neglected diseases.

10.3 Rheumatic Heart Disease

There are more than 68 million existing cases of RHD, causing 1.4 million deaths each year [12-15]. Case studies throughout Africa suggest that the majority of the disease burden is carried by children in developing countries, especially those in Sub-Saharan Africa (Figure 10.1).

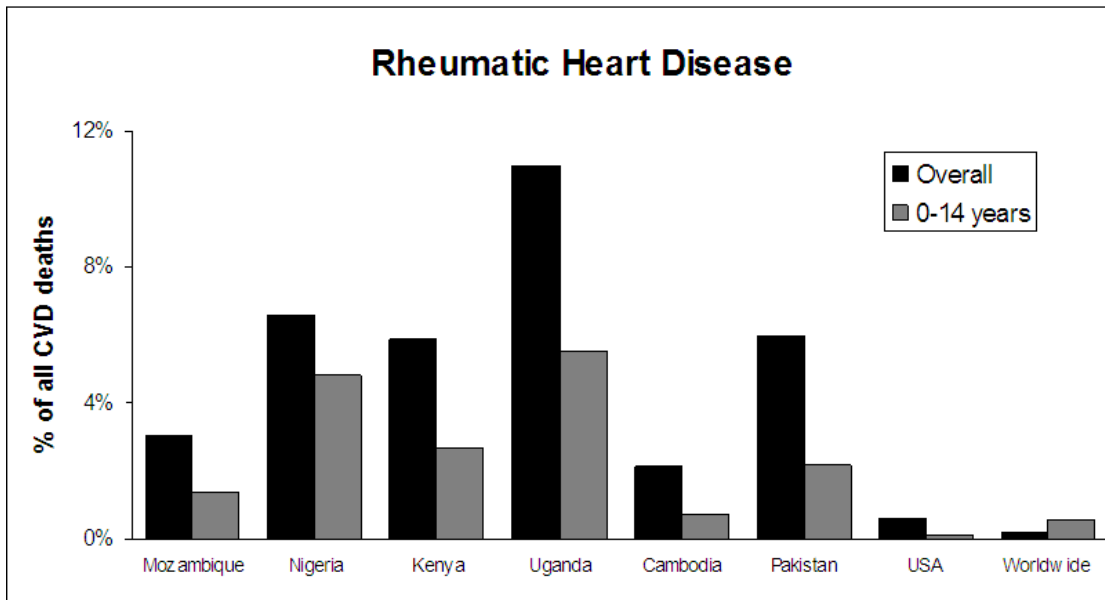


Figure 10.11 Mortality due to RHD in developing countries compared to Western nations.

The majority of sufferers in these countries are less than 15 years old [16-22].

According to the American Heart Association, in most of the developing world RHD is the single largest cause of hospital admissions for children and young adults [23]. RHD arises from untreated complications of rheumatic fever (RF), associated with group-A streptococcal pharyngitis in children [11,23]. It is thought that antibodies against the initial infection cross-react with proteins in the heart creating an autoimmune reaction, which propagates inflammation and self-destruction of the

valves and myocardium [24] [24]. Nine to thirty-nine percent of patients who contract acute rheumatic fever develop associated valve deficiency two to ten years after the initial febrile episode, creating a bimodal age distribution with peaks in late childhood and early adulthood. Twenty percent of patients with RHD will die before the age of five, and eighty percent before they reach 25 years old [25]. One of the most common manifestations of RHD is valve deformity, occurring in twenty-five to forty percent of chronic RHD patients [5,26] (Figure 10.2). Currently, the most common treatment for advanced stages of RHD is valve replacement, but both mechanical and bioprosthetic valves fail prematurely in these patients due to their young age and limited ability to access and manage anti-coagulation treatments [29,30]. The expense of replacement valves and long-term pharmaceutical strategies suggest that the methods now used to confront RHD valvular degeneration, imported from the first world, should be reconsidered within the African context.

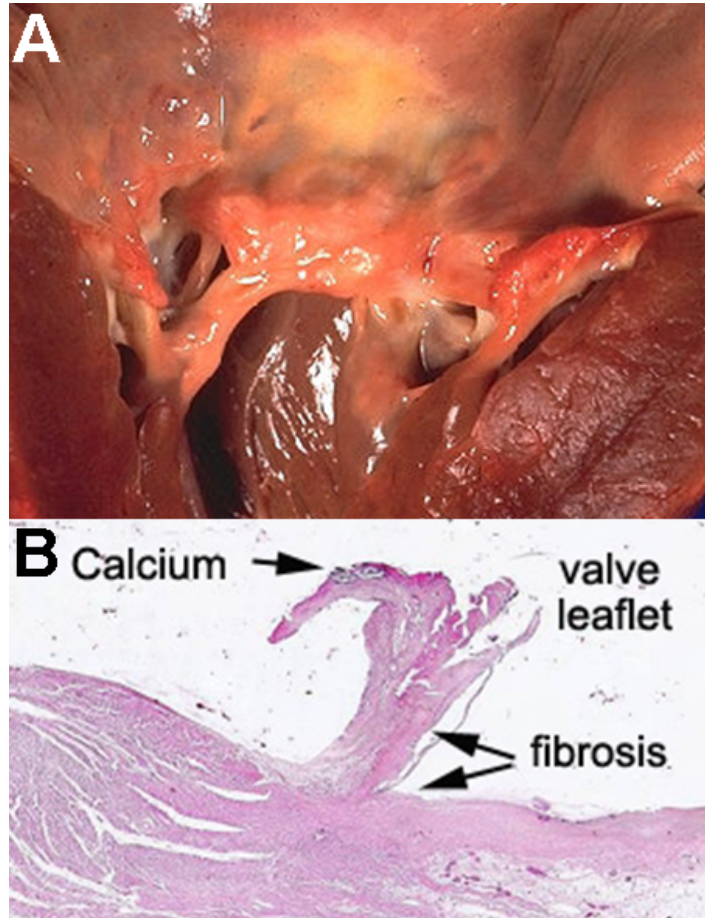


Figure 10.2 Valve deformity in rheumatic heart disease.

- A) A rheumatic mitral valve showing severe thickening of the leaflet and chordae tendoneae [27]. B) Hematoxylin and Eosin staining of a rheumatic mitral valve leaflet showing calcification, fibrosis, and leaflet thickening [28].

10.4 Endomyocardial Fibrosis

In the equatorial region of Africa, endomyocardial fibrosis has been found to be the second most frequent cause of acquired cardiovascular disease in young adults and children [16]. Recent studies have also found that EMF accounts for about twenty percent of all heart failure deaths in Uganda and Mozambique [7,16,31,32], with similar results from hospital-based studies in ten other African countries [3]. EMF is a restrictive cardiomyopathy generally characterized as a disorder of the tropical regions of the world. It is thought to begin as an initial feverish illness that is usually not of a severity to warrant medical presentation, especially in light of the high cost and inaccessibility of health care in developing countries. A latent phase follows, in which the fever subsides and there are no symptoms over a period of two to ten years. The disease asymptotically advances, leading to degeneration of the heart as ventricular and endocardial thrombi accumulate and impede the normal function of the valves. Concurrently, unknown mechanisms cause the tissues of the heart to remodel, forming fibrous scars, which further impede the ability of the heart to supply the body with adequate blood flow [33] (Figure 10.3).

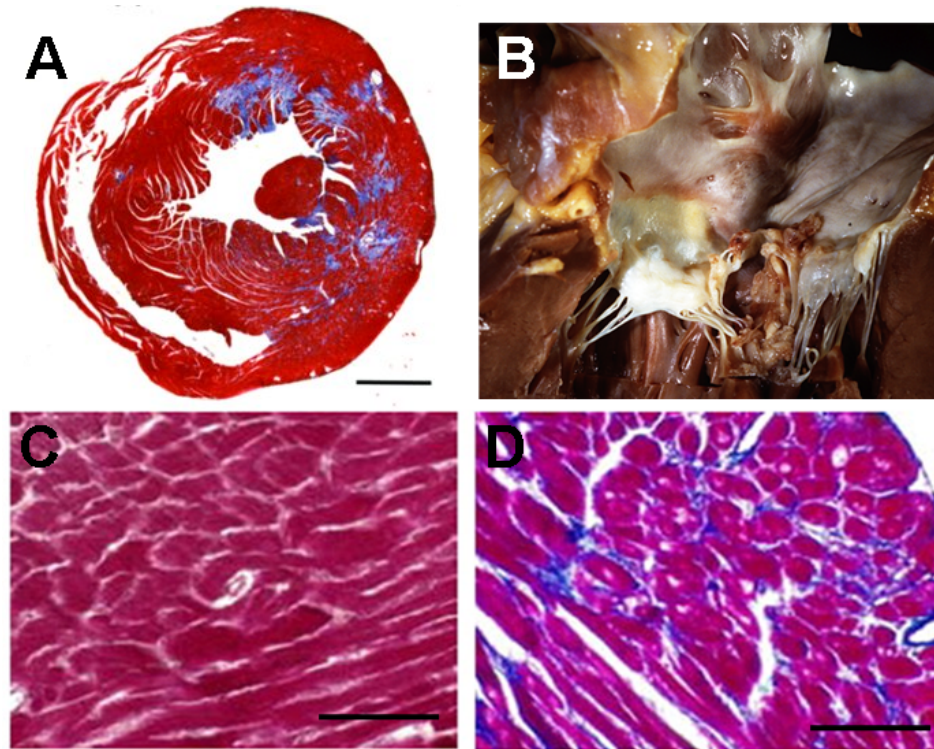


Figure 10.3 Pathology of endomyocardial fibrosis.

(A) A fibrosed mouse heart, in which Masson's trichrome staining illustrates excessive collagen fiber deposition (Bar = 1mm) [34]. (B) Regions of fibrosis accumulate on the myocardium, often mingling with the valve leaflets and chordae [35]. Masson's trichrome staining of normal (C) and fibrotic (D) myocardium reveals increased collagen deposition (blue) and fiber disorganization in diseased regions (Bar = 200 um) [36].

Despite the high incidence, little is known about the mechanisms or pathology of EMF. Most patients do not present until the onset of the severe symptoms caused by increasing fibrosis and inadequate blood flow such as venous hypertension, valvular stenosis, thromboembolism or arrhythmia [37]. In such advanced stages of the disease, costly surgical intervention becomes the sole viable treatment strategy, which is both unavailable and expensive in the regions where EMF is most prevalent [38]. Despite the need for new therapeutic approaches, the number of publications concerning EMF

has decreased since the 1980s [31], indicating that both a revival in interest and a novel approach to the disease are necessary.

10.5 Developmental Biology Perspectives

Large-scale studies conducted throughout Africa have emphasized the need for a new approach to understanding neglected conditions such as endomyocardial fibrosis and rheumatic heart disease. Both diseases degrade the normal function of valves in the heart, impairing cardiac output and effectively disabling the patient from contributing to their community. Developmental biology offers a promising new avenue towards understanding the neglected cardiovascular diseases of the developing world. As researchers unravel the embryonic blueprint of native valvulogenesis, a deeper understanding of the mechanisms of disease follows and fundamentally improved tissue engineering strategies may become possible.

The early heart is a single tube of endocardial cells surrounded by an outer layer of myocardium. In the first phases of development, the myocardium secretes a jelly-like matrix, forming protrusions, which swell into the lumen of the endocardial tube. The endocardial cells then begin to shed cell-to-cell contacts and migrate from the surface down into the matrix in a process called the endothelial to mesenchymal transition (EMT). Concurrently, new mesenchymal cells proliferate and begin to digest the jelly-like matrix and secrete a denser material in its place, causing the protrusions to swell further into the lumen. These larger protrusions are known as “cushions” due to their soft and rounded morphology.

The next phase of development differs between atrioventricular and semilunar valves. For atrioventricular valves, fenestrations between the cushion and myocardial wall begin to coalesce in a process called delamination, allowing the cushion to separate from the wall as it is remodeled into a dense leaflet connected only at the caudal edge and the chordae tendonae. In the semilunar valve, migration of the neural crest cells, retraction of the myocardial casing, myocardial apoptosis, and endocardial differentiation occur concurrently, creating a depression that deepens gradually on the superior face, progressively excavating or sculpting the leaflet cusps [39].

Embryonic development is 99% successful in creating perfectly functional hearts. Understanding why the 1% of malfunctions occur can elucidate the steps of valvulogenesis which are integral to the development of a healthy heart. Normal developmental mechanisms provide the blueprint for outlining how the heart and valves malfunction in disease states and suggest therapeutic avenues that capitalize on the innate mechanisms and potential of the native heart (Figure 10.4). Both the molecular signaling pathways and the remodeling transitions of valvulogenesis have been implicated in various pathologies such as EMF and RHD [40-43], and are discussed below.

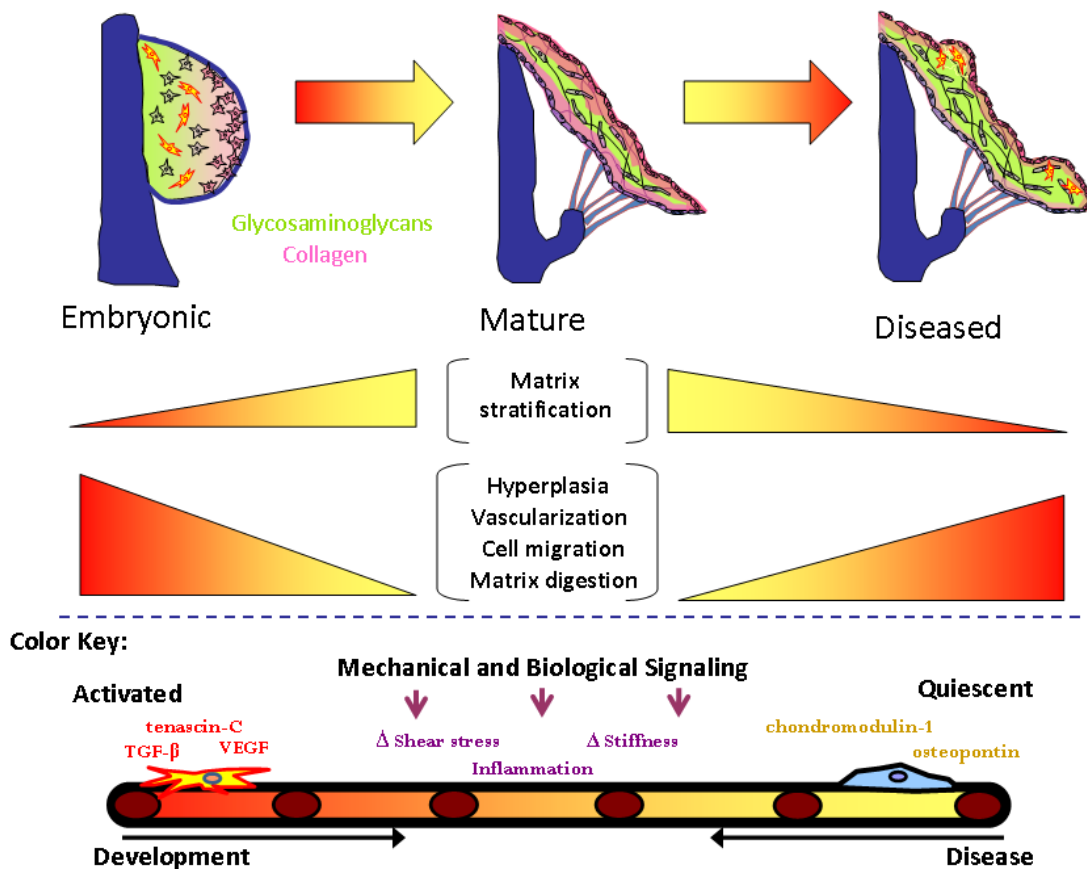


Figure 10.4 Similar pathways in valve development and disease.

Mechanisms such as vascularization, ECM organization, and cell migration are controlled by common molecules including, but not limited to, TGF- β , VEGF, chondromodulin-1, and tenascin-C.

Endomyocardial fibrosis and developmental biology

The endothelial to mesenchymal transition is an important phase in valvulogenesis during which quiescent endocardial cells migrate, change phenotype, and take on a new role. This same process has been shown in connection with fibrosis, most notably by Zeisberg et al. in 2007. Zeisberg showed that fibrosis arises from endothelial cells undergoing a transition to a mesenchymal then fibrotic phenotype in diseased tissue,

establishing a direct connection between EMF-like pathology and processes governing developing heart valves [44].

EMT is regulated in both processes by transforming growth factor beta (TGF- β), shown to be necessary in development for migration, matrix digestion, cell separation, and hyperplasia [45-47] and in pathology for fibrosis to occur [44]. TGF- β modulation of EMT has also been implicated in cardiac fibroblast to collagen metabolism [48], derivation of interstitial fibroblasts [49] [49], and myocardial fibrosis [50]. These studies point towards a direct link between the roles of TGF- β controlled EMT during development and endomyocardial fibrosis pathogenesis.

Other promising connections between valvulogenic pathways and EMF include the role of growth-stimulating angiotensin-II in conjunction with TGF- β [51-53], tenascin-C regulation of cell behavior in embryonic and pathological remodeling [54], and stimulation of EMT by endothelin-1 [55]. The etiology of fibrosis as regulated by these developmental signaling pathways offers a fresh perspective on the progression of EMF and possibly novel therapeutic approaches.

RHD and Developmental Biology

Various studies have connected RHD valvulitis and developmental pathways, specifically with regards to TGF- β modulation, chondromodulin-1, and structural changes [40,41,56,57]. Kim et al. showed a correlation between elevated levels of TGF- β 1 expression in rheumatic mitral valve leaflets and myofibroblast proliferation,

valvular fibrosis, inflammation, and calcification [56]. This suggests that the pathological mechanisms of RHD may be similar to embryonic processes by which progenitor cells activate, proliferate, and migrate under the influence of TGF- β .

Healthy cardiac valves abundantly express chondromodulin-1, an antiangiogenic molecule, whereas rheumatic valves exhibit increased vascularization and calcification in areas of downregulated chondromodulin-1 [41]. This correlation points to a link between normal valvular function and proper maintenance of chondromodulin pathways, marking a potential therapeutic strategy in exogenous administration of antiangiogenic drugs. One option is candesartan, which blocks angiotensin-II receptor type 1 and has been shown to increase left ventricular hypertrophy regression after valve replacement surgery [58].

In many RHD valvular pathologies and similar degenerative conditions such as myxomatous valve disease, the trilaminar, structured healthy valve reverts to a disorganized embryonic-like phenotype [42,59]. Healthy quiescent valvular interstitial cells become activated osteoblasts, driving calcification near sites of inflammation [56]. This is a complementary process to valvulogenesis, in which the mesenchymal cells associated with condensation and organization of the leaflets move towards an inactive phenotype. Current studies have shown that reactivation of embryonic signaling pathways in diseased valves promotes regression of degenerative characteristics such as stiffening and inflammation [59]. Controlling valve remodeling

and phenotypic changes using embryonic pathways could have exciting ramifications for RHD therapy.

The importance of the microenvironment in contributing to healthy cardiovascular development presents an opportunity for engineering to contribute to understanding of these clinical pathologies. Quantifying changes in micromechanical properties of the valves such as stiffness and extracellular matrix organization promises to elucidate both development and disease. Fluid dynamics, soft tissue biomechanics, and methodical quantitative analysis of contributing factors will complement the biological expertise of natural scientists in leading to a deeper understanding of these conditions and intervention strategies.

10.6 Paths Forward

Tissue engineered heart valves (TEHV) are the most promising therapy for the young patients of developing countries, offering both long-term viability and significant amelioration of the life-threatening aspects of valve pathologies. However, the field faces significant challenges in understanding the biomechanics and biology of growing valves in the pediatric applications, which are of greatest importance in the young patient populations of developing countries, problems which can only be solved by referencing the natural processes by which the body develops. These issues are neglected in the West because more than 90% of valve replacement surgeries are performed in patients over 50 years of age [60], making the economic case for developing a pediatric TEHV a much lower priority.

The potential for tissue-engineered valves for pediatric applications has been demonstrated in several studies, most recently with Weber et al.'s successful design and implantation of a marrow stromal cell-based autologous valve in non-human primates [61]. Creative rethinking may make the opportunities in this field particularly suited to the challenges and resources of Sub-Saharan Africa.

Tissue engineering can mean not only the comprehensive development of a fully functional valve, but also the experimental approach which uses biosynthetic platforms to recapitulate the native valvular environment in a tunable in vitro model. Principles from developmental biology such as those described above can be applied to these models in order to understand the parallels between valvulogenesis and RHD/EMF pathology. For example, cells could be isolated from a rheumatic valve, grown on a three-dimensional tissue engineered scaffold, treated with a TGF- β inhibitor and assessed for amelioration of inflammation. Researchers who are daily confronted with the realities of RHD and EMF-associated valvular pathology are uniquely suited to design low-cost experimental investigations which combine insights from developmental biology with the principles of tissue engineering in working towards a therapeutic solution for the young cardiac patients of the developing world.

REFERENCES

1. Yusuf S, Vaz M, Pais P. (2004) Tackling the challenge of cardiovascular disease burden in developing countries. *Am Heart J* 148:1-4.
2. Mathers C, Fat DM, Boerma J. (2004) The global burden of disease: 2004 update. WHO 2008.
3. Mayosi BM. (2007) Contemporary trends in the epidemiology and management of cardiomyopathy and pericarditis in sub-Saharan Africa. *Heart* 93:1176-1183.
4. Mutazind T. (1972) Survival after first presentation with endomyocardial fibrosis. *Br Heart J* 34:403-407.
5. Guilherme L, Ramasawmy R, Kalil J. (2007) Rheumatic fever and rheumatic heart disease: Genetics and pathogenesis. *Scand J Immunol* 66:199-207.
6. Mayosi B, Robertson K, Volmink J, et al. (2006) The Drakensberg declaration on the control of rheumatic fever and rheumatic heart disease in Africa. *S Afr Med J* 96:246.
7. Mocumbi AO, Ferreira MB, Sidi D, Yacoub MH. (2008) A population study of endomyocardial fibrosis in a rural area of Mozambique. *N Eng J Med* 359:43-9.
8. Yusuf S, Reddy S, Ounpuu S. (2001) Global burden of cardiovascular diseases: Part I: general considerations, the epidemiologic transition, risk factors, and impact of urbanization. *Circ* 104:2746-2753.
9. Moran M, Guzman J, Ropars AL, et al. (2009) Neglected Disease Research and Development: How Much Are We Really Spending? *PLoS Med* 6:0137-0146.
10. Carapetis JR, Steer AC, Mulholland EK, Weber M. (2005) The global burden of group A streptococcal diseases. *Lancet Infect Dis* 5:685-694.
11. Wayne AR, Schlant RC, Fuster V. (1998) *Hurst's The Heart, Arteries and Veins*. New York, McGraw-Hill, Health Professions Division.

12. Drakensberg Declaration on the Control of Rheumatic Fever and Rheumatic Heart Disease in the World. 2011.
13. Watkins DA, Zuhlke LJ, Engel ME, Mayosi BM. (2009) Rheumatic fever: Neglected again. *Science*. 324:37.
14. Paar J , Berrios NM, Rose JD, et al. (2010) Prevalence of rheumatic heart disease in children and young adults in Nicaragua. *Am J Cardiol* 105:809-814.
15. Rheumatic Fever and Rheumatic Heart Disease: Report of a WHO Expert Consultation, Geneva, 2004.
16. Freers J, MayanjaKizza H, Ziegler JL, Rutakingirwa M. (1996) Echocardiographic diagnosis of heart disease in Uganda. *Trop Doct* 26:125-128.
17. Anabwani GM, Bonhoeffer P. (1996) Prevalence of heart disease in school children in rural Kenya using colour-flow echocardiography. *East Afr Med J* 73:215-217.
18. Marijon E, Ou P, Celermajer DS, et al. (2007) Prevalence of rheumatic heart disease detected by echocardiographic screening. *New Eng J Med* 357:470-476.
19. Paar JA, Berrios NM, Rose JD, et al. Prevalence of Rheumatic Heart Disease in Children and Young Adults in Nicaragua. *Amer J Cardiol* 2010;105:1809-1814.
20. Sadiq M, Islam K, Abid R, et al. (2009) Prevalence of rheumatic heart disease in school children of urban Lahore. *Heart* 95:353-357.
21. Ansa VO, Ekott JU, Bassey EO. (2008) Profile and outcome of cardiovascular admissions at the university of Uyo Teaching Hospital, Uyo - A five year review. *Niger J Clin Pract* 11:22-24.
22. Roger VL, Go AS, Lloyd-Jones DM, Adams RJ, Berry JD, Brown TM, et al. (2011) Heart Disease and Stroke Statistics – 2011 Update. *Circulation* 123:e18-e209.

23. Dajani AS, Ayoub E, Bierman FZ, et al. (1992) Guidelines for the Diagnosis of Rheumatic Fever - Jones Criteria, 1992 Update. *JAMA* 268:2069-2073.
24. Cunningham MW. (2000) Pathogenesis of group A streptococcal infections. *Clin Microbiol Rev* 13:470-511.
25. Oli K, Asmera J. (2004) Rheumatic Heart Disease in Ethiopia: Could it be more malignant? *Ethiop Med J* 421-428.
26. WHO. (2004) *Rheumatic Fever and Rheumatic Heart Disease*. WHO technical report series.
27. Braun M. General and Systemic Histopathology: Rheumatic Valvulitis [Internet]. Indiana University, Medical Sciences Program.
28. Hammermeister K, Sethi GK, Henderson WG, Grover FL, Oprian FL, Rahimtoola S. (2000) Outcomes 15 years after valve replacement with a mechanical versus a bioprosthetic valve: final report of the Veterans Affairs randomized trial. *J Am Coll Cardiol* 36:1152-1158.
29. Zilla P, Brink J, Human P, Bezuidenhout D. (2008) Prosthetic heart valves: Catering for the few. *Biomaterials* 29:385-406.
30. Bukhman G, Ziegler J, Parry E. (2008) Endomyocardial Fibrosis: Still a Mystery after 60 Years. *PLoS Negl Trop Dis* 2:e97.
31. Connor DH, Somers K, Hutt MSR, Manion WC, Darbela PG. (1967) Endomyocardial Fibrosis in Uganda (Davies Disease): an Epidemiologic Clinical and Pathologic Study. *Amer Heart J* 74:687-709.
32. Mocumbi AO, Yacoub S, Yacoub MH. (2008) Neglected tropical cardiomyopathies: II. Endomyocardial fibrosis: myocardial disease. *Heart* 94:384-390.
33. Teekakirikul P, Eminaga S, Toka O, et al. (2010) Cardiac fibrosis in mice with hypertrophic cardiomyopathy is mediated by non-myocyte proliferation and requires TGF- β . *J Clin Invest* 120:3520-3529.

34. Burke AP. (2011) "Endocarditis." In *Practical Cardiovascular Pathology*, 1st ed., 349–63, Philadelphia, PA: Wolters Kluwer.
35. Niu JL, Azfer A, Rogers LM, Wang XH, Kolattukudy PE. (2007) Cardioprotective effects of cerium oxide nanoparticles in a transgenic murine model of cardiomyopathy. *Cardiovasc Res* 73;549-559.
36. Davies JNP, Ball JD. (1955) The pathology of endomyocardial fibrosis in Uganda. *Brit Heart J* 17:337-359.
37. Wright IG, Walker IA, Yacoub MH. (2007) Specialist surgery in the developing world: luxury or necessity? *Anaesthesia* 62:Suppl 184-189.
38. Butcher JT, Markwald RR. (2007) Valvulogenesis: the moving target. *Philos Trans R Soc London* 362:1489-1503.
39. Hakuno D, Kimura N, Yoshioka M, Fukuda K. (2009) Molecular mechanisms underlying the onset of degenerative aortic valve disease. *J Mol Med* 87:17–24.
40. Yoshioka M, Yuasa S, Matsumura K, Kimura K. (2006) Chondromodulin-I maintains cardiac valvular function by preventing angiogenesis. *Nature Med* 12:1151-1159.
41. Markwald RR, Norris RA, Moreno-Rodriguez R, Levine RA. (2010) Developmental basis of adult cardiovascular diseases: Valvular heart diseases. *Ann NY Acad Sci* 1188:177-183.
42. Shworak NW. (2004) Angiogenic modulators in valve development and disease: does valvular disease recapitulate developmental signaling pathways? *Curr Opin Cardiol* 19:140-146.
43. Zeisberg EM, Tarnavski O, Zeisberg M, et al. (2007) Endothelial-to-mesenchymal transition contributes to cardiac fibrosis. *Nature Med* 13:952-961.
44. Boyer AS, Ayerinkas II, Vincent EB, McKinney LA, Weeks DL, Runyan RB. (1999) TGF- β 2 and TGF- β 3 have separate and sequential activities during epithelial-mesenchymal cell transformation in the embryonic heart. *Dev Bio* 208:530-545.

45. Brown CB, Boyer AS, Runyan RB, Barnett JV. (1996) Antibodies to the type II TGF- β receptor block cell activation and migration during atrioventricular cushion transformation in the heart. *Dev Bio* 174:248-257.
46. Brown CB, Boyer AS, Runyan RB, Barnett JV. (1999) Requirement of type III TGF- β receptor for endocardial cell transformation in the heart. *Science* 283:2080-2082.
47. Chen K, Mehta JL, Li DY, Joseph L, Joseph J. (2004) Transforming growth factor- β receptor endoglin is expressed in cardiac fibroblasts and modulates profibrogenic actions of angiotensin II. *Circ Res* 95:1167-1173.
48. Goumans MJ, van Zonneveld AJ, ten Dijke P. (2008) Transforming Growth Factor beta-Induced Endothelial-to-Mesenchymal Transition: A Switch to Cardiac Fibrosis? *Trends Cardiovasc Med* 18:293-298.
49. Kania G, Blyszczuk P, Eriksson U. (2009) Mechanisms of cardiac fibrosis in inflammatory heart disease. *Trends Cardiovasc Med* 19:247-252.
50. Chen SL, Fang WW, Ye F, et al. (2004) Effect on left ventricular function of intracoronary transplantation of autologous bone marrow mesenchymal stem cell in patients with acute myocardial infarction. *Am J Cardiol* 94:92-95.
51. Chu PY, Mariani J, Finch S, et al. (2010) Bone Marrow-Derived Cells Contribute to Fibrosis in the Chronically Failing Heart. *Am J Pathol* 176:1735-1742.
52. Haudek SB, Cheng J, Du J, et al. (2010) Monocytic fibroblast precursors mediate fibrosis in angiotensin-II-induced cardiac hypertrophy. *J Mol Cell Cardiol* 49:499-507
53. Imanaka-Yoshida K, Hiroe M, Yoshida T. (2004) Interaction between cell and extracellular matrix in heart disease: Multiple roles of tenascin-C in tissue remodeling. *Histol Histopathol* 19:517-525.
54. Widyantoro B, Emoto N, Nakayama K. (2010) Endothelial cell-derived endothelin-1 promotes cardiac fibrosis in diabetic hearts through stimulation of endothelial-to-mesenchymal transition. *Circulation*. 121: 2379-2380.

55. Kim L, Kim DK, Yang WI, et al. (2008) Overexpression of transforming growth factor-beta 1 in the valvular fibrosis of chronic rheumatic heart disease. *J Korean Med Sci* 23:41-48.
56. Cunningham MW. (2003) Autoimmunity and molecular mimicry in the pathogenesis of post-streptococcal heart disease. *Front Biosci* 8:533-543.
57. Dahl JS, Videbaek L, Poulsen MK, et al. (2010) Effect of candesartan treatment on left ventricular remodeling after aortic valve replacement for aortic stenosis. *Am J Cardiol* 106:713-719.
58. Hinton RB, Lincoln J, Deutsch GH, et al. (2006) Extracellular matrix remodeling and organization in developing and diseased aortic valves. *Circ Res* 98:1431-1438.
59. Lewin M, Otto C. (2005) The bicuspid aortic valve - adverse outcomes from infancy to old age. *Circ* 111:832-834.
61. Weber B, Scherman J, Emmert MY, et al. (2011) Injectable living marrow stromal cell-based autologous tissue engineered heart valves: first experiences with a one-step intervention in primates. *Eur Heart J* 32:2830-2840.

Appendix A

Protocols

<u>Protocol</u>	<u>Page</u>
Sectioning and Slides	394
Russell-Movat Pentachrome Stain	396
Alizarin Red S	398
Hematoxylin & Eosin	399
Hematoxylin, Eosin, & Saffron	400
Von Kossa	401
Harvesting RNA & Protein from <i>ex vivo</i> aortic valve leaflets	403
PAVEC Cell culture media	404
PAVIC Cell culture media	406
Osteogenic Media	407
Isolation of Endothelial Cells from Porcine Aortic Valves	408
PAVEC Cell Culture	409
PAVIC Cell Culture	410
PAVEC Collagen Hydrogels	413
PAVIC Collagen Hydrogels	414
Alizarin Red S on Hydrogels	416
Apoptosis Assay (Hydrogels)	418
Proliferation Assay (Hydrogels)	420
Immunofluorescence (Paraffin sections)	422
Immunofluorescence (Cells on slides)	425
Immunofluorescence (Hydrogels)	426
Chemical Transfection (X-treme Gene)	427
Plasmid transformation/propagation	429
PAVEC electroporation	438
PAVEC transwell assay	440
Genotyping PCR (mouse tissue)	444
RNA Isolation	446
cDNA synthesis	447
q-rtPCR primer design	448
Quantitative rtPCR	449
Western Blot	451

Sectioning and Slides

By: Christopher Mosher, modified by EJJ

Time: ~30 min.

Materials: Wax-embedded sample, razor blade, microtome, paintbrush (Jingjing's shelf above Emily's bench), pizza box, hot plate, 1 L beaker, thermometer

Background:

Unifrost slides marked with a (+) have been treated with an adhesive. These slides are used for protein retrieval. If there is no (+), the slides may be used for H&E staining.

Protocol:

1. Use the razor blade to trim wax off the perimeter of the embedded sample so that it fits into the microtome
2. Switch the microtome lever to the right to unlock, load the blade and move it to the sample, and switch the lever back to the left
3. Remove the blade guards and take a section of the sample by turning the wheel clockwise, starting at 25 μm
4. Move to 15, 10, and eventually 6 μm
5. Take a 6 μm ribbon section using the microtome and a paintbrush. When using the paintbrush to remove wax, always stroke upwards away from the blade
6. Take as many ribbon sections as needed so that the sections penetrate the bulk of the sample. Place the sections in the pizza box
7. Heat water to 42°C in a 1 L beaker
8. Cut desired section of ribbon with the razor blade, and float the section on the surface of the water (NO FOLDS).
 - a. *Transfer the section to the water with a paintbrush
9. Dip the glass slide (be mindful of +) under the surface of the water and trap the section on top
10. Dry the slides upright in the cardboard box
11. Label the slides with a pencil
12. Clean the microtome bench and remove all wax scraps

Russell-Movat Pentachrome Stain

Time: ~3 hours

Background: Performing stain with American MasterTech Russell-Movat Pentachrome Stain Kit (Cat. #KTRMP) + purchased reagents (see below)

Verhoeff's Elastic Stain expires after 24 hours, and is prepared with 7.5 mL of each of the following:

1. 10% Alcoholic Hematoxylin (Corrosives cabinet)
2. Reagent Alcohol (not in kit, in flammables cabinet)
3. 10% Ferric Chloride (corrosives cabinet)
4. Universal Iodine Solution (Lugol's iodine solution, flammables cabinet)

Protocol:

1. Deparaffinize slides and hydrate through alcohols
 - a. 3 changes of Xylene, 3 min. each
 - b. 100% ethanol 5 min., 95% ethanol 2 min., 70% ethanol 2 min.
2. Rinse in running water for 2 min., followed by diH₂O for 2 min.
3. Place slide in **Verhoeff's Elastic Stain** for 15 min.
4. Rinse in lukewarm running water for 5 min., followed by 2 min. diH₂O
5. Differentiate in **2% Ferric Chloride**. Looking for black fibers, gray background
 - a. 1-2 minutes for mouse hearts
 - b. 30 seconds for valve leaflets (human or porcine)
6. Rinse slide in diH₂O for 2 min. and place in **5% Sodium Thiosulfate** for 1 min.
7. Rinse in lukewarm running water for 5 min.
8. Place in **3% Acetic Acid** for 3 min.
9. Place in **1% Alcian Blue Solution** for 20 min.
10. Rinse in lukewarm running water for 1 min., then in diH₂O for 2 min.
11. Place in **Crocein Scarlet-Acid Fuchsin** for 2 min.
12. Rinse through 3 changes of diH₂O, 1 min. each
13. Dip slide 5 times in **1% Acetic Acid**
14. Place in 2 changes of **5% Phosphotungstic Acid** for 2 min. each. Collagen is now a pale pink, ground substance turns from red to bluish. Check under microscope, and stop differentiation when connective tissue is clear but before the elastic fibers are de-stained.
15. Dip slide 5 times in **1% Acetic Acid**
16. Dehydrate through 3 changes of 100% EtOH, 2 min. each
17. Place in **Alcoholic Saffron Solution** for 15 min. →collagen turns yellow
 - a. Check Saffron solution for precipitation, if present, replace solution
18. Dehydrate through 3 changes of 100% EtOH, 1 min. each
19. Clear slide through 3 changes of Xylene, 1 min. each
20. Coverslip using permanent mounting media

Results

Elastic fibers, nuclei: **BLACK**

Collagen: **YELLOW**

Mucins: **BLUE TO GREEN**

Muscle: **RED**

Fibrinoid: **INTENSE RED**

Replacement reagents:

Universal Iodine: Sigma 62650

Reagent alcohol: 90% EtOH, 5% MeOH, 5% Isopropanol

Alcoholic saffron solution: Electron Microscopy Sciences #26395-10

Alizarin Red Staining Protocol for Paraffin Slides

Referenced from:

http://www.ihcworld.com/_protocols/special_stains/alizarin_red_s.htm

Prepared by: Kevin Hsu, 3-28-14

Stains for: Calcium deposits – orange-red

Preparation (Solutions):

1. Alizarin Red Solution – 25 mL – Change every month!
 - a. 0.5 grams Alizarin Red
 - b. 25mL Distilled water
 - c. Couple drops of 10% ammonium hydroxide
 - d. Add water, and Alizarin Red, mix well to dissolve the Alizarin Red. While it is mixing, use pH meter and dropwise addition of ammonium hydroxide to adjust pH to 4.1-4.3 range.
2. Acetone (100%) – 25mL
 - a. 25mL Acetone
3. Acetone-Xylene – 25mL
 - a. 12.5mL Acetone
 - b. 12.5mL Xylene

Procedure:

De-paraffinize slides using the following sequence:

1. 3 min xylene
2. 3 min xylene
3. 3 min xylene
4. 5 min 100% EtOH
5. 2 min 95% EtOH
6. 2 min 70% EtOH
7. Two changes of water, 30 seconds each

Apply the alizarin red stain

8. 2 min Alizarin Red Solution
9. Remove, lightly blot excess solution off slides
10. 30s Acetone
11. 30s Acetone-Xylene
12. 1.5 min Xylene
13. 1.5 min Xylene

Apply coverslip with permanent mounting medium

Hematoxylin & Eosin Stain

By: Caitlin Bowen, modified by EJF

- 1) Bake at 65 degrees for ~15 minutes or until wax melts
- 2) Let cool to room temp or until wax hardens again
- 3) Stain
 1. Xylene #1 15 min
 2. Xylene #2 5 – 10 min
 3. Xylene #3 5 min
 4. 100% EtOH 5 min
 5. 95% EtOH 2 min
 6. 75% EtOH 2 min
 7. dd water 2 min
 8. hematoxylin 6 min
 9. tap water 3 min
 10. 0.2% acid alcohol 20 sec
 11. Tap water 1.5 min
 12. 1% ammonia water 1 min
 13. Tap water 1.5 min
 14. 70% EtOH 1 min
 15. Alcoholic Eosin 2 min
 16. *Tap dry with paper towel*
 17. 95% EtOH 1 min
 18. 95% EtOH 1 min
 19. 100% EtOH 1 min
 20. 100% EtOH 1 min
 21. Xylene 3 min
- 4) 3 Drops of Permount per section, place cover slip & let dry overnight

Hematoxylin, Eosin, Saffron (HES) Staining Protocol (Time: about 2 hours)

By: Varsha Pramila, modified by EJJ

1. Place slide in oven for about **20 min** to melt off paraffin. Make sure oven is at 65 degrees Celsius.
2. Next, place in **xylene** (3 changes, 4 minutes each)
3. Place in **100% EtOH** for 5 minutes.
4. Place in **95% EtOH** for 2 minutes.
5. Place in **70% EtOH** for 2 minutes.
6. Place in **tap H₂O** for 2 minutes.
7. Place in **Harris's Hematoxylin** for 10 minutes.
8. Rinse in **running tap H₂O** for 3 minutes.
9. Place in **0.2% Acid Alcohol** for 20 seconds.
10. Rinse in **running tap H₂O** for 1.5 minutes.
11. Place in **1% Ammonia water** for 1 minute.
12. Rinse in **running tap H₂O** for 1.5 minutes.
13. Place in **70% EtOH** for 1 minute.
14. Place in **Alcoholic Eosin** for 4 minutes.
15. Rinse in **running tap H₂O** for 20 seconds.
16. Place in **100% EtOH** for 2 minutes.
17. Place in **Q Path alcoholic Saffron** for 30 minutes.
18. Place in **100% EtOH** (2 changes, 1 minute each)
19. Place in **xylene** for (3 changes, 2 minutes each)
20. Come out in xylene.
21. Put a drop of **Permount** on each sample and cover with glass slip.

The collagen is orangey-yellow due to saffron. Nuclei will be stained black.

von Kossa Staining Protocol for Calcium

Obtained from: http://www.ihcworld.com/protocols/special_stains/von_kossa.htm

Modified by EJJ, Kevin Hsu

Description: This technique is for demonstrating deposits of calcium or calcium salt so it is not specific for the calcium ion itself. In this method, tissue sections are treated with a silver nitrate solution and the silver is deposited by replacing the calcium reduced by the strong light, and thereby visualized as metallic silver.

Fixation: formalin fixed, paraffin embedded tissue sections or alcohol fixed, frozen sections.

Solutions and Reagents:

1% Aqueous Silver Nitrate Solution:

Silver nitrate ----- 1 g
Distilled water ----- 100 ml

5% Sodium Thiosulfate:

Sodium thiosulfate ----- 5 g
Distilled water ----- 100 ml

0.1% Nuclear Fast Red Solution:

Nuclear fast red ----- 0.1 g
Aluminum sulfate----- 5 g
Distilled water -----100 ml

Dissolve aluminum sulfate in water. Add nuclear fast red and slowly heat to boil and cool. Filter and add a grain of thymol as a preservative.

Procedure:

1. Deparaffinize paraffin sections and hydrate to water.
2. Rinse in several changes of distilled water.
3. Incubate sections with 1% silver nitrate solution in a clear glass coplin jar placed under ultraviolet light for 20 minutes (or in front of a 60-100 watt light bulb for 1 hour or longer). Note: If stain was weak or rinsed off in washing steps, it indicated the UV light was not strong enough. Longer staining is required for up to several hours.
4. Rinse in several changes of distilled water.
5. Remove un-reacted silver with 5% sodium thiosulfate for 5 minutes.
6. Rinse in distilled water.
7. Counterstain with nuclear fast red for 5 minutes.
8. Rinse in distilled water.
9. Dehydrate through graded alcohol and clear in xylene.
10. Coverslip using permanent mounting medium.

Results:

Calcium salts ----- black or brown-black

Nuclei ----- red

Cytoplasm ----- pink

Positive Controls:

16-18 days mouse embryo, calcium containing tissues or undecalcified bone.

Notes:

1. UV light usually gives stronger reaction so the calcium salts are often stained black. The regular 60-100 watt light bulb usually gives weaker reaction so the calcium salts are often stained brown-black.
2. Oxalate salts are usually believed to give a negative von Kossa staining.
3. A negative control may be needed when there is any doubt that the resulting black deposits are calcium. This is done by treating a test slide in 10% formic acid for 10 minutes prior to step 3. The test slide should show negative reaction.

Harvesting tissue from *ex vivo* porcine aortic valve leaflets

RNA isolation:

Rinse sample in PBS, 1x
Transfer sample to mortar and pestle
Add 2 mL liquid nitrogen (approximately)
Allow sample to flash freeze
Crush with pestle
Collect resulting powder with disposable spatula
Transfer to 1.5mL eppendorf tube
Add .35 mL RLT+1% beta-mercapthenol to tube, on top of sample
Vortex to mix
Flash freeze
Put on ice until move to -80C freezer
* Recommended to freeze in batches if processing > 6 samples.
Wash mortar and pestle with soap and water
Dry thoroughly
Spray mortar and pestle generously with 70% ethanol
Dry with kim wipe
Spray again
Allow to air dry
Repeat for remaining samples

Protein isolation:

Rinse sample in PBS, 1x
Transfer sample to mortar and pestle
Add 2 mL liquid nitrogen (approximately)
Allow sample to flash freeze
Crush with pestle
Collect resulting powder with disposable spatula
Transfer to 1.5mL eppendorf tube
Add 100uL of 2x Laemmli buffer, propelling sample to bottom of tube
Use pipet to ensure that all sample is submerged in buffer
Wash mortar and pestle with soap and water
Dry thoroughly
Spray mortar and pestle generously with 70% ethanol
Dry with kim wipe
Spray again
Allow to air dry
Repeat for remaining samples
*Freeze samples at -80C until ready for next step. Recommended to freeze in batches if processing > 6 samples.

Set heat block to 70C, allow to come to temp
Transfer samples from freezer to heat block
Incubate samples at 70C for 1 minute to thaw, then vortex to mix

Return samples to heat block and incubate at 70C for 10 minutes
Move samples to ice
Sonicate each sample for 10-15 seconds using CRK sonicator
*Keep samples on ice before and after sonications
*Clean sonication probe with water and kim wipe between each use
Spin down samples at ~14,000 rpm for 10 minutes at 4C (Fridge in CRK lab)
*Samples will have large amount of precipitate in bottom of tube after spin
Transfer supernatant to new, labeled 1.5mL eppendorf tube
Discard pellet (or keep, if you're worried about throwing anything away that might be useful)
Flash freeze pellet in liquid nitrogen
Store in -80C until ready for quantification

PAVEC Cell Culture Media

By: Chris Frendl, M.Eng., modified by EJJ

Materials:

10% FBS (stored in -20 °)

1% Pen/Strep (stored in -20 °)

250mg/L Heparin Sodium Salts (powder in 4 °deli fridge) *can be less for more developed cells

13.37 g/L of DMEM (powder in 4 °deli fridge)

3.7 g/L sodium bicarbonate (dry powder on shelf above pH meter)

18 Ω H₂O (85% of final volume)

PROTOCOL for 1 Liter:

- Thaw FBS and Pen/Strep in water bath
- Fill beaker w/stir-bar to ~850mL 18 Ω H₂O
- Measure out DMEM and add to beaker + H₂O on mixing plate
 - If clumps of DMEM occur 'shoot' apart with 18 Ω H₂O squeeze bottle
- Add sodium bicarbonate (solution should change from orange to red)
- Adjust pH to 7.2 with HCL
- Add Heparin 250 mg/L
- Add Pen/Strep 10mL/L
- Fill to 900ml with 18 Ω H₂O
- Filter through 2um vacuum filter in hood
- Add 100mL FBS to filtered media
- Label: INITIALS

PAVEC (Intent: cell culture type)

DMEM

DATE

+FBS

+Pen/Strep & Hep

STORE IN 4 °deli fridge (gone bad when color turns purple)

PAVIC media:

Same as PAVEC, but without heparin

Osteogenic Media Protocol (By Jen Richards, Ph.D., modified by EJF)

Supplements

β-Glycerophosphate disodium salt hydrate (Sigma G9891-10G)

L-Ascorbic acid (vitamin C) (Sigma A4544-25G)

Dexamethasone (D4902-25MG)

Supplement Concentrations:

β-Glycerophosphate: **10 mmol/L**

$$\frac{x \text{ grams}}{\text{L}} = \left(10 \times 10^{-3} \frac{\text{mol}}{\text{L}}\right) \left(216.04 \frac{\text{mol}}{\text{L}}\right) = \mathbf{2.16 \frac{g}{L}}$$

(molecular weight)

Ascorbic acid (vitamin C): **50 μg/ml**

$$\left(\frac{50 \times 10^{-6} \text{ g}}{10^{-3} \text{ L}}\right) \left(\frac{1000 \text{ mg}}{1 \text{ g}}\right) = \mathbf{50 \frac{mg}{L}}$$

Dexamethasone: **10⁻⁸ M (mol/L)**

$$\left(\frac{10^{-8} \text{ mol}}{\text{L}}\right) \left(\frac{392.46 \text{ g}}{\text{mol}}\right) \left(\frac{1000 \text{ mg}}{1 \text{ g}}\right) \left(\frac{1 \text{ L}}{1000 \text{ ml}}\right) = \mathbf{3.92 \times 10^{-6} \frac{mg}{ml}}$$

Preparing Supplements (to be added to normal culture media):

- Supplements to be added to media: 10 ml of β-Glycerophosphate and Vitamin C solution

1 ml 1 mM Dexamethasone

β-Glycerophosphate and Vitamin C solution (50 X concentration)

1. Start with 50 ml of 18 MΩ water

2. Add β-Glycerophosphate:

$$\left(\frac{2.16 \text{ g}}{\text{L}}\right) \left(\frac{1 \text{ L}}{1000 \text{ ml}}\right) (50 \text{ ml})(50) = \mathbf{5.4 \text{ g } \beta\text{GP}}$$

50X concentrated

3. Add Vitamin C:

$$\left(\frac{50 \text{ mg}}{\text{L}}\right) \left(\frac{\text{g}}{1000 \text{ mg}}\right) \left(\frac{1 \text{ L}}{1000 \text{ ml}}\right) (50 \text{ ml})(50) = \mathbf{0.125 \text{ g VitC}}$$

4. Mix well until completely dissolved

5. Aliquot into five 10 ml centrifuge tubes

6. Store at -20°C

1% Dexamethasone: stored at -20°C

When making osteogenic media, make 500 ml of normal culture medium, add 10 ml of supplement solution and 1 ml of Dexamethasone to media before sterile filtering.

Isolation of Endothelial Layer from Porcine Aortic Valves

Gould, R. A., Butcher, J. T. Isolation of Valvular Endothelial Cells. *J. Vis. Exp.* (46), e2158, doi:10.3791/2158 (2010).

1. Fill a sterile 35mm dish with 3mL of cold collagenase solution per valve (3 leaflets).
2. Place all three leaflets from the 15 mL tube into the dish filled with the collagenase solution.
3. Incubate the tissue for 5-10 minutes at 37°C.
4. Gently remove the endothelial layer by rotating a dry sterile swab onto the surface of the leaflet. The direction of rotation and amount of shear applied is critical for the purity of your sample. The rotation of the swab should be in an opposite direction to linear motion of your hand creating a controlled shear. This shear is what lifts the endothelial cells from the tissue. The amount of force applied should be enough to feel the resistance of the tissue but not penetrate the basement membrane.
5. Occasionally, dab the swab within the collagenase solution to dislodge cells from the tip fibers. After swabbing is complete, the texture of the endothelial layer should feel slightly smoother than before.
6. Collect the cell suspension/collagenase and transfer to a new sterile 15mL tube.
7. Centrifuge the tubes at 1000 rpm for 5 minutes to pellet any isolated cells and aspirate supernatant. If isolating interstitial cells as well, perform that protocol while these cells are being centrifuged.
8. Add 3 mL of endothelial porcine medium to the 15 mL tubes, centrifuge a second time, and aspirate media. This second centrifugation helps filter some of the unwanted material such as tip fibers.
9. Re-suspend the centrifuged endothelial cells in 5 mL of endothelial porcine medium and plate the cells in a pre-coated T-25 flask with collagen (use 1 flask per centrifuge tube).
10. Let the cells grow at least 2-3 days before changing the endothelial medium. This helps the cells recover and divide since the isolation process is fairly harsh and the cell yield may be low. It is critical to passage cells near confluence since contact inhibition could lead to cell transformation.

PAVIC isolation (following PAVEC isolation protocol)

Transfer swabbed leaflets to 5-8mL of collagenase II solution.

Incubate overnight at 37 C.

The next day, shake tube to homogenize cell solution, allow to settle.

Pipet collagenase+cell solution off the top of tube, transfer to clean tube

Spin down at 1000rpm for 5 min.

Pour off supernatant, resuspend in 15mL of PAVIC media, plate in T75 flask.

Grow 2-4 days, monitoring confluence.

Change media when 50% confluent.

Passage to new T75 when 90% confluent.

PAVEC Cell Culture

By: Schinthia Islam, edited by EJJ

Thawing cells, changing media, counting cells, passaging

Thawing Cells

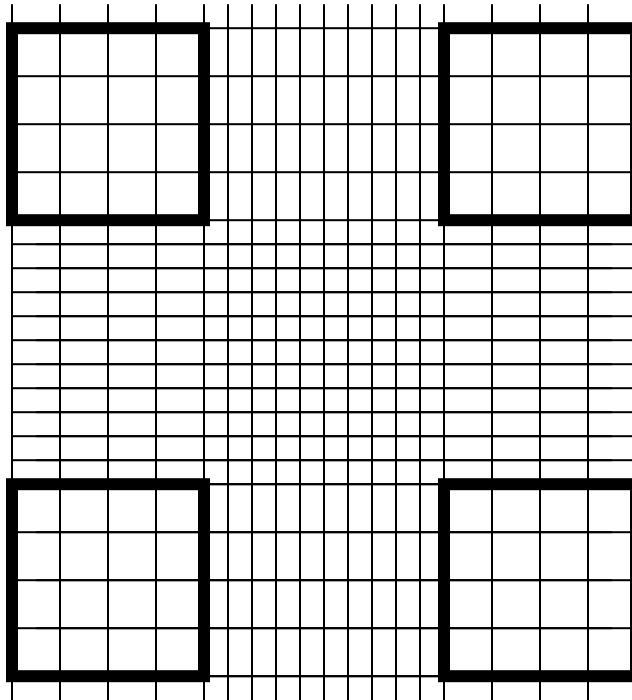
1. Prepare biosafety hood, wipe area with 70% ethanol. Warm standard culture media for PAVEC in water bath. Wipe empty beaker with ethanol, fill with 50-100 mL 100% bleach and place in hood.
2. Wipe closed bag of T-75 flasks (*located on shelf above centrifuge*) and place into hood. Do not open outside of hood or sterility will be lost. Remove one flask.
3. For porcine aortic valve endothelial cells (PAVEC), flasks must be coated with 3 mL collagen (125 uL stock collagen type I/10 mL 1X PBS) 30 minutes prior to plating to allow proper adhesion. Apply collagen to flask at least 20 minutes prior to beginning thawing process.
4. Obtain cryotube of PAVEC from the nitrogen storage tank (*located between 4 C and large -20 C fridge*). Check Cryofridge Storage Excel sheet on computer next to Zeiss microscope for most current location of PAVEC.
5. Wipe tube with ethanol and place in hood. Thaw immediately and transfer to 15 mL conical tube.
6. Dilute DMSO with 10 mL warm standard PAVEC media.
7. Centrifuge at 1000 rpm for 4 minutes.
8. Carefully aspirate supernatant without disturbing pellet and dispose in waste bleach beaker.
9. Resuspend by adding 15 mL fresh media to conical tube (5 mL for T-25 flask). At this stage, cells can be counted if desired (see below).
10. Aspirate collagen from flask and dispose in waste beaker.
11. Add to cell suspension to T-75 flask.
12. Place in dry 37 C incubator.

Changing Media

1. Media should be changed every 24-48 hours. Repeat hood and waste disposal preparation as normal.
2. Aspirate media from flask and dispose in waste bleach beaker.
3. Replenish flask with 12 mL warm standard PAVEC media (4 mL for T-25 flask).
4. Return to dry 37 C incubator.

Counting Cells

1. Carefully clean hemacytometer and glass cover slip (*located in drawer beneath light microscope*) with 70% ethanol and let air dry
2. Trypsinize cells and resuspend in media (Media volume = 3x trypsin volume)
3. Place glass cover slip on center of hemacytometer and slowly apply 10 uL of cell and media mixture to groove under edge of cover slip until a thin layer of solution forms underneath.
4. View under light microscope. Focus first on the center grid that contains the most horizontal and vertical lines.
5. Count cells in grid at the immediate upper and lower left and right corner of the center grid, as indicated below with the darkened boxes. Record four separate counts of cells.



6. Open “Hanging Drop Worksheet” in QuickRef Folder on any computer or search by file name.
7. Under “Cushion” column on the right, input counts for grids 1, 2, 3, and 4. Change suspension volume under “Cushion” on the left to whatever volume the 10 uL aliquot was originally taken from to determine total cell count (cells/flask) and concentration (cells/mL suspension) of entire suspension.
8. Carefully clean hemacytometer and glass cover slip with 70% ethanol.

Passaging Cells (1:3 expansion)

1. Cells are passaged when confluency is reached and the current flask has approximately 70-90% area covered in cells. At this stage, cells no longer grow exponentially and can be split to continue expansion.
2. Prepare biosafety hood, wipe area with 70% ethanol. Warm standard culture media for PAVEC, 1X PBS (25 mL 10X PBS in 225 mL 18M mΩ water, autoclaved), and trypsin in EDTA (*located on middle shelf in large -20 C fridge*) in water bath. Wipe empty beaker with ethanol, fill with 50-100 mL 100% bleach and place in hood.
3. Wipe closed bag of T-75 flasks (*located on shelf above centrifuge*) and place into hood. Do not open outside of hood or sterility will be lost. Three flasks will be needed.
4. Flasks must be coated with 3 mL collagen (50 ug/mL collagen type in sterile 18mO water) 20 minutes prior to plating to allow proper adhesion. Apply collagen to flask at least 10 minutes prior to beginning passaging process.
5. Aspirate media from current old flask and dispose into waste bleach beaker.
6. Add 10 mL 1X PBS to flask to rinse cells. Remove PBS and dispose in waste beaker.
7. Add 3 mL trypsin in EDTA to flask to remove the cells from the plate surface. Tap flask to aid in removal. Be mindful of time in contact with trypsin because excessive exposure will destroy the cells.
8. Place in dry 37 C incubator for 3 minutes (no more than 5 minutes or cells will die).
9. Take flask out of incubator and continue tapping. Solution should be cloudy with cells. Quickly check under light microscope to verify cells have been detached from plate bottom.
10. Deactivate trypsin by adding 3X volume (9 mL) warm standard PAVEC media to flask. Pipette up and down to homogenize.
11. Transfer cell suspension to 15 mL conical tube. Count cells at this stage if desired/needed.
12. Centrifuge at 1000 rpm for 5 minutes.
13. Prepare three T-75 flasks by removing collagen and adding 12 mL warm standard PAVEC media into each one.
14. After centrifugation, aspirate supernatant carefully without disturbing the pellet and dispose in waste beaker.
15. Resuspend cells by adding 9 mL warm standard PAVEC media to conical tube and pipette up and down to mix.
16. Add 3 mL of cell suspension to each of the three flasks. Label flasks properly with name, date, passage number, cell type, etc.
17. Place in 5% CO₂, 37 C incubator.

PAVIC Cell Culture

By: Katy Fang, edited by EJF

PAVIC Media Prep:

To make 1 L media [blue text is instructions to make 250 mL]:

1. Get DMEM-HG Powder (*light blue, in deli fridge on left*), 1% P/S (Pen-Strep) and 10% FBS (*in -20°C freezer*), sodium bicarbonate (*above scale/stirrer bench*), beaker and stir bar (*in drawer below bench*), 2 mm filter (*cell culture room cabinet*), pH probe and waste beaker
2. Thaw P/S and FBS aliquots in 37°C water bath
3. Rinse beaker with distilled water, fill with 890 [222.5] mL 18 MΩ water
4. Add entire packet of DMEM powder [3.35 g] with 18 MΩ water to rinse everything into beaker; stir on electric stirrer by Jen's bench
 - *Should turn solution orange → acidic pH
5. Add 3.7 g sodium bicarbonate [0.925 g] using a weighing boat
 - *Should turn solution red → neutral pH
 - *Make sure you can't see it at the bottom anymore (completely dissolved)
6. Remove pH probe from its buffer, rinse with 18 MΩ water, remove tape from probe
7. Turn on pH meter, bring probe into stirring media, press "Measure"
8. Add 1 M HCl drop-wise to decrease pH – aim for pH 7.2
 - *Solution will turn more orange
9. Rinse pH meter with 18 MΩ water, cover hole with tape, place probe back into buffer solution
10. Turn off pH meter – hold "on" button, wash pH waste beaker
11. Add 10 mL P/S [2.5 mL]
12. Check for total of 900 mL media [225 mL], top off with 18 MΩ water if needed
13. Prep cell culture fume hood
14. Spray FBS, filter, media with ethanol, place into fume hood
15. Connect the opaque white vacuum tube to the filter, turn on
16. Pour media into filter
17. Remove vacuum, turn off filter, add cap directly onto media beaker
18. Add 100 mL FBS [25 mL] to media
19. Swirl beaker without getting media bubbly or into cap
20. Label cap "DMEM, sterile", date, initials; label bottle with "DMEM+FBS+P/S", date, initials
21. Store media at 4°C, warm to 37°C before use

Thawing cells:

1. Prep cell culture fume hood, place waste bleach beaker into hood
2. Warm PAVIC media in 37°C water bath
3. Transfer 8.5 mL warmed PAVIC media to 15 mL conical tube
4. Wipe closed bag of T-75 flasks (*on shelf above centrifuge in cell culture room*), place in hood

5. Obtain cryotube of PAVIC, P3 cells from nitrogen storage tank (*between 4°C and -20°C fridges*); let nitrogen drain first
6. Thaw cryotube in water bath to triple point (small amount of ice left in tube ~1-2 minutes), spray with ethanol, place in hood
7. Transfer contents of cryotube to media tube (should be total of 10 mL)
8. Centrifuge at 1000 RPM for 5 minutes; **balance!**
9. Slowly decant supernatant without disturbing pellet, dispose in waste bleach beaker
10. Resuspend cells by adding 12 mL fresh media to conical tube (4 mL for T-25 flask)
- *Can count cells at this point
11. Add cell suspension to T-75 flask
12. Place in 37°C incubator

Changing media:

Should change media every 24-48 hours

1. Aspirate media from flask, dispose in waste bleach beaker
2. Replenish flask with 12 mL warm PAVIC media
3. Return to 37°C incubator

Passaging cells:

Instructions are for passing P4 to P5 (T-75 to T-175 flask)

If passaging P5 to P6, scale up all volumes by factor of 175:75 (e.g. 7 mL trypsin for 3 mL) To make 1x PBS, mix 25 mL 10x PBS in 225 mL 18 MΩ water, then autoclave

1. Check for 70-90% confluency (70-90% area covered in cells)
2. Prep cell culture fume hood, warm PAVIC media, 1x PBS, and trypsin in EDTA (*middle shelf in large -20°C fridge*), place waste bleach beaker into hood
- *Need 1 mL trypsin for every 25 cm² of growth area
3. Wipe with ethanol a closed bag of T-75 flasks and place into hood
4. Aspirate media from old flask, dispose into waste bleach
5. Add 5 mL 1x PBS to flask to rinse cells, remove PBS, dispose into waste bleach
6. Add 3 mL trypsin in EDTA to flask to remove cells from flask surface, tap flask against table
- *Don't want long exposure of cells to trypsin
7. Place in 37°C incubator for 3-5 minutes (no more than 5 minutes)
8. Take out flask, check under light microscope
- *Cells should be circular and floating around
9. Add 9 mL (3x volume of trypsin) of PAVIC media to flask to deactivate trypsin, pipette up and down
10. Transfer cell suspension to 15 mL conical tube
- *Can count cells at this point

11. Centrifuge at 1000 RPM for 5 minutes
12. Carefully aspirate supernatant, dispose in waste bleach
13. Resuspend cells by adding 22 mL warm PAVIC media to conical tube, pipette up and down
14. Add cell suspension to new T-175 flask
15. Label new flask with name, date, passage number, cell type; place in 37°C incubator

PAVEC Collagen Hydrogels

By: Christopher Mosher, edited by EJJ

Time: ~25 minutes

Materials: Collagen stock (2 mg/mL), FBS (10%), DMEM 3X, water, NaOH → all in 4C, 4-well plates

Background: PAVECs should be seeded onto collagen gels after the gels have been made. PAVICs are found within the native tissue, so they should be seeded within the collagen gel as the gel is formed.

Protocol:

1. Fill a bucket with ice and place the collagen stock, FBS, DMEM 3X, sterile water, and NaOH inside. Spray the bucket with EtOH and put it in the cell hood.
2. Use a spreadsheet for calculations: Desktop → Collagen only disk template new
3. Change the following:
 - a. # disks (put #+1) – ex: want to make 4 gels, put 5
 - b. Mixture Vol Per Disk: 0.30 mL (for a 4-well plate)
 - c. Gel Collagen Conc: 2 mg/mL
 - d. Stock Collagen Conc: 4.41 mg/mL
 - e. Chick Serum %: 0
 - f. FBS: 10%
4. Add calculated components to a 15 mL conical tube in the following order: DMEM 3X → MilliQ H₂O → FBS → Collagen → NaOH. Keep everything sterile.
5. Add 0.3 mL of the resulting solution per well in a 4-well plate. The Microsoft Excel calculator has an error, and inputting 5 disks gave enough solution to make 16 gels (four 4-well plates)
6. Incubate the well plates at 37C
7. Seed PAVEC on surface of each gel, 100,000 cells/cm²
*For a 24-well plate-sized gel, this is 100,000 cells/gel. Resuspend every 100,000 cells in 50uL of PAVEC media. Ex. 1 million cells should be resuspended in 0.5mL of media. Add 50uL of cell resuspension to each gel. Minimal amount of media in this technique causes seeded PAVEC to congregate in the center of the hydrogel, which is optimal for gel coverage.
8. Let adhere for > 4 hours, preferably overnight

PAVIC Collagen Hydrogels

By: Christopher Mosher, edited by EJJ

Time: ~40 min. (wait a few hours before adding media)

Materials: Collagen stock (2 mg/mL), FBS (10%), DMEM 3X (DMEM powder and sodium bicarbonate), sterile water, NaOH, 4-well plates, 0.1 M NaOH (from 5M stock) PAVIC cells and media

Background: See Collagen Hydrogel protocol. Interstitial cells will be dispersed throughout these gels.

Reagents:

3X DMEM: 2.01 g DMEM powder (4C) + 0.555 g sodium bicarbonate + 50 mL 18 Mohm water

NAOH 0.1M:

$$\begin{aligned} m_1 v_1 &= m_2 v_2 \\ (0.1 M)(50 mL) &= (5 M \text{ stock solution})(X mL) \\ X &= 1 mL \end{aligned}$$

Add 1 mL 5 M stock solution to 50 mL 18 Mohm water

Sterile filter the 3X DMEM and NADH 0.1M using a 60 mL slip-tip syringe (by microscope) and Acrodisc syringe filters (by water bath) in the cell hood. Use a stock solution of **sterile water** for this experiment.

Protocol:

1. Remove PAVIC cells from the 37C incubator
2. Pour the PAVIC media into a waste beaker with bleach, wash the T-75 flask with 5 mL PBS 1X (discard to bleach beaker), and add 3 mL trypsin to the flask
3. Incubate at 37C for 5 min., then add 9 mL PAVIC media (to dilute trypsin 3X) and transfer the solution to a 15 mL conical tube
4. Add 10 uL to a hemacytometer and count the cells

Want 400,000 cells/mL gel → Making 6 gels, 0.3 mL each

$$400,000 * 6 * 0.3 = 720,00 \text{ cells desired}$$

From hemacytometer: $36 * 10^4 = 360,000 \frac{\text{cells}}{\text{mL}}$

$$\frac{720,000 \text{ cells}}{360,000 \text{ cells/mL}} = 2 \text{ mL needed for gels}$$

5. Of the ~12 mL in the conical tube, transfer 2 mL to another 15 mL conical tube for gels
6. Spin down both tubes for 5 min. at 1,000 rpm
7. Add 9 mL PAVIC media to two T-75 flasks

8. Pour off the supernatant from the conical tube being used for cell plating and resuspend the pellet in 2 mL PAVIC media. Add 1 mL to each of the flasks from step 7. Incubate these flasks at 37C
 9. For gels, resuspend what has been calculated on Microsoft Excel spreadsheet (see protocol p. 10) .Continue the protocol on p. 10 from step 4
- After a few hours, remove the VIC gels from the incubator, add ½ mL PAVIC media to each well, and return to the incubator

Alizarin Red S Staining (Collagen Gels)

By: Jennifer Richards, Ph.D., modified by EJJ

Materials:

- **40 nM Alizarin Red S (ARS) stain**
- **10% Acetic Acid** (diluted in 18 mΩ H₂O)
- **10% Ammonium Hydroxide** (diluted in 18 mΩ H₂O)
- **4% PFA**

Staining Procedure

1. Wash gels with sterile PBS, fix in 4% PFA (overnight at 4°C or 1-2 hours at room temperature)
2. Aspirate 4% PFA, store gels at 4°C in 70% ethanol (EtOH) until staining begins
3. Aspirate EtOH, wash 3X in 1X PBS on shaker for 5 minutes each
4. Add 500 µl ARS dye to each gel. Incubate on shaker for 20 minutes at room temperature
5. Aspirate ARS dye, wash with 1X PBS on shaker until rinse solution is clear (1 hour to 1 week, depending on amount of calcification)
6. Aspirate the liquid
7. Take images of gel (with either Zeiss or Nikon camera)

Dye Extraction and Quantification

1. Add 400 µl of 10% acetic acid to each gel and incubate at room temperature for 30 minutes
2. Scrape the samples from each well, transferring to a 1.5 ml centrifuge tube. Vortex each sample for 30 seconds.
3. Heat samples in oven at 85°C for 10 minutes
4. Cool samples on ice for 5 minutes (do not open tubes until fully cooled)
5. Centrifuge samples at 13,500 RPM for 15 minutes
6. Make ARS standards (while samples are spinning)

High:

- Make a **2 mM solution** by diluting ARS 1:20 with 10% acetic acid
(50 µl ARS with 950 µl acetic acid)
- 2-fold serial dilution:
(2 mM, 1 mM, 500 µM, 250 µM, 125 µM, 62.5 µM, 31.3 µM)

Low:

- Make a **30 µM solution** by diluting the 2 mM ARS 1:66 with 10% acetic acid
(15 µl ARS (2 mM) with 985 µl acetic acid)
- 2-fold serial dilution:
(30 µM, 15 µM, 7.5 µM, 3.75 µM, 1.88 µM, 0.94 µM, 0.47 µM)

7. Transfer supernatant (400 μ l) from each tube to a new 1.5 ml centrifuge tube
8. Add 200 μ l of 10% ammonium hydroxide to each sample (pH 4.1-4.5)
9. Add 150 μ l of standards and samples in triplicate to clear 96 well plate
10. Use plate reader (Bonassar lab) to measure the dye absorbance at 405 nm
(Protocol: Butcher_ARS)
11. Determine the quantity of ARS in each sample using the standard curve

Apoptosis Assay (APO-BrdU TUNEL Assay)

By: Jennifer Richards, Ph.D., modified by EJF

Materials:

- **APO-BrdU TUNEL Assay Kit** (Invitrogen A23210)
 - **Positive control cells** (Component A, brown cap), fixed human lymphoma cell line (5 ml)
 - **Negative control cells** (Component B, white cap), fixed human lymphoma cell line (5 ml)
 - **Terminal deoxynucleotidyl transferase** (Component C, yellow cap) (45 μ l)
 - **5-Bromo-2'-deoxyuridine 5'-triphosphate (brdUTP)** (Component D, violet cap) (480 μ l)
 - Anti-BrdU mouse monoclonal antibody PRB-1, Alexa Fluor 488 conjugate (Component E, orange cap) (350 μ l)
 - **Propidium iodide/RNase A staining buffer** (Component F, amber bottle) (30 ml)
 - **Reaction buffer** (Component G, green cap) (0.6 ml)
 - **Wash buffer** (Component H, blue cap) (120 ml)
 - **Rinse bugger** (Component I, red cap) (120 ml)
- **1X Phosphate Buffered Saline (PBS)**
- **Draq5** (Biostatus Limited)

Method:

12. Wash gels once with warm PBS, then fix in 4% PFA for 24 hours (store at 4°C)
13. Aspirate 4% PFA, store gels at 4°C in 70% EtOH (until staining begins)
14. Aspirate EtOH, wash 3X in wash buffer (blue cap) on shaker for 5 minutes each (1X PBS is also ok)
15. Prepare a DNA labeling solution (total volume 50 μ l per gel)
 - 10 μ l reaction buffer (green cap)
 - 0.75 μ l TdT enzyme (yellow cap)
 - 8.0 μ l BrdUP (violet cap)
 - 31.25 μ l dH₂O
 - Note: this makes up 50 μ l of labeling solution – scale up volumes as needed for multiple samples
16. Incubate gels with 50 μ l DNA labeling solution for 2 hours at 37°C (oven or incubator)
 - Note: Incubation of labeling solution can also be carried out at room temperature overnight
17. Rinse with rinse buffer (red cap), 5 minutes on shaker
18. Aspirate, rinse once more with rinse buffer (red cap), 5 minutes on shaker
19. Add 100 μ l antibody (1:50 dilution in rinse buffer) to each gel, incubate for 1 hour in dark at room temperature

20. Incubate samples with 1:1000 dilution Draq5 in 1X PBS for 30 minutes
 - Note: this step can be combined with the previous (add Draq5 to the BrdU antibody solution)
21. Add 200 μ l of propidium iodine (amber bottle) to each sample, incubate in dark at room temperature for 30 minutes
22. Store in 1X PBS at 4°C until imaging
 - Note: samples are best imaged within 24 hours of staining

Proliferation Assay (BrdU Labeling)

By: Jennifer Richards, Ph.D., modified by EJF

Materials:

- BrdU Labeling Reagent (15 ml; Invitrogen 00-0103)
- 10X Phosphate Buffered Saline (PBS)
- 1.5 M Hydrochloric Acid
- Blocking Buffer (1X PBS / 5% BSA / 0.3% Triton X-100)
 - To make 500 ml of blocking buffer:
 - 50 ml 10X PBS
 - 25 ml 5% BSA (1.25 g BSA in 25 ml 1X PBS)
 - 420 ml dH₂O
 - 1.5 ml Triton X-100
 - Mix well, store at 4°C
- Antibody Dilution Buffer (1% BSA in 1X PBS)
 - To make 100 ml of buffer:
 - 1 g BSA
 - 100 ml 1X PBS
 - Mix well, store at 4°C
- Anti-BrdU mouse monoclonal antibody, Alexa Fluor 488 conjugate (350 µl; Invitrogen B35130)
- Draq5 (Biostatus Limited)

Method (Part 1) – Adding BrdU to Experiment

8. Add BrdU labeling reagent (1:100 dilution) to cell culture media
9. Sterile filter BrdU media before adding to gels
10. Add BrdU media to gels 12 hours prior to fixation (other cell types may need doubling time to be determined)
11. Incubate at 37°C

Method (Part 2) – Fixation and Staining

23. After 12 hours incubation with BrdU, aspirate media, wash once with warm PBS, then fix in 4% PFA for 24 hours (store at 4°C)
24. Aspirate 4% PFA, store gels at 4°C in 70% EtOH (until staining begins)
25. Aspirate EtOH, wash 3X in 1X PBS on shaker for 5 minutes each.
26. Add 1.5M HCl and incubate for 30 minutes at room temperature.
27. Aspirate HCl and wash 2X with 1X PBS on shaker for 5 minutes each.
28. Block samples in Blocking Buffer for 60 minutes at room temperature.
29. Aspirate blocking buffer, add conjugated antibody (anti-BrdU 488) to each sample
 - 1:100 dilution of antibody in 1% BSA
 - Add 50 µl to each sample
 - Incubate at room temperature in the dark for 2 hours
30. Incubate samples with 1:1000 dilution Draq5 in 1X PBS for 30 minutes

- Note: this step can be combined with the previous (add Draq5 to the BrdU antibody solution)
31. Store in 1X PBS at 4°C until imaging
- Note: samples are best imaged within 24 hours of staining

Immunofluorescence on paraffin sections

Melt wax by placing slides in 55C oven for ~10 minutes

*Set slides on their side, against the wall of a box, so that wax melts down, off the sample

Deparaffanization and Rehydration

1. Xylene, 3 changes for **3 minutes each**
 2. 100% ethanol, 1 changes, **5 minutes**
 3. 95% ethanol, 1 change, **2 minutes**
 4. 70% ethanol, 1 change, **2 minutes**
 5. Rinse gently in de-ionized water (gently pipette and aspirate dH₂O on sample)
- Circle each sample with hydrophobic pen, let dry
 - Optional antigen retrieval (protocol developed by Jingjing Zhou and Caitlin Bowen, Summer 2012):
 - Lay slides flat in container
 - Pipet enough 2N HCl to cover samples onto each slide
 - Incubate for 70 minutes at 37C
 - Aspirate 2N HCl
 - Pipet enough 0.1M Sodium Borate (pH 8.5) to cover samples onto each slide
 - Incubate for 12 minutes at Room Temp
 - Rinse 3x in PBS for 5 minutes each
 - Alternative antigen retrieval (developed by Jingjing Zhou)
 - Tri-sodium citrate buffer:
 - Weigh out 2.94g Tri-Sodium Citrate
 - Add 1000mL distilled water
 - pH to 6.0 with 1M HCl
 - Add 0.5mL Tween-20
 - Add Sodium Citrate buffer to tip box
 - Warm buffer by heating in microwave on High for 1 min
 - Add slides to dish
 - 5 min on “warm”
 - 5 min rest
 - 5 min on “warm”
 - 2 min rest
 - 2 min on “warm”
 - 20 min cool to RT
 - Rinse 1x in PBS
 - Apply enough 10% Goat serum (in 1X PBS) to cover sample (about 75uL per sample)
 - Incubate 60 min at 37°C or overnight at 4°C

Primary antibody application:

1. Make 100 μ L per sample of 1 $^{\circ}$ antibody (1:500 in antibody dilution buffer)
Antibody dilution buffer: 1% BSA in 1x PBS +0.3% Triton-X (Cell Signaling Tech)
*Note: If in doubt of pipetting small volumes, err on the side of higher concentration
2. Gently aspirate 1% BSA
3. Dry slide very carefully with a kim wipe by touching a corner of the wipe to the edge of the liquid on your sample
*Do NOT touch your samples with the kim wipe
4. Apply primary antibody
5. Incubate overnight (at least 8 hr) at 4 $^{\circ}$ C

Secondary antibody application:

Aspirate 1 $^{\circ}$ ab solution

Place slide(s) in dish (ex: pipet box lid) with enough PBS to cover

Wash 3x in PBS on shaker, 5 minutes each

While shaking, prepare 2 $^{\circ}$ ab solution:

Fluorescent antibody: 1:200

Draq 5: 1:1000

In solution of 1% BSA+PBS

Ex: 2.5 μ L goat anti-rabbit 568 + .5 μ L Draq 5 + 497 μ L 1% BSA+PBS = 500 μ L 2 $^{\circ}$ ab solution

Apply 100 μ L 2 $^{\circ}$ ab solution to each sample

Incubate for 30 minutes at room temperature, *cover with foil*

3 washes

Wash 3x in PBS on shaker, 5 minutes each

Dehydration (optional, unclear from the literature if this degrades your fluorescent signal or not):

70% ethanol, 1 change, 3 min

95% ethanol, 1 change, 3 min

100% ethanol, 2 changes, 3 min each

Xylene, 3 changes, 3 min each

Rinse gently in deionized water

Mounting

Remove ProLong Gold antifade reagent (Invitrogen P36934) from freezer, allow to come to room temp

Do not apply external heat

Remove excess liquid from specimen using kim wipe, as described above

Apply 1 drop of medium to the sample

Or to the slide if sample was mounted on a coverslip

Gently lower coverslip onto slide, avoid trapping air bubbles

Allow slides to cure 24 hrs at room temperature. *Protect from light!*

If necessary, seal the edges of the coverslip with nail polish (clear) or hot wax

Long term storage: RT, fridge, or -20 freezer

Prepared by: Emily J. Howell, 4.7.11

Edited: Calvin Knapp, 8.4.11

Edited: Emily Farrar (nee Howell) 6.12.13 with consultation with Caitlin Bowen

Edited: Emily Farrar (nee Howell) 6.28.13 with consultation with Caitlin Bowen
(alternative antigen retrieval, addition of antibody dilution buffer)

Immunofluorescence of cells on slides:

Cell culture: PAVEC

Divide slide into three sections and outline outer edge with hydrophobic pen
Sterilize under UV for > 30min
Apply ~100uL collagen (50ug/mL) to each section
Incubate at 37C for >20 min
Meanwhile, trypsinize and spin down cells
Resuspend cells in 200uL x (# of sections)
Ex. For 3 slides = 9 sections = 1.8mL
Aspirate excess collagen
Apply cells to each section
Let adhere for > 2 hours (until cell spreading is observed)
Ideally, let grow overnight.

Immunofluorescence:

Rinse with PBS
Fix in 4% PFA for 20 min at 37C or overnight at 4C
Rinse with PBS
Permeabilize with 0.5% Triton-X for 10 min on rotator
1 mL PBS + 5uL Triton-X
Wash 3x with PBS for 5 min on rotator
Block in 1% BSA for 30 min at room temp
Make primary antibody solution
1:100 primary antibody
+PBS
Aspirate BSA
Apply 100uL primary ab to each section, at 1:100 dilution
Incubate 1 hr at Room Temp
Wash 2x in PBS for 5 min on rotator
Make secondary antibody solution
1:100 secondary antibody
+1:100 Draq 5
+1% BSA
Apply 100uL secondary antibody to each section, at 1:100 dilution
Incubate 30 min at Room Temp
Apply small drop of ProLong Gold anti-fade mounting medium
Carefully apply coverslip
Fix for 24 hrs

Immunofluorescence on collagen hydrogels

Day 1

Fixation & Blocking

1. Aspirate medium
2. Wash once with PBS (repeat until pink color is gone from solution)
3. Add 4% PFA, incubate at least 4 hours at 4°C
 - PFA moves approximately 1 mm per hour
4. Aspirate 4% PFA, add PBS (or 70% EtOH if you want to store them for up to 2 wks)
5. Transfer gels from 4-well to 6-well plate (carefully, maintain up/down orientation) (not necessary)
6. Wash gels 3X in lots of PBS, 15 minutes each on rotator
7. Permeabilize with 0.2% Triton-X 100 for 10 minutes on rotator (10 mL PBS, 20 μ L Triton-X)
8. Wash 3X with PBS, 15 minutes each on rotator
9. Add blocking solution, incubate overnight at 4°C, **or 1 hour at 37°C**
 - 1% BSA in PBS (blocking solution, 2 mL/well) (recommended also 10% goat serum)

Day 2

10. Transfer gels back to 4-well plate
11. Aspirate blocking solution and add primary antibodies in PBS, 100 μ L/well
 - α SMA (spring biosciences, rabbit anti-human, 1:100)
 - QH1, for quail (mouse anti-human, 1:100)
 - *ex. Have 4 x 7 gels = 28 gels*
28 x 50 μ L = 1400 μ L (make 1600 μ L)
16 μ L QH1 antibody
16 μ L α SMA antibody
1568 μ L PBS
12. Incubate with primary antibody overnight at 4°C in a humidified chamber (fridge)

Day 3

13. Transfer gels to 6-well plate (maintain up/down orientation)
14. Wash 3X with PBS, 15 minutes each on rotator
15. Transfer gels back to 4-well plate
16. Add secondary antibody at 1:100 dilution in PBS + 1% BSA
 - 100 μ L per gel, 3 mL PBS, 30 μ L secondary antibodies (QH1: goat anti-mouse 568
 α SMA: goat anti-rabbit 488)
 - Additionally add Draq 5 at same time as secondary antibodies
 - Rhodamine Phalloidin at 1:40 dilution
17. Incubate with secondary antibody for 2 hours at RT
18. Transfer gels to 6-well plate
19. Wash 3X with PBS, 15 minutes each on rotator

20. Transfer gels back to 4-well plate
21. Add Draq 5, 1:1000, 100 μ L per gel
 - 3 mL PBS, 3 μ L Draq 5
22. Incubate for 30 minutes at RT
23. Store in 2 mL PBS

After final Draq 5 staining, to prepare gels for imaging:

If using Zeiss (images from bottom)

Transfer gels to a 6-well plate, in plenty of 18 MOhm deionized water

Bring downstairs:

6-well plate with gels

squirt bottle of 18 MO water

a few slides or coverslips

disposable spatula

4-well plates (with some PBS in them) for storing gels after imaging

Flash drive

Once downstairs, move gel carefully from well to slide, maintaining orientation

Squirt enough water onto the gel to keep it from sliding around... will this work? Practice before confocal training

Place slide carefully onto microscope stage

After imaging, transfer gel into its well in the 4-well plate, re-use slide

Roche X-tremeGene 9 Transfection (PAVIC, PAVEC, L-cell)

By: Caitlin Bowen, modified by EJJ

1. Culture cells on plate for 24 hours in antimicrobial-free media (No P/S, 5% serum)
2. Dilute the reagent with 1x DMEM to a concentration of 3 ul reagent/100 ul medium using a sterile tube and gentle mixing.
3. Add 1 ug of plasmid DNA to 100ul of diluted transfection reagent. Mix gently. *Use a minimum of 100 ul of diluted reagent; lower volumes may decrease the efficiency.*
4. Incubate the reagent/DNA mixture for 30 minutes at room temperature. Mix gently.
5. Add the reagent in a drop wise manner according to the chart. There is no need to remove the growth media. Gently swirl for 30 seconds to ensure even distribution.
6. Incubate for 18-72 hours.

Vessel	Total volume of media (ml)	Amount of transfection complex to add	Total DNA added (ug)
96-well plate	0.1	5 ul	0.05
48-well plate	0.3	15 ul	0.15
24-well plate	0.5	25 ul	0.25
6-well plate	2.0	100 ul	1
T-25 flask	6.0	300 ul	3

Bacterial Transformation of Plasmid in *E. coli*

By: Katy Fang

Preparation of LB broth: (feeds bacteria)

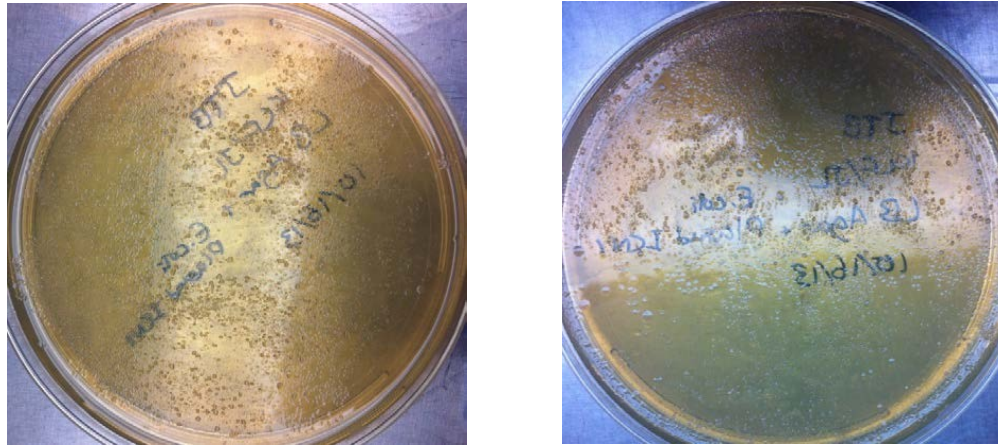
1. Get 500 mL glass bottle with purple screw top lid
2. Add 500 mL 18 M Ω water
3. Add 10 grams LB broth powder, mix well
4. Partially seal with lid (when it starts to tighten, pull off slightly), seal with autoclave tape, label with name, date, contents
5. Autoclave program: liquid cycle, 15 minutes, slow

Preparation of LB agar: (plates to grow bacteria)

1. Get 500 mL glass bottle with purple screw top lid
2. Add 50 mL 18 M Ω water or distilled (DI) water for each plate
3. Add 1 LB agar tablet for each plate, mix well until dissolved (manually or using stir bar)
4. Partially seal with lid (when it starts to tighten, pull off slightly), seal with autoclave tape, label with name, date, contents
5. Autoclave program: liquid cycle, 15 minutes, slow

6. Turn on fume hood (light and fan); before use, wipe with ethanol; wait 5 minutes for clean air to push out room air (spray everything with ethanol before placing it inside hood)
7. Open sterile petri dishes inside fume hood, label bottom and lid with name, date, contents
8. Thaw appropriate antibiotic (*on top shelf of -20°C freezer in "Transfection Reagents" box*)
 - A) 100x kanamycin (so for 100 mL agar, use 1 mL kan)
 - B) 1000x ampicillin (so for 100 mL agar, use 100 μ L amp)
9. After autoclave is finished, let cool to \sim 55°C (can touch bottle for 3 seconds with gloves)
10. Add antibiotic to agar, stir
11. While agar mixture is still warm, pour \sim 40-50 mL into each dish (as long as it covers the bottom of the plate, it should be fine)
12. Let agar cool and harden (color should lighten), place lid only partially on to prevent condensation from dripping onto agar
13. When solidified, you can store the plates in the 4°C cold room for long-term storage

Examples of plates with grown colonies



Transformation in NovaBlue Competent Cells:

1. Prepare ice bucket, 42°C water bath (place centrifuge tube with water in blue and grey heater next to Andrew's bench), and fume hood
2. For each set of plasmids, get ~10-20 μL of competent cells (each yellow tube should have ~50 μL) (*cells are in -80°C freezer in second compartment from the top*)
3. Thaw cells on ice for 2-5 minutes
 - *Don't touch the bottom of cells as heat from fingers can cause damage
 - *Perform all steps on ice to avoid heat shock unless told otherwise
4. Separate cells into separate tubes for each plasmid to be transformed (~10-20 μL cells each)
5. Thaw SOC medium at room temperature (*in "Transfection Reagents" box*)
6. Resuspend competent cells by flicking tube
7. Add 1 μL plasmid to each tube of competent cells
8. Incubate on ice for 5 minutes
9. Heat shock tubes in 42°C water bath for 30 seconds
10. Place back on ice for 2 minutes
11. Add ~60 μL SOC medium (if 10 μL cells) to competent cells tube (6 x volume of competent cells = volume of SOC medium to use), place back on ice
12. In fume hood, add cells + plasmid to plate
13. Using disposable bent plastic bacteria spreader, spread bacteria around surface of agar until bacteria is all over the plate and has become drier
14. Cover plate with lid and store in 37°C incubator upside-down (to prevent condensation from dripping onto bacteria) in Weill basement B07 for 12-16 hours

Selecting colonies for miniprep:

1. Prep fume hood
2. Get a 15 mL conical tube for each colony you plan on choosing
 - *Recommended: choose at least two colonies per plate
 - *Try to avoid huge colonies with a zone of space around them – these colonies may have grown so fast they ate the colonies around them, and they might not have antibiotic resistance anymore
3. Transfer 5 mL LB broth to tube, warm to room temperature (can use water bath in fume hood room)
4. Add corresponding concentration of antibiotic to broth (e.g. 5 mL broth = 5 μ L ampicillin)
5. Bend the tip of a sterile pipette tip (smallest tips work well), scrape one colony of bacteria and drop into conical tube
6. Place tubes onto rocking incubator at 37°C, leave overnight (or 8 hours)
7. Parafilm shut agar plates and store in cold room (at 4°C) until certain that plasmid has been isolated
 - *If plates are not very crowded with colonies, next time you can increase the volume of competent cells (original procedure suggests 50 μ L); on the contrary, if the plates are overcrowded (which is a bigger problem), use a lower volume of cells

Miniprep:

**Used to confirm presence of plasmid inside bacteria

1. Take 1.2 mL from 5 mL of bacterial culture and place into 2 mL microcentrifuge tube (in white box on shelf above centrifuge)
2. Spin at 13000 RPM for 1 minute
 - *If need to pause, freeze bacteria pellet at -80°C
3. Remove supernatant and resuspend in 250 μ L Buffer P1 (found on bottom shelf of deli fridge, small bottle is for miniprep)
 - *Make sure P1 has LyseBlue and RNase A added
 - *Place supernatant in container with bleach
4. Resuspend up and down multiple times until sufficiently mixed (~10 seconds)
5. Immediately after mixing P1, add 250 μ L Buffer P2 and invert 4-6 times to mix
 - *Solution should turn blue from LyseBlue reagent; if dark blue dots appear, did not mix well enough
 - *Do next step within 5 minutes; reaction shouldn't sit longer than 5 minutes
6. Add 350 μ L Buffer N3, invert 4-6 times to mix
 - *Don't add N3 tip to bleach → bad reaction
 - *N3 should make solution clear
7. Leave solution on ice for a few minutes, wait for white fluffy protein to precipitate out
8. Centrifuge for 10 minutes at 13000 RPM
9. Take out blue QIAprep spin columns

10. **Save** supernatant, apply to spin column, put entire thing into centrifuge
11. Centrifuge for 1 minute at 13000 RPM, **discard** flowthrough
 - *Do not add to bleach
 - *Filter tip has DNA – do not touch to anything
12. Wash spin column by adding 750 μ L Buffer PE
 - *Make sure ethanol has been added to PE before using
13. Centrifuge for 1 minute at 13000 RPM, **discard** flowthrough
14. Centrifuge again for 1 minute at 13000 RPM to dry membrane
15. Add small blue column to a dry new centrifuge tube, discard outer tube
16. Add 20-30 μ L DEPC water to center of spin column, let stand for 1 minute
 - *Instead of DEPC water, can use Buffer EB
 - *Be sure to switch pipette tips
17. Centrifuge for 1 minute at 13000 RPM
 - *Keep lids on; position sideways and flat against centrifuge so they don't break; cover with centrifuge lid so lids don't fly around
18. Discard column; bring samples, blank (DEPC water), 1 μ L pipette, and tips in ice bucket to Nanodrop (in Shen lab, Weill first floor)
 - *Expected concentration: ~80-100 ng/ μ L

Troubleshooting for Miniprep:

If miniprep is unsuccessful, a new trial can be improved by selecting multiple colonies from the current plate and retrying miniprep on all new colonies

Gel electrophoresis troubleshooting:

Make 60 mL gel with:

Agarose – 1% w/v gel

For 60mL gel, you need 0.6g agarose

Ethidium bromide (EtBr) – makes DNA fluoresce

Needs to stay in

fume hood

Ratio of 60 mL

gel:9 μ L EtBr

TAE (1x) buffer – rest of the volume

1. Weigh out agarose
2. Add agarose to 60 mL TAE
3. Using the microwave in the Shuler lab, microwave for 1 ½ minutes
4. Check. Heat for 30 more seconds if necessary
5. Add EtBr (should be done inside fume hood in the main room)
6. Pour solution into tray, wait for solidification

7. Precipitate nucleic acids in the same volume of isopropanol as sample (so you are doubling the volume of tubes)
8. Vortex to mix
9. Centrifuge at 13000 RPM for 3 minutes, pour off supernatant
10. Rinse walls with 500 μ L of 70% EtOH (tube in Emily's Styrofoam tray) – don't vortex
11. Centrifuge again at 13000 RPM for 3 minutes, pour off supernatant
12. Dry tube, resuspend in 10 μ L of Tris
13. Move 5 μ L of your DNA sample into small PCR tubes
14. Add 1 μ L Blue Juice into each PCR tube
15. Mix with the quick spinner
16. Take solidified gel out and place into electrophoresis machine
- *Gel should be completely submerged in the TAE buffer
17. Gently insert samples into wells – 5 μ L for the ladder (first sample), 6 μ L for the rest
- *Make sure pipette tip isn't too far into the well
18. Turn on electrophoresis machine
- *Should take 20 minutes
- *It is done when blue bands are on the bottom of the gel
19. Take finished gel to Shuler lab machine and use Quantity One software to image (protocol below)

Quantity One Software:

Go to Quantity One

Turn on machine (switch in back, lower left-hand side) Light mode: VPI white

Slide gel out of tray into machine

File: chemidoc

Open iris to increase light, zoom to adjust image

Set on machine: light source – Trans UV

Close iris almost all the way, then live/focus, then autoexpose

If blurry, close iris more

After gel is imaged, save in a folder, export as tiff image, click "Export"

Nanodrop:

1. Have ice bucket, samples, blank, pipette, and tips with you
2. Go into Nanodrop 2000
3. Cover Nanodrop surface with 1 μ L blank, cover
4. Click "blank," gently wipe nanodrop with Kimwipe
5. Cover scanner hole with 1 μ L sample
6. Type in name of sample, click "Measure"
7. Write value on tube, wipe down Nanodrop
8. Repeat steps 5-7 as needed (recommended: 3 runs per sample)

9. Export data as .xml, e-mail to yourself/Emily
- *Blank (DEPC) must be pure and fresh!

Inoculation of colony – prep for maxiprep:

Instructions for culturing in multiple tubes to increase chances of maxiprep success

1. Transfer 25 mL LB broth to each 50 mL conical tube
 2. Warm to room temperature in water bath
 3. Add corresponding concentration of antibiotic
 4. Transfer 250-300 μ L bacteria culture to each tube
- *If waiting a short time, use higher volume (300 μ L)
*If waiting a long time, use lower volume (250 μ L) (avoids overcrowding)
5. Repeat step 4 in another tube of broth
 6. Place conical tubes into 37°C shaking incubator in Weill basement overnight

Maxiprep:

Used to propagate plasmids

Pre-experiment:

Make sure Buffer P1 has RNase A and LyseBlue reagent added

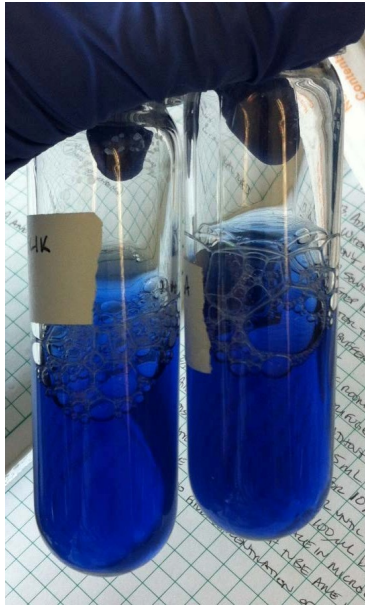
Chill Buffer P3 in 4°C fridge next to centrifuge in lab

Set ultracentrifuge in Shuler's lab to 4°C (probably take

~15 minutes) Label tubes, prepare ice bucket

Autoclave white lidded ultracentrifuge tubes

1. Prepare ice bucket, maxiprep kit, large bottle of Buffer P1 from fridge
 2. Remove bacteria cultures from incubator
 3. Add 25 mL culture to white lidded ultracentrifuge tube, label tubes
 4. Shuler's lab: weigh centrifuge tubes so weights are same to first decimal place (discard excess and pipette tips in beaker of bleach)
 5. Centrifuge for 15 minutes at 6000 RPM at 4°C (use F0650 rotor, make sure this is set on centrifuge)
- *Make sure not to put much more than 25 mL into one white-lidded centrifuge tube; tube might not be able to withstand much extra weight at this speed
6. Discard supernatant in bleach
- *Can pause here, freeze bacterial pellet in -20°C freezer
7. Resuspend bacteria pellet in 10 mL of Buffer P1
- *If you have multiple pellets of same plasmid, resuspend all pellets together in the same 10 mL of P1 – concentrates large amount of bacteria to make propagation easier
8. Mix sufficiently by resuspending up and down repeatedly
 9. Add 10 mL Buffer P2 to centrifuge tube, invert 4-6 times until cloudy solution is homogenous and clearer
- *Solution should turn blue
*Don't vortex to mix



After adding Buffer P2, solution turns a deep blue color



Immediately after adding Buffer P3, you can start to see the color change



Invert a few times, and the entire solution will turn white and clear

*Don't let solution sit longer than 5 minutes

10. Add 10 mL Buffer P3, invert 4-6 times or until mixed well enough (can shake but don't vortex), incubate in ice bucket for 20 minutes

*Make solution clear, white fluffy protein will precipitate out

11. Mix and weigh samples, centrifuge for 30 minutes at 20000xg (RCF) at 4°C

12. Immediately transfer supernatant to clean ultracentrifuge tubes

*Remove supernatant using 25 mL pipet tips, carefully keep in tips while cleaning tube

*Clean centrifuge tubes using distilled water (no soap), make sure all protein is out

13. Centrifuge supernatant 20000xg (RCF) for 15 minutes at 4°C

14. While centrifuge is running, place filter tips (QIAGEN-tip 500) from kit onto 50 mL conical tubes using the filter tip holder

15. Add 10 mL Buffer QBT to wash tip, allow to empty via gravity flow (should take about 3 minutes)

16. When centrifuge is finished, immediately place supernatant into filter tip

*Don't wait too long or else tip could dry out (though upper frit will protect column matrix)

17. When solution has stopped dripping, add 30 mL Buffer QC to tip (tip should hold at most 30 mL)

18. Repeat step 17 (need two 30 mL washes)

19. Continually empty out tubes in waste beaker or solutions will not go through filter

20. Place filter tips on clean centrifuge tubes, secure with tape, leave some air to allow filtering

*Clean tubes with distilled water again

21. Add 15 mL Buffer QF to elute DNA stuck in filter

22. Add 10.5 mL of room temperature isopropanol directly to centrifuge tube, **mix well** by shaking or else DNA will not precipitate out



23. Weigh and centrifuge at 15000xg (RCF) for 30 minutes at 4°C

*To help identify where DNA pellet will be, mark outside of tube with removable marker, centrifuge will push pellet to most outer edge furthest from center of centrifuge

*Isopropanol pellets will be glassy, difficult to identify, and easily detached from the side of the tube; even if you can't see it, it might still be there, and you should proceed with the following steps carefully

*Can also centrifuge at a higher RPM and/or for longer time

24. Remove supernatant slowly without disturbing DNA pellet

- *Remove supernatant into a clean centrifuge tube; if DNA pellet detaches accidentally, can centrifuge supernatant again to retry
- 25. Wash DNA pellet with 5 mL 70% ethanol, swirl around pellet
- 26. Centrifuge at 15000xg (RCF) for 10 minutes, gently decant supernatant
- 27. Air dry pellet for 5-10 minutes or until completely dry (ethanol can degrade pellet DNA)
- 28. Redissolve DNA pellet in 50 μ L DEPC water, place in new microcentrifuge tube
- *Make sure bottom and sides of tube are washed
- 29. Nanodrop to find concentration of DNA
- *Expected concentration >1000 ng/ μ

PAVEC Electroporation (Transfection)

By: Christopher Mosher, edited by EJJ

Time: ~45 min

Materials: PAVEC media, PAVEC electroporation media (5% FBS, no antibiotic (Pen-Strep)), PBS 1X, collagen stock (3.84 mg/mL) and 18 Mohm sterile water OR prepared collagen solution (50 ug/mL), E2 buffer, Resuspension buffer (all at 4C, E is top shelf and R is third shelf down), trypsin (-20C), 1 mL and 200 uL pipettes and tips, 1.5 mL autoclaved ependorf tube (1 per plasmid to be used), Neon Transfection System (100 uL kit includes tips and chamber) located under the cabinet in the cell room along with the power supply, electroporation pipette and chamber

Background: Electroporation passes current through the cell membrane in order to open pores for transfection. In the kit, the tips can be used two times and the chamber can be used ten times before replacing.

10 ug plamid/transfection, 1 million cells/transfection

110 uL R buffer/1 million cells

Calculations for collagen solution:

$$\begin{aligned}m_1 v_1 &= m_2 v_2 \\(50 \text{ ug})(50 \text{ mL}) &= (3.84 \text{ mg})(X \text{ mL}) \\(0.05 \text{ mg})(50 \text{ mL}) &= (3.84 \text{ mg})(X \text{ mL})\end{aligned}$$

$X = 0.651 \text{ mL}$ collagen stock to be added to 18 Mohm sterile water

Protocol (2 transfections at once):

1. Plug in power supply, then turn it on
2. Put the chamber in the base attached to the power supply
 - a. Ensure that the chamber contains 3 mL E2 buffer
3. Get bucket of ice and add to it E2 buffer, R buffer, plasmid (RelA used here is the P65 subunit of NF κ B), and collagen stock (3.84 mg/mL)/sterile water OR prepared collagen solution
4. Put PAVEC media, PAVEC E media, trypsin, and PBS 1X in the 37C water bath
5. If collagen solution is not prepared, make it by adding 0.651 mL collagen stock (3.84 mg/mL) to 50 mL 18Mohm sterile water (see above calculations)
6. Add 1 mL of 50 ug/mL collagen solution to two T-25 flasks for transfection, and 7 mL to a T-175 flask for plating cells pelleted but not used for transfection → Sit for 20 min. at room temperature
7. Use 2 million cells for two transfections (wash, trypsinize, dilute, spin down, remove supernatant, resuspend, COUNT CELLS → all from cell thawing protocols)
8. Pour collagen out of the three flasks. Add ~3.5 mL Electroporation media to the two T-25s, and ~22 mL PAVEC media to the T-175
9. Spin down 2 million cells and use 220 uL R buffer to resuspend the cell pellet

10. Add this solution to the ependorf tube along with 20 ug plasmid (6.7 uL in this case). Mix by stirring with pipette and flicking the tube
11. On the power source, select Database→5. Conditions: 1600 mV, 20 sec, 1 pulse, "PAVECRelA2" (or select alternative protocol for different plasmid)
12. Add solution from centrifuge to the gold pipette, put in chamber, press start only if there are no bubbles
13. *If there are bubbles, pipet solution back into tube and re-pipet, slowly and carefully
14. *Watch gold tip of pipet carefully after pressing start. If you see an orange spark, there was a bubble in the solution and the electroporation has not worked. Avoid this. If it happens, count this as one "use" of the tip and go back and repeat steps 12-13.
15. After the current is passed through the sample, pipet the solution gently into the prepared T-25 flask and swish around
16. Repeat for the remaining sample, and put both T-25s in the 37C incubator with the caps facing right, propped up on the edge of the incubator shelf so as to grow flask at a slant, encouraging endothelial cells to develop cell-cell contacts.
17. With the remaining cells, resuspend in 22 mL media in a T-175 and store in the 37C incubator.

PAVEC transwell protocol

Materials:

For cells:

- PAVEC (P4 to P6 is fine)
- PAVEC media
- Trypsin
- 50ug/mL collagen
- PBS

For gels:

- Stock collagen (3.5-4.0 mg/mL)
- 0.1M NaOH
- Sterile filtered 18MOhm water
- FBS (small aliquot)
- 3x D-MEM (with Sodium Bicarb added)

For post-experiment processing:

- Collagenase (aliquots in large -20 freezer)
- Autoclaved 1.5mL eppendorf tubes
- RLT buffer
- Beta-merc

Other:

- Autoclaved 1000uL tips
- 1000uL pipet
- Bleach
- BD Falcon™ Multiwell 24 well insert system. 3 µm pores, High Density PET

Membrane (351182)

- 24 well plate (x2)
- Desired treatment (ex. TNFa, TGFb)
- VWR plastic spatula (for transferring gels)

Directions:

Put PAVEC media, PBS, trypsin in water bath to warm

Prep work:

- In hood, transfer transwell insert to a new 24-well plate
- Add 100uL of 50ug/mL collagen to each membrane that you plan to use
 - *Coats the surface so VECs can adhere
- Incubate for at least 20 minutes

Make gels:

- Use “Collagen gel only disk template” spreadsheet from Quick Refs folder
- Enter number of gels, stock collagen concentration
- Enter 0.3mL for gel volume (is enough to come into contact with membrane)
- Print sheet
- Get ice bucket, put all gel materials on ice + 1 extra centrifuge tube for mixing
- In hood, add ingredients in order listed on spreadsheet to extra centrifuge tube
 - *EXCEPT add NaOH last

*Mix well, especially collagen and NaOH (should turn yellow, then pink)

Carefully pipet 300uL into each well of 24-well plate

*No bubbles!

*Shake/tap plate to spread gel if necessary

In hood, transfer transwell insert (coated with collagen) onto the gels while they are still liquid

Incubate gel + membrane + collagen coating for > 20 min

Obtain cells:

Trypsinize, count, and pellet cells as if you were passaging them

*Calculate number of cells needed using hemocytometer

*Use 100,000 cells/well (1e5)

Resuspend cells in enough PAVEC media for about 100uL/well

Seed cells onto transwell membrane

Treatment:

1 hour after seeding, add treatment in 300-500uL of media/well

Post-processing:

Prep work:

Thaw collagenase

Add 1.0mL of collagenase to desired number of 1.5mL eppendorf tubes, enough for 1/well

Incubate eppendorfs + collagenase at 37C, until needed

In non-sterile eppendorfs, add 350uL RLT buffer + 3.5uL beta-merc per tube (for RNA storage)

Coat desired number of wells in a 24 well plate with 50ug/mL collagen

Gels:

Remove transwell system from incubator

Gently lift transwell membrane insert off of gels

With plastic spatula, transfer gels either into collagenase (cell isolation/culture) or RLT buffer

Replace membrane onto 24 well plate

Put collagenase + gel into 37C incubator

Incubate 25 minutes

Spin down collagenase solution, 5 min at 1000 rpm

Aspirate supernatant

Resuspend in 100uL of PAVEC media

Plate each tube onto one well of a collagen-coated 24 well plate

Digest gels in RLT buffer by vortexing, then put in -80C

Cells:

Working with transwell membrane:

For samples for rtPCR:

Rinse each membrane with PBS (gently, but well)

add 50uL trypsin to each membrane well

Incubate for 10 min at 37C
Stop rxn with media
Pipet up media + trypsin + cells
Scrap membrane gently with pipet tip, rinse membrane well
with media
Transfer to empty eppendorf tube
Spin down in tabletop centrifuge for 5 min at 1000rpm
Aspirate media + trypsin
Rinse pellet/resuspend in sterile PBS
Spin down in tabletop centrifuge for 5 min at 1000rpm
Aspirate PBS
Resuspend in RLT buffer +beta merc solution, transfer to RLT buffer
centrifuge tube

Written by: Emily J Howell
Date: Oct 24, 2011

PCR for Mouse Genotyping

DNA Extraction – Mouse ear snip

- 1- Ear snips taken on when pups are ~14 days (14-21 days) old.
 - a. Ear snips are about 1-2 millimeter diameter
- 2- The ear snip is put in a tissue digesting mix composed of:
 - a. 87ul DEPC- treated Water
 - b. 10ul 10x PCR buffer
 - c. 3ul of ProK (**10mg/mL**)
- 3- The digesting solution is then:
 - a. Incubated at 55°C over-night in thermocycler
 - b. ProK is then boiled (to deactivate) in thermocycler
 - i. 98°C for 10 minutes and then held for 20min at 20°C
 - ii. “BOIL” program on thermocycler

DNA Extraction – Mouse Tail

- 1) 300 ul Tail Buffer/sample
- 2) 1:20-1:50 dilution of Proteinase K
- 3) Incubate at 55 degrees on heat block overnight
- 4) Add equal volume of isopropanol to each sample
- 5) Vortex to precipitate DNA
- 6) Spin @ 13000 RPM for 3 minutes
- 7) Pour off supernatant
- 8) Add 600 ul 70% EtOH to each sample
- 9) Spin @ 13000 RPM for 3 minutes
- 10) Pour off supernatant and let dry upside down for ~5 minutes
- 11) Add ~100ul ddH₂O (this can change to increase or decrease DNA concentration)

To load/run a thermocycler program

1. Highlight “FILES”, hit Enter
2. Highlight “LOAD”, hit Enter
3. Scroll down to your program, hit Enter
4. Check that program is what you want, hit Exit
5. Hit Enter (affirms you do not want to save)
6. Hit Start

PCR technique

- 1- Prepare Master Mix for specific #samples that will be run on gel in one tube
 - a. Thaw all vials at room temp, EXCEPT polymerase (thaw on ice)
 - b. Combine calculated volumes of H₂O, 2x GoTaq Green master mix, and primers in one eppendorf (1.5mL) tube
 - c. Put tube on ice

- 2- Dilute sample DNA in a 1:10 ratio
 - a. Pipet 1ul DNA from the digester tube + 9ul H₂O (1:10 dilution)
 - b. Transfer 1 uL of the diluted solution to a new tube
 - i. Place your pipet tip against the side wall of the tube and depress slowly, so that you can observe the entire volume exiting the tip
 - c. 1 uL of each diluted sample should be in each tube in the strip
 - d. Label tubes with mouse ID number
- 3- Add designated volume of Master Mix to each sample tube
 - a. Mix by pipetting up and down when withdrawing Master mix from the eppendorf tube
 - b. Mix well with DNA sample by pipetting up and down **gently** 3 times
- 4- Check tubes for any bubbles; clear bubbles with pipet tip (NEW tip each time)
- 5- Place strip tube caps firmly onto the tubes
- 6- Check the caps are completely secure – leakage will result in loss of your sample during cycling
- 7- Place strip tubes into thermocycler
 - a. Orient strips left to right, in center of cycler
- 8- Load appropriate program, hit Start
- 9- When program is finished (approx 2-2.5 hrs), use samples immediately or transfer tubes to the fridge (not freezer). Use within 3 days.

GoTaq PCR (20uL)			4/22/15
		# Reactions	7
GoTaq Mix	10 ul		70 ul
Nuclease-free H₂O	3 ul		21 ul
Primer Mix [10 uM]	2 ul		14 ul
DNA Template	5 ul		
	TOTAL	20 ul	105 ul

Go Taq Mix Ordering Options:

NEB Taq 2x Master Mix (NEB M0270L)

GoTaq® Green Master Mix (Promega M7122)

Gel electrophoresis:

Agarose gel:

Larger gel: up to 17 wells

60 mL TAE 1x buffer

1.2g agarose powder

4.5 uL Ethidium Bromide

For a smaller gel: up to 8 wells

30 mL TAE 1x buffer

0.6g agarose powder

2.25 uL Ethidium Bromide

Procedure:

1. Assemble gel mold (plate, clear tray, comb), set aside
2. Place 20uL pipet and tips in the fume hood
3. Combine TAE buffer and agarose powder in a 150 mL beaker
4. In the Shuler lab, microwave beaker for 1 minute on High
5. Remove beaker, swirl to mix
6. Microwave on High for an additional 0.5-1.5 min, checking periodically for complete disappearance of the agarose powder
7. Bring beaker back to the lab, place in the chemical fume hood
8. When beaker is cool enough to pick up with a gloved hand...
 - a. Using a 20uL pipet, add 4.5 uL of EthBr to the agar/TAE solution and swirl to mix
9. Pour hot agar solution into gel mold
 - a. Remove any air bubbles with a pipet tip
10. Let sit at room temperature for at least 15 minutes, or until solid and translucent
11. Gently remove comb
12. Transfer gel from mold to electrophoresis chamber using clear tray
13. Make sure the side of the gel with the comb holes is closest to the black lead
14. Loading samples:
 - a. Load desired ladder in the far left well
 - b. Load post-PCR DNA samples in remaining wells, noting which sample corresponds with which well
15. Close chamber, connect wires
16. Run for 50 min at 110V

RNA Isolation

By: Christopher Mosher, edited by EJJ

Time: ~1 hour

Materials (located by RNase free bench unless otherwise noted):

RNA isolation kit (includes QIAshredders with caps, RNeasy spin columns, RW1, RPE, 1.5 mL collection tubes), RNase Zap, RNase free water, RNase free 70% EtOH (Emily's bench), 1 mL pipette with RNase free tips, 1 mL RNase free centrifuge tubes, waste beaker (cabinet), kimwipe (Emily's bench), tube racks

Background:

Porcine Aortic Valve Leaflets were excised from pigs and placed in vessels for disruption and homogenization. Samples were flash frozen with LN₂ and broken down with a mortar and pestle, and stored at 4C.

Protocol:

1. Retrieve samples from -80C (2nd shelf down, right hand side)
2. Wipe down area and samples with RNase Zap
3. Vortex samples to mix
4. Centrifuge 30 seconds at 15,000 rpm
5. Transfer the supernatant (lysate, ~350 uL) to a QIAshredder spin column for each sample
6. Centrifuge 2 min. at 15,000 rpm
7. Remove QIAshredder from centrifuge, remove membrane and replace it with a lid from the kit (label the lids)
8. Centrifuge 3 min at 15,000 rpm to get protein/remaining contaminants to the bottom of the tube.
9. Return aortic valve leaflets to the -80C freezer
10. Transfer 300 uL of each sample to a RNase free centrifuge tubes
11. Transfer 300 uL (1 volume) of 70% EtOH to each tube, pipette up and down until viscosity change is no longer visible. DO NOT CENTRIFUGE
12. Transfer the volume (600 uL) to RNeasy spin columns
13. Centrifuge for 30 sec at 8,000 rcf
14. Discard flow through into a waste beaker (pour out of clear tube, tap the tube on a kimwipe to remove any excess)
15. Add 700 uL RW1 to each sample, use the same tip as long as you don't touch
16. Centrifuge 30 sec at 8,000 rcf
17. Remove the flow through as before
18. Add 500 uL RPE Buffer to each sample and centrifuge 30 sec at 8,000 rcf
19. Remove the flow through as before
20. Add 500 uL RPE Buffer to each sample and centrifuge for 2 min at 8,000 rcf
21. Transfer RNeasy spin column (pink membrane) into 2 mL collection tubes
22. Centrifuge for 1 min at full speed
23. Place RNeasy spin column into 1.5 mL collection tubes from the kit

24. Dilute with 30 uL RNase free water by adding directly to the membrane
25. Place tubes in centrifuge with clear lid facing inwards. Centrifuge for 1 min at 8,000 rcf
26. Wash the waste beaker, then use RNase Zap on hands
27. RNA solution is collected in 1.5 mL tubes after centrifugation. Add 2 uL of each sample to 0.5 mL tubes (black box above the RNA station) to be used with the NanoDrop
28. Store RNA samples at -80C

NanoDrop Protocol:

1. Put 2 uL samples on ice, take to the NanoDrop (Weill 130, LER) with gloves and RNase free water
2. Open NanoDrop 2,000 software → Nucleic Acid → No → Okay
3. Change “type” to RNA, type in sample ID, load 1 uL RNase free water onto the stage and click blank
4. Wipe the stage with a kimwipe, add 1 uL sample, and click measure. Repeat this step for all samples. When saving, use the date and nucleic acid, but add the sample name
5. Click Report, Export, and save as a Report, Excel SML spreadsheet (*.xml)

cDNA synthesis

Use iScript™ cDNA synthesis kit, according to manufacturer’s instructions:

Components	Volume per Reaction
5x iScript reaction mix	4 µl
iScript reverse transcriptase	1 µl
Nuclease-free water	x µl
RNA template (100 fg to 1 µg total RNA)*	x µl
<hr/>	
Total volume	20 µl

Reaction Protocol

Incubate complete reaction mix:
 5 minutes at 25°C
 30 minutes at 42°C
 5 minutes at 85°C
 Hold at 4°C (optional)

<http://www.bio-rad.com/webroot/web/pdf/lsr/literature/4106228C.pdf>

Q-rtPCR primer design

As taught by Gretchen Mahler and written by EJJ

1. Look up desired gene (Ensembl or PubMed)
 - a. Type in gene name and species (e.g. Sus Scrofa = pig)
2. In ensemble, Click on the red box where they have identified your gene
 - a. click on Transcript ID
 - b. choose cDNA in the left hand menu
3. Copy and paste the whole sequence into Word
 - a. Delete all spaces
 - b. Delete all but the first line of every 3 line segment (gets rid of complementary sequence and the protein transcription info)
4. Copy and paste entire sequence into Primer3
 - a. Sequence ID: animal name and gene name (e.g. Pig CDH11)
 - b. Product size: 100-150 (number of base pairs)
 - c. Click “pick primers”
5. Primers are chosen, denoted by >>> and <<<<
 - a. Amplicon is the information in between
 - b. Reverse primer is backwards and complementary to the section underlined by <<<<

Notes:

*Don't want primers too close to the beginning or end of the sequence. If this happens, restrict the base pairs Primer3 can choose from in the “include section” space

* Avoid sequences with long repetitions of G or C –could get primer dimers or folding

*Ideally, have G or C clamps at the end of your primers for secure bonding

6. Copy and paste amplicon into Word
7. Find where amplicon is in gene sequence (Ctl+F)
 - a. Amplicon should span blue/black region: this makes sure it crosses an intron-exon boundary, which excludes genomic DNA from amplification
 - b. cDNA doesn't have introns, so spanning a boundary between two exons insures you're only amplifying your cDNA
8. BLAST your amplicon using NIH website to check primer specificity
 - a. Select “nucleotide collection”
 - b. Paste in amplicon
 - c. Should see 100% match in your species of interest
 - d. Check that there are no other 100% matches

Quantitative Real Time PCR (Polymerase Chain Reaction)

By: Christopher Mosher, edited by EJJ

Time: ~3 hr.

Materials: PerfeCTa Sybr Green FastMix (Quanta) (-20C by computer, “Sybr Green” box), RNase/DNase free DEPC water, 1.5 mL tubes, tube rack, primers (forward and reverse, 4C in “Emily Working Primer Pig” Box), cDNA (-20C, small purple boxes with clear lids), white plastic well plate (on shelf above DNA area)

Background:

Transcriptase – transcribes entire library of genes

Polymerase – transcribes specific region of genes

Protocol:

1. Sign up for rtPCR machines for hours of use – most runs take ~2 hours. Best to do this 1-2 days ahead, if possible.
2. Choose samples to be run and genes of interest (always must include housekeeping gene, in our case 18S)
3. Draw plate layout in lab notebook (samples along rows, genes along columns – remember to run each gene in triplicate on each sample)
4. Get cDNA samples from -20C and primers from “Emily Working Primers Pig” box in bottom left of 4C. Need forward and reverse for each primer set.
5. Desktop → Quick Ref → rag Real Time PCR calculator
6. Enter #samples+1 into the “samples” row
7. Add appropriate Syber Green and 18 Mohm water from calculator results (given in uL)
8. Split the resulting mixture into 2 tubes (because we will use 2 primers) and pipette up/down
9. Add 22 uL (#samples+1) of forward and 22 uL of reverse primer into one of the two tubes containing the mixture
10. Add 22 uL of the other forward and reverse primer into the other tube containing the mixture (Each tube will contain Syber Green, water, and a primer set)
11. Add 19 uL of these master mixes to the appropriate wells (see figure below)
12. Add 1 uL of the control samples to the appropriate wells (see figure below)
13. Add cap strips and centrifuge in Shuler Lab (500 for 3 min.)
14. Put away cDNA at -20C, primers at 4C
15. Software: Bio-Rad CFX Manager (Desktop)
16. Emily → OK → MiniOpticon → Select Existing → Standard 54 → Next
 - a. 54 is the annealing temp, is actually 58
17. Create New → Highlight All → Select Syber → Sample Type Unknown
18. Experiment Settings: Targets=genes, Samples=C1-C7 (depends on experiment) *Give detailed names, to eliminate future confusion*

19. Load appropriate wells with sample and target names, clear unused wells, save with date, sample names and genes assayed
20. Start → Give data file a name, with date, sample names, and genes assayed.
This will take around 2 hours
21. Make sure you've signed up on the sheet behind the computer and return all materials, clean and straighten DNA area

Reaction Assembly

Component	Volume for 20- μ L rxn.	Final Concentration
PerfeCta SYBR Green FastMix (2X)	10.0 μ L	1x
Forward primer	variable	100 – 500 nM
Reverse primer	variable	100 – 500 nM
Nuclease-free water	variable	
Template	5 – 10 μ L	variable
Final Volume (μ L)	20 μ L	

Final reaction volume may vary from 10 to 50 μ L, scale all components proportionally.
After sealing each reaction, vortex gently to mix contents. Centrifuge briefly to collect components at the bottom of the reaction tube.

PCR Cycling Protocol

	Fast 2-Step Cycling	Fast 3-Step Cycling	Standard Cycling
Initial denaturation:	95°C, 30s *	95°C, 30s *	95°C, 2-3 min *
PCR cycling (30-45 cycles):	95°C, 3 to 5s	95°C, 3 to 5s	95°C, 10 to 15s
		55 to 65°C, 15s	
Collect data at end of extension step	60°C, 20 to 30s †	68 to 72°C, 10s †	60°C, 30 to 60s †
Melt Curve (dissociation stage)	Refer to instrument instructions (optional)		

<http://www.quantabio.com/pdf/manual/>

Western Blot

By: Jen Richards, Ph.D., edited by EJJ

Prepare Lysis Buffers

RIPA buffer (1 ml aliquots, store at -20°C)

Final concentration	Stock Concentration	20 ml
150 mM NaCl	2.5M	1.2 ml
50 mM Tris-HCl, pH 8.0	1M	1 ml
0.5% Sodium Deoxycholate	10%	1 ml
0.1% SDS	10%	0.2 ml
1% Igepal CA-630		0.2 ml
18 mΩ H ₂ O		16.4 ml

Protease/Phosphatase Inhibitors – *add to RIPA buffer on the day of experiment*

NaF (25 mM, 1:40 dilution from 1 M stock) – 25 μL in 1 ml RIPA

NaVO₄ (1 mM, 1:100 dilution from 100 mM stock) – 10 μL in 1 ml RIPA

Protease Inhibitor Cocktail (PIC) (1:500 dilution) – 2 μL in 1 ml RIPA (stored at -20°C)

Lysing Cells

2D Cultured Cells

1. Rinse cells twice with ice cold 1X PBS
2. Add lysis buffer (RIPA + protease/phosphatase inhibitors) to cells, incubate at room temperature for 15 minutes
3. Scrape cells and transfer to a microcentrifuge tube
4. Pipette solution several times to mix
5. Spin tubes at room temperature for 10 minutes at 15,000 rpm
6. Transfer supernatant to new microcentrifuge tubes, discard pellet
7. Flash freeze samples in liquid nitrogen
8. Store at -80°C

3D Collagen Gels

1. Warm 150μL of Laemmli buffer (per gel) to 70°C
2. Remove media from gels and rinse twice in ice cold 1X PBS
3. With pipette, transfer gel into a microcentrifuge tube
4. Spin down at 15,000rpm for 1 min at RT; discard supernatant
 - a. N.B. You can collect supernatant for later analysis of excreted proteins
5. Flash freeze pellets in liquid N₂
6. Add 150 μL of hot Laemmli buffer (70°C) to each gel. Vortex to mix and dislodge pellet
7. Incubate gels at 70°C for 10 minutes
8. Sonicate on ice 5-10 seconds per sample

9. Spin down at 4°C for 10 minutes at 16,000 rpm (CRK lab fridge mini centrifuge)
10. Collect the supernate and store at -80°C

Protein Quantification Assay

Consult Pierce compatibility table for appropriate assay for sample buffer

<http://www.piercenet.com/files/TR0068-Protein-assay-compatibility.pdf>

For RIPA buffer, use Pierce BCA Protein Assay Kit

For Laemmli buffer, use Pierce 660nm Protein Assay Kit

Protein Quantification Assay (Pierce 660nm Protein Assay Kit)

By: Christopher Mosher, edited by EJF

To make reagent: 500 mg IDCR + 10 mL 660 nm protein reagent (Western blotting shelf, above electrophoresis equipment)

1. Thaw protein samples from the -80 at room temperature
2. Vortex the protein sample and add 5 uL to the walls of microcentrifuge tubes
3. Wash the protein sample down with 45 uL of Laemmli Buffer
4. Pipette up and down to mix, and add 10 uL of the solution to the wells of a 96-well plate (N=4)
5. Add 150 uL of reagent (see above) to each well
6. Cover the well plate in Parafilm, shake to mix
7. Turn the plate reader on (Putnam Lab)
8. Open Gen5 software
9. Create new item: Experiment→Butcher_660 nm→Right click Plate1→Read
10. Plate ID: date, sample
11. Wait for tray to come out and computer to prompt you to load the plate.
Remove Parafilm and load, read
12. Save experiment under Desktop→Butcher Lab→Emily→660 nm Assay
13. Export to Microsoft Excel and save the experiment the same way, email to yourself

Protein Electrophoresis

Obtain 4-15% gradient gel from top left shelf of deli fridge (Bio-Rad 456-1085, 12-well, 20 μ L)

OR make your own gel to desired percentage as described below

Preparing Gel for Electrophoresis

1. Prepare gel-making apparatus

Materials: Casting frame and stand

Two glass plates (one is larger with white runners and one is shorter with longer tips)

Comb (thickness should match glass plate spacer thickness)

Pipettes (with long gel loading tips, VWR 1035-960-306)

15-50 mL conical tubes

Solutions: 18 m Ω H₂O

1.5 M Tris-HCl, pH 8.8

1 M Tris-HCl, pH 6.8

30% Acrylamide/BIS solution (stored at 4°C)

10% SDS

10% APS (make new every time)

TEMED (stored in flammable cabinet)

2. Assemble 2 clean glass plates. Place them in blue casting frame **on a hard surface (benchtop)** and screw into place when glass plates are both level at the bottom.

3. Insert casting frame on stand with rubber insert, and lock into place. Ensure that the glass plates have good seal against the rubber.

4. Make the **resolving (or separating) gel**

<i>Ingredients:</i>	<u>Amount of total gel</u>
18 m Ω H ₂ O	depends on gel %
1.5 M Tris	25%
30% acrylamide/BIS	depends on gel %
10% SDS	1%
Add just { 10% APS	1%
before pouring { TEMED	0.0667%

The amount of acrylamide/BIS added to the gel will depend on the desired gel percentage

Each gel requires about **7.5 mL** per gel. Gently mix by inversion before adding the APS and TEMED, then add these ingredients only when everything is completely ready to go. Invert a few times more to mix.

For 1 gel:

	8%	10%	12%	15%
18 mΩ H ₂ O	3.47 mL	2.975 mL	2.47 mL	1.725 mL
1.5 M Tris	1.875 mL	1.875 mL	1.875 mL	1.875 mL
30% acrylamide/BIS	2.0 mL	2.5 mL	3.0 mL	3.75 mL
10% SDS	75 μL	75 μL	75 μL	75 μL
10% APS	75 μL	75 μL	75 μL	75 μL
TEMED	5 μL	5 μL	5 μL	5 μL

5. Load gel solution with a pipet between glass plates, leaving about an inch at the top for the stacking gel. Make sure the gel is not leaking out of the bottom. If there is some leaking, keep adding gel solution until the gel level stabilizes. Add ~500 μL methanol to the top of the gel to straighten the top surface. Let the gel polymerize for about **20 minutes**.
6. When the gel is polymerized, pour the methanol out and rinse a few times with water. Blot dry with kimwipes (may need to absorb extra water at surface with kimwipe).
7. Make the solution for the **stacking gel (5%)**

Each gel requires 3 mL

		5% gel
	18 mΩ H ₂ O	2.1 mL
	1.0 M Tris	0.38 mL
	30% acrylamide/BIS	0.5 mL
	10% SDS	30 μL
Add just before pouring	{ 10% APS TEMED	30 μL
		3 μL

8. Transfer the solution to the top of the resolving gel between the glass plates. Make sure to suck out any bubbles that form. Fill the solution completely to the top of the glass plates. Place the comb into the space between the glass plates by sliding it in carefully. Avoid creating bubbles (note: some gel solution will spill out when inserting the comb). Let the gel polymerize for about **20 minutes**. If you are leaving the gel overnight, wrap in wet paper towels and put in plastic bag.
9. Make a 1X dilution of Running Buffer from 10X stock in a 1 L bottle (use 18 mΩ H₂O to dilute).
10. Make a 2 L of Transfer Buffer (you will need ~1.5 L, keep what you don't use today). Keep refrigerated until needed

	1 L	2 L
18 mΩ H ₂ O	700 mL	1400 mL

10X Transfer Buffer	100 mL	200 mL
Methanol	200 mL	400 mL

11. Remove casting frame from the stand (DO NOT remove glass plates). Place casting frame into the gel box. Fill the sealed area between the two gels with 1X running buffer, and then remove the combs from the gels. You should see bubbles in the wells left by the comb.
12. Wash out the wells with running buffer with a p200 pipette and a gel loading tip (be sure to wash away any remaining acrylamide/BIS).
13. Take out samples from -80°C and Precision Plus Protein WesternC Standards from -20°C to thaw.
14. Prepare Laemmli Sample Buffer to mix with samples. Use 1 part Laemmli with 1 part sample.
Example: For a 12 well comb, you will load about **20 µL of total sample (10 µL Laemmli, 10 µL sample)**. Add 50 µL β-mercaptoethanol for every 950 µL Laemmli buffer (as per product instructions). Mix in separate CLEAN microcentrifuge tubes.

Note: To use Li-Cor 4X protein sample buffer:

1. Calculate required amount of buffer to dilute each sample with 1 part buffer to 3 parts sample.
 - a. Ex: for 12-well comb, each well takes 15 µL of sample + 5 µL buffer =20 µL
 2. Prepare buffer by adding 1:10 β-mercaptoethanol to required amount of buffer
 - a. Ex: for 4 samples you will need 20 µL of buffer, so 18 µL buffer+2µL of β-merc).
 3. Mix well by vortexing
 4. Mass balance samples using protein quantification data
 5. Create mass-balanced sample aliquots for loading by combining the following in 200 µL PCR tubes:
Required amount of sample for desired # of µg + Laemmli or RIPA buffer up to 15 µL+ 5 µL buffer
4x protein loading buffer + β-mercaptoethanol keeps for 2 weeks at RT
15. Load 6-10 µL Protein Standards (ladder) to left-most well.
 16. Skip one well, then load 20 µL of Laemmli-buffered samples in each well with a p20 pipete and gel loading tips. Load samples SLOWLY to ensure samples do not spill over into adjoining wells. It is best to load samples alternating controls and treatments (for later analysis)

Standard (10 μ L) Control 1 Experiment 1 Control 2 Experiment 2

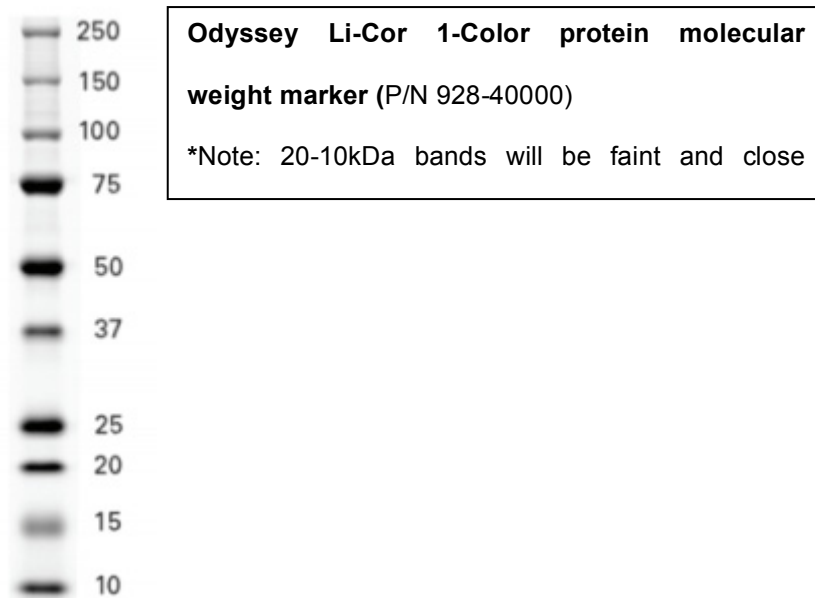
17. Fill the rest of the gel box with 1X running buffer, until buffer reaches “max fill” line on the box. Put the lid on the box and attach the electrode assembly to the power supply. *Be sure to attach the red cord to the red electrode, and the black cord to the black electrode.*

18. **Run at 100 V constant for 2.5 hours.**

Note: 1 hour is sufficient to separate bands of approximately 35-250kDa

1.5-2 hours are necessary to separate bands of < 35 kDa

Set chamber for 2.5 hours and stop run when desired separation of bands is observed in ladder

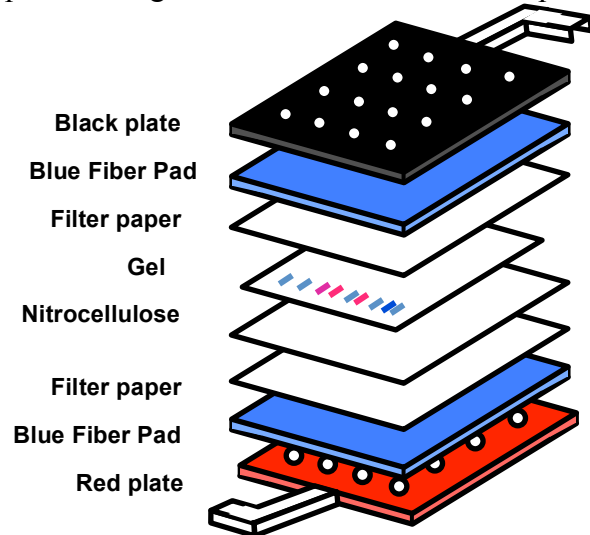


Gel Transfer

1. 10 minutes before electrophoresis is complete, prepare transfer materials: soak blue fiber pads, filter paper, and nitrocellulose membrane in transfer buffer in plastic container. Total soak time should be ~ 15 minutes.
2. When the proteins have reached the desired separation, stop electrophoresis and remove the casting frame from gel box. Unscrew the glass plates from casting frame (gel will remain between plates).

3. Carefully separate glass plates with plastic wedge tool. Cut off most of the top layer (stacking gel).

4. Layer the plates, fiber pads, filter paper, membrane and gel as depicted on the right. Keep everything soaked during layering. Remember your gel will “run to red” (charge moves from negative to positive), so have the nitrocellulose membrane between the gel and the red plate.



5. Roll the gel smooth (removing any bubbles from gel and transfer pads) with small rolling pin. Lock whole sandwich together and insert into gel box.
6. Place transfer tank with lid on in square ice bucket. Fill bucket around tank entirely with ice.
7. Fill entire tank (until max fill) with ice-cold 1X transfer buffer. Insert an ice pack and put top on transfer tank. Attach electrode apparatus.

8. **Run 30 min, 100 V constant** (note: avoid running for longer as gel can begin to melt)

Blot Staining

1. After gel has transferred, remove cassettes and mark the data and experiment on the membrane (**DO NOT** write anywhere close to the protein). **MAKE SURE** you are

wearing **CLEAN** gloves. Cut around the gel and detach gel from the nitrocellulose membrane, **making sure you only touch edges of membrane** (note: it is best to handle membrane with tweezers).

2. Wash with PBS-Tween, then block with ~10 mL Odyssey blocking buffer. Put on rocker for **1 hour**.
3. In a 15 ml conical tube, prepare 1° antibody. Dilute in Odyssey blocking buffer+0.1%Tween-20 1:1000-1:5000 (check the optimal antibody dilution as indicated with antibody instructions).

You only need enough antibody solution to cover the gel.

Large membrane in full size dish will require ~6-8mL of antibody solution

Half-size membrane in divided dish will require 2.5-3mL of antibody solution

GAPDH aliquots are stored in -20°C, small freezer, diluted 1:100 in water. Diluting these aliquots 1:200 in antibody dilution solution will give appropriate 1:20,000 dilution of GAPDH.

Note: you can add both primary antibodies (GAPDH and protein of interest) in the same solution, **as long as you have previously assessed each antibody for non-specific binding.*

4. After blocking, rinse membrane 4 times with PBS-Tween, 5 minutes each on the rocker, then add 1° antibody. Cover and rock slowly **overnight on rocker at 4°C**.

2° Antibody and Imaging

1. Wash the membrane with PBS-Tween 4 times for 15 minutes each on the rocker, then do a final wash with 1X PBS, rocking for 5 minutes.
2. In a conical tube, prepare 2° antibody for your protein of interest. For each membrane, combine 2.5-8 mL (depending on size of membrane) Odyssey blocking buffer, 0.1% Tween-20 (10 µL of Tween-20), 0.02% SDS (20 µL of 10% SDS) + 0.5 µL 2° antibody for a 1:20,000 dilution.
3. Add 2° antibody, cover with foil, and place on rocker at room temperature for 45 minutes.
4. Pour off antibody, then wash membrane with PBS-Tween, 4X for 5 minutes each on rocker. Do one final 5 minute wash with 1X PBS to ensure no Tween-20 remains on the membrane.
5. In a conical tube, prepare 2° antibody for GAPDH. For each membrane, combine 10 mL Odyssey blocking buffer, 0.1% Tween-20 (10 µL of Tween-20), 0.02% SDS (20 µL of 10% SDS) + 0.5 µL 2° antibody for a 1:20,000 dilution.

6. Add 2° antibody, keep covered with foil, and place on rocker at room temperature for 45 minutes.
7. Pour off antibody, then wash membrane with PBS-Tween, 4X for 5 minutes each on rocker. Do one final 5 minute wash with 1X PBS to ensure no Tween-20 remains on the membrane.
8. Walk blot to Biotech building, 3rd floor, to the Odyssey LICOR infrared imager. Image blot with Image Studio software (both red and green channels).
9. After imaging, rinse membrane a few times, then remove 1° and 2° antibodies by applying Restore Western Blot Stripping Buffer (8 mL). Rock for ~15 minutes.
9. Repeat primary and secondary antibody application for two new proteins of interest.

Solutions and Buffers:

Stock solutions for RIPA buffer

2.5 M NaCl

7.305 g in 50 ml 18 mΩ H₂O, store at room temperature

$$(0.05 L) \left(\frac{2.5 \text{ moles}}{L} \right) \left(\frac{58.44 \text{ g}}{\text{mol}} \right) = 7.305 \text{ g in } 50 \text{ ml H}_2\text{O}$$

1 M Tris-HCl, pH 8.0

6.057 g Tris base in 50 ml 18 mΩ H₂O

pH to 8.0 with high molar (12.1M) HCl, store at room temperature

$$(0.05 L) \left(\frac{1 \text{ mol}}{L} \right) \left(\frac{121.14 \text{ g}}{\text{mol}} \right) = 6.057 \text{ g in } 50 \text{ ml H}_2\text{O}$$

10% Sodium Deoxycholate

5 g in 50 ml 18 mΩ H₂O, store at room temperature

10% SDS

5 g in 50 ml 18 mΩ H₂O, store at room temperature

Protease/phosphatase inhibitors stock solutions

1 M NaF

0.4199 g in 10 ml 18 mΩ H₂O, store at -20°C in 25 μl aliquots

$$(0.01 L) \left(\frac{1 \text{ mol}}{L} \right) \left(\frac{41.99 \text{ g}}{\text{mol}} \right) = 0.4199 \text{ g in } 10 \text{ ml H}_2\text{O}$$

100 mM NaVO₄ (sodium orthovanadate) – prepare under a fume hood

$$(0.01 L) \left(\frac{100 \times 10^{-3} \text{ mol}}{L} \right) \left(\frac{183.91 \text{ g}}{\text{mol}} \right) = 0.184 \text{ g in } 10 \text{ ml H}_2\text{O}$$

0.184 g in <10 ml 18 mΩ H₂O

Set pH to 9.0 with HCl

Boil until colorless

Cool, and set pH to 9.0 again

Bring up to 10 ml with 18 mΩ H₂O

} Repeat this cycle until solution remains at

Store at -20°C in 10 μl aliquots

Protease Inhibitor Cocktail (PIC)

Aliquot into 15 μL and store at -20°C

Gel-making solutions

30% acrylamide/BIS (37.5:1) – store at 4°C in dark *Note: Gels used for protein are commonly 37.5:1 Acrylamide:BIS or 29:1 Acrylamide:BIS

Make ~250 ml, store at 4°C in dark

For a 37.5:1 acrylamide:bisacrylamide solution: 37.5 g Acrylamide } in 18
1 g Bisacrylamide } mΩ

For a 30% acrylamide:bisacrylamide (37.5:1) solution: $x(0.3) = 38.5$
 $x = 128.33 \text{ ml H}_2\text{O}$

Mix 37.5 g acrylamide and 1 g bisacrylamide with 128.33 ml 18 mΩ H₂O (will need to heat solution to ~37°C to dissolve). Cover with tin foil and store at 4°C. To make ~250 ml, double all ingredients.

1.5 M Tris-HCl, pH 8.8

36.34 g Tris base in 200 ml 18 mΩ H₂O
pH to 8.8 with high molar (12.1M) HCl, store at room temperature

$$(1.5 \text{ M}) \left(\frac{121.14 \text{ g}}{\text{L}} \right) \left(\frac{1 \text{ L}}{1000 \text{ ml}} \right) (200 \text{ ml}) = 36.34 \text{ g in } 200 \text{ ml H}_2\text{O}$$

1.0 M Tris-HCl, pH 6.8

24.22 g Tris base in 200 ml 18 mΩ H₂O
pH to 6.8 with high molar (12.1M) HCl, store at room temperature

$$(1.0 \text{ M}) \left(\frac{121.14 \text{ g}}{\text{L}} \right) \left(\frac{1 \text{ L}}{1000 \text{ ml}} \right) (200 \text{ ml}) = 24.22 \text{ g in } 200 \text{ ml H}_2\text{O}$$

10% Ammonium Persulfate (APS)

APS – 0.1 g
18 mΩ H₂O – 1 ml

Buffers

10X Running Buffer (use as stock – use 1X Running Buffer in experiments)

Tris base (250 mM) – 30.3 g/L
Glycine (1.92 M) – 144.1 g/L
SDS (1%) – 10 g/L
18 mΩ H₂O – 1 L

Store at room temperature

10X Transfer Buffer (use as stock – use 1X Transfer Buffer in experiments)

Tris base (250 mM) – 30.3 g/L
Glycine (1.92 M) – 144.1 g/L

18 mΩ H₂O – 1 L
Store at 4°C

Washes

1X PBS-0.1% Tween-20

18 mΩ H₂O – 900 mL
10X PBS – 100 mL
Tween-20 – 1 mL

Store at room temperature

1X PBS

10X PBS – 100 mL
18 mΩ H₂O – 900 mL

Store at room temperature

Materials:

Acrylamide (Sigma A9099-25G)

Ammonium Persulfate (APS) (Sigma A9164-25G)

Bisacrylamide (N-N'-methylenebisacrylamide) (Sigma M2022-25G)

Blotting Grade Blocker (Nonfat dry milk) (BioRad, 970-6404)

Glycine (Sigma G8898-500G)

IGEPAL CA-630 (Sigma 18896-50mL)

Methanol (Sigma 34860-1L)

Protease Inhibitor Cocktail (PIC) (Sigma P8340-1mL)

Sodium Chloride (NaCl) (Sigma S5886-500G)

Sodium Deoxycholate (Sigma D6750-10G)

SDS (Sodium Dodecyl Sulfate) (Shelton Scientific, IB07060, 100G)

Sodium Fluoride (NaF) (Sigma S7920-100G)

Sodium Orthovanadate (NaVO₄) (Sigma S6508-10G)

TEMED (N,N,N',N'-Tetra-methylethylenediamine) (BioRad 161-0801)

Tween-20 (Sigma P9416-100mL)

Pierce BCA Protein Assay Kit (Thermo Scientific, 23227)

Western Blotting Filter Paper (Thermo Scientific, 88600)

Nitrocellulose Membrane (Thermo Scientific, 88018)

Two channel protein marker (LICOR 928-40000)

Laemmli Sample Buffer (BioRad, 161-0737)

Odyssey Blocking Buffer (LICOR 928-40000)

Goat anti-mouse 800 (green) (LICOR 926-32210)

Goat anti-rabbit 680 (red) (LICOR 926-68071)

Restore Western Blot Stripping Buffer (Thermo Scientific, 21059)

1. Butcher JT, Markwald RR (2007) Valvulogenesis: the moving target.

Philosophical Transactions of the Royal Society B 362: 1489–1503.
doi:10.1098/rstb.2007.2130.

2. Farrar EJ, Butcher JT (2012) Valvular Heart Diseases in the Developing World: Developmental Biology Takes Center Stage. *The Journal of Heart Valve Disease* 21: 234–240.
3. Mahler GJ, Farrar EJ, Butcher JT (2013) Inflammatory Cytokines Promote Mesenchymal Transformation in Embryonic and Adult Valve Endothelial Cells. *Arteriosclerosis, Thrombosis, & Vascular Biology* 33: 121–130. doi:10.1161/ATVBAHA.112.300504/-/DC1.
4. Balachandran K, Alford P, Wylie-Sears J, Goss JA, Grosberg A, et al. (2011) Cyclic strain induces dual-mode endothelial- mesenchymal transformation of the cardiac valve. *Proceedings of the National Academy of Sciences*: 1–6.
5. Mahler GJ, Frenzl CM, Cao Q, Butcher JT (2014) Effects of shear stress pattern and magnitude on mesenchymal transformation and invasion of aortic valve endothelial cells. *Biotechnol Bioeng* 111: 2326–2337. doi:10.1002/bit.25291.
6. Yang J-H, Wylie-Sears J, Bischoff J (2008) Opposing actions of Notch1 and VEGF in post-natal cardiac valve endothelial cells. *Biochemical and Biophysical Research Communications* 374: 512–516. doi:10.1016/j.bbrc.2008.07.057.
7. Combs MD, Yutzey KE (2009) Heart valve development regulatory networks in development and disease. *Circulation Research* 105: 408–421.
8. Chen J-H, Yip CYY, Sone ED, Simmons CA (2009) Identification and Characterization of Aortic Valve Mesenchymal Progenitor Cells with Robust Osteogenic Calcification Potential. *The American Journal of Pathology* 174: 1109–1119. doi:10.2353/ajpath.2009.080750.
9. Visconti RP, Ebihara Y, LaRue AC, Fleming PA, McQuinn TC, et al. (2006) An in vivo analysis of hematopoietic stem cell potential. *Circulation Research* 98: 690–696.
10. Skowasch D, Schrempf S, Wernert N, Steinmetz M, Jabs A, et al. (2005) Cells of primarily extravalvular origin in degenerative aortic valves and bioprostheses. *European Heart Journal* 26: 2576–2580.
11. Nichols J, Zevnik B, Anastassiadis K, Niwa H (1998) Formation of

pluripotent stem cells in the mammalian embryo depends on the POU transcription factor Oct4. *Cell*.

12. Pesce M, Schöler HR (2001) Oct-4: Gatekeeper in the Beginnings of Mammalian Development. *STEM CELLS* 19: 271–278. doi:10.1634/stemcells.19-4-271.
13. Zeineddine D, Papadimou E, Chebli K, Gineste M, Liu J, et al. (2006) Oct-3/4 Dose Dependently Regulates Specification of Embryonic Stem Cells toward a Cardiac Lineage and Early Heart Development. *Developmental Cell* 11: 535–546. doi:10.1016/j.devcel.2006.07.013.
14. Shi G, Jin Y (2010) Role of Oct4 in maintaining and regaining stem cell pluripotency. *Stem Cell Research Therapy* 1: 39.
15. Sternecker J, Höing S, Schöler HR (2011) Concise Review: Oct4 and More: The Reprogramming Expressway. *STEM CELLS* 30: 15–21. doi:10.1002/stem.765.
16. Schöler HR, Dressler GR, Balling R, Rohdewohld H, Gruss P (1990) Oct-4: a germline-specific transcription factor mapping to the mouse t-complex. *The EMBO journal* 9: 2185.
17. Takahashi K, Yamanaka S (2006) Induction of pluripotent stem cells from mouse embryonic and adult fibroblast cultures by defined factors. *Cell*.
18. Liu K, Ji G, Mao J, Liu M, WANG L, et al. (2012) Generation of Porcine-Induced Pluripotent Stem Cells by Using OCT4 and KLF4 Porcine Factors.
19. Blin G, Nury D, Stefanovic S, Neri T, Guillevic O, et al. (2010) A purified population of multipotent cardiovascular progenitors derived from primate pluripotent stem cells engrafts in postmyocardial infarcted nonhuman primates. *The Journal of Clinical Investigation* 120: 1125. doi:10.1172/JCI40120.